The V_H Repertoire and Clonal Diversification of B cells in Myositis and Vasculitis

A Thesis submitted to the University of Glasgow for the degree of

Doctor of Philosophy

by

Donna McINTYRE, BSc., MSc.

Division of Immunology, Infection and Inflammation
Glasgow Biomedical Research Centre
Faculty of Medicine
University of Glasgow

January 2009

ABSTRACT

Autoimmune inflammatory reactions occur in a number of disorders to a variety of self antigens but the precise cellular and molecular mechanisms resulting in pathology are largely unresolved. In some instances T cell mediated reactions are thought to be the main contributors to disease mechanisms but it is becoming increasingly evident that B cells, and their cognate antibodies, play a significant and contributory role in disease pathogenesis. Therefore establishing the occurrence of highly-specific B cell antigen-driven adaptive immune responses within autoimmune disorders would provide a valuable understanding into the roles of B cells within these disorders.

The work of this study sought to determine the incidence of these B cell antigen-driven adaptive immune responses in the target tissues of the autoimmune disorders myositis and vasculitis, two autoimmune disorders characterised by a wide range of autoantibodies which have been implicated in the pathological mechanisms of these diseases. This study aimed to test the hypothesis that infiltrating B cells within the target tissue of myositis and vasculitis patients were being stimulated by antigen present within the tissue resulting in clonal diversification and affinity maturation mechanisms which would contribute to the pathological mechanisms of these disorders.

Initially the cellular phenotypes and organisations of the inflammatory infiltrating cell population were characterised by immunohistochemical techniques, with particular interest on the infiltrating B cell and plasma cell populations. No typical ectopic germinal centre structures were observed in the target tissues from either disorder; cellular aggregations varied from loose aggregations to dense cellular follicles. Both B cell and plasma cell phenotypes were included in these infiltrating populations in correlation with varying numbers of cells positive for helper, cytotoxic and regulatory T cell, follicular dendritic cell, macrophage and proliferating cell markers. Double fluorescent labelling of B cells with the Ki67 proliferation marker indicated the possible expansion and clonal diversification of these cells within the target tissues. To address the main objective of this study and the possible antigen-driven mechanisms and active participation of these infiltrating B cells within the target tissue of these

disorders, Ig gene repertoires, mutational characteristics, clonal diversification and affinity maturation were examined from infiltrating cells microdissected from areas of aggregation within the target tissues of both disorders. From the muscle infiltrating cells, Ig gene selections which were both patient and disease specific, mutational characteristics and oligoclonal expansion of B cells were observed establishing the involvement of muscle infiltrating B cells in the antigen-driven responses within inflamed muscle. Alternatively in the inflamed skin of vasculitis patients very few Ig gene rearrangements could be identified and no clonally related sequences or oligoclonal expansion of B cells were observed despite mutational characteristics indicating that antigen-driven diversification had occurred within these cells. Collectively the results indicate a role for B cells in the antigen-driven responses towards autoantigens within both disorders, either within an active antigen-driven response within the target tissue or at alternative sites resulting in cell migration into the target tissues.

In the final part of this study recombinant antigens were used to identify antigen-specific B and plasma cells within the inflammatory infiltrating cell population in some cases of myositis. Pilot experiments were conducted to establish the sequence characteristics of Ig genes from these antigen-specific cells.

Results of this study demonstrate the influence of B cell antigen-driven responses, either directly or indirectly, within the target tissues of myositis and vasculitis patients respectively, although the exact mechanisms leading to autoimmune reactions, and additional roles of B cells within these reactions, remain unresolved. The work presented from this study provides a foundation for further work to fully ascertain the role of B cells and antibodies within the target tissues of autoimmune disorders and in characterising the disease-associated antibodies, identifying stimulating antigens as well as assessing the effects of somatic hypermutation on the affinity and specificity of autoantigen specific antibodies. Increased understanding of B cells in these disorders will ultimately assist in the diagnosis and management of these diseases.

LIST OF CONTENTS

LIST OF FIGURES

Chapter 1

Chapter 2

Chapter 3

Chapter 4

Chapter 6

LIST OF TABLES

Chapter 1

Chapter 2

Chapter 3

Chapter 4

Chapter 6

ABBREVIATIONS

AASV	ANCA-associated systemic vasculitides
ADM	Amyopathic DM
AECA	Anti-Endothelial Cells Antibodies
AID	Activation-induced cytidine deaminase
ANA	Anti-Nuclear Antibody
ANCA	Antineutrophilic cytoplasmic antibody
APAAP	Alkaline phosphatase anti-alkaline phosphatase
APC	Antigen Presenting Cell
ARS	Aminoacyl-tRNA synthetase
AS	Ankylosing spondylitis
ASS	Antisynthetase syndrome
BAFF	B cell Activating Factor
BCR	B Cell Receptor
Biotin NHS	Biotin (Long Arm) N hydroxysuccinimide ester
bp	Base Pair
Bregs	Regulatory B cells
BSA	Bovine Serum Albumin
C	Constant Region
cDNA	Complementary DNA
CD	Clusters of Differentiation
CDR	Complementarity Determining Regions
CK	Creatine Kinase
CSR	Class Switch Recombination
CSS	Churg-Strauss syndrome
D	Diversity Region
DC	Dendritic Cell
DM	Dermatomyositis
DMSO	Dimethyl sulfoxide
dNTP	Deoxynucleoside triphosphate
DNA	Deoxyribonucleic acid
dsDNA	Double Stranded DNA
DZ	Dark Zone
EDTA	Ethylenediaminetetraacetic acid
ELISA	Enzyme-linked immunosorbent assay
ELP	Early lymphoid progenitors
ER	Endoplasmic Reticulum

FBS	Foetal Bovine Serum
FDC	Follicular dendritic cell
FR	Framework
GC	Germinal Centre
HEV	High endothelial venules
HSC	Hematopoietic stem cells
HSP	Henoch-Schönlein purpura
HT	Hashimoto's thyroiditis
Ig	Immunoglobulin
IC	Immune Complex
IBM	Inclusion Body Myositis
ICAM-1	Intercellular adhesion molecule-1
IFN	Interferon
IHC	Immunohistochemistry
IL	Interleukin
IPTG	Isopropyl-β-D-thiogalactopyranoside
J_H	Junctional Region
JAM	Junctional adhesion molecules
KD	Kawasaki Disease
LB	Luria Bertani
LCM	Laser Capture Microdissection
LZ	Light Zone
MAA	Myositis Associated Antigen
MG	Myasthenia Gravis
MHC I/II	Major Histocompatibility Complex I/II
M.O.M	Mouse on Mouse
MPA	Microscopic polyangitis
MPO	Myeloperoxidase
mRNA	Messenger RNA
MS	Multiple Sclerosis
MSA	Myositis Specific Antigen
MZ	Marginal Zone
NK	Natural Killer Cell
OA	Osteoarthritis
PAN	Polyarteritis nodosa
PBL	Peripheral Blood Lymphocytes
PBMC	Peripheral Blood Mononuclear Cells

PBS	Phosphate Buffered Saline
PCR	Polymerase Chain Reaction
PDC	Plasmacytoid Dendritic Cell
PM	Polymyositis
PR3	Proteinase 3
R	Replacement (Mutation)
RA	Rheumatoid Arthritis
RAG 1/2	Recombination-activating genes 1/2
RNA	Ribonucleic acid
RPM	Revolutions per minute
RSS	Recombination signal sequences
RT-PCR	Reverse Transcriptase PCR
S	Silent (Mutation)
scFV	Single Chain Fragment Variable
ssDNA	Single Stranded DNA
SHM	Somatic Hypermutation
SLE	Systemic Lupus Erythematosus
SRP	Signal Recognition Particle
SS	Sjögrens Syndrome
TBS	Tris Buffered Saline
TdT	Terminal deoxynucleotidyl transferase
TEM	Transendothelial migration
TGF-β	Transforming Growth Factor-β
TLR	Toll-like Receptor
TNF	Tumour Necrosis Factor
Tregs	Regulatory T cells
T1D	Type 1 Diabetes
V_H	Variable Heavy Chain
V_L	Variable Light Chain
WG	Wegener's granulomatosis
X-Gal	5-bromo-4-chloro-3-inodyl-β-D-galactopyranoside

In loving memory of my sister

Karen

1975-2009

Always in our thoughts

Forever in our hearts

ACKNOWLEDGEMENTS

I would like to thank my supervisors Prof. David Stott and Dr Max Field for giving me the opportunity to undertake this research and their help and guidance during the course of my PhD. In recent months I have been gratefully appreciative of the advice and support of Prof. Iain McInnes and Dr Alastair Gracie. I would also like to thank the Dr Robert Mairs' Charitiable Trust for funding this work.

I am grateful to the staff of the Dermatology Department at the Royal Infirmary, Glasgow and the staff of the Pathology Department, Western Infirmary, Glasgow for their assistance during different aspects of this research. In particular I would like to thank Linda MacKinnon for helping me locate archival biopsies and Dr Fiona Henriquez for her expertise with the Laser Capture Microdissection. My thanks also go to Prof. Paul Plotz, National Institute of Health, Betheseda, MD, USA and Prof. Bill Stimpson, Strathclyde University, Glasgow for their kind gifts of recombinant antigens and antibodies. I am gratefully appreciative of the advice from Dr Gary Sims, Dr Nancy Longo and Dr Daniel Russ, past and present contributors of the JOINSOLVER Programme, Dr Mohamed Uduman, CLIP administrator, Yale University and Dr Tony Speekenbrink, Clinical Microbiology, University of Glasgow for his help with statistical analysis. Prof. Thomas Kepler and Dr Joe Volpe, Duke University, also very kindly provided me with normal control data.

I received a lot of help from various people in the GBRC and would like to thank them all and let them know that it was very much appreciated. I am especially grateful to Miss Cecilia Lindestam, Dr Susan Short, Dr Michelle Bellingham, Dr Anne-Sophie Rouzière, Dr Arunima Mukhopadhay, Dr Su Crail and Dr Fi Stirling for helping and guiding me through all the bumps along the way.

Lastly I would like to thank my family and friends, in particular my parents, Sandra, Amy and Fraser for their constant love, support and patience. This also includes my sister Karen, who despite suffering her own troubles in the last couple of years, has been an unwavering source of love and support.

DECLARATION

This thesis represents original work carried out by the author, and has not been submitted in any form to any other University. Where materials have been received, due acknowledgement has been made in the text.

Donna McIntyre
January 2009

Chapter 1 – General Introduction

1.1 The Immune Response in Health and Autoimmunity

The immune system is the body's protection from infections and pathological agents and the damage they can cause by utilising a variety of cells and soluble factors. After breaching the initial physical and chemical barriers of the body, the immune system mediates the body's protection from invading pathogens using the innate and adaptive components of the immune system (1). The innate immune system is the body's immediate line of defence which occurs rapidly following infection with no specificity and limited memory. This component of the immune system is effective in defending against a large array of pathogens due to it's recognition of common pathogenic structural features. Invariant pathogen recognition receptors (PRRs), which include Toll-like receptors (TLRs), on effector cells such as macrophages, neutrophils, eosinophils, basophils, mast cells and dendritic cells recognise simple and regular molecular structures and patterns, pathogen-associated molecular patterns (PAMPs) on invading pathogens. The effector mechanisms of these cells, like phagocytosis, aim to eliminate and neutralise the invading pathogen. If these mechanisms fail, the adaptive immune responses are activated to enhance the protection generated by innate responses. In contrast to the innate immune system, the responses of adaptive immunity are antigen specific and exhibit memory, providing enhanced protection against re-infection of the pathogen, but occur in a time-delayed manner in comparison to the innate responses. Although these responses work by different mechanisms both can work in collaboration with each other through direct cell contacts and cytokine and chemokine interactions, ultimately shaping the nature of the immune response. The adaptive immune responses are mediated through the effector mechanisms of B and T cells; each expresses a receptor of unique antigen specificity, B cell Receptor (BCR) and T cell Receptor (TCR) respectively, following the random recombination of receptor gene segments. Selection and activation of these cells in the immune response can result in humoral and/or cell mediated immune responses. Humoral immunity mechanisms respond to extracellular antigens and results in the production of antigen-specific antibodies produced by B cells which can aid the eradication of pathogens by neutralisation, opsonisation and complement activation (1). Antigens bound to

the BCR of B cells are endocytosed, processed and presented on Major Histocompatibility Complex (MHC) class II molecules at the cell surface. These B cells become activated following interactions with antigen-specific $CD4^+$ T helper cells, which have previously been activated by antigen to differentiate into effector cells following antigen recognition and co-stimulation from antigen presenting cells (APCs) such as dendritic cells and macrophages, and recognise the antigens presented on the MHC class II molecules of B cells at the edges of lymphoid follicles in the periphery lymphoid organs. $CD4^+$ T helper cells activate B cells through a number of paired interactions at the cell surface. Key interactions include CD40 ligand (CD154) on T cells with CD40 on B cells. This interaction causes B cells to increase expression of co-stimulatory molecules, particularly of the B7 family (CD80/CD86), which interact with CD28 expressed on T cells which provides important signals to sustain T cell growth and differentiation. In addition to these interactions, $CD4^+$ T helper cells also secrete cytokines upon activation. T helper 1 cells secrete cytokine including IFN-γ and TNF-α while T helper 2 cells secrete cytokines including IL-4, 5, 10 and 13. These cytokines, in addition to other activation signals, can drive proliferation and differentiation of the cells as well as induce clonal expansion, isotype switching and synthesis and secretion of antibodies from B cells. In some instances, with T independent antigens, antibody production can be induced in the absence of T helper cells as these antigens provide sufficient B cell stimulation in the absence of T cells. Cell mediated mechanisms respond to antigens that are generated intracellularly, e.g. by virus infection, and presented on MHC molecules expressed on APCs (1). $CD8^+$ and $CD4^+$ cells are activated to differentiate into effector cells in the T cell rich zones of the peripheral lymphoid organs. In cell mediated immunity, $CD4^+$ T helper cells recognise antigens presented on MHC class II molecules by APCs and become activated through similar cell surface interactions that have been previously described like the CD40L-CD40 and B7-CD28 interactions and activate phagocytes. $CD4^+$ T helper 1 cells participate in macrophage activation, the secretion of IFN-γ by the T cell along with the co-stimulation via the CD40 ligand is sufficient to activate the macrophage and boost the antimicrobial mechanisms within the macrophages. In addition to macrophage activation, the IFN-γ released by the T helper 1 cells can also be used to activate other cells

involved in cell mediated immunity such as $CD8^+$ T cells and NK cells. $CD8^+$ T cells recognise pathogenic peptides presented by MHC class I molecules on APCs and are activated to release cytotoxic effector proteins such as perforins and granzymes, which induce cell death of the virus infected cell. $CD4^+$ T helper cells may also be required in the activation of $CD8^+$ T cells. In cases where sufficient co-stimulation is not provided by the APC, $CD4^+$ T cells may be required to provide extra help in the activation and stimulation of $CD8^+$ T cells through stimulation of the APC to upregulate the surface expression of B7 molecules which can increase the co-stimulation to $CD8^+$ T cells driving proliferation and differentiation of these cells in the cell mediated immune response. Regardless of which mechanism is mediating the immune response, any infection and the responding immune mechanisms will initiate an inflammatory reaction in response to the invading pathogen.

1.1.1 Inflammation

Inflammation is a major component of the body's defence mechanism and is a complex process initiated by physical, chemical, biological or immunological injury and the inflammatory response constitutes an important part in both the innate and adaptive immune responses (1). Inflammation involves activation of resident tissue cells and recruitment of immune cells from the circulation in response to inflammatory mediators such as cytokines and chemokines resulting in tissue disruption, both structurally and functionally.

The recruitment of B and T lymphocytes, and other inflammatory cells, to sites of inflammation is a multi-step process which includes tethering and rolling, activation, firm adhesion and transendothelial migration (TEM) of lymphocytes; a process which is mediated by chemokines and a number of adhesion molecules (**Figure 1.1**) (1-4). Circulating lymphocytes tether and role along endothelium as a result of low-affinity interactions with the selectin adhesion molecules (L-, P- and E-selectin) which effectively slow down the flow of the circulating lymphocytes. This brings lymphocytes into contact with the endothelial surface and allows them to sample the local environment. Activation molecules and stimulation of the cells leads to a firm adhesion to the endothelium while in the absence of stimuli the lymphocytes detach and remain

in the circulation. The firm adhesion of stimulated cells is mediated by the up-regulation of integrins which brings the adherent cell to arrest and allows progression to TEM. TEM is a complex process and the exact mechanisms are unresolved but it is dependent on the integrin binding to endothelial cells and the activation of lymphocytes by chemokines. TEM generally occurs through endothelial cell junctions, formed by the interactions of a number of adhesion molecules, including junctional adhesion molecules (JAMs) along increasing chemokine gradients. JAMs have been implicated in vascular inflammation as a result of redistribution to the apical surface to increase the adhesion of lymphocytes (5). The final obstacle in the recruitment of lymphocytes is the basement membrane but the mechanisms of this are incompletely understood. Release of endothelial cells into the circulation as a result of necrosis has been observed, intensifying the pathology at the endothelial surface and exacerbating inflammatory reactions (6-9). Resolution of inflammation aims to restore the injured tissue back to its normal state but in cases where the stimulating factors could not be removed, or by loss of regulation, chronic inflammation results in severe tissue damage and loss of function with progressing clinical symptoms. These chronic inflammatory reactions can occur due to defects in the body's regulatory processes of tolerance which results in immune and inflammatory responses against self components of the body resulting in autoimmune responses.

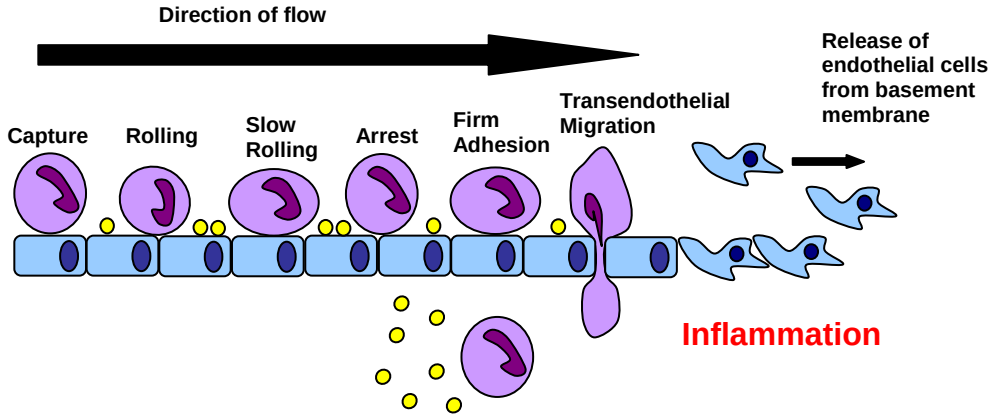

Figure 1.1 The Multistep Model of Lymphocyte Extravasation

Recruitment of lymphocytes to areas of inflammation occurs from a multistep process. Initially interactions between lymphocytes and adhesion molecules (selectins) slow the rate of lymphocyte movement along the endothelial surface. Chemokines (○) at the epithelial surface stimulate the lymphocyte and integrin binding halts the lymphocyte on the cell surface. Lymphocytes then migrate through the epithelial cell layer by transendothelial migration towards a source of chemokine production. Unstimulated cells detach from the endothelial surface and remain in the circulation. Chronic inflammation can result in endothelial cell necrosis causing them to detach from the basement membrane and enter the circulation. Adapted from 1-4.

1.1.2 Tolerance Mechanisms in Controlling Autoimmunity

Tolerance is the regulation of immune responses to antigens ensuring that immune responses to self-antigens are controlled and repressed while maintaining the capacity to exert an effective immune response against foreign antigens; essentially the discrimination between self- and non-self antigens. Tolerance is applied to cells with antigen-specific receptors, T and B cells, and is acquired following interaction of a self-antigen with an antigen-specific lymphocyte which results in signalling for cell inactivation. Due to the process of the antigen receptor generation by random recombination of receptor gene fragments, the development of autoreactive cells is a normal consequence. Between 20 and 50% of TCRs and BCRs generated are thought to bind with dangerously high affinity to self antigens; the work of one group found that 75% of gene rearrangements in immature B cells were autoreactive (10-12). Despite the generation of these autoreactive cells, tolerance mechanisms aim to regulate and arrest the development of these cells.

Tolerance is induced at a number of stages along lymphocyte development and differentiation pathways. To prevent immune responses towards self-antigens, developing T and B cells, with specificity towards self-antigens, undergo negative selection in early stages of development within the primary lymphoid organs, the thymus and bone marrow for T and B cells respectively, resulting in cell inactivation. This process of cell inactivation is known as central tolerance but such reactions can also be carried out in the periphery with mature lymphocytes, which have either escaped central tolerance mechanisms or became self-reactive as a result of further receptor-gene diversification processes in the periphery, resulting in peripheral tolerance. The lymphocyte tolerance mechanisms in these reactions can result in cell editing, deletion or inactivation (anergy) (1;11;12), but these mechanisms are not mutually exclusive and cells that were initially anergised may be deleted at a later stage. Upon detection of an autoreactive high affinity self antigen by BCR or TCR expressed on immature B cells or immature thymic T cells within the bone marrow and thymus respectively, the maturation of the cell is halted. Within the bone marrow homing and activation receptors such as CD62L and B cell activating factor (BAFF) are poorly expressed or induced. Conversely

recombination-activating gene 1 (RAG1) and RAG2 are continually expressed to allow the BCRs to be edited. Receptor editing involves the further rearrangement of the antigen specific receptor to alter the antigen specificity of the cells allowing the rescue of these cells from inactivation. For the antibody light (L) chains of B cells, upstream V_L and downstream J_L gene segments of the rearranged V_LJ_L can recombine to form a new V_LJ_L rearrangement (1). In heavy (H) antibody chains of B cells, due to the process of V(D)J recombination, discussed further in section 1.4, all unused D segments are deleted. For editing of the rearranged gene to occur, cleavage at cryptic recombination signal sequences (cRSS) located near the 3' end of the V_H gene results in formation of a double-stranded break. Following cleavage, recombination with a new V_H gene results in a new V(D)J rearrangement (13), reviewed (14). The receptor editing processes of central tolerance can also occur within the periphery as receptor revision. This peripheral tolerance mechanism, and its importance in tolerance, has been recently substantiated by the work of Wang and Diamond (15) reviewed (16). This study demonstrated the re-expression of RAG proteins, essential components of recombination processes, in peripheral autoreactive B cells in germinal centre (GC) responses but also following activation of autoreactive B cells by soluble antigen outside of the GC environment. This work follows previous studies which have identified RAG expressing B cells in the peripheral blood of lupus patients (17) and the synovial tissue of Rheumatoid Arthritis (RA) patients (18). Within T cell populations TCRs can stimulate an editing process which downregulates TCRs and allows RAG expression to continue to allow the offending TCR α-chain to be replaced or diluted with a second α-chain that is less self-reactive. If the receptor fails to edit sufficiently in both B and T cells, cell deletion occurs due to increased levels of BIM (BCL-2-interacting mediator of cell death) that inhibit the BCL-2 family of proteins which are essential for lymphocyte survival or activate death receptors such as Fas (11;12). Both editing and deletion processes occur within developing T cells but deletion appears to be the dominant process. Anergy is a process which leaves B and T cells in an unresponsive state and occurs when B and T cells recognise antigens without sufficient levels of co-stimulation, from helper T cells and APCs that are required for full cell activation. Several mechanisms of anergy have been documented and include

the downregulation and decreased display of BCRs and TCRs on the cell surface, the blocked transfer of new antigen receptors from the endoplasmic reticulum as well as increased expression of inhibitory receptors such as CD5 on both B and T cells and cytotoxic T-lymphocyte antigen 4 (CTLA-4) on T cells which are increased on self reactive cells and inhibit cell activation (1;11;12;19-21). An additional mechanism is also thought to play a role in tolerance, clonal ignorance in which B and T cells that have failed to be edited or trigger deletion co-exist with antigen without being affected by it as the self-reactive cells are either not in contact with the stimulating antigen or they binds so weakly that there is insufficient signalling to activate the cell. In the periphery, with large numbers of circulating B and T cells, self-reactive cells can fail to receive sufficient stimulation and activation factors such as BAFF and IL-7 for B cells and T cells respectively and are competitively deleted (22;23). In addition to regulating self-reactive cells that have escaped the central tolerance mechanisms, peripheral tolerance mechanisms also need to regulate a second generation of self-reactive cells that are produced within GC reactions, a result of the additional receptor gene diversification mechanisms. These cells potentially have an increased affinity for self antigens and have the potential to diversify into memory and long-lived plasma cells which would produce self-reactive antibodies indefinitely. GC reactions also have the potential to be a powerful stimulus for self-reactive cells in the production of autoantibodies by the presentation of self antigens within immune complexes. Little is known about the tolerance mechanisms that normally deal with self-reactive cells participating in GC reactions but it has been demonstrated that self-reactive BCRs induce subtle differences in the cell's responsiveness to chemokine gradients which excludes them from follicles and minimises the self-reactive cell's participation in germinal centre reactions (12;24).

Another aspect of tolerance is the role of regulatory T and B cells within peripheral tolerance. In recent years vast arrays of studies have been conducted on regulatory T cells (Tregs) and their ability to suppress rather than activate immune responses. These $CD4^+$ differentiated T cells can arise during normal T cell development and are thought to make up approximately 5-10% of the $CD4^+$ cell population but are committed to a regulatory fate in the thymus

after high-affinity binding to MHC molecules containing self peptides rather than being deleted or inactivated under the tolerance mechanisms described above (25). Once released into the periphery as a mechanism of tolerance, the exact mechanisms of suppression by these cells are not fully established. Studies have demonstrated that suppressive mechanisms include the regulation of responses by the IL-10 and TGF-β cytokines produced by these cells (26) and it has also been shown that they can affect the maturation and antigen-presentation capacity of DCs (27). Regulatory T cells have been classified as natural Tregs but adaptive Tregs have also been described which differentiate from a heterogeneous group of naïve $CD4^+$ T cells in the periphery under the influence of particular environmental conditions to elicit suppressive effects on auto-reactive responses.

Recently it has been shown that B cells may also have a suppressive and regulatory role in immune responses in addition to their role as positive regulators of immune responses. Most of the evidence for regulatory B cells presently comes from studies in autoimmune mouse models, such as EAE where they prevent the development of disease as well as reduce the severity of disease once it has been established, but the existence of a Breg cell subset has yet to be confirmed in humans. It is thought that these cells may suppress the activation and differentiation of T cells, disrupt the antigen-presenting function in DCs, promote autoantibody mediated clearance of apoptotic cells to reduce the autoantigenic load or induce the activity of Tregs (28;29). Studies have established that Bregs mediate their effects through IL-10 but what remains unclear is if this regulatory mechanism is a general property of multiple B cells subsets or if it is unique to a specific suppressive subset of B cells (28;30;31).

Although these mechanisms aim to remove and inactivate self-reactive T and B cells, and prevent the initiation of immune reactions towards self-antigens, not all of these cells are removed during these tolerance mechanisms under normal conditions. Self-reactive responses may also occur as some antigens may be ignored by these mechanisms as they are below the critical threshold and are present at too low a concentration or some antigens may be present at

immunologically privileged sites that do not elicit a destructive immune response under normal conditions. Disruption to the integrity of these tolerance mechanisms leads to the initiation of self-reactive responses within the body, resulting in specific B and T cell adaptive immune responses against self antigens leading to the development of autoimmune diseases.

1.1.3 Breaking of Self-Tolerance and the Autoimmune Response

A vast array of autoimmune disorders exists but the precise aetiology and initiating antigens of these responses is unknown in most cases. Autoimmune disorders can be broadly classified , based on the tissue or organ involved, as organ-specific like Multiple Sclerosis (MS), Myasthenia Gravis (MG), Type 1 Diabetes (T1D), Hashimoto's Thyroiditis (HT) with responses to organ specific autoantigens and the formation of tissue specific autoantibodies or non-organ-specific or systemic which includes Rheumatoid Arthritis (RA), Systemic Lupus Erythematosus (SLE), Inflammatory myopathies, such as Dermatomyositis (DM), Sjögrens Syndrome (SS) and various vasculitic disorders which affect multiple organs and generate autoantibodies that are not tissue specific, although not all autoimmune disorders can be classified according to these criteria (1). The initiation of autoimmune responses occurs when there is disruption of tolerance mechanisms and activation of self-reactive cells as previously described, although self-reactive cells are part of the normal cell repertoire and activation of self-reactive cells, at a low level, is physiological and crucial to the normal immune function and does not always necessarily lead to the development of a pathological response to self-antigens. Under normal conditions self-reactive cells help to shape and form the repertoire of mature lymphocytes. Autoreactive cells are part of the normal cell repertoire but with autoimmune disorders occurring in approximately 5% of the population a number of other susceptibility factors must also play a role in autoimmune disorders (1). Pathological autoimmune responses develop when a number of safe-guard and tolerance mechanisms are overcome or disrupted resulting in a sustained response towards self-antigen generating effector mechanisms that result in tissue damage. A combination of factors such as genetic predisposition and exposure to environmental triggers are thought to initiate autoimmune responses in addition to alterations in tolerance mechanisms.

Firstly, age and gender may play a role in the initiation of autoimmune responses. Autoantibodies are more prevalent in older people and certain autoimmune disorders have female or male bias. DM and SLE are more commonly observed in females, with a 9:1 female:male bias observed in SLE, whereas Ankylosing Spondylitis (AS) affects more male than female patients (1;32;33).

Genetic susceptibility factors can have various influences on the development of autoimmune disorders from a genetic predisposition from inherited MHC genes to polymorphisms of genes that are involved in maintenance of self-tolerance and immune regulation such as regulatory proteins. Many autoimmune disorders are heterogeneous with no one gene sufficient to initiate disease mechanisms. The most common evidence of a genetic predisposition is the higher incidence of disease in monozygotic twins, with a lower but still increased incidence in dizygotic twins and family members in relation to an unrelated population. Regardless of any other variables for the initiation of autoimmune reactions, predispositions of autoimmune disorders are associated with certain MHC alleles. MS and RA are associated with the DR2 and DR4 alleles respectively while SLE, SS, MG and Inclusion Body Myositis (IBM) have an association with the DR3 allele (1;34). Most autoimmune disorders have an association with MHC class II alleles but there are cases for a strong association with type I alleles, like B27 observed in over 90% of AS patients (35), reviewed (36). These particular alleles may contribute to the development of autoimmune reactions through the presentation of self antigens, or mimics, driving positive selection of autoreactive cells; the presence or absence of the appropriate MHC determines whether a potential autoantigen is presented and the occurrence of a response to the antigen. These alleles may only be expressed at low levels or have low affinity towards the antigen that would not drive a negative selection response but are present at a sufficient level and with sufficient affinity to drive positive selection. It may also be the case that the antigens presented on these alleles may fail to stimulate the formation of regulatory T cells or they are inefficiently presented.

Polymorphisms in a number of other genes have also been associated with the development of autoimmune reactions. Single-nucleotide polymorphisms (SNPs) have been observed in the *CTLA-4* and *PTPN22* genes (1;12;37;38). As previously mentioned CTLA-4 is an inhibitory receptor expressed on T cells. Lack of CTLA-4 has been shown to cause a large accumulation of self-reactive T cells in peripheral and nonlymphoid organs and causes disruption of both TCR-induced proliferation but also impairs the suppressive properties of Tregs. Defects in this gene caused by SNPs are associated with diseases such as T1D and Grave's disease (19). Similarly to CTLA-4, PTPN22, protein tyrosine phosphate nonreceptor type 22, is involved in suppression of T cell activation and SNPs within this gene are associated with T1D as well as RA and SLE (39;40). Mutations within the *AIRE* (autoimmune regulator) gene, which promotes the thymic expression of peripheral tissue-restricted genes, have been found to be responsible for autoimmune polyendocrinopathy-candidiasis-ectodermal dystrophy (APECED) which leads to destruction of multiple endocrine tissues (1;12;37;38). In addition to subtle mutational changes within genes, the deletion or overexpression of genes resulting in defects in cytokine production or signalling can also contribute to the pathogenesis of autoimmunity; overexpression of TNF-α is associated with arthritis and vasculitis while underexpression of the same cytokine is associated with SLE. Elevated BAFF levels have also been reported in a number of autoimmune disorders, including the inflammatory myopathies, in particular DM (41;42).

As well as these genetic mechanisms, defects may also occur in other aspects of the immune response. Defects in regulatory T cell functions have been described in SLE (43) and in MS patients where Treg populations are normal but their suppressive activity is defective (1;44). Several autoimmune disorders have also been associated with apoptosis. The process of programmed cell death is essential for the prevention of autoimmune reactions as this process is responsible for the removal of self-reactive cells and the downregulation of immune responses to self antigens. Impaired generation or clearance of apoptotic cells and alterations in apoptosis machinery can reduce resistance to normal processes of cell death and expose cytoplasmic and nuclear components that are normally sheltered from the immune system. Mutations

within Fas genes have been associated with autoimmune lymphoproliferative syndrome (ALPS), T1D and MS (1;38).

Breakdowns in tolerance and the initiation of autoimmune reactions have also been associated with a number of infections that can initiate autoimmune reactions by a number of pathways. For example, certain subsets of vasculitis have been associated with hepatitis B and C viruses as well as *Staphylococcus aureus* and parvovirus B19 infections (45), SLE has been associated with the Epstein-Barr virus (32;33) and Guillain-Barré syndrome is associated with *Campylobacter jejuni* infections (12;46;47). Infectious agents may directly activate autoreactive cells by presenting antigens that are cross-reactive with self antigens in a process of molecular mimicry. As a result, the immune response and resultant antibodies produced against the infectious agent are directed against self antigens. The structures of the infections agent and the self antigen do not need to be identical as long as they are sufficiently similar to be recognised by the same antigen receptor or antibody. Once self-reactive cells have been activated by these cross-reactive mechanisms, the effector functions of these cells can lead to tissue destruction. This mechanism has been shown for Guillain-Barré syndrome where antibodies produced in response to *C. jejuni* infections are directed towards components of the peripheral nerves (12;46;47). An infectious agent may not necessarily trigger a pathogenic autoimmune response directly; this may follow as a result of epitope spreading in the reaction. Epitope spreading is the diversification of the epitope specificity and extension of the autoreactive response from the initial focused epitope to new epitopes and new autoantigens (37;38;48). As a result of the immune response towards the initial infectious agent, previously hidden or cryptic epitopes of the autoantigen may be presented to the immune system, as well as a modified version of the initial epitope due to altered processing mechanisms, resulting in a cascade of autoreactive cells within the response and an extension of the self-reactive immune response to multiple epitopes. Epitope modification can also occur due to exposure to drugs or other chemical agents. These may modify self-components and result in the formation of neo-antigens which the immune system has never seen and therefore is not tolerant towards, eliciting an autoreactive immune response (1;37). Drug associated

disorders been observed in a number of autoimmune disorders, including SLE patients following exposure to procainamide, as well as a number of other drugs, and in myositis patients as a result of statin therapy (32;33;49).

The strong inflammatory response to infections may itself stimulate an autoreactive response as a result of non-specific activation of self reactive cells in a process known as bystander inflammation (37;38;48). The response to infections may result in tissue damage or cell death which may cause release, and increase the presentation, of potential autoantigens that have previously been sequestered from the immune system which stimulate the activation of autoreactive cells. The inflammatory mediators, such as cytokines, generated during the immune response could lead to the attraction, activation and expansion of autoreactive cells at sites of infection as well as stimulation of anergic cells which have previously been inactive, perpetuating the autoimmune response. It has also been described that stimulatory ligands released by the invading infectious agent, such as CpG dinucleotides, may stimulate antibody production from autoreactive B cells, stimulating the autoimmune response (12;50). These ligands are recognized by TLRs on B cells and partially substitute for T cell help promoting autoantibody production.

The adaptive immune responses involved during autoimmunity are incapable of removing the offending antigen therefore the immune responses persists with a constant supply of antigen resulting in amplification of the response which manifests as tissue damage as a result of the effector mechanisms. The effector mechanisms associated with autoimmune disorders are generally classified according to the scheme adopted for hypersensitivity reactions (1). Type I, IgE mediated, reactions do not seem to play a major role in autoimmune reactions but conversely Type II, autoantibody mediated, reactions are common. Autoantibodies bind to the cell surface and either alone via Fc receptor opsonisation or with the help of complement damage cells. This is observed in autoimmune hemolytic anaemia (AIHA) where IgG autoantibodies bind to red blood cells leading to rapid destruction of the cells. In Goodpasture's syndrome the IgG autoantibodies bind directly to cells in the tissue resulting in tissue damage. Within this type of reaction, the antibodies

can bind and either interfere or enhance the functional activity of the cell. In MG, the binding of autoantibodies to the acetylcholine receptor block the neuromuscular transmission from the receptor whereas in Grave's disease the autoantibodies continually stimulate production of thyroid hormone. Type III, immune complex (IC) mediated disorders result from circulation of ICs composed of soluble antigen and autoantibodies resulting in systemic manifestations. ICs are normally cleared in healthy individuals but clearance may be defective or may be overwhelmed by the continuous supply of autoantigens in self-reactive responses. ICs can mediate tissue damage by activation of complement or phagocytic cells through Fc receptors. These types of effector mechanisms have been observed in autoimmune disorders such as various vasculitic disorders and SLE where ICs are deposited in blood vessels and kidneys respectively. Finally Type IV, T cell mediated, mechanisms occur in disorders such as Type 1 diabetes and MS. These autoreactive T cells not only play a helper role in autoimmune development but also have a direct, cytotoxic, role in tissue damage similar to the mechanisms during a normal immune response.

As described above, autoimmune diseases are multifactoral and involve an extensive range of cells and effector mechanisms but B cells and their production of autoantibodies are frequently central to these mechanisms and autoimmune reactions. Some disorders are thought to be directly dependent on the actions of B cells while in some disorders it is thought that B cells merely play an accessory role. The full extent of B cell involvement and the precise role of these cells have not fully been established in a number of autoimmune diseases. Given the potential for B cells in GC reactions to generate and diversify high-affinity self-reactive B cells, and the resultant autoantibodies, as well as the identification of GCs as tertiary lymphoid organ (TLO) formations at ectopic sites adjacent to autoantigen sources in a number of autoimmune disorders, reviewed (51), the production of tissue-specific and/or disease relevant autoantibodies and development of effector mechanisms *in situ* is an important component of the autoimmune response in a number of disorders. Previous studies have identified autoreactive B cells generated in ectopic GCs in a number of autoimmune disorders including MG (52), SS (53) and HT (54)

and most recently in RA (55), but they have not yet been identified in a number of other autoimmune disorders such as myositis and vasculitis. Myositis, as well as vasculitis, discussed further in sections 1.2 and 1.3, are a series of systemic disorders with unknown aetiology that have been associated with aspects of the different genetic and environmental features discussed in this section that may disrupt self tolerance resulting in the formation of autoantibodies and leading to the initiation of autoimmune disease. The work presented in this thesis examines the loss of B cell tolerance in these disorders to determine if B cells are being locally stimulated by self-antigen leading to the production of potentially self reactive high affinity autoantibodies.

1.2 Myositis

Inflammatory myopathies, or myositis, are inflammatory disorders of the muscle composed of 3 principal subsets, dermatomyositis (DM), polymyositis (PM) and Inclusion body myositis (IBM) (56-68). Other forms of myositis have also been described and include giant cell myositis, eosinophilic myositis, granulomatous myositis, necrotizing myositis and drug-associated myositis, induced notably by HMG-CoA reductase inhibitors (statins) (49;56;69;70). A diagram representing normal muscle architecture, in cross-section, is shown in **Figure 1.2** and identifies the regions where inflammation and lymphocyte aggregation are observed within the 3 myositis subsets. Each of the 3 principal disorders is characterised by moderate to severe muscle weakness and mononuclear inflammatory cell infiltrates (59). Patients with myositis present with varying degrees of muscle weakness which may develop over weeks to months as a result of muscle inflammation. Diagnosis of myositis is based on the results of an electromyography, elevated muscle enzymes in serum (creatine kinase (CK)) by as much as 50 fold and a muscle biopsy to define histological changes. Concentrations of CK usually parallel the disease activity but normal levels may be found in some DM and IBM patients; continuous elevated CK levels have been reported during active PM (58;71). Inflammatory myopathies are systemic and often multi-organ illnesses, skin, heart, lungs, gastrointestinal tract and joints can all be affected in each disorder (56). Classification criteria for myositis was originally devised by Bohan and Peter (72;73) but this failed to distinguish between PM and IBM and the criteria has recently been revised

(58). Each of the 3 inflammatory myopathies have been seen in connection with various autoimmune and connective tissue diseases as well as being associated with malignancies (58); malignancy is thought to be associated with up to 45 % of adult DM patients (71). DM and PM have been reported in 4-16% of Systemic Lupus Erythematosus (SLE) cases with DM most commonly found, a retrospective study of myositis in SLE found that the muscle disease observed in SLE was similar, in a small sample size, to primary myositis disorders (61). The pathogenesis and mechanisms of cellular injury are still unresolved in myositis; possible mechanisms are summarized in **Figure 1.3**.

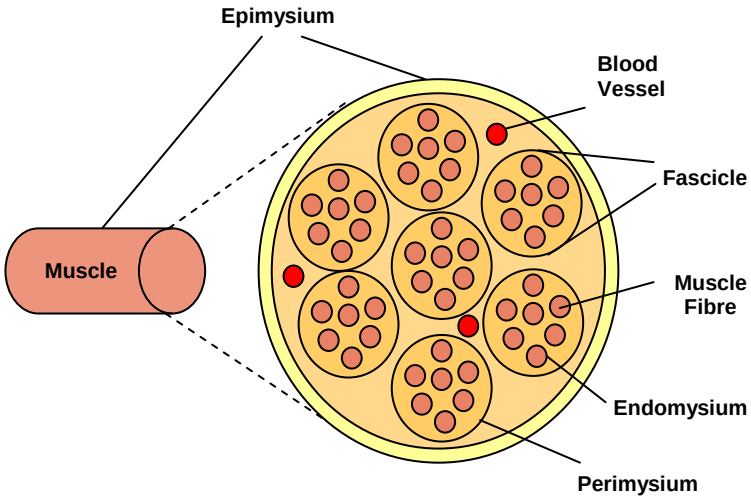

Figure 1.2 Transverse-Sectional Representation of Skeletal Muscle Tissue.

Muscle tissue consists of three dense layers of connective tissue. The outermost layer, encircling the whole muscle is the **epimysium**. The **perimysium** surrounds bundles, or **fascicles**, of individual muscle fibres. Within the fascicle each individual **muscle fibre** is surrounded by the **endomysium**. Muscles are well supplied with blood vessels and capillaries which are abundant within the endomysium surrounding each muscle fibre.

In inflammatory myopathies various patterns of lymphocytic infiltration are observed. In DM this pattern is largely perimysial/perivascular surrounding fascicles while in PM/IBM inflammatory infiltrates are largely endomysial and are found surrounding individual muscle fibres within fascicles.

1.2.1 Dermatomyositis (DM)

DM, found in both children and adults, is observed in women more than men and is the most common inflammatory myopathy (58;63). DM is characterised by a heliotrope rash on the upper eyelids, face or upper trunk accompanying or more commonly preceding proximal muscle weakness (63;74;75). Gottron rash is also observed in approximately 30% of DM patients; a raised rash or papules at the knuckles, prominent in metacarpophalangeal and interphalangeal joints (56;58;63;75). Inflammation is predominately perivascular and/or perimysial or in the interfascicular septae and around, rather than within, the muscle fascicles but can extend into the individual muscle fascicles along the endomysium at fascicle edges (Figure 1.2). Perivascular atrophy is another characteristic within DM patients, a result of degeneration and phagocytosis of muscle fibres often in

groups at the periphery of the fascicle at perimysial locations (60). Lymphocyte infiltrations in DM have a higher than normal percentage of B and $CD4^+$ cells compared to $CD8^+$ cells (58-60;65). The proximity of $CD4^+$ cells to B cells and macrophages and the absence of lymphocytic invasion into muscle fibres suggest that DM is a humorally mediated immune response, possibly towards microvessels. B cells observed within inflammatory myopathies are more commonly observed in muscle tissue from patients with DM compared to PM or IBM (65). The immune process in DM is thought to be directed against microvascular antigens in a process mediated by the complement C5b-9 membrane attack complex (MAC). Complement deposits result in necrosis of the endothelial cells leading to muscle fibre destruction (58-60). Complement activation occurs early in disease triggering the release of proinflammatory cytokines which upregulate VCAM-1 and ICAM-1 on endothelial cells and facilitates the transmigration of activated lymphoid cells to the perimysial and endomysial spaces (60).

Different subsets of DM have been described in patients (75-77); patients with amyopathic DM (ADM) display the classical cutaneous features of DM for prolonged periods of time without clinical evidence of muscle weakness and with normal muscle enzymes. Hypomyopathic DM (HDM) has also been described which is similar to ADM except that upon testing evidence of muscle inflammation is evident. These distinctive subsets have also been observed within juvenile myositis (78). DM is the most frequent inflammatory myopathy observed in children, approximately 85% of all juvenile inflammatory myopathies (78). The peak onset age of juvenile DM is approximately 7 years although a broad distribution is observed throughout childhood. 25% of cases have onset prior to age 5, and is primarily observed within girls although a similar incidence has been reported between boys and girls (63;78). Certain characteristics are observed in juvenile DM that are not frequent within the adult form of the disease; dystrophic calcification with calcium deposits in the skin, subcutaneous tissue or muscle are observed in 30% of patients (78). For both the adult form of the disease and juvenile DM the same major immunogenetic risk factors haven been identified which include HLA DRB1*0301 and it's linked allele DQA1*0501. In addition to similar risk factors, similar protective factors

have been identified in European Americans, DQA1*0201, *0101 and *0102 (78). The similar risk and protective factors observed between juvenile DM and the adult form suggest common elements within the disorders.

1.2.2 Polymyositis (PM)

PM is generally observed after the second decade of life and is best defined as a subacute myopathy that evolves over weeks to months and presents with symmetrical weakness of the proximal muscles (58). The actual onset of PM is hard to define as there are no early recognition signs such as the rash observed in DM. As a stand-alone disorder PM is uncommon and is more commonly observed in conjunction with other autoimmune and connective tissue disorders. PM is characterised by scattered necrotic and regenerating muscle fibres and endomysial inflammation with invasion and destruction of non-necrotic muscle fibres (Figure 1.2) (65;66). Inflammatory infiltrates mostly consist of $CD8^+$ T cells and macrophages which invade MHC class I antigen expressing muscle fibres leading to fibre necrosis via the perforin pathway suggesting the immune reactions target muscle fibres (56;58-60;63;65;66). MHC class I expression, absent from normal muscle fibres but found widespread in inflammatory myopathies (79), is thought to be induced by cytokines secreted by activated T cells and macrophages. The MHC class $I_{(muscle)}$: CD8 complex $_{(T\ cell)}$ is characteristic of PM. A proportion of the infiltrating cytotoxic $CD8^+$ T cells have been shown to be clonally expanded and suggest an antigen-driven T cell response. These cells have conserved amino acid sequences within the CDR3 region of the T cell receptor (TCR) while other infiltrating, non-invading cells are clonally diverse (59;65;67;80-84). Pathology within PM is a result of these clonally expanded $CD8^+$ T cells invading muscle fibres that express the MHC class I antigen which results in fibre necrosis via the perforin pathway (63). Cytotoxic $CD8^+$ T cells can release 3 cytotoxic proteins: perforin, granzyme and granulysin (65). Perforin may cause a leak in the sarcolemmal surface through which granzymes could invade the muscle to initiate fibre necrosis (65). This pathogenesis pathway has also been observed in perforin/granzyme expressing $CD4^+$ lymphocytes, reviewed (65), although perforin was found to be randomly distributed in the cytoplasm of $CD4^+$ cells in comparison to $CD8^+$ cells where perforin is located towards the target muscle

fibre (85) . The ER stress response pathway has also been proposed to result in muscle damage (86). Nagaraju *et al* (86) demonstrated that the ER stress response pathway was highly activated in human myositis and that overexpression of MHC class I, observed in muscle fibres, induces the ER response.

Immunohistochemical studies have demonstrated that few $CD20^+$ B cells are present within PM muscle biopsies in contrast to T cells which would indicate that humoral mediated immune responses do not play a major role within PM (87;88). Greenberg *et al* (89) examined the infiltration of $CD138^+$ plasma cells in PM muscle biopsies. In PM samples B cells displayed a mean density of 2.8 cells / mm^2, while $CD138^+$ plasma cells displayed a mean density of 11.0 cells / mm^2 which were predominately located in the endomysium. The identification of plasma cells within PM biopsies was confirmed by sequence analysis of Ig V-genes expressed by single plasma cells isolated by laser capture microdissection. Although the occurrence of plasma cells was established the functional role of these cells in PM was unclear until a subsequent study (90) demonstrated that infiltrating plasma cells in PM were clonally related and undergoing an antigen-driven response.

1.2.3 Inclusion Body Myositis (IBM)

In male patients over the age of 50 IBM is the most frequent inflammatory myopathy with distinctive atrophy and weakness of wrist and finger flexors and quadriceps and can often be asymmetrical (34;56;59;60;63;71;91). Although similar to PM, less frequent myofibre necrosis and increased invasion of non-necrotic fibres by lymphocytic infiltrates have been observed in IBM (65;66). Other features of IBM include rimmed vacuoles and groups of atrophic fibres (68). A strong association with HLA DR3 has been reported and is present in approximately 75% of cases (34). $CD8^+$ T cells are the dominant infiltrating cell which surround and invade MHC class I expressing muscle fibres, the characteristic MHC class I : CD8 complexes found within PM are also characteristic of IBM (59;60;63). Also the invading $CD8^+$ T cells within IBM have been demonstrated to be clonally expanded while non-invading infiltrating $CD8^+$ T cells were found to be clonally diverse (59;80;92-94). Amemiya *et al* (92)

demonstrated the clonal restriction of T cells within IBM and observed that these clonally related T cell sets persist over the course of the disease. It was also noted that identical rearrangements were found at different muscle biopsy sites of the same patient as well as in different patients implying a continued response to the same antigens. In addition to clonally expanded muscle infiltrating T cells within the muscle, evidence has demonstrated that these clones also recirculate into the blood (65;80;93) but this may also occur as a result of the same antigen being present at both sites leading, independently, to the expansion of T cells at both sites. IBM differs in its clinical presentation as the hallmarks of IBM are usually atrophy and weakness of the quadriceps and the wrist and finger flexors, producing distal rather than proximal weakness (56;68). In contrast to PM, IBM has a slowly progressing clinical course, over months to years and is unresponsive to treatment (34;60). Pathology associated with IBM is thought to occur by the same $CD8^+$ perforin/granzyme mechanism that is observed in PM but an additional pathological mechanism is thought to occur in IBM patients. Granular deposits are found to be distributed around vacuoles along with amyloid deposits, first identified in 1991, within or next to vacuoles, suggesting that two concurrent pathological processes are occurring within IBM (34;59;63).

As found within PM, infiltrating plasma cells were identified in biopsies taken from IBM patients (89). $CD138^+$ plasma cells displayed a mean density of 17.2 cells / mm^2 while B cells were observed at a mean density of 4.2 cells / mm^2. These infiltrating plasma cells were also found to be clonally related within IBM samples (90) indicating that an antigen–driven response was also occurring within IBM and that T cells may not be the only cell mediating an antigen-specific response within inflammatory myopathies and other autoimmune diseases.

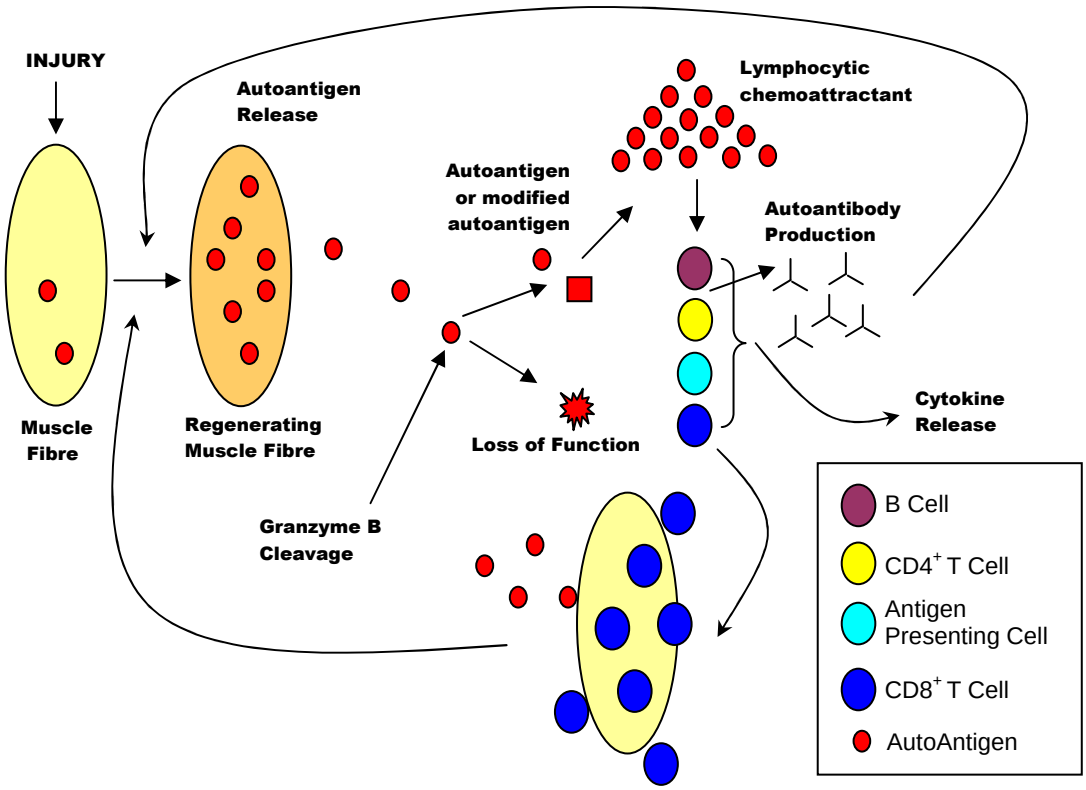

Figure 1.3 Possible Mechanisms of Pathology in Myositis

A muscle lesion induces the overexpression of autoantigens, most notably from regenerating muscle fibres. The released autoantigen may undergo conformational changes resulting in cleavage by granzyme B generating unique fragments that were still able to generate a high autoantibody titre response. Alterations in autoantigens may promote apoptosis within muscle fibres. Autoantigen fragments may exert chemotactic effects resulting in the influx of several cell types. B cell and $CD4^+$ T cells and may be stimulated to produce autoantibodies which could contribute to further pathology or $CD8^+$ T cells may surround and invade muscle fibres via the Granzyme : perforin pathway resulting in muscle fibre necrosis and further autoantigen release. Adapted from 95.

1.2.4 Autoantibodies and Autoantigens in Myositis

As with most autoimmune disorders different autoantibodies have been described within the myositis subsets DM and PM (95;96). Classically autoantibodies are absent from IBM although they have been detected in a small number of cases (95;97). The presence and diversity of these autoantibodies demonstrates the significance of B cell tolerance in the complexity of these disorders. Myositis autoantibodies can either be classified as myositis-specific autoantibodies (MSAs), specific for the muscle disorder myositis not specific for muscle tissue, or myositis-associated autoantibodies (MAAs) (95;96), **Table 1.1**. Generally individual patients comprise of a single MSA but may also have one or more MAAs (95). Most of these autoantibodies are directed to protein or ribonucleoprotein complexes involved in protein

synthesis, translocation or elongation. MAAs target antigens are primarily located in the nucleoplasm or nucleolus.

Myositis-Specific Autoantibodies (MSA)	Target Antigen	Myositis-Associated Autoantibodies (MAA)	Target Antigen
Anti-tRNA synthetases -	Aminoacyl-tRNA synthetases –		
Anti-Jo-1	Histidyl-tRNA synthetase	Anti-Ro60	Cellular Antigen Ro60/SSA
Anti-PL7	Threonyl- tRNA synthetase	Anti-Ro52	Cellular Antigen Ro52/SSA
Anti-PL12	Alanyl-tRNA synthetase	Anti-La	Cellular Antigen La/SSB
Anti-EJ	Glycyl-tRNA synthetase	Anti-RNP	Ribonucleoprotein
Anti-OJ	Isoleucyl-tRNA synthetase	Anti-Ku	Heterodimer bound to protein kinase
Anti-KS	Asparaginyl-tRNA synthetase	Anti-PM/Scl	Nucleolar macromolecular complex
Anti-JS	Glutaminyl-tRNA synthetase		
Anti-tRNA His Anti-tRNA Ala	tRNA His tRNA Ala		
Anti-Mi-2	Nuclear Helicase		
Anti-SRP	Signal-Recognition Particle		
Anti-FER	Elongation Factor 1α (eEF1α)		
Anti-KJ	30/34kDa Translocation Factor		
Anti-Wa	48kDa unknown peptide		

Table 1.1 Myositis-Specific Antigen (MSAs) and Myositis-Associated Antigens (MAAs)

Casciola-Rosen *et al* (98) recently examined autoantigen expression in normal and myositis tissues and observed increased levels of autoantigens in myositis affected muscle, particularly in regenerating muscle cells, compared to the low levels in control muscle. Low autoantigen expression in normal muscle indicates that an immune response, directed against myositis antigens, is unlikely to be initiated in normal, unperturbed normal muscle. Enhanced autoantigen expression was observed in muscle cells of an immature and regenerating phenotype. Despite the emergence of autoantigens in diseased muscle, no site of initiation for the immune response was identified although it was hypothesised that forms of proinflammatory muscle injury may induce muscle regeneration which in turn induces autoantigen expression resulting in pathology. The study suggests that damage focused on cells achieving repair produces a feed-forward loop mechanism where regenerating cells provide an ongoing antigen supply in the disease progression and therefore are targets for

attack in the autoimmune process. This may account for the well defined but patchy histological changes of myositis next to apparently normal areas of muscle. Previous studies by Casciola-Rosen *et al* (99) in SLE have demonstrated that the majority of autoantigens were effectively cleaved by granzyme B generating unique fragments that were still able to generate a high titre autoantibody response, illustrating the complexity of antigen-driven responses.

1.2.4.1 Aminoacyl-tRNA synthetases (ARS)

The most prevalent MSAs are directed against amino-acyl-tRNA-synthetases (ARS) (95;96;100). These molecules are cytoplasmic enzymes which catalyse the ATP-dependent binding of tRNAs to the corresponding amino acid, forming an aminoacyl-tRNA, so that the amino acid can be incorporated into a growing polypeptide chain. The presence of anti-ARS and its clinical manifestations has been termed antisynthetase syndrome (ASS) which consists of myositis (DM or PM), idiopathic interstitial lung disease (ILD), arthritis and Raynaud phenomenon (100;101). ASS carries a severe prognosis with a threefold increase in mortality compared to myositis without these antibodies (95). Anti-ARS antibodies are found in 16-26% of patients with inflammatory myopathies but the precise roles of these antibodies are still unresolved (100). The specific anti-ARS antibodies found in myositis patients are shown in Table 1.1. These antibodies are not cross-reactive and occur independently of one another (102). Anti-Jo-1 antibodies are the most prevalent antibodies found in myositis patients; they are found in 20-30% of patients while the other anti-ARS antibodies are only present in 1-3% of patients (100;103;104). The increased occurrence of anti-Jo-1 antibodies indicates that synthetases are not randomly targeted; targeting of these antibodies may be the result of increased expression or improved presentation (105). Anti-ARS antibodies are mainly observed in DM and PM patients and are rarely observed in IBM patients and in a pattern similar to other MSAs; only one type anti-ARS antibody is ever observed in each myositis patients (95;104). Anti-OJ and anti-KS antibodies have been shown to have a stronger association with ILD than with myositis and may distinguish a subtype of ASS (106), while anti-Jo-1 and anti-PL-12 has a strong association with ILD in patients with myositis (107;108). Levine *et al*

(107) recently addressed whether alterations in histidyl-tRNA synthetase expression and/or conformation was observed in the lung of affected patients. A unique, granzyme B cleavable form of histidyl-tRNA synthetase was located in the lung. The presence of this form in the lung and not within muscle focuses attention on the lung as the potential driving environment for immunity against histidyl-tRNA synthetase. Muscle may become targeted at later stages upon injury to muscle when histidyl-tRNA synthetase antigen levels are increased (98). ARSs can be classified into Class I and Class II synthetases based on overall structure, characteristic motifs and site of tRNA attachment (96;105). Most of the ARSs found in myositis patients, anti-Jo-1, -PL-7, -PL-12, -EJ and –KS, belong with Class 2 synthetases but anti-OJ is a Class 1 synthetase that exists as part of a multi-enzyme synthetase complex (96;105). Recent studies have identified two new anti-ARS antibodies, anti-phenylalanyl synthetase antibodies (anti-Zo) (109) and anti-tyrosyl antibodies (110).

ARS molecules have been shown to possess chemoattractant properties and generate an ARS-specific autoimmune response in myositis and ILD (105;111;112). Histidyl-tRNA synthetase and a 1-48 amino acid histidyl-tRNA synthetase peptide were chemotactic for human $CD4^+$, $CD8^+$ and IL-2 activated monocytes that express the CCR5 receptor but not for neutrophils or unstimulated monocytes that do not express CCR5 (111;112). Asparaginyl-tRNA synthetase was chemotactic for CCR3-expressing mononuclear cells. The chemoattractant properties of these proteins were only two to four folds higher over background levels and were not as efficacious as chemokines but were potent enough to induce migration *in vitro*. Both proteins were also chemotactic for immature dendritic cells (iDC) which express both CCR5 and CCR3. These findings suggest that the tRNA synthetases may participate in the initiation of an adaptive immune response which leads to the production of autoantibodies; by engaging receptors on iDCs the tRNA synthetases may be more likely to initiate T and B cell responses (111). The chemotactic activity of the tRNA synthetases for iDCs may initiate a cascade of immune events, beginning with the antigen presentation to T lymphocytes and production of B lymphocyte stimulating cytokines that results in the production of autoantibodies in some patients (111). These chemotactic effects were not observed for the

nonautoimmune synthetases aspartyl and lysyl-tRNA synthetases. Other autoantigens, such as La and ssDNA, were also examined but failed to induce leukocyte migration (112). The reasoning of targeting anti-ARSs or why some are targeted over others is largely unknown, as previously described it could result from differing expression, presentation or generation of unique fragments from granzyme B cleavage. The similarities in structure may suggest that a common structural factor is involved but it has been shown that antibodies to different synthetases do not crossreact (96;102).

Anti-Jo-1 antibodies are the most prevalent anti-ARS found in myositis patients and are a diagnostic marker for autoimmune myositis and a prognostic marker for disease severity (104;113;114). Anti-Jo-1 antibodies were first described in 1980 from the serum of a patient affected with PM (104). Formation of these antibodies could be attributed to molecular mimicry from infectious agents, Jo-1 shares structural homology with a protein, EC-RF4, from Epstein Barr virus and the RNA of picornavirus (95;115). It has been suggested that autoantibodies result from interaction of the synthetase with a virus during viral replication which leads to the presentation of the synthetase to the immune system in association with the foreign viral protein resulting in a break in tolerance. The major epitope of histidyl-tRNA synthetase, a 60 amino acid portion, is located at the amino terminus of the protein and is predicted to have a coiled-coil configuration (WHEP-TRS domain) and autoantibody binding affects the conformation of the N terminus (104;107;113). Studies on mutant histidyl-tRNA synthetase, to establish the effects on reactivity with anti-Jo-1 antibodies, demonstrated that anti-Jo-1 antibodies recognise multiple conformation dependent and independent epitopes which may have occurred as a result of fragmented histidyl-tRNA synthetase released from inflamed muscle (104). Anti-Jo-1 antibodies have been identified in patients before the onset of myositis (116), similar to that observed in other autoimmune disorders such as SLE (117). A patient's anti-Jo-1 status may change from positive to negative during the course of disease (104) and has been found to correlate with disease activity (118). The presence of anti-Jo-1 antibodies has been associated with the presence of anti-Ro52 antibodies and was first discovered in 1997 (119;120) and was later confirmed in a subsequent study (102). Rutjes *et al*

(120) found that 21% of the sera from myositis patients were reactive with Jo-1 while 20% was reactive with Ro52. Isolating anti-Jo-1 positive sera demonstrated a higher frequency of anti-Ro52 antibodies, 58%, a similar percentage to the 70% found in the study conducted by Frank *et al* (102). It was established this was not due to cross-reactivity since no competition could be detected for recombinant Jo-1 protein and affinity-purified anti-Ro52 and anti-Jo-1 antibodies did not cross react with each other. Anti-Ro52 antibodies were also shown to be associated with other antibodies (102;121); other anti-tRNA-synthetases, anti-SRP and anti-PM-Scl but are rarely detected in patients with anti-Scl70 or anti-centromere antibodies (121). The co-existence of these antibodies has recently been considered to generate a programmed cytokine imbalance in PM and DM patients (122). Hassan *et al* (122) demonstrated that female patients with anti-Jo-1 and anti-Ro52 antibodies had a higher TNF:IL-10 ratio. Elevated TNF cytokine levels have been observed in DM and PM and have been implicated in associated pathological mechanisms. IL-10 is also of interest in autoimmune diseases as it exerts anti-inflammatory properties in addition to stimulatory effects on B cells and autoantibody production. This elevated ratio was not observed within male patients or within patients who had anti-ANA or anti-RNP antibodies. Elevated ratios of these cytokines may contribute to the development or aggravation of chronic inflammation. Reasons for the association of anti-Jo-1 antibodies and anti-Ro52 antibodies remains unclear as tRNA synthetases charge their nucleic acids in the cytoplasm and Ro52 occurs primarily in the nucleus (119;120) but the concordance of these two apparently unrelated ribonucleoproteins may provide a greater insight into the aetiology or pathogenesis of inflammatory myopathies (119).

Recently Eloranta *et al* (123) demonstrated that immune complexes containing anti-Jo-1 or anti-Ro52/Ro60 autoantibodies may act as endogenous IFN-α inducers that activate IFN-α production from plasmacytoid dendritic cells (PDCs). This may suggest that the type 1 IFN system may play a role in the disease mechanism of myositis although different mechanisms may occur in different myositis subsets.

1.2.4.2 Mi-2

Anti-Mi-2 autoantibodies are classified as MSAs and were first identified in 1976 in a 60 year old female DM patient (124). These autoantibodies are directed to a nuclear macromolecule complex of eight peptides ranging from 34 to 240 kDa. The complete complex is involved in transcription (95;124). Mi-2 autoantibodies preferentially recognise the 240 kDa portion of this complex. Two different but highly homologous proteins, resembling the 240 kDa portion of the complex, were identified and were labelled Mi-2α and Mi-2β. Both of these proteins are recognised by anti-Mi-2 antibodies (96;124). These Mi-2α and Mi-2β components exert helicase and acetylase-deacetylase activities which regulate transcription factor binding to DNA (95). Mi-2β is part of a complex known as NURD (nucleosome remodelling deacetylase) (95;96). Immunogenetic studies have shown a strong correlation of anti-Mi-2 antibodies with HLA-DR7 and there is evidence that a tryptophan residue at position 9 of the HLA-DRβ chain is a common epitope essential for Mi-2 antibody production (124). Anti-Mi-2 antibodies have been identified in approximately 4-18% of patients with myositis, and are primarily observed in patients with DM (95;124;125). Hengstman *et al* (100) report the autoantibody occurrence within DM as 13 – 21% (100) and it had been reported that more than 90% of anti-Mi-2 positive patients had juvenile or adult-onset DM (95;124) and show a classic representation of DM (124). As previously mentioned in section 1.2.1 subsets of DM have been described, a lower frequency of the Mi-2 antibody have occasionally been reported in the DM subset amyopathic DM (ADM) (124). Hengstman *et al* (100) report that these antibodies have only been seen in 2 patients with PM and never in IBM. Additional studies (126;127) have established the presence of anti-Mi-2 antibodies in the sera of PM and IBM patients. Most studies examining anti-Mi-2 antibodies used the NM fragment of the Mi-2β autoantigen which is thought to contain the major antigenic epitope. A recent study used the four different fragments of the Mi-2β autoantigen, NT, NM, M and CT fragments, to characterise these autoantibodies in myositis patients (126;127). Using these 4 fragments the presence of anti-Mi-2 autoantibodies were found in a large number of PM and IBM patients and these antibodies did not appear to be a marker for a specific subset of myositis. This

study was unable to confirm that these antibodies were specific for DM in contrast to previous investigations.

1.2.4.3 Additional MSAs

In addition to the presence of autoantibodies towards the cytoplasmic amino-acyl-tRNA-synthetase enzymes, autoantibodies may also be directed towards the cognate tRNA, tRNA ^{His} and tRNA ^{Ala}. Anti- tRNA ^{Ala} is detected in the sera of most patients with anti-PL12 autoantibodies whereas tRNA ^{His} is present in approximately a third of patients with anti-Jo-1 (100).

Another MSA found within myositis patients is the anti-SRP autoantibody, which is directed against components of the signal recognition particle (SRP) (95;100;128). Antibodies target a cytoplasmic ribonucleoprotein composed of six peptides (SRP 9, 14, 19, 54, 68, 72) including a dominant 54 kDa peptide and of a small RNA molecule (7 SL RNA). SRP recognises signal sequences in the N-termini of secretary proteins or membrane proteins to regulate the translocation of newly synthesized proteins across the endoplasmic reticulum (ER) membrane. Anti-SRP antibodies are uncommon and are found in only 5% of myositis patients, predominately PM although the antibodies have been observed in a small proportion of DM and IBM patients (95;100). Autoantibodies are most frequently directed against the SRP 54 protein, those directed solely towards the 7 SL RNA may be markers for a less severe disease (95). Patients with anti-SRP antibodies generally have proximal muscle involvement and have been associated with cardiac involvement. These antibodies are characteristic of necrotizing myopathies (128).

As shown in Table 1.1, other MSAs have been identified which are directed to cytoplasmic antigens. These antibodies are extremely rare and not readily detectable but characteristically resemble antisynthetase syndrome (95). Anti-FER autoantibodies are directed towards an elongation factor, while the target antigen for anti-KJ antibodies is a translocation factor. Anti-Wa antibodies are directed towards a 48 kDa peptide with an unknown function.

1.2.4.4 MAAs

As shown in Table 1.1 many MAAs have been described in myositis patients. Anti-Ro and anti-La antibodies have been detected in approximately 4 to 58% and 3 to 6% of myositis patients respectively (95) and have also been observed in SLE and SS patients. These antibodies are generally associated with an anti-synthetase like syndrome in comparison to anti-SRP positive myositis. A faint association of anti-Ro antibodies has been observed in myositis patients with anti-Mi-2 and anti-PM-Scl antibodies. As described in section 1.2.4.1 it is generally anti-Ro52 antibodies that are observed within myositis patients, in conjunction with anti-Jo-1 antibodies.

Anti-RNP proteins target the 70 kDa peptide of an 11 peptide containing complex. This ribonucleoprotein protein also contains five small RNA's. These antibodies are also found in other disorders, such as SLE, SS and scleroderma but are found in 5-60% of myositis patients (95).

Antibodies to the Ku antigen have been reported in 3-19% of myositis patients (95). The Ku antigen is a heterodimer composed of one 70 kDa and one 80 kDa peptide bound to a 350 kDa DNA-dependent protein kinase. The overall function of this complex is unknown but is thought to be involved in DNA repair and VDJ recombination. This autoantibody has also been observed within other conditions, such as scleroderma, SS and undifferentiated connective tissue disease (95).

Anti-PM-Scl autoantibodies are observed in 5-25% of myositis patients and are directed against a nucleolar macromolecular complex composed of 11-16 peptides (95). This complex is an exosome whose exoribonucleases destroy RNA's. A 100 kDa peptide is the main target for these autoantibodies. This antibody in myositis in conjunction with overlap syndromes such as scleroderma contributes to 43-88% of cases of myositis associated with the autoantibody.

1.2.4.5 Novel Autoantigens

Recently a number of novel autoantibodies have been identified within myositis patients. Anti-56 kDa antibodies have been found in 60-86% of myositis

patients and are directed against a nuclear ribonucleoprotein complex (95;129). These antibodies are fairly specific for myositis but have also been described in other forms of connective tissue disease (95;129).

Sato *et al* (130), reviewed (129;131), identified autoantibodies to a 140 kDa peptide, CADM-140, in Japanese patients with clinically amyopathic dermatomyositis. CADM-140 antibodies were identified in 19% of DM patients; all of these patients were diagnosed with clinically amyopathic DM (C-ADM). These antibodies were found to be associated with rapidly progressive ILD.

Another novel antibody was identified within myositis patients (132), reviewed (129;131), directed to a 155 kDa protein. This antibody was identified in sera from children and adults with inflammatory myopathies and was found to precipitate with a 155 kDa protein along with a weaker 140 kDa protein on most samples. This anti-p155 antibody was strongly associated with myositis, more frequently within DM (29.4%) compared to PM (4.2%); it was also observed in 75% of cancer-associated DM patients (132). Within juvenile DM patients this anti-p155 antibody appeared to be more common than other defined autoantibodies. Although this antibody was largely found within myositis patients, it has been observed in one patient with SLE who demonstrated no signs of myositis.

More recently Kraj *et al* (133) identified an anti-155/140 antibody which was highly specific for DM and reacted simultaneously with two proteins of 155 and 140 kDa. In this study anti-155/140 antibodies were found in 13% of DM patients, a frequency slightly lower than anti-EJ antibodies but were comparable or higher than other MSAs that were examined in the study, including anti-Jo-1, anti-OJ, anti-PL-7, anti-Mi-2, anti-SRP and anti-CADM140 antibodies. As observed for other MSAs (95) the anti-155/140 antibody did not co-exist with other known MSAs. In this study the anti-155/140 antibody was associated with internal malignancy and skin manifestations typical of DM but were not associated with ILD, indicating a high expression of 155/140 kDa antigens in cancer, skin and muscle but is absent or poorly expressed in the lung. Kraj *et al* (133) deemed that this antibody was different to that identified by Sato *et al*

(130) and Targoff *et al* (132) as a result of immunodepletion studies and the ever presence of the 140 kDa precipitated protein which was not observed in every patient within the Targoff study (132).

Autoantibodies towards the small ubiquitin-like modifier 1 (SUMO-1) activating enzyme A and B subunits, SAE1 and SAE2 respectively, have recently been identified in DM patients (134). These proteins are involved in the posttranslational modification of specific proteins. Although these antibodies were only observed in two patients both patients presented with similar clinical features, severe skin disease and interstitial pneumonia, suggesting that these autoantibodies may identify a further discrete subset of DM patients.

1.2.5 Therapies in Myositis.

Treatment of inflammatory myopathies can be complex, partly because the specific target antigens are unknown, therefore traditionally therapy has been based on non-selective immunosuppression or immunomodulation. Improved muscle strength, normalised CK levels and remission or stabilisation are the primary goals in treatment of myositis disorders (135). DM has been found to be the most treatable myopathy while responses in PM have also been favourable but responses have found to vary. IBM is characteristically the most resistant myopathy to treatment (62;135;136). Corticosteroids, mostly prednisolone, are the standard initial treatment for these disorders, particularly in DM and PM although a recent case has reported clinical improvements in IBM (137), and have been used successfully for the last three decades. However the frequent side effects associated with the treatment results in a reduction or termination of the therapy and a switch, or a combined, approach with steroid-sparing immunosuppressive agents like methotrexate, azathioprine, cyclosporine A, cyclophosphamide and mycophenolate mofetil which have effects on various aspects of the immune response (62;91;135;136). Long-term use of steroid therapy may result in reappearance of muscle weakness without changes in CK levels, necrotizing myopathy, without a prominent infiltration of immune cells (71;91). No standard choice, combination or dose of these therapies is used and is influenced by a number of factors including disease severity and other underlying medical conditions. Intravenous immunoglobulin

therapy (IVIg) is also used in treatment strategies; the large range of antibodies from this therapy has a number of immunomodulatory effects in these disorders (135;138;139). Favourable responses with this treatment are mostly observed in DM and PM patients with no significant improvements in IBM patients, although some studies report limited effects (135;138). Recent, more selective, therapies include the use of monoclonal antibodies aimed at more selective targets including TNF-α blockers (Etanercept, Infliximab and Adalimumab), complement component C_5 (Eculizumab) as well as other cytokines, costimulatory and cell adhesion molecules (135). Another monoclonal antibody therapy being tested in inflammatory myopathies, which is relevant to the current study of this thesis, is Rituximab, a chimeric depleting antibody against the CD20 marker on B cells. Studies have shown favourable outcomes in myositis, after successful studies in other autoimmune disorders such as RA and SLE (140-149), although relapses in some myositis patients did occur after the return of B cells and depletion of autoantibody titres have been found to vary (150-153). The exact mechanism of this antibody is unknown but could involve depletion by either activation of complement, inducing cell-mediated lysis, by apoptosis, or increased sensitisation to cytotoxic agents and corticosteroids. Despite the mechanism of action the initial rationale for using the antibody in autoimmune disorders was to reduce the production of autoantibodies. It is also postulated that other B cell functions may be affected during therapy, such as antigen presentation, costimulatory and regulatory functions. Further studies are now underway with additional CD20 therapies, Ocrelizumab and Ofatumumab, a humanized CD20 monoclonal antibody as well as TRU-015, a single-chain polypeptide which binds to CD20. Other therapies aimed at B cells in autoimmune disorders include Epratuzumab, an anti-CD22 antibody and various therapies at the B cell activating factor BAFF/BLyS (154;155).

As well as treating inflammatory myopathies some therapeutic interventions, for other disorders, are known to cause or contribute to the pathogenesis of inflammatory myopathies. Although the exact mechanisms leading to pathology are unresolved the use of statins as well as corticosteroids have been found to result in inflammatory myopathies (49;56;69;70;156).

1.3 Vasculitis

Vasculitis is inflammation of blood vessel walls; this may occur as a primary process (primary vasculitis) or as a secondary feature of other diseases (secondary vasculitis) such as systemic autoimmune disease, inflammatory disease and connective tissue disease, which can include the inflammatory myopathies (157-162). A number of classification systems have been proposed to classify the varying forms of vasculitis, from the American College of Rheumatology (159;163) in 1990 and the Chapel Hill Consensus Conference in 1994 (164;165) reviewed (157-160;166). Additional classification schemes have been proposed based on the dominant blood vessel involved, the inflammatory cell primarily mediating vascular damage, the distinction between primary and secondary vasculitis and the incorporation of pathophysiological markers (157;162). Multiple pathogenic pathways are generally thought to mediate vasculitis disorders (33;157;158), many of which affect the skin resulting in cutaneous vasculitis due to the large vascular supply to the skin (167). The trigger that initiates inflammation or determines the location of vascular inflammation is unknown. The annual incidence of cutaneous vasculitis ranges from 39.6 to 59.8 per million (157) and can affect all ages. Cutaneous vasculitis is observed slightly less in men than women and is often seen in adults more often than children (157). The mean age of onset is 47 years in adults and 7 years among children (157). Vasculitis can have a wide range of clinical and pathological manifestations due to its capacity to affect vessels of different sizes, although considerable overlap exists (**Figure 1.4**) (157-162).

1.3.1 Large Vessel Disease (>150 μm)

Two distinct disorders have been identified that primarily affect larger vessels, Giant cell arteritis and Takayasu's arteritis. Both disorders involve granulomatosus inflammation, containing activated and antigen-driven T cells and macrophages, of the aorta and its major branches but Giant cell arteritis is generally observed in patients older than 50 years whereas Takayasu's arteritis commonly occurs in patients younger than 50 years old (168;169).

1.3.1.1 Kawasaki Disease (KD)

KD is an arteritis which can affect large, medium and small vessels, as with other vasculitic disorders the cause is unknown (168). It is primarily a childhood disorder and is associated with mucocutaneous lymph node syndrome. Infectious agents have been proposed as possible triggering agents for the disease in immature immune systems leading to the inability to clear certain pathogens. Boys younger than 5 years are most commonly affected (168;170). Oligoclonal IgA producing plasma cells have been recently identified in KD which were critical pathological mediators (167;169;171).

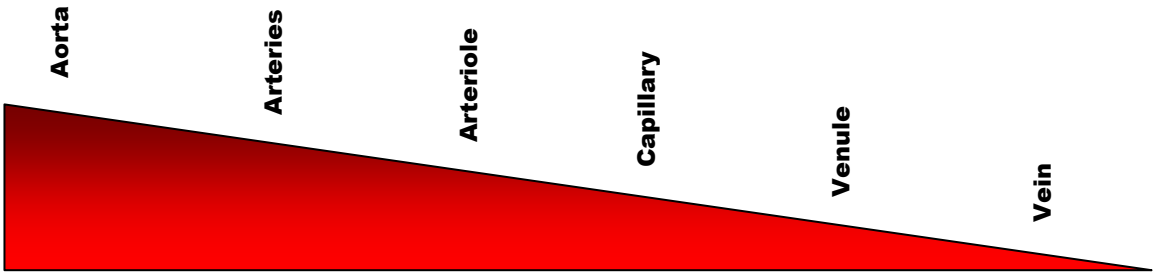

Large-Vessel Vasculitis

Giant-cell arteritis
Takayasu's arteritis

Medium-Vessel Vasculitis

Polyarteritis nodosa (PAN)
Kawasaki's Disease

Small-Vessel Vasculitis

Henoch-Scholein Purpura (HSP), Cryoglobulinemic vasculitis, leukocytoclastic vasculitis, Wegner's granulomatosis (WG), Churg-Strauss syndrome (CSS), Microscopic polyangitis

Figure 1.4 Classifications of Primary Vasculitis Disorders

Classification of the vasculitic disorders is based on the Chapel Hill Consensus Conference on the Nomenclature of Systemic Vasculitis (164;165). These disorders are classified, in part, based on the predominant vessel affected; however substantial overlap among different vasculitis disorders exists. Adapted from 159.

1.3.2 Medium Vessel Disease (50-150 µm)

1.3.2.1 Polyarteritis nodosa (PAN)

PAN is a necrotizing inflammatory disease of medium or small arteries and is observed in 2 to 9 cases per million annually (168;170). This vasculitic disorder is typically considered a medium vessel disorder although it is not restricted to

medium vessels and can be observed in smaller vessels. PAN can occur as a systemic disorder but cutaneous PAN represents 10% of cases (161). Patients, 20-50%, normally present with cutaneous manifestations such as livedo reticularis, nodules, ulcerations and digital ischemia as well as symptoms like fever, fatigue, myalgias, arthralgias and weight loss (168). GI tract, renal and myocardial involvement may occur within patients rendering the disease life threatening (168). This disease affects men more commonly than women and can occur at any age, maximum at 40-60 years (172). PAN been associated with hepatitis B infections (5 to 10 %) and streptococcal infection in children (161;170).

1.3.3 Small Vessel Disease (<50 µm)

Small vessel vasculitis presents with purpura, papules, vesicles and urticarial lesions. Although skin is the primary organ involved, involvement of the renal, musculoskeletal and gastrointestinal systems may occur depending on the disease (161). These vascular diseases are commonly associated with connective tissue diseases such as SLE, RA and SS (159;167;172-174). Small vessel vasculitis restricted to the skin, without systemic involvement, is classified as leukocytoclastic vasculitis. Histopathologically leukocytoclastic vasculitis manifests as segmental infiltration and disruption of the vessel wall by neutrophils, which is usually accompanied by extravasation of erythrocytes and endothelial cell swelling (159;167;172).

1.3.3.1 Henoch-Schonlein Purpura (HSP)

HSP represents approximately 10% of all cutaneous vasculitis cases. All cases demonstrate palpable purpura but is only the presenting sign in 50% of cases (168). Arthritis, gastrointestinal manifestations and nephritis are also observed within this subtype of vasculitis but all may not be present in a given patient. HSP is more common in childhood, primarily in boys aged 4 to 8 years old and is the most common form of systemic vasculitis in children (172). The incidence of HSP in children is approximately 14 cases per 100,000 per year (172). Diagnosis of HSP is conditional on the presence of IgA deposition within and around blood vessels (175), although these IgA deposits are not specific for HSP and are commonly found in other vasculitis disorders (175). Medium sized

vessels are rarely involved in HSP (172) and the pathogenesis associated with small vessels may be related to abnormal glycosylation of IgA. The precise mechanisms mediating pathology in HSP is unknown as is the significance of antiendothelial IgA antibodies, anticardiolipin antibodies and IgA antineutrophil cytoplasmic antibodies (ANCAs) which can all be detected in HSP.

1.3.3.2 Cryoglobulinemic vasculitis

Cryoglobulinemic vasculitis is associated with circulating, cold-precipitable antibodies, cryoglobulins. Mixed cryoglobulins consist of monoclonal IgM or polyclonal IgM directed against IgG. Cryoglobulin immune deposits affect small vessels, predominately in the skin and glomeruli (161;168). Patients present with erythematosus and papules often triggered by cold exposure or prolonged standing (175). In this type of vasculitis patients may also present with medium-sized vessel disease.

1.3.3.3 ANCA-associated Small Vessel Vasculitis

Wegener's granulomatosis (WG), Churg-Strauss syndrome (CSS) and Microscopic polyangitis (MPA) are 3 forms of small to medium vasculitis that are associated with ANCAs but lack deposits of immune complexes, therefore these syndromes are also described as pauci-immune syndromes (176;177).

1.3.3.3.1 Wegener's Granulomatosis (WG)

WG is a multisystem necrotizing granulomatosus vasculitis involving the upper and lower respiratory tract and the kidneys. Rapidly progressive renal disease can occur as a result of necrotising and crescentic glomerulonephritis (178). WG can occur at any age and affects both males and females. Generally the incidence of WG is 5 to 10 per million annually and 80-97% of cases are observed within Caucasian populations (168;172). Cutaneous manifestations like palpable purpura, oral ulcers, papulonecrotic lesions, subcutaneous nodules and ulcers develop in 46 to 66% of cases, parallel disease activity in other organs and are the presenting sign in approximately 10% of patients (168;175). Renal disease, a necrotizing pauci-immune glomerulonephritis, develops in 80% of cases. Cutaneous WG vasculitis is associated with active, rapidly progressive disease and higher frequency of renal and joint disease

compared to WG patients without cutaneous vasculitis (175). Diagnosis of WG is based on clinical features, biopsy and the presence of ANCA, described further in section 1.3.4. Up to 80% of WG patients are c-ANCA positive, while 10-15% of WG patients are p-ANCA positive. A small percentage of WG patients are ANCA negative, these patients tend to have a better prognosis (168;172).

1.3.3.3.2 Churg-Strauss Syndrome (CSS)

CSS, also known as allergic granulomatosus, is a rare necrotizing vasculitis which is usually associated with asthma and eosinophilia (168;175). Clinically and pathologically this vasculitis disorder resembles PAN, MPA and WG but has distinct features, asthma and tissue eosinophilia, making it a separate entity (175). CSS affects small to medium vessels and is reported to occur in 3 people per million (168). Vasculitis occurs as the final distinct phase during disease progression, after allergic rhinitis (asthma) and eosinophilic lung infiltration, but may occur up to 30 years after initial symptoms (168;172). Vasculitis affects the lungs and heart in addition to peripheral nerves and skin. Cutaneous manifestations are reported in 60 to 70% of cases and include not only erythematosus lesions but also ulcers, livedo reticularis and facial oedema (168). Renal involvement is also observed within CSS but is less severe than that observed in WG. Diagnosis of CSS is based on clinical presentations, skin, lung and kidney biopsies and blood eosinophilia. For CSS the presence of ANCA is not a diagnostic property as it is in WG. 50% of CSS patients are ANCA negative; the remaining patients are equally positive for both subtypes of ANCAs (168), this suggests that CSS may exist as two distinct disease entities.

1.3.3.3.3 Microscopic Polyangitis (MPA)

MPA is a pauci-immune nongranulomatosus small and medium vessel vasculitis most often associated with progressive renal disease (168;175). 90% of patients have renal disease in the form of pauci-immune necrotising and crescentic vasculitis (178). Although disease can occur within medium sized vessels in MPA, the disease is often restricted to small vessels (175). Features of MPA are similar to that of WG except that upper respiratory tract involvement is rarely observed (168). Palable purpura is found in 46% of patients at

presentation, nodular lesions are not found within MPA and presentation of this should direct diagnosis towards WG or CSS (168). Skin disorders are observed in 65% or less of patients; in 15% of cases cutaneous disease is the presenting clinical feature (175). Skin biopsies from MPA patients closely resemble leukocytoclastic vasculitis and HSP. Distinction between disorders is established by the presence of p-ANCA within MPA and the absence of immunoglobulin and complement localisation to vessel walls (175). p-ANCA levels correlate with disease activity (175).

1.3.4 Anti-Neutrophilic Cytoplasmic Antibodies (ANCA)

Anti-neutrophilic cytoplasmic antibodies (ANCA) are predominately IgG autoantibodies directed against antigenic targets of primary granules of neutrophils and monocyte lysosomes (178) and are implicated in the pathogenesis of ANCA-associated systemic vasculitides (AASV), necrotizing small vessel vasculitis with a paucity of immune complexes in conjunction with the presence of ANCAs (6;178). Titres of these antibodies appear to precede clinical disease activity and rising levels of these antibodies during remission phases of the disease are indicative of relapses (179-181). Indirect immunofluorescence established two patterns of staining with ANCAs; a diffuse cytoplasmic staining of neutrophils and monocytes, but not lymphocytes, (c-ANCA) and a perinuclear staining (p-ANCA). Two main target antigens were identified from these two ANCAs, c-ANCAs are generally directed against proteinase 3 (PR3), while p-ANCAs are directed against myeloperoxidase (MPO) (6;113;178;182). PR3 is a 29-30 kDa serine protease consisting of 288 amino acids (182). The structure of PR3 shows considerable homology to neutrophil elastase. Under inflammatory conditions PR3 is released extracellularly, together with other granule constituents and oxygen radicals which can degrade collagens, proteoglycans and other connective tissue constituents. PR3-cANCA recognise restricted epitopes on PR3 involving the catalytic site and interfere with the enzyme inactivation (182). MPO is a covalently linked dimer with a molecular weight of 140 kDa localised in the azurophilic granules of neutrophils and lysosomes, making up almost 5% of the total protein content of the neutrophil. MPO catalyses the formation of intracellular toxic products, such as hydrogen peroxide and oxygen radicals,

which are effective in killing phagocytosed bacteria and viruses. ANCA-associated vasculitic disorders are characterised by neutrophil infiltration. Falk *et al* (183) demonstrated that neutrophils express PR3 and MPO on their surface when primed with low dose proinflammatory cytokines. Neutrophils become fully activated when incubated with sera from PR3-ANCA and MPO-ANCA positive patients and produce reactive oxygen species as well as release lytic enzymes including PR3 and elastase. Ohlsson *et al* (184) demonstrated a strong increase, 10 fold, in mRNA levels for PR3 in monocytes from patients with AASV compared to both healthy controls and SLE disease controls. These high mRNA levels do not necessarily indicate increased total PR3 protein levels. Isolation of neutrophils from the bloodstream demonstrated that different individuals differ in their expression of membrane PR3 (mPR3) (185). Most individuals contain a heterogeneous population of neutrophils with both positive and negative neutrophils for PR3 membrane expression, the proportion of these cells are stable and may be genetically determined (185). In WG or in other inflammatory conditions patients have an elevated proportion of mPR3-positive neutrophils (185;186).

ANCAs have been implicated in the pathology of AASV. A direct link between ANCA and the development of glomerulonephritis and vasculitis was demonstrated in an MPO knockout mouse model where passive transfer of mouse MPO was sufficient to induce the disorders in knockout mice (187), reviewed (6;157;178;185;188). The pathogenic potential of these antibodies was confirmed by transfer of purified anti-MPO IgG into RAG2 knockout mice which developed focal necrotizing and crescentic glomerulonephritis with a paucity of glomerular Ig deposition in the absence of functional T or B lymphocytes, although renal lesions were not as widespread as positive control mice. This may indicate that additional factors are required to enhance the inflammatory response. A subsequent study demonstrated that mice depleted of neutrophils were completely protected from anti-MPO induced glomerulonephritis (185). Additionally transfer of recombinant murine PR3 into PR3 and neutrophil knockout mice generated murine PR3-specifc polyclonal antibodies although antibody transfer into wild-type mice did not induce vasculitis (6;176;185;188). An aggravated local immune response was

observed supporting PR3 mediated tissue damage. Comparison of these MPO and PR3 mouse models may indicate that anti-MPO and anti-PR3 have different mechanisms of action. In addition to mouse studies, a human study reported that a newborn child developed glomerulonephritis and pulmonary haemorrhage 48 hours after delivery from a mother with MPO-ANCA microscopic polyangitis (188). MPO-ANCA IgG was found in the child's blood concluding that transplacental transfer of MPO-ANCA IgG resulted in the glomerulonephritis and pulmonary haemorrhage.

The mechanisms generating ANCAs are unresolved; Pendergraft *et al* (189), reviewed (159;178;185;188;190), suggested the generation of ANCAs may result from autoantigen complementarity. In patients with inflammatory vascular disease the patients generated antibodies to the autoantigen, PR3, as well as antibodies to a peptide translated from the antisense, or complementary, DNA strand of PR3 (cPR3). The study was based on the hypothesis that the antigen that initiates the sequence of events leading to autoimmunity is not an autoantigen, but rather the complementary, antisense, peptide or a mimic of this peptide. This complementary peptide initiates the autoantibody production. Following this an anti-idiotype response occurs. The resulting anti-idiotypes react with the antigen derived from the sense peptide and whose amino acid sequence is complementary to the sequence of the initiating, antisense, antigen. This theory was confirmed in mouse models where mice immunised with a complementary human peptide, cPR3 whose structure mirrors that of PR3, produced antibodies against that peptide, cPR3, as well as to the peptides sense counterpart, PR3. The structure of cPR3 mirrors that of PR3

At least two separate signalling pathways are thought to be involved in the activation of neutrophils by ANCA (6;178;179). The $F(abs')_2$ portion of ANCA IgG activates a G-protein coupled receptor pathway while the Fc portion of the antibody binds to the constitutively expressed FcγRIIa and FcγRIIIb receptors of the neutrophil, activating Syk kinase and protein kinase C-β and mediates calcium release.

1.3.5 Antiendothelial Cell Antibodies (AECA)

Antibodies directed against endothelial cells (AECA) have been detected in the sera of patients with vasculitis (173), they have also been found in myositis with vascular injury resulting in myofibre damage (58). AECAs are a heterogeneous group of antibodies directed against a variety of endothelial cell antigenic membrane proteins. Endothelial cell dysfunction and persistent local inflammation is considered to be an early event which subsequently leads to the development and progression of vascular wall disorders, such as vasculitis (7), but may also play a significant role in other disorders like myositis. The endothelium participates in homeostatic mechanisms including regulation of vascular tone and directing biological responses such as leukocyte trafficking to inflammatory sites, Figure 1.1, (7). The mechanisms of AECA are thought to include complement or antibody dependent cellular cytotoxicity, induction of endothelial cell apoptosis and upregulation of adhesion molecules resulting in continued recruitment of leukocytes, but the exact role of AECAs in vasculitis is largely unresolved (176;191). Certain forms of endothelial injury are associated with ANCA. Endothelial cells may express, process and present ANCA antigens to cytotoxic T cells. Previous studies have demonstrated that endothelial cells develop an activated phenotype in ANCA-associated vascular injury with enhanced expression of adhesion molecules, ICAM-1 & VCAM-1, that promote interaction with circulatory inflammatory cells (7). An association of ANCA-associated vasculitis and endothelial cells had been proposed by Woywodt *et al* (6;8) who demonstrated that patients with ANCA-associated vasculitis have high numbers of circulating endothelial cells compared to controls. It was also observed that these endothelial cells had undergone necrosis indicating that they detached from the basement membrane as a result of a direct, active and pathogenic mechanism but the exact role of this in vasculitis is unresolved.

Stromal cells such as fibroblasts and smooth muscle (SM) cells can also produce biologically active proteins that act to regulate endothelial cell function (192), thus the interactions of stromal cells with endothelial cells at the sites of inflammation are likely to be important in the initiation and maintenance of the local inflammatory response and determination of site specificity. Baiu *et al*

(193) studied the role and pathogenicity of anti-SM antibodies in vasculitis. Vasculitis was induced by adoptive transfer of SM-stimulated lymphocytes and the production of autoantibodies targeting blood vessels and the pathogenicity of these autoantibodies was established. Results demonstrated the development of small vessel vasculitis in mice accompanied by the presence of pathogenic antibodies reactive with vascular smooth muscle as well as the persistence and expansion of activated, potentially pathogenic, B cells. These results were confirmed as a result of serum transfer experiments. The anti-SM antibodies were shown to recognise intracellular antigens which has also been observed in human patients (193) suggesting that other mechanisms resulting in damage to vascular cells need to occur first in order for B cells to be exposed to the intracellular antigen. Other antibodies found in vasculitis patients, such as anti-Ro, La, DNA or RNP, may be associated with underlying disorders in these patients.

1.3.6 Pathogenesis of Vasculitis

The pathogenesis of vasculitis includes different immune mechanisms that cause leukocytes to adhere to endothelial cells, penetrate into vessel walls and release injurious products resulting in vessel wall injury. Like the classification of vasculitis disorders, the mechanisms of pathogenesis have also been classified into 4 types (157;158;162). The first major pathogenic mechanism in vasculitic syndromes is termed allergic vasculitis and is strongly associated with atopic disorders. In vasculitic disorders such as urticarial vasculitis and CSS activated Th2 lymphocytes play a central role through their production of cytokines to mediate the accumulation of mast cells, basophils and eosinophils. Bridging of IgE receptors on these cells leads to the secretion of inflammatory and toxic mediators. Antibody-mediated vasculitis is another major pathogenic mechanism, especially in ANCA-associated vasculitis as previously described. The third pathogenic mechanism in vasculitis is immune-complex vasculitis. Immune complexes are associated with cutaneous lesions of vasculitic disorders and are observed in HSP, cryoglobulinemic vasculitis, leukocytoclastic vasculitis and PAN. 80% of direct immunofluorescence examinations are positive for IC or complement deposition (157). Deposition of IC results in complement activation and release of anaphylatoxins C3a and C5a

that recruit inflammatory cells, in particular neutrophils and mast cells which are necessary for the progression of IC-mediated vascular damage. This process is also highly regulated by adhesion molecules. T cell hypersensitivity vasculitis is the final classification of immunopathogenic mechanisms. These mechanisms are largely seen in large vessel vasculitic disorders or granulomatous vasculitides but lack the IC deposition and ANCA association. Although the immune mechanism of pathogenesis has been classified, more than one immune mechanism may be involved over the course of a single disease as well as the occurrence of overlap syndromes.

1.3.7 Therapies in Vasculitis

Therapeutic strategies within vasculitis disorders are similar to those described for myositis disorders in section 1.2.5. Currently corticosteroid and immunosuppressive therapies, as previously described, are the foundation of treatments strategies but the regime and combination of treatments is dependent on a number of factors including vasculitis severity and underlying medical conditions (157;159). Similarly to myopathies the exact pathogenic mechanisms and target antigens are still being defined, therefore treatments to date are non-selective but new selective therapies are being studied in different vasculitic disorders. TNF-α treatments, Infliximab and Entanercept, have shown promise in some treatments while being disappointing in others and have also been related to the development of autoimmune processes (157;194-201). TNF-α could mediate the endothelial dysfunction in vasculitis therefore such targeted therapy could improve endothelial functions in these disorders. B cell depletive therapy using Rituximab has also shown promising results in vasculitic disorders in a number of studies (148;157;159;177;202-206). Depletion of B cells in the patients included in these studies were accompanied by partial or complete remission and decreased autoantibody levels with few side effects which further substantiates the role of B cells in such autoimmune disorders. Additional B cell therapies targeting CD20, CD22 and BAFF could also impact on these disorders (154;155).

The aetiology of most autoimmune disorders is largely unknown, including myositis and vasculitis. Many different factors have been implicated in the different cellular and molecular mechanisms associated with autoimmune

disorders, including the involvement of B cells, the central theme of this study. The participation and significance of B cells in these mechanisms are substantiated by the occurrence of autoantibodies and immune complexes within autoimmune disorders as well as the recent clinical improvements observed using B cell depletive therapies.

1.4 B cells

B cells, along with T cells, were first identified in 1960 (207) and participate in adaptive immune responses by mediating humoral immunity through the release of antigen specific antibodies. B cells originate in the bone marrow from undifferentiated hematopoietic stem cells (HSC), which have the capacity to develop into all lymphohematopoietic lineages, and undergo a process of maturation from early lymphoid progenitors (ELP) to common lymphoid progenitors (CLP) by the increased expression of IL-7Rα (208). CLPs are also the precursor cells for natural killer (NK) cells, dendritic cells (DCs) and T lymphocytes (208;209). In B cell diversification CLPs then diversify through pro-B cell and pre-B cell maturation to an immature B cell stage leading to a mature B cell (**Figure 1.5**) (154;208-213). Mature B cells them become activated by a relevant antigen and co-stimulatory factors and migrate to germinal centres to differentiate into memory cells and plasma cells which are all specific for the original antigen (154;208-213). Plasma cells are antibody-secreting cells which are no longer in cell cycle and generally reside within the bone marrow. Within this phenotype of cells there are long-lived and short-lived plasma cells (209;213-216). Prior to plasma cell differentiation activated B cells transition into activated cells, termed plasmablasts, which secrete antibodies but still remain in cell cycle. Similarly to plasma cells these can be divided into short and long-lived categories. The exact relationship between these cell types remains to be defined. Memory cells can also be differentiated into antibody secreting cells by repeated antigenic challenge resulting in reactivation, rapid proliferation and mutation of memory B cells (209;213). B cell generation depends on signalling through the c-kit, Flt3 and IL-7 receptors and development control is exerted by a network of key transcription factors that include PU.1, Ikaros, Bcl11a, E2A, EBF, Foxp1 and Pax5 (217-219); in the absence of these regulators B cell development is severely affected. During the

life span of B cells they circulate between peripheral blood and tissue, on contact with antigen B cells undergo their final stages of development (207;208).

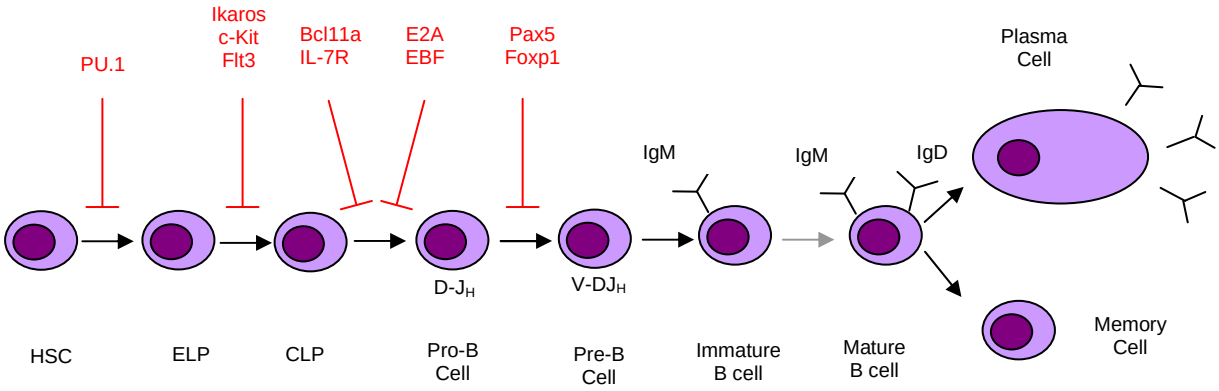

Figure 1.5 Differentiation Pathway of B Cells

The maturation of B cells occurs in two phases, antigen-independent in the bone marrow and antigen-dependent in the periphery. Stem cells diversify into lymphoid progenitors which further differentiate into pro-B cells before pre-B cells are formed where a rearranged VDJ unit is expressed at the cell surface with a surrogate light chain. Immature B cells are formed, still within the bone marrow, that express IgM which evolve into mature B cells expressing IgM and IgD. The terminal differentiation steps occur within germinal centre reactions in secondary lymphoid organs where naïve B cells are activated to differentiate into memory B cells and plasma cells. Markers in red signify where loss of transcription factors arrests B cell development; the grey arrow represents the transition of B cells from the bone marrow to the peripheral compartments. Adapted from 217.

1.4.1 B Cell Gene Repertoire Development

During the course of B cell development various gene segments rearrange to establish the repertoire of the immunoglobulins (Ig) expressed on the B cell surface (**Figure 1.5 & 1.6**). The Ig's produced by B cells are composed of 2 heavy polypeptide chains and 2 light polypeptide chains, kappa or lambda, made up by a combination of gene segments. The germline variable (V) region of the IgH, heavy, chain are coded by the V_H (variable), D (diversity) and J_H (joining) gene segments located on chromosome 14 in humans (220-224). The variable and joining gene segments for lambda light chains are located on chromosome 22 while the kappa gene segments are located on chromosome 2. 7 V_H families exist based on sequence homology of at least 80% (225-228), with approximately 51 functional gene segments. Approximately 27 functional D_H gene segments make up 7 D_H families based on sequence homology, which range from 11 to 37 base pairs in length (229), while 6 J_H genes are present within the genome. Kappa and lambda have 7 and 10 different V gene families respectively with approximately 40 and 30 gene segments respectively (**Table 1.2)**. 5 kappa J gene segments are found in the kappa locus with a single

constant kappa gene while four pairs of functional J lambda and constant genes are found within the lambda locus.

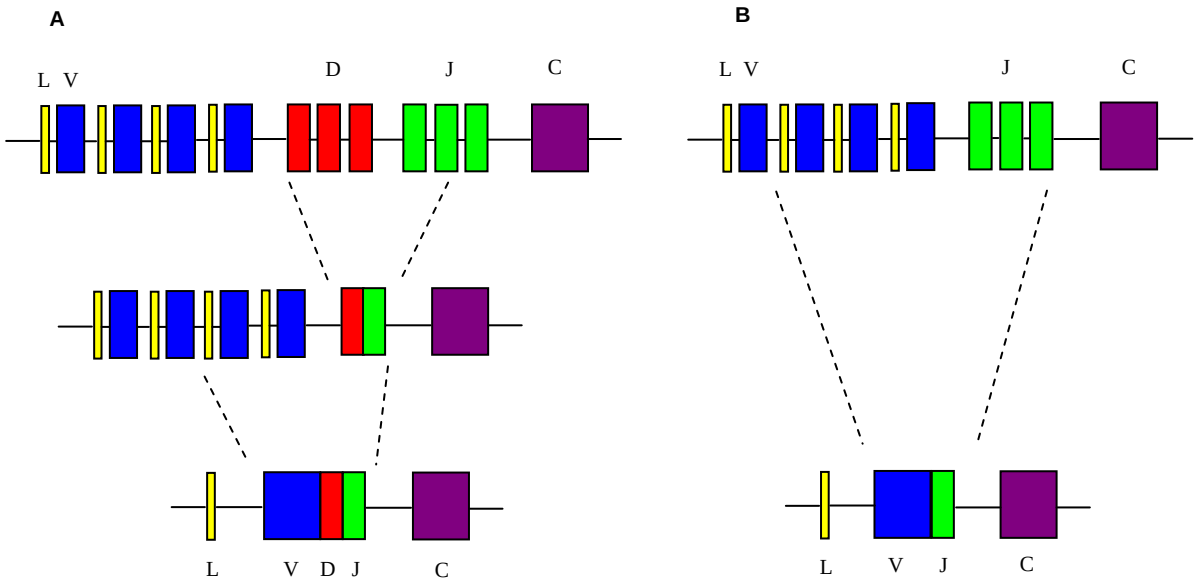

Figure 1.6 A simplified Diagram of Gene Rearrangement Processes of Heavy (A) and Light (B) Chain Immunoglobulin Genes

In the gene rearrangement process heavy chains are rearranged first (**A**). Initially one of the D gene segments is translocated to one of the several J gene segments forming a DJ gene combination. A V gene segment, with its own corresponding leader (L) sequence, is then translocated to the DJ segment to form a VDJ variable gene segment. After completion of the heavy chain rearrangements light chain rearrangements are completed (**B**). One of the V gene segments with its corresponding leader (L) sequence is translocated to a J gene segment creating a VJ gene segment encoding the complete light chain variable region. The kappa chain is rearranged first, if this produces a non-functional rearrangement a lambda rearrangement then occurs. A primary RNA transcript is then produced from the rearranged DNA. Splicing then occurs to remove the intervening introns and bring together the VDJ/VJ segments with the constant (C) exons. The kappa gene locus contains only one constant gene whereas each J segment of the lambda locus is associated with a different constant lambda region. Adapted from 1.

Gene segments combine to form functional immunoglobulin genes in a recombination reaction termed V(D)J recombination (**Figure 1.6**) (1;220;230-234). These rearrangements are guided by conserved non-coding DNA sequences that are found adjacent to the points where recombination takes place. These conserved sequences consist of a heptamer (5'CACAGTG3') followed by a nonconserved region, spacer, which is either 12 or 23 nucleotides long (**Figure 1.7A**). The conserved length of the spacer corresponds to one or two turns of the DNA double helix respectively. This is then followed by a second conserved nonamer sequence (5'ACAAAAACC3'). The heptamer-spacer-nonamer combination is also known as the recombination signal sequences (RSSs). Recombination of gene segments follows the 12/23 rule where only a gene segment flanked by a RSS with a 12 base pair (bp) spacer can be joined to one flanked by a 23 bp spacer RSS; D_H gene segments can be

joined to a J_H gene segments and a V_H gene segment to a D_H gene segment but V_H gene segments cannot be joined to J_H gene segments as they are both flanked by 23 bp spacers whereas D_H gene segments are flanked by 12 bp spacers. The mechanisms of V(D)J recombination bring together a 12 bp spaced and a 23 spaced RSS (**Figure 1.7B&C**). The DNA molecule is then broken in two places and rejoined in a different configuration. The gene segments join to form a coding joint while the remainder of the DNA in a hairpin loop form a signal joint creating a circular piece of chromosomal DNA which is lost during cell division. Rearrangement of immunoglobulin genes is a multistep enzymatic process and starts with the binding of products from the recombination-activating genes, RAG1 and RAG2, whose expression is unique to lymphoid cells, and high-mobility group proteins (HMG) to RSSs, following the 12/23 rule. The endonuclease activity of the RAG protein complexes produces two single-strand DNA breaks just 5' of the bound RSSs leaving a free 3'-OH group at the end of each coding segment. This 3'-OH then hydrolyses the phospodiester bond on the complementary uncut strand forming double-strand breaks, which are held tightly in a complex by the RAG proteins. These form a hairpin by joining to the cut end of its complementary strand on the other side of the break. The two RSSs are precisely joined by DNA ligase IV to form the signal joint. To complete the rearrangement of the gene segments the DNA hairpin is nicked open by a single-stranded break by the RAG proteins, this can occur at various points along the hairpin creating sequence variability when the sequences join. The DNA repair enzymes, DNA-dependent protein kinase (DNA-PK) and the Ku heterodimer (Ku70:Ku80) modify the opened hairpins by removing nucleotides by exonuclease activity and adding non-templated (N) nucleotides by terminal deoxynucleotidyl transferase, TdT, or templated (P) nucleotides. DNA ligase IV joins the processed ends to generate a continuous double-stranded DNA, reconstituting a chromosome which includes the rearranged gene.

The majority of gene segments do not join in phase with the reading frame resulting in non-functional rearrangements. Also inappropriate gene rearrangements, approximately 75%, produce recognition to self antigens resulting in apoptosis or anergy of cells at the pre-B stage. These cells may be

rescued by receptor editing, a dominant mechanism in B cell tolerance. Secondary Ig gene rearrangements occur, which are RAG-mediated, altering the specificity of an autoreactive B cell at the immature B cell stage (233;235;236).

V_H Family	**V_H1**	**V_H2**	**V_H3**	**V_H4**	**V_H5**	**V_H6**	**V_H7**			
	10	3	23	11	2	1	1			
D_H Family	**D_H1**	**D_H2**	**D_H3**	**D_H4**	**D_H5**	**D_H6**	**D_H7**			
	5	4	5	4	4	4	1			
J_H Family	**J_H1**	**J_H2**	**J_H3**	**J_H4**	**J_H5**	**J_H6**				
	1	1	1	1	1					
V_κ Family	**$V_\kappa1$**	**$V_\kappa2$**	**$V_\kappa3$**	**$V_\kappa4$**	**$V_\kappa5$**	**$V_\kappa6$**				
	19	9	7	1	1	3				
J_κ Family	**$J_\kappa1$**	**$J_\kappa2$**	**$J_\kappa3$**	**$J_\kappa4$**	**$J_\kappa5$**					
	1	1	1	1	1					
V_λ Family	**$V_\lambda1$**	**$V_\lambda2$**	**$V_\lambda3$**	**$V_\lambda4$**	**$V_\lambda5$**	**$V_\lambda6$**	**$V_\lambda7$**	**$V_\lambda8$**	**$V_\lambda9$**	**$V_\lambda10$**
	5	5	9	3	3	1	2	1	1	1
J_λ Family	**$J_\lambda1$**	**$J_\lambda2$**	**$J_\lambda3$**	**$J_\lambda7$**						
	1	1	1	1						

$V_\kappa7$, $J_\lambda4$, 5 and 6 are considered non-functional

Table 1.2 Distribution of V_H, V_κ and V_λ Functional Genes

The assembly of different gene segments in V(D)J recombination and the random pairing of heavy and light chains provide the diverse gene repertoire of the B cell. This diversity is further enhanced by exonuclease activity removing nucleotides and addition of up to 20 non-templated (N) or up to 4 templated (P) nucleotides, inverted repeats of V, D or J coding ends, at joining sequences within the CDR3 region generating the most diverse region of the Ig rearrangement (**Figure 1.7C**) (237;238). Additional mechanisms are also employed to further increase diversity following exposure to antigen, somatic hypermutation leading to affinity maturation and receptor revision. Receptor revision in the periphery, similar to that of receptor editing in the bone marrow, can also increase the diversity through secondary recombination of low affinity immunoglobulin genes to alter the specificity and affinity towards antigen (233;239;240).

1.4.2 V_H Repertoire from Healthy Individuals

Studies have been conducted within normal, healthy individuals to establish the normal repertoire of immunoglobulin genes which allow the modifications to the repertoire to be established within autoimmune diseases (241-250). Some of

these studies have demonstrated that the frequency of gene usage was similar to that of the germline complexity (241-243). Guigou *et al* (245) first used *in situ* hybridization, on cDNA libraries from peripheral blood samples, using Ig DNA probes specific for V_H1 to V_H6 to analyse the expression pattern of V_H families in the human adult repertoire of two healthy patients. Results produced an expression gradient for V_H genes; V_H3 (52%) > V_H4 (19%) > V_H1 (11%) > V_H5 (10%) > V_H6 (5%) > V_H2 (3%). This gradient of gene usage is comparable to the complexity of functional germline genes within each family although bias for activated B cells is possible. Brezinschek *et al* (241;242) in subsequent studies used single-cell PCR analysis on genomic DNA to analyse the heavy chain repertoire of human peripheral B cells. In functional repertoires V_H3 was used most frequently followed by V_H4, V_H1, V_H5, V_H2 and V_H6, an ordering similar to the number of functional genes within each V_H family. This preferential use of V_H3 gene segments was not found in non-functional repertoires. Selection for particular individual V_H germline genes was also reported. V_H3-23, V_H4-59, V_H4-39, V_H3-07, V_H3-30, V_H1-18, V_H3-30*03, V_H3-34 and V_H3-09 were over-represented in these repertoires and were found to be expressed by more than 50% of B cells. A limitation of these studies was the low number of patients involved which may not fully represent the true diversity of the Ig repertoire.

The most recent study examining the V_H gene repertoire was conducted using nearly 6,500 functional human Ig heavy chain genes which aimed to represent the natural Ig diversity and was compared to 325 non-functional genes (251). This study involves a larger set of genes than was previously examined, including the previous studies by Brezinchek *et al* (241;242). Clonally related gene duplicates and genes of autoimmune origin were filtered from the dataset of sequences isolated from the Genbank nucleotide database in addition to genes of perinatal origin, due to the known gene segments and CDR3 biases. The study established that functional gene rearrangements more closely resembled the genomic complexity compared to the non-functional gene rearrangements. The data from functional genes support that of previous findings (241;242) that V_H3 gene segments are used most frequently, followed in descending order by V_H4, V_H1, V_H5, V_H2, V_H6 and V_H7 which is also similar to the germline complexity. Also in support of previous findings the gene segment

V_H3-23 was most frequently used followed by the V_H4-34 gene segment in this study. Analysis of D_H gene segments demonstrated a significant departure of the proportions within functional and non-functional from the germline complexity at both the family and individual gene segments usage level. The functional repertoire of D_H demonstrated that D_H3 gene segments were most frequently used followed by D_H2, D_H6, D_H1, D_H5, D_H4 and finally D_H7. Due to the difficulties in assigning D_H gene segments in rearranged Ig genes, the normal repertoire of D_H gene segments had not been extensively studied prior to this study. The repertoire of J_H gene segments was also found to correlate with previous studies with the J_H4 gene segments most frequently used followed by J_H6, J_H5, J_H3, J_H1 and J_H2. As very few J_H gene segments are present within the genome, the repertoires observed within the functional, as well as the non-functional, were found to differ significantly from the germline complexity. In addition to the repertoires of the individual gene segments the study also examined D-J segments pairings. Several pairings were found to occur statistically above expected values, including D_H2-2 to J_H6 and J_H2, D_H1-14to J_H1 and J_H5, D_H5-24 to J_H4 and D_H7-27 to J_H3. Overall it was observed that several 5'D_H gene segments paired with increase frequency to the most 3'J_H gene segments (J_H5 and 6) while with decreased frequency to closer chromosomal segments (J_H1-4). However, some 3'D_H gene segments did show an increased frequency of pairings with the closest J_H gene segments and a decreased frequency in pairing with the furthest J_H5 and J_H6 gene segments. In addition to establishing the normal repertoire the study hypothesised that multiple D-J successive recombinations may occur before translocation of the V_H gene, although very little evidence for this mechanism had been found.

Conversely studies have been conducted in healthy individuals that demonstrate that the peripheral B cell repertoire differs from the gene frequency within the germline and biased expression of certain V_H families have been observed in certain individuals (246-248;250). Huang *et al* (246) demonstrated a selection for V_H1 and V_H5 gene segments with a selection against V_H3 family genes in cDNA libraries from 2 patients. Suzuki *et al* (250) assessed the contribution of individual V_H3 and 4 gene segments to the human antibody repertoire. Synthetic oligonucleotide probes, which were specific to individual

V_H gene segments within rearranged genomic DNA, were used to assess 8 individual V_H3 and 9 individual V_H4 gene segments in the PBL repertoire of two healthy patients. Of the eight individual V_H3 gene segments assessed the V_H3-23 and V_H3-30 gene segments were rearranged more frequently than expected based on germline complexity which accounted for approximately 17% and 20% of V_H3 gene rearrangements in both subjects respectively. In both subjects the eight V_H3 gene segments analysed accounted for over 50% of the V_H rearrangements, an increase from the 16 to 30% predicted based on V_H3 gene numbers. V_H4-34 was shown to be over-expressed in one of the subjects, accounting for more than 25% of the sequences isolated. This rearrangement with another two V_H4 rearrangements, V_H4-31 and V_H4-4b, accounted for more than 50% of the V_H4 rearrangements. Conversely V_H4-17, V_H4-55 and V_H4-28 were rarely found. The work of this study suggests that a limited number of V_H gene segments dominate the V_H repertoire but due to the polymorphic nature of these segments the dominance of individual V_H gene segments will differ between individuals. The repertoire was analysed after an 8 month intermission and little change in the V_H repertoire was observed indicating that the utilization of these V_H gene segments was a stable feature in the V_H repertoire of this subject. The over-representation of the V_H4-34 gene was also noted in another study into the normal adult human peripheral blood B cell repertoire. Kraj *et al* (247) established the representation of the V_H4-34 gene in the repertoire of two healthy individuals. V_H family distribution was found not to significantly differ from expected values based on the germline complexity but in both the cDNA library and rearranged Ig DNA library V_H4-34 gene segments were over-represented relative to other V_H4 gene segments accounting for 25 and 70% of DNA sequences in the two patients.

Previous work on biased subsets of V_H gene segments within peripheral repertoires led Kraj *et al* (248) to assess the human V_H repertoire at different stages of B cell development. The study compared the V_H3 and V_H4 gene representation of pre-B, immature B and preimmune mature B cells from two healthy individuals. Within pre-B cells there was a large representation of V_H4 gene segments. V_H4-34 was the most prominent and accounted for over 20% of sequences in both patients. V_H4-59 was also highly prominent within V_H

repertoires while V_H4-31, V_H4-4b and V_H4-61 were very low within both repertoires. For the V_H3 repertoire a biased representation of certain V_H3 gene segments, V_H3-23 and V_H3-30, was observed at the pre-B cell stage and this was carried through to mature B cell stages. Other genes such as V_H3-11 were highly prominent at early B cell stages but were rare in later B cells stages while V_H3-20 were very infrequent in early B cell stages but this increased in the mature B cell population. V_H3-15 was shown to be highly frequent on immature B cells compared to pre-B cells but this was not observed at later stages of B cell development. The authors suggest that bias within the V_H repertoire is established at the earliest pre-B cells stage resulting from preferential rearrangement which may later be modified by V_H gene-mediated mechanisms such as effective surrogate light chain pairing and ligand mediated selection.

Many mechanisms for these reported bias gene usage repertoires have been proposed (247;252;253). These mechanisms include chromosomal positions, accessibility to recombinase machinery, and the presence of gene-specific promoter or enhancer sequences in addition to a greater number of gene copies in the germline. It has also been shown that preferential use of certain V_H elements may result from cellular selection due to antigen binding. Gu *et al* (254) established that the recruitment of newly generated B cells into the long-lived peripheral B cell population is mediated through positive selection by internal and/or external ligands. Despite these previous studies the most recent and comprehensive study (251) has illustrated that the Ig repertoire is similar to the germline complexity.

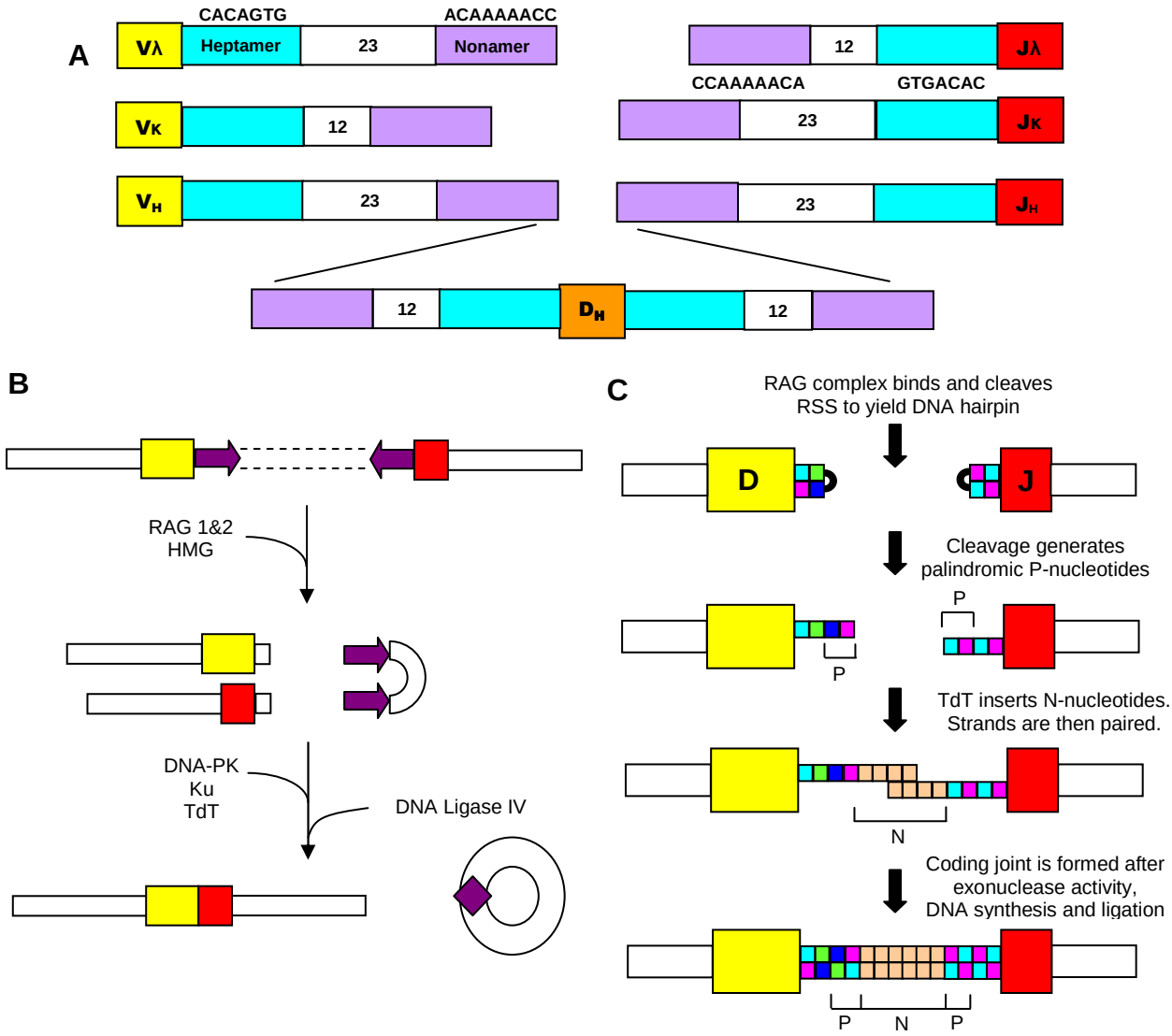

Figure 1.7 A simplified diagram of the mechanisms of V(D)J recombination

Figure 1.7A – Conserved heptamer ( ) and nonamer ( ) sequences flank the gene segments of the heavy and light chains. These are separated by a spacer of either 12 base pairs or 23 base pairs. In V(D)J recombination a 12/23 rule is in place to ensure that only a gene segment flanked with a 12bp spacer can be joined with a 23bp spacer. Heptamer – spacer – nonamer combinations are known as recombination signal sequences (RSSs)

Figure 1.7B&C – Ig rearrangement is a multistep process, initially RAGs and HMG bind to RSSs ( ) and bring the regions together before causing single stranded DNA breaks resulting in hairpin structures at the ends of the Ig gene segments. A number of proteins (DNA-PK, Ku) bind to the hairpins and the sequences are cleaved at random and additional bases are added by TdT to generate diverse ends. DNA ligase IV ligates the gene segments forming a coding joint. The cleaved DNA circularises forming a signal joint which is lost during cell division. Adapted from 1.

1.4.3 Somatic Hypermutation (SHM)

The release of B cells into the periphery from the bone marrow allows B cells to recirculate through peripheral lymphoid tissues and to come into contact with their cognate antigens resulting in B cell activation. Activated B cells can enter primary lymphoid follicles leading to the formation of germinal centres (GCs), also containing antigen-specific T cells. Within GCs the B cells undergo two distinct immunoglobulin gene diversification processes; somatic hypermutation

(SHM) and class switch recombination (CSR), although SHM has been demonstrated to occur outside GCs in animal models that cannot develop GCs (255). SHM introduces non-template point mutations in the variable region of Ig heavy and light chains, a process which underlies the process of affinity maturation, generating an immunoglobulin with an altered, higher or lower, affinity for its cognate antigen (256). The full workings of SHM have yet to be established although some mechanisms have been elucidated. Activation-induced cytidine deaminase (AID) plays a significant role in SHM, as well as CSR. AID is a B cell specific molecule that plays a central role in adaptive immunity by initiating SHM (257-261). Although AID functions as a DNA mutator it is predominately located in the cytoplasm of B cells but nuclear localisation and export signals allows transfer between the nucleus and cytoplasm (261). Mutations are confined to a 1 to 2 kilobase region in the rearranged immunoglobulin genes of which the variable region defined the 5' boundary of the hypermutation region. Mutations begin approximately 150 bp downstream of the transcription start site but the mutational frequency is not constant and decreases exponentially with increasing distance from the transcription start site (262). Point mutations generally occur in SHM, although insertions and deletions are occasionally observed, at a rate of $1x10^{-3}$ mutations per base per generation (261;263). Transition mutations (a pyrimidine (C or T) to pyrimidine base change or a purine (A or G) to purine base change) occur approximately twice as frequently as transversion mutations (a pyrimidine to purine base change and vice versa) and a high proportion of these arise in mutational hotspot motifs. Mutations are often seen in conjunction with WRCY motifs (W=A/T, R=A/G and Y=C/T) or its complement RGYW (264). AID initiates SHM by the deamination of C nucleotides, on single strand DNA, resulting in a U.G mismatch. Following this DNA polymerases can insert an A nucleotide opposite the U nucleotide to generate C>T or G>A transition mutations following replication, the mismatch could be removed by the UNG (uracil-DNA glycosylase), base-excision repair (BER) mechanism, to create an abasic site that can then be bypassed by error-prone polymerases (η or ζ) to give rise to both transition and transversion mutations or the mismatch can be targeted by the mismatch repair (MMR) to initiate an error-prone polymerase

mediated mutation process that introduces A-T and G-C mutations that are proximal but not located within hot spots. (257-259;262)

1.4.4 Class Switching Recombination (CSR)

Class switching recombination (CSR) is also initiated by AID, although the exact role of AID is unknown (257;261;265;266). CSR is a process that changes the Cμ constant regions to another constant region (Cγ, Cα or Cε) to define the Fc mediated functions but allows the antibody to retain its specificity and affinity for antigen. Tight regulation of CSR is required as abnormal levels of IgG, IgA or IgE favour the onset of autoimmune and allergic disorders such as SLE and asthma (265). CSR results from DNA recombination between switch (S) region DNA segments located upstream of each C gene and deletion, circularisation, of the intervening DNA. The choice of which S region serves as recipient for CSR is determined by which cytokines are released by the helper T cells that interact with the IgM-producing B cell (261). Evidence suggests that once AID deaminates C to U in both the donor and recipient S region, the resulting mismatch recruits all the same enzymes that are recruited during SHM to create ssDNA breaks with CSR a result of DNA repair and germline transcription (257;261;265;266). It has also been proposed that AID generates dsDNA breaks, generated by closely spaced single-strand breaks, with the recruited enzymes and additional enzymes are recruited to complete the process of CSR by nonhomologous end joining (261). It has been recently demonstrated that AID is expressed in bone marrow pre-B cells and immature B cells initiated by the signalling through BCR and TLRs (266) providing an innate population of IgG and IgA expressing cells that could be involved in receptor editing of self-reactive immature B cells.

1.4.5 Germinal Centres

GCs are composed of a network of B cells, FDC and $CD4^+$ T cells whose interactions result in the B cell humoral immune response in secondary lymphoid tissues and the generation of antigen-specific antibodies. The microenvironments of GCs are essential in the development of normal B cell immune responses as they provide an infrastructure that captures and stores antigen, drives B cell division and maturation, selects B cells with antigen

specific high affinity receptors and differentiates cells into memory B cells and Ig-secreting plasma cells. GCs are derived from 1-3 B cells clones (267). Small recirculating follicular B cells are displaced to the outer edge of the network of FDCs to form the follicular mantle (268). GCs first appear at day 4-5 postimmunisation, achieve maximum cell numbers by day 10-11 and decline after about 3 weeks (269). Antigen stimulated B cells within secondary lymphoid tissues migrate to the edges of B cell follicles where they interact with T helper cells and begin to form GCs (270). Classically mature GC reactions are a two-stage process, firstly B cells form the GC dark zone and begin to proliferate, during proliferation B cells undergo somatic hypermutation to diversify the antibody variable region to produce variants with different affinities to the specified antigen (268;269;271-273). Following this, B cells termed centroblasts convert to smaller, non-proliferating centrocytes with surface expression of mutated Igs and migrate to the GC light zone where they encounter a network of FDC, that present native antigen in the form of immune complexes, and $CD4^+$ T cells, that provide helper signals to promote B cell proliferation and differentiation, and undergo intense selection. Selection is based on competition for antigen; only those B cells with an increased affinity for antigen can undergo isotype switching and be selected to differentiate into memory B cells or plasma cells. FDCs with successfully bound high affinity B cells switch off the apoptotic machinery of these high affinity B cells (273). The majority of B cells die through apoptosis and are immediately taken up by germinal centre tingible-body macrophages as somatic mutations result in a lower affinity for the specified antigen or the B cells may even become reactive with self antigens. Over the course of the GC reaction the light zone is continuously replenished by migration of GC B cells from the dark zone. It is also thought that selected centrocytes can return to the dark zone for further rounds of division and somatic mutations giving rise to the cyclic re-entry model (268;274). The organisation of light and dark germinal centre zones is mediated by CXCR4 and CXCR5. Allen *et al* (275) demonstrated that CXCR4 was essential for the segregation of dark and light zones, CXCR4 was more abundant on centroblasts rather than centrocytes and was required for centroblast localization in the dark zone where its ligand, SDF1/CXCL12, was more abundant in comparison to the light zone. Conversely CXCR5 helped

direct CXCL13-positive cells to the light zone but this was not essential for segregation of zones. The study proposed that centroblasts downregulate CXCR4 and differentiate into centrocytes and migrate towards the light zone while centrocytes upregulate CXCR4 to allow re-entry into the dark zone.

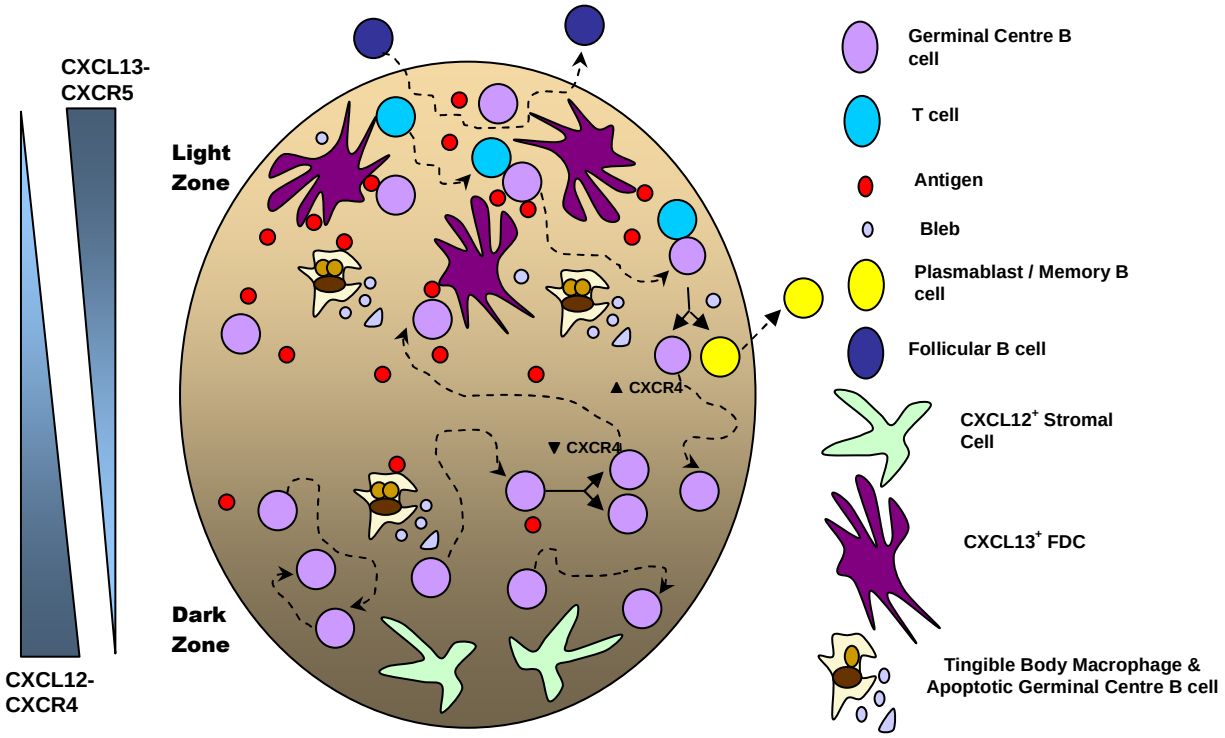

Figure 1.8 Germinal Centre Organisation and Reactions

Germinal Centre (GC) reactions occur within two distinct zones of the GC; the Light Zone (LZ) and the Dark Zone (DZ). The DZ is composed of GC B cells, a sparse network of stromal cells, GC T cells and tingible-body macrophages (TBM). The LZ is composed of GC B cells, a dense network of FDCs, GC T cells and TBMs. GC B cells migrate within their respective compartments as well as moving between compartments by regulating CXCR4 levels. Antigen is displayed on FDCs as immune complexes (IC). GC B cells cycle within the DZ through cell proliferation and cell death. Reducing CXCR4 levels cells from the DZ can migrate to the LZ where GC B cells rapidly move within the FDC network to be selected as high affinity GC B cells. From the LZ, GC B cells either undergo apoptosis, exit the GC to differentiate into plasma cells or memory cells or they return to the LZ, a result of increasing CXCR4 levels. Recent evidence had found that follicular B cells may enter GCs scanning the antigens present and may be recruited to an ongoing GC reaction if they have a higher affinity towards antigen. Adapted from 276.

Classically GC mechanisms defined GC B cells as centroblasts and centrocytes within the DZ and LZ respectively. Centroblasts were thought to undergo a rapid process of proliferation and somatic mutation before differentiating into centrocytes within the LZ where selection of high affinity antigen B cells were selected. The cycle of mutation and selection required to isolate high-affinity GC B cells led to the cyclic re-entry model where GC B cells migrate between zones between each phase of mutation and selection.

Recent studies have used two-photon laser-scanning fluorescent microscopy to capture the movement and behaviour of B cells in germinal centres and present GC mechanisms which are in contrast to the previous GC mechanisms (276-278), reviewed (274;279;280) (**Figure 1.8**). Allen *et al* (276;279) tracked germinal centre B cells in mouse lymph nodes, in a perfusion chamber. Initially it was demonstrated that germinal centre B cells possessed highly dynamic

shapes, extending dendritic processes when they moved in contrast to the spherical phenotype characteristic of naïve B cells. Tracking analysis indicated that GC B cells were highly motile, similar to that of follicular mantle B cells and in contrast to plasma cells which demonstrated little motility. This motility was partially dependent on the chemokine CXCL13, expressed by FDCs. The behaviour of B cells in the dark and light zones were examined and it was demonstrated that GC B cells stayed within the dark or light zone although 5-8% travelled from one zone to another per hour. Cell division and cell death were observed in both regions of the germinal centre, in contrast to the classic model of germinal centre reactions mentioned previously. Schwickert *et al* (278) and Hauser *et al* (277) also tracked the movement of germinal centre B cells, but these were conducted in live mice that had received fluorescently labelled antigen specific B cells. Similar to Allen *et al* (276) the studies demonstrated that GC B cells were highly motile and re-circulate within the dark and light zones but Schwickert (278) demonstrated that bi-directional movement between zones occurred but at a higher frequency of 26% per hour in contrast to 5-8% per hour described by Allen *et al* (276) and Hauser *et al* (277). Schwickert *et al* (278) also demonstrated that the contact between antigen bearing FDCs and antigen specific B cells was short lived, in the light zone, but frequent suggesting that B cells were crawling along FDCs scanning for antigen. This is in contrast to naïve B and T cells which stop moving when they initially encounter antigen. The study also demonstrated that follicular B cells are frequent visitors to the GC compartment indicating that B cells may scan antigen trapped within the confines of germinal centres. In addition to this it was found that high-affinity antigen-specific B cells can be recruited to an ongoing germinal centre reaction which would enhance competition and ensure that rare high-affinity B cells, not initially recruited into the germinal centre reaction, might gain the opportunity to participate within antibody responses. This is in contrast to lower-affinity B cells which could not easily colonise an established germinal centre. This mechanism has recently been substantiated by Bende *et al* (281) who analysed the B cell composition of 48 GCs of reactive lymph nodes from 3 different donors and demonstrated that single, hypermutated B cell clones were found in multiple GCs, along with the offspring

from these clones. These results indicated the repeat involvement of antigen-experienced B cells within GC reactions.

Allen *et al* (276) concluded that the rates of interchange between the two zones and the bi-directional movements were consistent with the cyclic re-entry model. Conversely Hauser *et al* (277) concluded that there was not sufficient migration between each cell division to substantiate the cyclic re-entry model and instead favoured the intrazonal model (**Figure 1.9)**. Within this model most cells stay resident in the dark or light zones and selection in each of the zones occurs independently. In a more recent study statistical and functional modelling approaches were applied to the two-photon data to formulate a migration model which also incorporated chemokine receptor expression levels (282). Collectively these results demonstrate diverse germinal centre models which differ from the conventional and classic models.

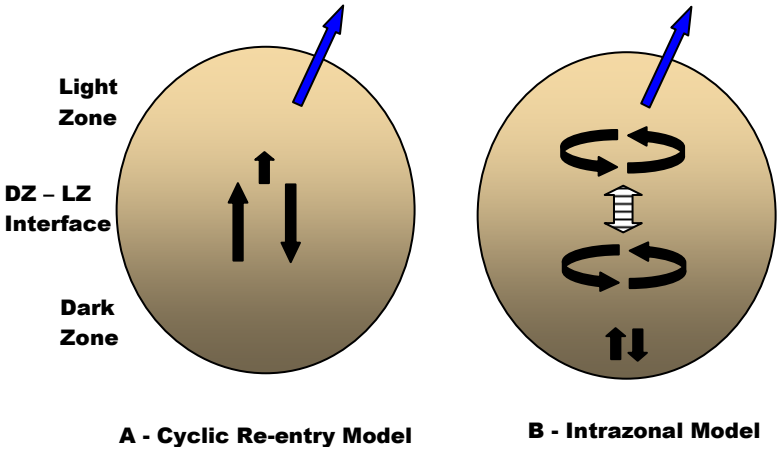

Figure 1.9 Migration Models for Germinal Centre Reactions

Previous findings on GC reactions implied that GC B cells which succeed in the selection process return to the dark zone for further division following a cyclic re-entry model (**A**). Recent studies have found that intra-zonal recirculation (**B**) may be the predominant mode of migration within GCs. This model suggests that GC B cell migration is parallel to, rather than perpendicular to the DZ – LZ interface with infrequent exchanges between the zones.

Solid arrows indicate strong movement of GC B cells, dashed arrows indicate a less prominent movement. Blue arrows indicate cells exiting the GC. Adapted from 277.

Analogs of germinal centre structures with comparable proliferation, mutation and apoptotic reactions, ectopic GCs, have been identified in non-lymphoid tissues in a variety of diseases, MG (52), SS (283), RA (284), HT (54) and breast cancer (285). The biological functions of this lymphoid neogenesis have been implicated in the pathology of autoimmune diseases by the generation of autoantibodies from autoreactive B cells although the steps leading to auto-antibody production remain elusive. Abnormal GC reactions have been observed in SLE which are thought to play a central role in SLE pathogenesis (286).

1.4.6 Role of B cells in Myositis and Vasculitis

The autoimmune origin and the role of B cells remain uncertain in myositis and vasculitis. The autoimmune origins of these disorders are supported by the disease's association with other autoimmune diseases, production of autoantibodies, formation of immune complexes and the response of the disease to B cell depletive therapies. In a recent study the role of B cells has been established in myositis where the study aimed to distinguish DM from PM by B cell activation (287). The study examined RP105, a leucine-rich repeat molecule, structurally similar to Toll-like receptors, located on the surface of B cells that was found to transmit an activation signal for B cell proliferation and resistance to apoptosis, this molecule is lost upon activation. SLE patients were found to have increased numbers of RP105 negative cells in peripheral blood, a phenotype of B cells consistent with that of activated B cells or germinal centre B cells, therefore the study investigated if DM and PM could be distinguished from one another by establishing the surface expression of RP105 on circulating B cells in both myopathies. The results showed a noticeably increased percentage of RP105 negative cells in DM compared to PM, 33.0% compared to 5.8%, suggesting the expansion of RP105 negative B cells is a hallmark of DM and indicating that B cells have a fundamental role in the pathogenesis of DM different from that of PM. Recent studies indicate RP105 regulates antigen-presenting functions and Treg development in a model of collagen-induced arthritis (288). In vasculitis, the work of Baiu *et al* (193) implicated a role for B cells in the pathophysiology of vasculitis as does the presence of immune-complex formations and many autoantibodies within vasculitic lesions.

Pathogenic roles for B cells in both myositis (DM) and vasculitis are substantiated by the recent studies using the B cell depletive therapy, Rituximab (149-151). Pilot studies indicated that Rituximab is an efficient treatment of DM as the resulting B cell depletion reduced DM symptoms (150-152). Improvements in muscle strength were observed as well as decreased levels of creatine kinase and a reduction in skin rashes but these symptoms reappeared during relapse associated with a return of circulating B cells. Although preliminary, and from a small sample size, these results emphasise the role of B

cells in the pathogenesis of DM. A recent study has also demonstrated the use of Rituximab in the treatment of 4 Juvenile DM patients, with and without myositis specific autoantibody (MSA) production (152). Clinical improvement was observed in three of the patients while the fourth had progression of the disease indicating that B cells are not fully accountable for the pathogenesis associated with myositis. Similar results have also been observed in Rituximab use in SLE and RA (149). Additional studies have demonstrated remission as a result of the Rituximab treatment in ANCA-associated vasculitic (148;157;159;177;202-206).

Collectively evidence from the studies described above substantiate a role for B cells in myositis and vasculitis but the exact mechanisms of B cells and their role in disease pathogenesis in these disorders remain unresolved.

1.5 Hypothesis and Aim of Study

The core objective of this study was to establish a role for B cells in the autoimmune disorders of myositis and vasculitis. By assessing the V_H antibody repertoire and clonal diversification of infiltrating B cells and plasma cells this study could examine the hypothesis that infiltrating lymphocytes within the muscle and vasculature were being locally stimulated by endogenous or exogenous antigens contributing to the pathological mechanisms of these disorders. Therefore the following main aims of this study were addressed:

- Identify infiltrating B cells and plasma cells within the inflammatory target tissue of myositis and vasculitis patients (Chapters 3 and 5).
- Establish the Ig gene repertoires of these muscle and skin infiltrating B cells and determine if gene selections are occurring (Chapters 4 and 5).
- Identify clonally related sets of sequences to indicate if B cell antigen-driven responses occur in the target tissues of myositis and vasculitis patients (Chapters 4 and 5).
- Identify and characterise infiltrating antigen specific cells and determine the Ig repertoire of these cells (Chapter 6).

Chapter 2 – Materials and Methods

2.1 Materials

All chemicals were supplied by Sigma-Aldrich (St. Louis, MO, USA) and Griener Bio-One (Kremsmuenster, Austria), Sarstedt (Numbrecht, Germany) and StarLab (UK) supplied the plasticware unless otherwise stated.

2.2 Identification of Cellular Infiltrates in Myositis and Vasculitis Biopsies

2.2.1 Patients and Samples

Muscle and skin tissue biopsies were obtained from patients undergoing diagnostic biopsies for myositis or vasculitis, following informed consent. Ethical approval was obtained from North Glasgow Hospital Research Ethics Committee. Samples, at time of biopsy, were embedded in Tissue-Tek OCT compound (Sakura Finetek, Torrance, CA) and snap-frozen in dry ice and ethanol and stored at -70℃. Alternatively archival muscle biopsies from previous diagnostic procedures, conducted by Dr W Behan, were obtained from the Pathology Department, Western Infirmary, Glasgow. Biopsies had been embedded in OCT and either stored in liquid nitrogen or at -70℃. To obtain retrospective consent for these samples to be used for research purposes amendments to the original ethical approval were completed and the medical records department for each patient's hospital was contacted to obtain information of the patients General Practitioner to allow the patient's contact information to be sought.

A total of 28 myositis patients, plus a control biopsy from a healthy patient, were selected from archival records. Sample MYO1 had already been selected and gave consent for the study. From the 28 patients selected 9 were deceased at the commencement of the study. To allow these samples to be used within the study the patient details were blinded and the samples number selected to the investigator by Linda MacKinnon, Pathology Department, Western Infirmary, Glasgow. From the 9 samples only 6 could be obtained from the archival stores, 3 could not be located or had been sent away. Four patients could not be found within any medical records departments therefore consent could not be sought from the patients and there was no confirmation if the patient was living or deceased therefore the samples were not included in the study. For

the remaining 15 patients, including the control patient, consent for the samples to be used in the study was requested. From these requests consent was given by 13 patients. From these, 10 of the samples could be obtained from archival stores, 3 could not be located or had been sent away. For 2 patients, MYO5 and MYO18, records indicated that each patient had 2 separate biopsies conducted. For patient MYO5 a further biopsy was conducted 3 years following a diagnostic biopsy and for patient MYO18 a second biopsy was conducted a year following the diagnostic biopsy. For these patients both biopsies were sought but only the biopsies following the diagnostic procedure could be obtained, the diagnostic biopsies could not be located. From the archival selection a total of 17 muscle samples from 16 different myositis patients and 1 control patient (**Table 2.1**) were used within the study. These samples, plus the sample from patient MYO1 who had already been included in the study, resulted in a total of 17 myositis biopsies being used within the study with the addition of a control sample. A summary of the pathology reported in these 17 myositis biopsies is shown in **Table 2.2**. Each sample was examined using immunohistochemical techniques for the presence of B cells and plasma cells and those with evident cellular infiltrates were examined further.

An additional muscle biopsy was obtained (MYO4) during the duration of the study but due to storage and transit conditions the sample was unable to be included in the study.

8 skin biopsies were obtained during diagnostic procedures from the Dermatology Department, Royal Infirmary, Glasgow. Only 3 of these biopsies could be used for the vasculitis study (**Table 2.3**). Pathologists from the Royal Infirmary hospital reported no active vasculitis within 3 of the biopsies and problems with sample handling meant an additional 2 could not be included in the study. The remaining 3 skin biopsies had active vasculitis confirmed by the Pathology Department, Royal Infirmary. As previously mentioned, each sample was examined using immunohistochemical techniques for the presence of B cells and plasma cells and those with evident cellular infiltrates were examined further.

2.2.2 Tissue Sectioning

Serial frozen sections (8 µm) were cut with a Shandon cryostat and were mounted on positively charged slides (Menzel Glaser, Germany or VWR, UK). Sections were air dried for at least 1 hour, fixed in acetone for 10 minutes and stored at -70℃ with a desiccant.

Sample	Diagnosis	M/F	Age at Diagnosis	Disease Duration From Diagnosis	CK at Biopsy IU/ml Normal Range up to 150 IU/ml	CRP at Biopsy (mg/L) Normal Range <10	Autoantibody Profile	Therapies at time of Biopsy	Family History	Other Features
MYO1	DM	F	40	0	142	NR	ANA NR, ENA Negative, Jo-1 Negative, Weakly Positive Anti-DNA (52U/ml, normal range <30U/ml)	No Prednisolone at biopsy, other medication unknown	No Significant Family History Recorded	Skin Rash for 8 months prior to biopsy. 6 week history of weakness in shoulder muscles prior to biopsy.
MYO3	PM	M	80	0	897	30	ANA 1:2560, RNP/Sm Positive, Jo-1 Positive, RF and Centromere Negative	Clopidogrel and NSAID (Name not apparent in notes)	None	Prostate Cancer (Previous Surgery, No medical treatment). Died with pericarditis.
MYO5	PM (With Sjogren's Syndrome)	F	40	3.5 years	1031	<6	ANA 1:40 (2000) Pattern Homogenous ANA Negative (2001) ENA Negative RF 294 (2000) (Normal Range 1-15 IU/ml)	Prednisolone 2.5mg daily IVIg every 8 weeks	Brother - Reiter's Syndrome Cousin - SLE	Diagnostic muscle biopsy conducted April 2000, CK 800 IU/ml. Patient also diagnosed with Sjogren's Syndrome (2000). Prednisolone started at 40mg daily, reduced to 2.5mg at second biopsy, October 2003. IVIg therapy began September 2000 (2g/kg). CK levels started to rise in January 2001 and reached 650 IU/ml in October 2001 despite steroid and IVIg therapy. Past Infection with EBV.
MYO6	PM	M	63	0	919	<6	ANA Negative ENA Negative RF<22	GTN & Tildiem (Angina) Nexium (GI Upsets) Co-proximal (Analgesia)	No Significant Family History Recorded	Muscular pains began around 2 years prior to biopsy, CK levels increased from 260 IU/ml (18 months prior to biopsy) to 967 IU/ml (10 months prior to biopsy) with normal CKMB. Previous statin therapy, discontinued 2 years prior to biopsy. Past medical history includes hiatus hernia, duodenal ulcer, angina, paraumbilical hernia, sleep apnoea syndrome
MYO7	PM	M	50	0	8390	NR	ANA Positive, ENA Negative, Jo-1 Negative	No Prednisolone at biopsy, other medication unknown	No Significant Family History Recorded	Pain and weakness noticed in shoulder and wrist a year prior to biopsy. Arthralgia

Cont…

Sample	Diagnosis	M/F	Age at Diagnosis	Disease Duration From Diagnosis	CK at Biopsy IU/ml Normal Range up to 150 IU/ml	CRP at Biopsy (mg/L) Normal Range <10	Autoantibody Profile	Therapies at time of Biopsy	Family History	Other Features
MYO16	DM	F	33	0	1076	7	ANA Positive (1:5120) Pattern Nucleolar (probable Topoisomerase 1), ENA Positive, Anti-DNA Negative	Oral Contraceptive Pill, Diclofenac	No Significant Family History Recorded	Past medical history of postural hypotension, no drug therapy received. Two year history of polyarthralgia and onset of Raynaud's disease just prior to biopsy.
MYO17	PM Diagnosis reported as IBM, 6 years following biopsy.	F	66	0	2716	NR	Scleroderma / Myositis Screen Negative, ANA Negative, ENA Ro Negative, ENA La/Sm/RNP Negative, RF<22	No Prednisolone at biopsy and no record of any other therapy at time of biopsy. Patient received a 7 day trial 40mg Prednisolone (8 months prior to biopsy) for Dyspnoea.	No Significant Family History Recorded	Pathologist noted that the degree of inflammatory cell infiltrate within the biopsy was greater than normal. IBM also suspected. Exacerbation of myositis occurred 4 years post biopsy, despite therapy. Biopsy was reviewed 6 years post biopsy, Diagnosis IBM. Past medical history includes Rheumatic Fever as a child, Cholecystectomy (1975), Hysterectomy (1981), Bowens Disease (1996), treated surgically, Asthma (1997). Following diagnosis, prednisolone therapy initiated. Additional therapies included Azathioprine, IVIg and Methotrexate were used but stopped due to lack of effect, patient continued with Cyclosporin therapy.
MYO19	PM	F	62	0	Elevated in a single occasion to 400 but normal at time of biopsy	NR	ANA Positive (1:2560) Pattern Nucleolar, ENADNA Negative, ENA Negative	Methotrexate 15mg/week and oral corticosteroid (dose not specified)	NR	Past medical history includes seronegative inflammatory synovitis. Patient received corticosteroid injection following knee aspiration in July 2001. At this time recent medical history included excision of basal cell carcinoma at the right medial canthus. Previous to this past medical history includes appenicectomy (1957), anxiety and depression (1967-1969), Varicose vein injection (1972), hallux valgus repair (1986), hypertension (1992) and Potts fracture of left ankle (1996).

Cont…

Sample	Diagnosis	M/F	Age at Diagnosis	Disease Duration From Diagnosis	CK at Biopsy IU/ml Normal Range up to 150 IU/ml	CRP at Biopsy (mg/L) Normal Range <10	Autoantibody Profile	Therapies at time of Biopsy	Family History	Other Features
MYO23	PM	F	45	0	5829	46	Jo-1 Positive, ANA, ENA, RF and Centromere Negative	Steroid therapy for 1 week which was stopped 2 weeks prior to biopsy. Thyroxine	No Significant Family History Recorded	5 week history of diffuse swelling of both lower limbs with weakness prior to biopsy. Hyperthyroidism (partial resection)
MYO24	PM	F	59	0	6623	No Record at Biopsy, Reported at 13, 6 weeks after biopsy	ANA negative Ro/La/Sm/RNP/Jo/ Scl70 Negative	120mg Prednisolone (im) given 4 days prior to biopsy. 18 month treatment with statins, stopped a week prior to biopsy. Losartan 25mg, Metformin 1.5gms, Bendrofluazide 2.5mg, Glicazide 160mg, Salbutamol. Previous treatment for pernicious anaemia.	NR	Past Medical History includes hypertension, asthma, Type II diabetes and pernicious anaemia. Diagnosed with adenocarcinoma of endometrium (Grade II) April 2006. Died May 2006, second day post op myocardial infarction.
MYOC **Patient deceased and clinical notes destroyed**	PM	M	66 (At Biopsy)	-	2500-3000	NR	NR	Treatments at biopsy unknown. Previous statin and steroid therapy.	No History of muscle disease	Six month history of muscle weakness and cramping at time of biopsy. Past medical history includes a long history of cardiac problems.

Cont…

Sample	Diagnosis	M/F	Age at Diagnosis	Disease Duration From Diagnosis	CK at Biopsy IU/ml Normal Range up to 150 IU/ml	CRP at Biopsy (mg/L) Normal Range <10	Autoantibody Profile	Therapies at time of Biopsy	Family History	Other Features
MYOE **Patient deceased and clinical notes destroyed**	Chronic Inflammatory Myopathy (Pathology consistent with PM)	F	49	0	NR	46	Anti-DNA + (Feb 03, 10 months prior to biopsy), Anti-Mitochondrial Negative (Dec 02), Anti-Smooth Muscle Negative (Dec 02), Anti-Gastric Parietal Cell Negative (Dec 02)	Had been on Prednisolone (40mg) for four months prior to biopsy. Stopped Steroid therapy for around 6 weeks resumed on 20mg, at time of biopsy patients was on 10mg. Other medications include thyroxine (50mg), Clarithromycin (500mg), Citalopram (40mg) and Viscotears.	NR	8 month history of symmetrical joint pain in shoulders, elbows, wrists, hands, knees and feet prior to biopsy. Past medical history includes Bell's palsy, pneumonia and hypothyroidism. Patient was admitted with acute bronchitis approximately 4 weeks prior to biopsy.
MY025		F	37							Control Sample from Healthy Volunteer
MYO2 **Patient deceased and clinical notes destroyed**	Inflammatory Myopathy (Pathology consistent with PM)	F	77 (At Biopsy)	-	17203	173	Not Known	Prednisolone 60mg (Just prior to biopsy)	NR	At time of biopsy patient had a recent myocardial infarct, cardiac arrest and then resuscitation. At this time patient had obvious proximal weakness. CK was previously normal.
MYOA	Inflammatory Myopathy (possible IBM)	F	70	0	694	50 (A month prior to biopsy)	ANA 1/2560, Anti-mitochondria, Anti-smooth muscle and Anti-gastric parietal cell. Anti-SRP Negative, Anti-Jo-1 NR	Atenolol, Dihydrocodeine, oxytetracycline, Vioxx, Frusemide	No Significant History	Medical History includes Fibromyalgia, Pulmonary TB, Primary biliary Cirrhosis, Hypertension, OA knees and Pulmonary fibrosis. Died cerebral haemorrhage 15/01/04

Cont…

Sample	Diagnosis	M/F	Age at Diagnosis	Disease Duration From Diagnosis	CK at Biopsy IU/ml Normal Range up to 150 IU/ml	CRP at Biopsy (mg/L) Normal Range <10	Autoantibody Profile	Therapies at time of Biopsy	Family History	Other Features
MYOD	DM	F	75	0	>3000	NR	ENA Negative, DNA <30U/ml, ANCA Negative, ANA NR	No Prednisolone at biopsy, other medication unknown	NR	Four week history of weakness in arms and legs. Heliotrope rash on hands. One year post biopsy a chest x-ray revealed a lung tumour (Right hand side at the hilum). Diagnosis of DM associated with underlying lung tumour.
MYO18	PM	F	52	13 months	597	NR (at time of biopsy)	ANA 1:40, nucleolar RF Normal ENA Negative	Prednisolone 15mg Co-Codamol Omeprazole 20mg Alendronate 70mg once weakly	No Significant History	Diagnostic Biopsy conducted January 2001, CK 11226, CRP <5, Prednisolone started at 60mg daily, reduced to 15mg daily. Second Biopsy conducted February 2002
MYO21	PM	M	64	0	783	36	ANCA Positive (pANCA-MPO) RF Negative ANA Negative	Prednisolone 60mg (Just prior to biopsy) Other medications include: Enalapril (10mg od), Isosorbide Mononitrate (60mg od), Sertraline (50mg od), Simvastatin (40mg od), Nicorandil (20mg), Montellukast (10mg od), Serertide 500, Salbutamol	NR	Marked Eosinophilia (10, normal range <0.4110^9/l). No deterioration in chest symptoms. Medical History includes Polyarteritis nodosa (PAN) with cutaneous involvement, asthma and Ischaemic heart disease. Myocardial Infarction 6 years prior.

Table 2.1 Myositis Patients

M, Male; F, Female; CK, Creatine Kinase; CRP, C-Reactive Protein; NR, No Record.

Sample	Fibre Size Variation	Necrotic Fibres (Undergoing Phagocytosis)	Basophilic / Regenerating Fibres	Internal Nuclei	Perivascular Atrophy	HLA	Inflammatory Infiltrate			Presence of Vacuoles	Presence of Inclusions	Fibrosis
							✓/×	Location	Invasion of Fibres			
MYO1	-	✓	✓	✓	-	✓	✓	Perivascular	-	✓	-	-
MYO3	✓	✓	✓ Occasional	-	-	-	✓	-	-	-	-	Minimal
MYO5	✓	✓	✓ Occasional	✓	×	✓	✓	Surrounding Necrotic Fibres	-	-	-	-
MYO6	✓ Mild	✓ (✓)	-	✓	×	✓	✓	Surrounding Necrotic Fibres & Perimysial BV	✓	-	-	-
MYO7	-	✓ (✓)	×	✓	×	-	✓	Perimysial	-	-	×	-
MYO16	✓ Mild	✓ (✓)	✓ Rare	✓ Occasional	×	-	✓	Surrounding Necrotic Fibres	-	-	-	-
MYO17	✓	✓	✓	✓	-	-	✓	Endomysial, Surrounding Necrotic and Regenerating Fibres	-	✓	(✓ Reported 2004, 6 years after biopsy)	-
MYO19	-	✓ (✓)	✓ Rare	-	×	✓	✓	Surrounding Necrotic Fibres & Perimysial BV. Not in Perifascicular region.	-	-	×	-
MYO23	✓	✓	✓	-	×	✓	✓	-	-	-	-	-
MYO24	✓	✓	✓	✓	-	✓	✓	Surrounding Necrotic Fibres	-	-	×	-
MYOC	✓	✓	✓	✓	-	✓	✓	Surrounding necrotic fibres in each fascicle	✓	-	×	✓
MYOE	-	✓ (✓)	✓ Mild	-	-	✓	✓	Surrounding Necrotic Fibres and BV	-	-	-	✓
MYO2	-	✓	✓	-	-	✓	✓	Endomysial	✓		-	✓
MYOA	✓	✓ Occasional	✓ Occasional	✓	✓	✓	✓	Surrounding Necrotic Fibres	-	-	-	✓
MYOD	✓	✓	-	✓ Mild	✓	-	×	-	-	✓ Occasional	-	-
MYO18	×	✓ (✓)	✓	-	-	-	×	-	-	-	-	-
MYO21	✓ Mild	✓ (✓)	✓	-	×	✓	✓	Endomysial	-	-	-	-

Table 2.2 Myositis Pathological Summary

- No record or discussion of feature in pathology report

Sample	Diagnosis	M/F	Age at Diagnosis	Disease Duration at Biopsy	CK at Biopsy IU/ml Normal Range up to 150 IU/ml	CRP at Biopsy (mg/L) Normal Range <10	Autoantibody Profile	Therapies at time of Biopsy	Family History	Other Features
VAS1	Cutaneous Vasculitis (With Sjogren's Syndrome)	F	59	8 months	NR	NR	ANA 1:2560, speckled Ro & La Positive	Beclomethasome and Salbutamol	Ischaemic heart disease & Thyroid Disease	Diagnostic Biopsy conducted in Jun 04 and found features of leukocytoclastic vasculitis. In June 04, RF positive and atypical c-ANCA positive. Past Medical history includes childhood chest infections, hyperthyroidsm and asthma.
VAS6	Leukocytoclastic Vasculitis of lower limbs and scalp	M	43	0	NR	7	ANA Negative ANCA negative	Sulphasalazine 500mg daily, Kenalog 40mg, Indocid, Imipramine, Diazepam, DF-118, Zantac	Mother - Post-traumatic epilepsy Father - Angina	Background of Ankylosing Spondylitis
VAS7	Henoch-Schonlein Purpura. Biopsy confirmed Leukocytoclastic Vasculitis	M	49	0	NR	20	ANA Negative RF Negative Atypical c-ANCA moderately positive (MPO and PR3 negative) Mitochondrial Negative Smooth muscle Negative Gastric Parietal cell Negative Liver kidney microsomal Negative Glomerular basement membrane Negative	Spironalactone, Warfarin, Vitamin B Co Strong, Thiamine, Folate, Biprobase	No Significant Family History Noted	Polyarthralgia (Left Hand, Right Wrist, Both elbows, knees and ankles) IgA 9.9g/l (Normal Range 0.8-4) IgG 21.5g/l (Normal Range 6-16) IgM 6.7 (Normal Range 0.5-2) Positive E Coli Blood culture - May 05 Long History of excess alcohol. Past Medical History includes Liver Cirrhosis,Recurrent DVT's, Pleural Effusion, Folate Deficiency and Borderline Protein C Deficiency

Table 2.3 Vasculitis Patients

M, Male; F, Female; CK, Creatine Kinase; CRP, C-Reactive Protein; NR, No Record.

2.2.3 Immunohistochemistry

Slides from -70℃ were thawed at room temperature for 30 minutes in a staining vessel containing anhydrous silica gel. To fix sections slides were transferred to acetone for 10 minutes and then allowed to dry. Sections were circled with a PAP pen (Immedge Pen, Vector Laboratories, Burlingame, CA, USA) and allowed to dry for 5 minutes. 100 µl of 2% bovine serum albumin/ Tris-buffered saline (2%BSA/TBS) was added to each section to block for 30 minutes. All incubations were carried out at room temperature in a humidified chamber. Blocking solution was poured off and 100 µl of 2% BSA/TBS containing mouse anti-human primary antibody (DAKO, Denmark) was added to each section (**Table 2.4**). Negative control experiments were performed using antibodies with matched isotypes. Sections were incubated for 1 hour. The primary antibody solution was poured off and sections were washed twice in TBS (**Section 2.5**) for 5 minutes. Following washing 100 µl of 2% BSA/TBS containing 5 µl of rabbit anti-mouse IgG secondary antibody (DAKO) was added to each section and was incubated for 30 minutes. After the secondary antibody was poured off and sections were washed twice in TBS for 5 minutes 100 µl of 2% BSA/TBS containing 2 µl of alkaline phosphatase anti-alkaline phosphatase (APAAP) was added to each section and was incubated for 30 minutes. Sections were again washed twice in TBS for 5 minutes. 100 µl of substrate was then added to each section and allowed to develop for 20 minutes. Substrate solution contained 10 µl of 5% New Fuchsin in 2 M HCl, 25 µl of 0.7 M sodium nitrite, 3.5 ml of Buffer E (0.05 M Tris, 0.9% NaCl, pH 9.7), 1.25 ml of 0.2M 2-amino-2-methyl-1,3-propanediol (AMPD), 50 µl of 40 mg/ml levamisol, 30 µl of Naphthol AS-BI phosphate and 100 µl of 2M HCl. Following substrate incubation sections were washed twice in TBS for 5 minutes and once in sterile distilled water for 5 minutes. Sections were counter-stained with Mayer's Haemotoxylin and washed in Scotts tap water substitute (**Section 2.5**) to allow proper colour development, except for sections with Ki67 staining. As this is a nuclear marker haemotoxylin staining would camouflage the signal. Sections were viewed using a Nikon (Melville, NY) Diaphot inverted microscope and images were taken using a JVC 3-CCD camera. The analog signal from the camera was converted into a digital signal using an ADS Tech (Ireland) Pyro A/V link convertor and images were taken using Adobe Premier Elements

software. Sections were stored in a wet chamber at 4℃ for microdissection. Sections not used for microdissection were mounted using glycerol gelatine.

Initially sections at intervals of between 40 to 80 μm were stained for $CD20^+$ B cells and plasma cells to determine the presence of these cell phenotypes throughout the collection of serial sections obtained from the biopsy; n=3-7 depending on tissue availability. Serial sections surrounding areas of infiltrating B cells and/or plasma cells were then used to establish the infiltration of the other cell phenotypes. Representative images of these cellular infiltrations are presented in this thesis. Semi quantitative analysis of cellular infiltration of the various cell phenotypes was conducted, described further in Tables 3.1 and 5.1.

Antibody Specificity	Source	Species	Clone	Isotype	Dilution
CD20	DAKO[a]	Mouse Monoclonal	L26	-IgG2a	1:50
FDC	DAKO	Mouse Monoclonal	CAN.42	-IgM	1:100
Plasma Cell	DAKO	Mouse Monoclonal	V538c	-IgG1	1:200
CD3	DAKO	Mouse Monoclonal	T3-4B5	-IgG1	1:100
CD4	DAKO	Mouse Monoclonal	MT310	-IgG1	1:20
CD8	DAKO	Mouse Monoclonal	Dk25	-IgG1	1:100
Ki67	DAKO	Mouse Monoclonal	MIB-1	-IgG1	1:100
FoxP3	AB CAM[b]	Mouse Monoclonal	236A/E7	-IgG1	1:40
CD68 (Macrophage)	DAKO	Mouse Monoclonal	EMB11	-IgG1	1:100
-IgG1 Isotype Control	DAKO	Mouse Monoclonal	DAK-G01		Same as primary antibody concentration
-IgG2a Isotype Control (Anti-Aflatoxin)	Kind gift from Prof Stimpson, Strathclyde University, Glasgow				1:50
-IgM Isotype Control	DAKO	Mouse Monoclonal	DAK-G08		1:100

a – Denmark, b – Cambridge, UK

Table 2.4 Primary Antibodies used in Immunohistochemistry

2.2.4 Immunofluorescence

Double immunofluorescent staining on frozen serial sections was carried out using the Mouse on Mouse (M.O.M) Immunodetection Immunofluorescent Kit (Vector Laboratories, Burlingame, CA, USA) designed to fluorescently detect several mouse primary antibodies on the same tissue whether or not the tissue is of mouse origin. Primary antibodies used for fluorescent staining were the same as those described in Table 2.4 of section 2.2.3, although some antibody concentrations were optimized for multiple immunofluorescent staining, **Table 2.5**. Frozen sections were thawed at room temperature for 30 minutes in a staining vessel containing anhydrous silica gel. To fix sections slides were transferred to acetone for 10 minutes and then allowed to dry. Sections were circled with a PAP pen (Vector Laboratories) and allowed to dry for 5 minutes. All incubations were carried out at room temperature in a humidified chamber. Sections were incubated for 15 minutes with avidin blocking solution (Vector Laboratories) and briefly washed in TBS before a 15 minute incubation with biotin blocking solution (Vector Laboratories). They were then washed twice for 2 minutes in TBS before a 5 minute incubation with a working solution of M.O.M diluent to allow all non-specific protein sites to be blocked. After a 5 minute incubation excess M.O.M diluent was removed and sections were incubated for 30 minutes with the first primary antibody, Table 2.5, in M.O.M diluent. Sections were again washed twice in TBS for 2 minutes. A working solution of biotinylated Horse Anti-Mouse Ig reagent in M.O.M diluent was then applied to each section and incubated for 10 minutes followed by two washes in TBS for 2 minutes. A working solution of fluorescein avidin DCS was then applied to each section for 5 minutes before two 5 minute washes in TBS. For staining of the second antigen sections were again blocked with avidin and biotin blocking solutions for 15 minutes to prevent the interaction of the second set of labelling reagents with the first set of labelling reagents. Sections were washed twice for 2 minutes in TBS before sections were incubated for 1 hour with a working solution of M.O.M mouse Ig blocking reagent. After two 2 minute washes sections were again incubated with a working solution of M.O.M diluent for 5 minutes to block any non-specific protein binding sites. Excess M.O.M diluent was removed and sections were incubated for 30 minutes with M.O.M diluent containing the second primary antibody. After two 2 minute washes in TBS

sections were incubated for 10 minutes with a working solution of Anti-Mouse Ig reagent in M.O.M diluent. Following two 2 minute washes sections were incubated for 10 minutes with Texas Red Avidin DCS (20 µg/ml). After two final 5 minute washes sections were mounted in VECTASHIELD hardset mounting medium (Vector Laboratories) and viewed using a Zeiss Axiovert S100 microscope with a Zeiss Plan-NEOFLUAR 63x lens (Carl Zeiss Ltd., Welwyn Garden City, UK). For each view, 5 images were taken at 0.5 micron intervals and Openlab software (Improvision) was used to deconvolve the images.

Antibody Specificity	Source	Species	Clone	Isotype	Dilution
CD20	DAKO[a]	Mouse Monoclonal	L26	-IgG2a	1:100
Plasma Cell	DAKO	Mouse Monoclonal	V538c	-IgG1	1:200
CD3	DAKO	Mouse Monoclonal	T3-4B5	-IgG1	1:100
CD4	DAKO	Mouse Monoclonal	MT310	-IgG1	1:100
CD8	DAKO	Mouse Monoclonal	Dk25	-IgG1	1:100
Ki67	DAKO	Mouse Monoclonal	MIB-1	-IgG1	1:100
FoxP3	AB CAM[b]	Mouse Monoclonal	236A/E7	-IgG1	1:20
CD68 (Macrophage)	DAKO	Mouse Monoclonal	EMB11	-IgG1	1:100
-IgG1	DAKO	Mouse Monoclonal	DAK-G01		Same as primary antibody concentration
-IgG2a (Anti-Aflatoxin)	Kind gift from Prof. Stimpson, Strathclyde University, Glasgow				1:100

a – Denmark, b – Cambridge, UK

Table 2.5 Primary Antibodies used in Immunofluorescence

2.3 V_H-Gene Repertoire of Infiltrating B Cells in Myositis and Vasculitis Samples

2.3.1 Microdissection and DNA preparation

To establish the antibody repertoire of the B cells and/or plasma cells in the cellular infiltrates the stained areas resembling B cell and plasma cell aggregates were microdissected under a Nikon Diaphot inverted microscope (Melville, NY). To avoid contamination a fresh lancet was used for each section excised and discarded if it came into contact with any other site. DNA was released by proteinase K digestion using the QIAGEN DNA Micro Kit (QIAGEN, Sussex, UK) according to manufactures instructions. Briefly, microdissected tissue was added to 180 µl Lysis Buffer ATL and 20 µl Proteinase K. Microdissected samples were incubated at 56℃ for approximately 4 hours to allow lysis. Following lysis 200 µl of Buffer AL containing 1 µg of carrier RNA was added to each sample and mixed by pulse vortexing for 15 seconds. 200 µl of 100% ethanol was then added to each sample and after mixing thoroughly samples were incubated at room temperature for 5 minutes. Lysates were then transferred to a QIAamp MinElute column and centrifuged at 8000 rpm for 1 minute to allow binding of the DNA to the column membrane. The DNA bound to the column was washed firstly with 500 µl of Buffer AW1 by centrifugation at 8000 rpm for 1 minute and then 500 µl of Buffer AW2 by centrifugation at 8000 rpm for 1 minute. Columns were then centrifuged at 14, 000 rpm for 3 minutes to dry the membrane. To elute the DNA 20 µl of PCR Grade Water (Roche, Mannheim, Germany) was added to each column and allowed to incubate for 5 minutes at room temperature before a final centrifugation at 14, 000 rpm for 1 minute to release the DNA from the membrane. For extremely small areas that were microdissected, cell lysis occurred in a total volume of 25 µl Buffer ATL/Proteinase K containing 10 µl Proteinase K. An additional 25 µl of Buffer ATL was added to each sample following a 3 hour incubation at 56℃. 50 µl of Buffer AL was then added to each sample which again contained 1 µg of carrier RNA. After pulse-vortexing for 15 seconds samples were mixed with 50 µl 100% ethanol and allowed to incubate at room temperature for 5 minutes. The remainder of the protocol was as described above. Alternatively excised tissue was digested in 30 µl of Proteinase K (0.7 mg/ml, Roche, Mannheim, Germany) at 50℃ for 1 hour and the enzyme was inactivated at 95℃ for 10 minutes. This

method was used for analysis of sample MYO1. Samples were either stored at -20℃ or used directly in nested PCR reactions.

2.3.2 Peripheral Blood Mononuclear Cell (PBMC) Isolation

For positive control PCR and analysis of patient's peripheral blood, PBMCs were isolated from blood samples containing the anticoagulant heparin using Lymphoprep (Axis Shield, Oslo, Norway), a sterile and endotoxin tested solution for the isolation of pure lymphocyte suspensions. Lymphoprep results in aggregation of erythrocytes, increasing their sedimentation rate allowing them to be isolated after centrifugation, as leukocyte sedimentation is only slightly affected and can therefore be removed from the upper layer (**Figure 2.1**). An equal volume (6 mls) of 0.9% NaCl was used to dilute the blood. 6 mls of the diluted blood was then layered over 3 mls of lymphoprep and centrifuged at 800 x g for 20 minutes without brake, or 30 minutes without brake if the blood had been collected over a 2 hour time frame. After centrifugation PBMCs form a distinct band at the sample/medium interface, also known as the buffy coat, and were removed using a glass Pasteur pipette. The upper serum layer was removed and stored at -20℃ after PBMCs were remove d. The fraction of PBMCs was diluted in 10 mls 0.9% NaCl and centrifuged at 250 x g for 10 minutes twice. The pellet was then resuspended in 200 µl PBS (**Section 2.5**).

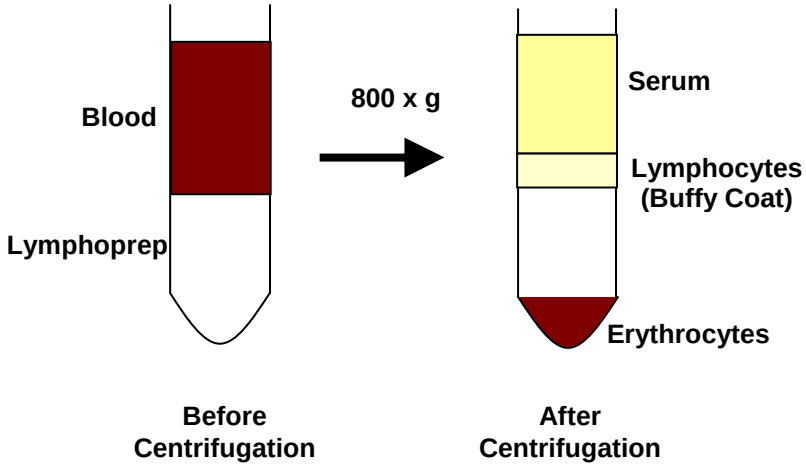

Figure 2.1 Removal of lymphocytes from peripheral blood

To establish the repertoire of lymphocytes from peripheral blood samples, lymphocytes were separated with the use of Lymphoprep (Axis Shield, Norway). Lymphoprep is a ready made, sterile, and endotoxin tested solution which allows the isolation of pure lymphocyte suspensions. The mixing of blood with lymphoprep causes aggregation of the erythrocytes, increasing their sedimentation rate. The lymphoprep solution only slightly affects the sedimentation rates of lymphocytes and therefore after centrifugation the erythrocytes, with their increased sedimentation rate, collect at the base of tube while lymphocytes form a distinct band at the sample/medium interface allowing the lymphocyte suspension to be removed. Adapted from Lymphoprep (Axis Shield, Norway) datasheet.

2.3.3 Lymphocyte Cryopreservation

In cases where additional blood samples were taken from patients, lymphocytes were extracted as described in section 2.3.2 but were either resuspended in 1 ml Foetal Bovine Serum (FBS) supplemented with 10% dimethyl sulfoxide (DMSO) or 1 ml 60% wash buffer (RPMI supplemented with 1% Penicillin/Streptomycin and 1% 200 mM L-Glutamine) supplemented with 30% Foetal Bovine Serum and 10% DMSO and transferred to a 1.5 ml cryovial (Starstedt, Numbrecht, Germany). The lymphocytes were cooled at approximately 1°C a minute in a freezing container (Nalgene Nunc, Abingdon, UK) containing isopropanol to a final temperature of -80°C. The lymphocytes were kept at -80°C for 24 hours before being transferred to liquid nitrogen for long-term storage. The tissue culture medium and supplements were obtained from Invitrogen (Paisley, UK).

2.3.4 Sera Isolation

Blood collected from patients in the absence of any anticoagulant was stored at 4℃ for at least 30 minutes to allow the clot to re duce. The blood clot was then removed and the remaining serum was centrifuged at 3000 rpm for 10 minutes to remove any remaining erythrocytes. The serum supernatant was then removed and stored at -20℃.

2.3.5 Genomic DNA Isolation

PBMC DNA was extracted from the resuspended fraction after PBMC isolation, section 2.3.2, using a QIAamp DNA mini kit (QIAGEN, Sussex, UK), according to manufacturers instructions. In summary, 20 µl of QIAGEN proteinase K was added to 200 µl of buffy coat sample. 200 µl of Buffer AL was then added to sample and mixed by pulse vortexing for 15 seconds. Samples were then incubated for 10 minutes at 65℃ to ensure maximum lysis. 200 µl of 100% ethanol was then added to the sample and mixed for 15 seconds by pulse vortexting. The sample mixture was then added to the QIAamp spin column and columns were centrifuged at 8,000 rpm for 1 minute. 500 µl of Buffer AW1, wash buffer, was added to the column and the column was again centrifuged for 1 minute at 8, 000 rpm. 500 µl of Buffer AW2, wash buffer, was then added to the column and the column was centrifuged for 1 minute at 13, 000 rpm.

Columns were then centrifuged at 13, 000 rpm for an additional 3 minutes to remove any residual Buffer AW2. Columns were transferred to 1.5 ml microcentrifuge tubes and 200 µl Buffer AE was added and allowed to stand for 1 minute before being centrifuged for 1 minute at 13, 000 rpm. DNA concentration was measured as described in section 2.3.11 and DNA was stored at -20℃. 10 µl of DNA, for positive control purposes or for analysing a patient PBL, was used in each PCR reaction as described in Section 2.3.7.

2.3.6 Primers

Primers for nested PCR were synthesised by Operon Biotechnologies (Huntsville, AL, USA), **Tables 2.7 and 2.8**. For use in PCR, primers were synthesised at 0.2 µmole, desalted and arrived lyophilized and were reconstituted in PCR grade H_2O (Roche, Mannheim, Germany) to produce a stock concentration of 100 µM (100 pmol/µl). Primer stock concentrations were stored at -20℃. For use in PCR, working solutions of a total combined concentration of 20 µM (20 pmol/µl) were prepared as per **Table 2.6**. For primary PCR reactions all V_H leader sequences were combined in one working solution but for secondary PCR reactions each set of V_H family primers were combined to produce family specific working solutions to allow for family specific amplification. All J family primers were also combined. Working concentrations of primers were also stored at -20℃.

Number of primers in working solution	µl of each primer required for final concentration of 20 µM	µl of 50 mM Tris-HCl pH 8.0	µl of sterile PCR grade H_20
1	4	6	10
2	2	6	10
3	1.33	6	10
4	1	6	10
5	0.8	6	10
11	1	27.5	37.5

Table 2.6 Volumes for preparing primer working concentrations (20 µM)

2.3.7 Nested PCR

Immunoglobulin genes from infiltrating B cells and plasma cells were amplified by a nested PCR system (**Figure 2.2**) that ensures that only rearranged Ig V-genes were amplified and has been used previously within the laboratory to successfully analyse the repertoire of Ig V-genes from B cell clusters and germinal centres in SS (283), MG (52), breast cancer (285) and SLE (289). Primers were designed to amplify all known functional, rearranged human V_H genes and are shown in **Tables 2.7 and 2.8**. To avoid contamination of samples and PCR reagents all procedures prior to primary PCR amplification were performed in a clean laboratory prior to where post amplification steps were carried out. All PCR reactions were prepared in a Captair™Bio Biocap™RNA/DNA hood (Erlab, France). Filter tips were also used in sample preparation to limit PCR contamination as well as the use of a Microman M10 pipette with sterilised and disposable pipette capillaries and pistons in transferring DNA from primary to secondary PCR reactions. Microman pipettes are equipped with a positive displacement mechanism that isolates the aspirated liquid from the body of the pipette with prevents the sample-to-sample contamination that can result from aerosols (290). The disposable pistons and capillaries are the only feature to make contact with the aspirated liquids therefore protecting against contamination from one sample to another.

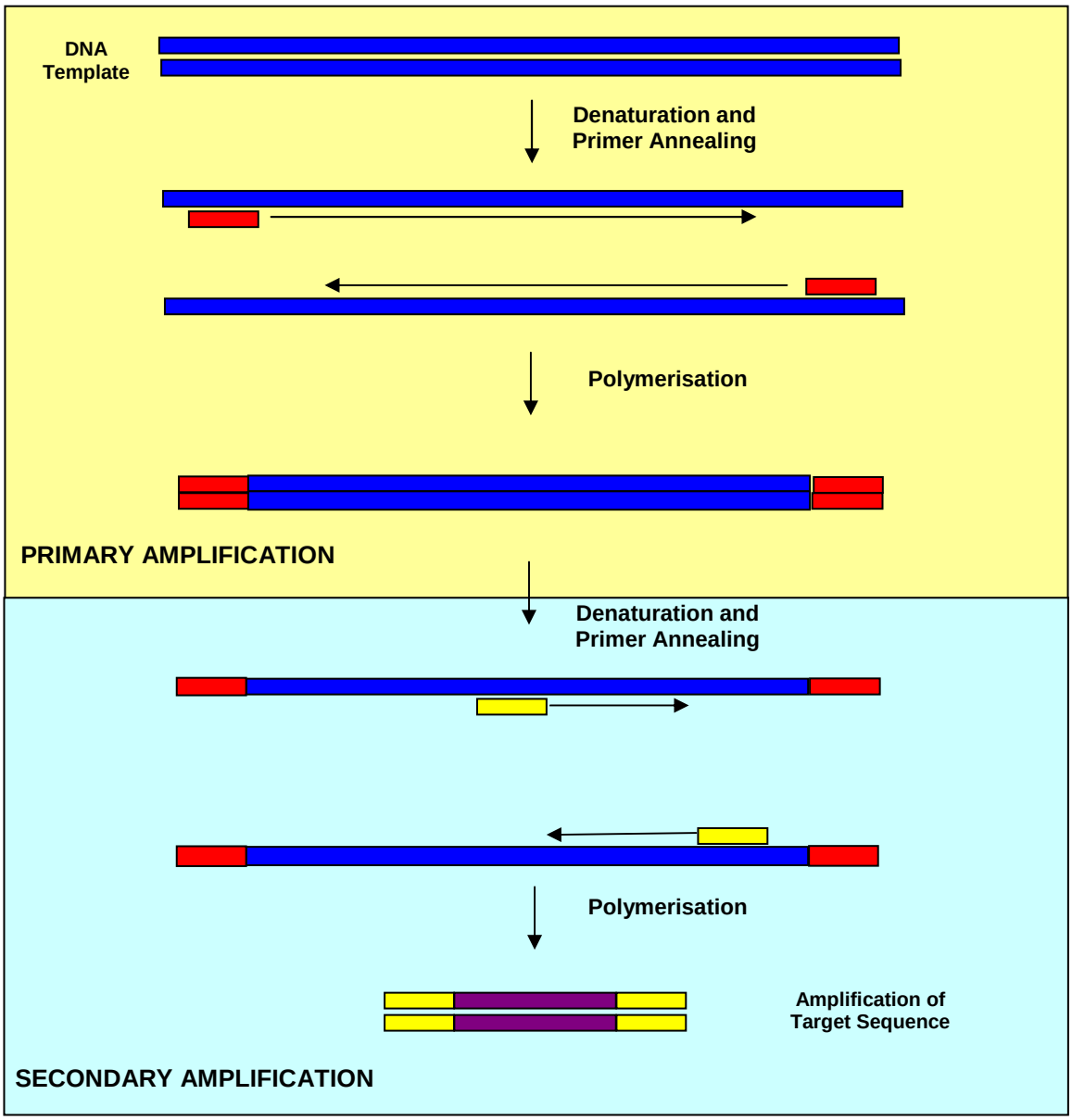

Figure 2.2 A simplified Diagram of Nested Polymerase Chain Reaction (PCR)

The Polymerase Chain Reaction (PCR) was used to amplify a specific sequence of DNA using primers, each complementary to the DNA target sequence ( ). Target DNA was amplified through a series of cycles of denaturation to separate target DNA, primer annealing to target DNA and polymerisation of the target DNA For this series of cycles Mg^{2+}, each deoxynucleoside triphosphate (dNTP), PCR buffer and the thermostable DNA polymerase, *Taq*, are required in addition to the template DNA. To increase the specificity of immunoglobulin gene amplification a second round of PCR was carried out in a process of nested PCR. In the second phase of cycles a new set of primers ( ) were used that anneal within the fragments produced in the first round of PCR. The use of nested PCR increased the specificity by ensuring that only the target sequence was amplified from the mixture from the first round; as only the target sequence should contain both sets of primer-binding sites.

2.3.7.1 Nested PCR – V_H Chain Amplification

For primary amplification 10 µl of DNA was amplified in a reaction volume of 50 µl with 10 pmole of V_H leader primer mixture, 10 pmole of universal J_H primer, 2.6 U DNA polymerase, 2.5 mM $MgCl_2$ and 200 µM dNTP's in conjunction with hot-start ampli-wax Gem 50 beads (Applied Biosystems, Foster City, CA). The conditions used for 35 cycles were, after an initial 2 minute hot start, 94℃ for 1 minute, 50℃ for 1 minute and 72℃ for 2 minutes fo llowed by one cycle of 72℃ for 15 minutes. The reactions were conducted on a Trio-Thermoblock (Biometra, Tampa, FL) or Tprofessional Thermocycler (Biometra) using the Expand High Fidelity PCR System (Roche, Mannheim, Germany). The Expand High Fidelity PCR System contains a unique combination of thermostable Taq DNA polymerase and Tgo DNA polymerase, providing a thermostable DNA polymerase with proofreading activity to generate PCR products of high yield, fidelity and specificity. For secondary amplification 2 µl of primary amplification product was used as a template in reactions similar to primary PCR reactions except 20 pmole of each V_H family and J_H primer mixes were used. Conditions for 40 cycles were 94℃ for 1 minute, after an init ial 2 minute hot start at 94℃, 61℃ for 1 minute for V_H 1, 2 and 3 primers or 65℃ for 1 minute for V_H 4, 5 and 6 primers and 72℃ for 2 minutes followed by one cy cle of 72℃ for 15 minutes.

	Primer Name	Sequence
V_H Leader primers	HUVH1L	TCA CCA TGG ACT GGA CCT GGA G
	HUVH1L.2	TCA CCA TGG ACT GGA TTT GGA GG
	HUVH2L	ACC ATG GAT ATA CTT TGT TCC ACG
	HUVH2L.2	ACC ATG GAC ACA CTT TGC TCC ACG
	HUVH2L.3	ACC ATG GAC ACA CTT TGC TAC ACA
	HUVH3L	ACC ATG GAG TTT GGG CTG AGC TG
	HUVH3L.2	ACC ATG GAA CTT GGG CTC CGC TG
	HUVH4L	AAG AAC ATG AAA CAC CTG TGG TTC
	HUVH4L.2	AAG AAC ATG AAG CAC CTG TGG TTT
	HUVH5L	ATC ATG GGG TCA ACC GCC ATC CT
	HUVH6L	ACA ATG TCT GTC TCC TTC CTC ATC
Universal J_H primer	HUJHUNI	CTC ACC TGA GGA GAC GGT GAC CGG

Table 2.7 Leader Primer Sequences for primary amplification round in Nested PCR

	Primer Name	Sequence
V_H Family primers		
V_H 1	HUVH1.1	CAG GTG CAG CTG GTG CAG TCT GG
	HUVH1.2	CAR ATG CAG CTG GTG CAG TCT GG
	HUVH1.3	GAG GTC CAG CTG GTA CAG TCT GG
V_H 2	HUVH2	CAG ATC ACC TTG AAG GAG TCT GG
	HUVH2.1	CAG GTC ACC TTG ARG GAG TCT GG
V_H 3	HUVH3.1	GAG GTG CAG CTG GTG GAG TCT GG
	HUVH3.2	GAG GTG CAG CTG TTG GAG TCT GG
	HUVH3.3	GAG GTG CAG CTG GTG GAG ACT GG
	HUVH3.4	GAG GTG CAG CTG GTG GAG TCT CG
V_H 4	HUVH4	CAG GTG CAG CTG CAG GAG TCG GG
	HUVH4.1	CAG CTG CAG CTG CAG GAG TCS GG
	HUVH4.2	CAG GTG CAG CTA CAR CAG TGG GG
V_H 5/ V_H 7	HUVH5/7	SAG GTG CAG CTG GTG CAR TCT GG
V_H 6	HUVH6.1	CAG GTA CAG CTG CAG CAG TCA GG
J_H primers	HUJH1	TGA GGA GAC GGT GAC CAG GGT GC
	HUJH3	TGA AGA GAC GGT GAC CAT TGT CCC
	HUJH4	TGA GGA GAC GGT GAC CAG GGT TCC
	HUJH6	TGA GGA GAC GGT GAC CGT GGT CC

Table 2.8 Family Primer Sequences for secondary amplification round in Nested PCR

2.3.8 Agarose Gel Electrophoresis

PCR products were separated through 1.5% electrophoresis grade Ultra Pure Agarose (Invitrogen, Paisley, UK) in TBE (**Section 2.5**) and visualised with ethidium bromide (0.5 µg/ml) under UV light. Samples were diluted with 6X Blue-Orange Gel loading dye (Promega, Madison, WI, USA) and the size of products was determined using a 10 KB ladder (Bioline, London UK). PCR products were visualised under UV light using KODAK Gel logic 200 and KODAK 1D Image Analysis software (KODAK, Rochester, NY, USA). Products of approximately 350-400 base pairs were expected.

2.3.9 Gel Extraction

DNA (20 µl) to be extracted and purified was run on a 1.5% agarose gel (**Section 2.5**) and DNA fragments were excised with a sterile sharp scalpel. To eliminate any cross contamination a fresh scalpel was used for each DNA sample. DNA was extracted using the QIAquick Gel Extraction Kit (QIAGEN, Sussex, UK) according to manufactures instructions. In summary, after the weight of the gel slice was determined, 3 volumes of Buffer QG was added to 1 volume of gel (100 mg ~ 100 µl) and gel extracts were incubated at 50℃ for 10 minutes to allow the gel slice to completely dissolve. To aid dissolution of the agarose gel slice samples were vortexed every 2-3 minutes. After incubation 1 gel volume of isopropanol was added to each sample and mixed. Samples were then applied to the QIAquick column and centrifuged at 13, 000 rpm for 1 minute to allow DNA to bind to the column membrane. QIAquick columns contain uniquely-designed silica gel membranes which adsorb DNA in the presence of high salt concentrations and at approximately pH 7.5. This uniquely-designed membrane allows the removal of unwanted primers and impurities. 0.5 ml Buffer QG was applied to each column and centrifuged for 1 minute at 13, 000 rpm to remove all traces of agarose. 0.75 ml Buffer PE was then applied to the QIAquick column and allowed to stand for 5 minutes before a 1 minute centrifugation at 13, 000 rpm. Buffer PE, containing ethanol, removes the high salt concentrations from the column to allow for DNA elution. Columns were then centrifuged for an additional minute to remove any residual ethanol from Buffer PE. Columns were then transferred to 1.5 ml microcentrifuge tube and 30 µl of Buffer EB (10 mM Tris-Cl, pH 8.5) was added

to the membrane to elute DNA. After a 1 minute incubation samples were centrifuged for 1 minute at 13, 000 rpm and eluted DNA was stored at -20℃.

2.3.10 Cloning of Rearranged Immunoglobulin Genes

The TA cloning kit Dual promoter with pCR®II vector (Invitrogen, Paisley, UK) provided a one-step cloning approach for the direct insertion of V_H PCR products into a plasmid vector. *Taq* polymerase used in PCR reactions provided a nontemplate-dependent addition of a single deoxyadenosine (A) to the 3' ends of each PCR product. The linearized plasmid vector was supplied with additional single 3' deoxythymidine (T) residues allowing effective ligation of PCR product with the plasmid vector. The use of the TA cloning kit Dual promoter with pCR®II vector eliminates the use of PCR primers that contain restriction sites, eliminates any enzymatic modifications of the PCR product and allows transcription from either direction of the insert.

2.3.10.1 Ligation into Dual Promoter pCR®II Vector

Ligation efficiencies were optimised within a 10 µl ligation reaction to contain 6 µl DNA, 2 µl pCR®II vector (25 ng/µl) (**Figure 2.3**), 1 µl 10X Ligation buffer and 1 µl T4 DNA Ligase (4.0 Weiss units). Ligation reactions were incubated overnight at 14℃ using the Trio-Thermoblock (Biome tra, Tampa, FL) PCR machine.

2.3.10.2 Transformation into One Shot TOP10F' Chemically Competent *E. coli*

2 µl of the ligation reaction was pipetted into one 50 µl vial of One shot TOP10F' chemically competent cells (Invitrogen, Paisley, UK) and was mixed by gentle stirring. Vials were incubated for 30 minutes on ice before being heat shocked at 42℃ for 30 seconds. 250 µl of room temperature S.O.C medium (Invitrogen) was added to each vial of competent cells and vials were shaken at 37℃ for 1 hour at 225 rpm in a shaking incubator. LB plates (25 g/l Miller's Lab Broth Base (Invitrogen) supplemented with 15 g/l agar (Oxoid, Basingstoke, UK) containing Kanamycin (Gibco) (50 µg/ml)) were equilibrated at 37° for 30 minutes then 40 µl 100 mM IPTG (Roche, Mannheim, Germany) and 40 µl 40 mg/ml X-Gal (Roche, Mannheim, Germany) were spread on each plate and

allowed to soak into plates. Following the 1 hour incubation 50 µl and 200 µl of each transformation vial was plated onto LB plates and plates were incubated overnight at 37℃ before being moved to 4℃ to allo w proper colour development. Alternatively 75 µl from each transformation vial was plated onto LB plates.

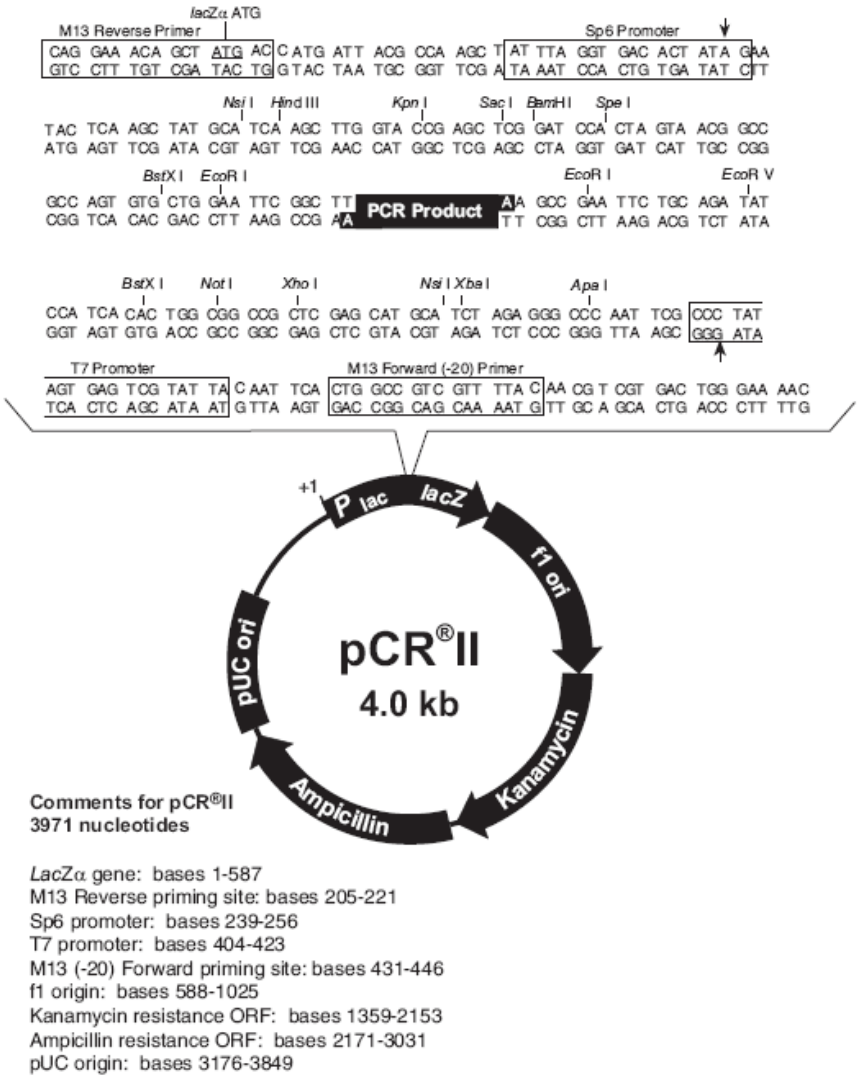

Figure 2.3 pCR®II Vector

The TA cloning kit Dual promoter with pCR®II vector provided a one-step cloning approach for the direct insertion of V_H PCR products into a plasmid vector. The linearized plasmid vector was supplied with additional single 3' deoxythymidine (T) residues allowing effective ligation of PCR product with the plasmid vector as *Taq* polymerase used in PCR reactions provides a nontemplate-dependent addition of a single deoxyadenosine (A) to the 3' ends of each PCR product.

The disruption of the *lacZ* gene by the PCR product allows for colour screening of colonies as vectors containing a PCR insert would not be able to transcribe the *lacZ* gene therefore the colonies would be white whereas empty colonies with no PCR insert would be blue as transcription could occur from the *lacZ* promoter. *lacZ* encodes the enzyme β-galactosidase enzyme which can be induced by isopropyl-β-D-thiogalactopyranoside (IPTG) and utilizes the substrate 5-bromo-4-chloro-3-inodyl-β-D-galactopyranoside (X-gal) to yield a blue product.

pCR®II vector also contains a number of primer annealing sites for sequencing of the PCR insert, M13F and M13R, as well as a number of restriction sites, i.e. *EcoR1*, to allow for the presence and size of inserts within each plasmid to be determined. Restriction digestion of the pCR®II vector containing the appropriate insert produced digested fragments of approximately 400 base pairs. Adapted from TA cloning kit Dual promoter with pCR®II vector User Guide (Invitrogen, Paisley, UK).

2.3.11 Nucleic Acid Concentration

The concentration of nucleic acids was determined using a Beckman DU640 spectrophotometer by measuring the absorbance of the sample at a wavelength of 260 nm. The absorbance at 280 nm was also determined and the ratio of 260 nm / 280 nm assesses the purity of the sample. A range of 1.6 to 1.9 was expected for DNA samples, a lower value of ratio indicated protein contamination as protein absorbs more strongly at 280 nm. To determine the nucleic acid concentration (µg/ml) the absorbance at 260 nm was multiplied by 50 and then by the dilution factor.

2.3.12 Sequencing and Analysis of Rearranged V_H Genes

2.3.12.1 Analysis of Transformants

2.3.12.1.1 Overnight Cultures

For analysis of positive clones single white colonies were picked from LB plates and were grown overnight in 3 mls LB broth (25 g/l, Invitrogen, Paisley, UK) supplemented with 50 µg/ml kanamycin (Gibco). Cultures were incubated and shaken at 37℃ at 225 rpm. After an overnight incu bation glycerol stocks were produced from each culture for long-term storage. 1 ml glycerol stocks were produced containing 15% sterile glycerol and stored at -80℃. Plasmid DNA was purified using QIAprep Miniprep kit (QIAGEN, Sussex, UK), as described in section 2.3.12.1.2, from the remaining culture after bacterial cells were harvested after a 10 minute centrifugation at 13, 000 rpm.

2.3.12.1.2 Plasmid DNA Extraction (Miniprep)

Plasmid DNA was isolated using QIAprep Miniprep kit (QIAGEN, Sussex, UK), a system based on alkaline lysis of bacterial cells which utilises a unique silica-gel membrane system. After harvesting and resuspension of bacterial cells in Buffer P1 (50 mM Tris-Cl, pH8.0, 10 mM EDTA, 100 µg/ml RNase A), the cells were lysed in Buffer P2 (200 mM NaOH, 1%SDS (w/v)) by gently inversion of microcentrifuge tube. The lysate was then neutralised by the addition of Buffer N3 (acidic potassium acetate) and gently mixed until the solution became cloudy. Samples were then centrifuged for 10 minutes at 13, 000 rpm resulting in a compact white pellet. The remaining supernatants were applied to the QIAprep spin columns and centrifuged for 1 minute at 14, 000 rpm. The columns were washed with 0.5 ml Buffer PB and centrifuged again for 1 minute

at 13, 000 rpm. After addition of 0.75 ml Buffer PE columns were left to stand for 3 minutes before a 1 minute centrifugation at 13, 000 rpm. Columns were then centrifuged for an additional minute at 13, 000 rpm to remove residual wash buffer. Columns were then transferred to 1.5 ml microcentrifuge tubes and 50 µl of filter sterile distilled water was added to each column to elute the plasmid DNA from the column. After a 1 minute incubation columns were centrifuged for 1 minute at 13, 000 rpm and eluted DNA was stored at -20℃.

2.3.12.1.3 EcoR1 Restriction Digestion of Plasmid DNA

To check the presence and size of inserts within each plasmid EcoR1 restriction digest (G↓AATTC) was conducted on each plasmid after purification. In a 10 µl reaction 5 µl of each purified plasmid was mixed with 3 µl water and 1 µl reaction buffer and 1 µl EcoR1 Restriction enzyme (10 U/µl) (Invitrogen, Paisley, UK). Reactions were incubated at 37℃ for 1 hour. The presence of an insert was determined by agarose gel electrophoresis, as described in Section 2.3.8. 1.5% agarose gel was used and inserts approximately 400 bp were expected.

2.3.12.1.4 Measurement of DNA Concentration

A DNA concentration for each purified plasmid was calculated as described in section 2.3.11.

2.3.12.2 Sequencing

DNA sequencing was performed by The Sequencing Service (School of Life Sciences, University of Dundee, Scotland, www.dnaseq.co.uk) using Applied Biosystems Big-Dye Ver 3.1 chemistry on an Applied Biosystems model 3730 automated capillary DNA sequencer. 200-300 ng of each plasmid DNA sample was sent for each sequencing reaction and plasmids were sequenced from the M13F and M13R regions of the plasmid using primers, **Table 2.9**, supplied by The Sequencing Service, Dundee. The Sequencing Service also included a gc melt within the sequencing reactions to ensure efficient sequencing.

	Primer Name	Sequence
Sequencing Primers	**M13F**	GTAAAACGACGGCCAGTG
	M13R	GGAAACAGCTATGACCATG

Table 2.9 Primers used for sequencing of pCR®II plasmid

2.3.12.3 Sequence Analysis

Sequence results, text files and electropherograms, obtained from The Sequencing Service, Dundee were checked and analysed using Chromas Lite software (Technelysium Pty Ltd, Australia). The text file sequence was checked against the electropherogram for each sequence to ensure no anomalies had occurred during reading of the sequence. The corresponding human germline genes were identified by searching the IMGT database using the JOINSOLVER software (http://joinsolver.niams.nih.gov) for the best matching genes in a Kabat data format (291). JOINSOLVER was specifically developed to analyze the CDR3 region of the immunoglobulin genes, a region fundamental in identifying clonally related sequences, and to provide a more accurate assessment of D segments. JOINSOLVER initially searches for D germline sequences. The human D germline gene database employed includes all D gene segments from the IMGT database in addition to the reverse and DIR germline genes. JOINSOLVER identifies codon 93 as the beginning of CDR3 by searching for the conserved motif sequence TAT TAC TGT which comprises codons 90 to 92 of the V_H gene. If this conserved motif is not found the search is reinitiated with an allowance for one base change, if this fails homologies to the germline genes are used to find the most likely start of the CDR3 region. Once the V_H end of the CDR3 had been identified, the J_H border of the CDR3 was determined using the conserved motif C TGG GG at the 3' end of the CDR3 region. Once the CDR3 region has been established V_H, J_H and D gene assignment was conducted. The V_H and J_H regions are scored with an alignment score, a score of +5 is assigned for a nucleotide match with a score of -4 for a mismatch between the unknown sequence and germline sequence. Following V_H and J_H assignment, the D segment assignment is conducted using a consecutive nucleotide matching system. Matches to the D segment are

scored and sorted based on the V_H-J_H distance, the distance in nucleotides between the end of the V_H segment and the beginning of the J_H segment. A Monte Carlo simulation was used to establish the minimal D segment match length required to assign a D segment (**Table 2.10**), this was found to depend on the V_H-J_H distance. These minimal match lengths were used in conjunction with the V_H-J_H distance of the sequence to determine if the highest scored D segment could be statistically assigned to the immunoglobulin rearrangement with a 95% probability that the match was not from random chance. In some instances a mismatch was found within the D segment, disrupting the consecutive match length. To allow a higher percentage of D genes to be assigned statistically advice was sought and followed according to the criteria kindly provided by Dr Gary Sims, a contributor to the development of the JOINSOLVER software (**Figure 2.4**). JOINSOLVER also conducts junction analysis at the VD and DJ junctions to assign P nucleotides, inverted repeats at germline encoded ends and N nucleotides, nontemplated junctional additions.

Assignment of V_H, D and J_H gene segments and mutational numbers were also analysed for all sequences using IMGT/V-QUEST software (http://imgt.cines.fr)(292;293) with a search for insertions and deletions. Any deviations from JOINSOLVER assignments were noted. IMGT, the international ImMunoGeneTics information system® was created in 1989 by the Laboratoire d'ImmunoGénétique Moléculaire (LIGM) (Université Montpellier II and CNRS) at Montpellier, France. It is a high-quality integrated knowledge resource specialising in immunoglobulins (IG), T cell receptors (TR) and major histocompatibility complex's (MHC) and deals with all the IG and TR nucleotide sequences published in the DDBJ, EMBL and GenBank databases. IMGT/V-QUEST (V-QUEry and STandardization) is an integrated on-line software programme which analyses IG and TR rearranged nucleotide sequences. IMGT/V-QUEST first identifies the locus to which the sequence belongs and then identifies the V, D and J genes and alleles by best alignment score of the input sequence with the IMGT reference directory. The programme first aligns the V-region, then the J-region and finally the D-region. The junction of these sequences, CDR3, encompasses the sequence between the V-region conserved cysteine (2^{nd}- CYS) at position 104 and the J-region conserved

tryptophan (J-TRP) at position 118 found within the Trp-Gly-X-Gly conserved motif. IMGT/JunctionAnalysis, an integrated system in IMGT/V-QUEST performs analysis of the V-D-J junction.

V_H-J_H Distance (bp)	Minimal D Segment Match Length Required (bp) at a stringency of 0.05 (To allow a 95% probability that the match was not from random chance)
8	8
9-11	8
12-23	9
24-27	9
28-75	10
76-79	10

Table 2.10 Assignment of D gene segments based on V_H-J_H distance and D segment match length

For each sequence the V_H-J_H distance is calculated using the JOINSOLVER software, in order to assign the best matching D gene segment with a 95% probability the associated number of minimal match lengths must be observed within the D segment sequence.

For each mismatch in a sequence add 2 to the minimal D segment match length.

eg. if the consecutive match required is 8. (x=match; o=mismatch)
oxxxxxxxo 7 match = not significant
oxxxxxxxxo 8 match = significant
oxxxxxoxxxo 8/9 match = not significant
oxxxxxxoxxxo 9/10 match = not significant
oxxxxxxxoxxxo 10/11 match = significant
oxxxxxoxxoxxxxxo 12/14 match = significant

Figure 2.4 Additional Criteria for assignment of D gene segments

Figure 2.4 demonstrates supplementary criteria used in the statistical assignment of D gene segments in immunoglobulin rearrangements found within myositis and vasculitis samples, kindly provided by Dr Gary Sims, a contributor to the development of the JOINSOLVER software. These criteria describe the additional match length required when a mismatch disrupts the consecutive match length observed within the segment to allow a D gene assignment with a 95% probability that the match was not from random chance.

The V_H, D, J_H gene usage distribution of functional gene rearrangements was analysed by determining the percentage usage of each gene family within infiltrating B cells and/or plasma cells of myositis and vasculitis samples. These gene distributions were compared to the baseline germline complexity and to published normal distributions from studies conducted by Volpe and Kepler (251). The number of single point mutations within each variable gene segment of functional gene rearrangements were also analysed and given as a

percentage of the total number of sequences. Base differences within the first 24 bases of sequence were disregarded as this part of the sequence binds the 5' V_H primer. In addition to mutational numbers, the location of mutations were analysed between Framework regions (FR) and Complementary Determining Regions (CDR). The number of mutations in each segment was expressed as a percentage of the total length of the segment to correct for the longer lengths observed within the framework regions. The approximate base positions of each region is summarised in **Figure 2.5**. As well as analysing the location of mutations within variable gene segments the types of mutation were also analysed. The numbers of mutations resulting in an amino acid change (replacement, R, mutation) were calculated in V_H gene segments along with the number of silent, S, mutations where a nucleotide change does not result in an amino acid change within the sequence. Each mutation within the sequence was handled independently on a base-by-base method (**Figure 2.6**) rather than a codon-by-codon method. This corresponds to the method used by the JOINSOLVER software for calculating R and S mutational numbers; confirmed in consultation with Dr Nancy Longo and Dr Daniel Russ (National Institute of Health, Bethesda, MD, USA), two authors of the JOINSOVLER software (291). Statistical analysis of these R and S mutational numbers for antigen-driven selection was conducted according to Hershberg *et al* (294) and the corresponding computer programme (http://clip.med.yale.edu/selection) which demonstrates an improved method for detecting selection by mutational analysis of Ig V region sequences. The software uses a focused binomial test which accounts for known biases of somatic hypermutation at two levels, the impact of local sequence context on mutability and the transition bias, in order to establish positive or negative mutational selections within the sequence with high specificity and increased sensitivity. Use of this software required the V_H gene segments of the immunoglobulin sequences obtained from The Sequencing Service to be converted to a FASTA format with the IMGT unique format including gaps. These sequences were initially analysed using IMGT/V-QUEST software (292;293) to confirm the V_H gene segment assignment and were aligned with the corresponding germline gene. Both sequences were entered into the software with the germline gene following the input query sequence and the CDR regions were selected manually to correspond to Kabat

nomenclature. The software calculated the number of R and S mutations within FR and CDR1 and 2 regions independently as well as testing for positive and negative selections for each of these mutations in both the FR and CDRs. The use of this software also allowed the number of independent mutations and selection to be analysed in sets of clonally related sequences. All sequences were entered into the software with the germline V_H sequence following the clonally related sequences. CDR3 lengths in addition to P and N nucleotides and exonuclease activity at the VD and DJ junctions were also calculated and expressed as a mean value ± SEM. For assignment of P and N nucleotides these values were checked for each sequence as the criteria for handling mismatches within the D segment, as previously described, resulted in a change to the P and N nucleotide numbers. Clonally related sequences were identified on the basis of identical VDJ gene rearrangements, CDR3 regions and junctional sequences. Genealogical trees were constructed by analysis of shared and unshared mutations within these sequences. In some instances the best matching and highest scoring V_H gene alignment for clonally related sets were not always assigned, some alternative and lower scoring sequence matches were used to correlate with clonally related sequence sets where the same CDR3, junctional rearrangements and common mutational patterns as the other isolated sequences were found, the clonally related gene was generally found to be the 4-6th best matching gene segment.

The text file sequence and gene alignments for all sequences are given in Appendix 1.

2.3.12.3.1 PCR Error Rate

The number of base changes regarded as significant was based on the PCR error rate for the polymerase, previously calculated (52), as less than one base per 4 V_H genes.

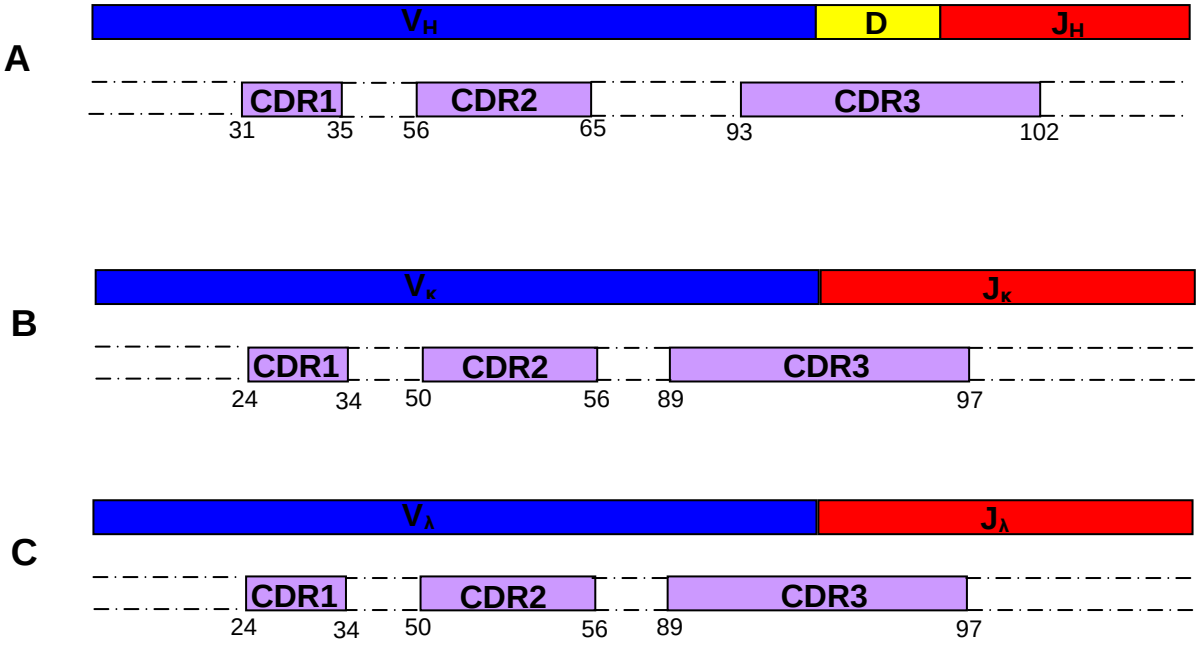

Figure 2.5 A simplified Diagram of Immunoglobulin Gene Segments for Sequence Analysis

Figure 2.5 demonstrates the different gene segments that form the rearranged V_H (**A**), V_λ (**B**) and V_κ (**C**) genes. Within these rearrangements there are areas of variability known as Complementarity Determining Regions (CDR) which are flanked by less variable Framework Regions (FR). Figures represent approximate codon locations of CDRs. CDRs constitute the antigen binding site with CDR3 being the most hypervariable as it is generated by the recombination of different gene segments, VDJ in heavy chains and VJ in light chains.

For sequence analysis the number and type of mutations within variable gene segments, FR and CDRs were compared. Base differences within the first 24 bases of sequence were disregarded as this part of the sequence binds the 5' V_H primer. CDR3 was not incorporated into mutational analysis due to the difficulty in distinguishing point mutations and junctional variation as a result of gene recombination. Clonally related sequences were identified on the basis of identical VDJ gene rearrangements, CDR3 regions and junctional sequences.

Sequence mutation

GGA->GAC (Gly->Asp)

Base-by-base method

GGA -> GAA - mutation in the 2nd base (Gly->Glu) 1 R
GGA -> GGC - mutation in the 3rd base (Gly -> Gly) 1 S

Codon-by-codon method would only generate 1 R mutation

Figure 2.6 Calculation of Replacement (R) and Silent (S) mutations on a base-by-base method

Figure 2.6 demonstrates the criteria used to assign each point mutation as Replacement (R) or Silent (S) with the V_H segment of rearrangements. For this study each mutation is taken independently on a base-by-base method, in this example this concluded with 1 R and 1 S mutation within the codon. If the assignment of R and S mutations had been on a codon-by-codon basis this would only represent 1 R mutation.

2.3.13 Statistical Analysis

Statistical analysis was conducted using GraphPad Prism 4 (GraphPad Software Inc., San Diego CA, USA) and after consultation with Dr Tony Speekenbrink (Statistics Analyses Advisor to the Clinical Microbiology Department, University of Glasgow). P values less than 0.05 were deemed significant. All p values are given in **Appendix 2**.

The distribution of V_H, D_H and J_H family usage, as well as individual V_H and D_H gene usage, was compared to published normal PBL values (251) and the germline complexity using Pearson's Chi square analysis to determine a statistical selection for or against particular gene families, or individual genes, expressed on infiltrating cells from the muscle or skin. Absolute values obtained for each V_H, D_H and J_H family, as well as individual genes, were used to construct contingency tables in the GraphPad software for each V_H, D_H and J_H family and tested for selection against the values of the corresponding family in the normal PBL and the germline complexity.

CDR3 lengths, P and N nucleotides and exonuclease activity were analysed in functional and non-functional sequences using a two-tailed unpaired t-test. The One-way analysis of variance test was used in conjunction with Tukey-Kramer multiple comparison post test to determine any statistical difference between mean CDR3 lengths in mutated sequences. These statistical tests allowed any statistical difference in the mean CDR3 lengths of the 4 different mutational groups (0-2, 3-10, 11-20 and 20+) to be established as well as correcting for multiple comparisons within the same data set, this eliminates the Type 1 errors that occur when statistical tests are used repeatedly.

Statistical analysis of R and S mutations was conducted as described previously in section 2.3.12.3. Briefly a focused binomial test was used to calculate the parameters of the null model of mutation and test for positive and negative selection in the CDR and FW separately. P values less than 0.05 were deemed significant.

2.4 Identification of Antigens Driving the Immune Response in Myositis Patients

2.4.1 Protein Biotinylation

50 µg of recombinant proteins to be biotinylated, **Table 2.11**, were mixed and incubated for 2 hours with 5 µl of 1 mg/ml Biotin (Long Arm) N hydroxysuccinimide ester – water soluble (NHS) (Vector Laboratories), dissolved in 100 mM bicarbonate buffer pH 8.5 or 1X PBS. After 2 hours the biotinylation reaction was stopped by the addition of 1 ml 10% glycine in H_20. To remove excess biotin, samples were dialyzed against 100 mM bicarbonate buffer pH 8.5 or 1X PBS using 0.5 ml-3 ml Slide-A-Lyzer Dialysis cassettes (Pierce, Rockford, IL, USA). Initially cassette membranes were rehydrated in dialysis buffer for 30 seconds to increase the flexibility of the membrane. Cassettes were checked for leaks by injecting sterile distilled water into the cassette immediately prior to the addition of the sample. After removal of the distilled water samples were injected into cassettes using a syringe filled with the sample and an 18-gauge 1-inch beveled needle. Excess air was removed from the cassette to allow maximal sample solution contact with the dialysis buffer. Dialysis was carried out at 4℃ and dialysis buffer was changed after 3 hours, then after overnight followed by a further 2 hour incubation in dialysis buffer. To remove samples syringes with an 18-gauge 1-inch beveled needle were filled with air at least equal in volume to the sample. The air was then discharged into the cassette to allow the membranes of the cassette to separate. The cassette was then rotated to allow the biotinylated sample to be drawn back into the syringe. Biotinylated proteins were aliquoted and stored at -20℃. BSA was also biotinylated by the above procedure to use as a control in experiments.

2.4.2 Dot Blot

To verify biotinylation of recombinant proteins an aliquot of the protein was serially diluted 1:10 until a final dilution of 1:100, 000. 10 µl neat biotinylated protein (50 µg/ml) and each serial dilution were spotted onto Hybond™-N nylon membrane (Amersham Life Sciences, Buckinghamshire, England). Proteins were allowed to soak into the membrane before the membrane was blocked with 1X Casein in TBS/Tween (Section 2.5) for 30 minutes. The membrane

was washed twice for 10 minutes each in TBS/Tween then for 10 minutes in TBS. The membrane was then incubated with 5 ml ABComplex AP reagent (Vector Laboratories) for 30 minutes. The reagent consists of 5 ml TBS with 2 drops of Reagent A, Avidin DH, and 2 drops of Reagent B, biotinylated alkaline phosphatase H. The reagent was mixed 30 minutes prior to use and allowed to stand at room temperature. Membrane was washed twice for 10 minutes each in TBS/Tween then for 10 minutes in TBS before incubating with 5 ml Alkaline phosphatase substrate as described in section 2.2.3 and 2.5 or 5 ml of Vector Blue Alkaline Phophatase Substrate III (Vector Laboratories). A working solution of Vector Blue substrate consisting of 5 mls 100 mM Tris-HCl pH 8.2, 2 drops Reagent 1, 2 drops Reagent 2 and 2 drop of Reagent 3 was prepared immediately prior to use and membrane was incubated for 20 minutes of until colour development. Membranes were then washed 3 times in TBS for 10 minutes. All incubations were carried out at room temperature. Non-biotinylated BSA was used as a negative control.

RECOMBINANT PROTEIN	SOURCE
Jo-1	A kind gift from Prof. Paul Plotz, National Institute of Health, Bethesda, MD, USA
Calf Thymus DNA	Sigma (St. Louis, MO, USA)
Sm/RNP	The Binding Site (UK)
Scl-70	The Binding Site (UK)

Table 2.11 Recombinant Proteins for biotinylation to identify antigen specific cells

2.4.3 Antigen Specific Staining

Slides from -70℃ were thawed at room temperature f or 30 minutes in a staining vessel containing anhydrous silica gel. To fix sections slides were transferred to acetone for 10 minutes and then allowed to dry. Sections were circled with a PAP pen (Immedge Pen, Vector Laboratories) and allowed to dry for 5 minutes. They were then incubated for 15 minutes with avidin blocking solution (Vector Laboratories) and briefly washed in TBS before a 15 minute incubation with biotin blocking solution (Vector Laboratories). Sections were then washed twice for 5 minutes in TBS. 100 µl of 1X Casein (Vector Laboratories) was added to

each section to block for 15 minutes. Blocking solution was poured off and 100 µl of 20 µg/ml biotinylated recombinant protein was added to sections, with appropriate negative controls, and incubated for 1 hour. The sections were then washed 3 times in TBS for 5 minutes and then incubated with 100 µl of ABComplex AP Reagent (Vector laboratories) solution for 30 minutes. The reagent consists of 5 mls TBS with 2 drops of Reagent A, Avidin DH, and 2 drops of Reagent B, biotinylated alkaline phosphatase H. Reagent was mixed 30 minutes prior to use and allowed to stand at room temperature. Sections were washed 3 times in TBS for 5 minutes then incubated with 5 mls Alkaline phosphatase substrate as described in section 2.2.3 and 2.5. Following substrate incubation sections were washed twice in TBS for 5 minutes and once in sterile distilled water for 5 minutes. All incubations were carried out at room temperature in a humidified chamber. Biotinylated BSA as a negative control on myositis sections and biotinylated antigen was also used on tonsil sections as a negative control.

2.4.4 Double Immunofluorescent Antigen Specific Staining

Double Immunofluorescent immunohistochemistry for antigen specific cells was performed as described in section 2.2.4 using 2 µg/ml recombinant protein (Table 2.11). Use of the biotinylated recombinant proteins eliminated the need for using M.O.M biotinylated Anti-Mouse Ig reagent therefore this step was eliminated where appropriate before the appropriate detecting solution was applied to each section. Biotinylated BSA was used on sample sections as a negative control.

2.4.5 Laser Capture Microdissection

Laser capture microdissection (LCM) was performed using a PixCell® IIe Laser Capture Microdissection System (Arcturus Bioscience Inc, Mountain View, CA) to direct the low-powered infrared laser through the CapSure® HS (Arcturus) caps to melt the film onto the cell of interest (**Figure 2.7A**). CapSure® HS caps are coated with a special thermoplastic film which melts onto the surface of the target cell when pulsed with the infrared light from the laser. This film also absorbs the laser radiation ensuring that any infrared radiation that does penetrate the polymer does not create or catalyse any chemical alterations to

the DNA/RNA of the sample ensuring its integrity for further downstream applications. CapSure® HS caps contain a 12 µm discontinuous circular ridge that sits on the surface of the tissue ensuring the cap is elevated above the sample microdissection (**Figure 2.7B**). This ensures that the only part of the film that comes into contact with the sample is that which has been melted by the laser onto the cell of interest. The ExtracSure Extraction device is placed on the caps after capture of the cells of interest and seals around the perimeter of the cap surface and covers the circular ridge that was in contact with the sample during LCM. Extraction buffer can then be safely added to ExtracSure device to allow extraction of DNA (**Figure 2.7C-A**). For RNA extraction the ExtracSure device was not required. 100 µl of lysis buffer is placed in a 0.5 ml microcentrifuge tube and inverted to allow cell lysis (**Figure 2.7C-B**). Taken from PixCell® IIe Laser Capture Microdissection System User Guide, Arcturus Bioscience Inc, Mountain View, CA.

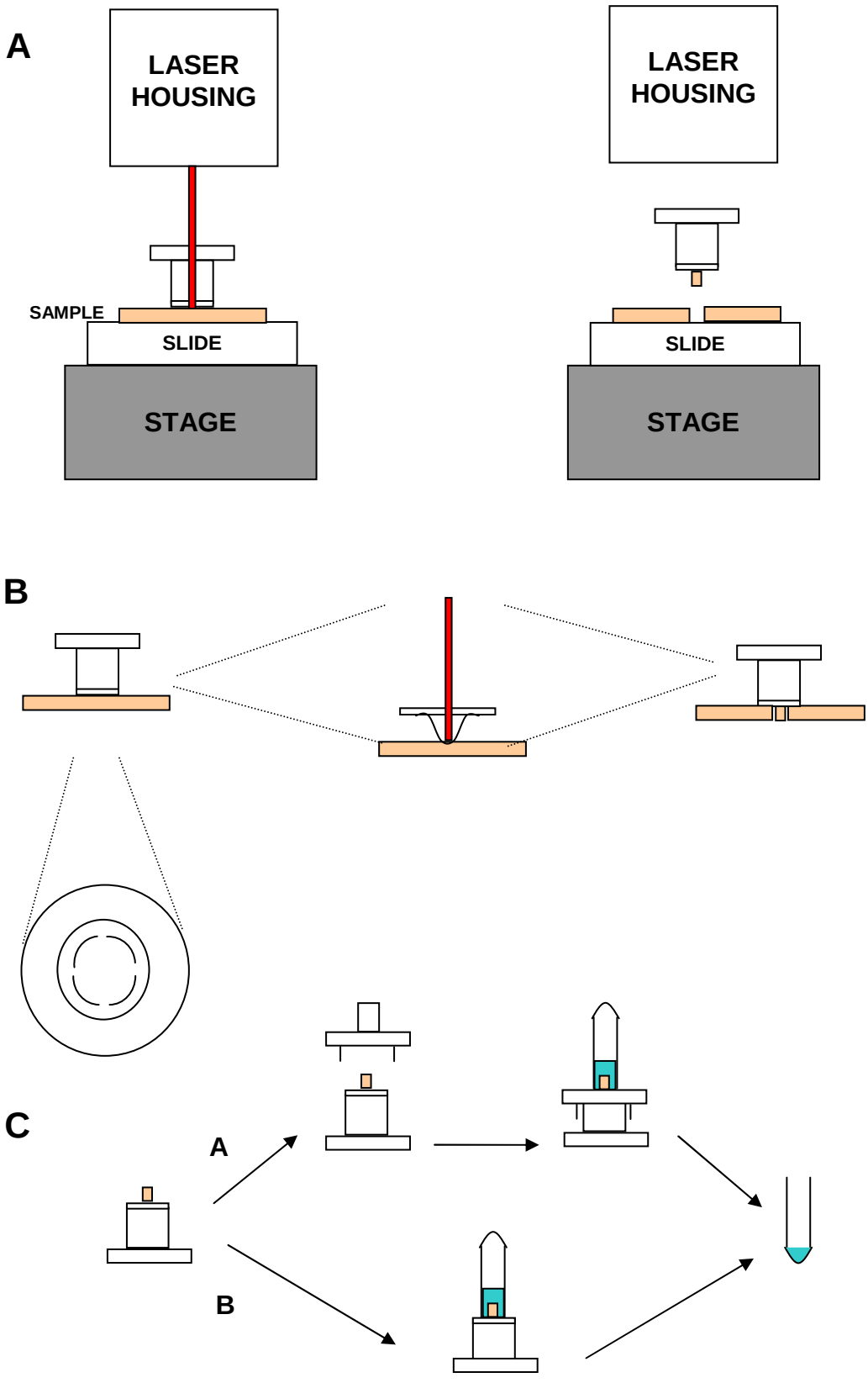

Figure 2.7 A simplified diagram of Laser Capture Microscopy (LCM)

Figure 2.7 A simplified diagram of Laser Capture Microscopy (LCM)

Laser capture microdissection (LCM) to isolate single cells was performed using a PixCell® IIe Laser Capture Microdissection System (Arcturus Bioscience Inc, Mountain View, CA). A low-powered infrared laser is passed through CapSure® HS caps (**Figure 2.7A**) over the cell which is to be dissected. CapSure® HS caps are coated with a special thermoplastic film which melts onto the surface of the target cell when pulsed with the infrared light from the laser (**Figure 2.7B**). For extraction of genomic DNA the ExtracSure Extraction device is placed on the caps after capture of the cells of interest and seals around the perimeter of the cap surface and filled with DNA extraction buffer (**Figure 2.7C-A**). The ExtracSure Extraction device is not required for RNA isolation (**Figure 2.7C-B**); alternatively 100 µl of lysis buffer is placed in a 0.5 ml microcentrifuge tube and inverted to allow cell lysis. Adapted from (295) and PixCell® IIe Laser Capture Microdissection System User Guide, Arcturus Bioscience Inc, Mountain View, CA.

2.4.5.1 Immunohistochemistry for LCM

Immunohistochemical staining for LCM was performed as described in section 2.2.3, although incubation times were reduced and antibody concentrations were increased. This was to ensure efficient transfer and quality of nucleic acid obtained during microdissection. Sections were also dehydrated as moisture present within the sample can impede transfer efficiency. Briefly, slides from -70℃ were thawed at room temperature for 15 minutes in a staining vessel containing anhydrous silica gel. To fix sections slides were transferred to acetone for 10 minutes and then allowed to dry. Sections were circled with a PAP pen (Immedge Pen, Vector Laboratories) and allowed to dry for 5 minutes. Sections were rehydrated in TBS for 30 seconds. 100 µl of 2% BSA/TBS was added to each section to block for 15 minutes. Blocking solution was poured off and 100 µl of 2% BSA/TBS containing mouse anti-human primary antibody (DAKO) was added to each section (**Table 2.12**) and incubated for 15 minutes. Negative control experiments were performed using antibodies with matched isotypes. The primary antibody solution was poured off and sections were washed twice in TBS for 30 seconds. Following washing 100 µl of 2% BSA/TBS containing 10 µl of rabbit anti-mouse IgG secondary antibody (DAKO) was added to each section and was incubated for 10 minutes. After secondary antibody was poured off and sections were washed twice in TBS for 30 seconds 100 µl of 2% BSA/TBS containing 4 µl of alkaline phosphatase anti- alkaline phosphatase (APAAP) was added to each section and was incubated for 10 minutes. Sections were again washed twice in TBS for 30 seconds. 100 µl of substrate solution, as per section 2.2.3 and 2.5, was then added to each section and allowed to develop for 20 minutes. Following substrate incubation sections were washed twice in TBS for 5 minutes and once in sterile distilled water for 1 minute. Sections were counter-stained with Mayer's Haemotoxylin and washed in Scotts tap water substitute to allow proper colour development. All incubations were carried out at room temperature in a humidified chamber. For laser microdissection sections were dehydrated in 75% ethanol for 1 minute, followed by 95% ethanol for 1 minute and then 100% ethanol for 1 minute. Finally sections were incubated for 5 minutes with Histoclear (National Diagnostics). They were then allowed to air dry, under a fume hood, and stored

desiccated. For antigen-specific cells staining was carried out as described in section 2.4.3.

Antibody Specificity	Source	Species	Clone	Isotype	Dilution
CD20	DAKO	Mouse Monoclonal	L26	-IgG2a	1:25
Plasma Cell	DAKO	Mouse Monoclonal	V538c	-IgG1	1:100
-IgG1 Isotype Control	DAKO	Mouse Monoclonal	DAK-G01		1:100
-IgG2a Isotype Control (Anti-Aflatoxin)	Kind gift from Prof Stimpson, Strathclyde University, Glasgow				1:25

Table 2.12 Primary Antibodies used for staining LCM sections

2.4.5.2 Laser Microdissection

Microdissection for single cells was performed using a spot size of 7.5 µM, power of 70 mV and 1 ms duration. Cells were transferred to CapSure® HS caps.

2.4.5.3 RNA Purification

Isolation of RNA from microdissected single cells was performed using Absolutely RNA Nanoprep Kit (Stratagene, La Jolla, CA. USA). The nanoprep RNA purification method utilizes a guanidine thiocyanate lysis buffer which acts as a strong protein denaturant to allow cell lysis and prevention of RNA degradation by ribonucleases (RNases). After transfer to the nano-spin cup, RNA is bound to the silica-based fibre matrix and RNA sample is treated with DNase to remove contaminating DNA and several washes removes DNase and other proteins resulting in RNA suitable for cDNA synthesis. Briefly, 0.7 µl β-Mercaptoethanol (14.2 M) was added to 100 µl lysis buffer for each sample in a 0.5 ml Eppendorf. The CapSure® cap containing laser-captured cell is snapped onto each microcentrifuge tube. Each tube was inverted and vortexed for 30 seconds to allow cell lysis. 100 µl of 70% ethanol was then added to each sample and mixed by pulse vortexing. The entire lysate was then transferred to

an RNA-binding nano-spin cap and centrifuged for 60 seconds at 12,000 g. After discarding the filtrate 300 µl of 1x Low-Salt Wash Buffer was added to each cap and centrifuged at 12, 000 g for 60 seconds. After removal of the filtrate the cap was centrifuged for 2 minutes to dry out the fibre matrix. Each sample was then incubated with 15 µl DNase solution (2.5 µl reconstituted RNase-Free DNase 1 with 12.5 µl DNase Digestion Buffer) at 37℃ for 15 minutes. 300 µl 1x High-Salt Wash Buffer was then added to each sample and centrifuged for 60 seconds at 12, 000 g. This was repeated twice with 300 µl Low-Salt Wash Buffer before a 3 minute centrifugation to dry out the fibre matrix. 10 µl Elution Buffer was then added to each sample and incubated for 2 minutes at room temperature. Total RNA was eluted after centrifugation at 12,000 g for 5 minutes.

2.4.5.4 cDNA Synthesis

cDNA synthesis was performed using the AffinityScript Multiple Temperature cDNA synthesis Kit (Stratagene, La Jolla, CA. USA). First strand cDNA synthesis reaction was performed using the total RNA sample from section 2.4.5.3; 5.7 µl RNase-free water was added to the purified RNA before 1 µl of constant region gene specific primers (100 ng/µl) were added. The reaction was incubated at 65℃ for 5 minutes. Constant region primers were synthesised by Operon Biotechnologies (Huntsville, AL, USA) and were as previously described by Wang and Stollar (296) (**Table 2.13**). After 5 minutes reactions were allowed to cool to room temperature to allow primers to anneal to RNA. Once cooled to room temperature 2 µl of 10x AffinityScript RT buffer was added to each reaction followed, in order, by 0.8 µl dNTP mix (25 mM each), 0.5 µl RNase Block Ribonuclease Inhibitor (40 U/µl) and 1 µl of AffinityScript Multiple Temperature Reverse Transcriptase. Reactions were incubated for 60 minutes at 42℃. Reactions were stopped by incubating for 15 minutes at 70℃. cDNA synthesis reactions were stored on ice for subsequent PCR reactions.

	Primer Name	Sequence
Constant Region Primers	**HuCmu**	GCAGGAGACGAGGGGGA
	HuCgamma	AGGGYGCCAGGGGGAA
	HuCkappa	AACAGAGGCAGTTCCAGA
	HuClambda	TGTGGCCTTGTTGGCTTG

Table 2.13 Constant Region Primers for cDNA synthesis

2.4.5.5 V_H Nested PCR on single cells

V_H amplification from cDNA isolated from single infiltrating cells was carried out as previously described in section 2.3.7. PCR products were visualised as described in section 2.3.8 and extraction and cloning were performed as described in sections 2.3.9, 2.3.10 and 2.3.12.

2.5 Buffers

Tris-Buffered Saline (TBS)	20 mM Tris Base 137 mM NaCl 2.7 mM KCl pH 7.4
TBS/Tween	20 mM Tris Base 137 mM NaCl 2.7 mM KCl pH 7.4 0.1% Tween 20
Phosphate Buffered Saline (PBS)	137 mM NaCl 10 mM phosphate 2.7 mM KCl
Buffer E	0.05 M Tris Base 0.9% NaCl pH 9.7
Alkaline Phosphate Substrate for Immunohistochemistry	10 µl of 5% New Fuchsin in 2 M HCl 25 µl of 0.7 M sodium nitrite 3.5 mls of Buffer E 1.25 mls of 0.2 M 2-amino-2-methyl-1,3-propanediol (AMPD) 50 µl of 40 mg/ml levamisol 30 µl of Naphthol AS-BI phosphate 100 µl of 2 M HCl
Scotts Tap Water Substitute	0.35% $NaHCO_3$ 0.2% $MgSO_4$
Complete RPMI	RPMI Medium 1% Penicillin/Streptomycin 1% 200mM L-Glutamine) 30% Foetal Bovine Serum +10% DMSO for Lymphocyte Cryopreservation
TBE Electrophoresis Buffer	45 mM Tris base 45 mM Boric Acid 1 mM EDTA
Agarose Gel	1.5% electrophoresis grade Ultra Pure Agarose (Invitrogen) 1 x TBE 0.5 µg/ml Ethidium Bromide

Chapter 3 - Phenotypic Characterisation of Cellular Infiltrates in Myositis Patients

3.1 Introduction

As discussed in Chapter 1 the presence and phenotypes of cellular infiltrates have previously been studied in myositis (87-89;297;298). The roles, interactions, degree of infiltration and organisation of these cells have yet to be fully understood in these autoimmune disorders. Including myositis, a variety of different cellular phenotypes have been identified in different autoimmune inflammatory reactions, these include B cells, either in their B cell state or in their differentiated plasma cell state. These cells have been implicated in the pathogenesis of autoimmune disorders but their precise role in contributing to autoimmune pathology is largely unknown.

To investigate the role of B cells in myositis and examine the Ig gene repertoire and clonal diversification of infiltrating cells the occurrence of these B cells and plasma cells within the target tissues of these disorders was initially determined. Therefore immunohistochemical studies were conducted to address the central aim of this chapter;

- Establish the occurrence and organisation of $CD20^+$ B cells and plasma cells within the infiltrating cellular population of the muscle.
- Identify proliferating $Ki67^+$ B cells within the muscle to indicate the possible expansion and clonal diversification of these cells within the muscle.
- Determine the degree of infiltration, organisation and proliferation of additional cell phenotypes (T cells (CD3, CD4, CD8), macrophages (CD68), Follicular dendritic cells (FDC), proliferating cells (Ki67) and regulatory T cell (FoxP3)) within muscle samples.

The work described in this chapter demonstrates that a large variety of cellular phenotypes was present within inflammatory reactions in myositis and are summarised in Table 3.1.

Sample	Diagnosis	Germinal Centre Formation	Cellular Aggregation	CD20	Plasma Cell	FDC	CD3	CD4	CD8	FoxP3	CD68	Ki67	-IgG1	-IgG2a	-IgM
MYO1	DM	-	+++	++	++	-	++	++	+	++	++	++	-	-	-
MYO3	PM	-	+++	+	++	+	++	+++	+	-	++	+	-	-	-
MYO5	PM	-	-	+	++	+	++	++	++	-	++	+	-	-	-
MYO6	PM	-	++	+	+	-	++	+	+	-	++	+	-	-	-
MYO7	PM	-	++	+	++	-	+	+++	+	-	+++	+	-	-	-
MYO16	DM	-	+++	+++	++	-	++	++	+	-	+++	+	-	-	-
MYO17	PM/IBM	-	++	+	++	+	+++	++	+	+	++	+	-	-	-
MYO19	PM	-	++	+	++	-	++	++	+	-	++	+	-	-	-
MYO23	PM	-	+	+	++	+	+	++	+	-	++	+	-	-	-
MYO24	PM	-	++	- (+ IF only)	+++	-	++	++	+	+	++	+	-	-	-
MYOC	PM	-	+	+	++	-	++	+++	++	-	++	+	-	-	-
MYOE	Myopathy (PM)	-	+	+	++	-	++	++	++	-	++	++	-	-	-
MYO25	Control	-	N/A	-	-	-	-	-	-	-	+	-	-	-	-
MYO2	Myopathy (PM)	-	+	-	-								-	-	
MYOA	Myopathy (IBM)	-	N/A	-	-								-	-	
MYOD	DM	-	N/A	-	-								-	-	
MYO18	PM	-	-	-	-								-	-	
MYO21	PM	-	+	-	-								-	-	

Table 3.1 Immunohistochemistry Summary Table from Myositis Samples

Table 3.1 provides a summary overview of the immunohistochemistry profiles observed from each sample for each myositis patient. The table summarises the infiltration of each cell phenotype observed throughout the entire biopsy (n=3-7 sections for each cell phenotype depending on tissue availability) and is not based solely on the representative images presented in Figures 3.1, 3.5, 3.7, 3.9, 3.11, 3.13, 3.15, 3.17, 3.19, 3.21, 3.23, 3.25, 3.27 and 3.28. Comparisons were made between cell phenotypes in the same patient and not between different patients. For germinal centre formation, – represents the absence of these structures within the muscle sections. The extent of cellular aggregation of infiltrating cells was established for each sample and was based on semi quantitative observations; - represents no cellular aggregation with a widespread scattering of lymphocytes throughout the muscle section; +, ++, +++ represents an increasing degree of aggregation of lymphocytes respectively observed within the muscle sections. N/A was applied to samples where no or very little infiltration was present. Immunohistochemistry summary profiles were based on semi-quantitative observations of cellular infiltration; - indicates where cell phenotypes were absent from the infiltrating population while +, ++, +++ represent increasing numbers of cell phenotypes respectively within the muscle infiltrating population. Areas highlighted in yellow indicate where proliferating cell phenotypes were observed from fluorescent double immunohistochemistry (IF) experiments, these experiments were not included in the semi quantitative analysis and were used solely to establish the population of proliferating cells. Areas in grey indicate where cell phenotypes were not tested for.

3.2 Characterisation of Cellular Infiltrates in Inflammatory Myopathies

3.2.1 Sample MYO1

Six extensive regions of cellular infiltration were observed through serial sections of sample MYO1 with additional scattered infiltration throughout the section between the muscle fibres. No characteristic germinal centre structures were observed; areas of infiltration appeared as loose aggregates of cells situated between muscle fibres, mainly in perimysial and/or perifascicular regions of the muscle. In region 1 (**Figure 3.1**), as well as other regions of infiltration, $CD20^+$ (**A**), $CD3^+$ (**D**), $CD4^+$ (**E**), $CD8^+$ (**F**) and $Ki67^+$ (**G**) cells were identified with plasma cell staining (**C**) mostly concentrated in the six regions but were also identified lightly scattered throughout the section in endomysial locations. Very few FDCs (**B**) appeared to be present within the infiltrating cell population. In addition, a large infiltration of $CD68^+$ (**H**) cells was observed as well as an infiltration of $FoxP3^+$ cells (**I**) throughout sections examined. These cell markers were observed in each of the areas of cell aggregation as well as additional scattered staining throughout the muscle section. Staining sections with the appropriate negative controls (**J-L**) identified virtually no staining in the regions identified by the other cellular stains although small amounts were observed throughout the section. A large proportion of B cells, $CD4^+$ cells and plasma cells were observed which may suggest a humoral, ectopic germinal centre response was occurring within the sample but no germinal centre structures or FDCs were observed. Although CD8 staining was observed cell numbers appeared reduced in comparison to other cell types.

Double staining experiments to characterise the nature of proliferating cells within sample MYO1 showed that the majority of proliferating cells were $CD3^+$ (**B**) or $CD4^+$ (**C**) cells (**Figure 3.2**). There was the presence of an occasional proliferating $CD20^+$ cell throughout the MYO1 sections. **Figure 3.3** (**A & B)** shows that $FoxP3^+$ cells are included in the population of proliferating cells. Negative control experiments with the antibody isotype controls showed no non-specific staining within sections (**Figure 3.4**).

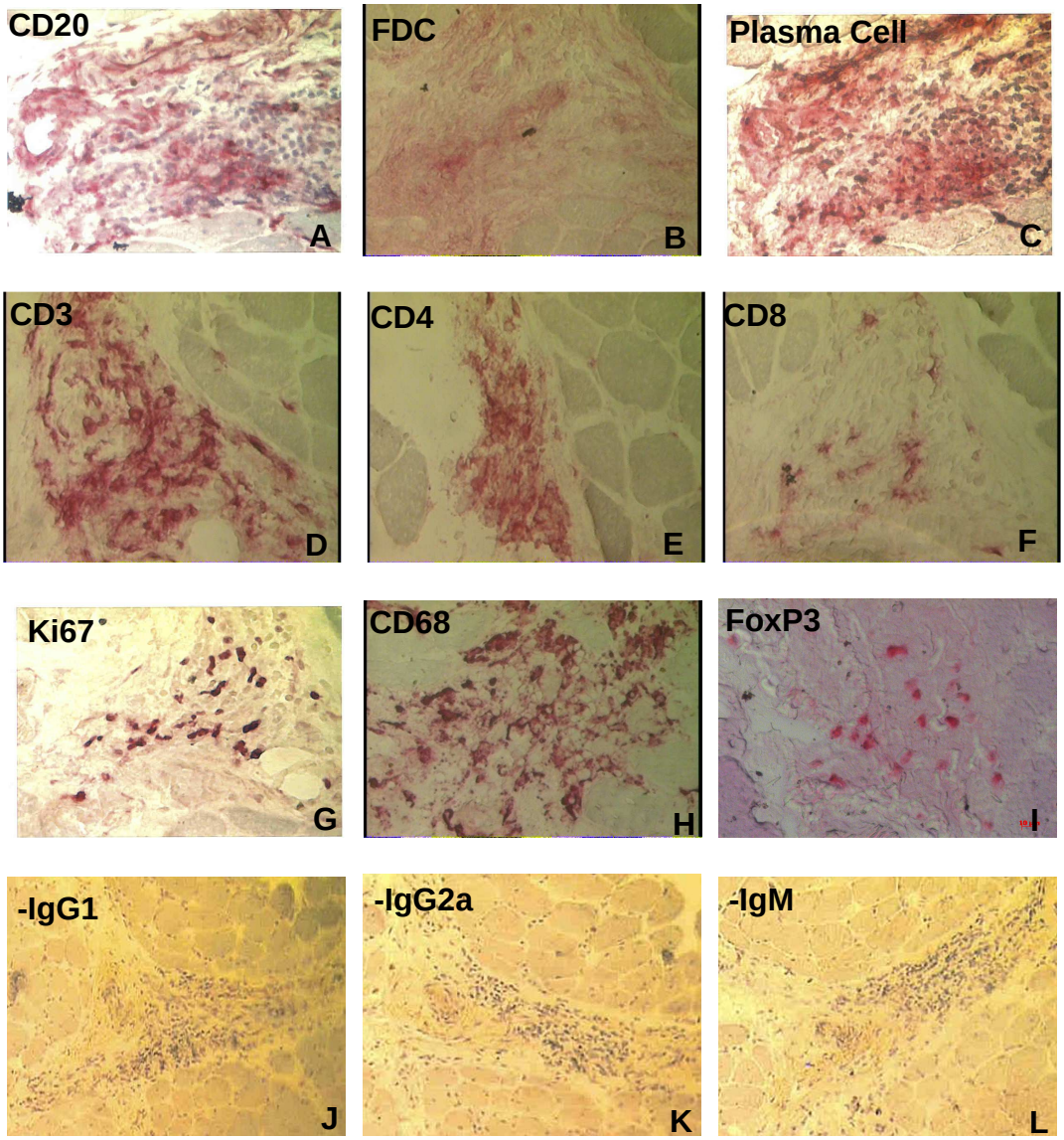

Figure 3.1 Immunohistochemistry of serial muscle sections of sample MYO1

A representative example of serial muscle sections from sample MYO1 stained for CD20 (**A**), FDC (**B**), Plasma cells (**C**), CD3 (**D**), CD4 (**E**), CD8 (**F**), Ki67 (**G**), CD68 (**H**), FoxP3 (**I**), IgG1 Negative control (**J**), IgG2a Negative control (**K**), IgM Negative control (**L**) and visualised by APAAP and New Fuschin substrate to establish cellular infiltrates within the muscle section. Images A – I: 400X; Images J-L: 100X

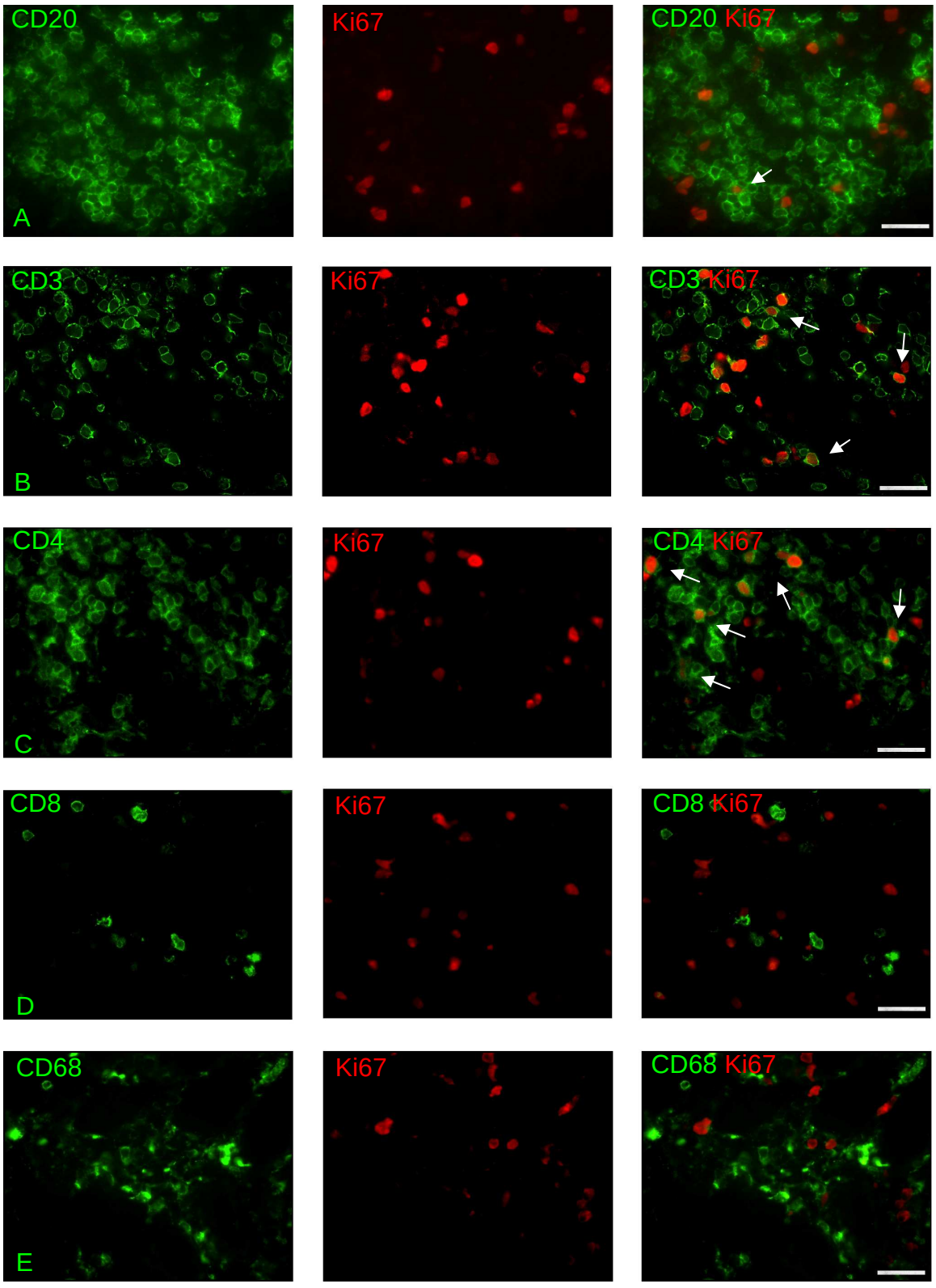

Figure 3.2 Double Immunohistochemical staining of serial muscle sections of sample MYO1

A representative example of serial muscle sections from sample MYO1 stained for CD20 (**A**), CD3 (**B**), CD4 (**C**), CD8 (**D**), CD68 (**E**) and visualised by Fluorescein Avidin D before all sections were stained with Ki67 and visualised by Texas Red Avidin D. This allowed the type of proliferating cells within the myositis sample to be identified. Images were taken at 630X; Scale Bar represents 15 µm. Arrows identify proliferating cells within the sections.

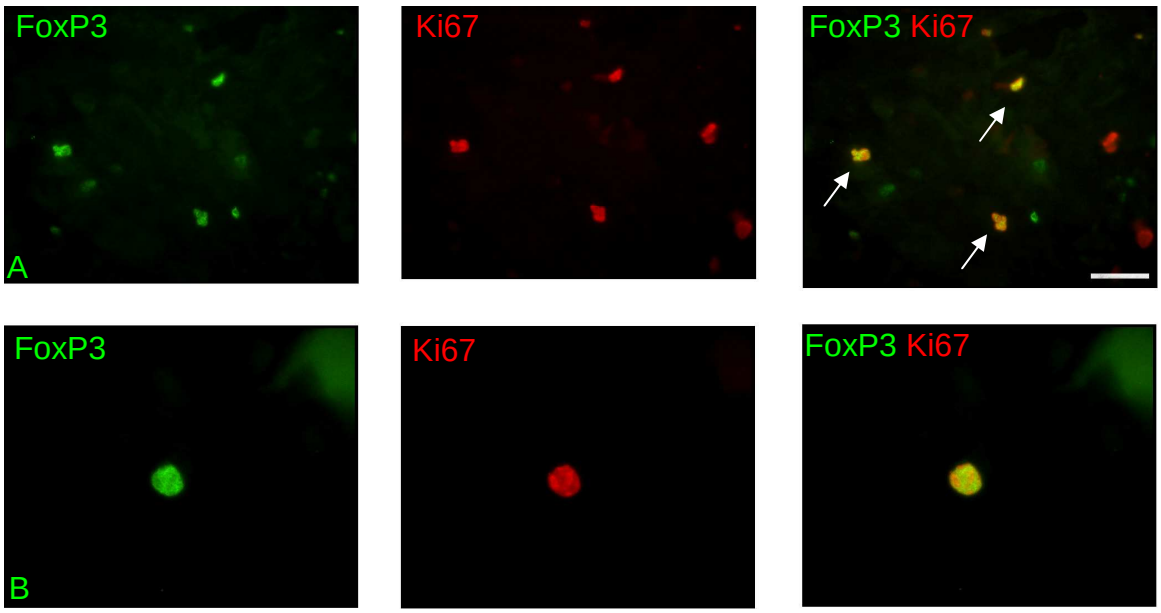

Figure 3.3 Double Immunohistochemical staining of serial muscle sections of sample MYO1 with Anti-FoxP3

A representative example of serial muscle sections from sample MYO1 stained for FoxP3 (**A&B**) and visualised by Fluorescein Avidin D before all sections were stained with Ki67 and visualised by Texas Red Avidin D. This allowed any FoxP3 proliferating cells within the myositis sample to be identified. Images were taken at 630X (**A**) and 1000X (**B**). Scale Bar (**A**) represents 15 µm, no Scale Bar was calibrated at 1000X. Arrows identify proliferating cells within the sections.

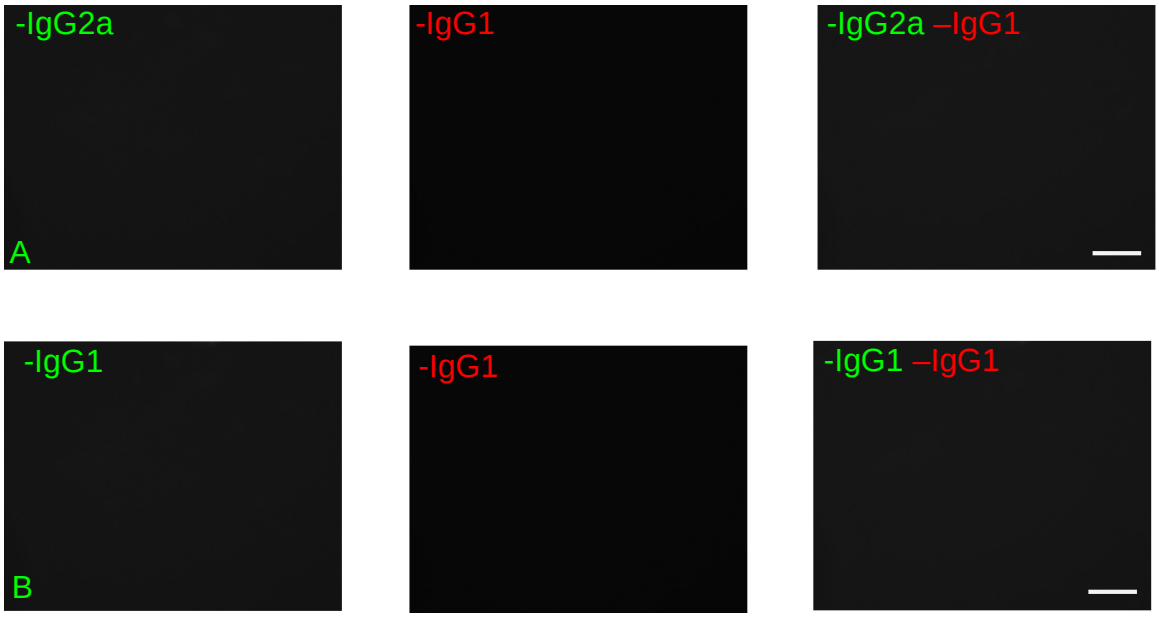

Figure 3.4 Double Immunohistochemical staining of serial muscle sections of sample MYO1 with negative control isotype antibodies

A representative example of serial muscle sections from sample MYO1 stained with –IgG2a isotype control (**A**) or –IgG1 isotype control (**B**) and visualised by Fluorescein Avidin D before all sections were stained with –IgG1 isotype control and visualised by Texas Red Avidin D. This allowed any non-specific staining within the myositis sample to be identified. Images were taken at 630X. Scale Bar represents 15 µm.

3.2.2 Sample MYO3

Immunohistochemical staining of sample MYO3 produced a different pattern of staining in comparison to sample MYO1 (**Figure 3.5**). Two distinct regions of infiltration at endomysial locations were observed with varied degrees of cellular infiltration in addition to scattered staining throughout the section. Staining for $CD20^+$ (**A**) cells and FDCs (**B**) produced a very diffuse pattern of staining but there appeared to be a low infiltration of these cell classes present within the sample. A large infiltration of plasma cells (**C**) was observed throughout the section. These were aggregated in the regions of distinct infiltration but plasma cells were also observed scattered throughout the entire section. A large proportion of cells appeared to be $CD3^+$ (**D**) and $CD4^+$ (**E**) cells, in some instances the occurrence of $CD4^+$ cells appeared to be greater than that of $CD3^+$ cells. $CD8^+$ (**F**) cells were present within sample MYO3 but these appeared to be reduced in comparison to the numbers of $CD3^+$ and $CD4^+$ cells. A large infiltration of $CD68^+$ (**H**) cells was also present within the sample; in addition to being aggregated in dense areas of infiltration, these cells were also scattered throughout the whole section. Proliferating cells were observed within the sample using the Ki67 proliferation marker (**G**), as with the other cell markers staining was observed within the cellular aggregates as well as throughout the whole section. No $FoxP3^+$ (**I**) cells were evident within sample MYO3. Staining of section with negative control isotype antibodies showed no non-specific staining (**J-L**).

Identification of $Ki67^+$ cells by double staining experiments showed the presence of $CD3^+$ (**B**) and $CD8^+$ (**D**) proliferating cells throughout the section at the areas of cellular aggregation (**Figure 3.6**). Figure 3.6 represents a small area of the whole section but these proliferating cells were observed in other areas of cellular aggregation. No other type of proliferating cell was observed within the sections stained. Negative control staining produced no non-specific staining.

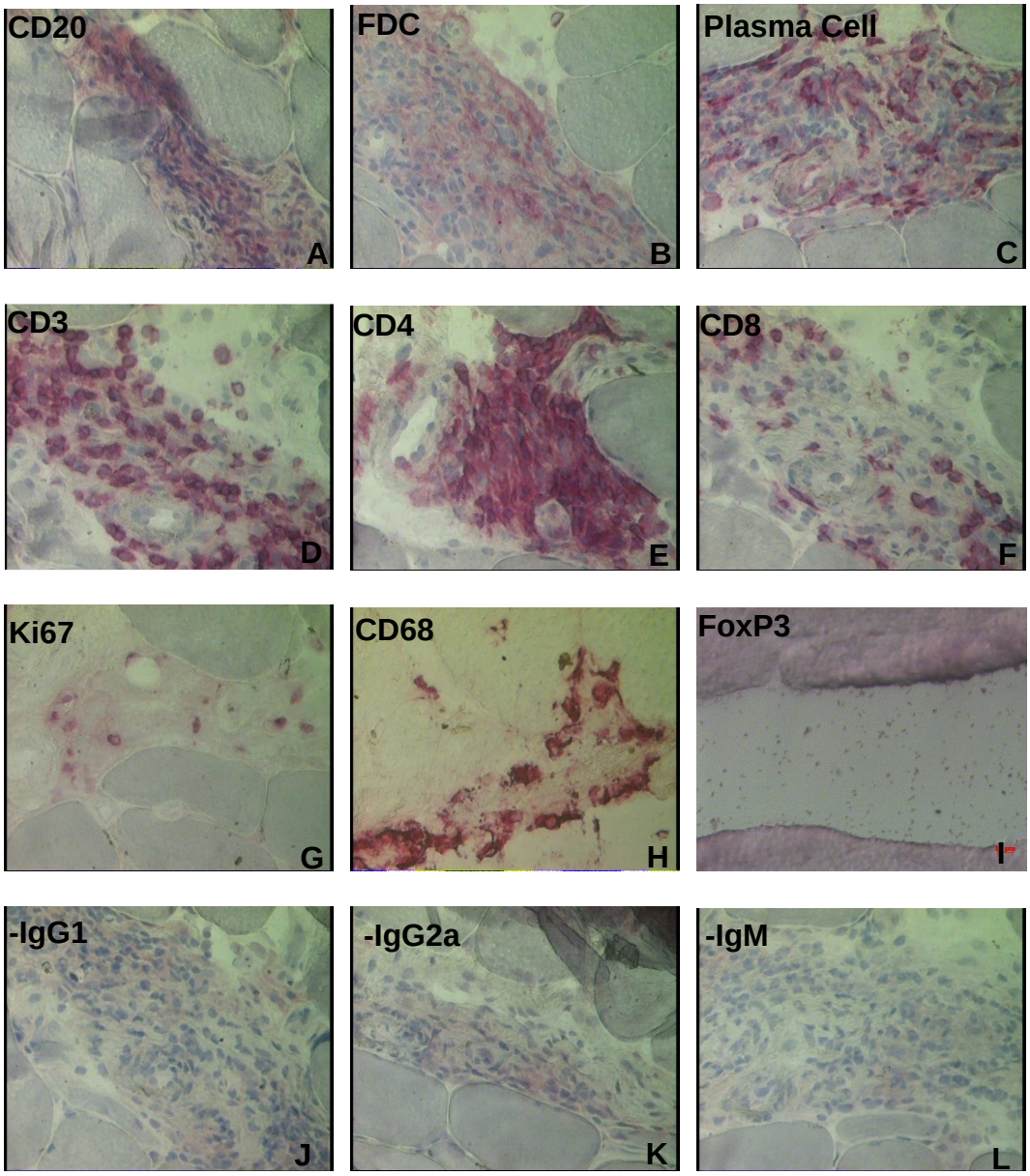

Figure 3.5 Immunohistochemistry of serial muscle sections of Sample MYO3.

A representative example of serial muscle sections from sample MYO3 stained for CD20 (**A**), FDC (**B**), Plasma cells (**C**), CD3 (**D**), CD4 (**E**), CD8 (**F**), Ki67 (**G**), CD68 (**H**), FoxP3 (**I**), IgG1 Negative control (**J**), IgG2a Negative control (**K**), IgM Negative control (**L**) and visualised by APAAP and New Fuschin substrate to establish cellular infiltrates within the muscle section. Images A – L: 400X

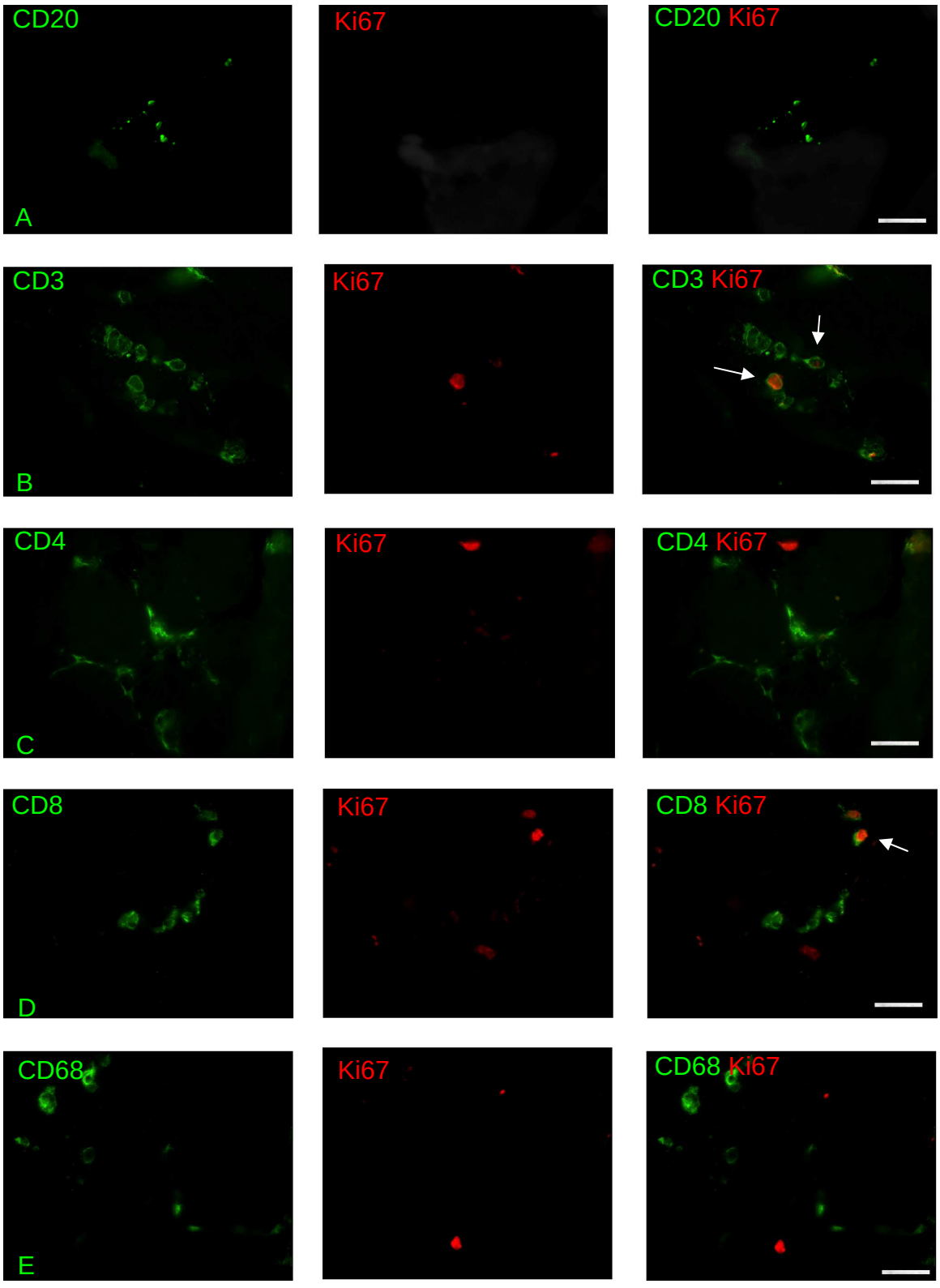

Figure 3.6 Double Immunohistochemical staining of serial muscle sections of sample MYO3

A representative example of serial muscle sections from sample MYO3 stained for CD20 (**A**), CD3 (**B**), CD4 (**C**), CD8 (**D**), CD68 (**E**) and visualised by Fluorescein Avidin D before all sections were stained with Ki67 and visualised by Texas Red Avidin D. This allowed the type of proliferating cells within the myositis sample to be identified. Images were taken at 630X; Scale Bar represents 15 µm. Arrows identify proliferating cells within the sections.

3.2.3 Sample MYO5

Analysis of cellular infiltrates within sample MYO5 produced a largely endomysial pattern of staining, characterisation of cellular phenotypes was similar to that of sample MYO3 (**Figure 3.7**). There was very little evidence of $CD20^+$ (**A**) cells and FDCs (**B**) within the sample. A large proportion of infiltrating cells were plasma cells (**C**) or $CD3^+$ (**D**), $CD4^+$ (**E**) and $CD8^+$ (**F**) cells. As seen in MYO3 a large infiltrate of $CD68^+$ (**H**) cells was observed. $Ki67^+$ (**G**) cells were present within the myositis biopsy but no $FoxP3^+$ (**I**) cells were evident throughout the sections examined. Negative control experiments were clear with no non-specific staining (**J-L**). In contrast to sample MYO3 cells were not formed in loose aggregates with additional scattered staining throughout the section. In sample MYO5 there was a large endomysial infiltrate of cells throughout the entire section which did not appear to aggregate at any particular region within the muscle biopsy.

Proliferating $CD3^+$ (**B**), $CD8^+$ (**D**) and $CD68^+$ (**E**) cells were observed within the sample (**Figure 3.8**). No proliferating $CD20^+$ cells were observed within the sections examined but proliferating cells were found to be located next to $CD20^+$ cells (**Figure 3.8A**). Negative control staining produced no non-specific staining.

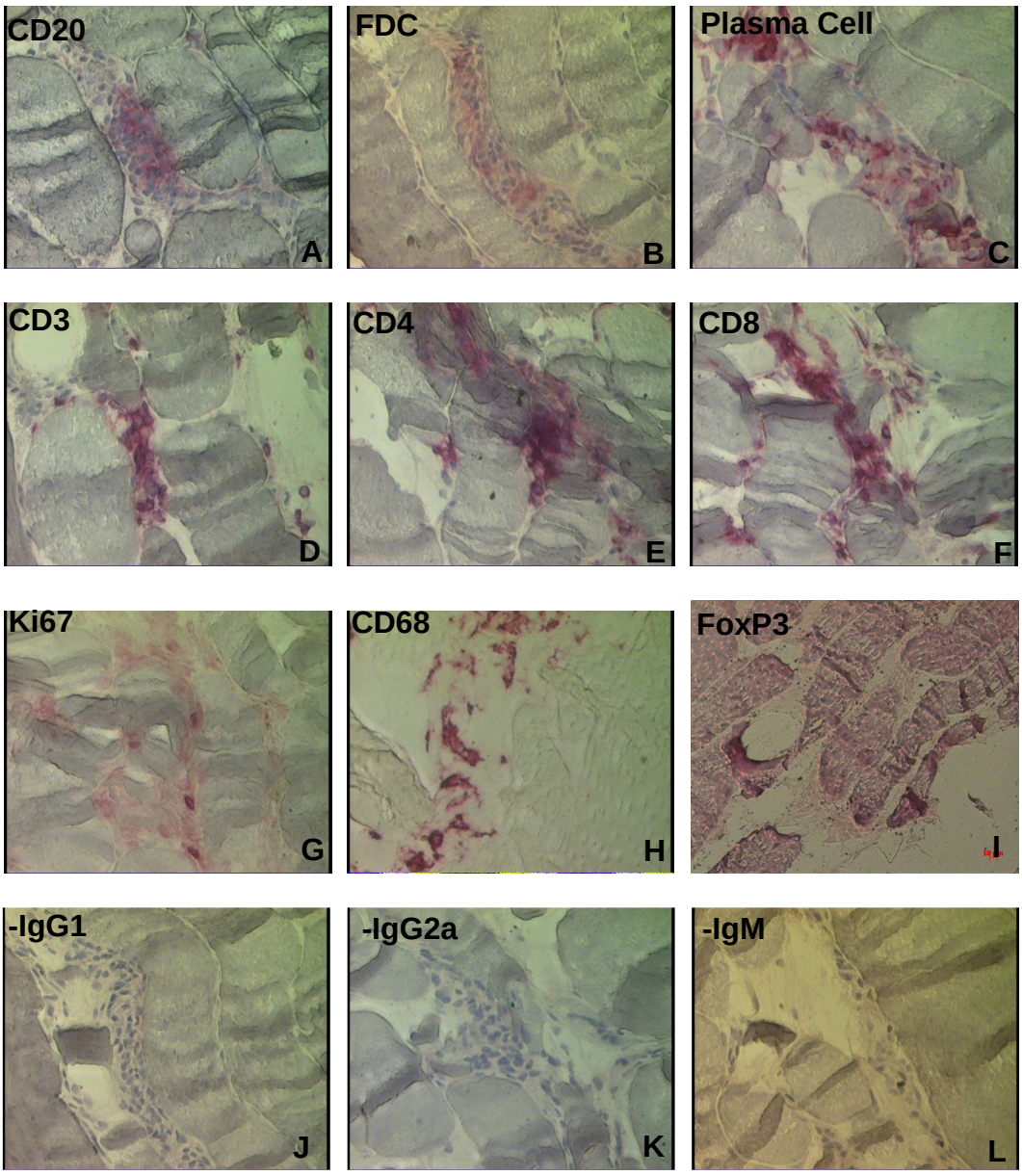

Figure 3.7 Immunohistochemistry of serial muscle sections of Sample MYO5.

A representative example of serial muscle sections from sample MYO5 stained for CD20 (**A**), FDC (**B**), Plasma cells (**C**), CD3 (**D**), CD4 (**E**), CD8 (**F**), Ki67 (**G**), CD68 (**H**), FoxP3 (**I**), IgG1 Negative control (**J**), IgG2a Negative control (**K**), IgM Negative control (**L**) and visualised by APAAP and New Fuschin substrate to establish cellular infiltrates within the muscle section. Images A – L: 400X

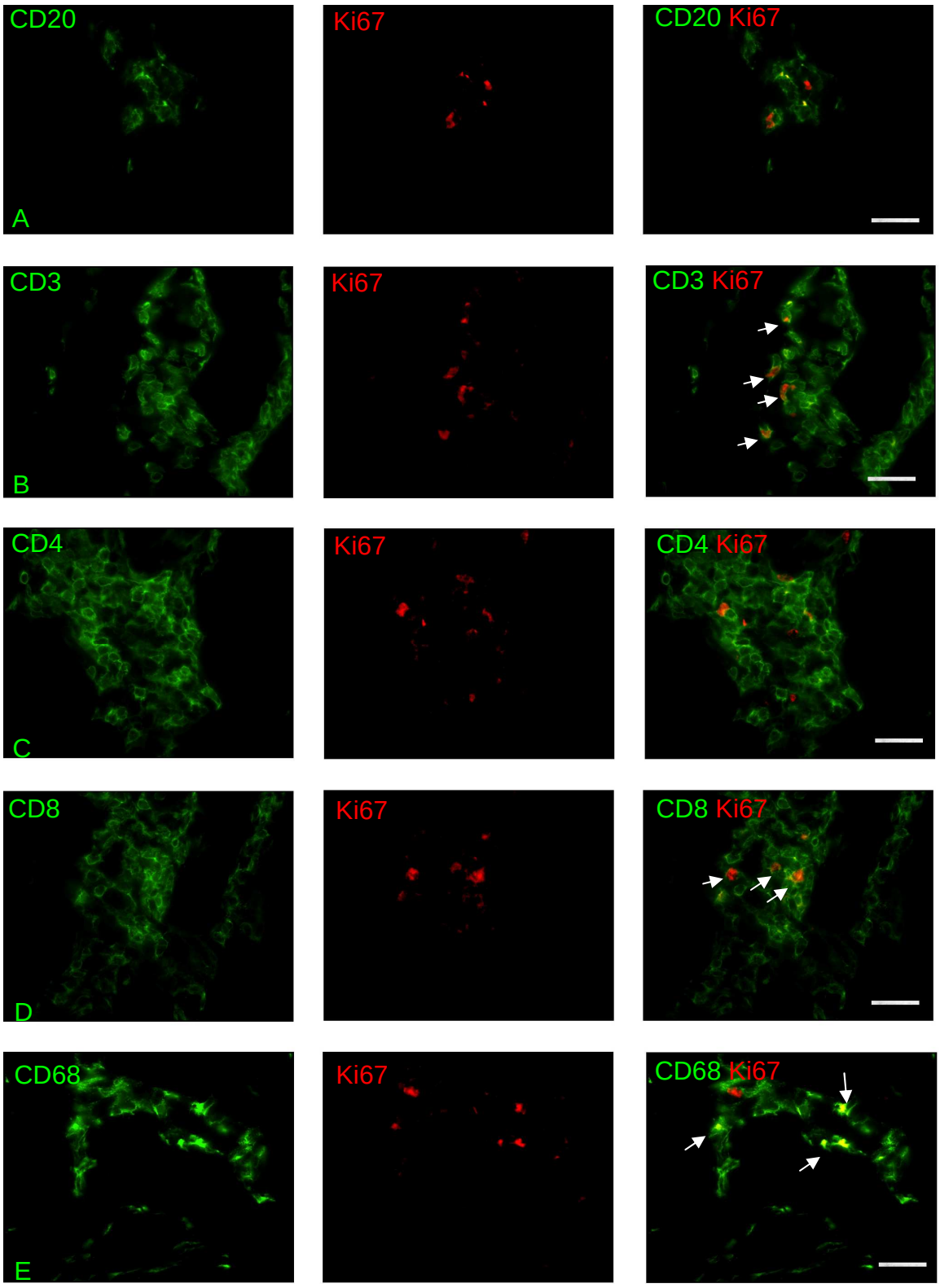

Figure 3.8 Double Immunohistochemical staining of serial muscle sections of sample MYO5

A representative example of serial muscle sections from sample MYO5 stained for CD20 (**A**), CD3 (**B**), CD4 (**C**), CD8 (**D**), CD68 (**E**) and visualised by Fluorescein Avidin D before all sections were stained with Ki67 and visualised by Texas Red Avidin D. This allowed the type of proliferating cells within the myositis sample to be identified. Images were taken at 630X; Scale Bar represents 15 µm. Arrows identify proliferating cells within the sections.

3.2.4 Sample MYO6

In sample MYO6 there was no extensive region of cellular infiltration. Cells present within the sample appear to surround the muscle fibres in an endomysial pattern (**Figure 3.9**). Immunohistochemistry experiments produced largely diffuse areas of staining but some of the cells stained were identified as $CD20^+$ (**A**) cells in addition to $CD3^+$ (**D**), $CD4^+$ (**E**) and $CD8^+$ (**F**) cells. No staining was observed for FDCs (**B**) but plasma cells (**C**) were evident amongst the infiltrating cells. No proliferating cells (**G**) were evident within this area of aggregation in sample MYO6; a few proliferating cells were observed in other areas of infiltration. There was a large infiltration of $CD68^+$ (**H**) cells within the sample. $FoxP3^+$ (**I**) cells were not present. Negative control isotype antibodies produced no non-specific staining (**J-L**).

Although few proliferating cells were present within sample MYO6, those that were present appeared to be $CD68^+$ cells (**Figure 3.10E**). No other proliferating cell type was observed in the serial sections analysed of sample MYO6. As with the previous staining experiments no non-specific staining was present.

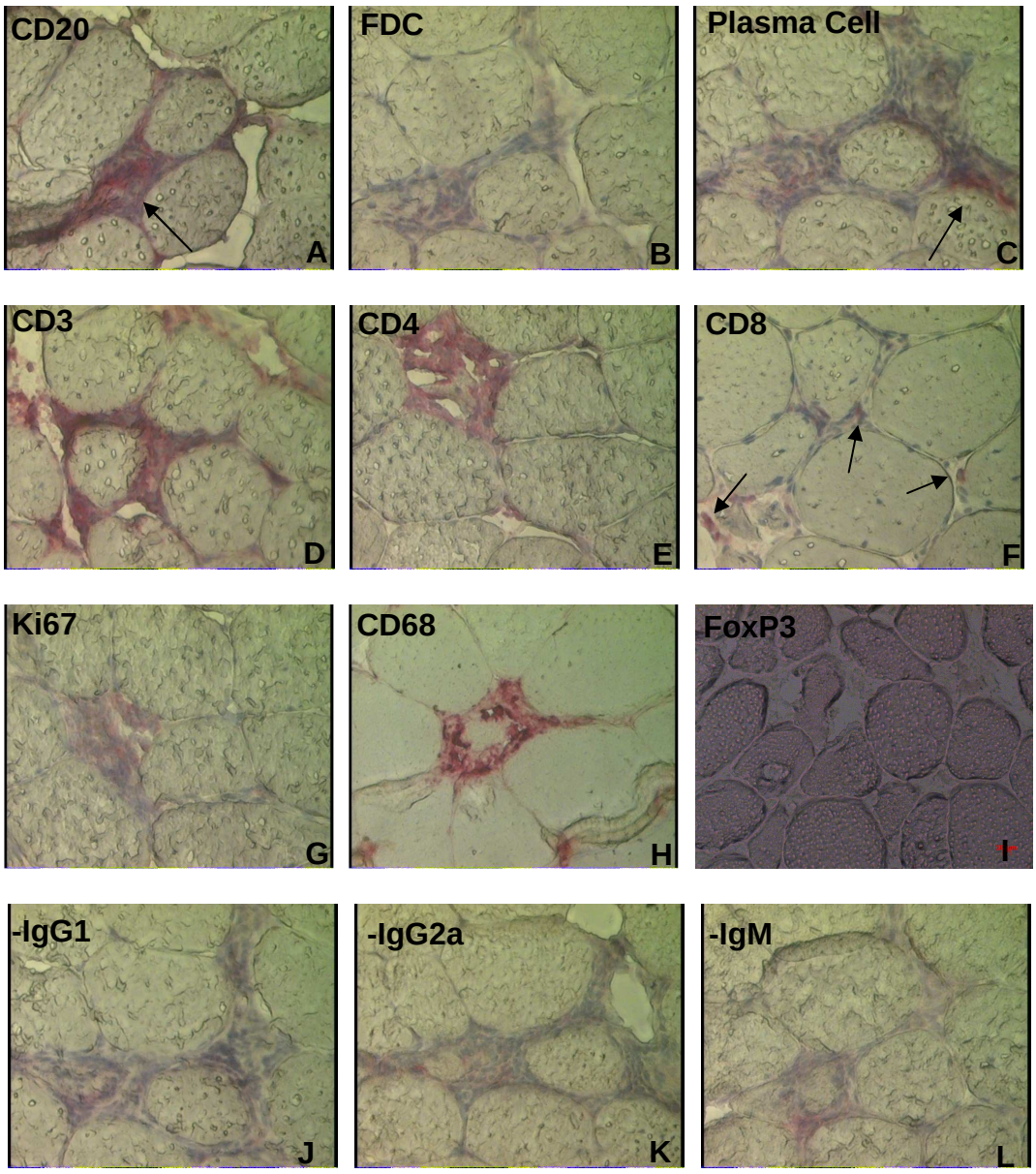

Figure 3.9 Immunohistochemistry of serial muscle sections of Sample MYO6.

A representative example of serial muscle sections from sample MYO6 stained for CD20 (**A**), FDC (**B**), Plasma cells (**C**), CD3 (**D**), CD4 (**E**), CD8 (**F**), Ki67 (**G**), CD68 (**H**), FoxP3 (**I**), IgG1 Negative control (**J**), IgG2a Negative control (**K**), IgM Negative control (**L**) and visualised by APAAP and New Fuschin substrate to establish cellular infiltrates within the muscle section. Images A – L: 400X

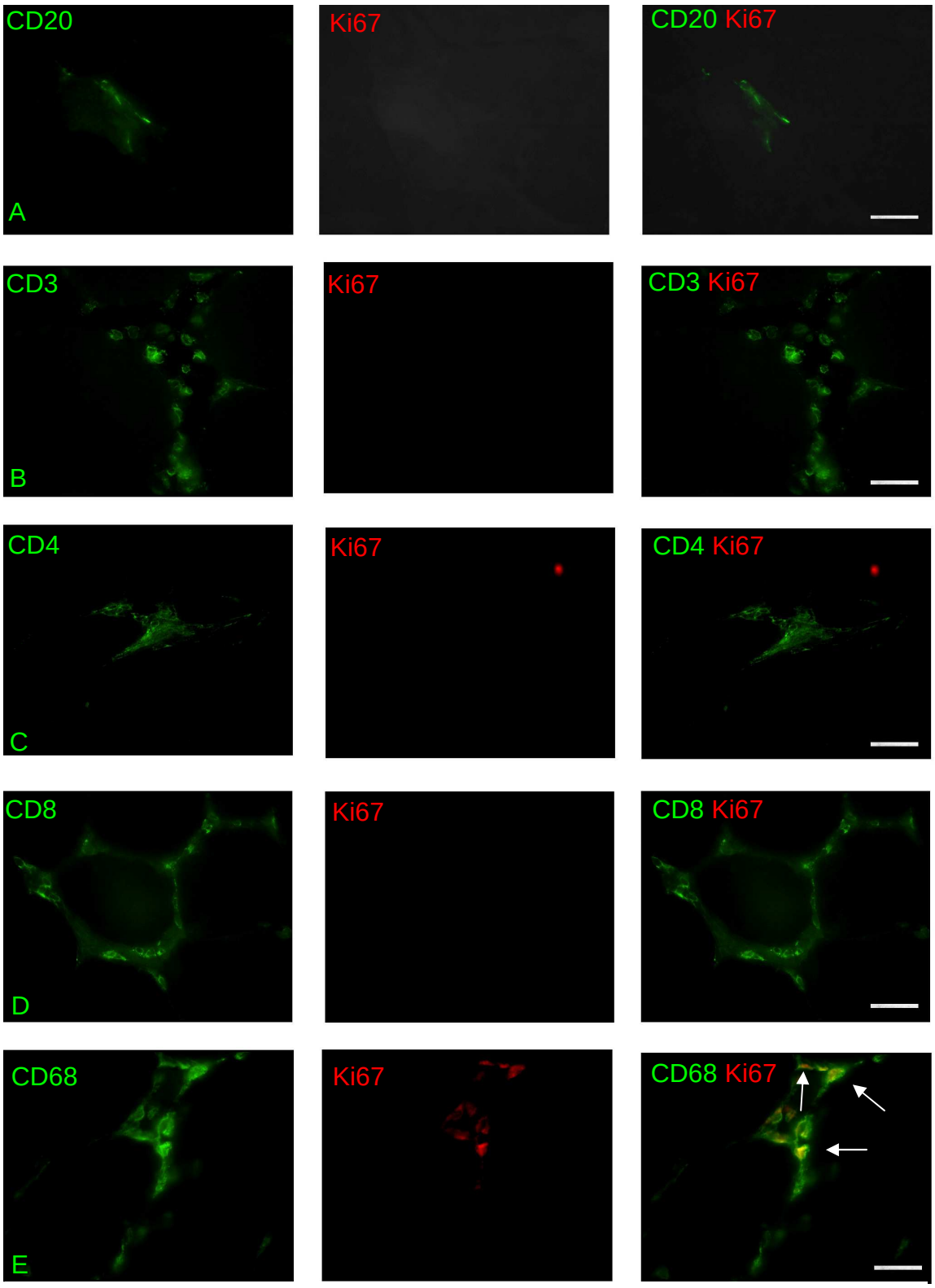

Figure 3.10 Double Immunohistochemical staining of serial muscle sections of sample MYO6

A representative example of serial muscle sections from sample MYO6 stained for CD20 (**A**), CD3 (**B**), CD4 (**C**), CD8 (**D**), CD68 (**E**) and visualised by Fluorescein Avidin D before all sections were stained with Ki67 and visualised by Texas Red Avidin D. This allowed the type of proliferating cells within the myositis sample to be identified. Images were taken at 630X; Scale Bar represents 15 µm. Arrows identify proliferating cells within the sections.

3.2.5 Sample MYO7

Immunohistochemical staining of sample MYO7 (**Figure 3.11**) demonstrated that infiltrating cells were present throughout the entire section, between muscle fibres, but did appear to form approximately three regions of aggregation, although some of these areas appeared to be damaged during section cutting. Within the cellular infiltrates very few $CD20^+$ (**A**) cells or FDCs (**B**) were present. A large proportion of the cells were identified as plasma cells (**C**) or $CD4^+$ (**E**) cells. The number of cells observed using the CD4 marker appeared to be greater than that observed for both $CD3^+$ (**D**) and $CD8^+$ (**F**) cells, as observed in sample MYO3. There was a large infiltrate of $CD68^+$ (**H**) cells present within sample MYO7. Very few $Ki67^+$ (**G**) cells were present with no evidence of $FoxP3^+$ (**I**) cells. Negative control experiments were clear from non-specific staining (**J-L**).

Double staining experiments showed that the proliferating cells present within the muscle sample were $CD3^+$ (**B**), $CD8^+$ (**D**) and $CD68^+$ (**E**) cells (**Figure 3.12**). Occasionally a proliferating $CD4^+$ (**C**) cell was observed throughout the section. Negative control staining was clear.

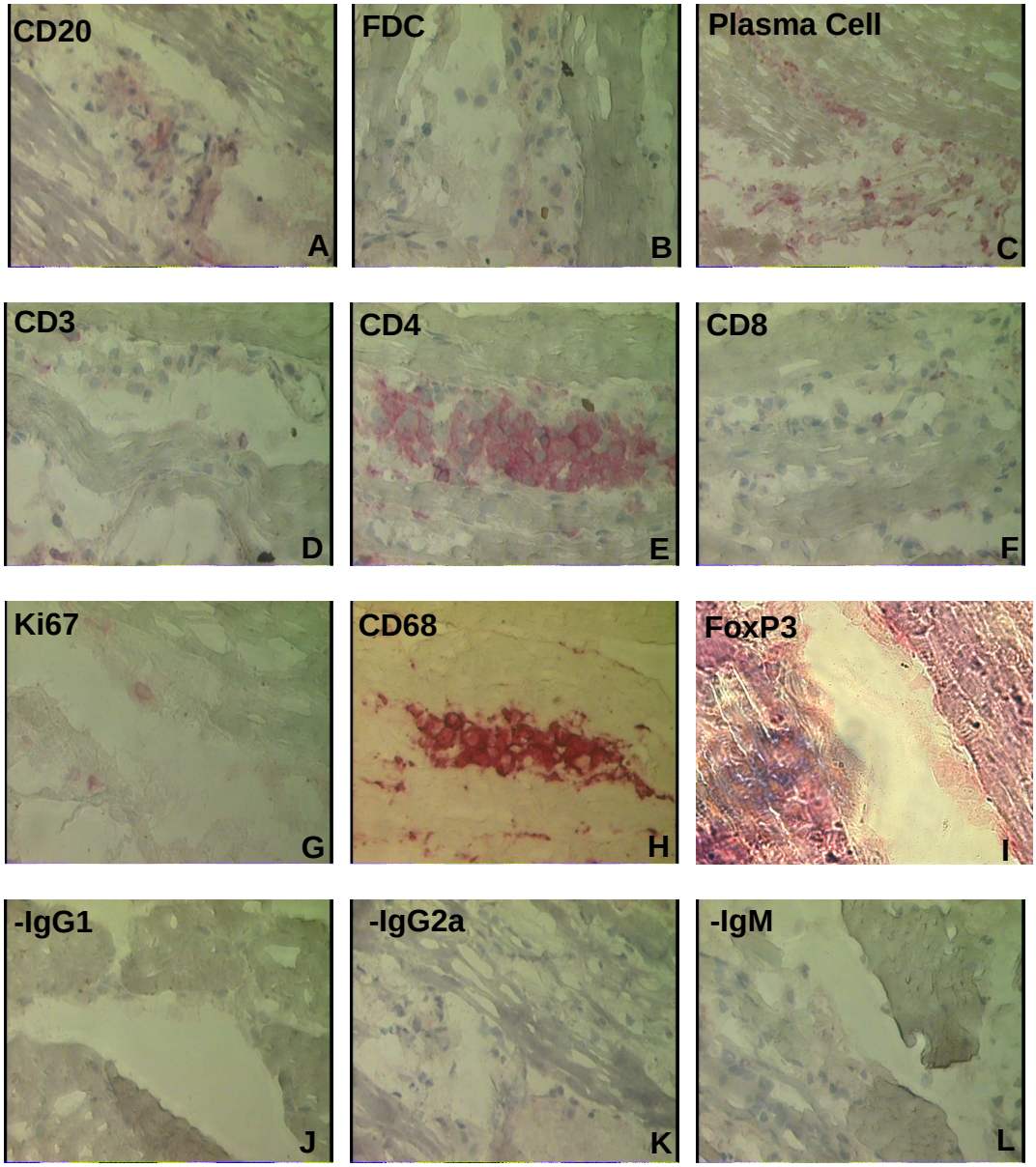

Figure 3.11 Immunohistochemistry of serial muscle sections of Sample MYO7.

A representative example of serial muscle sections from sample MYO7 stained for CD20 (**A**), FDC (**B**), Plasma cells (**C**), CD3 (**D**), CD4 (**E**), CD8 (**F**), Ki67 (**G**), CD68 (**H**), FoxP3 (**I**), IgG1 Negative control (**J**), IgG2a Negative control (**K**), IgM Negative control (**L**) and visualised by APAAP and New Fuschin substrate to establish cellular infiltrates within the muscle section. Images A – L: 400X

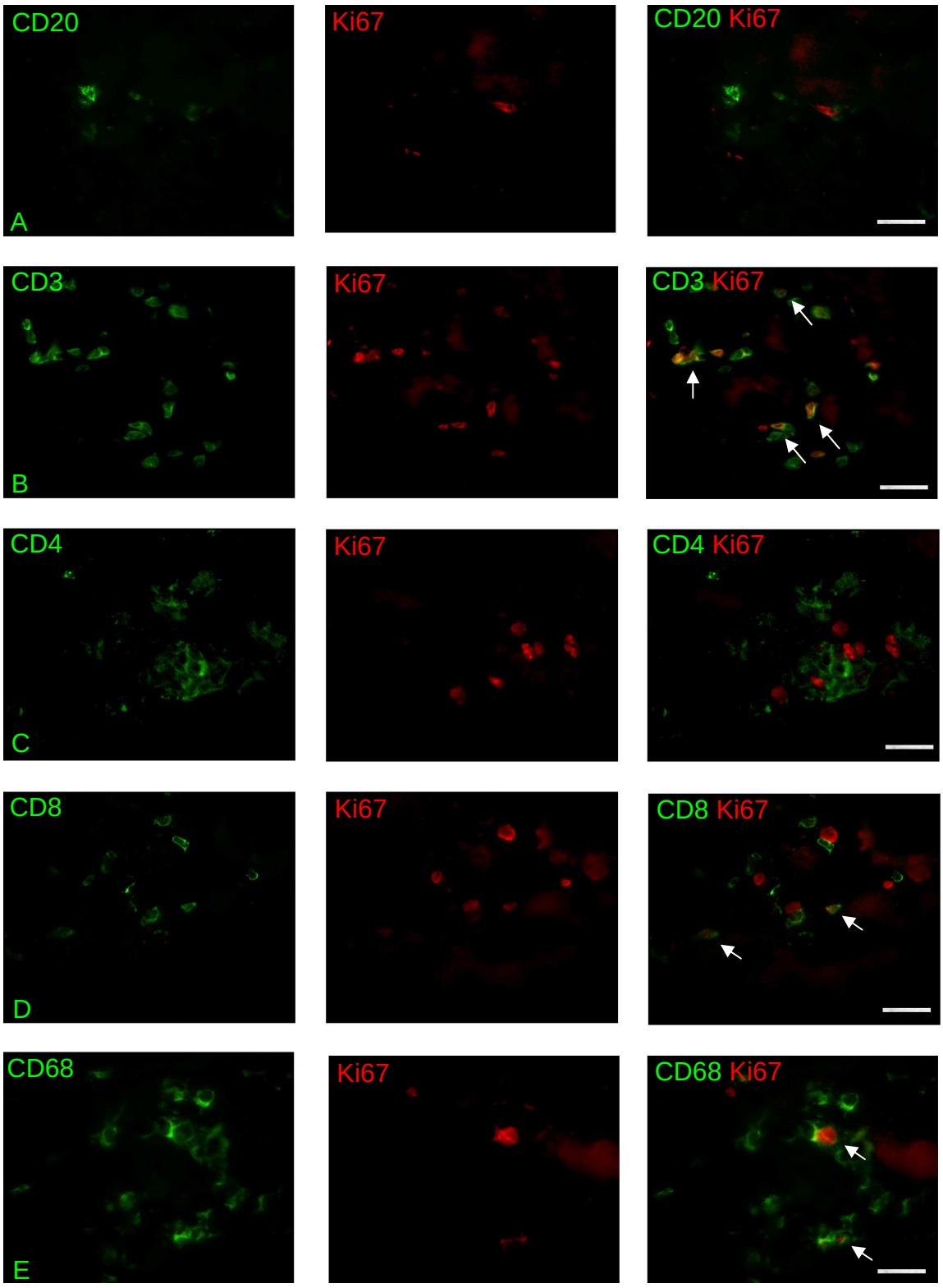

Figure 3.12 Double Immunohistochemical staining of serial muscle sections of sample MYO7

A representative example of serial muscle sections from sample MYO7 stained for CD20 (**A**), CD3 (**B**), CD4 (**C**), CD8 (**D**), CD68 (**E**) and visualised by Fluorescein Avidin D before all sections were stained with Ki67 and visualised by Texas Red Avidin D. This allowed the type of proliferating cells within the myositis sample to be identified. Images were taken at 630X; Scale Bar represents 15 µm. Arrows identify proliferating cells within the sections.

3.2.6 Sample MYO16

Within sample MYO16 three main regions of perimysial/perifascicular cellular infiltration were observed with additional scattered infiltration (**Figure 3.13**). Although infiltrates were largely focused at the fascicle edges, a number of individual muscle fibres at one area of aggregation were surrounded by infiltrating cells. One of the main regions of cellular infiltration displayed considerable $CD20^+$ (**A**), $CD3^+$ (**D**), $CD4^+$ (**E**) cells and plasma cell (**C**) infiltrates, as well as $Ki67^+$ (**G**) cells with reduced cellular $CD8^+$ (**F**) staining in comparison to other cell types. The $CD20^+$ cells formed a very dense follicle of cells situated between muscle fibres. In other regions the infiltrating $CD20^+$ cells were more loosely aggregated. A large infiltration of $CD68^+$ (**H**) cells was also present within sample MYO16. These cells types were evident within the regions of aggregation but were also dispersed throughout the entire section. No $FoxP3^+$ (**I**) cells or FDCs (**B**) were present within the infiltrating population. This pattern of infiltration was observed in the other regions of cellular aggregation but there was a reduction in the presence of $CD20^+$ cells in the other regions compared to that observed in the region mentioned above. Negative control stains with appropriate isotype controls produced no non-specific staining (**J-L**).

Identification of the proliferating cells by double staining identified the $Ki67^+$ cells as $CD3^+$ (**B**), $CD4^+$ (**C**), $CD8^+$ (**D**) and $CD68^+$ (**E**) cells (**Figure 3.14**). No proliferating $CD20^+$ (**A**) cells were observed in serial sections of the sample although the large areas of aggregation observed within immunohistochemistry experiments, Figure 3.13, could not be located in the later sections used for the immunofluorescence experiments. As previously described no non-specific staining was observed within the sample.

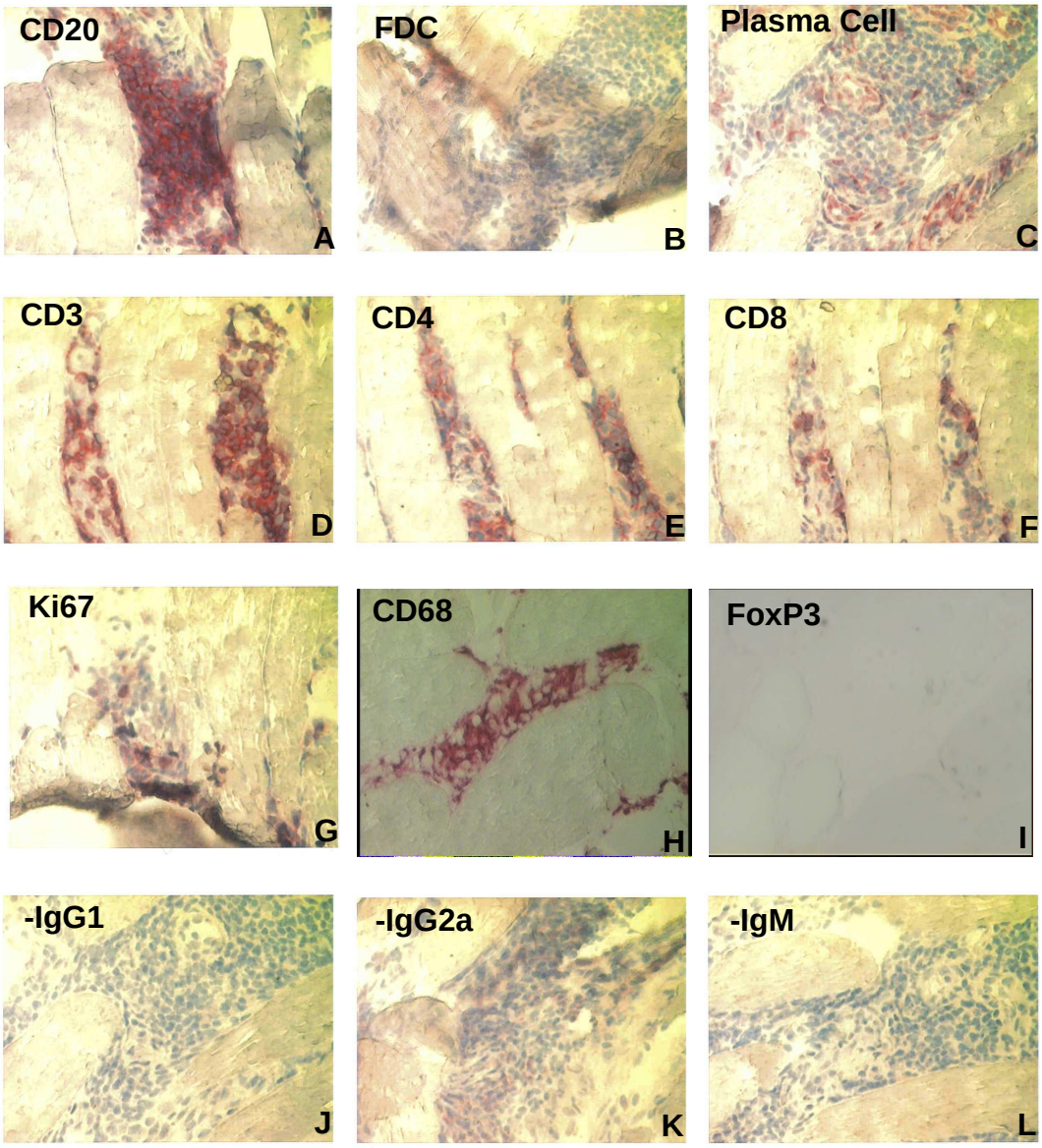

Figure 3.13 Immunohistochemistry of serial muscle sections of Sample MYO16.

A representative example of serial muscle sections from sample MYO16 stained for CD20 (**A**), FDC (**B**), Plasma cells (**C**), CD3 (**D**), CD4 (**E**), CD8 (**F**), Ki67 (**G**), IgG1 Negative control (**H**), IgG2a Negative control (**I**), IgM Negative control (**J**) and visualised by APAAP to establish cellular infiltrates within the muscle section. Images A – J 400X

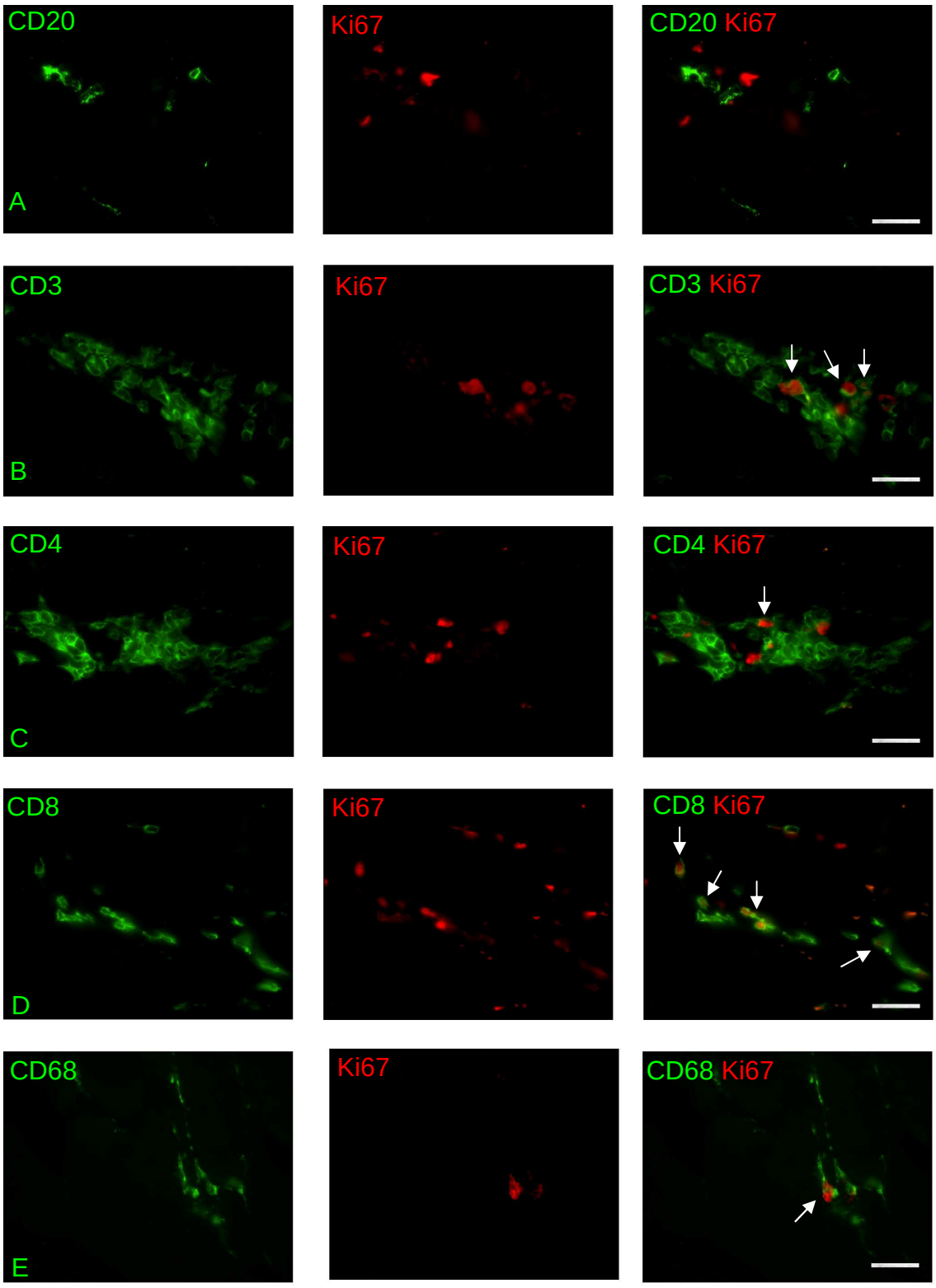

Figure 3.14 Double Immunohistochemical staining of serial muscle sections of sample MYO16

A representative example of serial muscle sections from sample MYO16 stained for CD20 (**A**), CD3 (**B**), CD4 (**C**), CD8 (**D**), CD68 (**E**) and visualised by Fluorescein Avidin D before all sections were stained with Ki67 and visualised by Texas Red Avidin D. This allowed the type of proliferating cells within the myositis sample to be identified. Images were taken at 630X; Scale Bar represents 15 µm. Arrows identify proliferating cells within the sections.

3.2.7 Sample MYO17

Identification of cellular infiltrates within sample MYO17 showed many small areas of aggregation as well as scattered areas of cellular infiltration throughout the section at endomysial locations. One extensive area of cellular infiltration between muscle fibres was observed within sample MYO17 (**Figure 3.15**). $CD3^+$ (**D**), $CD4^+$ (**E**) cells and plasma cells (**C**) dominated the cellular infiltrate with positive but reduced numbers of $CD8^+$ (**F**) cells. Very few $CD20^+$ (**A**) cells or FDCs (**B**) were observed within the sample in comparison to $CD3^+$, $CD4^+$ and plasma cell staining. Proliferating $Ki67^+$ (**G**) cells were present within the sample as well as a large infiltrate of $CD68^+$ (**H**) cells. $FoxP3^+$ (**I**) staining showed the presence of an occasional positive cell. Some light diffuse staining was observed with the negative control isotype antibodies but the staining for cell markers are clearly specific due to the differences in staining intensity (**J-L**).

Proliferating cells were shown to include $CD20^+$ (**A**), $CD3^+$ (**B**), $CD4^+$ (**C**), $CD8^+$ (**D**) and $CD68^+$ (**E**) cells (**Figure 3.16**). Negative control experiments with the antibody isotype controls showed no non-specific staining within sections.

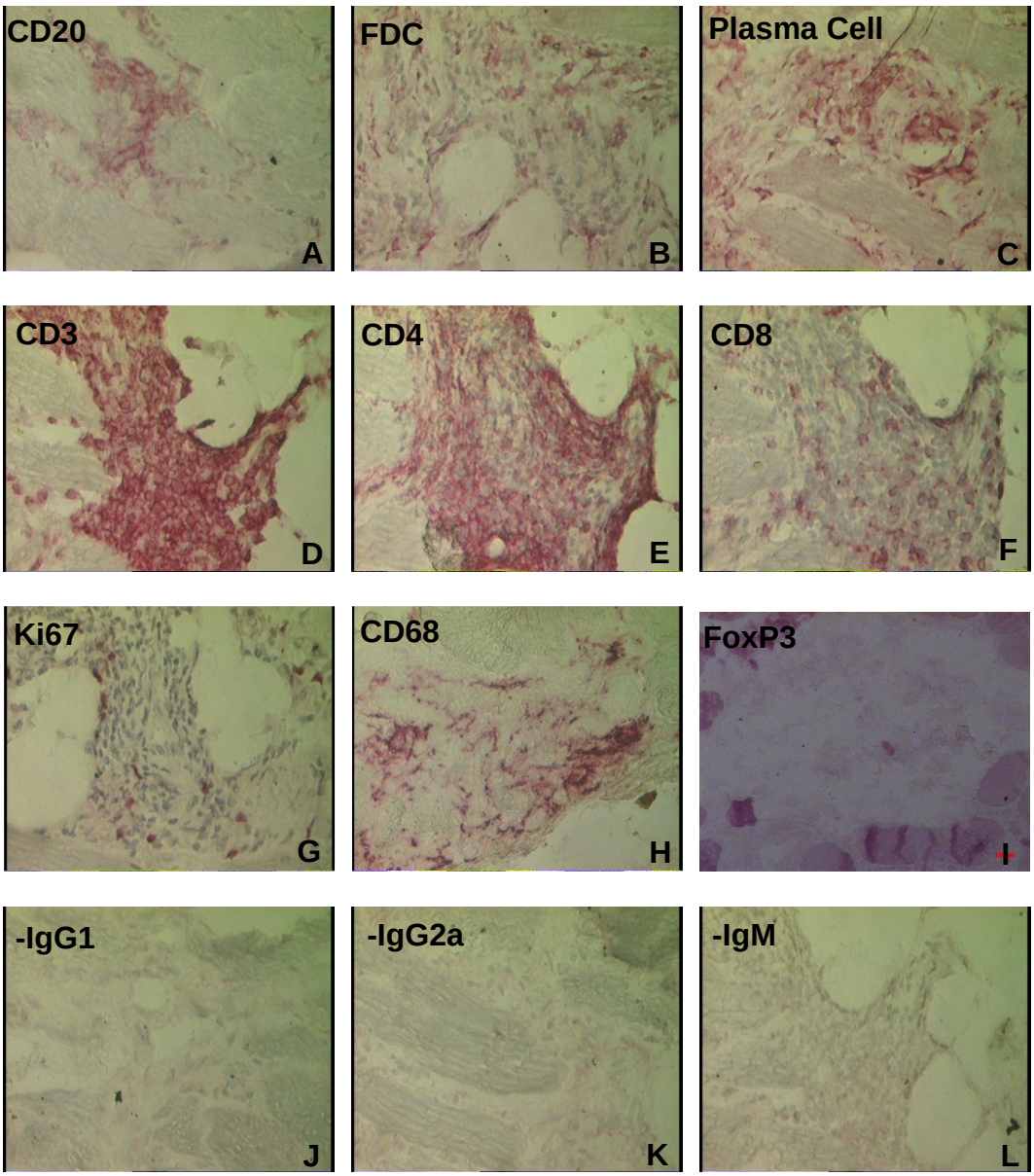

Figure 3.15 Immunohistochemistry of serial muscle sections of Sample MYO17.

A representative example of serial muscle sections from sample MYO17 stained for CD20 (**A**), FDC (**B**), Plasma cells (**C**), CD3 (**D**), CD4 (**E**), CD8 (**F**), Ki67 (**G**), CD68 (**H**), FoxP3 (**I**), IgG1 Negative control (**J**), IgG2a Negative control (**K**), IgM Negative control (**L**) and visualised by APAAP and New Fuschin substrate to establish cellular infiltrates within the muscle section. Images A – L: 400X

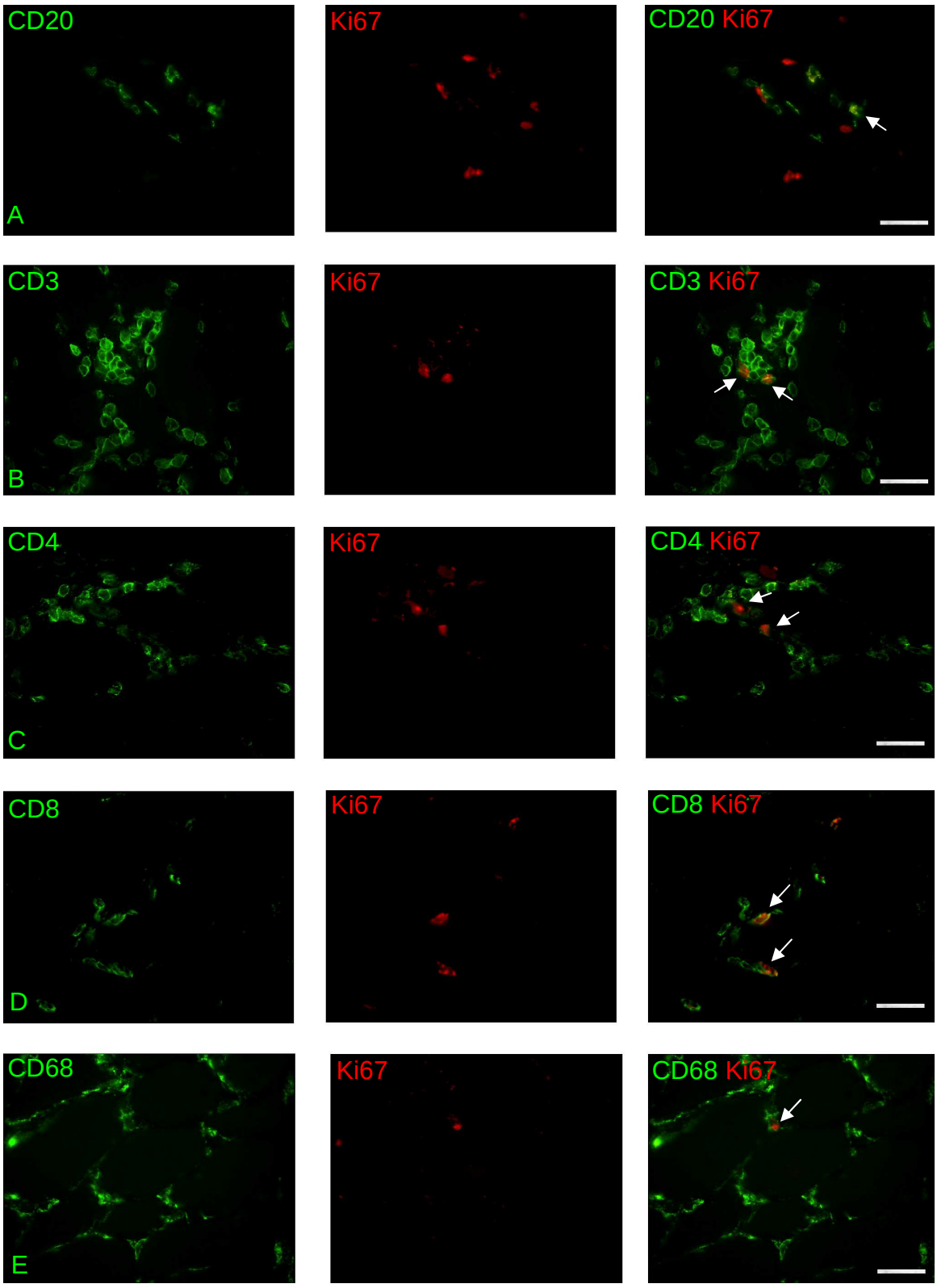

Figure 3.16 Double Immunohistochemical staining of serial muscle sections of sample MYO17

A representative example of serial muscle sections from sample MYO17 stained for CD20 (**A**), CD3 (**B**), CD4 (**C**), CD8 (**D**), CD68 (**E**) and visualised by Fluorescein Avidin D before all sections were stained with Ki67 and visualised by Texas Red Avidin D. This allowed the type of proliferating cells within the myositis sample to be identified. Images were taken at 630X; Scale Bar represents 15 µm. Arrows identify proliferating cells within the sections.

3.2.8 Sample MYO19

Numerous small areas of endomysial infiltration were observed within sample MYO19 which appeared to vary in cell density, with additional scattered staining throughout the sample. As demonstrated in **Figure 3.17** all the regions displayed positive staining for CD20 (**A**), CD3 (**D**), CD4 (**E**), CD8 (**F**), Ki67 (**G**) cell markers and plasma cells (**C**). As previously observed in some other myositis samples no staining was observed for FDCs (**B**) and CD8 staining was reduced in comparison to other cell types. A large infiltration of $CD68^+$ (**H**) cells but no $FoxP3^+$ (**I**) cells were observed throughout sections examined for this sample. Staining sections with the appropriate negative controls (**J-L**) identified virtually no staining in the regions identified by the other cellular stains.

Double staining identified the proliferating cells within the muscle as a collection of $CD20^+$ (**A**), $CD3^+$ (**B**), $CD4^+$ (**C**) and $CD8^+$ (**D**) cells (**Figure 3.18**). No proliferating $CD68^+$ (**E**) cells were observed throughout the sample. Negative control experiments were clear of non-specific staining.

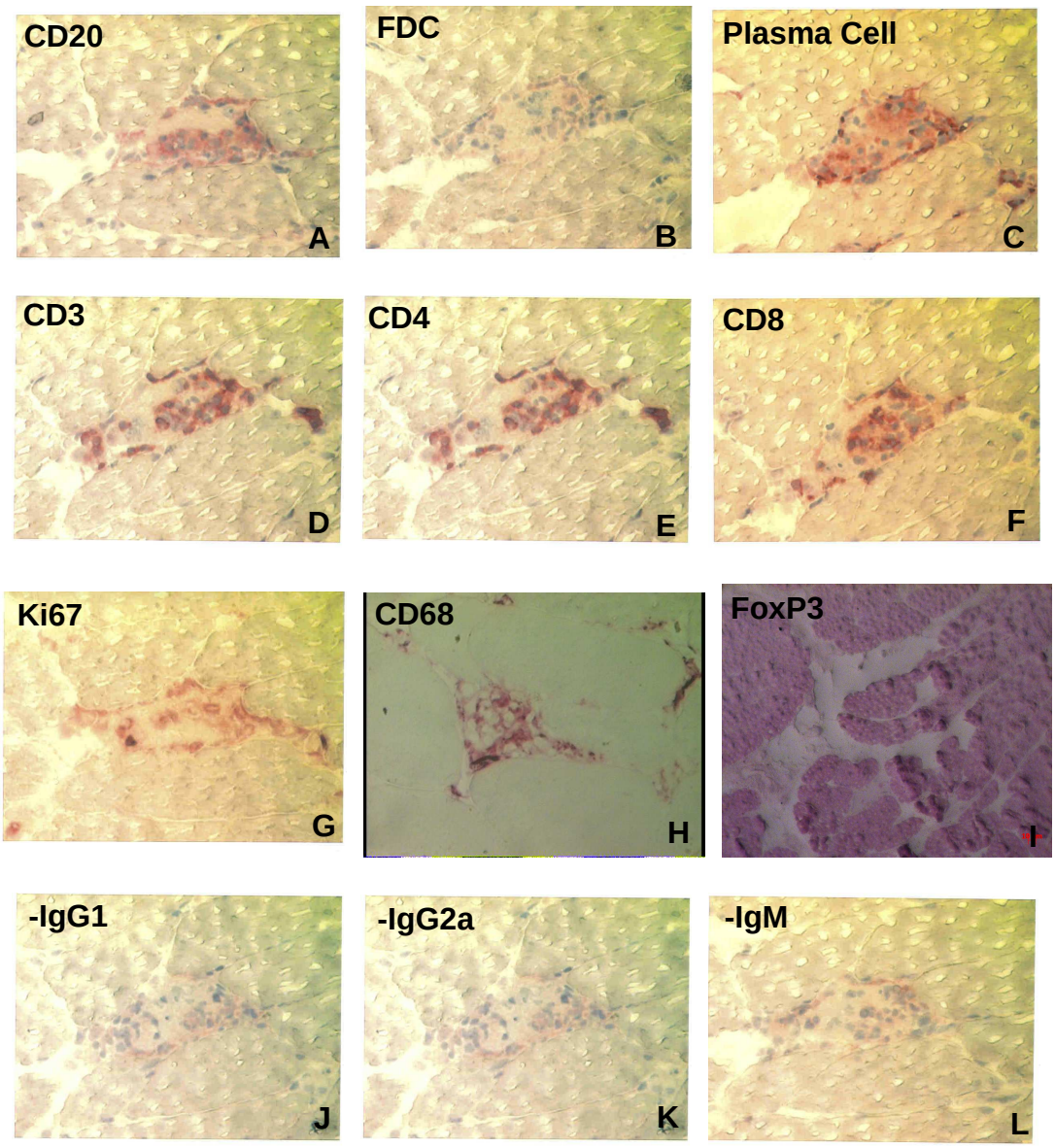

Figure 3.17 Immunohistochemistry of serial muscle sections of Sample MYO19.

A representative example of serial muscle sections from sample MYO19 stained for CD20 (**A**), FDC (**B**), Plasma cells (**C**), CD3 (**D**), CD4 (**E**), CD8 (**F**), Ki67 (**G**), CD68 (**H**), FoxP3 (**I**), IgG1 Negative control (**J**), IgG2a Negative control (**K**), IgM Negative control (**L**) and visualised by APAAP and New Fuschin substrate to establish cellular infiltrates within the muscle section. Images A – L: 400X

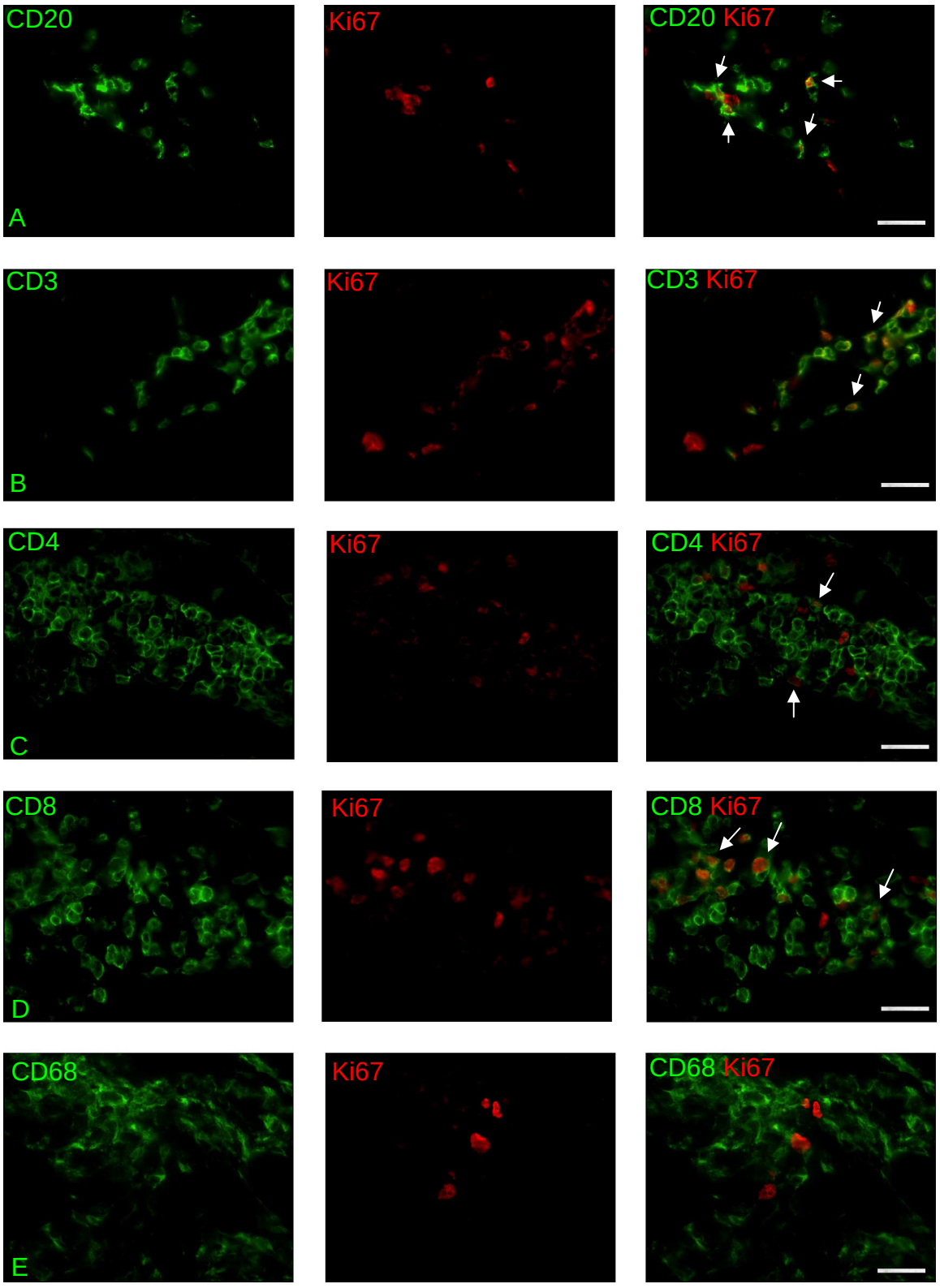

Figure 3.18 Double Immunohistochemical staining of serial muscle sections of sample MYO19

A representative example of serial muscle sections from sample MYO19 stained for CD20 (**A**), CD3 (**B**), CD4 (**C**), CD8 (**D**), CD68 (**E**) and visualised by Fluorescein Avidin D before all sections were stained with Ki67 and visualised by Texas Red Avidin D. This allowed the type of proliferating cells within the myositis sample to be identified. Images were taken at 630X; Scale Bar represents 15 µm. Arrows identify proliferating cells within the sections.

3.2.9 Sample MYO23

For sample MYO23 no dense region of cellular infiltration was observed and infiltrating cells appeared to be in very small numbers throughout the entire section between muscle fibres in endomysial locations (**Figure 3.19**). Of the cells that were present a large proportion were identified as plasma cells (**C**), $CD4^+$ (**E**) and $CD68^+$ (**H**) cells. Some of the infiltrating cells were identified as $CD20^+$ (**A**), $CD3^+$ (**D**) and $CD8^+$ (**F**) cells as well as FDCs (**B**). Some of the infiltrating cells were proliferating with the presence of $Ki67^+$ (**G**) cells. No $FoxP3^+$ (**I**) cells were found within the section. The use of negative control isotype antibodies produced no non-specific staining (**J-L**).

Double immunohistochemical experiments demonstrated that proliferating cells within sample MYO23 were $CD3^+$ (**B**), $CD8^+$ (**D**) or $CD68^+$ (**E**) cells (**Figure 3.20**). Negative control experiments were clear of non-specific staining.

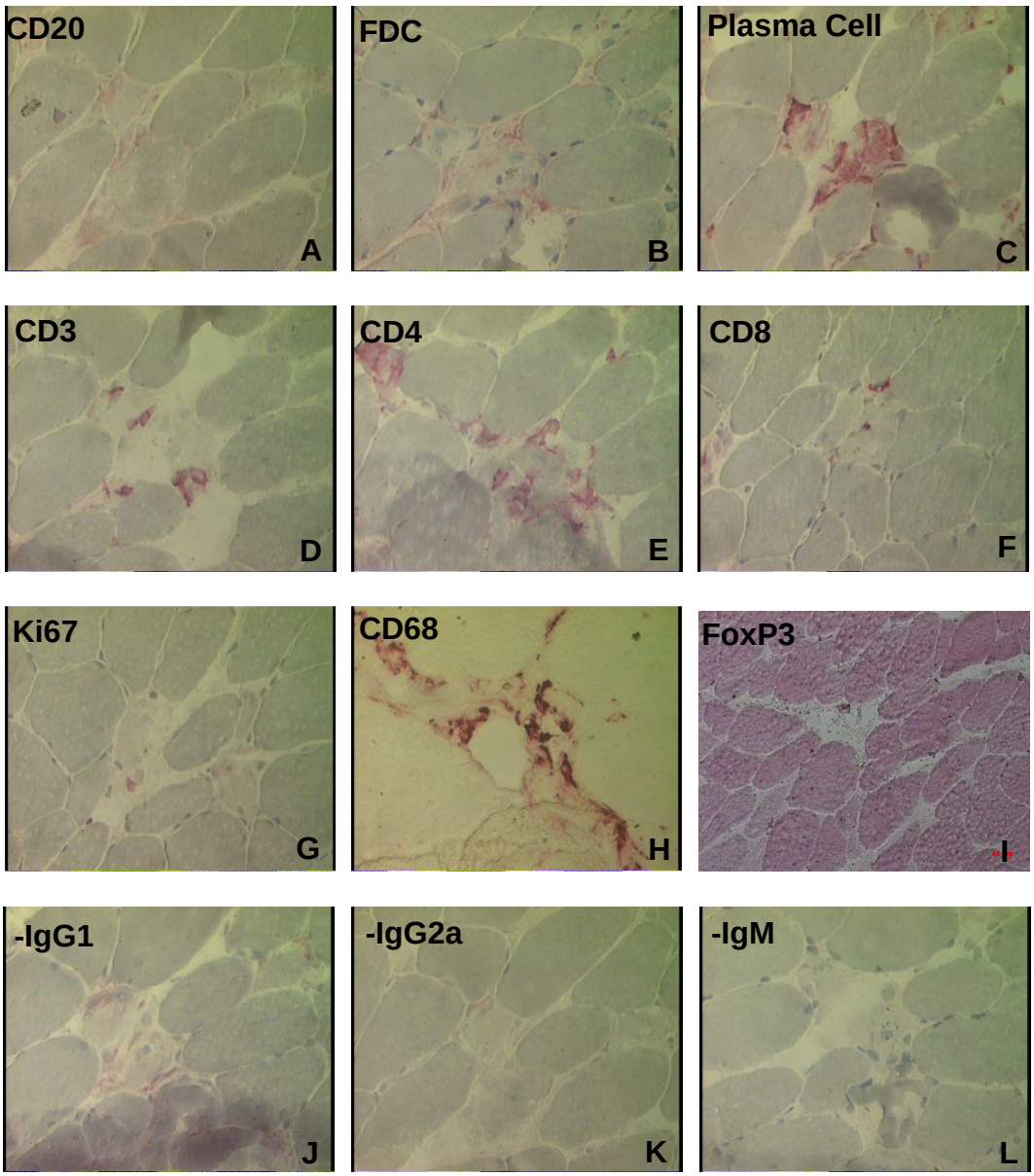

Figure 3.19 Immunohistochemistry of serial muscle sections of Sample MYO23.

A representative example of serial muscle sections from sample MYO23 stained for CD20 (**A**), FDC (**B**), Plasma cells (**C**), CD3 (**D**), CD4 (**E**), CD8 (**F**), Ki67 (**G**), CD68 (**H**), FoxP3 (**I**), IgG1 Negative control (**J**), IgG2a Negative control (**K**), IgM Negative control (**L**) and visualised by APAAP and New Fuschin substrate to establish cellular infiltrates within the muscle section. Images A – L: 400X

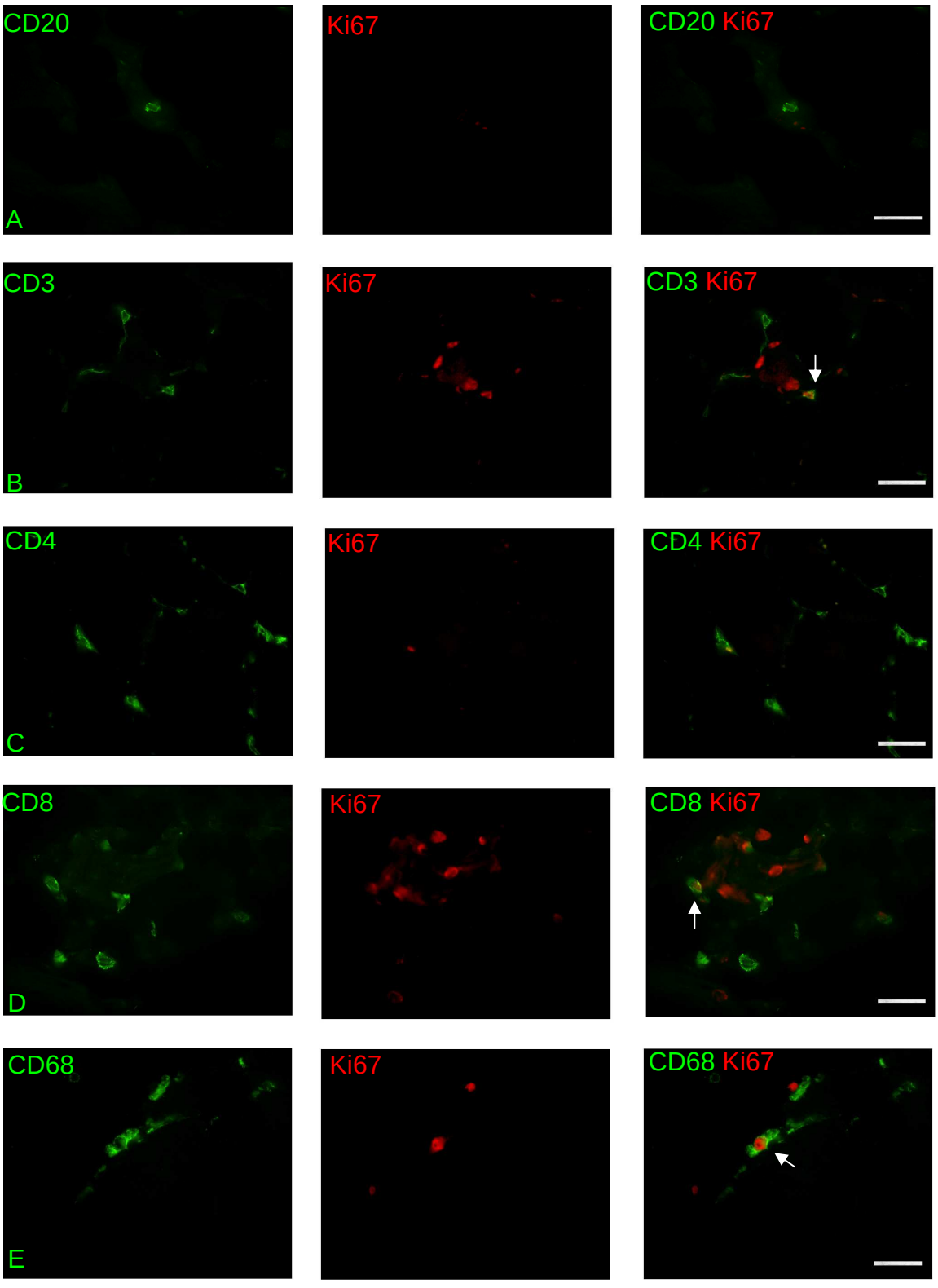

Figure 3.20 Double Immunohistochemical staining of serial muscle sections of sample MYO23

A representative example of serial muscle sections from sample MYO23 stained for CD20 (**A**), CD3 (**B**), CD4 (**C**), CD8 (**D**), CD68 (**E**) and visualised by Fluorescein Avidin D before all sections were stained with Ki67 and visualised by Texas Red Avidin D. This allowed the type of proliferating cells within the myositis sample to be identified. Images were taken at 630X; Scale Bar represents 15 µm. Arrows identify proliferating cells within the sections.

3.2.10 Sample MYO24

For sample MYO24 plasma cells (**C**) and $CD68^+$ (**H**) cells dominated the population of infiltrating cells (**Figure 3.21**). Diffuse staining was observed for $CD20^+$ cells (**A**) and FDCs (**B**) with no clear representation of these cells being present within sample MYO24, although $CD20^+$ cells were later identified in immunofluorescent experiments (**Figure 3.22**). $CD3^+$ (**D**) and $CD4^+$ (**E**) cells were evident within the sample. These cells formed a few small areas of cellular aggregation but additional cells were dispersed through the whole section between the muscle fibres. $CD8^+$ (**F**) cells were also present within the sample but the staining was reduced in comparison to that of CD3 and CD4 cell markers. $Ki67^+$ (**G**) cells were present within the sample with also the occasional $FoxP3^+$ (**I**) cell. All negative control staining experiments were clear of non-specific staining (**J-L**).

Identification of the proliferating cells within sample MYO24 by double staining showed that some of the infiltrating $CD20^+$ (**A**) and $CD4^+$ (**C**) cells were proliferating within sample MYO24 (**Figure 3.22**). Negative control experiments with the antibody isotype controls showed no non-specific staining within sections

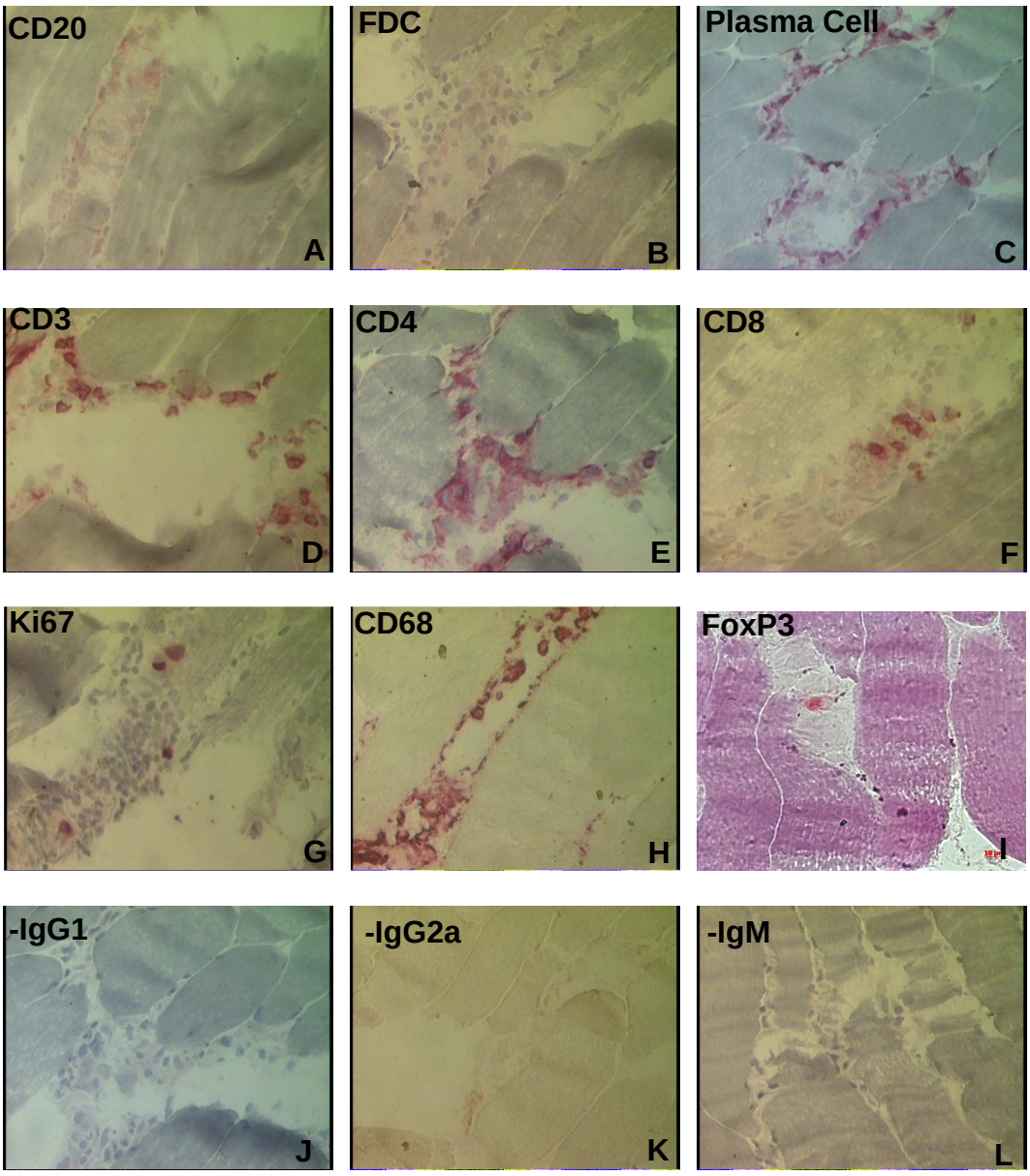

Figure 3.21 Immunohistochemistry of serial muscle sections of Sample MYO24.

A representative example of serial muscle sections from sample MYO24 stained for CD20 (**A**), FDC (**B**), Plasma cells (**C**), CD3 (**D**), CD4 (**E**), CD8 (**F**), Ki67 (**G**), CD68 (**H**), FoxP3 (**I**), IgG1 Negative control (**J**), IgG2a Negative control (**K**), IgM Negative control (**L**) and visualised by APAAP and New Fuschin substrate to establish cellular infiltrates within the muscle section. Images A – L: 400X

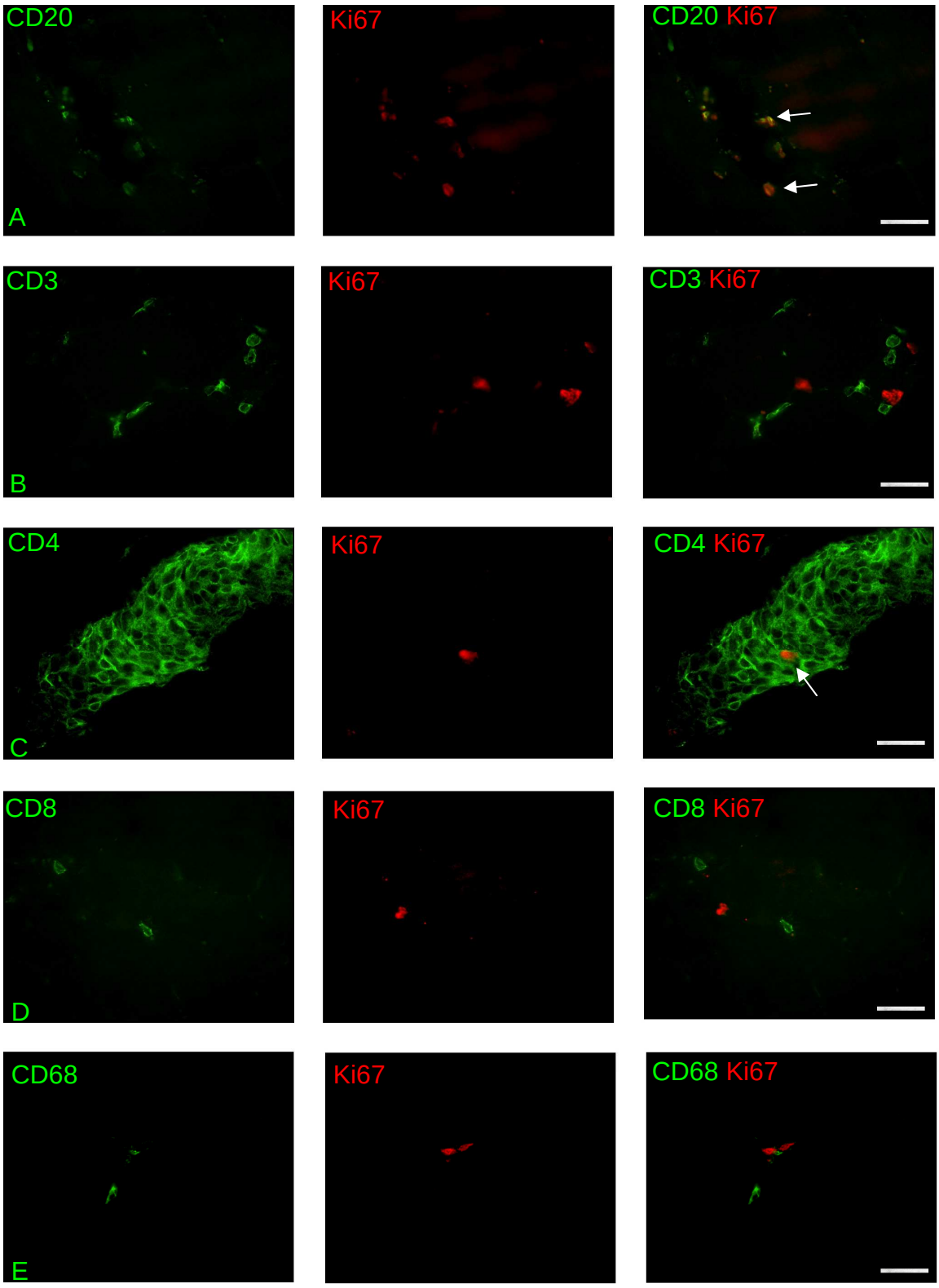

Figure 3.22 Double Immunohistochemical staining of serial muscle sections of sample MYO24

A representative example of serial muscle sections from sample MYO24 stained for CD20 (**A**), CD3 (**B**), CD4 (**C**), CD8 (**D**), CD68 (**E**) and visualised by Fluorescein Avidin D before all sections were stained with Ki67 and visualised by Texas Red Avidin D. This allowed the type of proliferating cells within the myositis sample to be identified. Images were taken at 630X; Scale Bar represents 15 µm. Arrows identify proliferating cells within the sections.

3.2.11 Sample MYOC

MYOC cellular infiltration was observed throughout the entire section, in an endomysial pattern, with small areas of aggregation (**Figure 3.23**). No FDCs (**B**) were observed within the section and there was very little staining observed for $CD20^+$ (**A**) cells. $CD3^+$ (**D**) and $CD8^+$ (**F**) cells were found within the muscle as well as $CD4^+$ (**E**) cells but the staining of $CD4^+$ cells was greater than that observed for the CD3 cell marker, similar to that observed in other samples. Also present within sample MYOC were $CD68^+$ (**H**) and a small number of $Ki67^+$ (**G**) cells. For sample MYOC no $FoxP3^+$ (**I**) staining was observed within the section. Negative control experiments produced no non-specific within the section (**J-L**).

Very few proliferating $Ki67^+$ cells were evident within sample MYOC, the phenotype of those that were present could not be identified from the sections examined (**Figure 3.24**). Negative control experiments produced no non-specific staining.

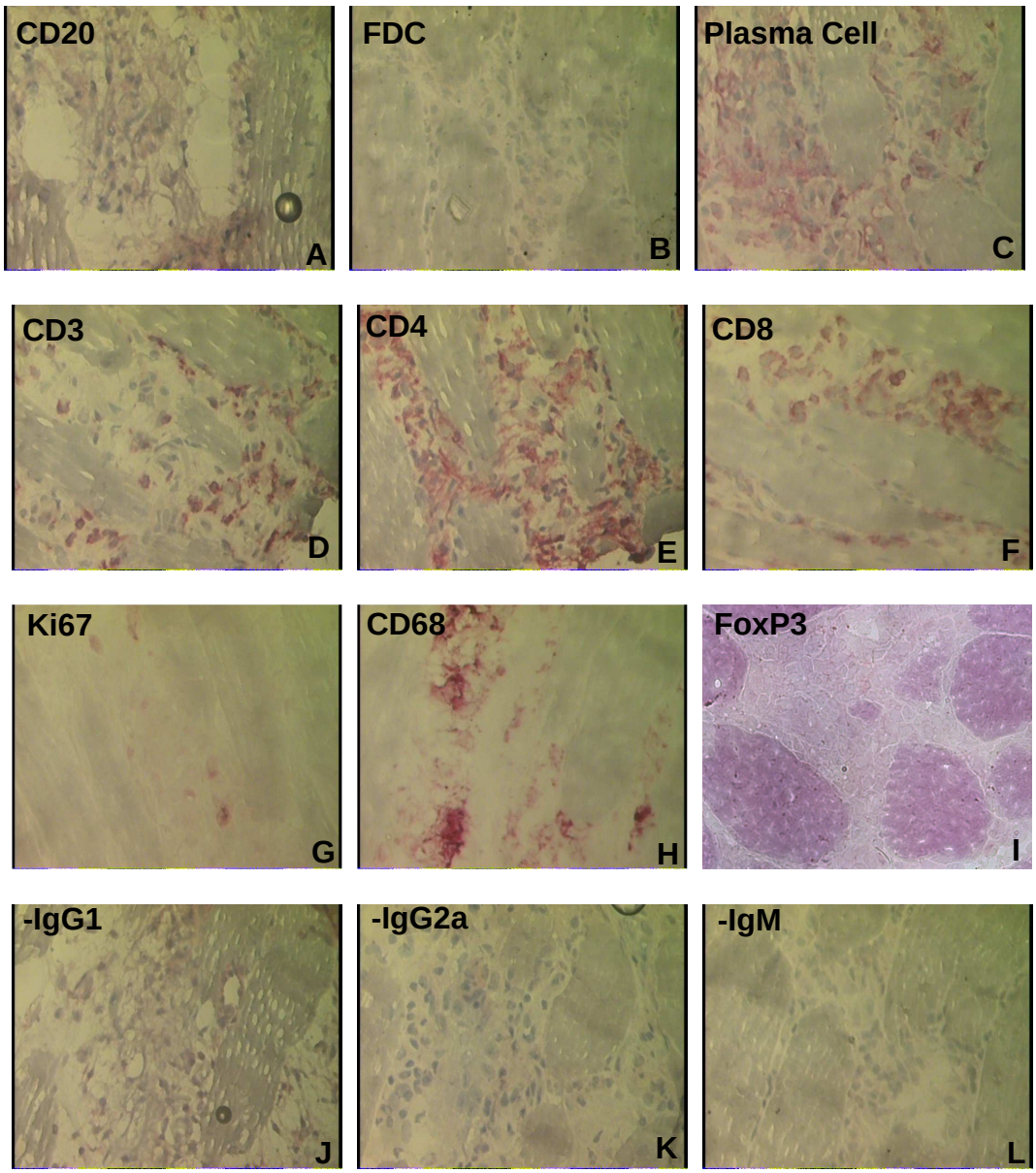

Figure 3.23 Immunohistochemistry of serial muscle sections of Sample MYOC.

A representative example of serial muscle sections from sample MYOC stained for CD20 (**A**), FDC (**B**), Plasma cells (**C**), CD3 (**D**), CD4 (**E**), CD8 (**F**), Ki67 (**G**), CD68 (**H**), FoxP3 (**I**), IgG1 Negative control (**J**), IgG2a Negative control (**K**), IgM Negative control (**L**) and visualised by APAAP and New Fuschin substrate to establish cellular infiltrates within the muscle section. Images A – L: 400X

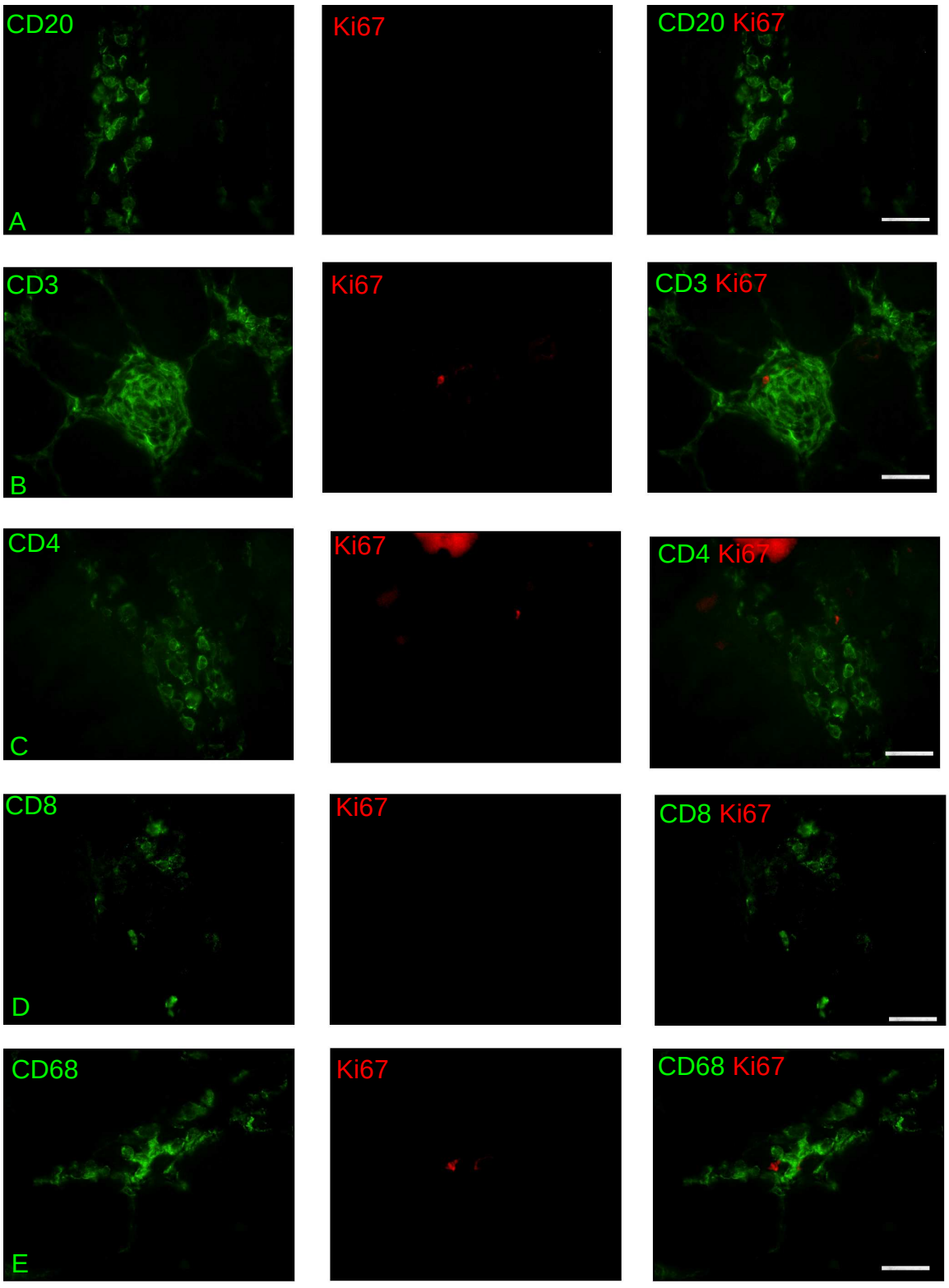

Figure 3.24 Double Immunohistochemical staining of serial muscle sections of sample MYOC

A representative example of serial muscle sections from sample MYOC stained for CD20 (**A**), CD3 (**B**), CD4 (**C**), CD8 (**D**), CD68 (**E**) and visualised by Fluorescein Avidin D before all sections were stained with Ki67 and visualised by Texas Red Avidin D. This allowed the type of proliferating cells within the myositis sample to be identified. Images were taken at 630X; Scale Bar represents 15 µm. Arrows identify proliferating cells within the sections.

3.2.12 Sample MYOE

Immunohistochemical staining within sample MYOE showed that there were small numbers of $CD20^+$ (**A**) cells within the cellular infiltrate of the sample (**Figure 3.25**). Cells infiltrating the sample were quite diffuse with small areas of aggregation which were distributed between the muscle fibres. As with previous myositis samples no FDCs (**B**) were present within the infiltrating population of cells but plasma cells (**C**), $CD3^+$ (**D**), $CD4^+$ (**E**), $CD8^+$ (**F**), $Ki67^+$ (**G**), and $CD68^+$ (**H**) cells were present. Comparing the $CD4^+$ staining with $CD3^+$ staining showed that again there was a slightly greater infiltration of $CD4^+$ cells in comparison to that of $CD3^+$ cells. $FoxP3^+$ (**I**) infiltrating cells were not found within the sample. Non-specific staining was not observed by the use of isotype negative control antibodies (**J-L**).

Double staining experiments identified that some of the proliferating cells were $CD20^+$ (**A**) cells but a large proportion of the proliferating cells were of other cell phenotypes (**Figure 3.26**). $CD3^+$ (**B**), $CD4^+$ (**C**) and $CD68^+$ (**E**) proliferating cells were identified within sample MYOE as were a few $CD8^+$ (**D**) proliferating cells. Negative control experiments were clear of non-specific staining. The large cluster of $CD20^+$ cells observed by immunofluorescent staining experiments could not be found in the remaining serial sections of sample MYOE to allow for possible microdissection.

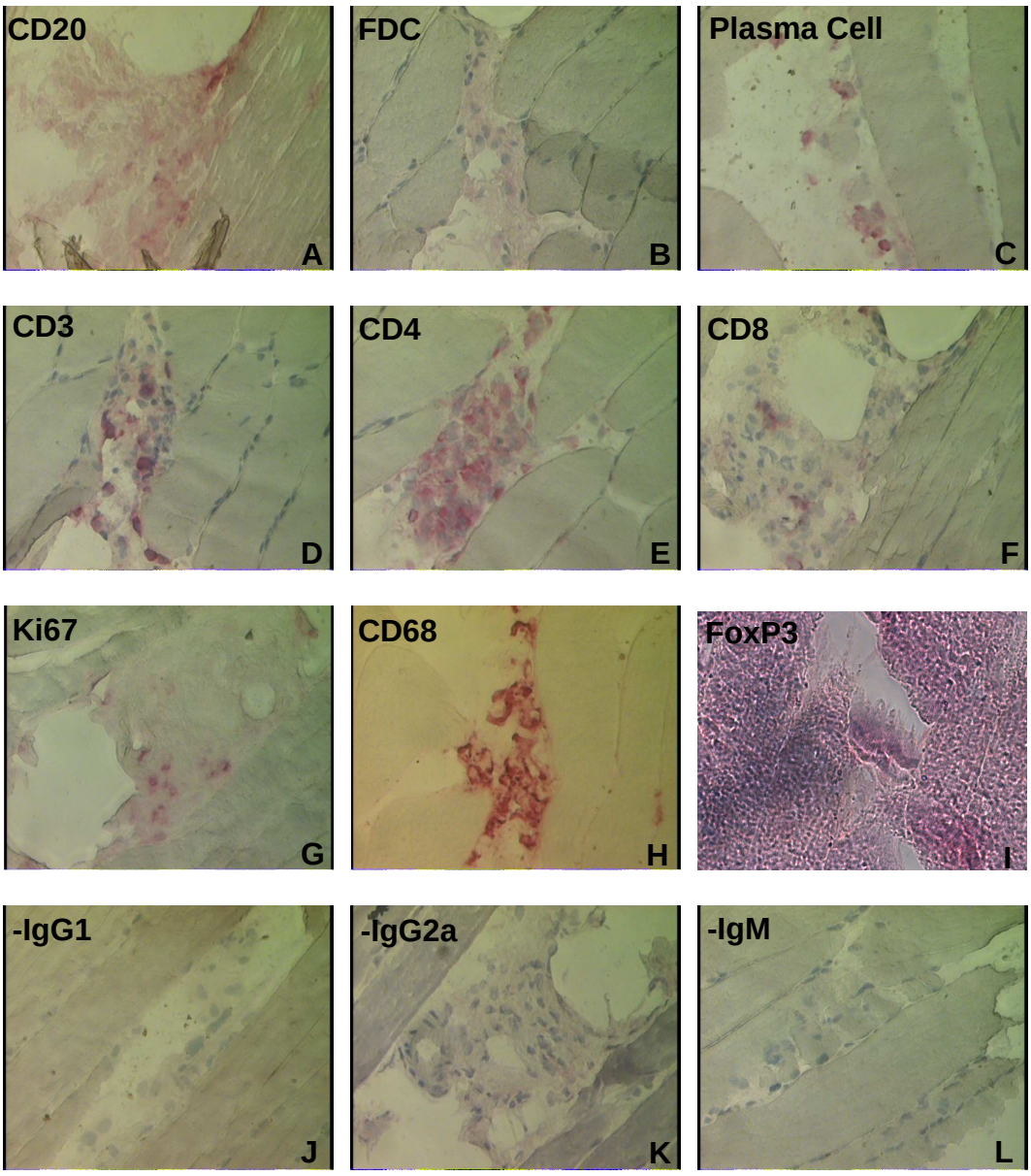

Figure 3.25 Immunohistochemistry of serial muscle sections of Sample MYOE.

A representative example of serial muscle sections from sample MYOE stained for CD20 (**A**), FDC (**B**), Plasma cells (**C**), CD3 (**D**), CD4 (**E**), CD8 (**F**), Ki67 (**G**), CD68 (**H**), FoxP3 (**I**), IgG1 Negative control (**J**), IgG2a Negative control (**K**), IgM Negative control (**L**) and visualised by APAAP and New Fuschin substrate to establish cellular infiltrates within the muscle section. Images A – L: 400X

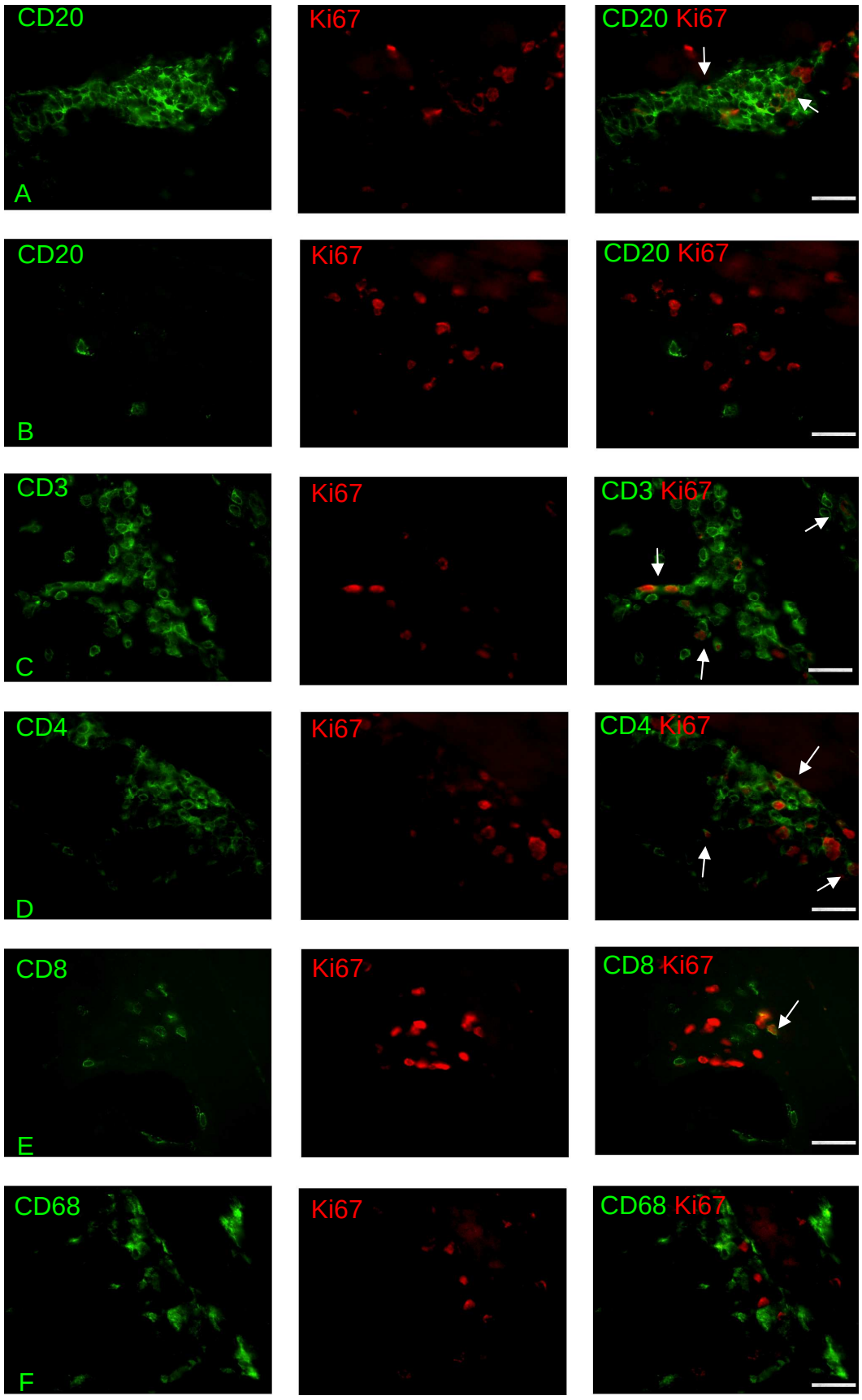

Figure 3.26 Double Immunohistochemical staining of serial muscle sections of sample MYOE

A representative example of serial muscle sections from sample MYOE stained for CD20 (**A-B**), CD3 (**C**), CD4 (**D**), CD8 (**E**), CD68 (**F**) and visualised by Fluorescein Avidin D before all sections were stained with Ki67 and visualised by Texas Red Avidin D. This allowed the type of proliferating cells within the myositis sample to be identified. Images were taken at 630X; Scale Bar represents 15 µm. Arrows identify proliferating cells within the sections.

3.2.13 Sample MYO25

Sample MYO25 was obtained from a healthy volunteer and was used as a control to identify any infiltrating cells within normal muscle. As shown in **Figure 3.27** no cell marker was identified within the normal muscle sections apart from the presence of some $CD68^+$ cells (**H**). As very few cell types were identified within sample MYO25 and with no $Ki67^+$ (**G**) cells found within the control section no double staining experiments were conducted.

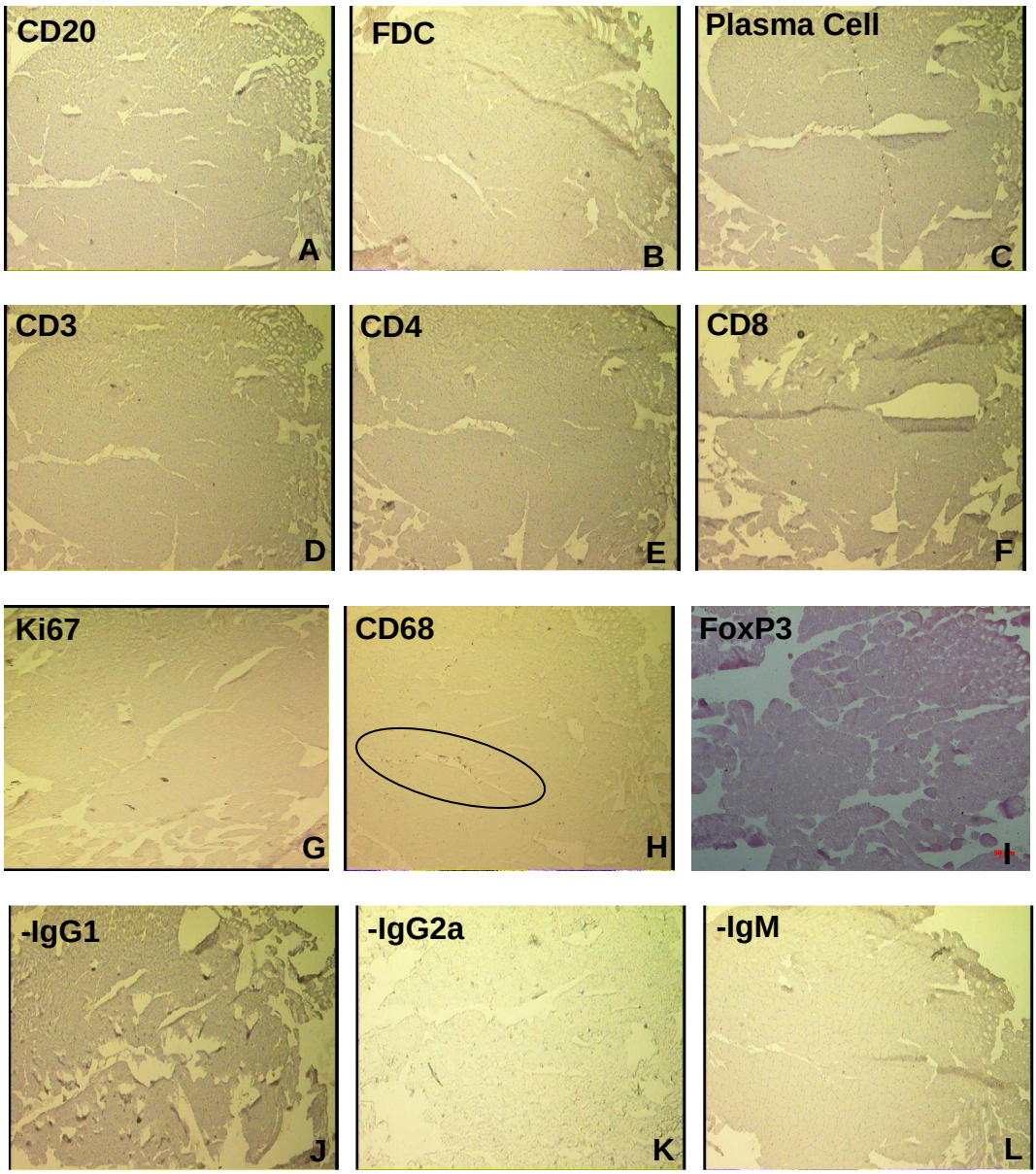

Figure 3.27 Immunohistochemistry of serial muscle sections of Sample MYO25.

A representative example of serial muscle sections from sample MYO25 stained for CD20 (**A**), FDC (**B**), Plasma cells (**C**), CD3 (**D**), CD4 (**E**), CD8 (**F**), Ki67 (**G**), CD68 (**H**) denoted by circle, FoxP3 (**I**), IgG1 Negative control (**J**), IgG2a Negative control (**K**), IgM Negative control (**L**) and visualised by APAAP and New Fuschin substrate to establish cellular infiltrates within the muscle section. Images A – L: 40X

3.2.14 Samples MYO2, MYOA, MYOD, MYO18 and MYO21

From the 17 myositis samples included in this study 5 samples did not contain a sufficient cellular infiltrate in serial sections that warranted further experiments (**Figure 3.28**). As the central aim of the work described in this chapter was to identify B cells and plasma cells to allow Ig gene repertoires and clonal diversification to be established, no further immunohistochemical analysis was conducted on these samples after the use of the CD20 and plasma cell markers revealed that these cell phenotypes were absent from the inflammatory infiltrating population. For sample MYO2 a large cellular infiltrate was observed in the muscle sections although this was very widespread between the muscle fibres in an endomysial pattern with no definite areas of aggregation observed. No B cells or plasma cells were clearly evident in the infiltrating population, a very light diffuse staining was observed while using the CD20 marker but this was non-specific and the same diffuse staining was also evident using in the negative control experiments. This may be the result of tissue damage that was observed in the sections as a result of tissue sectioning. Cellular infiltrates were also observed in samples MYO18 and MYO21, the degree of infiltration in these samples was substantially reduced in comparison to sample MYO2 but areas of cellular aggregation were observed. As previously mentioned no $CD20^{+}$ or plasma cells were evident within these samples. Use of additional cellular markers on these samples would have characterised the cellular phenotypes of the infiltrating population in these samples but as the aim of the study and central objective of this chapter was to identify B cells and plasma cells these experiments were not concluded. The identification of a cellular infiltrate within sample MYO18 is in contrast to the biopsy pathology report (**Table 2.2**) which indicated that no inflammatory infiltrate was observed. An inflammatory infiltrate was absent from the sections analysed for samples MYOA and MYOD, therefore no $CD20^{+}$ or plasma cells were found within these samples. The absence of an inflammatory infiltrate in sample MYOA was again in contrast to that reported within the biopsy pathology report which did report the presence of cells infiltrating the muscle biopsy. As with MYO18, the sections used in the analysis of MYOA were obtained from a different depth of muscle tissue compared to that used in the initial pathological assessment and may therefore account for the differences observed.

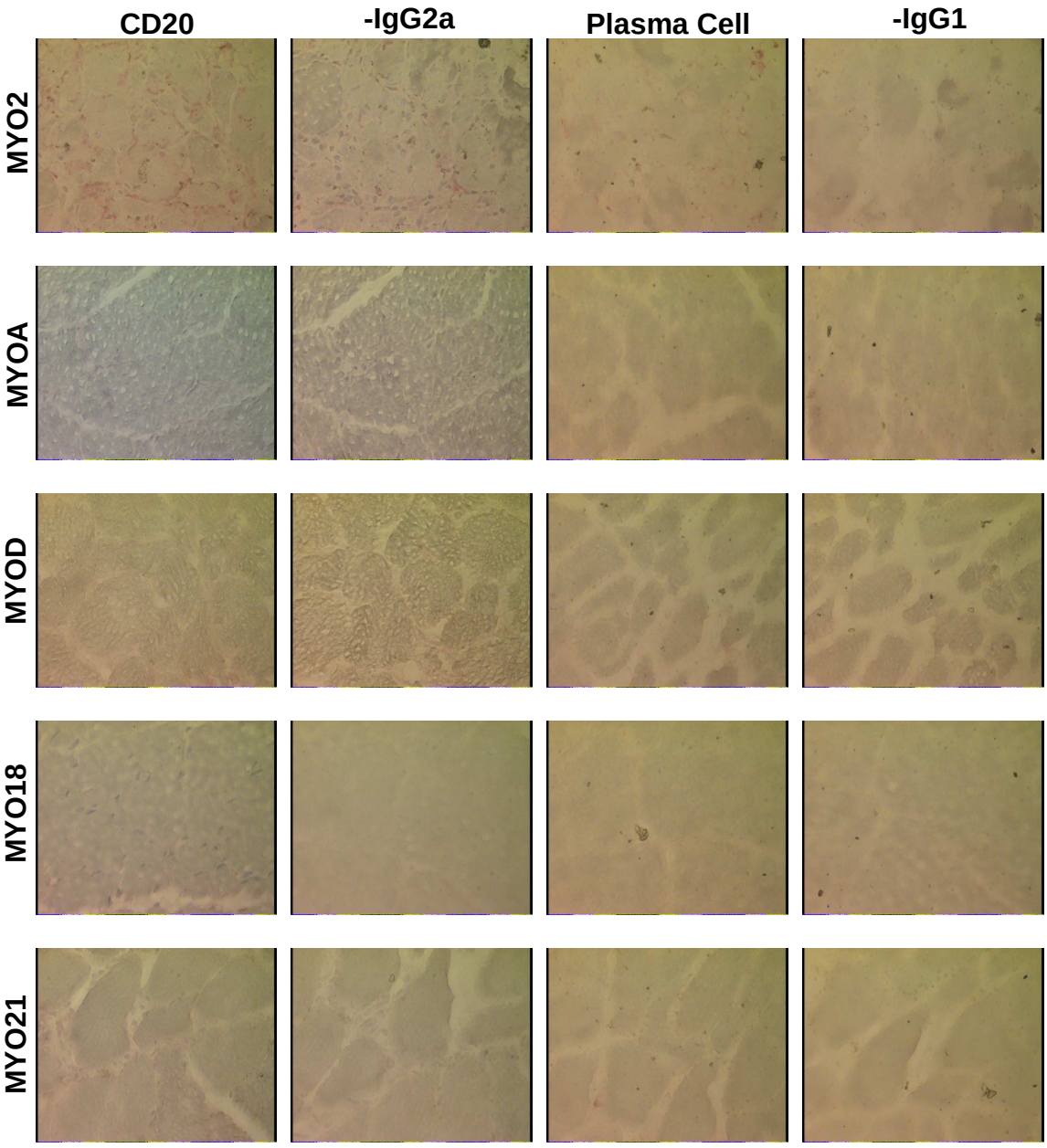

Figure 3.28 Immunohistochemistry of serial muscle sections of samples MYO2, MYOA, MYOD, MYO18 and MYO21

A representative example of serial muscle sections from the above samples stained for CD20, IgG2a Negative control, Plasma cells and IgG1 Negative control and visualised by APAAP and New Fuschin substrate to establish cellular infiltrates within the muscle section. From consecutive staining experiments from these serial sections no $CD20^{+}$ or plasma cells were observed within these sections, therefore no further analysis was conducted. Images at 400X.

3.3 Discussion

Identification and characterisation of B cells and plasma cells within the muscle infiltrating inflammatory population of cells was the main objective of the work presented in this chapter, this would allow further experiments to establish the Ig gene rearrangements expressed on muscle infiltrating B cells and plasma cells and determine if these cells were being locally stimulated within the muscle by assessing the somatic hypermutation and clonal diversification mechanisms. As well as these initial experiments to identify B cells, additional cell markers and double immunohistochemical experiments were conducted to identify and characterise follicular dendritic cells, macrophages, various T cell subsets and proliferating cells. The results of this chapter demonstrate that $CD20^+$ B cells and plasma cells were a substantial part of the muscle infiltrating population but that the infiltration of these cells as well as the other cell phenotypes identified was different between patients and myositis subsets.

Characterisation of inflammatory infiltrates in different myositis subsets have previously been established (87-89;297;298) with continuous studies facilitating the classification of muscle infiltrating populations to improve the understanding in the role of these cells within the disease mechanisms of the inflammatory myopathies. The current study supports the traditional observations as well as implicating additional roles for newly classified cells subsets, based on recent studies, of cellular infiltrates within inflammatory myopathies. Identification of proliferating cell phenotypes within the muscle disorders may also indicate the active participation of these cells in the pathogenesis of these disorders.

Unlike other studies investigating ectopic germinal centre type responses and the stimulation of B cells within the target tissues of various autoimmune disorders, such as MG (52), SS (283) and RA (284), no characteristic germinal centre type structures were observed within this study. Previous studies in muscle have not reported these structures and infiltrates, as previously described in Chapter 1, localise between or around muscle fibres either at perivascular, perimysial or endomysial sites depending on the myositis subset. Cellular infiltrates within this study were found to either form dense follicles of cells or loose aggregations, either perimysial or endomysial depending on the

myositis subset, with no distinct structure or pattern and additional scattered staining throughout the entire sample.

In the current study B cells were found to constitute a significant component of the inflammatory infiltrate in all samples examined, regardless of the myositis subset. These cells were either in their $CD20^+$ B cells state or differentiated plasma cell state and some of the $CD20^+$ B cells were found to be proliferating within the muscle. The heaviest infiltration of $CD20^+$ B cells were found in samples MYO1 and MYO16 corresponding to the diagnosis of these patients (Table 2.1). Both patients had a diagnosis of DM where larger populations of B cells are generally found in comparison to PM and IBM, as previously described in Chapter 1. Although at smaller and limited populations, $CD20^+$ B cell populations were observed in the majority of the patients who were diagnosed as PM and/or IBM. In 4 of these patients proliferating $CD20^+$ B cells were also observed which may indicate their active participation in an immune response.

In addition to these correlations plasma cells were evident within all samples of this study in varying degrees, regardless of the myositis diagnosis implicating a role for these variant B cell derived cells within these disorders. These results concur with recent studies further characterising inflammatory infiltrates within the myositis subsets as well as microarray studies which identified Ig transcripts, only transcribed in B cells and their progeny, in IBM and PM (89;299;300). Although B cells were identified in DM biopsies in earlier studies with very few present in PM and IBM (87;88), plasma cells were not identified in these studies for either myositis subset. The presence of plasma cells within inflammatory infiltrates was only recently studied in PM and IBM. Greenberg *et al* (89) identified few or no B cells within the infiltrating cell repertoire of inflammatory myopathies but did demonstrate the presence of $CD138^+$ plasma cells in the IBM and PM samples, confirmed by sequence analysis of Ig V-genes expressed by single laser dissected cells. These studies show that in IBM and PM plasma cells outnumber B cells by a factor of 4. A greater infiltration of plasma cells was observed within IBM samples in comparison to PM samples. It was also calculated that IBM had a mean of 0.84 times as many B cells and 4.3 times as many plasma cells compared to untreated

patients with DM. The numbers of $CD138^+$ plasma cells were also found to be smaller than the number of $CD3^+$ T cells. Recent studies have demonstrated the occurrence of autoantibodies in IBM reactive to a muscle constituent suggesting the involvement of a humoral immune response (97). The role of these plasma cells in this humoral immune response remains unclear. Despite implicating the participation of plasma cells in inflammatory myopathies the study did not show if plasma cell antibody production was a primary effector mechanism for muscle damage, any antigen specificity of the response and where the maturation of B cells into these plasma cells occurs. A question therefore remains on the role of these matured B cells within inflammatory myopathies. As plasma cells traditionally reside and secrete antibodies from the bone marrow (1) the presence of these cells within inflamed muscle may suggest an active pathological mechanism in these disorders, but why these cells locate to the inflamed muscle remains unresolved. Further studies would establish if non-specific infiltration of these cells occurs due to the formation of a suitable niche as a result of the inflammatory reaction, if antigen-specific cells, plasmablasts, are recruited and mature within the inflamed muscle or if complete ectopic germinal centre type responses occur within the muscle resulting in selection, diversification and maturation of B cells within the muscle.

The main objective of this study was to establish if B cell antigen-driven responses were occurring within inflamed muscle, reactions similar to germinal centre responses characterised by Ig gene selection, SHM and clonal diversification. For such reactions a population of FDCs would be expected similar to that observed in other studies of ectopic germinal centre responses (52;283;284) in order for antigen presentation and activation of high affinity B cells. Very few FDCs were identified within the samples of the current study; immunohistochemical analysis only identified these cells in 4 myositis patients within the study and demonstrated no distinct relationship with other cell types. These patients were diagnosed within PM or IBM and not DM where B cells are traditionally thought to play a greater role compared to PM and IBM. These findings may implicate that additional cell phenotypes substitute and take over the antigen presenting role of FDCs in muscle inflammatory reactions or may suggest that antigen-driven, germinal centre responses may not be occurring

within the target tissue of these myositis disorders although somatic mutation and activation of autoreactive B cells has been found to occur outwith the germinal centre response (301).

While the main intention of the work presented in this chapter was the identification of B cells and plasma cells in the muscle, additional cell phenotypes were also studied to examine the complexity of the immune response. Within myositis subsets $CD8^+$ cells are largely found in IBM and PM, demonstrating an endomysial pattern of infiltration while $CD4^+$ cells are generally characteristic of DM and display a perivascular/perimysial pattern of infiltration (87;88). In this study $CD3^+$, $CD4^+$ and $CD8^+$ cells, some proliferating ($Ki67^+$), were found in all autoimmune disorders studied and generally correlated with previous studies. $CD4^+$ cells are known to function through molecular mechanisms during contact with antigen presenting cells, in particular activation and maturation of B cells and production of cytokines while the function of $CD8^+$, cytotoxic, cells is largely undefined. These cells induce cell death, which is largely absent from muscle biopsies (302), through Fas, perforin and granzyme mechanisms. Perforin has been implicated in the pathogenesis of myositis with an increased expression in DM and PM compared to controls (85). In this study an additional subset of infiltrating T cells was examined, $FoxP3^+$ regulatory T cells (Tregs). The exact mechanisms of these cells are unknown but they are believed to play a pivotal role in controlling immune responses, maintenance of T cell homeostasis and controlling organ-specific autoimmune disorders. This T cell subset has not been extensively studied in inflammatory myopathies and the results of this chapter demonstrate that they are largely absent from the muscle infiltrating population. A considerable infiltration of these cells was only evident in 1 myositis specimen (MYO1, Figure 3.1) while a limited population were evident in 1 other patient (MYO24, Figure 3.21). Studies have occurred within other systems and have suggested that regulatory T cells may affect the maturation and antigen presentation capacity of DCs (27) and have also been shown to be defective in SLE patients (43). A novel type of regulatory T cells, $CD4^+$ $CD57^+$ $FoxP3^-$, has recently been reported in germinal centres of human tonsil tissues (303) and found to enhance the survival of GC B cells and have suppressive effects on

conventional $CD4^+$ $CD57^-$ T cells; an 80% reduction in cellular proliferation was observed. This collection of results established the dual role of $CD4^+$ $CD57^+$ T cells in promoting germinal centre B cell responses while suppressing conventional T cell responses. The presence or absence of regulatory T cells from inflammatory populations in muscle may play a role in the mechanisms in the muscle but additional studies would be required.

Although exact figures of cellular infiltrations were not calculated, some samples appeared to have greater staining for $CD3^+$ and $CD4^+$ cells in comparison to $CD8^+$ staining, regardless of the diagnosis. This is in contrast to previous studies where a larger population of $CD8^+$ cells were observed in PM and IBM (87;88). In some cases $CD4^+$ cells were more abundant than $CD3^+$ cells which is clearly illustrated for samples MYO3 (Figure 3.5), MYO7 (Figure 3.11) and MYOC (Figure 3.23). This correlates with other studies investigating cellular infiltrates in autoimmune inflammatory reactions (297). These studies have demonstrated that these $CD4^+$ cells may not all be the predicted $CD4^+$ T helper cells and may in fact be plasmacytoid dendritic cells (PDCs) which may be an important component in the myositis pathological mechanisms. While conventional or myeloid DCs are potent antigen-presenting cells and assist the adaptive immune response, PDCs play an important role in the innate immune response and are capable of producing interferon-α/β in quantities 200-1000 fold greater than other cell types which stimulates production of intracellular proteins capable of providing defence against pathogens (298). Greenberg *et al* (297) identified and studied $CD123^+$ BDCA-2^+ IFN-α^+ PDCs in DM muscle specimens and implicated these cells to the pathophysiology of DM. These cell types were abundant in 10 of 14 DM patients and were also present in muscle sections that lacked inflammatory cells with standard hematoxylin and eosin stains in routine clinical histopathological studies. These immunohistochemical results demonstrate that infiltrating PDCs are characteristic of DM. An upregulation of 86% of interferon-α and –β inducible genes was also observed in DM patients compared to 15% in other inflammatory myopathies in addition to the identification of MxA, an interferon-α/β-inducible protein in DM patients. These interferon signatures have recently been observed in peripheral blood samples of DM patients (304;305) and were also observed in PM patients in

one study (305). Qualitative analysis of 14 DM patients showed that 13 of these patients produced greater expression of CD4 compared to CD3. The study showed that there were approximately 5.3 times more $CD4^+$ cells than $CD3^+$ cells, suggesting that PDCs account for at least 30-90% of $CD4^+$ cells and they outnumber $CD4^+$ T cells by at least a factor of 2. More recent studies (306;307) identified these cells within the skin of DM patients. Wenzel *et al* (306) used anti-CD123 monoclonal antibodies and MxA to analyse the PDC infiltrating DM skin lesions and established that there was a significant increase of MxA expression in the epidermis and in the inflammatory infiltrate. $CD123^+$ cells, with plasmacytoid morphology, were found to heavily infiltrate the DM skin lesions compared to low levels observed in normal samples. McNiff *et al* (307) also identified PDCs within skin lesions of DM patients and established that this pattern was distinct from that observed in lupus erythematosus. Recently DCs have been identified in IBM, in addition to DM and PM (298), as well as in Juvenile DM (308). Greenberg *et al* (298) identified BDCA-1 positive cells (myeloid DCs) in IBM and PM specimens, widely distributed as well as loose aggregations of cells. Loose aggregations of cells were typically endomysial, which surrounded or invaded myofibres. Very few PDCs (BDCA-2 positive) were observed in these cell aggregations, myeloid DC numbers were 3 fold higher than that of PDCs. Similar numbers of myeloid and plasmacytoid cells were observed in perivascular and perimysial locations. Conversely in DM PDC numbers were 16 fold and 3 fold higher than myeloid DCs in endomysial and perivascular sites respectively. The precise role of DCs in inflammatory myopathies and other disorders has yet to be fully established. Myeloid DCs are generally believed to return to lymph nodes where they present antigen and activate, or suppress, helper T cells. PDCs are thought to have an immunomodulation role but have also been shown to act as antigen presenting cells (309) and have been shown to be critical for the generation of plasma cells and antibody responses (310), which may play a significant role in the pathophysiology of inflammatory myopathies.

The PDCs from Greenberg *et al* (297;298) were characterised as $CD4^+$, $CD68^+$, $CD123^+$ and BDCA-2^+ but CD68 was used as a cellular marker for infiltrating macrophages within this study therefore no definitive distinction can be made

between the two cellular phenotypes in this study. Further clarification of these cells types, with the use of additional cell markers, would be required to fully establish and evaluate the impact of both cell phenotypes on inflammatory myopathies. Double immunohistochemical studies within the current study demonstrated the presence of proliferating $CD68^+$ cells in some myositis patients, suggesting an active participation in the immune response. Previous studies (311) have found increased numbers of proliferating alveolar macrophages were observed in DM, PM patients as well as in systemic sclerosis patients compared to healthy volunteers. Recently macrophages in the lesion areas of atherosclerosis and RA patients have been found to express granzyme B, a cytotoxic protein thought to contribute to muscle pathology commonly found in $CD8^+$ T cells (312). A recent study has also demonstrated that human B cells can transfer BCR-targeted antigen to human macrophages and that the macrophages were able to capture B cell-derived membrane and/or intact intracellular proteins along with the antigen by a mechanism other that phagocytosis which is mediated by SR-A, class A scavenger receptors (313). The study postulates that this transfer of antigen from specific B cells to other APCs results in a more focused immune response and may indicate a possible immune mechanism within inflamed muscle.

Although characterisation of the muscle infiltrating populations provides valuable insights into inflamed muscle immune reactions, the effects of therapy on the inflammatory infiltrates needs to be considered. Under ideal conditions muscle specimens would be obtained from patients who had not received immunomodulatory therapy but as shown in Table 2.1 various patients were receiving various therapies at the time of biopsy which may alter the infiltration of inflammatory cells in muscle or the degree of muscle pathology observed within the specimens. As described in Chapter 1 statin therapy has been found to contribute to muscle pathology (49;69;70), although the mechanism of this has not been determined. Patients MYO24 and MYOC were both receiving statin therapy which may impact on the degree of muscle damage as well as the degree of cellular infiltration. The degree of muscle damage observed in sample MYO24 was found to exceed the damage observed by statin therapy, as observed by the reporting pathologist. Within the same report the non-

conspicuous infiltrate observed in this sample was attributed to the steroid therapy, 120 mg prednisolone intra-muscular injection. Corticosteroid therapy suppresses both cell-mediated and humoral immunity. In humoral immunity corticosteroids have been shown to reduce Ig concentrations (314;315) as well as influence the function of various cell phenotypes including PDCs and T cells (316). The use of steroid therapy could reduce or alter the cellular infiltrates observed within muscle inflammation and alter the true heterogeneity of the immune reactions. In this study 8 patients (MYO 5, 19, 23, 24, C, E, 2, 18) were receiving steroid therapy at the time of biopsy. Despite the influence of therapy significant inflammatory infiltrates, in particular B cells and plasma cells were observed in a number of these samples (MYO5, 19, 23, C, E). Other immunosuppressive therapies, such as methotrexate, may also disguise the true heterogeneity of the response. Underlying medical conditions and family history may also play a role in the results presented in this chapter. 3 of these patients (MYO3, 24, D – Table 2.1) had underlying carcinomas while patient MYO19 was treated for inflammatory synovitis. Patient MYO5 also had a background of Sjögrens syndrome and a strong family history of autoimmune disease which may come into play while assessing the mechanism of the muscle inflammation observed within such patients. A final consideration would be the area selected for biopsy, due to the large area affected by the inflammation and the small specimen obtained for diagnosis and these studies, considerable difference may be observed between different muscle sites.

To summarise, the work presented in this chapter demonstrates that B cells and their differentiated counterpart's plasma cells are substantial within the infiltrating inflammatory population of myositis disorders. The characterisation of proliferating B cells may indicate the active participation of these cells in the muscle response. B cells and plasma cells were identified in association with a number of additional cell phenotypes, illustrating the complexity of immune reactions within muscle. The identification of B cells and plasma cells within these samples allowed further work to be conducted to determine if B cells play an active role in antigen-driven responses within the inflamed muscle.

Chapter 4 - V_H-Gene Repertoire and Clonal Diversification of Muscle Infiltrating B Cells in Myositis

4.1 Introduction

As previously discussed in Chapter 1, the role of B cells and plasma cells, and the antibodies they produce, in the autoimmune disease of myositis is still unresolved although B cells have been thought to contribute to the pathological immune response at these sites of inflammation. The work conducted in Chapter 3, in addition to previously published work, classified the phenotypes of infiltrating cells in the inflammatory reactions of myositis of which B cells, and their differentiated counter-parts plasma cells, were prominent. Despite the presence of these cells within the inflammatory infiltrate no characteristic germinal centre formations, the typical sites of somatic hypermutation and clonal diversification, were observed at these ectopic sites. What remains unclear is the role of these B cells and plasma cells within the inflammatory infiltrate; therefore the work of this chapter aims to establish a role for these cells within myositis samples. To determine if infiltrating lymphocytes were being stimulated locally to respond to an endogenous antigen resulting in tissue damage, areas of significant B cell and plasma cell infiltration established in Chapter 3 were microdissected from tissue sections. The rearranged Ig gene amplification from the DNA of these cells was used to address the following key aims of the chapter;

- Establish the Ig gene repertoire of infiltrating B cells and plasma cells to determine if positive, or negative, gene selection was occurring within infiltrating cells.
- Analyse V_H gene point mutations (number, location and category) to establish if clonally related B cells, with shared VDJ and CDR3 sequences, are present within the muscle inflammatory infiltrate undergoing an antigen-driven B cell response.

For the results of this chapter the patients were studied individually in addition to collective myositis analysis.

4.2 V_H Repertoire and Sequence Analysis in Myositis

4.2.1 Sample MYO1

4.2.1.1 V_H Gene Repertoire of Infiltrating B Cells from MYO1

B cell aggregates from frozen sections from sample MYO1 were microdissected and the Ig rearrangements were amplified by nested PCR (**Figure 4.1**), cloned and sequenced. Over 150 sequences were analysed from the 6 different regions of cellular infiltration observed and the best matching germline genes were identified (**Table 4.1**). The gene usage distribution of functional gene rearrangements was analysed from 57 sequences as multiple copies of genes arose within the same regions of cellular infiltration (**Figure 4.2**). Using absolute values in Chi square analysis, significant selections were observed for V_H2 and V_H3 genes against the normal control values (**Figure 4.2A**). No other selections were observed against normal control values or the germline composition. Despite the selection for V_H2 and V_H3 genes, the V_H gene distribution followed the distribution pattern of that described in the normal control data, $V_H3>V_H4>V_H1>V_H2>V_H5>V_H6>V_H7$ (251). D_H gene assignments were conducted as described in section 2.3.12.3, V-J lengths and consecutive D match lengths are shown in Table 4.1. D_H genes could be assigned to 66.7% of the sequences isolated from sample MYO1. Comparing the distribution of these genes to both the normal control values and the germline composition demonstrated that there was no selection for or against any D_H gene families (**Figure 4.2B**). Selections against J_H1 and J_H2 genes were observed within the sequences (**Figure 4.2C**), but these were only significant against the germline composition. Analysis of the J_H gene usage compared to normal control values revealed no positive or negative J_H gene selections within the infiltrating repertoire.

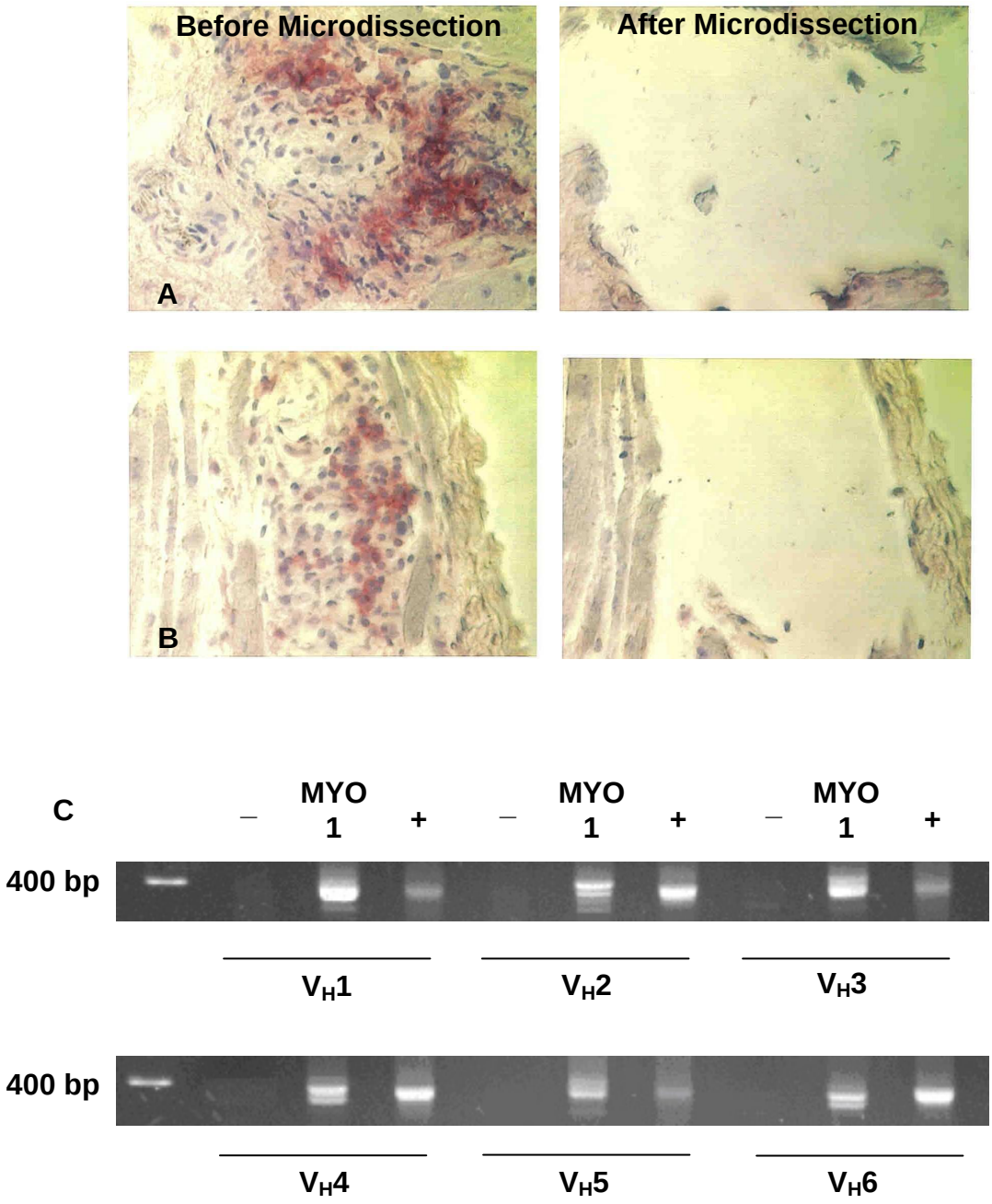

Figure 4.1 Microdissection of infiltrating B cells and amplification of V_H-gene rearrangements from Sample MYO1

Six areas of B cell and plasma cell infiltration were microdissected from sample MYO1. Figure 4.1A and B demonstrates the microdissection of 2 regions of cellular infiltration. Images were taken at 400X. DNA released from these microdissections was amplified using a Nested PCR system (Figure 4.1C), as previously described in Chapter 2. – indicates negative control PCR reactions where DNA was substituted with water while + indicates positive control PCR reactions using peripheral blood mononuclear cells isolated from peripheral blood of a healthy individual. Results show amplification of all 6 V_H families.

Region	V_H Gene	D_H Gene	J_H Gene	Number of Isolated Sequences	Number of Point Mutations	CDR3	V-J Length (bp)	Consecutive D length (bp) (+Mismatches)
1	1-46*01	3-10*01	5*02	1	1	ARSVWFRELLEVQNWFDP	33	18(+1)
	3-07*01	No D gene Assignment	6*02	1	12	AREGKEGYGMDV	12	10(+3)
	3-23*01	5-12*01	3*02	1	0	AKGGGYDWGDDAFDI	24	12
	3-30*04	4-17*01	3*02	1	11	AKDFGYDYGDYLYDAFDI	34	16
	3-43*01	3-10*01	5*02	(1)	1	AKDPYSGSYYATGST	28	22
	3-48*01	3-22*01	3*02	(1)	0	ARGSMVL**WDLI	27	12
	3-66*01	No D gene Assignment	6*02	1	0	ARERALYYYGMDV	10	5
	4-39*01	No D gene Assignment	4*02	1	0	ARHGLSEPYQQPPGYRFDY	40	12(+3)
	4-59*01	3-22*01	5*02	(1)	0	ARA*TYYYDSSGYYSTTGST	38	29
	4-59*01	6-13*01	6*02	1	2	ARHGKKQQLTRNYYYGMDV	28	11
	5-51*03	No D gene Assignment	6*02	1	27	VRHAPYYFYGMDV	22	5
2	3-09*01	6-13*01	4*02	(1)	0	AKDIPF*GIAAAGTLPPPGTS*L	53	20
	3-33*01	3-22*01	4*02	4	10, 11, 11, 12	AREFYDTSGYWEDC	33	19(+1)
	4-59*01	1-1*01	5*02	1	0	ARVLYNWNGGFGRFDP	30	13
3	3-30*04	No D gene Assignment	3*02	(1)	29	AIDRLAG*	17	7
	3-30*04	No D gene Assignment	4*02	4	11, 12, 12, 14	ARDRRGGWEGYFDY	21	6
	3-30*04	No D gene Assignment	4*02	(1)	13	ARDRGGGMGGLL*L	22	8
	3-30*04	No D gene Assignment	6*01	1	11	ARDR	3	6
	3-30*04	No D gene Assignment	6*01	1	11	ARDRRGG	13	6
4	2-05*01	No D gene Assignment	2*01	1	0	AHSRARLEGYFDL	17	6
	3-07*02	6-19*01	6*02	2	12, 13	ARDLGSSGWHVNPEMFYYHAMDV	54	13
	4-04*02	No D gene Assignment	4*02	1	19	ARGQLGNFDS	22	8
	4-31*03	3-22*01	5*01	1	8	ARGNYDMTSDS	20	9
	5-a*01	4-23*01	5*01	1	10	ARHGADYGGNPEGFDS	31	15
5	1-46*01	1-26*01	4*02	1	0	ARTRIVGATRSIDY	32	18
	1-69*04	1-26*01	4*03	1	0	ARTRIVGATRSIDY	32	18
	1-69*04	3-16*02	4*02	1	0	ARDVWEIFGSGSYPYFDY	34	10
	1-69*09	3-16*02	4*02	1	0	ARDVWEIFGSGSYPYFDY	34	10
	2-05*10	1-1*01	5*02	2	20, 21	AHRLGGYSWNDGWFDP	31	14(+1)
	2-05*01	No D gene Assignment	6*02	2	7, 8	ARREFSWGMDV	17	7
	3-15*01	3-10*01	4*02	4	11, 12, 13, 13	TTDTRPRLGEFFYFWVGYFDP	54	10
	3-23*01	No D gene Assignment	6*02	2	33, 44	VKNSGSGKPYYYAMDV	37	7
	3-30*03	6-19*01	4*02	2	0, 1	AFSDNSGYHN	25	11(+1)
	3-30*04	3-3*01	4*02	2	0, 1	ARDVHDFWSGYHFDY	26	19
	3-48*02	2-21*01	3*02	1	0	ARDYPDCGGDCSPYDAFDI	33	18
	3-66*01	2-21*01	3*02	2	26, 31	ARDYPDCGGDCSPYDAFDI	33	18

Cont…

Region	V_H Gene	D_H Gene	J_H Gene	Number of Isolated Sequences	Number of Point Mutations	CDR3	V-J Length (bp)	Consecutive D length (bp) (+Mismatches)
6	1-08*01	2-8*02	6*02	1	0	ARGRYCTGGVCYRDASYYYYGMDV	42	27
	1-18*01	No D gene Assignment	6*02	1	15	ARTQTPDLYAIFGHYYGMDV	40	10(+1)
	2-05*01	3-3*01	4*02	(1)	12	AHILAYYDFCSA*SPLLALT	54	15
	3-11*03	4-17*01	6*02	2	0, 1	ARDKPYGDSRNNWYYYYYGMDV	33	11
	3-23*01	1-26*01	4*02	1	0	AKDEGWVVGATKAPFDY	33	15
	3-30*03	6-19*01	4*02	1	0	AKLGSYNSGRDY	25	11 (+1)
	3-49*03	2-2*01	4*02	1	17	TRGNHLYCSSHSCYWDS	48	21(+4)
	4-b*02	No D gene Assignment	5*02	1	14	ARDDLPIRFDP	16	5
	4-04*02	No D gene Assignment	4*02	1	5	ARVTTGFFFDY	18	7
	4-59*01	5-12*01	5*02	1	17	ARQGTVGSAYSGSDP	35	14(+1)
	4-59*01	6-19*01	6*02	1	5	ARRRGGWYSSGHRGNYGMDV	37	14

Table 4.1 Heavy chain genes identified from myositis sample MYO1

Best matching germline sequences were identified from aligning sequences in the IMGT database using JOINSOLVER software from regions 1 to 6 within the MYO1 myositis section. The total number of sequences isolated is given in the 5th column of the table; non-functional rearrangements indicated in brackets. Identical sequences with the same V_H, D_H, J_H, CDR3 and base mutations were only counted once. CDR3 amino acid sequences were also identified using the JOINSOLVER software; * indicates the presence of a stop codon within the CDR3. V-J lengths and consecutive D match lengths (bp) were also identified using the JOINSOLVER software and allowed assignment of the D_H genes as described in section 2.3.12.3.

In addition to determining the gene assignments using the JOINSOLVER software, the IMGT/V-QUEST algorithm was also used to verify the gene assignments for this sample as well as all other samples in the study. For the majority of sequences the gene assignments matched the JOINSOLVER software but in some cases IMGT/V-QUEST determined a different match for part of the gene rearrangement or detected deletions or insertions within the sequence altering the gene assignment (**Appendix 1**). In cases where JOINSOLVER was unable to assign a D gene with statistical significance the region was also examined using the IMGT/V-QUEST software but no additional D gene assignments could be made with confidence. In contrast to JOINSOLVER, IMGT/V-QUEST failed to find a rearrangement for the sequence in region 3 using V_H3-30*04 (CDR3-ARDRRGG) and was only able to identify the same V_H gene segment. Also in region 3 with another Ig using the V_H3-30*04 (CDR3-ARDR) IMGT/V-QUEST categorised this sequence as non-functional and was not able to identify any D gene segments. In region 5 for the Ig using the V_H1-69*09 D_H3-16*01 J_H4*02 rearrangement IMGT/V-QUEST assigned the D gene as 3-10*01 which was the 2nd highest matching score in

JOINSOLVER but D_H3-16*01 had a higher consecutive match. If mismatches were incorporated into the analysis of the D_H3-10*01 gene it would have a D consecutive match length of 14 with 1 mismatch which may therefore indicate that the D_H3-10*01 gene should be assigned although no mismatch analysis had to be conducted on the D_H3-16*01 gene for it to be statistically assigned. The D_H3-16*01 gene was not identified in the top 5 matched using the IMGT/V-QUEST software. Also IMGT/V-QUEST assigned the J_H segment as 2P*01 but also suggested the gene segments of 6*01 and 6*02, these genes were found to be outwith the 6 best matching genes in JOINSOLVER with the 6*01 and 6*02 genes generating negative alignment scores. The 4*02 gene segment identified by JOINSOLVER was the 4th best matching gene in IMGT/V-QUEST. For the Ig rearrangement V_H3-15*01 D_H3-10*01 J_H4*02 in region 5 both JOINSOLVER and IMGT/V-QUEST identified two J_H genes that could possibly be assigned to the rearrangement, 4*02 and 5*02. In JOINSOLVER and IMGT/V-QUEST the 4*02 gene had a score of 195 while the 5*02 gene had a score of 192. Although the 5*02 gene had a greater number of consecutive matches both sequences exhibited a higher number of germline matches therefore either gene could be assigned, mismatches could be interpreted as mutations. Insertions and deletions were detected in Ig rearrangement V_H3-23*01 D_H3-10*01 J_H6*02 with 44 mutations. Once these had been resolved the gene rearrangement was revealed to be non-functional in IMGT/V-QUEST with the same gene assignments but with 34 mutations. 33 of these mutations were common between this sequence and the other sequence with the same gene rearrangement shown in Table 4.1 but an additional silent mutation was observed in codon 88 at the 3rd nucleotide position. A deletion was also detected in the CDR2 for both sequences with the V_H3-66*01 D_H2-21*01 J_H3*02 in region 5. Once the deletions had been restored the Ig rearrangement obtained was V_H3-48*02 D_H2-21*01 J_H3*02 in both the JOINSOLVER and IMGT/V-QUEST software although IMGT/V-QUEST also determined the J_H segment may also be assigned as J_H6*02 which exhibited a higher consecutive match in IMGT/V-QUEST. These sequences contained 1 and 11 mutations with no common mutations between the sequences.

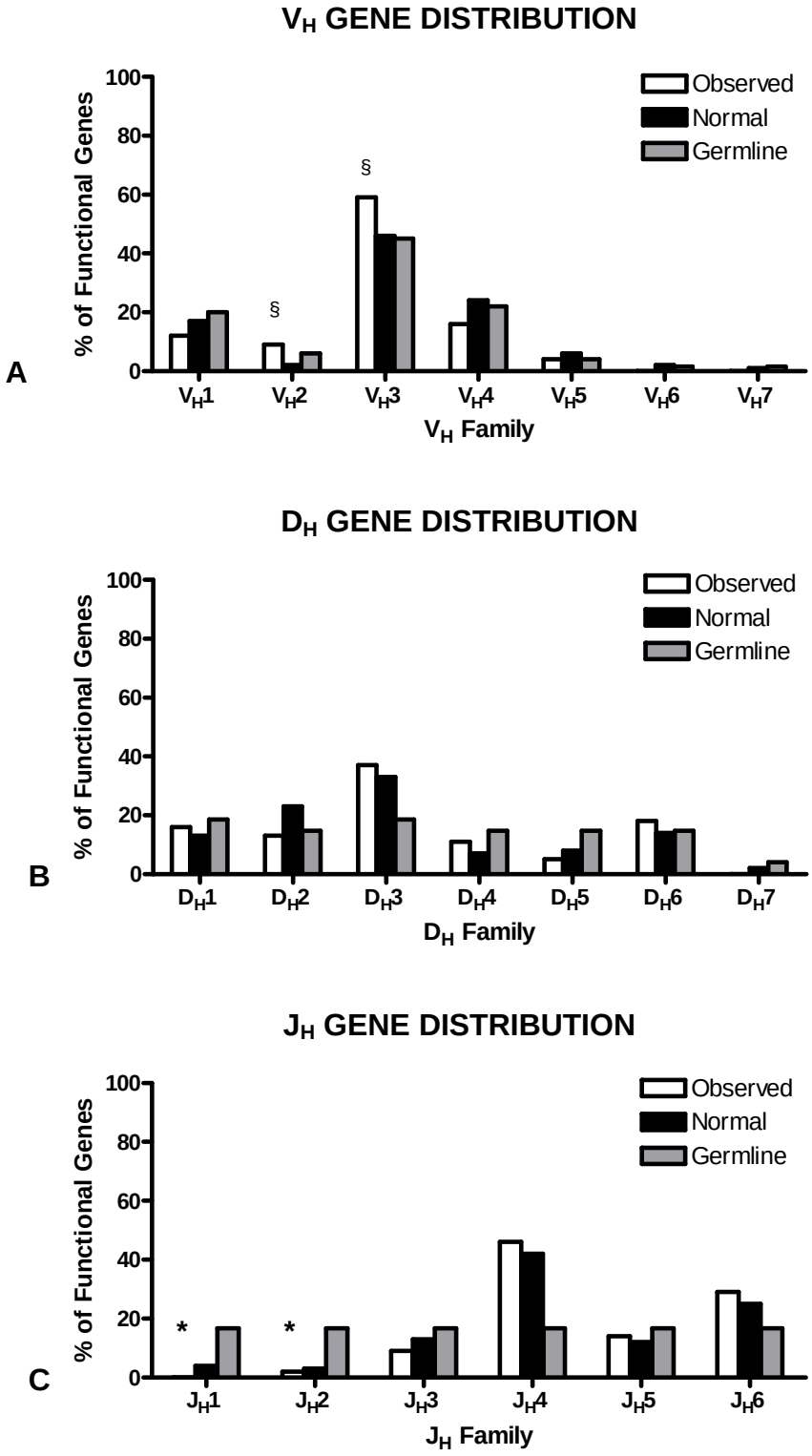

Figure 4.2 V_H Gene Family Usage of MYO 1

V_H gene family usage. Distribution of functional genes was compared with published normal control values from Volpe and Kepler (251) as well as the germline complexity assuming every germline gene is capable of producing a functional rearrangement. Absolute values were used in Chi Square Analysis to determine gene selections. § represent a significant difference from normal control values; * represent a significant difference from the germline ($p<0.05$).

4.2.1.2 Mutational Analysis of B Cell Ig Sequences of Sample MYO1

Numbers of mutations within the V_H gene segment of the functional gene rearrangements were analysed (**Figure 4.3A**). Results demonstrate that approximately 30 to 40% of sequences are virtually non-mutated with only 0 to 2 mutations within the V_H segment of the gene rearrangement while a further 30 to 40% contains 11 to 20 mutations within the V_H segment. Sequences containing 3 to 10 and over 20 mutations were found in approximately 10% of the infiltrating cells respectively. In addition to mutational numbers, the location of mutations was analysed between Framework regions (FR) and Complementarity Determining Regions (CDR) regions (**Figure 4.3B**). The number of mutations in each segment was expressed as a percentage of the total length of the segment. Results demonstrate a higher percentage of mutations within CDR regions compared to framework regions for rearranged genes. A higher percentage of mutations were observed in CDR1 compared to CDR2.

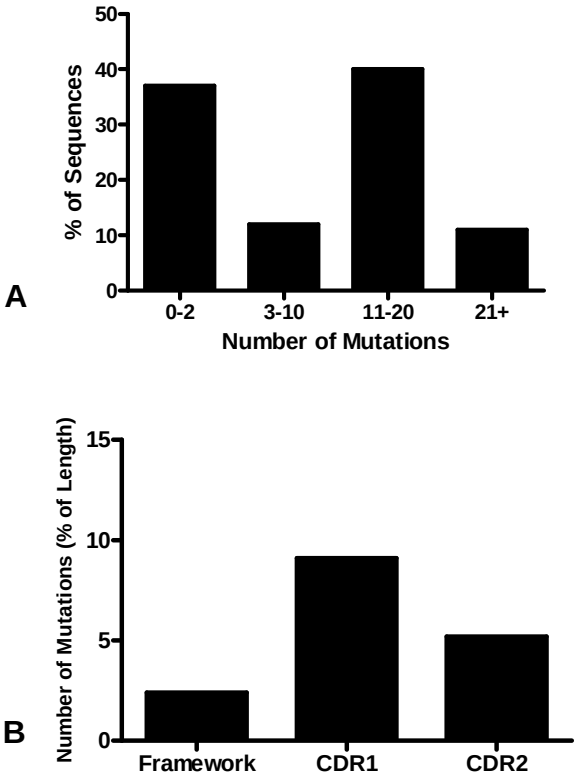

Figure 4.3 Numbers of Mutations and Mutational Distribution of Functional Sequences in MYO1

Figure 4.3A - The number of mutations within functional rearranged genes were analysed collectively from all 6 regions of cellular infiltration. Base differences within the first 24 bases of sequence were disregarded as this part of the sequence binds the 5' V_H primer. Graph demonstrates sequences within cellular infiltrates show a diverse distribution of mutational numbers.

Figure 4.3B - The locations of mutations observed within functional rearranged genes were categorised as being within FR or CDR regions. The numbers of mutations within these regions were expressed as a percentage of the entire length of the region to correct for the longer lengths observed within the framework regions. Graph demonstrates a higher percentage of mutations within CDR regions compared to framework regions.

The type of mutations, replacement and silent, in the V_H gene segment of the immunoglobulin gene were also analysed (**Table 4.2**), according to the revised method by Hershberg *et al* (294) described in section 2.3.12.3. This updated

analysis determined if positive or negative mutational selections were occurring within each sequence of the infiltrating repertoire. A significant selection was only observed in 8 of the sequences from all 6 regions. The only sequence which demonstrated selection in the CDRs was a non-functional rearrangement in region 3; results revealed a negative selection within the CDR. All remaining sequences with a significant selection also demonstrated negative selection but in these sequences the negative selection was observed in the framework regions of the sequences.

4.2.1.3 CDR3 Analysis

Analysis of the VDJ junctional area within the sequences demonstrated that the mean amino acid CDR3 length within functional sequences was 15.3 ± 0.5 (ranging from 4 to 24 amino acids) which was not significant against the non-functional repertoire (ranging from 8 to 23 amino acids) (**Table 4.3**). The CDR3 length was also analysed in relation to the number of V_H mutations observed within the sequence (**Figure 4.4**). The average CDR3 length was calculated for sequences in particular mutational ranges, as previous studies have shown a reduced CDR3 length in highly mutated sequences (238). For this sample no significant changes in the CDR3 length were observed for the different mutational groups. The numbers of P and N nucleotides at the VD and DJ junctions were also analysed (**Table 4.3**), from the sequences isolated in this sample no significant difference in these nucleotides was observed between the functional and non-functional sequences. There was also no significant difference in the numbers of P and N nucleotides between the VD region of the junction and the DJ region. Exonuclease activity at the 3' of the V_H gene segment was shown to be significantly lower from the $5'D_H$ and $5'J_H$ exonuclease activity in the functional repertoire. No significant differences in exonuclease activity between the functional and non-functional repertoires were observed at any point of the junction.

Region	V_H Gene	D_H Gene	J_H Gene	Number of Isolated Sequences	Number of Point Mutations	R-CDR	S-CDR	pCDR	p-CDR	R-FW	S-FW	pFW	p-FW
1	1-46*01	3-10*01	5*02	1	1	0	0	0.47626	**-0.52374**	0	1	0.674002	**-0.326**
	3-07*01	No D gene Assignment	6*02	1	12	4	2	0.44397	**0.988952**	3	3	0.670119	**-0.1031**
	3-23*01	5-12*01	3*02	1	0	-	-	-	**-**	-	-	-	**-**
	3-30*04	4-17*01	3*02	1	11	6	0	0.47645	**0.141781**	3	2	0.672622	**-0.7284**
	3-43*01	3-10*01	5*02	(1)	1	0	0	0.45644	**0**	1	0	0.678704	**0.6787**
	3-48*01	3-22*01	3*02	(1)	0	-	-	-	**-**	-	-	-	**-**
	3-66*01	No D gene Assignment	6*02	1	0	-	-	-	**-**	-	-	-	**-**
	4-39*01	No D gene Assignment	4*02	1	0	-	-	-	**-**	-	-	-	**-**
	4-59*01	3-22*01	5*02	(1)	0	-	-	-	**-**	-	-	-	**-**
	4-59*01	6-13*01	6*02	1	2	0	0	0.44001	**-0.31358**	0	2	0.656452	**-0.118**
	5-51*03	No D gene Assignment	6*02	1	27	6	2	0.43118	**-0.66779**	11	8	0.700775	**-0.0924**
2	3-09*01	6-13*01	4*02	(1)	0	-	-	-	**-**	-	-	-	**-**
	3-33*01	3-22*01	4*02	4	10	3	1	0.46759	**-0.6274**	2	4	0.673935	**-0.0473**
					11	3	1	0.46759	**-0.44768**	2	5	0.673935	**-0.0198**
					11	3	1	0.46759	**-0.6274**	3	4	0.673935	**-0.0982**
					12	3	1	0.46759	**-0.44768**	3	5	0.673935	**-0.0453**
	4-59*01	1-1*01	5*02	1	0	-	-	-	**-**	-	-	-	**-**
3	3-30*04	No D gene Assignment	3*02	(1)	29	2	3	0.47645	**-0.02004**	16	8	0.672622	**-0.3824**
	3-30*04	No D gene Assignment	4*02	4	11	2	3	0.47645	**-0.34645**	4	2	0.672622	**-0.1747**
					12	3	3	0.47645	**-0.59353**	4	2	0.672622	**-0.1747**
					12	2	3	0.47645	**-0.22438**	4	3	0.672622	**-0.0883**
					14	3	3	0.47645	**-0.59353**	6	2	0.672622	**-0.3876**

Cont…

Region	V_H Gene	D_H Gene	J_H Gene	Number of Isolated Sequences	Number of Point Mutations	R-CDR	S-CDR	pCDR	p-CDR	R-FW	S-FW	pFW	p-FW
	3-30*04	No D gene Assignment	4*02	(1)	13	2	3	0.47645	**-0.34645**	6	2	0.672622	**-0.3876**
	3-30*04	No D gene Assignment	6*01	1	11	2	3	0.47645	**-0.34645**	4	2	0.672622	**-0.1747**
	3-30*04	No D gene Assignment	6*01	1	11	2	3	0.47645	**-0.34645**	4	2	0.672622	**-0.1747**
4	2-05*01	No D gene Assignment	2*01	1	0	-	-	-	**-**	-	-	-	**-**
	3-07*02	6-19*01	6*02	2	12	6	2	0.44221	**0.338457**	2	2	0.668099	**-0.1162**
					13	6	2	0.44221	**0.338457**	3	2	0.668099	**-0.2156**
	4-04*02	No D gene Assignment	4*02	1	19	6	2	0.43349	**0.8366**	6	5	0.665093	**-0.1415**
	4-31*03	3-22*01	5*01	1	8	3	0	0.43271	**0.253968**	4	1	0.653402	**0.55407**
	5-a*01	4-23*01	5*01	1	10	1	2	0.45272	**-0.1871**	4	3	0.702728	**-0.1197**
5	1-46*01	1-26*01	4*02	1	0	-	-	-	**-**	-	-	-	**-**
	1-69*04	1-26*01	4*03	1	0	-	-	-	**-**	-	-	-	**-**
	1-69*04	3-16*02	4*02	1	0	-	-	-	**-**	-	-	-	**-**
	1-69*09	3-16*02	4*02	1	0	-	-	-	**-**	-	-	-	**-**
	2-05*10	1-1*01	5*02	2	20	2	2	0.44387	**-0.08592**	9	7	0.6816	**-0.1155**
					21	2	3	0.44387	**-0.05531**	9	7	0.6816	**-0.0652**
	2-05*01	No D gene Assignment	6*02	2	7	4	1	0.44837	**0.320677**	1	1	0.681376	**-0.2722**
					8	5	1	0.44837	**0.185831**	1	1	0.681376	**-0.2722**
	3-15*01	3-10*01	4*02	4	11	5	1	0.43976	**0.320397**	4	2	0.659501	**-0.6303**
					12	5	1	0.43976	**0.320397**	4	2	0.659501	**-0.6303**
					13	5	1	0.43976	**0.320397**	5	2	0.659501	**-0.8228**
					13	5	2	0.43976	**0.505038**	4	2	0.659501	**-0.369**
	3-23*01	No D gene Assignment	6*02	2	33	9	6	0.45266	**-0.45643**	9	9	0.650002	**-0.0071**
					44	9	6	0.45266	**-0.28386**	18	11	0.650002	**-0.1018**

Cont…

Region	V_H Gene	D_H Gene	J_H Gene	Number of Isolated Sequences	Number of Point Mutations	R-CDR	S-CDR	pCDR	p-CDR	R-FW	S-FW	pFW	p-FW
	3-30*03	6-19*01	4*02	2	0	-	-	-	-	-	-	-	-
					1	0	1	0.46606	**-0.53394**	0	0	0.674321	**-0.3257**
	3-30*04	3-3*01	4*02	2	0	-	-	-	-	-	-	-	-
					1	0	1	0.476452	**-0.523548**	0	0	0.672622	**-0.327378**
	3-48*02	2-21*01	3*02	1	0	-	-	-	-	-	-	-	-
	3-66*01	2-21*01	3*02	2	26	12	4	0.46522	**0.340486**	5	5	0.668169	**-0.0208**
					31	15	3	0.46522	**0.185352**	6	7	0.668169	**-0.0193**
6	1-08*01	2-8*02	6*02	1	0	-	-	-	-	-	-	-	-
	1-18*01	No D gene Assignment	6*02	1	15	6	2	0.47674	**0.279322**	6	1	0.688086	**-0.8666**
	2-05*01	3-3*01	4*02	(1)	12	3	2	0.44837	**0.807761**	6	1	0.681376	**-0.8999**
	3-11*01	4-17*01	6*02	2	0	-	-	-	-	-	-	-	-
					1	1	0	0.47238	**0.472384**	0	0	0.664488	**0**
	3-23*01	1-26*01	4*02	1	0	-	-	-	-	-	-	-	-
	3-30*03	6-19*01	4*02	1	0	-	-	-	-	-	-	-	-
	3-49*01	2-2*01	4*02	1	17	5	2	0.44618	**0.529547**	8	2	0.663604	**1.00709**
	4-b*02	No D gene Assignment	5*02	1	14	3	0	0.42687	**0.474147**	9	2	0.653301	**0.26984**
	4-04*02	No D gene Assignment	4*02	1	5	1	0	0.44897	**-0.74359**	2	2	0.659438	**-0.5379**
	4-59*01	5-12*01	5*02	1	17	4	3	0.44001	**-0.18652**	2	8	0.656452	**-0.0003**
	4-59*01	6-19*01	6*02	1	5	1	1	0.44001	**-0.50574**	1	2	0.656452	**-0.1343**

Table 4.2 Analysis of Replacement and Silent Mutations and Positive and Negative Selection in Sample MYO1

Replacement and silent mutations within the immunoglobulin sequences and antigen-driven selection were determined according to Hershberg *et al* (294) and the corresponding computer programme (http://clip.med.yale.edu/selection). This improved method of analysis uses a focused binomial test to establish positive or negative mutational selections within the sequence with high specificity and increased sensitivity accounting for known biases within the immunoglobulin gene sequence. R-CDR and S-CDR represents the number of replacement and silent mutations within the CDR respectively. pCDR represents the probability of having a R mutation in the CDR given all the mutations in the sequence except R mutations within the FW while p-CDR is the p-value of the focused binominal test on the CDR. Conversely R-FW and S-FW represents the number of replacement and silent mutations within the FW respectively. pFW represent the probability of having a R mutation in the FW given all the mutations in the sequence except R mutations within the CDR while p-FW is the p-value of the focused binominal test on the FW. If the number of R mutations is less than expected the software will test for negative selection and p-values will be preceded by a negative sign or if the number of mutations is more than expected the software will test for positive selection. p-values <0.05 are highlighted in yellow and were deemed significant for selection.

CDR3 Length	Functional	15.3 ± 0.5			
	Non-Functional	16.1 ± 1.9			
		VD Junction		DJ Junction	
P Nucleotide	Functional	0.6 ± 0.1		0.4 ± 0.1	
	Non-Functional	1.4 ± 0.7		0.4 ± 0.4	
N Nucleotide	Functional	8.7 ± 0.8		7.7 ± 0.9	
	Non-Functional	6 ± 1.5		10.2 ± 4.1	
		3' V_H	5' D_H	3' D_H	5'J_H
Exonuclease Activity	Functional	1.2 ± 0.2	5.6 ± 0.8 $^{\theta}$	4.7 ± 0.5	4.9 ± 0.6$^{\theta}$
	Non-Functional	2 ± 0.7	2.2 ± 1.2	6.2 ± 2.9	4.6 ± 1.6

Table 4.3 CDR3 and Junctional Analysis in Sample MYO1

The mean amino acid length of the CDR3, the mean nucleotide numbers corresponding to P and N nucleotides as well as the mean number of germline nucleotides lost due to exonuclease activity were calculated from the junctional regions of all immunoglobulin sequences from sample MYO1. Results are given as the Mean ± SEM, statistical significance was established using an unpaired t-test. Θ represents a significant difference from 3'V_H.

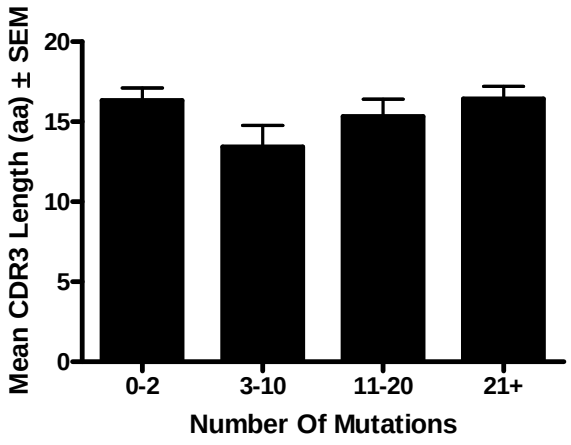

Figure 4.4 Mean CDR3 Lengths in Relation to V_H Mutational Numbers

The mean CDR3 length was calculated for immunoglobulin sequences according the number of mutations within the V_H segment of the gene rearrangement to establish any relationship between mutational number and CDR3 length. Results are given as Mean amino acid CDR3 length ± SEM. Groups were compared for statistical significance using the Tukey-Kramer test for multiple comparisons. The graph demonstrates that no significant changes in CDR3 length were observed at the various number of mutations. p-values <0.05 would have been deemed significant.

4.2.1.4 Clonal Diversification in MYO1

Two clonally related sequences were identified in region 5 of sample MYO1 (**Figure 4.5A&B**). These sequences shared the same VDJ gene segments, the same CDR3 amino acid sequence, the same junctional sequences and also contained 14 common replacement mutations and 8 common silent mutations. Analysis of the common and independent mutations (**Table 4.4**) of these two clonally related sequences demonstrated that there was a significant negative

selection within the framework regions of these sequences. A positive selection was occurring within the CDRs but this was not significant. As previously described, IMGT/V-QUEST detected deletions within these sequences, which not only changed the V_H gene assignment but also the number of point mutations. Taking the sequence alignments and changes suggested by IMGT/V-QUEST indicates that these sequences would not be clonally related.

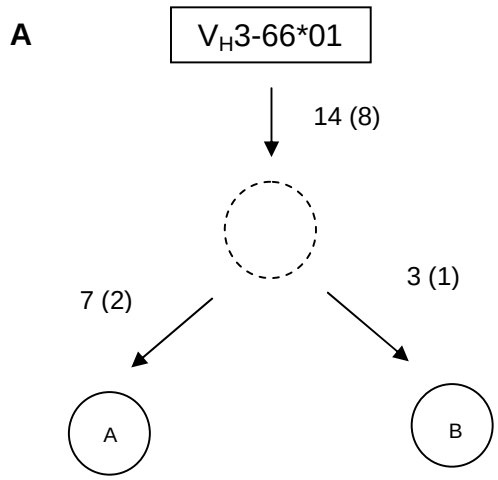

B

```
Germline3-66*01     GAGGTGCAGCTGGTGGAGTCTGGGGGAGGCTTGGTCCAGCCTGGGGGGTCCCTGAGACTC
CloneA              GAGGTGCAGCTGGTGGAGTCTGGGGGAGGCTTGGTACAGCCTGGGGGGTCCCTTAGAGTC
CloneB              GAGGTGCAGCTGGTGGAGTCTGGGGGAGGCTTGGTACAGCCTGGGGGGTCCCTGAGACTC

                                                 ← CDR1 →
Germline3-66*01     TCCTGTGCAGCCTCTGGATTCACCGTCAGTAGCAACTACATGAGCTGGGTCCGCCAGGCT
CloneA              TCCTGTGCAGCCTCTGGATTCACTTTCACTAAGGCCTGGATGAACTGGGTCCGCCAGGCT
CloneB              TCCTGTGCAGCCTCTGGATTCACCTTCAGTAGCTATAGCATGAACTGGGTCCGCCAGGCT

                                          ← ↓ AGT          CDR2 →
Germline3-66*01     CCAGGGAAGGGGCTGGAGTGGGTCTCAGTTATTTATAGCGGTGGTAGCACATACTACGCA
CloneA              CCAGGGAAGGGGCTGGAGTGGGTTTCATACATTAGTAGTAGTAGTACCATATACTACGCA
CloneB              CCAGGGAAGGGGCTGGAGTGGGTTTCATACATTAGTAGTAGTAGTACCATATACTACGCA

                    ──────────→
Germline3-66*01     GACTCCGTGAAGGGCAGATTCACCATCTCCAGAGACAATTCCAAGAACACGCTGTATCTT
CloneA              GACTCTGTGAAGGGCCGATTCACCATCTCCAGAGACAATGCCAAGAACTCACTGTATCTG
CloneB              GACTCTGTGAAGGGCCGATTCACCATCTCCAGAGACAATGCCAAGAACTCACTGTATCTG

                                                      CDR3 →
Germline3-66*01     CAAATGAACAGCCTGAGAGCCGAGGACACGGCTGTGTATTACTGTGCGAGAGA
CloneA              CAAATGAACAGCCTGAGAGACGAGGACACGGCTGTGTATTACTGTGCGAGAGA
CloneB              CAAATGAACAGCCTGAGAGACGAGGACACGACTGTGTATTACTGTGCGAGAGA
```

Figure 4.5 Clonal Proliferation in Sample MYO1

2 B cell sequences isolated from sample MYO1 demonstrated somatic hypermutation and clonal proliferation (**A&B**). **Figure A** - The letters in the circles refer to individual sequences isolated from each B cell clone. Numbers indicate the minimum number of mutations required between each sequence with bracketed figures representing additional silent mutations. The dashed circle represents a hypothetical intermediate whose sequence was not found amongst the isolated sequences. **Figure B** - The DNA sequences of the clonally related sequences were aligned using ClustalW software to highlight the common and independent mutations. CDR regions are highlighted in yellow, replacement mutations in blue and silent mutations in purple. The sequence in red above the alignment within the CDR2 regions indicated the deletion detected by the IMGT/V-QUEST software.

R-CDR	S-CDR	pCDR	p-CDR	R-FW	S-FW	pFW	p-FW
17	4	0.46522	**0.139067**	7	7	0.668169	**-0.0177**

Table 4.4 Analysis of Replacement and Silent Mutations and Positive and Negative Selection in Clonally Related B Cells in Sample MYO1

The number of replacement and silent mutations and the presence of any positive and negative selection were conducted as per Hershberg *et al* (294) as previously described in section 2.3.12.3 and Table 4.2. For clonally related sequences mutations shared across the sequences are only counted once and p values are calculated for the clone as a single entity. R-CDR/FW and S-CDR/FW represent the number of replacement and silent mutations in the CDR and FW respectively. pCDR represents the probability of having a R mutation in the CDR given all the mutations in the sequence except R mutations within the FW while pFW represents the probability of having a R mutation in the FW given all the mutations in the sequence except R mutations within the CDR and p-CDR/FW represent the p-value of the focused binominal test on the CDR and FW respectively. A negative sign indicates negative selection. p-values <0.05 are highlighted in yellow and were deemed significant.

As shown in Table 4.1 a number of sequences demonstrated different mutational patterns but shared common gene segment usage and CDR3 and junctional sequences; these were not deemed to be clonally related as the rate of base changes fell within the PCR error rate of one base per 4 V_H genes (52).

4.2.2 Sample MYO3

4.2.2.1 V_H Gene Repertoire of Infiltrating B Cells

For sample MYO3 one large area of infiltrating cells was microdissected and amplification of V_H1-6 families was carried out by nested PCR (**Figure 4.6**). From the extensive region of infiltration in sample MYO3 sequence results produced 17 functional sequences (**Table 4.5**) which showed a selection for V_H1 gene segments, approximately 60% of the sequences isolated belonged to the V_H1 family, which was significant against both normal control values and the germline complexity (**Figure 4.7A**). Figure 4.7A demonstrates an apparent reduced selection for V_H3 and V_H4 gene segments but this reduction was not significant against normal control values or the germline complexity when the absolute values were used in the Chi square analysis. No gene segments were observed within the infiltrating repertoire for V_H2, V_H5, V_H6 and V_H7 families, similarly this was not significant against both sets of control values. D_H genes could be assigned to 41.2% of the genes from the infiltrating repertoire. The repertoire of these genes almost mirrors the distribution of the normal control values and the germline complexity (**Figure 4.7B**); no significant selections were observed within the genes isolated from the muscle sections from sample MYO3 except for the selection of D_H3 genes which were significant against the germline complexity but were not significant against the normal control values. For J_H family segments a selection for J_H5 gene segments was observed which was significant against normal control values but not the germline complexity (**Figure 4.7C**). No other significant selections were observed for any other J_H gene family within cellular infiltrates of MYO3.

Comparing the V, D and J gene assignments from the JOINSOLVER software to that from the IMGT/V-QUEST produced no discrepancies between the two softwares.

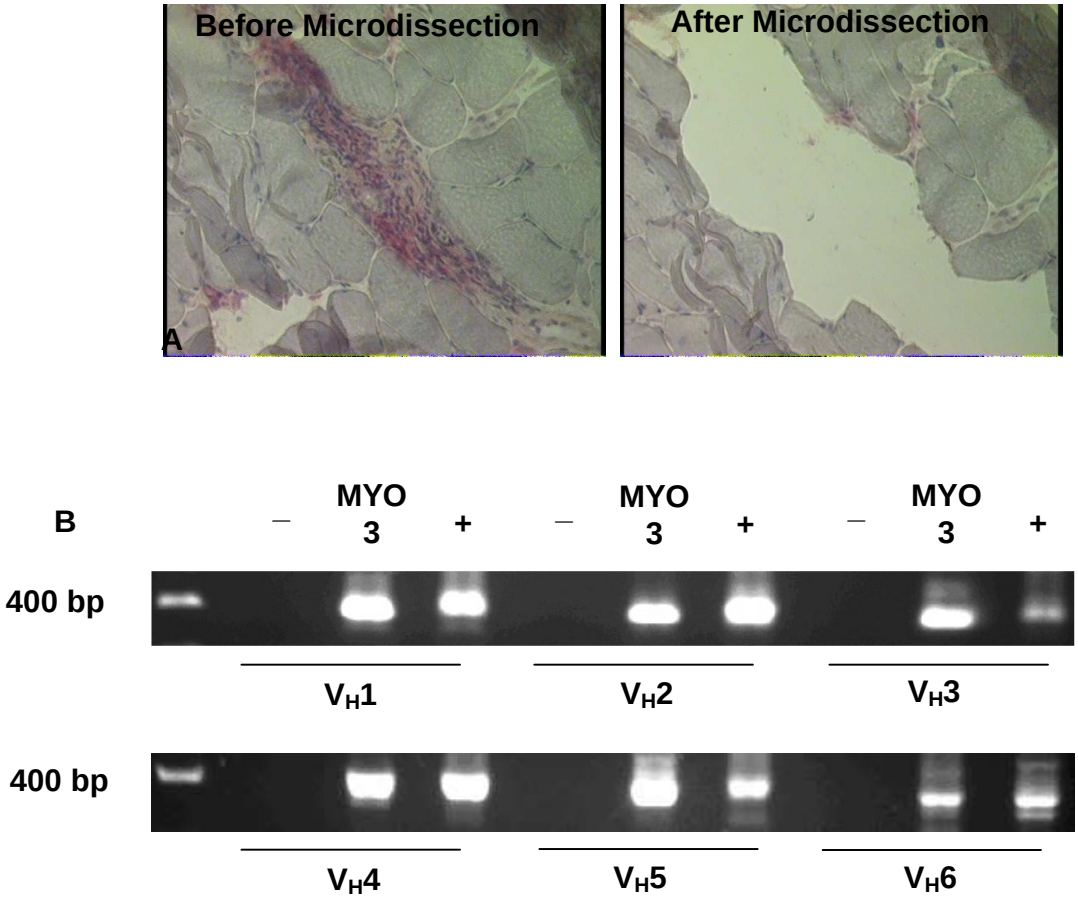

Figure 4.6 Microdissection of infiltrating B cells and amplification of V_H-gene rearrangements from Sample MYO3

The region of B cell and plasma cell infiltration was microdissected from sample MYO3. Figure 4.6A demonstrates the microdissection of the region of cellular infiltration. Images were taken at 200X. DNA released from these microdissections was amplified using a Nested PCR system (Figure 4.6B), as described in Chapter 2. – indicates negative control PCR reactions where DNA was substituted with water while + indicates positive control PCR reactions using peripheral blood mononuclear cells isolated from peripheral blood of a healthy individual. Results show amplification of all 6 V_H families.

V_H Gene	D_H Gene	J_H Gene	Number of Isolated Sequences	Number of Point Mutations	CDR3	V-J Length (bp)	Consecutive D length (bp) (+Mismatches)
1-03*01	3-22*01	4*02	2	0	ASGDSSGYTLDY	23	14
				2	ASGDSSGYTLDY	23	14
1-46*01	No D gene Assignment	5*02	2	10	AARVPVDSVMSSDH	39	6
				11	AARVPVDSVMSSDH		
1-69*01	5-24*01	4*02	1	14	ARDTRRDVYNSGYDY	36	17 (+1)
1-69*02	No D gene Assignment	5*02	1	23	AARVPVDSVMSSDH	39	6
1-69*04	No D gene Assignment	4*02	1	10	ARDSVGGTGY	18	6
1-69*09	No D gene Assignment	4*02	1	22	AARIASGDSSYFDY	27	8
1-69*09	No D gene Assignment	5*02	1	24	AARVPVDSVMSSDH	39	6
1-69*09	No D gene Assignment	4*02	1	25	ANGAAGYYDD	24	5
3-07*02	2-15*01	6*03	1	15	ARKTGRGGSRPWYNRYYYMDV	39	11
3-11*03	No D gene Assignment	6*02	1	1	ARDLSMVYYYYGMDV	14	5
3-30*03	No D gene Assignment	4*02	1	18	AKEEEVRSSAPPVFDY	35	8
3-49*03	No D gene Assignment	5*02	1	19	CRYYPSWFDP	30	7
4-34*12	3-10*01	6*02	1	12	ARGPRNYYRTGRRERDFYYYYGMDV	44	17 (+2)
4-39*01	1-26*01	4*02	1	5	ARRKARVGASQAFDY	29	11
4-59*01	3-22*01	2*01	1	12	ARTPYYYDSTGYYYPLVGFDL	47	30(+1)

Table 4.5 Heavy chain genes identified from myositis sample MYO3

Best matching germline sequences were identified from aligning sequences in the IMGT database using JOINSOLVER software from the MYO3 myositis section. The total number of sequences isolated is given in the 4th column of the table; non-functional rearrangements indicated in brackets. Identical sequences with the same V_H, D_H, J_H, CDR3 and base mutations were only counted once. CDR3 amino acid sequences were also identified using the JOINSOLVER software. V-J lengths and consecutive D match lengths (bp) were also identified using the JOINSOLVER software and allowed assignment of the D_H genes as described in section 2.3.12.3.

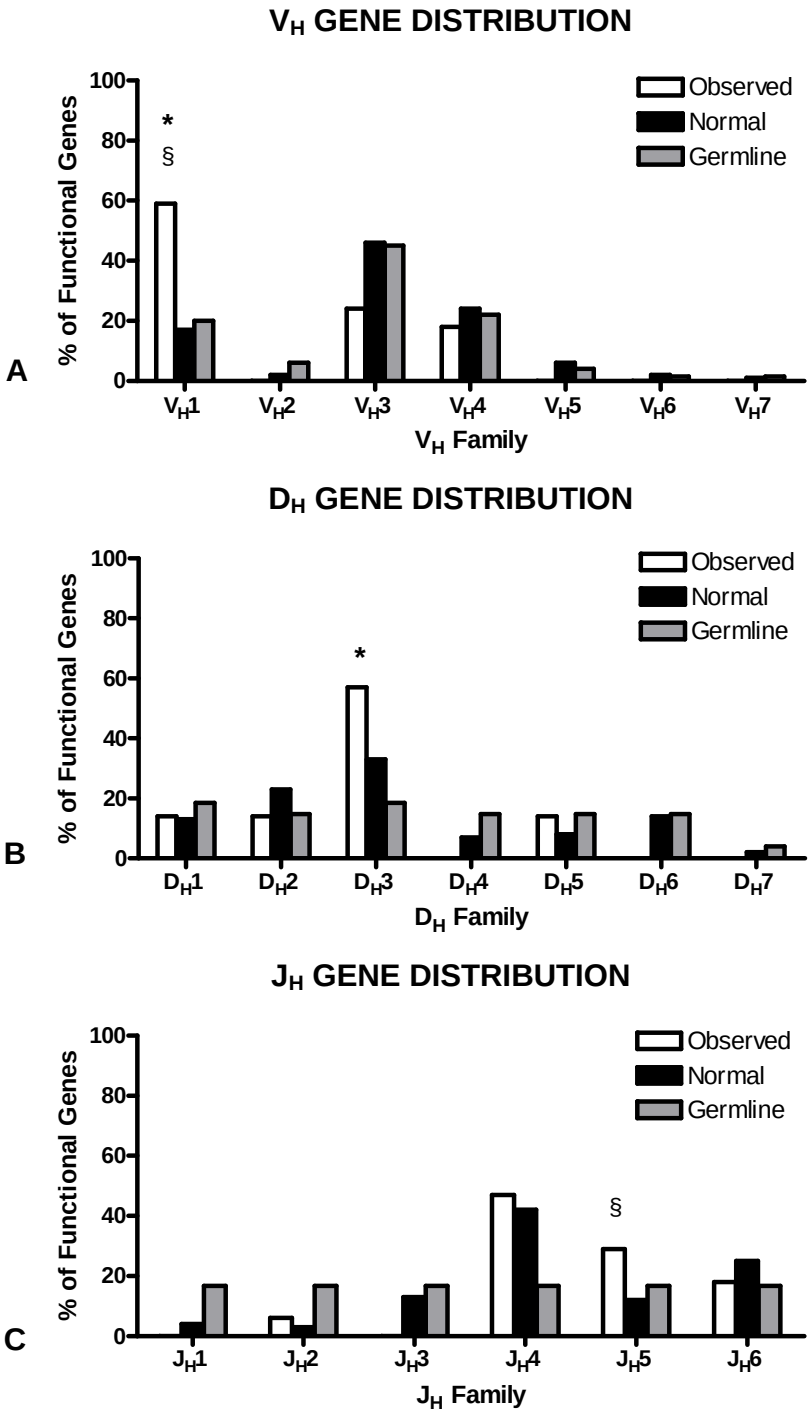

Figure 4.7 V_H Gene Family Usage of MYO3

V_H gene family usage. Distribution of functional genes was compared with published normal control values from Volpe and Kepler (251) as well as the germline complexity assuming every germline gene is capable of producing a functional rearrangement. Absolute values were used in Chi Square Analysis to determine gene selections. § represent a significant difference from normal control values; * represent a significant difference from the germline ($p<0.05$).

4.2.2.2 Mutational Analysis of B Cell Ig Sequences of Sample MYO3

Over 50% of the sequences isolated from sample MYO3 were highly mutated with mutational numbers over 11 per sequence (**Figure 4.8A**), which may indicate the infiltration of memory cells. Just fewer than 20% of sequences were virtually non-mutated with only 0 to 2 per sequence indicating the presence of a naïve population of cells with the remainder of sequences containing between 3 and 10 mutations throughout the V_H segment of the gene rearrangement. Examining the percentage of mutations within framework and CDR regions demonstrates, like the previous sample, that there were a higher percentage of mutations within CDR regions of gene sequences, with the highest percentage of these mutations found within the CDR1 region (**Figure 4.8B**).

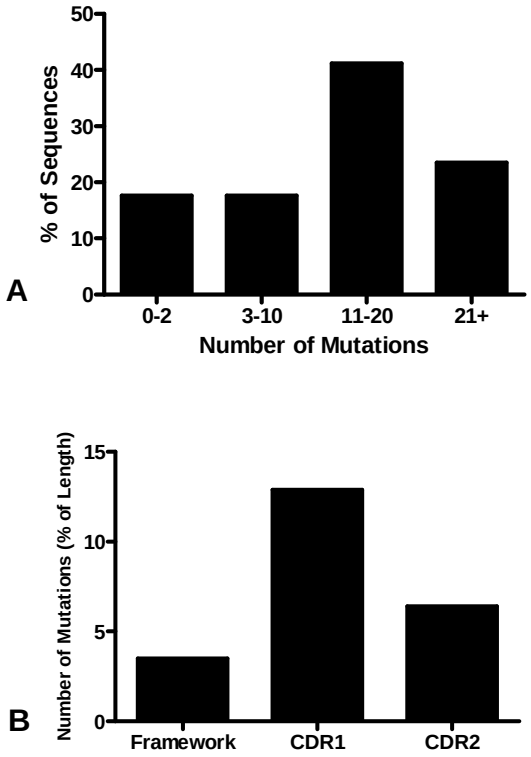

Figure 4.8 Numbers of Mutations and Mutational Distribution of Functional Sequences in MYO3

Figure 4.8A - The number of mutations within functional rearranged genes were analysed in sample MYO3. Base differences within the first 24 bases of sequence were disregarded as this part of the sequence binds the 5' V_H primer. Graph demonstrates sequences within cellular infiltrates show a diverse distribution of mutational numbers.

Figure 4.8B - The locations of mutations observed within functional rearranged genes were categorised as being within FR or CDR regions. The numbers of mutations within these regions were expressed as a percentage of the entire length of the region to correct for the longer lengths observed within the framework regions. Graph demonstrates a higher percentage of mutations within CDR regions compared to framework regions.

Analysis of replacement and silent ratios in the V_H region were analysed as previously described. From 17 sequences significant selections were only found within 2 of the sequences; positive selection within the CDR was observed within 1 of the sequences while negative selection in the FW was observed within the other sequence (**Table 4.6**). All other positive and negative selections within the CDR and regions were not significant.

V_H Gene	D_H Gene	J_H Gene	Number of Isolated Sequences	Number of Point Mutations	R-CDR	S-CDR	pCDR	p-CDR	R-FW	S-FW	pFW	p-FW
1-03*01	3-22*01	4*02	2	0	-	-	-	**-**	-	-	-	**-**
				2	0	0	0.47127	**0**	2	0	0.70269	**0.49377**
1-46*01	No D gene Assignment	5*02	2	10	0	0	0.47626	**-0.0752**	6	4	0.674	**-0.6191**
				11	1	0	0.47626	**-0.1539**	5	5	0.674	**-0.2677**
1-69*01	5-24*01	4*02	1	14	7	1	0.44858	**0.05775**	5	1	0.67095	**0.85185**
1-69*02	No D gene Assignment	5*02	1	23	9	1	0.46421	**0.599**	6	7	0.67462	**-0.065**
1-69*04	No D gene Assignment	4*02	1	10	8	1	0.46613	**0.01279**	1	0	0.67556	**-0.6489**
1-69*09	No D gene Assignment	4*02	1	22	6	4	0.4646	**-0.6319**	7	5	0.67435	**-0.0566**
1-69*09	No D gene Assignment	5*02	1	24	10	1	0.4646	**0.45103**	6	7	0.67435	**-0.0654**
1-69*09	No D gene Assignment	4*02	1	25	8	3	0.4646	**0.95751**	8	6	0.67435	**-0.089**
3-07*02	2-15*01	6*03	1	15	2	2	0.44221	**-0.2033**	6	5	0.6681	**-0.1353**
3-11*03	No D gene Assignment	6*02	1	1	0	0	0.47238	**-0.5276**	0	1	0.66449	**-0.3355**
3-30*03	No D gene Assignment	4*02	1	18	9	2	0.46606	**0.31422**	3	4	0.67432	**-0.0451**
3-49*03	No D gene Assignment	5*02	1	19	9	2	0.44618	**0.08515**	6	2	0.6636	**-0.6685**
4-34*12	3-10*01	6*02	1	12	3	0	0.41289	**0.92298**	5	4	0.65315	**-0.5497**
4-39*01	1-26*01	4*02	1	5	0	0	0.42497	**-0.1901**	2	3	0.66224	**-0.264**
4-59*01	3-22*01	2*01	1	12	2	1	0.44001	**-0.3081**	4	5	0.65645	**-0.1109**

Table 4.6 Analysis of Replacement and Silent Mutations and Positive and Negative Selection in Sample MYO3

Replacement and silent mutations within the immunoglobulin sequences and antigen-driven selection were determined according to Hershberg *et al* (294) and the corresponding computer programme (http://clip.med.yale.edu/selection). This improved method of analysis uses a focused binomial test to establish positive or negative mutational selections within the sequence with high specificity and increased sensitivity accounting for known biases within the immunoglobulin gene sequence. R-CDR and S-CDR represents the number of replacement and silent mutations within the CDR respectively. pCDR represents the probability of having a R mutation in the CDR given all the mutations in the sequence except R mutations within the FW while p-CDR is the p-value of the focused binominal test on the CDR. Conversely R-FW and S-FW represents the number of replacement and silent mutations within the FW respectively. pFW represent the probability of having a R mutation in the FW given all the mutations in the sequence except R mutations within the CDR while p-FW is the p-value of the focused binominal test on the FW. If the number of R mutations is less than expected the software will test for negative selection and p-values will be preceded by a negative sign or if the number of mutations is more than expected the software will test for positive selection. p-values <0.05 are highlighted in yellow and were deemed significant for selection.

4.2.2.3 CDR3 Analysis

Analysis of the CDR3 in these sequences could only be conducted within the functional repertoire as no non-functional sequences were isolated (**Table 4.7**). For these sequences the mean amino acid CDR3 length was 14.8 ± 1 (ranging from 10 to 25 amino acids). The mean CDR3 lengths were also compared between the different mutational groups but no significant differences in the CDR3 length was observed (**Figure 4.9**). Comparison of the P and N nucleotides at the VD and DJ junctions were not significant but a significant increase in exonuclease activity was observed at the 5' of the J_H gene segment compared to the exonuclease activity observed a the 3' end of the V_H gene. No further significant differences were observed.

CDR3 Length	**Functional**	14.8 ± 1			
	Non-Functional	N/A			
		VD Junction		**DJ Junction**	
P Nucleotide	**Functional**	0.9 ± 0.4		0.4 ± 0.2	
	Non-Functional	N/A		N/A	
N Nucleotide	**Functional**	6.9 ± 1.1		9.4 ± 1.7	
	Non-Functional	N/A		N/A	
		3' V_H	**5' D_H**	**3' D_H**	**5'J_H**
Exonuclease Activity	**Functional**	1.9 ± 0.5	5.1 ± 1.7	5.8 ± 1.4	6.1 ± 0.7$^{\theta}$
	Non-Functional	N/A	N/A	N/A	N/A

Table 4.7 CDR3 and Junctional Analysis in Sample MYO3

The mean amino acid length of the CDR3, the mean nucleotide numbers corresponding to P and N nucleotides as well as the mean number of germline nucleotides lost due to exonuclease activity were calculated from the junctional regions of all immunoglobulin sequences from sample MYO3. Results are given as the Mean ± SEM, statistical significance was established using an unpaired t-test. Instances where no non-functional sequences were identified and values could not be calculated were recorded as non applicable (N/A). Θ represents a significant difference from 3'V_H.

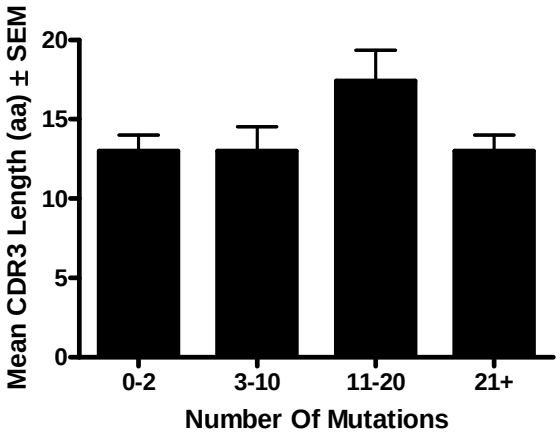

Figure 4.9 Mean CDR3 Lengths in Relation to V_H Mutational Numbers

The mean CDR3 length was calculated for immunoglobulin sequences according the number of mutations within the V_H segment of the gene rearrangement to establish any relationship between mutational number and CDR3 length. Results are given as Mean amino acid CDR3 length ± SEM. Groups were compared for statistical significance using the Tukey-Kramer test for multiple comparisons. The graph demonstrates that no significant changes in CDR3 length were observed at the various number of mutations. p-values <0.05 would have been deemed significant.

4.2.2.4 Clonal Diversification in MYO3

Two clonally related sequences from sample MYO3 were observed (**Figure 4.10**). In addition the common VDJ gene segments, CDR3 composition and junctional sequences, these clonally related sequences shared 4 replacement mutations and 3 silent mutations. No other clonally related sequences were observed within sample MYO3. Analysis of the R and S mutations (**Table 4.8**) showed that there was no significant selection observed within the CDR and FW regions although a non-significant negative selection was observed in both regions.

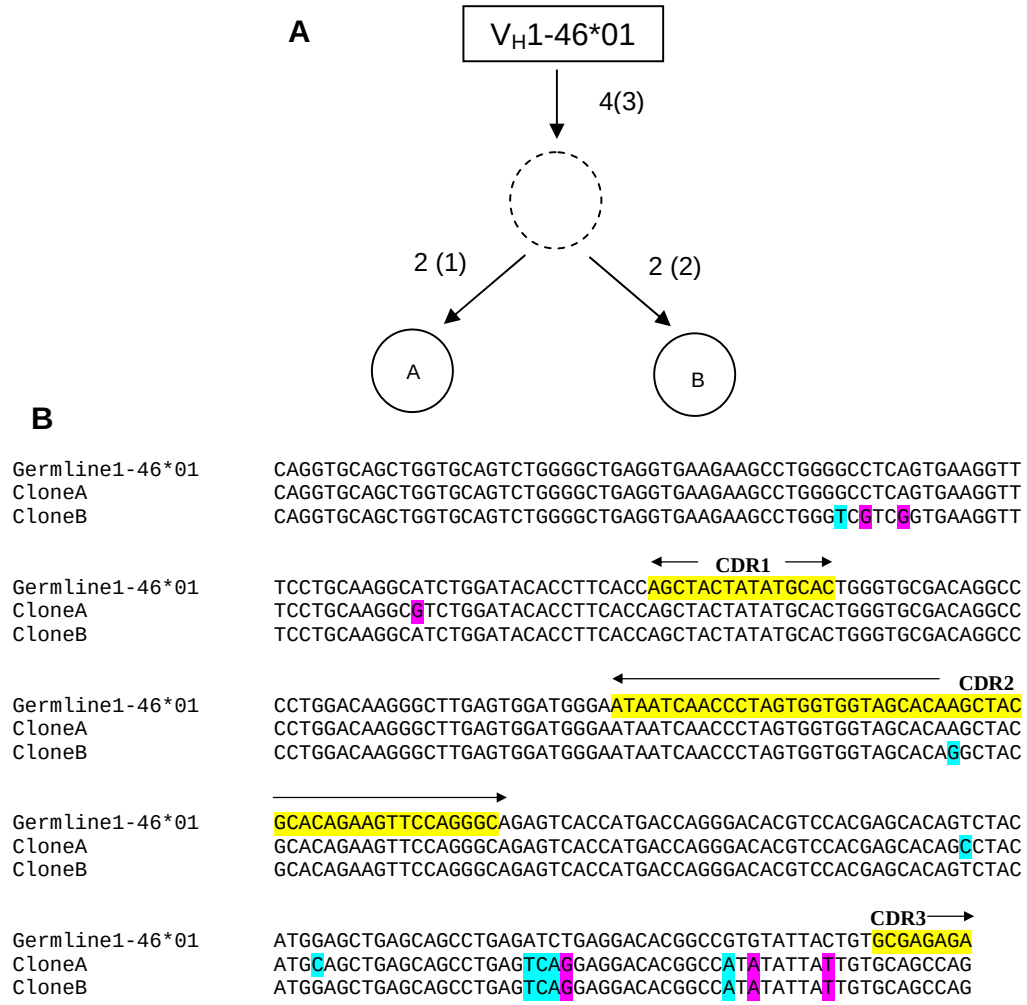

Figure 4.10 Clonal Proliferation in Sample MYO3

Two B cell sequences isolated from sample MYO3 demonstrated somatic hypermutation and clonal proliferation (**A&B**). **Figure A** - The letters in the circles refer to individual sequences isolated from each B cell clone. Numbers indicate the minimum number of mutations required between each sequence with bracketed figures representing additional silent mutations. The dashed circle represents a hypothetical intermediate whose sequence was not found amongst the isolated sequences. **Figure B** - The DNA sequences of the clonally related sequences were aligned using ClustalW software to highlight the common and independent mutations. CDR regions are highlighted in yellow, replacement mutations in blue and silent mutations in purple.

R-CDR	S-CDR	pCDR	p-CDR	R-FW	S-FW	pFW	p-FW
1	0	0.47626	**-0.0904**	7	6	0.674	**-0.3167**

Table 4.8 Analysis of Replacement and Silent Mutations and Positive and Negative Selection in Clonally Related B Cells in Sample MYO3

The number of replacement and silent mutations and the presence of any positive and negative selection were conducted as per Hershberg *et al* (294) as previously described. For clonally related sequences mutations shared across the sequences are only counted once and p values are calculated for the clone as a single entity. R-CDR/FW and S-CDR/FW represent the number of replacement and silent mutations in the CDR and FW respectively. pCDR represents the probability of having a R mutation in the CDR given all the mutations in the sequence except R mutations within the FW while pFW represents the probability of having a R mutation in the FW given all the mutations in the sequence except R mutations within the CDR and p-CDR/FW represent the p-value of the focused binominal test on the CDR and FW respectively. A negative sign indicates negative selection. p-values <0.05 were deemed significant.

4.2.3 Sample MYO5

4.2.3.1 V_H Gene Repertoire of Infiltrating B Cells

Biopsy material from patient MYO5 used in this study was a second biopsy conducted 3 years after the initial diagnostic biopsy due to a flare up of myositis. As described in Chapter 3 no well-defined areas of infiltration were observed within sections, cellular infiltration was observed throughout the entire sample. Consequently the whole section was used to establish the gene repertoire used by infiltrating B and plasma cells (**Figure 4.11**). 22 functional gene rearrangements were used to establish the gene usage distribution (**Table 4.9**), multiple copies of the same gene were isolated from the repertoire but these were only counted as one. A selection against V_H1 gene segments and a selection for V_H5 gene segments were observed significant against both normal control values and the germline complexity (**Figure 4.12A**). A difference of approximately 20% was observed for each family respectively. No other gene family displayed significant differences between the two sets of control data. D_H genes could be identified in 40.9% of the sequences isolated from the inflammatory infiltrate in sample MYO5. The distribution mirrored the normal control distribution as well as the germline complexity and no significant selections were observed for any D_H gene family (**Figure 4.12B**). Similarly no selection was observed for any of the J_H gene family segments and the repertoire of the inflammatory infiltrate mirrored the gene distribution of normal control values and the germline complexity (**Figure 4.12C**).

From the sequences isolated from the inflammatory infiltrate in sample MYO5 no discrepancies in gene assignment was observed between the JOINSOLVER and IMGT/V-QUEST software's.

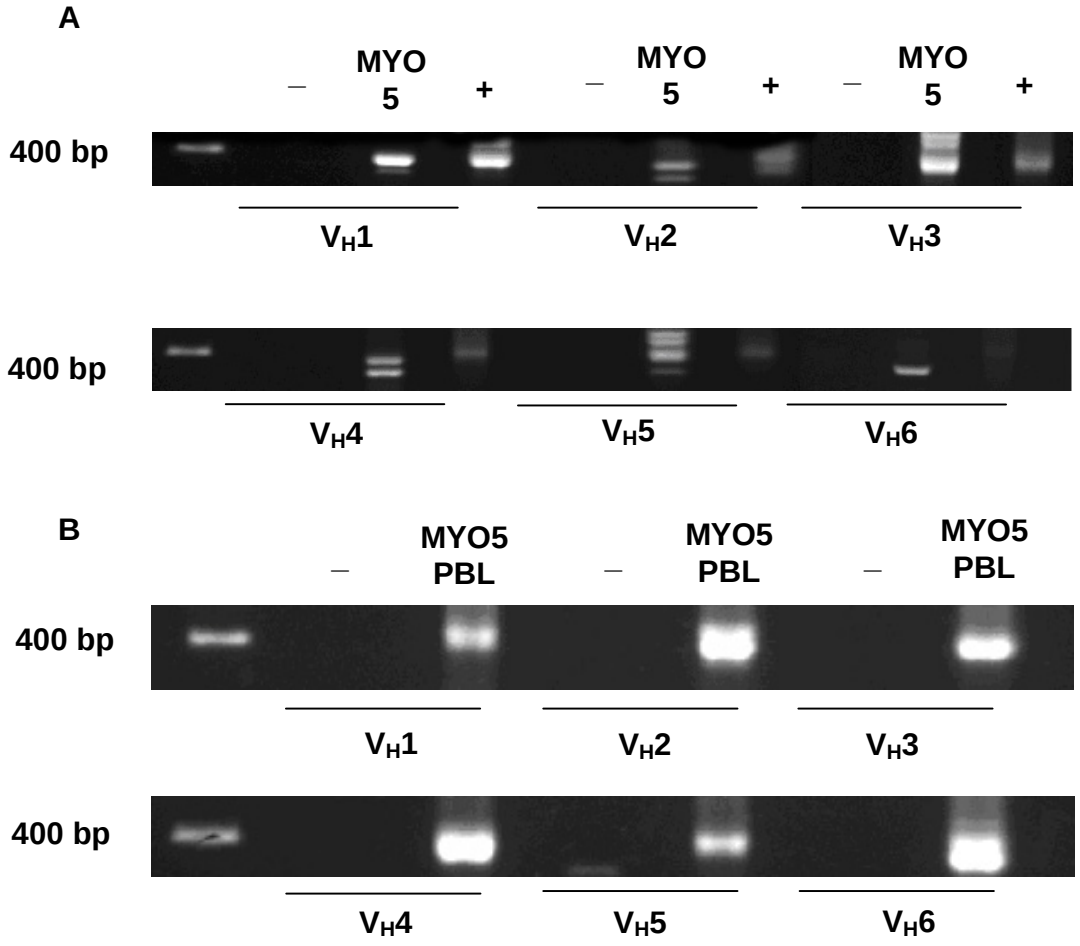

Figure 4.11 Amplification of V_H-gene rearrangements from Sample MYO5

As no distinct aggregation of infiltrating cells was observed within sample MYO5 and infiltrating cells were observed throughout the whole section, the whole section was used to obtain DNA. DNA released from the section was amplified using a Nested PCR system, as described in Chapter 2. PCR reactions were conducted for DNA isolated from the muscle sections (Figure 4.11A) in addition to DNA isolated from PBL (Figure 4.11B). – indicates negative control PCR reactions where DNA was substituted with water while + indicates positive control PCR reactions using peripheral blood mononuclear cells isolated from peripheral blood of a healthy individual. Results show amplification of all 6 V_H families for both types of DNA tested.

V_H Gene	D_H Gene	J_H Gene	Number of Isolated Sequences	Number of Point Mutations	CDR3	V-J Length (bp)	Consecutive D length (bp) (+Mismatches)
2-70*04	No D gene Assignment	5*02	1	14	SRTYLTNGYDP	26	6
3-30*04	1-7*01	4*02	2	4, 5	ARGGGYNWTYRVSGYCDS	46	14(+1)
3-30*04	3-22*01	4*02	1	13	ARDITYSDDDTGGYYYPI	43	25 (+4)
3-30*04	5-12*01	6*02	2	16, 19	ARGVGGSSGYDLPWYSSYGMDV	43	17(+2)
3-30*09	No D gene Assignment	6*02	1	21	ARDRYSHAYYSGVDV	29	9
3-30*09	No D gene Assignment	6*02	1	21	ARDRYSHAYYSGMDV	28	8
3-53*01	3-22*01	4*02	2	18, 18	ARDHDANSYYYEGSAY	42	10
3-72*01	No D gene Assignment	5*02	1	17	ARDLNGLGRN	21	8
3-73*02	No D gene Assignment	4*02	1	26	TRWAPKTGGLDY	30	7
4-34*01	No D gene Assignment	4*02	3	25, 27, 28	ARCLMGNYLH	22	6
4-59*01	No D gene Assignment	4*02	1	10	AKGGGDTALLFGN	35	6
5-51*01	No D gene Assignment	3*02	4	12, 25, 31, 32	ARAKCSAGQCRLPEAFDM	51	8
5-51*01	6-19*01	4*02	2	4, 5	ARQGRSSGWYWSDFDY	31	16

Table 4.9 Heavy chain genes identified from myositis sample MYO5

Best matching germline sequences were identified from aligning sequences in the IMGT database using JOINSOLVER software from the MYO5 myositis section. The total number of sequences isolated is given in the 4th column of the table; non-functional rearrangements indicated in brackets. Identical sequences with the same V_H, D_H, J_H, CDR3 and base mutations were only counted once. CDR3 amino acid sequences were also identified using the JOINSOLVER software. V-J lengths and consecutive D match lengths (bp) were also identified using the JOINSOLVER software and allowed assignment of the D_H genes as described in section 2.3.12.3.

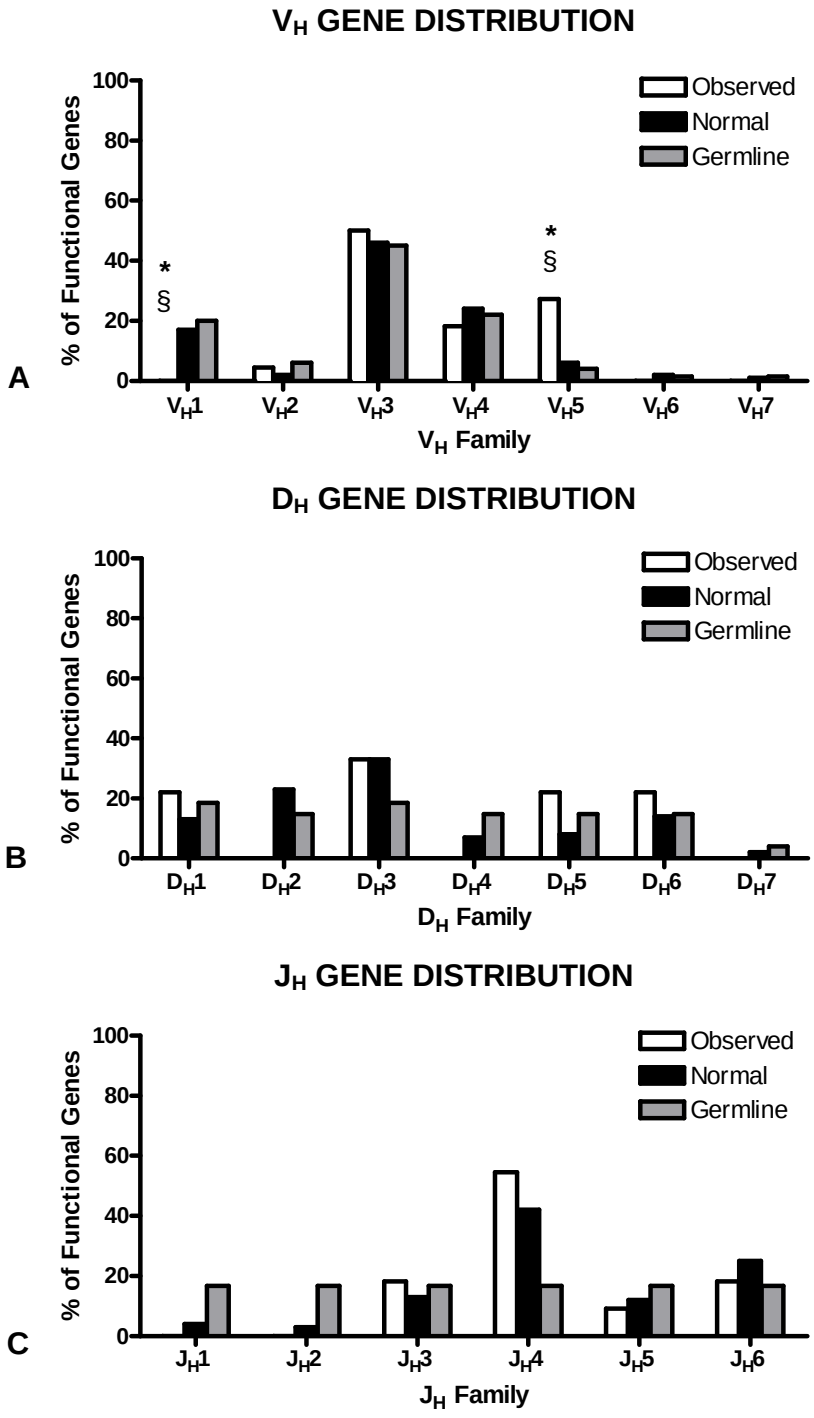

Figure 4.12 V_H Gene Family Usage of MYO5

V_H gene family usage. Distribution of functional genes was compared with published normal control values from Volpe and Kepler (251) as well as the germline complexity assuming every germline gene is capable of producing a functional rearrangement. Absolute values were used in Chi Square Analysis to determine gene selections. § represent a significant difference from normal control values; * represent a significant difference from the germline ($p<0.05$).

4.2.3.2 Mutational Analysis of B Cell Ig Sequences of Sample MYO5

Mutational numbers within functional rearrangements demonstrated that a highly mutated population was present within sample MYO5 which may represent a memory cell population, approximately 75% of cells isolated from the muscle contained over 11 mutations (**Figure 4.13A**). There was a very low presence of naïve cells within the muscle with no sequences being isolated with 0 to 2 mutations, all remaining sequences had between 3 and 10 mutations per sequence. Analysis of mutation locations demonstrated a higher percentage of mutations within CDR regions in comparison to framework regions (**Figure 4.13B**), a higher percentage of mutations was observed within CDR1 regions.

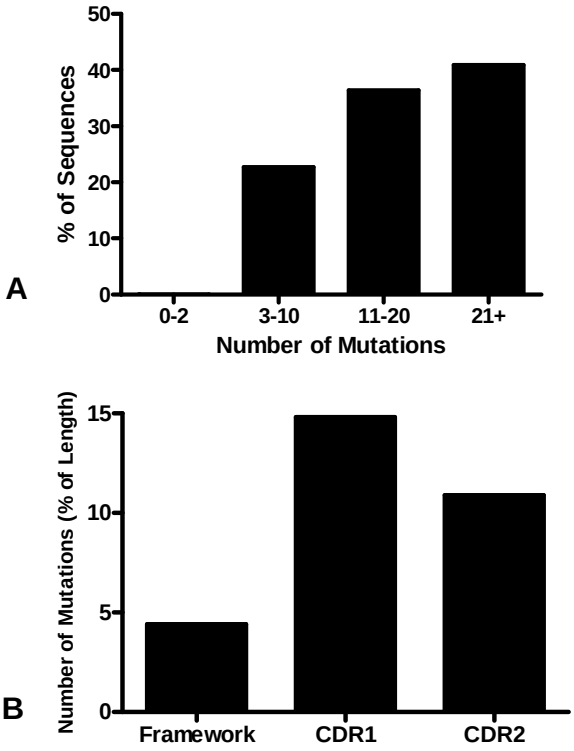

Figure 4.13 Numbers of Mutations and Mutational Distribution of Functional Sequences in MYO5

Figure 4.13A - The number of mutations within functional rearranged genes were analysed in sample MYO5. Base differences within the first 24 bases of sequence were disregarded as this part of the sequence binds the 5' V_H primer. Graph demonstrates sequences within cellular infiltrates of sample MYO5 do not contain any naïve cells and that the population within sample MYO5 are highly mutated.

Figure 4.13B - The locations of mutations observed within functional rearranged genes were categorised as being within FR or CDR regions. The numbers of mutations within these regions were expressed as a percentage of the entire length of the region to correct for the longer lengths observed within the framework regions. Graph demonstrates a higher percentage of mutations within CDR regions compared to framework regions.

Based on the replacement and silent mutations within the sequences (**Table 4.10**) selection was observed in 5 of the 22 sequences isolated from sample MYO5. Two of these sequences demonstrated positive selection within the CDR while the remaining 3 sequences demonstrated negative selection in the FW regions. In the other 17 sequences positive and negative selection were observed in both the CDR and FW region but these selections were not significant.

V_H Gene	D_H Gene	J_H Gene	Number of Isolated Sequences	Number of Point Mutations	R-CDR	S-CDR	pCDR	p-CDR	R-FW	S-FW	pFW	p-FW
2-70*04	No D gene Assignment	5*02	1	14	8	1	0.46004	**0.03713**	4	1	0.67539	**-0.9339**
3-30*04	1-7*01	4*02	2	4	3	0	0.47645	**0.32957**	0	1	0.67262	**-0.3274**
				5	3	0	0.47645	**0.61536**	0	2	0.67262	**-0.1072**
3-30*04	3-22*01	4*02	1	13	5	0	0.47645	**0.23822**	6	2	0.67262	**0.68795**
3-30*04	5-12*01	6*02	2	16	6	2	0.47645	**0.4565**	6	2	0.67262	**-0.6256**
				19	6	2	0.47645	**0.87298**	7	4	0.67262	**-0.3219**
3-30*09	No D gene Assignment	6*02	1	21	12	3	0.47758	**0.06524**	4	2	0.67244	**-0.1751**
3-30*09	No D gene Assignment	6*02	1	21	12	3	0.47758	**0.06524**	4	2	0.67244	**-0.1751**
3-53*01	3-22*01	4*02	2	18	8	3	0.45711	**0.08369**	7	0	0.65885	**0.81907**
				18	8	3	0.45711	**0.16134**	6	1	0.65885	**-0.6915**
3-72*01	No D gene Assignment	5*02	1	17	3	3	0.45531	**-0.3487**	7	4	0.65729	**-0.2354**
3-73*02	No D gene Assignment	4*02	1	26	14	1	0.47416	**0.04699**	6	5	0.66265	**-0.2564**
4-34*01	No D gene Assignment	4*02	3	25	6	1	0.42123	**0.76861**	12	6	0.65376	**-0.8267**
				27	7	2	0.42123	**-0.7963**	9	9	0.65376	**-0.0672**
				28	7	2	0.42123	**-0.6576**	9	10	0.65376	**-0.0385**
4-59*01	No D gene Assignment	4*02	1	10	3	0	0.44001	**0.51005**	5	2	0.65645	**0.79209**
5-51*01	No D gene Assignment	3*02	4	12	1	1	0.43137	**-0.2215**	6	4	0.70065	**-0.2864**
				25	5	5	0.43137	**-0.4626**	10	5	0.70065	**-0.0642**
				31	7	6	0.43137	**-0.4775**	11	7	0.70065	**-0.0148**
				32	7	6	0.43137	**-0.4775**	12	7	0.70065	**-0.023**
5-51*01	6-19*01	4*02	2	4	1	1	0.43137	**0.86274**	2	0	0.70065	**-0.8712**
				5	1	1	0.43137	**0.86274**	3	0	0.70065	**0.89384**

Table 4.10 Analysis of Replacement and Silent Mutations and Positive and Negative Selection in Sample MYO5

Replacement and silent mutations within the immunoglobulin sequences and antigen-driven selection were determined according to Hershberg *et al* (294) and the corresponding computer programme (http://clip.med.yale.edu/selection). This improved method of analysis uses a focused binomial test to establish positive or negative mutational selections within the sequence with high specificity and increased sensitivity accounting for known biases within the immunoglobulin gene sequence. R-CDR and S-CDR represents the number of replacement and silent mutations within the CDR respectively. pCDR represents the probability of having a R mutation in the CDR given all the mutations in the sequence except R mutations within the FW while p-CDR is the p-value of the focused binominal test on the CDR. Conversely R-FW and S-FW represents the number of replacement and silent mutations within the FW respectively. pFW represent the probability of having a R mutation in the FW given all the mutations in the sequence except R mutations within the CDR while p-FW is the p-value of the focused binominal test on the FW. If the number of R mutations is less than expected the software will test for negative selection and p-values will be preceded by a negative sign or if the number of mutations is more than expected the software will test for positive selection. p-values <0.05 are highlighted in yellow and were deemed significant for selection.

4.2.3.3 CDR3 Analysis

As no non-functional sequences were identified in the infiltrating repertoire in sample MYO5 no comparisons could be made between these sequences and the functional sequences of the cells infiltrating the muscle. The mean amino acid CDR3 length was calculated at 15.5 ± 0.8 (ranging from 10 to 22 amino acids) (**Table 4.11**). As demonstrated in Figure 4.13A no non-mutated sequences were found within the infiltrating repertoire therefore the mean CDR3 length could only be examined for the 3 different ranges of highly mutated sequences (**Figure 4.14**). Using the Tukey-Kramer multiple comparison test no significant difference in the CDR3 length was observed between the different mutational groups. Like the previous samples no significant differences were observed for the P and N nucleotides at the VD and DJ junctions but in similarity to the other myositis samples a significant difference was observed for the exonuclease activity between the two junctional areas with a significant increase in exonuclease at the 5' end of the J_H gene segments and the 5'D_H region compared to the 3'V_H region (Table 4.11). There is also a significant difference in the DJ junction between the genes with an increased exonuclease activity at the 5'J_H compared to the 3' D_H.

CDR3 Length	**Functional**	15.5 ± 0.8			
	Non-Functional	N/A			
		VD Junction		**DJ Junction**	
P Nucleotide	**Functional**	0.3 ± 0.2		0.2 ± 0.1	
	Non-Functional	N/A		N/A	
N Nucleotide	**Functional**	8.2 ± 1.3		9.6 ± 0.5	
	Non-Functional	N/A		N/A	
		3' V_H	**5' D_H**	**3' D_H**	**5'J_H**
Exonuclease Activity	**Functional**	0.2 ± 0.1	6.3 ± 2.8$^{\theta}$	0.9 ± 0.6	6.2 ± 1.4 $^{\theta\text{Ж}}$
	Non-Functional	N/A	N/A	N/A	N/A

Table 4.11 CDR3 and Junctional Analysis in Sample MYO5

The mean amino acid length of the CDR3, the mean nucleotide numbers corresponding to P and N nucleotides as well as the mean number of germline nucleotides lost due to exonuclease activity were calculated from the junctional regions of all immunoglobulin sequences from sample MYO5. Results are given as the Mean ± SEM, statistical significance was established using an unpaired t-test. Instances where no non-functional sequences were identified and values could not be calculated were recorded as non applicable (N/A). Θ represents a significant difference from 3'V_H while Ж represents a significant difference from 3' D_H.

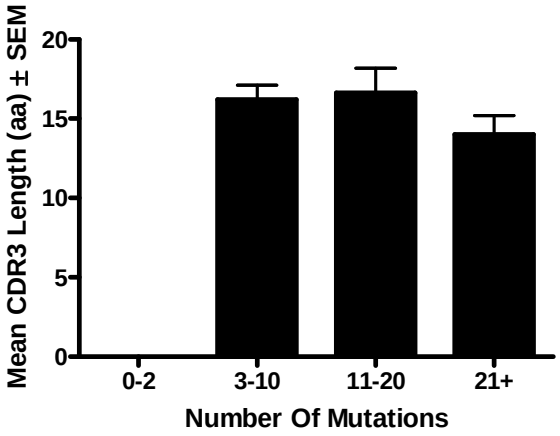

Figure 4.14 Mean CDR3 Lengths in Relation to V_H Mutational Numbers

The mean CDR3 length was calculated for immunoglobulin sequences according the number of mutations within the V_H segment of the gene rearrangement to establish any relationship between mutational number and CDR3 length. Results are given as Mean amino acid CDR3 length ± SEM. Groups were compared for statistical significance using the Tukey-Kramer test for multiple comparisons. The graph demonstrates that no significant changes in CDR3 length were observed at the various number of mutations. p-values <0.05 would have been deemed significant.

4.2.3.4 Clonal Diversification in MYO5

Four clonally related sets of genes were observed from sample MYO5 (**Figure 4.15A-H**). These clonally related sets of genes utilise V_H gene segments from V_H families 3, 4 and 5 and indicate a B cell antigen-driven response. The use of varying V_H families may also indicate an antigen-driven response to different antigens. Each set of clonally related sequences share the same VDJ gene rearrangement, CDR3 and junctional composition as well as common replacement and silent mutations. For clonal tree A clonal variants A and E share 1 replacement mutation between them but do not share the other R and S mutations indicated within the genealogical tree indicating that they are formed during different clonal lineages. The only sets of clonally related sequences which demonstrated a significant selection was the clonally related sequences from Figure 4.15A (**Table 4.12**); a significant negative selection was observed within the framework region when all the mutations from the clone were analysed as a single entity. Despite the individual sequence of clone D from Figure 4.15D exhibiting negative selection in the framework regions when analysed individually this was no longer significant when the other mutations of the clone were taken into consideration.

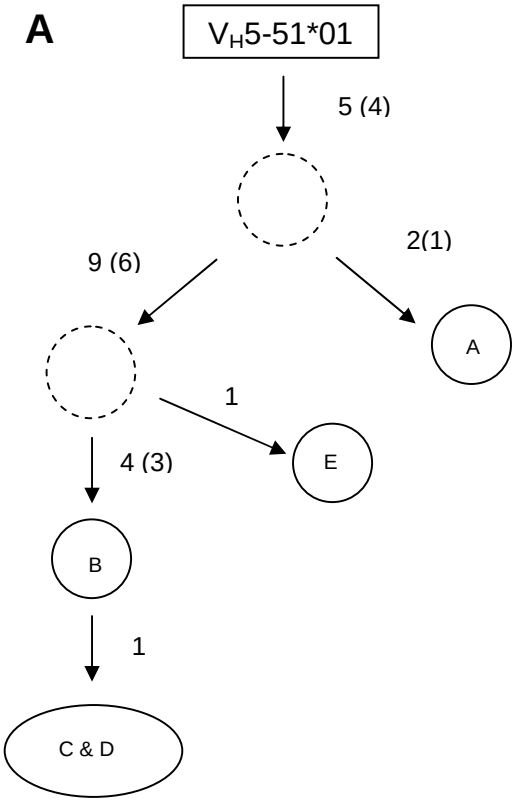
A
V_H5-51*01
5 (4)
9 (6)
2(1)
A
1
E
4 (3)
B
1
C & D

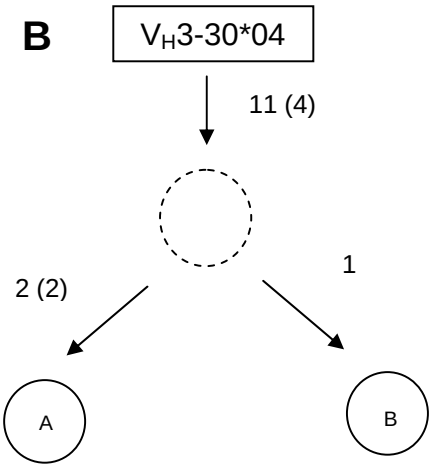
B
V_H3-30*04
11 (4)
2 (2)
1
A
B

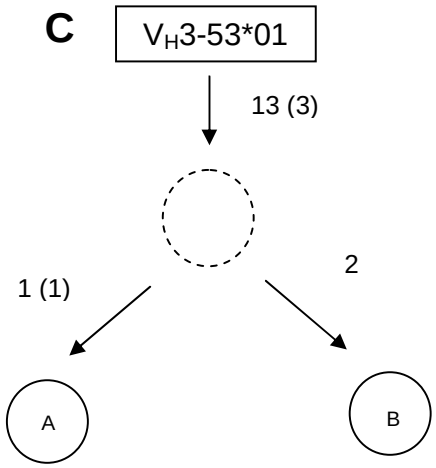
C
V_H3-53*01
13 (3)
1 (1)
2
A
B

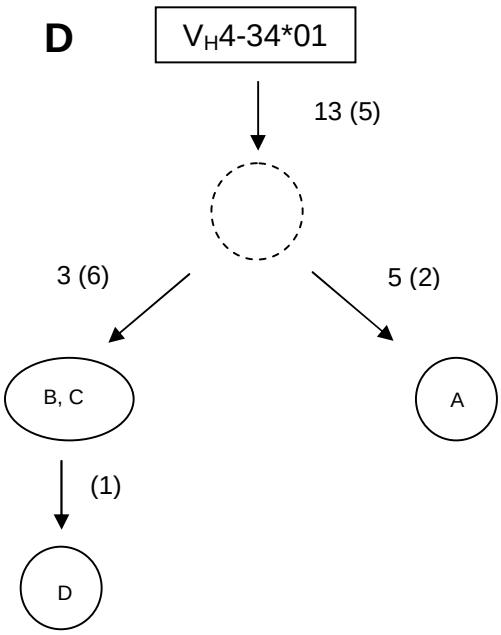
D
V_H4-34*01
13 (5)
3 (6)
5 (2)
B, C
A
(1)
D

E

```
Germline5-51*01     GAGGTGCAGCTGGTGCAGTCTGGAGCAGAGGTGAAAAAGCCCGGGGAGTCTCTGAAGATC
CloneA              GAGGTGCAGCTGGTGCAGTCTGGAGCAGAGGTGAAAAAGCCCGGGGAGTCTCTGAAGATC
CloneB              GAGGTGCAGCTGGTGCAGTCTGGAGCAGAGGTGAAAAAGCCCGGGGAGTCTCTGAAGATC
CloneC&D            GAGGTGCAGCTGGTGCAGTCTGGAGTAGAGGTGAAAAAGCCCGGGGAGTCTCTGAAGATC
CloneE              GAGGTGCAGCTGGTGCAGTCTGGAGCAGAGGTGAAAAAGCCCGGGGAGTCTCTGAAGATC

                                                  ← CDR1 →
Germline5-51*01     TCCTGTAAGGGTTCTGGATACAGCTTTACCAGCTACTGGATCGGCTGGGTGCGCCAGATG
CloneA              TCCTGTAAGGCTTCTGGATACAGCTTTACCAGCTACTGGATCGGCTGGGTGCGCCAGATG
CloneB              TCCTGTAAGGGTTCTGGATATAGTTTTCCCAACTTTTGGATCGGCTGGGTGCGCCAGCTG
CloneC&D            TCCTGTAAGGGTTCTGGATATAGTTTTCCCAACTTTTGGATCGGCTGGGTGCGCCAGCTG
CloneE              TCCTGTAAGGCTTCTGGATACAGCTTTACCAGCTACTGGATCGGCTGGGTGCGCCAGATG

                                                  ←————————————————— CDR2
Germline5-51*01     CCCGGGAAAGGCCTGGAGTGGATGGGGATCATCTATCCTGGTGACTCTGATACCAGATAC
CloneA              CCCGGGAAAGGCCTGGAGTGGATGGGGATCATCTATCCTGGTGACTCTGATAGTAGATAC
CloneB              CCCGGGAAAGGCCTGCAGTACGTGGGTATGATTCATCCTGGTGAATCTGACACCAGATAT
CloneC&D            CCCGGGAAAGGCCTGCAGTACGTGGGTATGATTCATCCTGGTGAATCTGACACCAGATAT
CloneE              CCCGGGAAAGGCCTGCAGTACGTGGGTATGATTCATCCTGGTGAATCTGACACCAGATAT

                    ————————→
Germline5-51*01     AGCCCGTCCTTCCAAGGCCAGGTCACCATCTCAGCCGACAAGTCCATCAGCACCGCCTAC
CloneA              AGCCCGTCCTTCCAAGGCCAGGTCACCATCTCAGCCGACAAGTCCCTGAGGACAGCCTAT
CloneB              AGTCCAGCCTTCCAAGACCAGGTCACCATCTCAGCCGACAAGTCCCTGAGGACAGCCTAT
CloneC&D            AGTCCAGCCTTCCAAGACCAGGTCACCATCTCAGCCGACAAGTCCCTGAGGACAGCCTAT
CloneE              AGTCCAGCCTTCCAAGACCAGGTCACCATCTCAGCCGACAAGTCCCTGAGGACAGCCTAT

                                                  CDR3 →
Germline5-51*01     CTGCAGTGGAGCAGCCTGAAGGCCTCGGACACCGCCATGTATTACTGTGCGAGACA
CloneA              CTGCAGTGGAGCAGCCTGAAGGCCTCGGACACTGCCGTGTTTTATTGTGCGCGGGC
CloneB              CTGCAGTGGAGCAGCCTGAAGGCCTCGGACACTGCCGTGTTTTATTGTGCGCGGGC
CloneC&D            CTGCAGTGGAGCAGCCTGAAGGCCTCGGACACTGCCGTGTTTTATTGTGCGCGGGC
CloneE              CTGCAGTGGAGCAGCCTGAAGGCCTCGGACACTGCCGTGTTTTATTGTGCGCGGGC
```

F

```
Germline3-30*04     CAGGTGCAGCTGGTGGAGTCTGGGGGAGGCGTGGTCCAGCCTGGGAGGTCCCTGAGACTC
CloneA              CAGGTGCAGCTGGTGGAGTCTGGGGGAGGCGTGGTCCAGCCTGGGAGGTCCCTGAGACTC
CloneB              CAGGTGCAGCTGGTGGAGTCTGGGGGAGGCGTGGTCCAGCCTGGGAGGTCCCTGAGACTC

                                                  ← CDR1 →
Germline3-30*04     TCCTGTGCAGCCTCTGGATTCACCTTCAGTAGCTATGCTATGCACTGGGTCCGCCAGGCT
CloneA              TCCTGTGCAGCCTCTGGGTTCATCTTCAGTAACTTTGCTATGCACTGGGTCCGCCAGGCT
CloneB              TCCTGTGCAGCCTCTGGATTCACCTTCAGTGACTATGCTATGCACTGGGTCCGCCAGGCT

                                                  ←————————————————— CDR2
Germline3-30*04     CCAGGCAAGGGGCTGGAGTGGGTGGCAGTTATATCATATGATGGAAGTAATAAATACTAC
CloneA              CCAGGCAAAGGGGCTGGAGTGGGTGGCAGTTATATCGTATGCTGGAACTAATAAAGACTAC
CloneB              CCAGGCAAGGGGCTGGAGTGGGTGGCAGTTATATCGTATGCTGGAACTAATAAAGACTAC

                    ————————→
Germline3-30*04     GCAGACTCCGTGAAGGGCCGATTCACCATCTCCAGAGACAATTCCAAGAACACGCTGTAT
CloneA              GCAGACTCCGTTAAGGACCGATTCACCATCTCGAGAGACAATTCCAAGAACACGCTGTAT
CloneB              GCAGACTCCGTTAAGGACCGATTCACCATCTCGAGAGACAATTCCAAGAACACGCTGTAT

                                                  CDR3 →
Germline3-30*04     CTGCAAATGAACAGCCTGAGAGCTGAGGACACGGCTGTGTATTACTGTGCGAGAGA
CloneA              CTGGAAATGAACAACCTGAGACTTGAAGACACGGCTTTGTTTTACTGTGCGAGAGG
CloneB              CTGGAAATGAACAACCTGAGACTTGAAGACACGGCTTTGTTTTACTGTGCGAGAGG
```

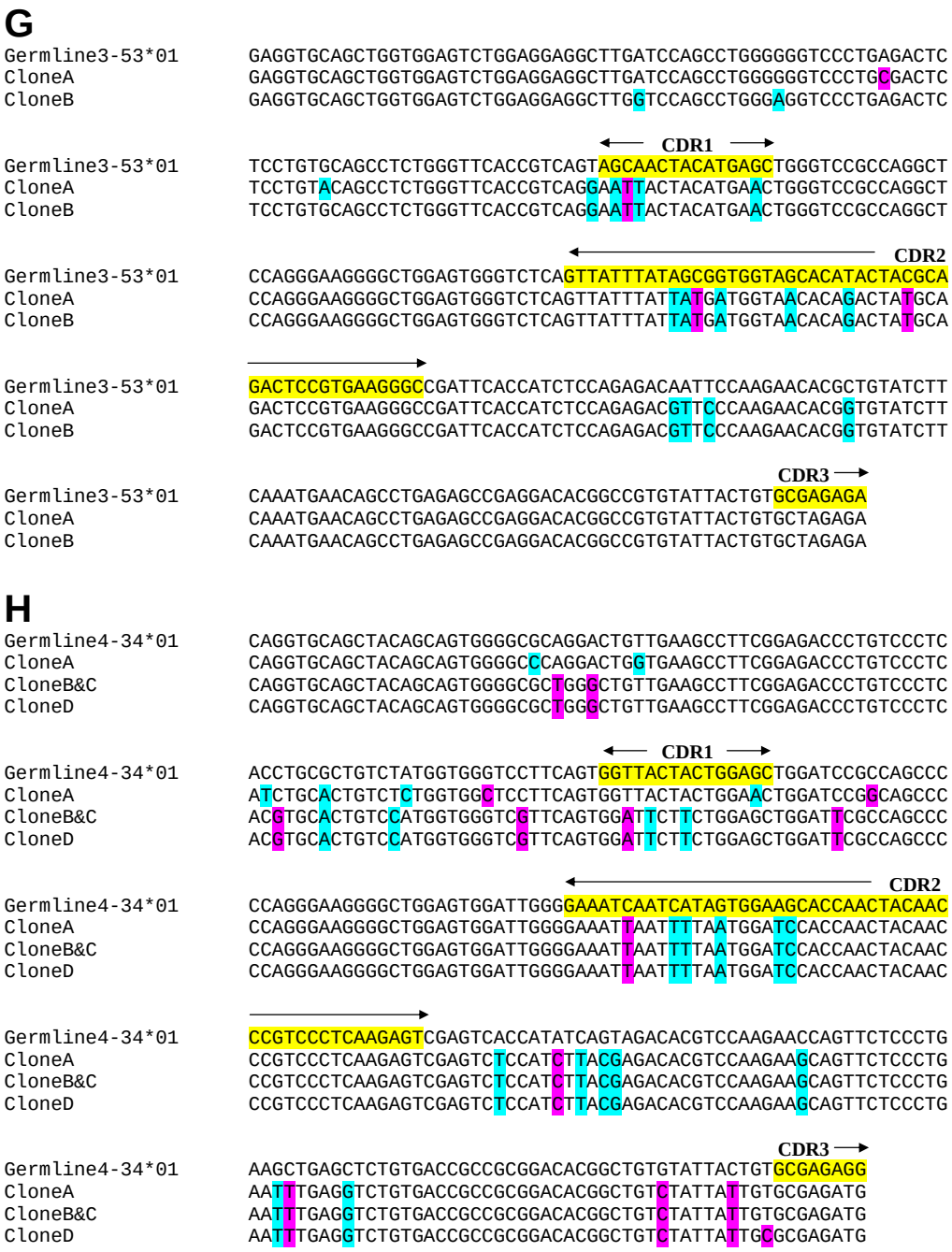

Figure 4.15 Clonal Proliferation in Sample MYO5

4 sets of sequences were isolated from sample MYO5 demonstrated somatic hypermutation and clonal proliferation (**A-H**). **Figure A-D** - The letters in the circles refer to individual sequences isolated from each B cell clone. Numbers indicate the minimum number of mutations required between each sequence with bracketed figures representing additional silent mutations. The dashed circle represents a hypothetical intermediate whose sequence was not found amongst the isolated sequences. **Figure E-H** - The DNA sequences of the clonally related sequences were aligned using ClustalW software to highlight the common and independent mutations. CDR regions are highlighted in yellow, replacement mutations in blue and silent mutations in purple.

V_H Gene	D_H Gene	J_H Gene	R-CDR	S-CDR	pCDR	p-CDR	R-FW	S-FW	pFW	p-FW
5-51*01	No D gene Assignment	3*02	9	7	0.44751	**-0.6002**	12	7	0.69597	**-0.0142**
3-30*04	5-12*01	6*02	7	2	0.47645	**0.66553**	7	4	0.67262	**-0.3219**
3-53*01	3-22*01	4*02	8	3	0.45711	**0.16134**	8	1	0.65885	**0.97999**
4-34*01	No D gene Assignment	4*02	8	2	0.42123	**-0.5993**	13	12	0.65376	**-0.0699**

Table 4.12 Analysis of Replacement and Silent Mutations and Positive and Negative Selection in Clonally Related B Cells in Sample MYO5

The number of replacement and silent mutations and the presence of any positive and negative selection were conducted as per Hershberg *et al* (294) as previously described. For clonally related sequences mutations shared across the sequences are only counted once and p values are calculated for the clone as a single entity. R-CDR/FW and S-CDR/FW represent the number of replacement and silent mutations in the CDR and FW respectively. pCDR represents the probability of having a R mutation in the CDR given all the mutations in the sequence except R mutations within the FW while pFW represents the probability of having a R mutation in the FW given all the mutations in the sequence except R mutations within the CDR and p-CDR/FW represent the p-value of the focused binominal test on the CDR and FW respectively. A negative sign indicates negative selection. p-values <0.05 were deemed significant.

4.2.3.5 V_H Repertoire from Myositis PBL

A blood sample was obtained from patient MYO5 allowing the gene repertoire within the blood to be determined (**Figure 4.11**); although this was taken 3 years after the second biopsy was conducted. Approximately 50 sequences have been isolated from the PBL repertoire (**Table 4.13**). Within the PBL a selection for gene segments V_H1 and 2 was observed which were significant against the published normal control values but were not significant against the germline complexity (**Figure 4.16A**). A selection against V_H4 segments was observed within the patient's blood sample which was significantly decreased in comparison to published normal control values and the selection was also significant against the germline complexity. The D_H gene repertoire was assessed from the 41.9% of sequences where a D gene could statistically be assigned (**Figure 4.16B**). As shown in Figure 4.16B this gene repertoire almost mirrors that of the normal control repertoire as well as the germline complexity, the only significant difference observed was a selection for the D_H3 gene segments but this was only significant against the germline complexity and not the normal control values. Analysis of the J_H gene repertoire demonstrated a selection for J_H2 and J_H4 gene segments which

were used significantly higher in the MYO5 PBL repertoire compared to the normal control values (**Figure 4.16C**). A selection against the use of J_H1 and J_H6 gene segments was also observed within the PBL repertoire. For J_H6 this decline was significant against normal control values but not the germline complexity whereas the decline in J_H1 family usage was only significant against the germline complexity and not the normal control repertoire.

For some sequences isolated from the PBL from patient MYO5 anomalies were detected between the JOINSOLVER and IMGT/V-QUEST software. For the V_H1-69*01 D_H5-12*01 J_H5*02 gene rearrangement IMGT/V-QUEST identified a different highest D_H gene match and assigned D_H3-22*01 to the rearrangement. In JOINSOLVER this gene was the 3rd best matching gene with only 8 consecutive nucleotides compared to the 9 observed for the D_H5-12*01 gene which were sufficient to assign the D_H gene statistically. Using the IMGT/V-QUEST software the D_H5-12*01 gene was the 2nd best matching gene and had a match score of 25 compared to 69 for the D_H3-22*01 gene. For the non-functional gene rearrangement using the V_H2-26*01 gene with 30 mutations, IMGT/V-QUEST assigned a different D_H gene segment to this rearrangement. Instead of assigning the D_H2-21*02 gene a D_H2-15*01 gene was assigned, this was found to be the 3rd best matching D_H gene segment using JOINSOLVER. Another difference was also observed with another non-functional gene, IMGT/V-QUEST failed to find a rearrangement for the V_H3-23*01 J_H1*01 identified using JOINSOLVER and was only able to identify the V_H segment of the rearrangement. IMGT/V-QUEST was also able to detect a deletion within the functional V_H3-66*01 D_H6-19*01 J_H5*02 rearrangement with 56 mutations. This single codon deletion was observed within the CDR2. When this deletion had been restored into the rearrangement both JOINSOLVER and IMGT/V-QUEST aligned the sequence to a V_H3-21*01 D_H6-19*01 J_H5*02 rearrangement with a total of 44 mutations, junctional sequences were common between both alignments.

V_H Gene	D_H Gene	J_H Gene	Number of Isolated Sequences	Number of Point Mutations	CDR3	V-J Length (bp)	Consecutive D length (bp) (+Mismatches)
1-03*01	No D gene Assignment	4*02	1	0	ARIHQEGPDY	17	8
1-03*01	No D gene Assignment	3*02	1	19	ARAGHTVPNNAFDI	23	6
1-18*01	2-21*02	3*02	1	17	ARDNVVVTVTTAFDI	24	14
1-46*01	2-21*02	4*02	(1)	46	AECGGDCLYFD*	33	15
1-46*01	3-22*01	2*01	1	2	ARVWNYYDSSGYYVGYFDL	36	26
1-46*01	No D gene Assignment	5*02	1	31	ARGGGYGYIWFDP	19	6
1-69*01	3-22*01	4*01	1	10	ARAYYSDSSGYGPFDN	39	24(+1)
1-69*01	3-3*02	2*01	1	1	ARTEWLLSSYWYFDL	21	14
1-69*01	3-3*02	6*02	2	37, 38	ARSSPFQNFWSALSYREAFYYAMDV	60	12
1-69*01	3-9*01	4*02	1	19	ARCSTHYDDLSGYNMAYYFDY	43	20(+3)
1-69*01	No D gene Assignment	1*01	(1)	25	ARDYRPKTSS	13	5
1-69*01	5-12*01	5*02	1	21	ARNFYDNSGYNWFDP	24	9
1-69*01	No D gene Assignment	6*02	1	25	ARAQFSYVAYIYYFYAMDV	40	8
1-69*06	No D gene Assignment	3*02	1	33	ARGRGNNSEGFDI	31	6
1-69*06	No D gene Assignment	5*02	1	10	ARDERYIGEVMTTNWFDP	31	7
1-69*06	2-8*01	4*02	1	0	ARAPQGRKNCTNGVCYTGGT	49	25
2-05*01	No D gene Assignment	4*02	1	2	AHRSNGPLFDY	20	6
2-26*01	2-15*01	6*02	(1)	0	ARTDIVVVVAANPPSLLTTVWT	44	23
2-26*01	2-21*02	5*02	(1)	30	TRTTESWWWLLRDDRGST(cc)	48	15(+1)
2-26*01	No D gene Assignment	4*02	2	0, 1	ARIPELDRWYLFDY	23	8
2-26*01	No D gene Assignment	5*02	2	19, 20	ARINREGWIGLG	30	6
3-07*02	No D gene Assignment	4*02	1	0	ARDWWLDNY	17	7
3-21*01	2-2*01	3*02	1	30	ARDGLPAARDI	22	11
3-21*01	No D gene Assignment	5*02	1	30	ARGVGMPGNPVFRFDP	32	5
3-21*01	No D gene Assignment	3*02	1	0	ARDDSTSPGSAFDI	21	8
3-21*01	6-19*01	5*02	1	21	ARGVAMAGTRVCTFDP	36	12(+1)
3-23*01	No D gene Assignment	1*01	(1)	15	ARWRGIS(cg)	21	5
3-23*01	3-10*01	2*01	1	0	AKNPNMVRDLRGVWYFDL	33	11
3-23*01	4-17*01	2*01	1	1	AKDSGVDYGAHGGLWYFDL	34	10
3-30*04	No D gene Assignment	3*01	2	23, 26	ARESVPNCGAGTCHPRDRAFDV	45	9
3-30*04	3-3*01	4*02	1	30	AREEGRQNTDFWSGYVFDC	54	17
3-30*04	3-3*02	2*01	1	1	ARTEWLLSSYWYFDL	21	14
3-48*01	No D gene Assignment	4*02	1	21	ARAGFFEPHFDF	33	7

Cont…

V_H Gene	D_H Gene	J_H Gene	Number of Isolated Sequences	Number of Point Mutations	CDR3	V-J Length (bp)	Consecutive D length (bp) (+Mismatches)
3-66*01	6-19*01	5*02	1	56	TRGLAVAGTGVLCFDP	39	11
3-73*01	No D gene Assignment	4*02	1	23	ARPSAAYTSTWPGDY	45	7
4-34*01	4-17*01	5*02	1	4	ARGGYGDYLKWFDP	22	12
4-34*01	No D gene Assignment	6*02	1	13	ARALGF	11	6
5-51*01	No D gene Assignment	4*02	1	35	AAFDTHAGARFLY	33	7
5-51*01	No D gene Assignment	4*02	1	22	TRLDTDAGAKFEY	36	7
5-51*01	No D gene Assignment	3*02	1	15	ARHSMYTFPDDALDK	37	6
5-51*01	5-24*01	4*02	1	0	ARQDSRDGYNPFDY	25	17
6-01*01	No D gene Assignment	4*02	2	0, 7	ARGGAGEDFDY	15	7
6-01*01	No D gene Assignment	5*02	1	23	ARGFLKLGFDP	28	8

Table 4.13 Heavy chain genes identified from the PBL sample of myositis patient MYO5 PBL

Best matching germline sequences were identified from aligning sequences in the IMGT database using JOINSOLVER software from the MYO5 PBL sample. The total number of sequences isolated is given in the 4th column of the table; non-functional rearrangements indicated in brackets. Identical sequences with the same V_H, $D_{H,}$ $J_{H,}$ CDR3 and base mutations were only counted once. CDR3 amino acid sequences were also identified using the JOINSOLVER software; * indicates the presence of a stop codon within the CDR3. V-J lengths and consecutive D match lengths (bp) were also identified using the JOINSOLVER software and allowed assignment of the D_H genes as described in section 2.3.12.3.

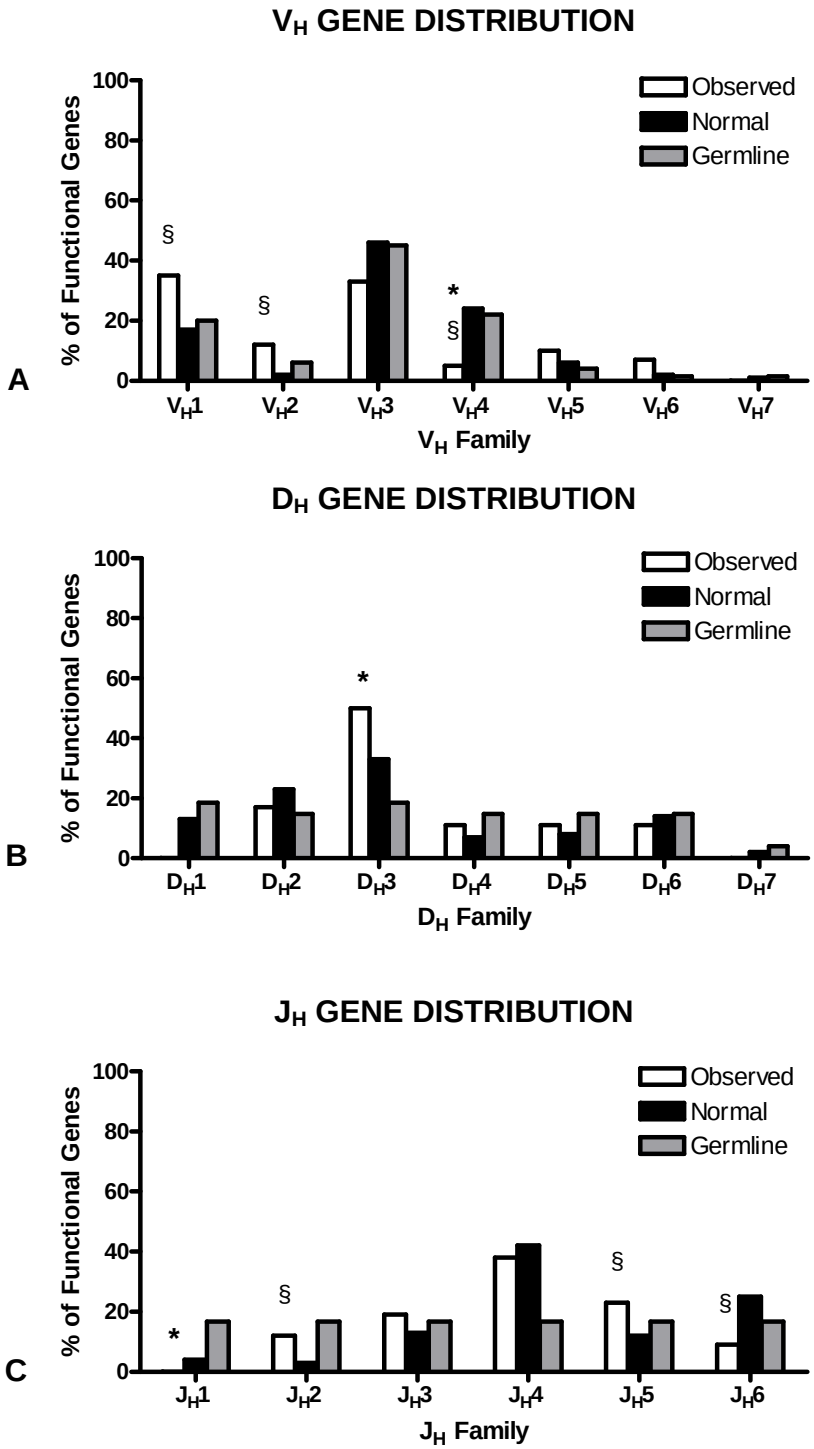

Figure 4.16 V_H Gene Family Usage of MYO5 PBL

V_H gene family usage. Distribution of functional genes was compared with published normal control values from Volpe and Kepler (251) as well as the germline complexity assuming every germline gene is capable of producing a functional rearrangement. Absolute values were used in Chi Square Analysis to determine gene selections. § represent a significant difference from normal PBL values; * represent a significant difference from the germline ($p<0.05$).

4.2.3.6 Mutational Analysis of B Cell Ig Sequences Isolated from PBL

Mutational numbers within rearranged genes demonstrated a variety of mutational numbers within PBL sequences (**Figure 4.17A**). Over 40% of sequences were highly mutated with over 21 mutations within V_H gene segments. Over 30% of cells were from a naïve population with between 0 and 2 mutations. The remainder of sequences contain between 3 and 20 mutations. Mutational distribution (**Figure 4.17B**) percentages within framework and CDR regions show that there were a higher percentage of mutations within CDR regions compared to framework regions. Comparing mutational distributions between CDR regions show that there were a higher percentage of mutations within CDR1.

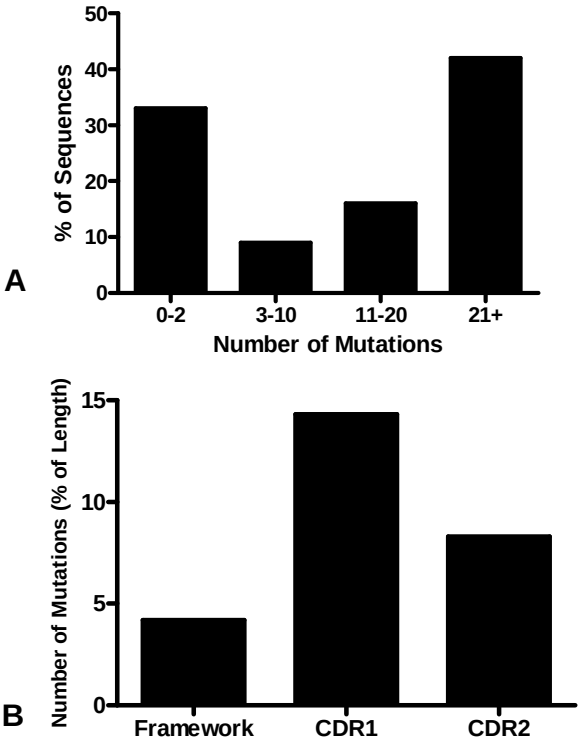

Figure 4.17 Numbers of Mutations and Mutational Distribution of Functional Sequences in MYO5 PBL

Figure 4.17A - The number of mutations within functional rearranged genes were analysed in the PBL sample of MYO5. Base differences within the first 24 bases of sequence were disregarded as this part of the sequence binds the 5' V_H primer. Graph demonstrates sequences within cellular infiltrates show a diverse distribution of mutational numbers.

Figure 4.17B - The locations of mutations observed within functional rearranged genes were categorised as being within FR or CDR regions. The numbers of mutations within these regions were expressed as a percentage of the entire length of the region to correct for the longer lengths observed within the framework regions. Graph demonstrates a higher percentage of mutations within CDR regions compared to framework regions.

Analysis of the R and S mutations from Ig sequences isolated from the PBL (**Table 4.14**) demonstrated negative selection within the framework regions of 10 of the sequences. Positive selection in the CDR was observed in 3 of the sequences while 1 sequence demonstrated negative selection within the CDR. This sequence also exhibited negative selection in the FW regions.

V_H Gene	D_H Gene	J_H Gene	Number of Isolated Sequences	Number of Point Mutations	R-CDR	S-CDR	pCDR	p-CDR	R-FW	S-FW	pFW	p-FW
1-03*01	No D gene Assignment	4*02	1	0	-	-	-	-	-	-	-	-
1-03*01	No D gene Assignment	3*02	1	19	6	1	0.47127	**0.63617**	8	4	0.70269	**-0.4975**
1-18*01	2-21*02	3*02	1	17	7	0	0.47674	**0.31052**	6	4	0.68809	**-0.5539**
1-46*01	2-21*02	4*02	(1)	46	11	2	0.47626	**-0.7247**	21	12	0.674	**-0.3563**
1-46*01	3-22*01	2*01	1	2	0	0	0.47626	**-0.5237**	1	1	0.674	**-0.652**
1-46*01	No D gene Assignment	5*02	1	31	9	5	0.47626	**-0.672**	10	7	0.674	**-0.037**
1-69*01	3-22*01	4*01	1	10	4	2	0.44858	**-0.9895**	1	3	0.67095	**-0.0181**
1-69*01	3-3*02	2*01	1	1	0	0	0.44858	**-0.5514**	0	1	0.67095	**-0.3291**
1-69*01	3-3*02	6*02	2	37	11	1	0.44858	**0.77525**	14	11	0.67095	**-0.1641**
				38	10	2	0.44858	**-0.7636**	14	12	0.67095	**-0.0644**
1-69*01	3-9*01	4*02	1	19	9	2	0.44858	**0.15835**	5	3	0.67095	**-0.2767**
1-69*01	No D gene Assignment	1*01	(1)	25	10	2	0.44858	**0.1692**	9	4	0.67095	**-0.5608**
1-69*01	5-12*01	5*02	1	21	7	4	0.44858	**0.88572**	6	4	0.67095	**-0.0695**
1-69*01	No D gene Assignment	6*02	1	25	11	1	0.44858	**0.26589**	6	7	0.67095	**-0.0695**
1-69*06	No D gene Assignment	3*02	1	33	7	4	0.44956	**-0.492**	14	8	0.67148	**-0.1623**
1-69*06	No D gene Assignment	5*02	1	10	2	1	0.44956	**-0.8508**	5	2	0.67148	**-0.7688**
1-69*06	2-8*01	4*02	1	0	-	-	-	-	-	-	-	-
2-05*01	No D gene Assignment	4*02	1	2	1	0	0.44387	**0.44387**	1	0	0.6816	**0.6816**
2-26*01	2-15*01	6*02	(1)	0	-	-	-	-	-	-	-	-
2-26*01	2-21*02	5*02	(1)	30	10	4	0.46263	**0.44118**	12	4	0.68432	**-0.4245**
2-26*01	No D gene Assignment	4*02	2	0	-	-	-	-	-	-	-	-
				1	0	0	0	-	1	0	0.74726	**0.74726**

Cont…

V_H Gene	D_H Gene	J_H Gene	Number of Isolated Sequences	Number of Point Mutations	R-CDR	S-CDR	pCDR	p-CDR	R-FW	S-FW	pFW	p-FW
2-26*01	No D gene Assignment	5*02	2	19	9	1	0.46263	**0.1913**	5	4	0.68432	**-0.2384**
				20	9	1	0.46263	**0.30178**	5	5	0.68432	**-0.126**
3-07*02	No D gene Assignment	4*02	1	0	-	-	-	**-**	-	-	-	**-**
3-21*01	2-2*01	3*02	1	30	12	5	0.5135	**0.93998**	7	6	0.65938	**-0.0219**
3-21*01	No D gene Assignment	5*02	1	30	10	3	0.5135	**-0.5886**	8	9	0.65938	**-0.0202**
3-21*01	No D gene Assignment	3*02	1	0	-	-	-	**-**	-	-	-	**-**
3-21*01	6-19*01	5*02	1	21	7	6	0.49658	**-0.6483**	5	3	0.66123	**-0.0241**
3-23*01	No D gene Assignment	1*01	(1)	15	6	1	0.45266	**0.22144**	6	2	0.65	**0.94618**
3-23*01	3-10*01	2*01	1	0	-	-	-	**-**	-	-	-	**-**
3-23*01	4-17*01	2*01	1	1	0	0	0.45265	**-**	1	0	0.65000	**0.65000**
3-30*04	No D gene Assignment	3*01	2	23	10	1	0.47645	**0.03902**	10	2	0.67262	**0.48789**
				26	6	1	0.47645	**-0.5693**	11	8	0.67262	**-0.2576**
3-30*04	3-3*01	4*02	1	30	11	3	0.47645	**0.98399**	7	9	0.67262	**-0.0079**
3-30*04	3-3*02	2*01	1	1	0	0	0.47645	**-0.5235**	0	1	0.67262	**-0.3274**
3-48*01	No D gene Assignment	4*02	1	21	5	3	0.51637	**-0.1685**	6	7	0.6621	**-0.0222**
3-66*01	6-19*01	5*02	1	56	17	7	0.46522	**-0.9478**	19	13	0.66817	**-0.0209**
3-73*01	No D gene Assignment	4*02	1	23	3	4	0.47416	**-0.0347**	8	8	0.66265	**-0.0186**
4-34*01	4-17*01	5*02	1	4	0	0	0.42123	**-0.5788**	3	1	0.65376	**0.75232**
4-34*01	No D gene Assignment	6*02	1	13	3	0	0.42123	**-0.8171**	5	5	0.65376	**-0.3309**
5-51*01	No D gene Assignment	4*02	1	35	14	3	0.43137	**0.0339**	14	4	0.70065	**-0.7216**
5-51*01	No D gene Assignment	4*02	1	22	8	1	0.43137	**0.00717**	13	0	0.70065	**0.05484**

Cont…

V_H Gene	D_H Gene	J_H Gene	Number of Isolated Sequences	Number of Point Mutations	R-CDR	S-CDR	pCDR	p-CDR	R-FW	S-FW	pFW	p-FW
5-51*01	No D gene Assignment	3*02	1	15	2	2	0.43137	**-0.4749**	8	3	0.70065	**-0.5078**
5-51*01	5-24*01	4*02	1	0	-	-	-	**-**	-	-	-	**-**
6-01*01	No D gene Assignment	4*02	2	0	-	-	-	**-**	-	-	-	**-**
				7	5	0	0.47248	**0.09678**	1	1	0.65538	**-0.6893**
6-01*01	No D gene Assignment	5*02	1	23	9	2	0.47248	**0.81772**	5	7	0.65538	**-0.0272**

Table 4.14 Analysis of Replacement and Silent Mutations and Positive and Negative Selection in Sample MYO5 PBL

Replacement and silent mutations within the immunoglobulin sequences and antigen-driven selection were determined according to Hershberg *et al* (294) and the corresponding computer programme (http://clip.med.yale.edu/selection). This improved method of analysis uses a focused binomial test to establish positive or negative mutational selections within the sequence with high specificity and increased sensitivity accounting for known biases within the immunoglobulin gene sequence. R-CDR and S-CDR represents the number of replacement and silent mutations within the CDR respectively. pCDR represents the probability of having a R mutation in the CDR given all the mutations in the sequence except R mutations within the FW while P-CDR is the p-value of the focused binominal test on the CDR. Conversely R-FW and S-FW represents the number of replacement and silent mutations within the FW respectively. pFW represent the probability of having a R mutation in the FW given all the mutations in the sequence except R mutations within the CDR while p-FW is the p-value of the focused binominal test on the FW. If the number of R mutations is less than expected the software will test for negative selection and p-values will be preceded by a negative sign or if the number of mutations is more than expected the software will test for positive selection. p-values <0.05 are highlighted in yellow and were deemed significant for selection.

4.2.3.7 CDR3 Analysis

No significant changes were observed in the CDR3 length between the functional and non-functional populations (**Table 4.15**) as well as between the different mutational groups within the functional population (**Figure 4.18**). Similarly no significant differences were observed for the P and N nucleotide additions between the two populations or between the two different junctional regions within each population. As seen within the Ig sequences of the myositis infiltrating repertoire a significant difference was observed for the exonuclease activity. A significant increase in this activity was observed at the 5' end of the D_H and J_H gene in comparison to the 3'V_H gene in the functional population. A significant change was also observed at the 3'V_H gene junction between the functional and non-functional populations. A significant increase in exonuclease activity was observed in the non-functional sequences at the 3'V_H region compared to the functional sequences. This increase in exonuclease activity may have resulted in a frameshift resulting in a non-functional rearrangement.

CDR3 Length	**Functional**	15.2 ± 6			
	Non-Functional	13.8 ± 2.7			
		VD Junction		**DJ Junction**	
P Nucleotide	**Functional**	1.0 ± 0.2		0.8 ± 0.2	
	Non-Functional	0.3 ± 0.3		0	
N Nucleotide	**Functional**	7.8 ± 1.5		7.9 ± 1.4	
	Non-Functional	4.7 ± 2.2		12 ± 5.1	
		3' V_H	**5' D_H**	**3' D_H**	**5'J_H**
Exonuclease Activity	**Functional**	1.6 ± 0.3*	5.1 ± 0.9$^{\theta}$	5.8 ± 1.0	4.9 ± 0.7$^{\theta}$
	Non-Functional	3.7 ± 0.7	5.3 ± 1.8	5.3 ± 0.7	7.3 ± 3.3

Table 4.15 CDR3 and Junctional Analysis in Sample MYO5 PBL

The mean amino acid length of the CDR3, the mean nucleotide numbers corresponding to P and N nucleotides as well as the mean number of germline nucleotides lost due to exonuclease activity were calculated from the junctional regions of all PBL immunoglobulin sequences from sample MYO5. Results are given as the Mean ± SEM. * indicates a significant difference between functional and non-functional sequences established using an unpaired t test. Θ represents a significant difference from 3'V_H.

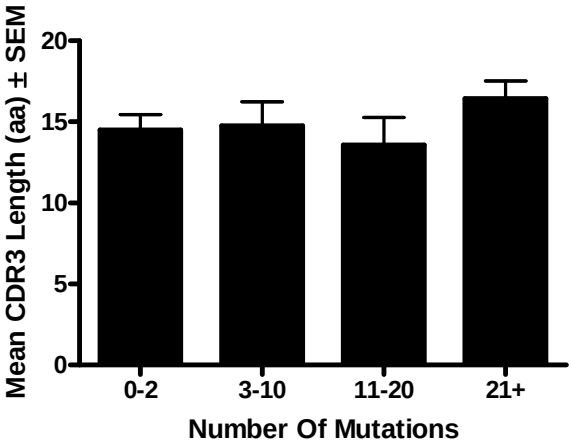

Figure 4.18 Mean CDR3 Lengths in Relation to V_H Mutational Numbers

The mean CDR3 length was calculated for immunoglobulin sequences according the number of mutations within the V_H segment of the gene rearrangement to establish any relationship between mutational number and CDR3 length. Results are given as Mean amino acid CDR3 length ± SEM. Groups were compared for statistical significance using the Tukey-Kramer test for multiple comparisons. The graph demonstrates that no significant changes in CDR3 length were observed at the various number of mutations. p-values <0.05 would have been deemed significant.

No clonally related sets of genes were isolated from the PBL population but as the sequences isolated represent only a small fraction of the overall PBL population the presence of clones within the isolated sequences was not anticipated. In cases where multiple genes were isolated from the PBL repertoire which shared VDJ gene assignments and junctional sequences these sequences only differed or shared 1 mutation and were therefore not deemed clonally related.

4.2.3.8 Comparison of Myositis Muscle V_H Repertoire with Myositis PBL Repertoire

Comparing the infiltrating cell repertoire from the muscle to that of the published repertoire of normal control values demonstrated selections for and against certain gene segments (**Figure 4.12**). As a blood sample was obtained from this patient the V_H gene repertoire of the muscle infiltrating B cells was also compared to the patients own PBL repertoire (**Figure 4.19**). Although this is from a small percentage of the whole PBL repertoire, and a larger number of sequences would be required for a more accurate comparison, it does demonstrate a selection for and against gene families. For V_H gene family segments there was a selection against V_H1 in the muscle repertoire in comparison with the PBL repertoire as there was a significant increase of these gene families evident within the PBL (**Figure 4.19A**). No other selections were significant for the V_H gene families despite the appearance of selection for V_H3, V_H4 and V_H5 family genes; these were not significant when the absolute values were used in Chi square analysis although a p-value of 0.0574 (**Appendix 2**) was observed for V_H5 family genes which may represent a significant selection for these genes segments if a larger population of sequences had been isolated from each sample. D_H1 gene segments were significantly selected for within the muscle repertoire and this selection for D_H1 was not observed within the PBL repertoire (**Figure 4.19B**). No significant changes in the J_H repertoire was observed between the muscle and PBL Ig populations (**Figure 4.19C**).

A larger number of sequences from the PBL repertoire is required to provide a more accurate representation of entire PBL repertoire and to fully determine if the selections for and against gene segments are in fact present between muscle and PBL repertoires. In addition to comparing the V_H repertoires between the muscle infiltrating population and the PBL population, comparing the individual gene rearrangements used in each population demonstrated that no similar gene rearrangements were found in both the muscle and blood B cell populations.

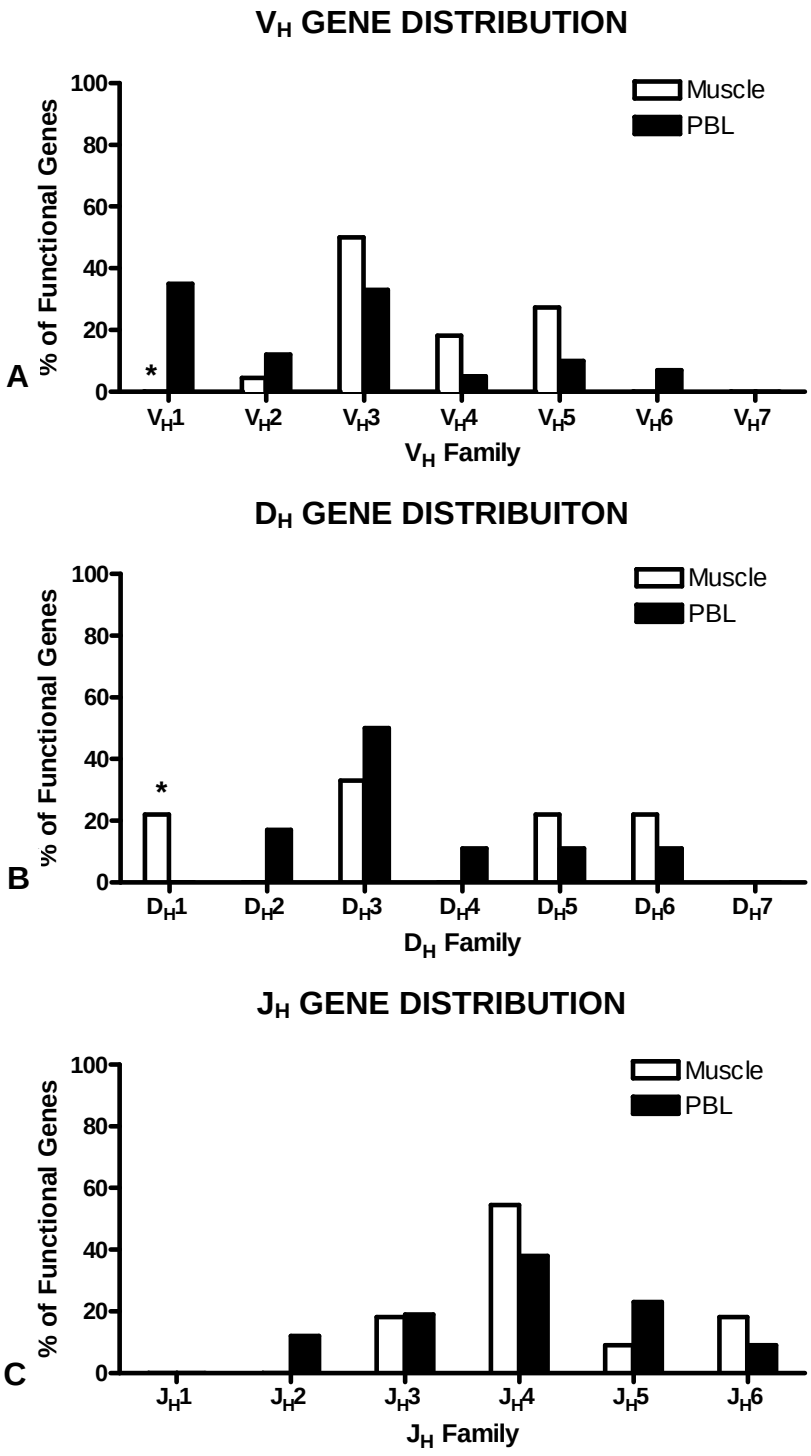

Figure 4.19 V_H Gene Family Usage of MYO5 muscle and PBL

V_H gene family usage. Distribution of functional genes from infiltrating cells within the muscle were compared to the patients own PBL repertoire. * represent a significant difference from myositis PBL values ($p<0.05$).

4.2.4 Sample MYO6

Areas of cellular infiltration within sample MYO6 were microdissected and the DNA released was amplified for all 6 V_H families by nested PCR (**Figure 4.20**). Despite the presence of B cells and plasma cells within the infiltrating population only 1 sequence could be found within various regions of the sample (**Table 4.16A**). This sequence utilised the V_H3-72*01 gene segment, in addition to the J_H4*02 gene segment; no D gene assignment could be statistically assigned. The isolated sequence contained 15 mutations, with the higher percentage of these mutations being present within the CDR2 region. Analysis of the R and S mutations indicates a negative selection in the FW regions of this sequence (**Table 4.16B**), negative selection was also found within the CDR but this was not significant. Analysis of the junctional region of this sequence could not be completed as no D_H gene could be statistically assigned. No changes in gene assignments were observed using the IMGT/V-QUEST software.

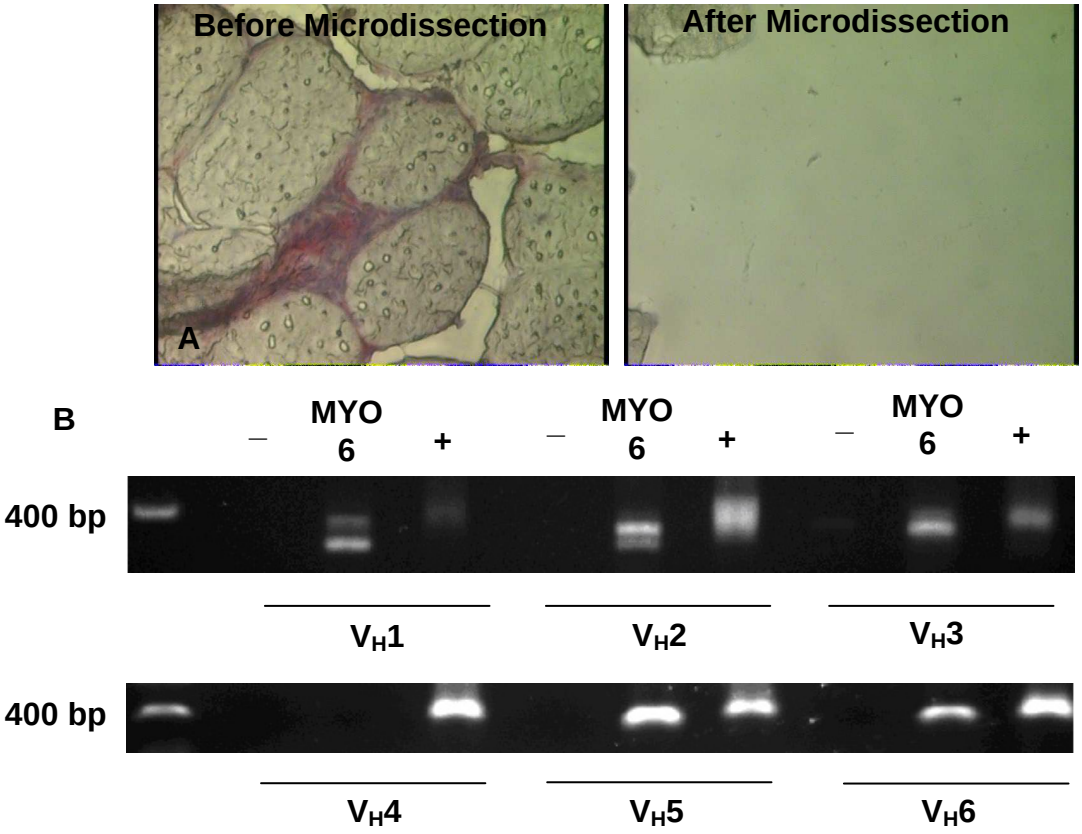

Figure 4.20 Microdissection of infiltrating B cells and amplification of V_H-gene rearrangements from Sample MYO6

The region of B cell and plasma cell infiltration was microdissected from sample MYO6. Figure 4.20A demonstrates the microdissection of the region of cellular infiltration. Images were taken at 400X. DNA released from these microdissections was amplified using a Nested PCR system (Figure 4.20B), as described in Chapter 2. – indicates negative control PCR reactions where DNA was substituted with water while + indicates positive control PCR reactions using peripheral blood mononuclear cells isolated from peripheral blood of a healthy individual. Results show amplification for VH1, 2, 3, 5 and 6 families.

A

V_H Gene	D_H Gene	J_H Gene	Number of Isolated Sequences	Number of Point Mutations	CDR3	CDR3 Length (aa)	Mutational Distribution (% of length)			V-J Length (bp)	Consecutive D length (bp) (+Mismatches)
							Framework	CDR1	CDR2		
3-72*01	No D gene Assignment	4*02	1	15	ARVVEGVVSRDVLDY	15	3.6	0	8.3	30	8

B

R-CDR	S-CDR	pCDR	p-CDR	R-FW	S-FW	pFW	p-FW
3	2	0.45531	**-0.2424**	4	6	0.65729	**-0.0271**

Table 4.16 A&B Sequence Analysis from Sample MYO6

Table 4.16A - Best matching germline sequences were identified from aligning sequences in the IMGT database using JOINSOLVER software from the MYO6 myositis section. Identical sequences with the same V_H, D_H, J_H, CDR3 and base mutations were only counted once. V-J lengths and consecutive D match lengths (bp) were also identified using the JOINSOLVER software and allowed assignment of the D_H genes as described in section 2.3.12.3.

The number of mutations within functional rearranged genes were analysed collectively from all region of dissected cellular infiltration. Base differences within the first 24 bases of sequence were disregarded as this part of the sequence binds the 5' V_H primer.

The locations of mutations observed within functional rearranged genes were categorised as being within FR or CDR regions. The numbers of mutations within these regions were expressed as a percentage of the entire length of the region to correct for the longer lengths observed within the framework regions.

Table 4.16B - The number of replacement and silent mutations and the presence of any positive and negative selection was conducted as per Hershberg *et al* (294) as previously described. R-CDR/FW and S-CDR/FW represent the number of replacement and silent mutations in the CDR and FW respectively. pCDR represents the probability of having a R mutation in the CDR given all the mutations in the sequence except R mutations within the FW while pFW represents the probability of having a R mutation in the FW given all the mutations in the sequence except R mutations within the CDR and p-CDR/FW represent the p-value of the focused binominal test on the CDR and FW respectively. A negative sign indicates negative selection. p-values <0.05 were deemed significant.

4.2.5 Sample MYO7

Areas of cellular infiltration microdissected from MYO7 (**Figure 4.21**) produced only 2 different functional gene rearrangements (**Table 4.17A**). Both sequences isolated were from the V_H3 gene family, V_H3-66*01 and V_H3-74*01. D_H3-3*01 was the only D gene that could be statistically assigned in the V_H3-66*01 rearrangement along with the J_H5*02 gene segment while the other gene rearrangement utilised the J_H6*02 segment. No changes were observed using IMGT/V-QUEST. The V_H3-74*01 was non-mutated but the other functional gene contained 9 V_H mutations, with the higher percentage of these mutations present within the CDR2 region. Analysis of R and S mutations demonstrated no significant selection was present in either the CDR or FW regions (**Table 4.17B**). As no D gene could be assigned to the V_H3-74*01 rearrangement no junctional analysis could be conducted. Analysis in the V_H3-66*01 rearrangement found that 0 and 1 P nucleotides and 1 and 9 N nucleotides were present at the VD and DJ junctions respectively. Exonuclease activity was calculated to have removed 2, 1, 9 and 4 nucleotides from the 3' V_H, 5'D_H, 3'D_H and 5'J_H regions of the junction respectively.

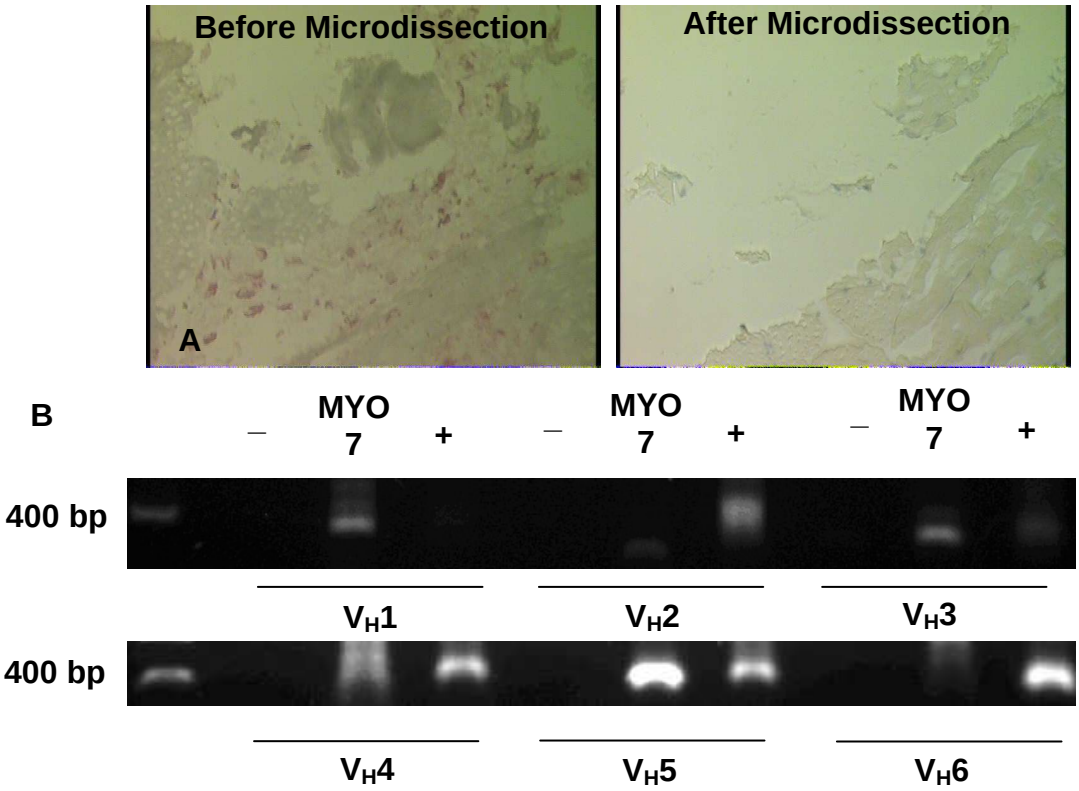

Figure 4.21 Microdissection of infiltrating B cells and amplification of V_H-gene rearrangements from Sample MYO7

The region of B cell and plasma cell infiltration was microdissected from sample MYO7. Figure 4.21A demonstrates the microdissection of the region of cellular infiltration. Images were taken at 400X. DNA released from these microdissections was amplified using a Nested PCR system (Figure 4.21B), as described in Chapter 2. – indicates negative control PCR reactions where DNA was substituted with water while + indicates positive control PCR reactions using peripheral blood mononuclear cells isolated from peripheral blood of a healthy individual. Results show amplification for V_H1, 3, 4 and 5 families.

A

V_H Gene	D_H Gene	J_H Gene	Number of Isolated Sequences	Number of Point Mutations	CDR3	CDR3 Length (aa)	Mutational Distribution (% of length)			V-J Length (bp)	Consecutive D length (bp) (+Mismatches)
							Framework	CDR1	CDR2		
3-66*01	3-3*01	5*02	1	9	ARILRSLEWSTGGWFDP	17	2.3	0	7.8	32	20 (+1)
3-74*01	No D gene Assignment	6*02	1	0	ARGELVKRADYYYGMDV	17	0	0	0	22	8

B

V_H Gene	D_H Gene	J_H Gene	R-CDR	S-CDR	pCDR	p-CDR	R-FW	S-FW	pFW	p-FW
3-66*01	3-3*01	5*02	3	1	0.46522	**0.87**	3	2	0.66817	**-0.4153**
3-74*01	No D gene Assignment	6*02	-	-	-	**-**	-	-	-	**-**

Table 4.17 A&B Sequence Analysis from Sample MYO7

Table 4.17A - Best matching germline sequences were identified from aligning sequences in the IMGT database using JOINSOLVER software from the MYO7 myositis section. Identical sequences with the same V_H, D_H, J_H, CDR3 and base mutations were only counted once. V-J lengths and consecutive D match lengths (bp) were also identified using the JOINSOLVER software and allowed assignment of the D_H genes as described in section 2.3.12.3.

The number of mutations within functional rearranged genes were analysed collectively from all region of dissected cellular infiltration. Base differences within the first 24 bases of sequence were disregarded as this part of the sequence binds the 5' V_H primer.

The locations of mutations observed within functional rearranged genes were categorised as being within FR or CDR regions. The numbers of mutations within these regions were expressed as a percentage of the entire length of the region to correct for the longer lengths observed within the framework regions.

Table 4.17B - The number of replacement and silent mutations and the presence of any positive and negative selection was conducted as per Hershberg *et al* (294) as previously described. R-CDR/FW and S-CDR/FW represent the number of replacement and silent mutations in the CDR and FW respectively. pCDR represents the probability of having a R mutation in the CDR given all the mutations in the sequence except R mutations within the FW while pFW represents the probability of having a R mutation in the FW given all the mutations in the sequence except R mutations within the CDR and p-CDR/FW represent the p-value of the focused binominal test on the CDR and FW respectively. A negative sign indicates negative selection. p-values <0.05 were deemed significant.

4.2.6 Sample MYO16

4.2.6.1 V_H Repertoire of Infiltrating B Cells

As shown in **Figure 4.22**, two significant areas of infiltration within sample MYO16 were microdissected and the DNA released from these areas was amplified in a nested PCR protocol for V_H amplification. The sequences isolated from these areas, as well as a third area of infiltration, are shown in **Table 4.18**. To establish the gene repertoire within sample MYO16, and to allow comparisons with normal control values and the baseline germline complexity, the sequence data from all regions was combined. From 36 functional gene rearrangements there was a significant selection for V_H3 family gene segments against both the normal control values and the germline complexity (**Figure 4.23A**). No significant differences were observed for the other V_H gene families against either set of the control values. In this sample D_H gene assignments could be completed in 47.2% of the sequences. From this repertoire a selection for D_H6 genes was observed which was significant against both the normal control values and germline complexity (**Figure 4.23B**), no other selection was observed. A positive selection for J_H3 gene segments was observed within J_H family members (**Figure 4.23C**). This selection was significant against normal control values but not against the germline complexity. Other selections observed within the infiltrating muscle repertoire in sample MYO16 was a decreased selection for the J_H1 and J_H2 genes but these were only significant against the germline complexity and not the normal control values.

The discrepancies observed between JOINSOLVER and IMGT/V-QUEST for these sequences was observed for the V_H3-15*01 J_H6*03 gene rearrangement with 1 mutation from region 5, IMGT/V-QUEST also suggest the 2P*01, 4*03 and 4*01 J_H gene assignment (**Appendix 1**). These three genes were the only genes that IMGT/V-QUEST could assign and they were not found to be within the best 5 matches using the JOINSOLVER software. For the V_H3-11*01 J_H6*03 gene rearrangements in region 6 with 11 and 13 mutations the best matching V_H germline gene in both JOINSOLVER and IMGT/V-QUEST was V_H3-48*01, with fewer mutations, which resulted in an increased score of 1389 compared to 1326 in

JOINSOLVER and 1372 compared to 1309 in IMGT/V-QUEST. In these instances the V_H3-11*01 gene was shown to be the 4th and 6th best matching gene but as these genes were rearranged with the same D and J gene segments in addition to the same CDR3 and junctional sequence composition as the other V_H3-11*01 gene rearrangements these sequences were considered to be assigned the V_H3-11*01 gene segment instead of the V_H3-48*01 gene segment.

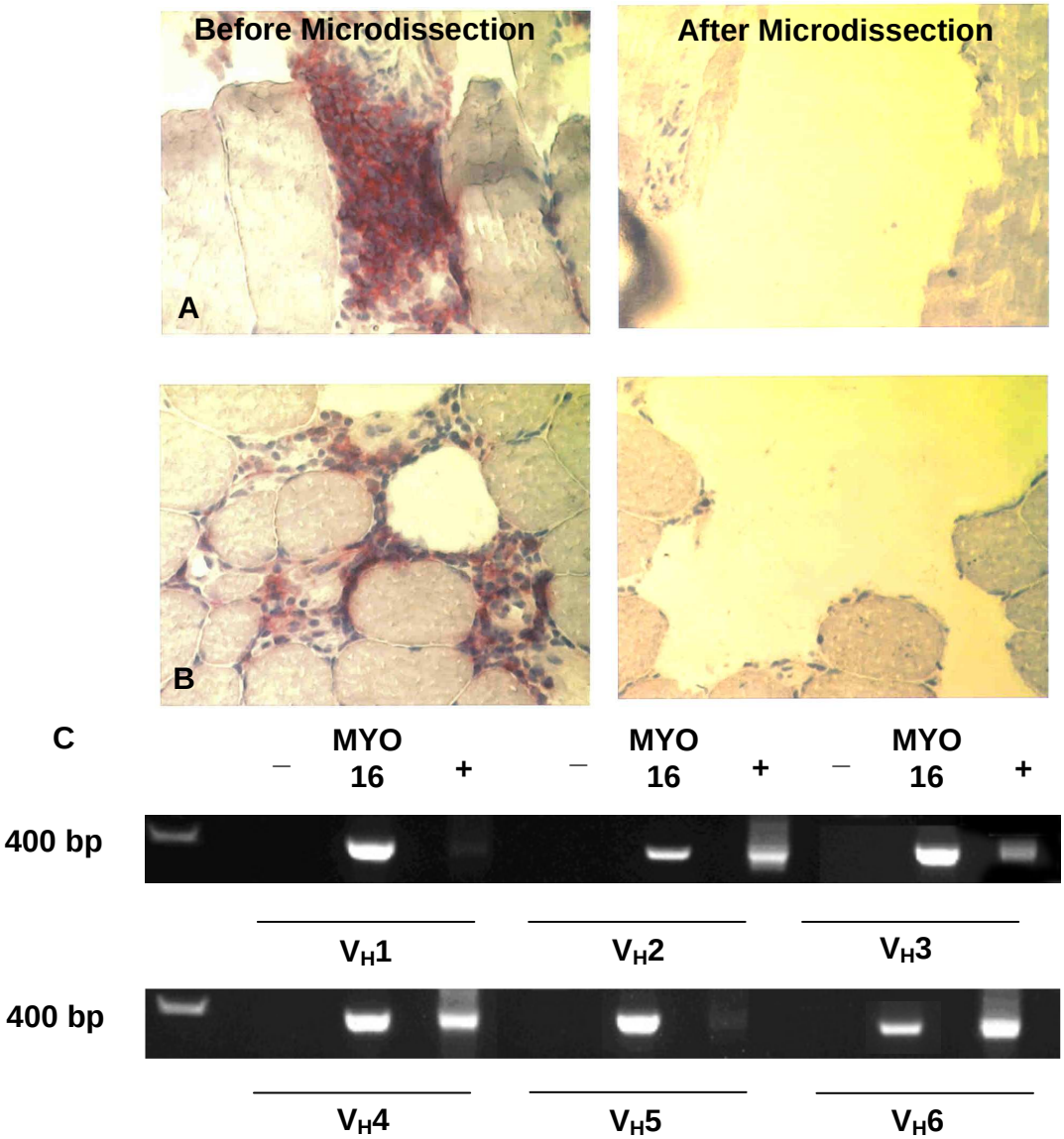

Figure 4.22 Microdissection of infiltrating B cells and amplification of V_H-gene rearrangements from Sample MYO16

Three regions of B cell infiltration were microdissected from sample MYO16. Figure 4.22A and B demonstrates the microdissection of 2 regions of cellular infiltration. Images were taken at 400X. DNA released from these microdissections was amplified using a Nested PCR system (Figure 4.22C), as described in Chapter 2. – indicates negative control PCR reactions where DNA was substituted with water while + indicates positive control PCR reactions using peripheral blood mononuclear cells isolated from peripheral blood of a healthy individual. Results show amplification of all 6 V_H families.

Region	V_H Gene	D_H Gene	J_H Gene	Number of Isolated Sequences	Number of Point Mutations	CDR3	V-J Length (bp)	Consecutive D length (bp) (+Mismatches)
1	3-09*01	6-6*01	4*02	5	0, 1, 1, 1, 1	AKDIGGQLVLGGVHYFDY	32	11
	4-59*01	6-13*01	4*02	2	0, 2	ARVIAAAGKAAAYFDY	28	14
	4-59*03	6-13*01	4*02	1	1	ARVIAAAGKAAAYFDY	32	14
5	1-46*01	No D gene Assignment	4*03	(1)	2	SRVIPGFPLDRFD	41	7
	1-46*01	6-6*01	4*02	1	1	ARGGYSSSSGDY	28	15
	3-07*01	No D gene Assignment	3*02	10	24, 32, 32, 33, 33, 33, 33, 33, 33, 34	SRVIPGFPLDRFDI	33	7
	3-07*01	3-3*01	4*03	1	1	ARVGYYDFWGGWGFDY	31	22(+1)
	3-15*01	3-3*01	4*02	1	13	ARVGYYDFWSGWGFDY	38	23
	3-15*01	No D gene Assignment	6*03	1	1	TTDLGELPYYYYYMDV	16	8
	3-15*01	No D gene Assignment	6*03	1	2	TTDLGELPYYYYMDV	16	6
	4-34*01	3-10*01	5*02	1	0	ARVSKITMVRGVIIKRGWFDP	43	27(+1)
6	1-18*01	3-9*01	4*02	1	0	ARVRYDGILTGYDDY	34	15
	3-11*01	No D gene Assignment	6*03	6	0, 1, 3, 3, 11, 13	AREYGRSLWLTQYYYYMDV	28	9
	3-48*01	2-21*01	6*03	2	0,1	AREVVVVIATPLSDYYYMDV	32	18
	3-48*01	No D gene Assignment	6*03	1	1	AREYGRSLWLTQYYYYMDV	28	9
	3-48*03	4-4*01	4*02	1	6	ARGFFPNYSNYGNLLGS	44	12
	4-61*01	6-13*01	6*03	1	2	ARETSPGYSSSWYGSYYYYYMDV	36	21

Table 4.18 Heavy chain genes identified from myositis sample MYO16

Best matching germline sequences were identified from aligning sequences in the IMGT database using JOINSOLVER software from the MYO16 myositis section. The total number of sequences isolated is given in the 5th column of the table; non-functional rearrangements indicated in brackets. Identical sequences with the same V_H, D_H, J_H, CDR3 and base mutations were only counted once. CDR3 amino acid sequences were also identified using the JOINSOLVER software. V-J lengths and consecutive D match lengths (bp) were also identified using the JOINSOLVER software and allowed assignment of the D_H genes as described in section 2.3.12.3.

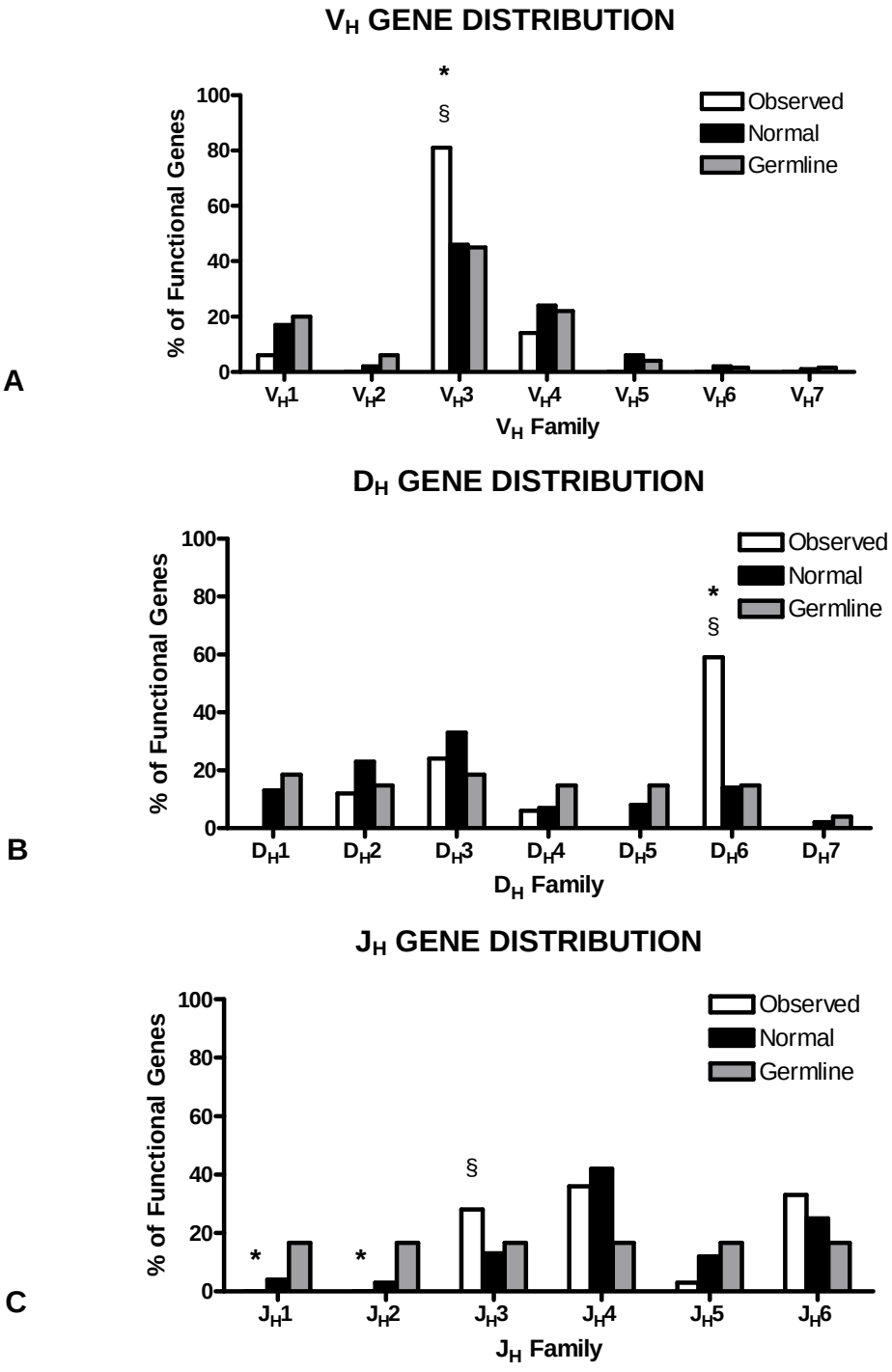

Figure 4.23 V_H Gene Family Usage of MYO16

V_H gene family usage. Distribution of functional genes was compared with published normal control values from Volpe and Kepler (251) as well as the germline complexity assuming every germline gene is capable of producing a functional rearrangement. Absolute values were used in Chi Square Analysis to determine gene selections. § represent a significant difference from normal control values; * represent a significant difference from the germline ($p<0.05$).

4.2.6.2 Mutational Analysis of B Cell Ig Sequences of Sample MYO16

Results of mutational numbers within functional rearrangements show that over 60% of sequences isolated from sample MYO16 were essentially non-mutated (0-2 mutations) while over 20% of sequences were highly mutated, containing over 21 mutations (**Figure 4.24A**). The remainder of the sequences contain between 3 and 20 mutations. Results suggest the presence of a largely naïve population, possibly due to a recent migration from the PBL, as well as the presence of a number of highly mutated, possibly memory cells. As seen with previous samples there were a higher percentage of mutations within CDR regions (**Figure 4.24B**) in comparison to framework regions. There were a similar percentage of mutations between CDR1 and CDR2 regions.

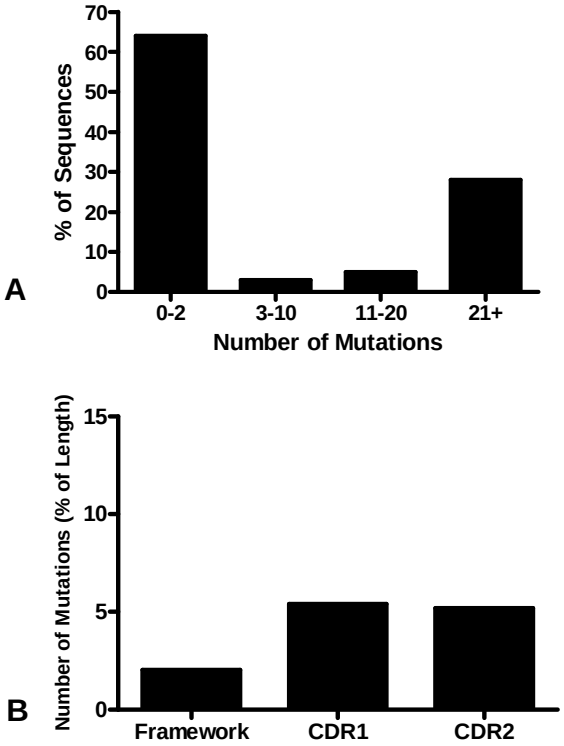

Figure 4.24 Numbers of Mutations and Mutational Distribution of Functional Sequences in MYO16

Figure 4.24A - The number of mutations within functional rearranged genes were analysed collectively from all 3 regions of cellular infiltration within sample MYO16. Base differences within the first 24 bases of sequence were disregarded as this part of the sequence binds the 5' V_H primer. Graph demonstrates sequences within cellular infiltrates were primarily from a naïve population of infiltrating cells with some highly mutated sequences also present.

Figure 4.24B - The locations of mutations observed within functional rearranged genes were categorised as being within FR or CDR regions. The numbers of mutations within these regions were expressed as a percentage of the entire length of the region to correct for the longer lengths observed within the framework regions. Graph demonstrates a higher percentage of mutations within CDR regions compared to framework regions.

Negative selection was observed in the FW regions of two of the isolated sequences; both of these sequences share the same VDJ gene rearrangement and junctional composition. Negative selection in the FW was also observed in a 3rd sequence in sample MYO16 but in contrast to the other 2 sequences a negative selection was also observed in the CDR of this sequence. All other sequences demonstrated both positive and negative selection within the CDR and FW regions but these were not statistically significant.

Region	V_H Gene	D_H Gene	J_H Gene	Number of Isolated Sequences	Number of Point Mutations	R-CDR	S-CDR	pCDR	p-CDR	R-FW	S-FW	pFW	p-FW
1	3-09*01	6-6*01	4*02	5	0	-	-	-	**-**	-	-	-	**-**
					1	0	0	0.46314	**-0.53685**	0	1	0.67146	**-0.3285**
					1	0	0	0.46314	**-0.53685**	0	1	0.67146	**-0.3285**
					1	0	0	0.46314	**-**	1	0	0.67146	**-0.6714**
					1	0	0	0.46314	**-**	1	0	0.67146	**-0.6714**
	4-59*01	6-13*01	4*02	2	0	-	-	-	**-**	-	-	-	**-**
					2	1	0	0.44001	**0.44001**	1	0	0.65645	**0.65645**
	4-59*03	6-13*01	4*02	1	1	0	0	0.44024	**-**	1	0	0.65722	**0.65722**
5	1-46*01	No D gene Assignment	4*03	(1)	2	0	0	0.47626	**-0.5237**	1	1	0.674	**-0.652**
	1-46*01	6-6*01	4*02	1	1	0	0	0.47626	**0**	1	0	0.674	**0.674**
	3-07*01	No D gene Assignment	3*02	10	24	11	2	0.44397	**0.16557**	6	5	0.67012	**-0.1312**
					32	14	2	0.44397	**0.17902**	8	8	0.67012	**-0.0537**
					32	14	2	0.44397	**0.12036**	9	7	0.67012	**-0.1422**
					33	14	3	0.44397	**0.3412**	7	9	0.67012	**-0.0084**
					33	14	2	0.44397	**0.17902**	9	8	0.67012	**-0.0829**
					33	14	2	0.44397	**0.17902**	9	8	0.67012	**-0.0829**
					33	14	2	0.44397	**0.17902**	9	8	0.67012	**-0.0829**
					33	15	2	0.44397	**0.12446**	8	8	0.67012	**-0.0537**
					33	14	2	0.44397	**0.17902**	9	8	0.67012	**-0.0829**
					34	14	2	0.44397	**0.25277**	9	9	0.67012	**-0.0468**
	3-07*01	3-3*01	4*03	1	0	-	-	-	**-**	-	-	-	**-**
					1	0	0	0.44397	**0**	1	0	0.67012	**0.67012**
	3-15*01	3-3*01	4*02	1	13	0	0	0.43976	**-0.0097**	5	8	0.6595	**-0.0496**
	3-15*01	No D gene Assignment	6*03	1	1	0	0	0.43976	**-0.5602**	0	1	0.6595	**-0.3404**
	3-15*01	No D gene Assignment	6*03	1	2	2	0	0.43976	**0.19339**	0	0	0.6595	**0**
	4-34*01	3-10*01	5*02	1	0	-	-	-	**-**	-	-	-	**-**

Cont…

Region	V_H Gene	D_H Gene	J_H Gene	Number of Isolated Sequences	Number of Point Mutations	R-CDR	S-CDR	pCDR	p-CDR	R-FW	S-FW	pFW	p-FW
6	1-18*01	3-9*01	4*02	1	0	-	-	-	**-**	-	-	-	**-**
	3-11*01	No D gene Assignment	6*03	6	0	-	-	-	**-**	-	-	-	**-**
					1	0	0	0.48848	**-**	1	0	0.66592	**0.66592**
					3	0	0	0.48848	**-0.2617**	1	2	0.66592	**-0.2975**
					3	0	0	0.48848	**-0.5115**	2	1	0.66592	**1.03506**
					11	6	1	0.48848	**0.31078**	2	2	0.66592	**-0.2566**
					13	6	1	0.48848	**0.71789**	2	4	0.66592	**-0.0526**
	3-48*01	2-21*01	6*03	2	0	-	-	-	**-**	-	-	-	**-**
					1	0	0	0.51636	**-**	1	0	0.6621	**0.6621**
	3-48*01	No D gene Assignment	6*03	1	1	0	0	0.49992	**-0.5001**	0	1	0.66392	**-0.3361**
	3-48*03	4-41*01	4*02	1	6	4	1	0.49491	**0.43894**	0	1	0.66764	**-0.1105**
	4-61*01	6-13*01	6*03	1	2	1	0	0.4489	**0.4489**	1	0	0.65022	**0.65022**

Table 4.19 Analysis of Replacement and Silent Mutations and Positive and Negative Selection in Sample MYO16

Replacement and silent mutations within the immunoglobulin sequences and antigen-driven selection were determined according to Hershberg *et al* (294) and the corresponding computer programme (http://clip.med.yale.edu/selection). This improved method of analysis uses a focused binomial test to establish positive or negative mutational selections within the sequence with high specificity and increased sensitivity accounting for known biases within the immunoglobulin gene sequence. R-CDR and S-CDR represents the number of replacement and silent mutations within the CDR respectively. pCDR represents the probability of having a R mutation in the CDR given all the mutations in the sequence except R mutations within the FW while p-CDR is the p-value of the focused binominal test on the CDR. Conversely R-FW and S-FW represents the number of replacement and silent mutations within the FW respectively. pFW represent the probability of having a R mutation in the FW given all the mutations in the sequence except R mutations within the CDR while p-FW is the p-value of the focused binominal test on the FW. If the number of R mutations is less than expected the software will test for negative selection and p-values will be preceded by a negative sign or if the number of mutations is more than expected the software will test for positive selection. p-values <0.05 are highlighted in yellow and were deemed significant for selection.

4.2.6.3 CDR3 Analysis

The muscle infiltrating population of B cells in this sample only produced 1 non-functional rearrangement, as a result the unpaired t-test could not be used to determine if a significant difference occurs between the CDR3 lengths and junctional sequences of these sequences; the unpaired t-test requires more than 1 value in the non-functional group. As shown in Table 4.20 the mean CDR3 length of functional sequences was 16.7 ± 0.4 amino acids (ranging from 12 to 23 amino acids), while the non-functional gene had a CDR3 length of 13 amino acids. Analysis of the CDR3 lengths in correlation with the V_H mutations of the sequences demonstrated a significant decrease in the CDR3 length in highly mutated, 21+, sequences (**Figure 4.25**). This significant decrease in CDR3 length was observed for all 3 previous mutational groups. The different sequence features of the junctional regions were also analysed. In the functional population of sequences a significant difference was observed for the removal of nucleotides by exonuclease activity between the VD and DJ junctional regions but not for the addition of P or N nucleotides in the junctions. As only 1 non-functional sequence was isolated in this sample a statistical comparison between functional and non-functional sequences could be conducted. Within the functional population a significant increase of exonuclease activity at the 5'D_H and 5'J_H regions of the junction was observed compared to the 3'V_H region.

CDR3 Length	**Functional**	16.7 ± 0.4			
	Non-Functional	13			
		VD Junction		**DJ Junction**	
P Nucleotide	**Functional**	0.4 ± 0.2		0.6 ± 0.2	
	Non-Functional	N/A		N/A	
N Nucleotide	**Functional**	6.2 ± 0.9		8.9 ± 1.1	
	Non-Functional	N/A		N/A	
		3' V_H	**5' D_H**	**3' D_H**	**5'J_H**
Exonuclease Activity	**Functional**	1.1 ± 0.4	4.3 ± 0.7$^{\theta}$	2.7 ± 0.7	4 ± 0.6$^{\theta}$
	Non-Functional	N/A	N/A	N/A	N/A

Table 4.20 CDR3 and Junctional Analysis in Sample MYO16

The mean amino acid length of the CDR3, the mean nucleotide numbers corresponding to P and N nucleotides as well as the mean number of germline nucleotides lost due to exonuclease activity were calculated from the junctional regions of all immunoglobulin sequences from sample MYO16. Results are given as the Mean ± SEM, statistical significance was established using an unpaired t-test. Θ represents a significant difference from 3'V_H.

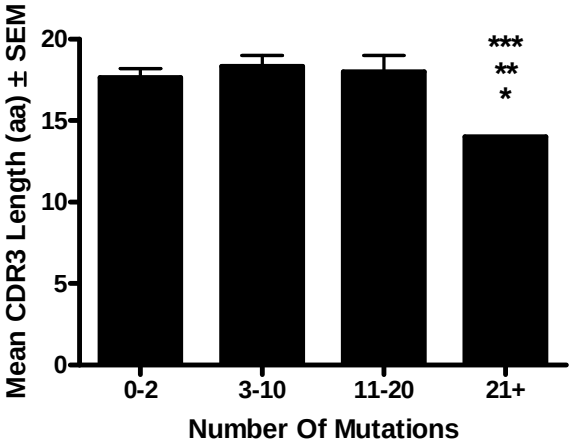

Figure 4.25 Mean CDR3 Lengths in Relation to V_H Mutational Numbers

The mean CDR3 length was calculated for immunoglobulin sequences according the number of mutations within the V_H segment of the gene rearrangement to establish any relationship between mutational number and CDR3 length. Results are given as Mean amino acid CDR3 length ± SEM. Groups were compared for statistical significance using the Tukey-Kramer test for multiple comparisons. The graph demonstrates significant changes in CDR3 length for sequences containing over 20 mutations. This reduction in CDR3 length was significant against sequences containing 0-2 mutations (*), 3-10 mutations (**) and 11-20 mutations (***). p-values <0.05 were deemed significant. * was calculated at <0.001.

4.2.6.4 Clonal Diversification in MYO16

Within sample MYO16 two clonally related sets of sequences were discovered (**Figure 4.26**). This provides evidence of B cell clonal proliferation and mutation within cellular infiltrates of muscle inflammation. These clones contained V_H3 family gene segments, V_H3-07*01 and V_H3-11*01, within the functional gene rearrangements. These clones were isolated from different regions of the muscle section; there was no evidence from the sequences isolated to suggest that clonally related B cells were migrating between different cellular aggregates suggesting that clones were generated independently in different cell clusters. In the clonal genealogical tree in Figure 4.26A 1 silent mutation was observed in the clonal branch consisting of clones C-J but this silent mutation was also observed in clone L. As clones C-J did not contain the additional replacement mutation found in clones K and L this would suggest that the mutations were formed during different and branch mutational lineages.

A

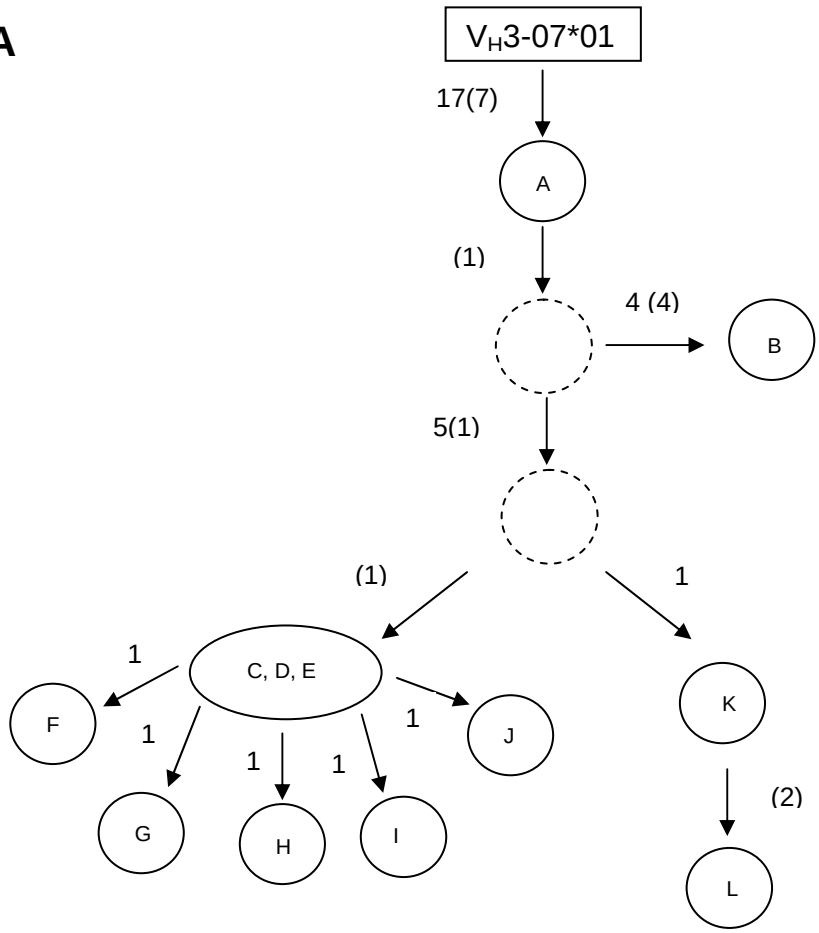
V_H3-07*01
17(7)
A
(1)
4 (4)
B
5(1)
(1)
1
1
C, D, E
F
1
1
1
1
J
G
H
I
K
(2)
L

B

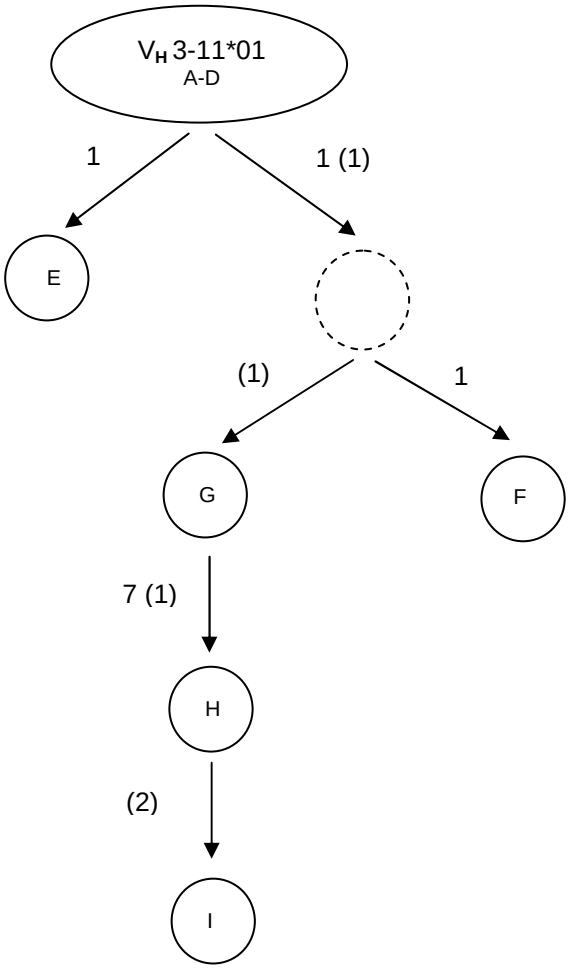
V_H 3-11*01
A-D
1
1 (1)
E
(1)
1
G
F
7 (1)
H
(2)
I

C

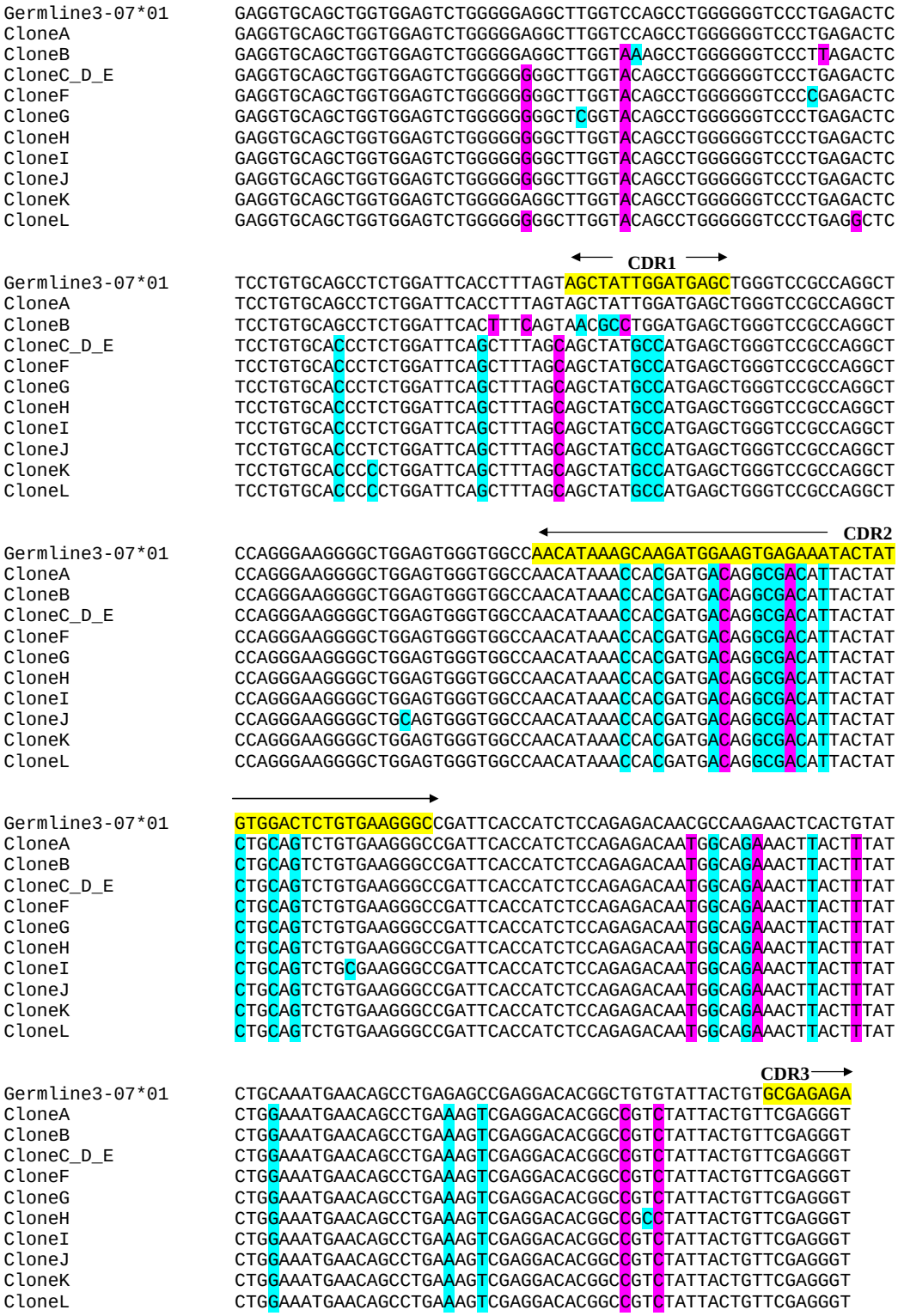
Germline3-07*01 GAGGTGCAGCTGGTGGAGTCTGGGGGAGGCTTGGTCCAGCCTGGGGGGTCCCTGAGACTC
CloneA GAGGTGCAGCTGGTGGAGTCTGGGGGAGGCTTGGTCCAGCCTGGGGGGTCCCTGAGACTC
CloneB GAGGTGCAGCTGGTGGAGTCTGGGGGAGGCTTGGTAAAGCCTGGGGGGTCCCTTAGACTC
CloneC_D_E GAGGTGCAGCTGGTGGAGTCTGGGGGGGGCTTGGTACAGCCTGGGGGGTCCCTGAGACTC
CloneF GAGGTGCAGCTGGTGGAGTCTGGGGGGGGCTTGGTACAGCCTGGGGGGTCCCCGAGACTC
CloneG GAGGTGCAGCTGGTGGAGTCTGGGGGGGGCTCGGTACAGCCTGGGGGGTCCCTGAGACTC
CloneH GAGGTGCAGCTGGTGGAGTCTGGGGGGGGCTTGGTACAGCCTGGGGGGTCCCTGAGACTC
CloneI GAGGTGCAGCTGGTGGAGTCTGGGGGGGGCTTGGTACAGCCTGGGGGGTCCCTGAGACTC
CloneJ GAGGTGCAGCTGGTGGAGTCTGGGGGGGGCTTGGTACAGCCTGGGGGGTCCCTGAGACTC
CloneK GAGGTGCAGCTGGTGGAGTCTGGGGGAGGCTTGGTACAGCCTGGGGGGTCCCTGAGACTC
CloneL GAGGTGCAGCTGGTGGAGTCTGGGGGGGGCTTGGTACAGCCTGGGGGGTCCCTGAGGCTC
CDR1
Germline3-07*01 TCCTGTGCAGCCTCTGGATTCACCTTTAGTAGCTATTGGATGAGCTGGGTCCGCCAGGCT
CloneA TCCTGTGCAGCCTCTGGATTCACCTTTAGTAGCTATTGGATGAGCTGGGTCCGCCAGGCT
CloneB TCCTGTGCAGCCTCTGGATTCACTTTCAGTAACGCCTGGATGAGCTGGGTCCGCCAGGCT
CloneC_D_E TCCTGTGCACCCTCTGGATTCAGCTTTAGCAGCTATGCCATGAGCTGGGTCCGCCAGGCT
CloneF TCCTGTGCACCCTCTGGATTCAGCTTTAGCAGCTATGCCATGAGCTGGGTCCGCCAGGCT
CloneG TCCTGTGCACCCTCTGGATTCAGCTTTAGCAGCTATGCCATGAGCTGGGTCCGCCAGGCT
CloneH TCCTGTGCACCCTCTGGATTCAGCTTTAGCAGCTATGCCATGAGCTGGGTCCGCCAGGCT
CloneI TCCTGTGCACCCTCTGGATTCAGCTTTAGCAGCTATGCCATGAGCTGGGTCCGCCAGGCT
CloneJ TCCTGTGCACCCTCTGGATTCAGCTTTAGCAGCTATGCCATGAGCTGGGTCCGCCAGGCT
CloneK TCCTGTGCACCCCTGGATTCAGCTTTAGCAGCTATGCCATGAGCTGGGTCCGCCAGGCT
CloneL TCCTGTGCACCCCTGGATTCAGCTTTAGCAGCTATGCCATGAGCTGGGTCCGCCAGGCT
CDR2
Germline3-07*01 CCAGGGAAGGGGCTGGAGTGGGTGGCCAACATAAAGCAAGATGGAAGTGAGAAATACTAT
CloneA CCAGGGAAGGGGCTGGAGTGGGTGGCCAACATAAACCACGATGACAGGCGACATTACTAT
CloneB CCAGGGAAGGGGCTGGAGTGGGTGGCCAACATAAACCACGATGACAGGCGACATTACTAT
CloneC_D_E CCAGGGAAGGGGCTGGAGTGGGTGGCCAACATAAACCACGATGACAGGCGACATTACTAT
CloneF CCAGGGAAGGGGCTGGAGTGGGTGGCCAACATAAACCACGATGACAGGCGACATTACTAT
CloneG CCAGGGAAGGGGCTGGAGTGGGTGGCCAACATAAACCACGATGACAGGCGACATTACTAT
CloneH CCAGGGAAGGGGCTGGAGTGGGTGGCCAACATAAACCACGATGACAGGCGACATTACTAT
CloneI CCAGGGAAGGGGCTGGAGTGGGTGGCCAACATAAACCACGATGACAGGCGACATTACTAT
CloneJ CCAGGGAAGGGGCTGCAGTGGGTGGCCAACATAAACCACGATGACAGGCGACATTACTAT
CloneK CCAGGGAAGGGGCTGGAGTGGGTGGCCAACATAAACCACGATGACAGGCGACATTACTAT
CloneL CCAGGGAAGGGGCTGGAGTGGGTGGCCAACATAAACCACGATGACAGGCGACATTACTAT
Germline3-07*01 GTGGACTCTGTGAAGGGCCGATTCACCATCTCCAGAGACAACGCCAAGAACTCACTGTAT
CloneA CTGCAGTCTGTGAAGGGCCGATTCACCATCTCCAGAGACAATGGCAGAAACTTACTTTAT
CloneB CTGCAGTCTGTGAAGGGCCGATTCACCATCTCCAGAGACAATGGCAGAAACTTACTTTAT
CloneC_D_E CTGCAGTCTGTGAAGGGCCGATTCACCATCTCCAGAGACAATGGCAGAAACTTACTTTAT
CloneF CTGCAGTCTGTGAAGGGCCGATTCACCATCTCCAGAGACAATGGCAGAAACTTACTTTAT
CloneG CTGCAGTCTGTGAAGGGCCGATTCACCATCTCCAGAGACAATGGCAGAAACTTACTTTAT
CloneH CTGCAGTCTGTGAAGGGCCGATTCACCATCTCCAGAGACAATGGCAGAAACTTACTTTAT
CloneI CTGCAGTCTGCGAAGGGCCGATTCACCATCTCCAGAGACAATGGCAGAAACTTACTTTAT
CloneJ CTGCAGTCTGTGAAGGGCCGATTCACCATCTCCAGAGACAATGGCAGAAACTTACTTTAT
CloneK CTGCAGTCTGTGAAGGGCCGATTCACCATCTCCAGAGACAATGGCAGAAACTTACTTTAT
CloneL CTGCAGTCTGTGAAGGGCCGATTCACCATCTCCAGAGACAATGGCAGAAACTTACTTTAT
CDR3
Germline3-07*01 CTGCAAATGAACAGCCTGAGAGCCGAGGACACGGCTGTGTATTACTGTGCGAGAGA
CloneA CTGGAAATGAACAGCCTGAAAGTCGAGGACACGGCCGTCTATTACTGTTCGAGGGT
CloneB CTGGAAATGAACAGCCTGAAAGTCGAGGACACGGCCGTCTATTACTGTTCGAGGGT
CloneC_D_E CTGGAAATGAACAGCCTGAAAGTCGAGGACACGGCCGTCTATTACTGTTCGAGGGT
CloneF CTGGAAATGAACAGCCTGAAAGTCGAGGACACGGCCGTCTATTACTGTTCGAGGGT
CloneG CTGGAAATGAACAGCCTGAAAGTCGAGGACACGGCCGTCTATTACTGTTCGAGGGT
CloneH CTGGAAATGAACAGCCTGAAAGTCGAGGACACGGCCGCCTATTACTGTTCGAGGGT
CloneI CTGGAAATGAACAGCCTGAAAGTCGAGGACACGGCCGTCTATTACTGTTCGAGGGT
CloneJ CTGGAAATGAACAGCCTGAAAGTCGAGGACACGGCCGTCTATTACTGTTCGAGGGT
CloneK CTGGAAATGAACAGCCTGAAAGTCGAGGACACGGCCGTCTATTACTGTTCGAGGGT
CloneL CTGGAAATGAACAGCCTGAAAGTCGAGGACACGGCCGTCTATTACTGTTCGAGGGT

D

```
Germline3-11*01     CAGGTGCAGCTGGTGGAGTCTGGGGGAGGCTTGGTCAAGCCTGGAGGGTCCCTGAGACTC
CloneA-D            CAGGTGCAGCTGGTGGAGTCTGGGGGAGGCTTGGTCAAGCCTGGAGGGTCCCTGAGACTC
CloneE              CAGGTGCAGCTGGTGGAGTCTGGGGGAGGCTTGGTCAAGCCTGGAGGGTCCCCGAGACTC
CloneF              CAGGTGCAGCTGGTGGAGTCTGGGGGAGGCTTGGTACAGCCTGGAGGGTCCCTGAGACTC
CloneG              CAGGTGCAGCTGGTGGAGTCTGGGGGAGGCTTGGTACAGCCTGGGGGGTCCCTGAGACTC
CloneH              CAGGTGCAGCTGGTGGAGTCTGGGGGAGGCTTGGTACAGCCTGGGGGGTCCCTGAGACTC
CloneI              CAGGTGCAGCTGGTGGAGTCTGGGGGAGGCTTGGTACAGCCTGGGGGGTCCCTGAGACTC

                                                  ← CDR1 →
Germline3-11*01     TCCTGTGCAGCCTCTGGATTCACCTTCAGTGACTACTACATGAGCTGGATCCGCCAGGCT
CloneA-D            TCCTGTGCAGCCTCTGGATTCACCTTCAGTGACTACTACATGAGCTGGATCCGCCAGGCT
CloneE              TCCTGTGCAGCCTCTGGATTCACCTTCAGTGACTACTACATGAGCTGGATCCGCCAGGCT
CloneF              TCCTGTGCAGCCTCTGGATTCACCTTCAGTGACTACTACATGAGCTGGATCCGCCAGGCT
CloneG              TCCTGTGCAGCCTCTGGATTCACCTTCAGTGACTACTACATGAGCTGGATCCGCCAGGCT
CloneH              TCCTGTGCAGCCTCTGGATTCACCTTCAGTAGCTATAGCATGAACTGGGTCCGCCAGGCT
CloneI              TCCTGTGCAGCCTCTGGATTCACCTTCAGTAGCTATAGCATGAACTGGGTCCGCCAGGCT

                                                  ← CDR2 ──────────
Germline3-11*01     CCAGGGAAGGGGCTGGAGTGGGTTTCATACATTAGTAGTAGTGGTAGTACCATATACTAC
CloneA-D            CCAGGGAAGGGGCTGGAGTGGGTTTCATACATTAGTAGTAGTGGTAGTACCATATACTAC
CloneE              CCAGGGAAGGGGCTGGAGTGGGTTTCATACATTAGTAGTAGTGGTAGTACCATATACTAC
CloneF              CCAGGGAAGGGGCTGGAGTGGGTTTCATACATTAGTAGTAGTGGTAGTACCATATACTAC
CloneG              CCAGGGAAGGGGCTGGAGTGGGTTTCATACATTAGTAGTAGTGGTAGTACCATATACTAC
CloneH              CCAGGGAAGGGGCTGGAGTGGGTTTCATACATTAGTAGTAGTAGTAGTACCATATACTAC
CloneI              CCAGGGAAGGGGCTGGAGTGGGTTTCATACATTAGTAGTAGTAGTAGTACCATATACTAC

                    ──────────→
Germline3-11*01     GCAGACTCTGTGAAGGGCCGATTCACCATCTCCAGGGACAACGCCAAGAACTCACTGTAT
CloneA-D            GCAGACTCTGTGAAGGGCCGATTCACCATCTCCAGGGACAACGCCAAGAACTCACTGTAT
CloneE              GCAGACTCTGTGAAGGGCCGATTCACCATCTCCAGGGACAACGCCAAGAACTCACTGTAT
CloneF              GCAGACTCTGTGAAGGGCCGATTCACCATCTCCAGGGACAACGCCAAGAACTCACTGTAT
CloneG              GCAGACTCTGTGAAGGGCCGATTCACCATCTCCAGGGACAACGCCAAGAACTCACTGTAT
CloneH              GCAGACTCTGTGAAGGGCCGATTCACCATCTCCAGGGACAACGCCAAGAACTCACTGTAT
CloneI              GCAGACTCTGTGAAGGGCCGATTCACCATCTCCAGAGACAATGCCAAGAACTCACTGTAT

                                                  CDR3 →
Germline3-11*01     CTGCAAATGAACAGCCTGAGAGCCGAGGACACGGCCGTGTATTACTGTGCGAGAGA
CloneA-D            CTGCAAATGAACAGCCTGAGAGCCGAGGACACGGCCGTGTATTACTGTGCGAGAGA
CloneE              CTGCAAATGAACAGCCTGAGAGCCGAGGACACGGCCGTGTATTACTGTGCGAGAGA
CloneF              CTGCAAATGAACAGCCTGAGAGTCGAGGACACGGCCGTGTATTACTGTGCGAGAGA
CloneG              CTGCAAATGAACAGCCTGAGAGCCGAGGACACGGCCGTGTATTACTGTGCGAGAGA
CloneH              CTGCAAATGAACAGCCTGAGAGCCGAGGACACGGCCGTGTATTACTGTGCGAGAGA
CloneI              CTGCAAATGAACAGCCTGAGAGCCGAGGACACGGCCGTGTATTACTGTGCGAGAGA
```

Figure 4.26 Clonal Proliferation in Sample MYO16

Two sets of sequences were isolated from sample MYO16 demonstrated somatic hypermutation and clonal proliferation (**A-D**). **Figure A&B** - The letters in the circles refer to individual sequences isolated from each B cell clone. Numbers indicate the minimum number of mutations required between each sequence with bracketed figures representing additional silent mutations. The dashed circle represents a hypothetical intermediate whose sequence was not found amongst the isolated sequences. **Figure C&D** - The DNA sequences of the clonally related sequences were aligned using ClustalW software to highlight the common and independent mutations. CDR regions are highlighted in yellow, replacement mutations in blue and silent mutations in purple.

Analysis of the replacement and silent mutations of these clones indicates that positive selection occurs within the CDR while negative selection occurs in the FW regions of the sequences (**Table 4.21**). These selections were only significant for the V_H3-07*01 clone for negative selections in the framework regions; no other selection was statistically significant. This negative selection was also observed in two of the individual sequences of this clone when the sequences were analysed independently (**Table 4.19**).

V_H Gene	D_H Gene	J_H Gene	R-CDR	S-CDR	pCDR	p-CDR	R-FW	S-FW	pFW	p-FW
3-07*01	No D gene Assignment	3*02	18	3	0.44397	**0.24823**	14	12	0.67012	**-0.0397**
3-11*01	No D gene Assignment	6*03	6	1	0.41326	**0.39307**	4	4	0.69174	**-0.1382**

Table 4.21 Analysis of Replacement and Silent Mutations and Positive and Negative Selection in Clonally Related B Cells in Sample MYO16

The number of replacement and silent mutations and the presence of any positive and negative selection was conducted as per Hershberg *et al* (294) as previously described. For clonally related sequences mutations shared across the sequences are only counted once and p values are calculated for the clone as a single entity. R-CDR/FW and S-CDR/FW represent the number of replacement and silent mutations in the CDR and FW respectively. pCDR represents the probability of having a R mutation in the CDR given all the mutations in the sequence except R mutations within the FW while pFW represents the probability of having a R mutation in the FW given all the mutations in the sequence except R mutations within the CDR and p-CDR/FW represent the p-value of the focused binominal test on the CDR and FW respectively. A negative sign indicates negative selection. p-values <0.05 were deemed significant.

4.2.7 Sample MYO17

From sample MYO17 only two functional sequences were isolated from multiple microdissections and DNA amplification (**Figure 4.27**). Table 4.22A details the characteristics of the two different isolated sequences. V_H3-30*03 and V_H6-01*01 gene segments were used in these sequences along with J_H4*02 and J_H5*02 respectively. A D_H gene, D_H3-9*01, could only be assigned to the V_H3-30*03 gene rearrangement; the consecutive D match length was not sufficient in the V_H6*01 gene rearrangement for a gene to be statistically assigned. Both V_H3 and V_H6 genes isolated from this sample were mutated, as shown in Table 4.22; they contained 12 and 5 mutations respectively. Examination of these mutations demonstrated that they were congregated mostly within CDR regions of the sequence. For the V_H3 gene these were mostly within the CDR1 region of the sequence while, conversely for the V_H6 gene, mutations were solely located within the CDR2 region of the sequence. Negative selection was observed in both the CDR and FW regions of both sequences (**Table 4.22B**) after analysis of the R and S mutations but these selections were not statistically significant. Analysis of the junctional characteristics from the V_H3-30*03 gene rearrangement where a statistical D_H match could be made revealed that no P nucleotides were present at with the VD or DJ junctions for either sequence. The number of N nucleotides assigned was 7 and 9 at the VD and DJ regions respectively while the mean exonuclease activity at the 3'V_H, 5'D_H, 3'D_H and 5'J_H region was 4, 0, 9 and 5 respectively.

The gene assignments using the JOINSOLVER software match those of the IMGT/V-QUEST software for both sequences isolated from sample MYO17.

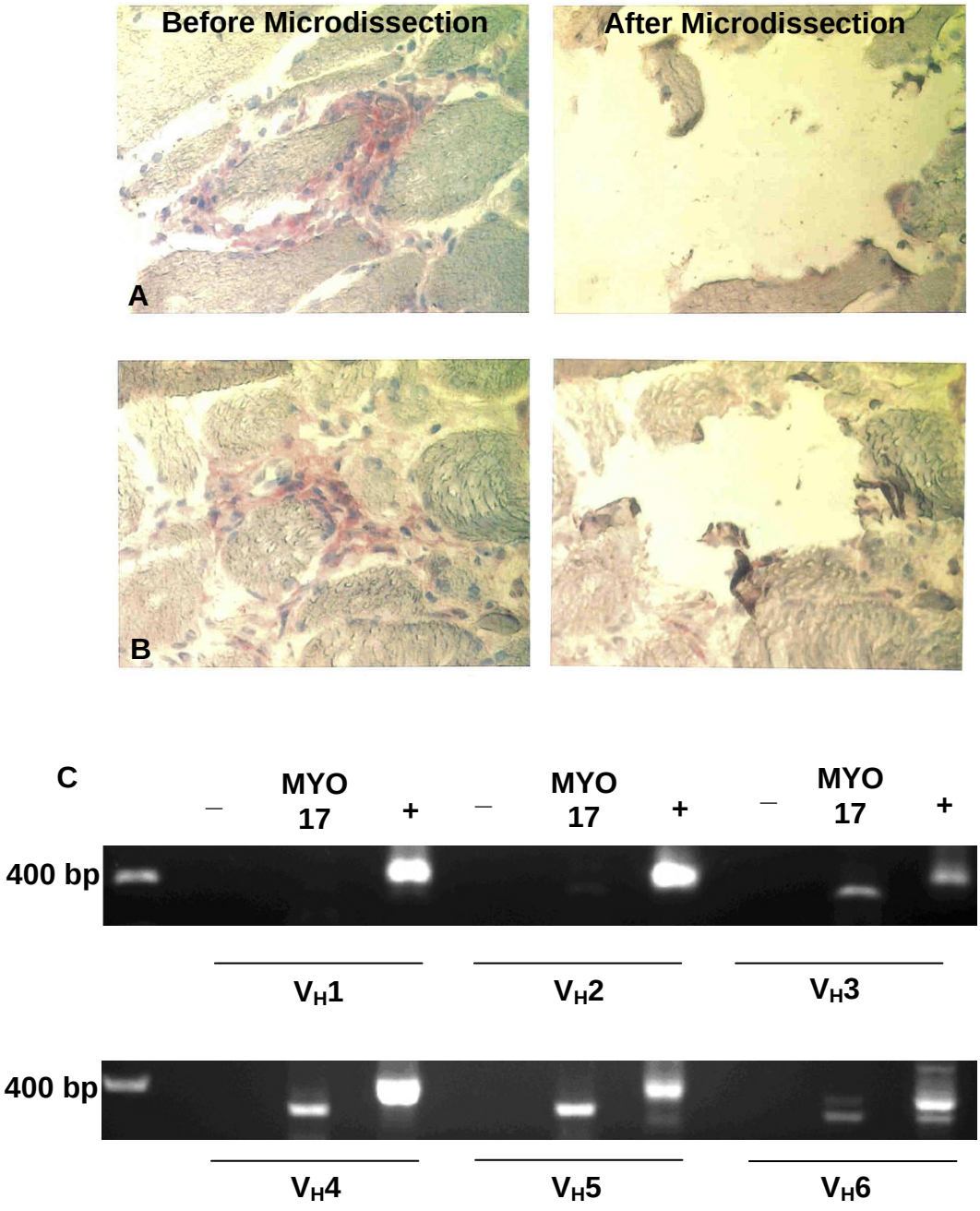

Figure 4.27 Microdissection of infiltrating B cells and amplification of V_H-gene rearrangements from Sample MYO17

Regions of B cell and plasma cell infiltration were microdissected from sample MYO17. Figure 4.27A and B demonstrates the microdissection of 2 regions of cellular infiltration. Images were taken at 400X. DNA released from these microdissections was amplified using a Nested PCR system (Figure 4.27C), as described in Chapter 2. – indicates negative control PCR reactions where DNA was substituted with water while + indicates positive control PCR reactions using peripheral blood mononuclear cells isolated from peripheral blood of a healthy individual. Results show amplification of V_H 3, 4, 5 and 6 families.

A

V_H Gene	D_H Gene	J_H Gene	Number of Isolated Sequences	Number of Mutations	CDR3	CDR3 Length (aa)	Mutational Distribution (% of length)			V-J Length (bp)	Consecutive D length (bp) (+Mismatches)
							Framework	CDR1	CDR2		
3-30*03	3-9*01	4*02	1	12	ATGAYYDILSGARPFDY	17	3.2	13.3	5.6	38	20(+2)
6-01*01	No D gene Assignment	5*02	1	5	VRSPLKQWLEP	11	1.8	0	1.8	29	6

B

V_H Gene	D_H Gene	J_H Gene	R-CDR	S-CDR	pCDR	p-CDR	R-FW	S-FW	pFW	p-FW
3-30*03	3-9*01	4*02	4	1	0.46606	**-0.908**	3	4	0.67432	**-0.0977**
6-01*01	No D gene Assignment	5*02	0	1	0.47248	**-0.1468**	2	2	0.65538	**-0.278**

Table 4.22 A&B Sequence Analysis from Sample MYO17

Table 4.22A - Best matching germline sequences were identified from aligning sequences in the IMGT database using JOINSOLVER software from the MYO17 myositis section. Identical sequences with the same V_H, D_H, J_H, CDR3 and base mutations were only counted once. V-J lengths and consecutive D match lengths (bp) were also identified using the JOINSOLVER software and allowed assignment of the D_H genes as described in section 2.3.12.3.

The number of mutations within functional rearranged genes were analysed collectively from all region of dissected cellular infiltration. Base differences within the first 24 bases of sequence were disregarded as this part of the sequence binds the 5' V_H primer.

The locations of mutations observed within functional rearranged genes were categorised as being within FR or CDR regions. The numbers of mutations within these regions were expressed as a percentage of the entire length of the region to correct for the longer lengths observed within the framework regions.

Table 4.22B - The number of replacement and silent mutations and the presence of any positive and negative selection was conducted by Hershberg *et al* (294) as previously described. R-CDR/FW and S-CDR/FW represent the number of replacement and silent mutations in the CDR and FW respectively. pCDR represents the probability of having a R mutation in the CDR given all the mutations in the sequence except R mutations within the FW while pFW represents the probability of having a R mutation in the FW given all the mutations in the sequence except R mutations within the CDR and p-CDR/FW represent the p-value of the focused binominal test on the CDR and FW respectively. A negative sign indicates negative selection. p-values <0.05 were deemed significant.

4.2.8 Sample MYO19

As described in Chapter 3 both $CD20^+$ cells and plasma cells were identified within sample MYO19. Despite the microdissection and DNA amplification (**Figure 4.28**) of various areas of infiltration within sample MYO19 only 1 functional rearranged sequence could be isolated (**Table 4.23A**). This gene used the 3-21*01 V_H gene segment along with D_H3-22*01 and J_H3*02 in this functional rearrangement. As described in Table 4.14 the sequence isolated from sample MYO19 only contained 4 mutations throughout the entire sequence. These mutations were solely within framework regions of the sequence with CDR regions remaining non-mutated. Based on these mutations negative selection was observed within both the CDR and FW regions but these were not significant selections (**Table 4.23B**). Only 1 P nucleotide was present in this rearrangement at the DJ region of the junction. 14 and 15 N nucleotides were present at the VD and DJ junctions respectively while 2, 6, 13 and 4 nucleotides were removed respectively from the 3'V_H, 5'D_H, 3'D_H and 5'J_H region.

No changes in gene assignment were observed for this sequence using the IMGT/V-QUEST software.

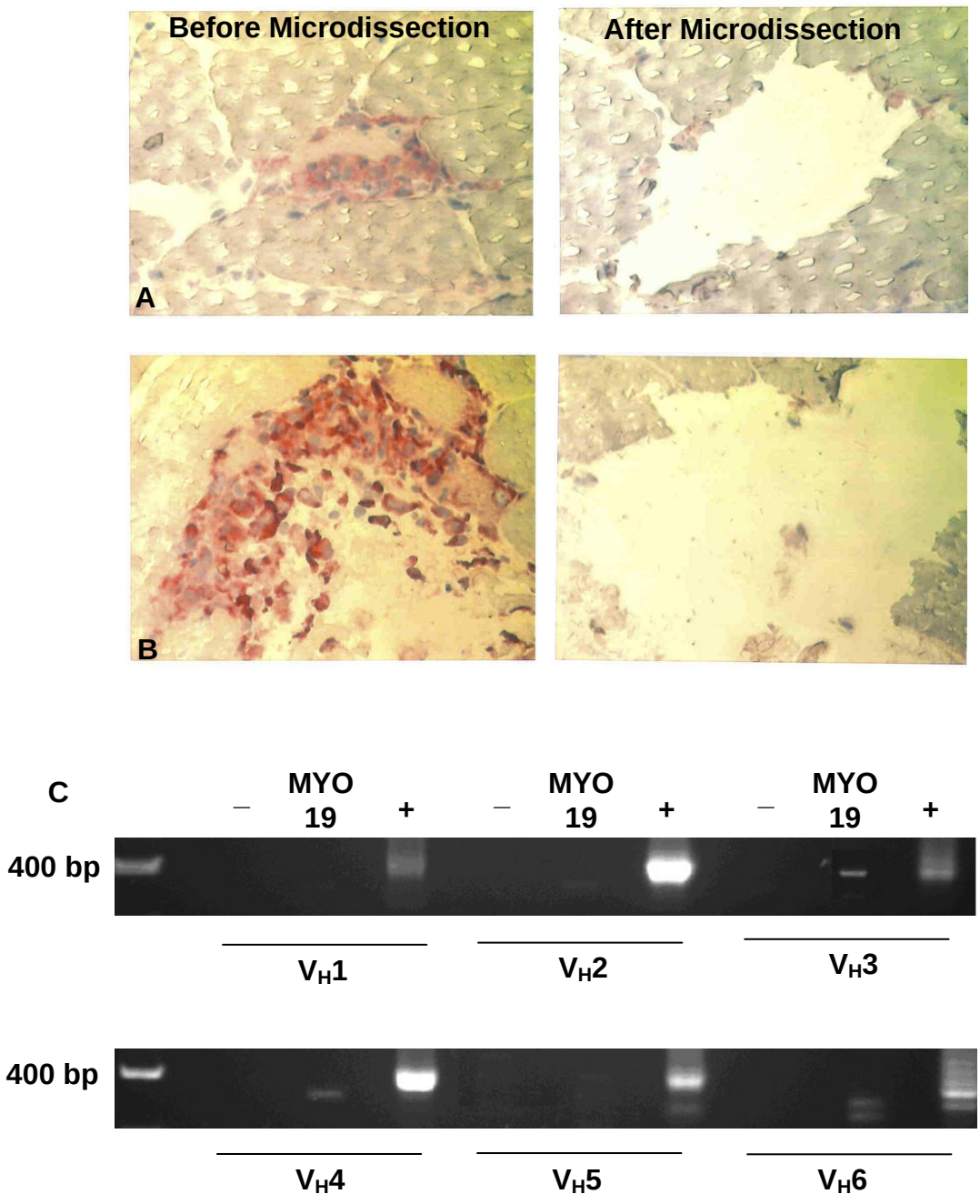

Figure 4.28 Microdissection of infiltrating B cells and amplification of V_H-gene rearrangements from Sample MYO19

Regions of B cell and plasma cell infiltration were microdissected from sample MYO19. Figure 4.28 A and B demonstrates the microdissection of 2 regions of cellular infiltration. Images were taken at 400X. DNA released from these microdissections was amplified using a Nested PCR system (Figure 4.28C), as described in Chapter 2. – indicates negative control PCR reactions where DNA was substituted with water while + indicates positive control PCR reactions using peripheral blood mononuclear cells isolated from peripheral blood of a healthy individual. Results show amplification of V_H 3,4 and 6 families.

V_H Gene	D_H Gene	J_H Gene	Number of Isolated Sequences	Number of Point Mutations	CDR3	CDR3 Length (aa)	Mutational Distribution (% of length)			V-J Length (bp)	Consecutive D length (bp) (+Mismatches)
							Framework	CDR1	CDR2		
3-21*01	3-22*01	3*02	1	4	ARPLSTPYDSRSASAAAFDI	20	1.8	0	0	42	12

R-CDR	S-CDR	pCDR	p-CDR	R-FW	S-FW	pFW	p-FW
0	0	0.5135	**-0.1151**	1	3	0.65938	**-0.1312**

Table 4.23 A&B Sequence Analysis from Sample MYO19

Table 4.23A - Best matching germline sequences were identified from aligning sequences in the IMGT database using JOINSOLVER software from the MYO19 myositis section. Identical sequences with the same V_H, D_H, J_H, CDR3 and base mutations were only counted once. V-J lengths and consecutive D match lengths were also identified using the JOINSOLVER software and allowed assignment of the D_H genes as described in section 2.3.12.3.

The number of mutations within functional rearranged genes were analysed collectively from all region of dissected cellular infiltration. Base differences within the first 24 bases of sequence were disregarded as this part of the sequence binds the 5' V_H primer.

The locations of mutations observed within functional rearranged genes were categorised as being within FR or CDR regions. The numbers of mutations within these regions were expressed as a percentage of the entire length of the region to correct for the longer lengths observed within the framework regions.

Table 4.23B - The number of replacement and silent mutations and the presence of any positive and negative selection was conducted as per Hershberg *et al* (294) as previously described. R-CDR/FW and S-CDR/FW represent the number of replacement and silent mutations in the CDR and FW respectively. pCDR represents the probability of having a R mutation in the CDR given all the mutations in the sequence except R mutations within the FW while pFW represents the probability of having a R mutation in the FW given all the mutations in the sequence except R mutations within the CDR and p-CDR/FW represent the p-value of the focused binominal test on the CDR and FW respectively. A negative sign indicates negative selection. p-values <0.05 were deemed significant.

4.2.9 Sample MYO23

4.2.9.1 V_H Repertoire of Infiltrating B Cells

Due to the low numbers of infiltrating cells within sample MYO23 and with no distinctive region of cellular aggregation it was not possible to obtain information from specific areas of the MYO23 sample. As a result the gene repertoire of the whole section was determined after nested PCR reactions amplified the V_H rearrangements from infiltrating cells (**Figure 4.29**). A total of 9 different functional genes were isolated from the infiltrating population which consisted of 4 different gene rearrangements with different mutational patterns (**Table 4.24**). Despite the small number of genes identified the repertoire of these genes was compared to both sets of control values (**Figure 4.30**), except for the D_H genes as there was not enough D_H genes (4) identified to allow a statistical comparison to be conducted. For V_H genes only V_H3 and V_H4 gene segments were used within these rearrangements which resulted in a significant selection for the V_H3 gene segments which was significant against both the normal control values and the germline complexity. A significant selection for J_H2 and J_H5 genes was observed which was only significant against normal control values and not the germline complexity when the absolute values were used in the Chi square analysis. A selection against J_H4 gene segments was also observed which again was only significant against the normal control values and not the germline complexity. As only a small number of sequences could be isolated from the muscle section these selections may not be representative of the entire population within the whole area of inflammation.

For all sequences isolated from sample MYO23 the gene assignments by JOINSOLVER matched those of IMGT/V-QUEST. The only change to gene assignments arose in the V_H3-33*01 J_H5*02 sequence with 18 mutations. This gene sequence was the 4th best matching gene for this sequence in both JOINSOLVER and IMGT/V-QUEST. The difference between these sequences was a score of 10 using JOINSOLVER and a score of 9 using IMGT/V-QUEST, which represented 1 base difference. The 4th best matching gene was used as this gene shared CDR3, junctional and J_H compositions with other sequences.

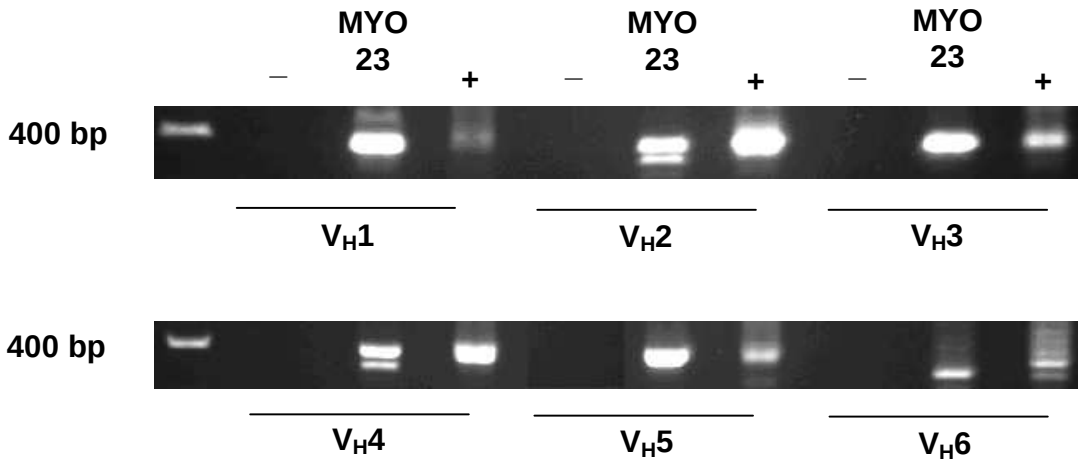

Figure 4.29 Amplification of V_H-gene rearrangements from Sample MYO23

As no distinct area of aggregation from infiltrating cells was observed within sample MYO23 and infiltrating cells were observed throughout the whole section, the whole section was used to obtain DNA. DNA released from the section was amplified using a Nested PCR system, as described in Chapter 2. – indicates negative control PCR reactions where DNA was substituted with water while + indicates positive control PCR reactions using peripheral blood mononuclear cells isolated from peripheral blood of a healthy individual. Results show amplification of all 6 V_H families.

V_H Gene	D_H Gene	J_H Gene	Number of Isolated Sequences	Number of Point Mutations	CDR3	V-J Length (bp)	Consecutive D length (bp) (+Mismatches)
3-07*01	6-19*01	2*01	3	5, 6, 7	ARGYTSGWYSANWYFDL	27	19(+2)
3-33*01	No D gene Assignment	5*02	4	8, 9(X2), 18	AKDSNRARPGWFDP	25	6
3-33*03	6-19*01	2*01	1	9	ARGYTSGWYSATWYFDL	28	19(+2)
4-04*07	No D gene Assignment	2*01	1	10	ARVDSRRQVWSPNWYFDL	34	6

Table 4.24 Heavy chain genes identified from myositis sample MYO23

Best matching germline sequences were identified from aligning sequences in the IMGT database using JOINSOLVER software from the MYO23 myositis section. The total number of sequences isolated is given in the 4th column of the table; non-functional rearrangements indicated in brackets. Identical sequences with the same V_H, D_H, J_H, CDR3 and base mutations were only counted once. CDR3 amino acid sequences were also identified using the JOINSOLVER software. V-J lengths and consecutive D match lengths (bp) were also identified using the JOINSOLVER software and allowed assignment of the D_H genes as described in section 2.3.12.3.

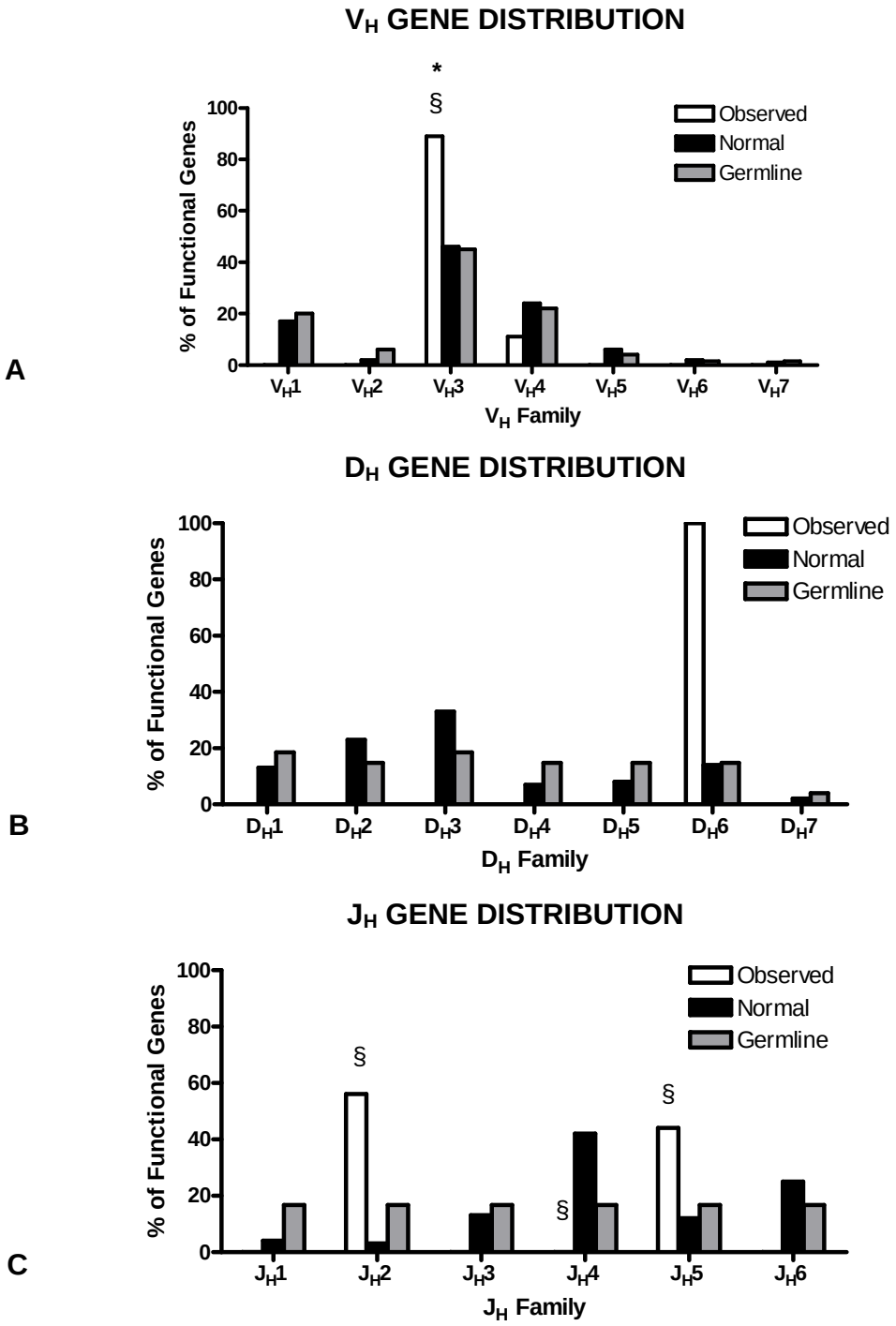

Figure 4.30 V_H Gene Family Usage of MYO23

V_H gene family usage. Distribution of functional genes was compared with published normal control values from Volpe and Kepler (251) as well as the germline complexity assuming every germline gene is capable of producing a functional rearrangement. Absolute values were used in Chi Square Analysis to determine gene selections. § represent a significant difference from normal control values; * represent a significant difference from the germline ($p<0.05$).

4.2.9.2 Mutational Analysis of B Cell Ig Sequences of Sample MYO23

Examining the number of mutations within functional rearrangements (**Figure 4.31A**) showed that the majority of sequences contained between 3 to 10 mutations while a small percentage, approximately 10% contained between 11 and 20 mutations. Sequences with 0 to 2 mutations or over 21 mutations were not found within the infiltrating repertoire. Analysis of mutational location (**Figure 4.31B**) demonstrated that there were a higher percentage of mutations within CDR regions of the gene in comparison to framework regions. Between CDR regions CDR1 possessed a higher percentage of mutations in comparison to CDR2.

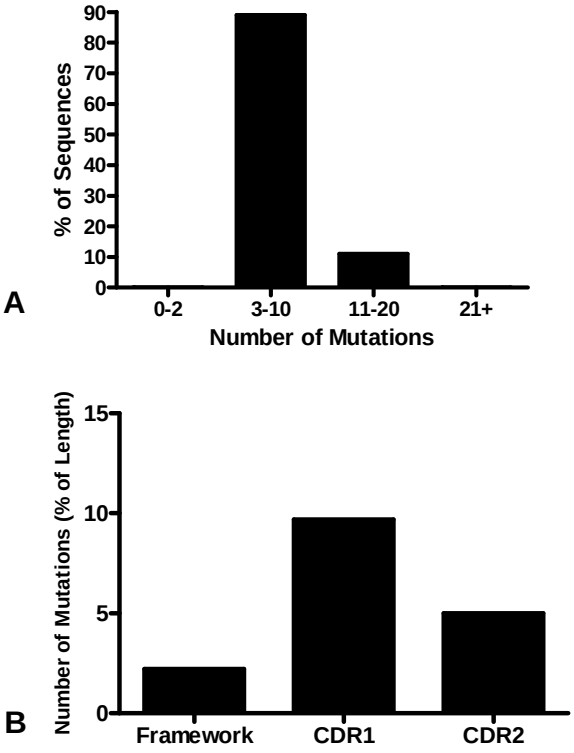

Figure 4.31 Numbers of Mutations and Mutational Distribution of Functional Sequences in MYO23

Figure 4.31A - The number of mutations within functional rearranged genes were analysed collectively from the whole sample of cellular infiltration within sample MYO23. Base differences within the first 24 bases of sequence were disregarded as this part of the sequence binds the 5' V_H primer. Graph demonstrates sequences within cellular infiltrates are not from a naïve population but rather a highly mutated population.

Figure 4.31B - The locations of mutations observed within functional rearranged genes were categorised as being within FR or CDR regions. The numbers of mutations within these regions were expressed as a percentage of the entire length of the region to correct for the longer lengths observed within the framework regions. Graph demonstrates a higher percentage of mutations within CDR regions compared to framework regions.

From these mutations positive and negative selections were observed in both the CDR and FW regions, the only significant selections were found in the gene rearrangements using the V_H3-33*01 and V_H3-33*03 gene segments (**Table 4.25**). These selections were shown to be negative within the framework regions of the sequences.

V_H Gene	D_H Gene	J_H Gene	Number of Isolated Sequences	Number of Point Mutations	R-CDR	S-CDR	pCDR	p-CDR	R-FW	S-FW	pFW	p-FW
3-07*01	6-19*01	2*01	3	5	2	0	0.44397	**0.50381**	2	1	0.67012	**-0.9537**
				6	3	0	0.44397	**0.27233**	2	1	0.67012	**-0.9537**
				7	2	0	0.44397	**0.50381**	4	1	0.67012	**0.60288**
3-33*01	No D gene Assignment	5*02	4	8	2	2	0.46759	**-0.2431**	0	4	0.67394	**-0.0012**
				9	2	2	0.46759	**-0.2431**	1	4	0.67394	**-0.0065**
				9	2	2	0.46759	**-0.2431**	1	4	0.67394	**-0.0065**
				18	6	2	0.46759	**-0.7825**	4	6	0.67394	**-0.0195**
3-33*03	6-19*01	2*01	1	9	2	2	0.46654	**-0.3726**	2	3	0.67113	**-0.0491**
4-04*07	No D gene Assignment	2*01	1	10	5	1	0.43938	**0.31935**	2	2	0.65629	**-0.2761**

Table 4.25 Analysis of Replacement and Silent Mutations and Positive and Negative Selection in Sample MYO23

Replacement and silent mutations within the immunoglobulin sequences and antigen-driven selection were determined according to Hershberg *et al* (294) and the corresponding computer programme (http://clip.med.yale.edu/selection). This improved method of analysis uses a focused binomial test to establish positive or negative mutational selections within the sequence with high specificity and increased sensitivity accounting for known biases within the immunoglobulin gene sequence. R-CDR and S-CDR represents the number of replacement and silent mutations within the CDR respectively. pCDR represents the probability of having a R mutation in the CDR given all the mutations in the sequence except R mutations within the FW while p-CDR is the p-value of the focused binominal test on the CDR. Conversely R-FW and S-FW represents the number of replacement and silent mutations within the FW respectively. pFW represent the probability of having a R mutation in the FW given all the mutations in the sequence except R mutations within the CDR while p-FW is the p-value of the focused binominal test on the FW. If the number of R mutations is less than expected the software will test for negative selection and p-values will be preceded by a negative sign or if the number of mutations is more than expected the software will test for positive selection. p-values <0.05 are highlighted in yellow and were deemed significant for selection.

4.2.9.3 CDR3 Analysis

The mean amino acid CDR3 length from these sequences is shown in **Table 4.26**. No non-functional sequences were isolated from the infiltrating repertoire and therefore the CDR3 lengths in the two populations could not be compared. Previous analysis with the CDR3 lengths in this study has examined the CDR3 lengths in different mutational groups. As shown in **Figure 4.31A** all the mutations from these sequences fell into only 2 of the mutational groups which did not allow the statistical multiple comparison test to be conducted as 3 or more groups are required for the comparison. Analysis of the P and N nucleotides as well as the exonuclease activity can only be conducted on gene rearrangements where a D gene has been assigned. As this was the case for only 4 sequences which exhibited the same junctional composition no statistical comparisons could be conducted but the number of the different nucleotides are shown in Table 4.26.

CDR3 Length	**Functional**	15.7 ± 0.6			
	Non-Functional	N/A			
		VD Junction		**DJ Junction**	
P Nucleotide	**Functional**	0		0	
	Non-Functional	N/A		N/A	
N Nucleotide	**Functional**	0		7.3 ± 0.3	
	Non-Functional	N/A		N/A	
		3' V_H	**5' D_H**	**3' D_H**	**5'J_H**
Exonuclease Activity	**Functional**	2 ± 0	0	0	2.3 ± 0.3
	Non-Functional	N/A	N/A	N/A	N/A

Table 4.26 CDR3 and Junctional Analysis in Sample MYO23

The mean amino acid length of the CDR3, the mean nucleotide numbers corresponding to P and N nucleotides as well as the mean number of germline nucleotides lost due to exonuclease activity were calculated from the junctional regions of all immunoglobulin sequences from sample MYO23. Results are given as the Mean ± SEM, statistical significance was established using an unpaired t-test. Instances where no non-functional sequences were identified and values could not be calculated were recorded as non applicable (N/A).

4.2.9.4 Clonal Diversification in MYO23

Despite the low numbers of isolated sequences from sample MYO23, four clonally related sequences were found within the infiltrating repertoire (**Figure 4.32**). These sequences shared the same VDJ gene rearrangement as well as common junctional areas. In these clonally related sequences clone K and clone L share 1 replacement mutation but do not contain the other additional mutations, after branching of the clonal tree, indicated in Figure 4.32 which indicates that the mutations were formed during different and branch mutational lineages. As shown in **Table 4.27** these mutations indicate that negative selection was occurring in both the CDR and FW regions but this selection was only significant in the framework regions.

V_H Gene	D_H Gene	J_H Gene	R-CDR	S-CDR	pCDR	p-CDR	R-FW	S-FW	pFW	p-FW
3-33*01	No D gene Assignment	5*02	6	3	**0.46759**	-0.4743	5	7	0.67394	**-0.0086**

Table 4.27 Analysis of Replacement and Silent Mutations and Positive and Negative Selection in Clonally Related B Cells in Sample MYO23

The number of replacement and silent mutations and the presence of any positive and negative selection were conducted as per Hershberg *et al* (294) as previously described. For clonally related sequences mutations shared across the sequences are only counted once and p values are calculated for the clone as a single entity. R-CDR/FW and S-CDR/FW represent the number of replacement and silent mutations in the CDR and FW respectively. pCDR represents the probability of having a R mutation in the CDR given all the mutations in the sequence except R mutations within the FW while pFW represents the probability of having a R mutation in the FW given all the mutations in the sequence except R mutations within the CDR and p-CDR/FW represent the p-value of the focused binominal test on the CDR and FW respectively. A negative sign indicates negative selection. p-values <0.05 were deemed significant.

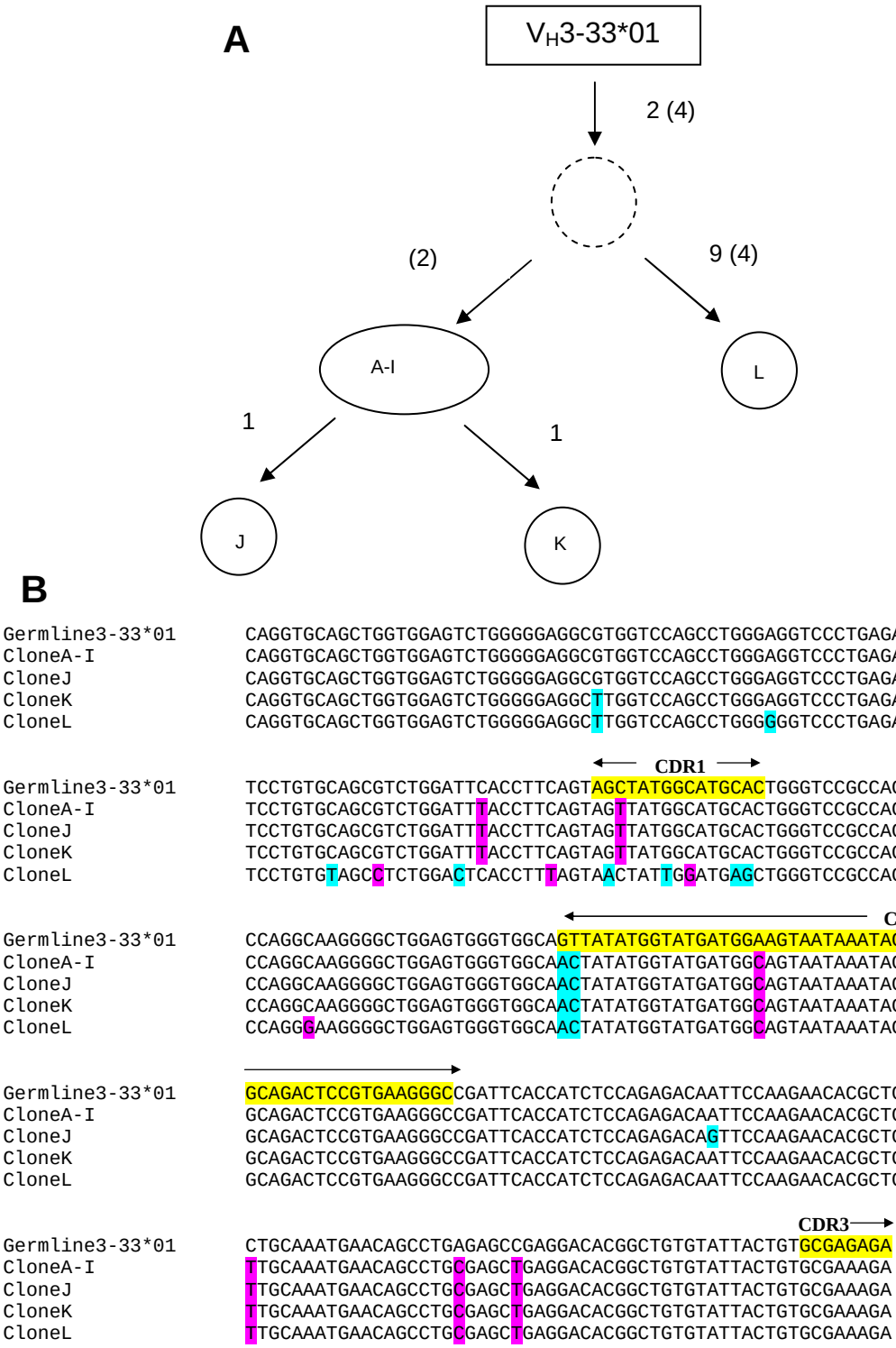

Figure 4.32 Clonal Proliferation in Sample MYO23

A set of sequences was isolated from sample MYO23 which demonstrated somatic hypermutation and clonal proliferation. **Figure A** - The letters in the circles refer to individual sequences isolated from each B cell clone. Numbers indicate the minimum number of mutations required between each sequence with bracketed figures representing additional silent mutations. The dashed circle represents a hypothetical intermediate whose sequence was not found amongst the isolated sequences. **Figure B** - The DNA sequences of the clonally related sequences were aligned using ClustalW software to highlight the common and independent mutations. CDR regions are highlighted in yellow, replacement mutations in blue and silent mutations in purple.

4.2.10 Sample MYO24

Infiltrating B cells were not observed within sample MYO24 but their differentiated counter-parts plasma cells were identified within the infiltrating population. These areas of plasma cells were microdissected and the resultant DNA was amplified for V_H1-6 families (**Figure 4.33**). Despite the presence of amplification bands for the V_H5 family no functional rearrangement sequences could be identified from these or subsequent microdissections.

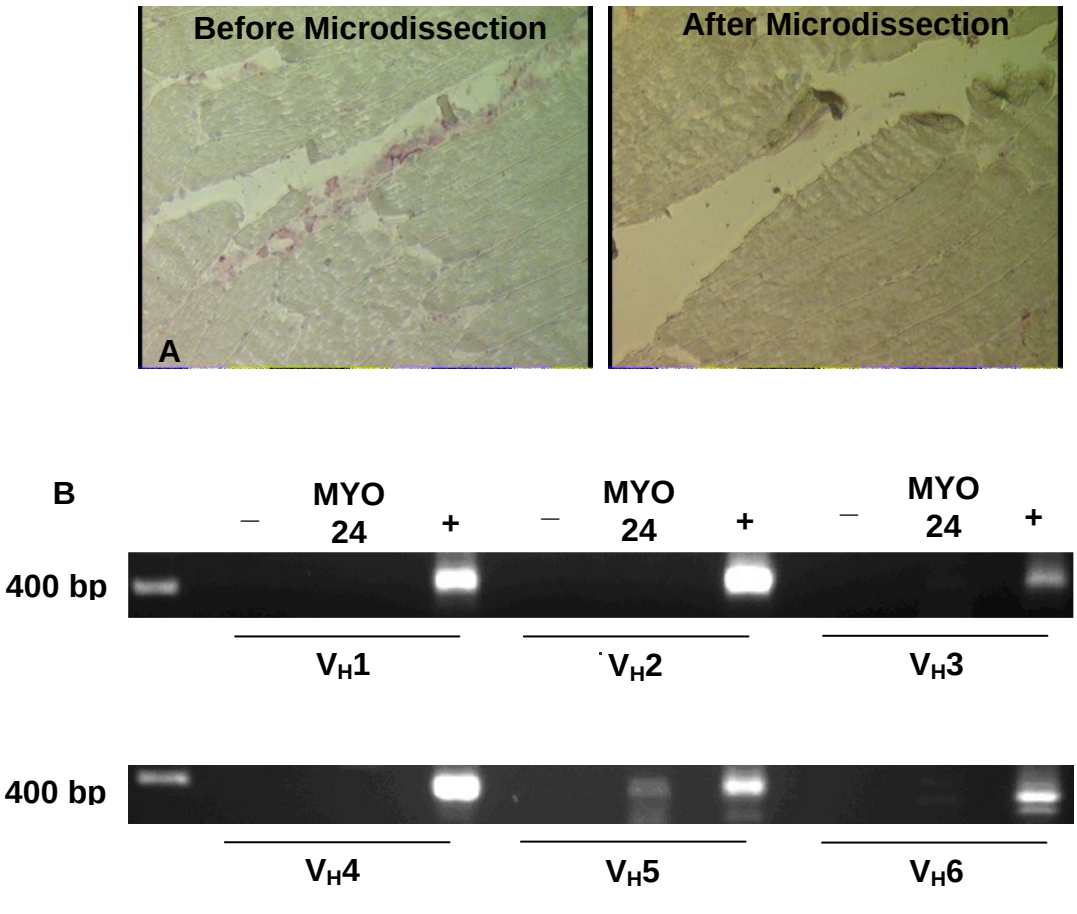

Figure 4.33 Microdissection of infiltrating B cells and amplification of V_H-gene rearrangements from Sample MYO24

The region of plasma cell infiltration was microdissected from sample MYO24. Figure 4.33A demonstrates the microdissection of the region of cellular infiltration. Images were taken at 200X. DNA released from these microdissections was amplified using a Nested PCR system (Figure 4.33B), as described in Chapter 2. – indicates negative control PCR reactions where DNA was substituted with water while + indicates positive control PCR reactions using peripheral blood mononuclear cells isolated from peripheral blood of a healthy individual. Results show amplification of V_H 5 family genes.

4.2.11 Sample MYOC

Aggregates of infiltrating cells in sample MYOC were microdissected and the DNA amplified for all 6 V_H families (**Figure 4.34**). Despite the various areas of infiltration within sample MYOC, and the presence of both $CD20^+$ cells and plasma cells, only 1 gene rearrangement was isolated from various microdissections, **Table 4.28A**. This gene used the 3-33*01 V_H gene segment along with J_H2*01 in its functional rearrangement, no D_H gene could be statistically assigned. The rearrangement contained a CDR3 length of 13 amino acids. This gene rearrangement was isolated for every clone checked and from various sections and regions of the sample but was not evident in any other samples tested therefore could not be the result of contamination. The sequence isolated from MYOC was highly mutated with a total of 47 mutations throughout the V_H gene segment. Examining the distribution of these mutations (**Table 4.28A**), the majority of mutations were located within the CDR2 region. Mutational percentages within framework regions of the sequence were similar to that of the CDRs. Analysis of the R and S mutations within this sequence demonstrate a significant negative selection in the framework regions of this sequence (**Table 4.28B**). A positive selection was observed in the CDR but this was not significant. As no D_H gene could be assigned to this Ig rearrangement the sequence composition, P and N Nucleotides, in the junctional regions of the sequence could not be identified. The lack of different gene rearrangements and clonally related sequences may indicate that memory cells are infiltrating the muscle and are proliferating without mutating.

From the sequence isolated from the inflammatory infiltrate in sample MYOC no discrepancies in gene assignment was observed between the JOINSOLVER and IMGT/V-QUEST software's.

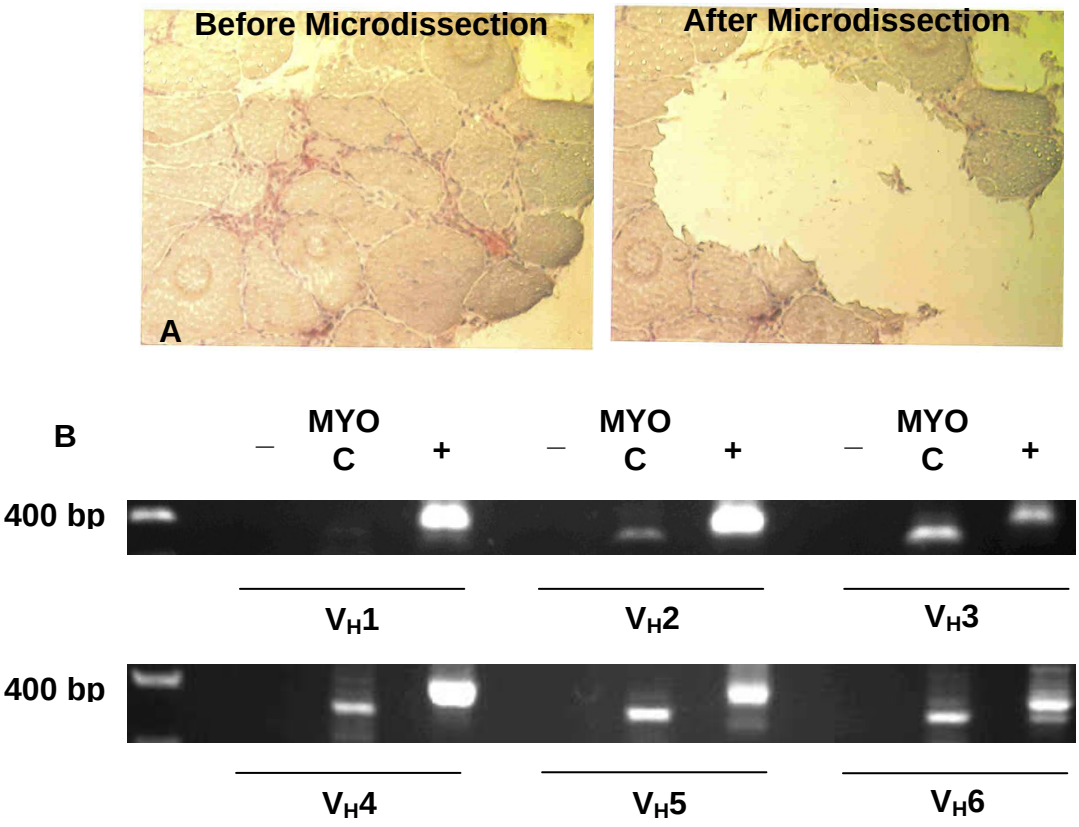

Figure 4.34 Microdissection of infiltrating B cells and amplification of V_H-gene rearrangements from Sample MYOC

The region of B cell and plasma cell infiltration was microdissected from sample MYOC. Figure 4.34A demonstrates the microdissection of the region of cellular infiltration. Images were taken at 200X. DNA released from these microdissections was amplified using a Nested PCR system (Figure 4.34B), as described in Chapter 2. – indicates negative control PCR reactions where DNA was substituted with water while + indicates positive control PCR reactions using peripheral blood mononuclear cells isolated from peripheral blood of a healthy individual. Results show amplification of all 6 V_H families.

A

V_H Gene	D_H Gene	J_H Gene	Number of Isolated Sequences	Number of Point Mutations	CDR3	CDR3 Length (aa)	Mutational Distribution (% of length)			V-J Length (bp)	Consecutive D length (bp) (+Mismatches)
							Framework	CDR1	CDR2		
3-33*01	No D gene Assignment	2*01	1	47	ARAIHITAWSFDL	13	12.2	13.3	33.3	29	7

B

R-CDR	S-CDR	pCDR	p-CDR	R-FW	S-FW	pFW	p-FW
15	5	0.46759	**0.85564**	16	11	0.67394	**-0.0438**

Table 4.28 A&B Sequence Analysis from Sample MYOC

Table 4.28A - Best matching germline sequences were identified from aligning sequences in the IMGT database using JOINSOLVER software from the MYOC myositis section. Identical sequences with the same V_H, D_H, J_H, CDR3 and base mutations were only counted once. V-J lengths and consecutive D match lengths (bp) were also identified using the JOINSOLVER software and allowed assignment of the D_H genes as described in section 2.3.12.3.

The number of mutations within functional rearranged genes were analysed collectively from all region of dissected cellular infiltration. Base differences within the first 24 bases of sequence were disregarded as this part of the sequence binds the 5' V_H primer.

The locations of mutations observed within functional rearranged genes were categorised as being within FR or CDR regions. The numbers of mutations within these regions were expressed as a percentage of the entire length of the region to correct for the longer lengths observed within the framework regions.

Table 4.28B - The number of replacement and silent mutations and the presence of any positive and negative selection were conducted as per Hershberg *et al* (294) as previously described. R-CDR/FW and S-CDR/FW represent the number of replacement and silent mutations in the CDR and FW respectively. pCDR represents the probability of having a R mutation in the CDR given all the mutations in the sequence except R mutations within the FW while pFW represents the probability of having a R mutation in the FW given all the mutations in the sequence except R mutations within the CDR and p-CDR/FW represent the p-value of the focused binominal test on the CDR and FW respectively. A negative sign indicates negative selection. p-values <0.05 were deemed significant.

4.2.12 Sample MYOE

From the microdissections and DNA amplification of infiltrating plasma cells in sample MYOE (**Figure 4.35**), that were previously described in Chapter 3, only 2 different functional rearrangements were isolated from various microdissections within sample MYOE (**Table 4.29A**). One of the isolated genes used the V_H1-f*01 gene along with the D_H2-2*01 and J_H4*02 while the other gene isolated used the 3-09*01 V_H gene with an unidentified D_H gene while J_H6*02 completing the functional rearrangement. The V_H1 gene rearrangement contained 6 mutations, only 1 of these was within the CDR region of the sequence. Conversely the V_H3 gene rearrangement contained a total of 36 mutations. As described in Table 4.29A mutations were distributed within all regions of the functional gene, 12.2% of the framework regions of the sequence contained mutations while 31.1% of CDR regions of the sequence contained mutations. Analysis of the R and S mutations of these sequences demonstrated that negative selection was occurring in both the CDR and FW regions of these sequences, but these selections were not deemed significant (**Table 4.29B**). Both sequences contained similar CDR3 lengths with only 1 amino acid difference between the two sequences which may be representative of a common antigenic epitope. As no D_H gene could be assigned to the V_H3-09*01 gene rearrangement, P and N nucleotides at the VD and DJ regions of the junctions as well as exonuclease activity at the V_H5' and J_H3' regions could not be assigned. For the other isolated gene from sample MYOE no P nucleotides were identified as either of the VD or DJ junctions while 6 and 11 N nucleotides were observed at the VD and DJ respectively. There appeared to be no exonuclease activity at the 5'V_H end of the rearrangement but 8, 4 and 5 nucleotides were removed by exonuclease activity at the 5'D_H, 3'D_H and 3'J_H regions of the rearrangement.

No anomalies between the JOINSOLVER and IMGT/V-QUEST algorithms were observed.

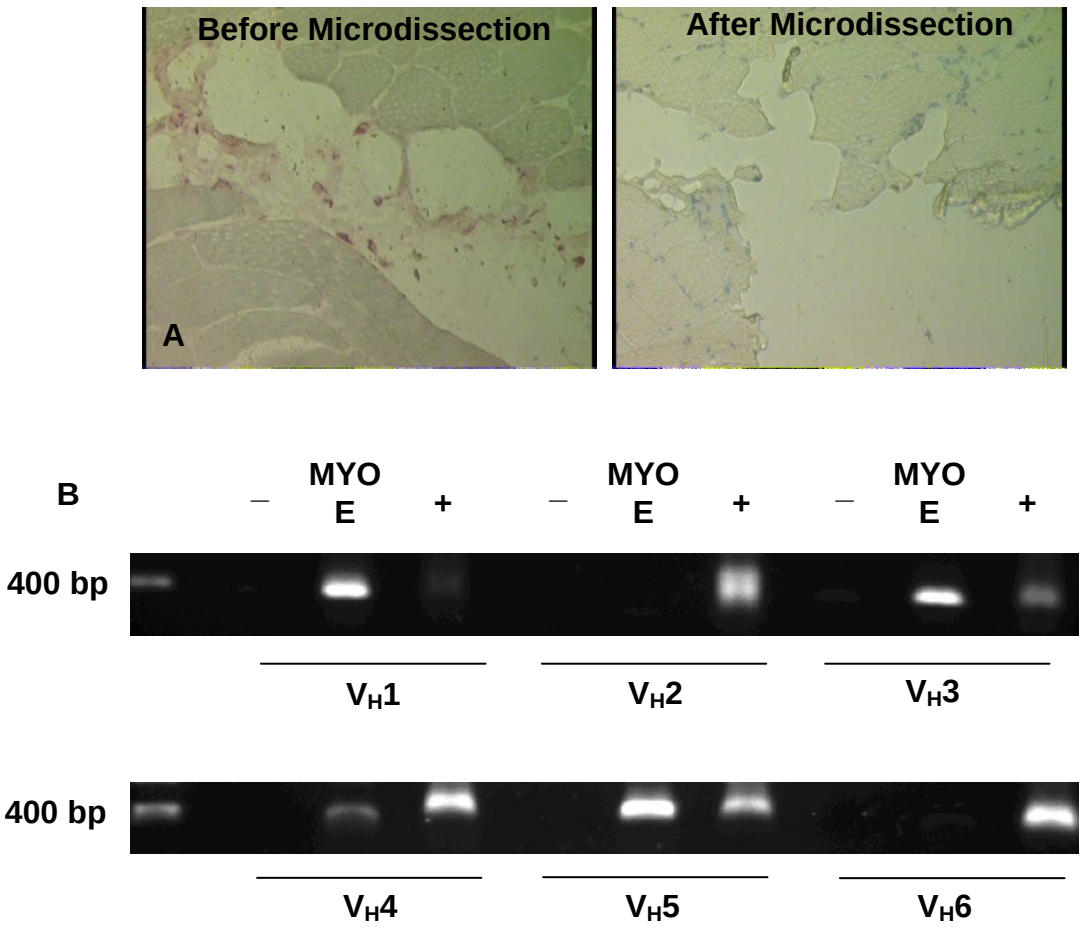

Figure 4.35 Microdissection of infiltrating B cells and amplification of V_H-gene rearrangements from Sample MYOE

The region of plasma cell infiltration was microdissected from sample MYOE. Figure 4.35A demonstrates the microdissection of the region of cellular infiltration. Images were taken at 200X. DNA released from these microdissections was amplified using a Nested PCR system (Figure 4.35B), as described in Chapter 2. – indicates negative control PCR reactions where DNA was substituted with water while + indicates positive control PCR reactions using peripheral blood mononuclear cells isolated from peripheral blood of a healthy individual. Results show amplification of V_H 3, 4 and 5 families.

A

V_H Gene	D_H Gene	J_H Gene	Number of Isolated Sequences	Number of Point Mutations	CDR3	CDR3 Length (aa)	Mutational Distribution (% of length)			V-J Length (bp)	Consecutive D length (bp) (+Mismatches)
							Framework	CDR1	CDR2		
1-f*01	2-2*01	4*02	1	6	ATGRVVVPAATASIFDF	17	2.3	6.7	0	44	19
3-09*01	No D gene Assignment	6*02	1	36	VQDVSRLTDLWRSMDV	16	12.2	20	11.1	38	7

B

V_H Gene	D_H Gene	J_H Gene	R-CDR	S-CDR	pCDR	p-CDR	R-FW	S-FW	pFW	p-FW
1-f*01	2-2*01	4*02	1	0	0.42032	**-0.8133**	3	2	0.68787	**-0.6761**
3-09*01	No D gene Assignment	6*02	7	2	0.46315	**-0.3223**	16	11	0.67147	**-0.1822**

Table 4.29 A&B Sequence Analysis from Sample MYOE

Table 4.29A - Best matching germline sequences were identified from aligning sequences in the IMGT database using JOINSOLVER software from the MYOE myositis section. Identical sequences with the same V_H, D_H, J_H, CDR3 and base mutations were only counted once. V-J lengths and consecutive D match lengths (bp) were also identified using the JOINSOLVER software and allowed assignment of the D_H genes as described in section 2.3.12.3.

The number of mutations within functional rearranged genes were analysed collectively from all region of dissected cellular infiltration. Base differences within the first 24 bases of sequence were disregarded as this part of the sequence binds the 5' V_H primer.

The locations of mutations observed within functional rearranged genes were categorised as being within FR or CDR regions. The numbers of mutations within these regions were expressed as a percentage of the entire length of the region to correct for the longer lengths observed within the framework regions.

Table 4.29B - The number of replacement and silent mutations and the presence of any positive and negative selection was conducted as per Hershberg *et al* (294) as previously described. R-CDR/FW and S-CDR/FW represent the number of replacement and silent mutations in the CDR and FW respectively. pCDR represents the probability of having a R mutation in the CDR given all the mutations in the sequence except R mutations within the FW while pFW represents the probability of having a R mutation in the FW given all the mutations in the sequence except R mutations within the CDR and p-CDR/FW represent the p-value of the focused binominal test on the CDR and FW respectively. A negative sign indicates negative selection. p-values <0.05 were deemed significant.

4.2.13 Sample MYO25 (Myositis Control Sample from Healthy Volunteer)

Immunohistochemical studies to identify any infiltrating cell populations within control muscle demonstrated that only a few $CD68^+$ cells were present within the control muscle sample. To further substantiate this finding DNA was released from an entire section of the control sample and the DNA was amplified for all 6 V_H families by nested PCR (**Figure 4.36**). Analysis of these PCR products on an agarose gels showed that no amplification products were observed from the control muscle sample. Consequently no further work was carried out with this sample.

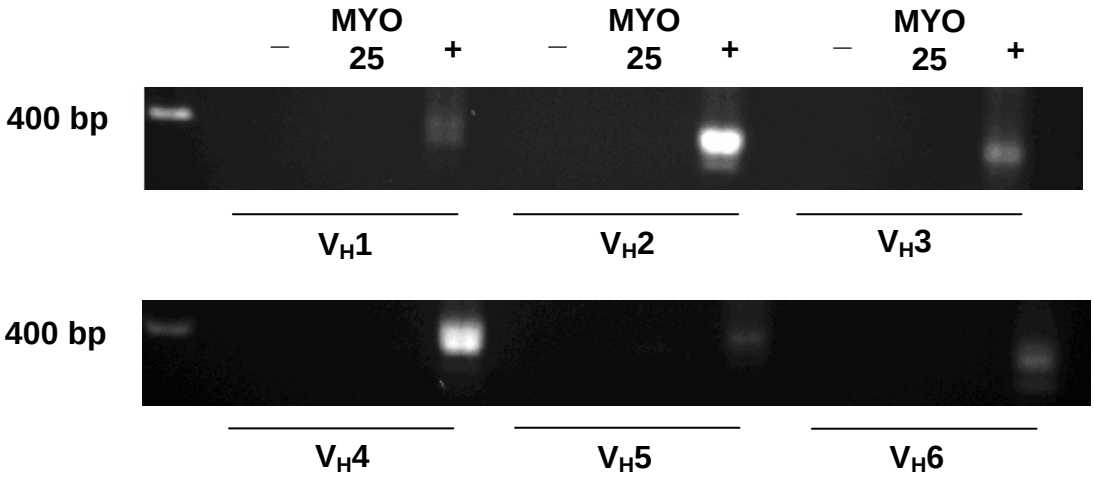

Figure 4.36 Amplification of V_H-gene rearrangements from Sample MYO25

As no distinct aggregation of infiltrating cells was observed within sample MYO25 and infiltrating cells were observed through out the whole section, the whole section was used to obtain DNA. DNA released from the section was amplified using a nested PCR system, as previously described in Chapter 2. – indicates negative control PCR reactions where DNA was substituted with water while + indicates positive control PCR reactions using peripheral blood mononuclear cells isolated from peripheral blood of a healthy individual. Results show no amplification for all 6 V_H families.

4.2.14 V_H Repertoire in Myositis

In addition to determining the repertoire of infiltrating B cells and plasma cells in individual patients the gene usage distribution and mutational patterns were also examined collectively for all patients, as well as in the DM and PM myositis subsets, to establish if any particular gene family was used preferentially in functional gene rearrangements. As shown in Chapter 2 (Table 2.1) there was some discrepancy in the diagnosis of patient MYO17 between PM and IBM in the clinical notes, therefore the sequences generated from this sample were not included in the PM subset but were for the full collective set of sequences. Collective examination of all sequences to establish a common gene selection between the different myositis subsets illustrated a selection for V_H3 gene segments compared to normal control values, which was also observed for the sequences identified from DM patients (**Figure 4.37A**). A selection for V_H2 gene segments and a selection against V_H1 and V_H4 gene segments, against normal control values, were also observed in sequences from DM patients. No significant positive or negative selections were observed for the sequences isolated from PM patients, the repertoire mirrored that of the normal control values as well as the germline values. A comparison of the DM and PM repertoires revealed a significant difference for the use of V_H5 gene segments between the 2 myositis subsets. Examining the use of individual gene segments indicated that in the myositis collective repertoire there was selection for the use of various gene segments, V_H3-11, 3-15, 3-30, 3-33, 3-66 and 3-7, while selection against V_H1-2, 3-23 and 4-34 was observed compared to the frequency observed for normal control values, although variations in the allele use of each gene were observed. For the DM repertoires a selection for V_H2-5, 3-11, 3-15, 3-30, 3-66, 3-7 and 3-9 and against V_H4-34 was observed while in the PM repertoire a selection for the use of gene segments V_H1-f, 3-30, 3-33, 3-72 and 5-51 and against the use of V_H3-23 was observed compared to normal control values. For D_H family genes, genes could be statistically assigned in 52.7, 59.1 and 41.8% of the sequences from the myositis, DM and PM collective sets respectively. A selection for D_H6 gene segments against normal control values was observed for both the myositis collective repertoire and the DM repertoire, while a decline in the use of D_H2 gene segments against normal controls was also observed within infiltrating cells for the myositis collective

repertoire (**Figure 4.37B**). Similarly with the individual V_H gene segments, selection for the use of D_H gene segments was observed. In the myositis collective repertoire a selection for the use of D_H3-22 and 6-6 was observed while a selection against D_H2-2 and 6-19 was also observed. In the DM repertoire the only selection found was a selection for the use of gene segment D_H6-6 while in the PM repertoire positive selections were observed for the use of D_H1-7, 3-22, 5-12, 5-24 and 6-19 gene segments. As previously discussed variations in the allele use within these genes were observed. Selection against the use of J_H1 gene segments was observed for the myositis and DM collective repertoires against normal control values (**Figure 4.37C**). These were also significant against the germline values for both sets of sequences as well as the PM sequence collection. A selection against the use of J_H2 gene segments was also observed in the DM sequences which were only significant against germline values, conversely a selection for the use of the J_H2 as well as J_H5, gene segments was observed for sequences isolated from the PM patients which was significant against normal control values. A comparison of the DM and PM sequence repertoire demonstrated a significant difference in the use of J_H2, 5 and 6 gene segments. A significant increase in the use of J_H2 and J_H5 gene segments was observed in the PM repertoire compared to the DM repertoire while a selection for J_H6 gene segments was observed in the DM repertoire compared to the PM repertoire.

The numbers of point mutations within the whole collective myositis repertoire were found to have a diverse number of mutations and similar distribution in each mutational group (**Figure 4.38A**). Conversely the sequences in the DM repertoire were found to be largely a naïve population of cells with almost 50% of sequences containing 0 to 2 mutations in the V_H region, although a considerable proportion of the sequences from infiltrating cells were highly mutated. Very few naïve cells were found in the PM repertoire, less than 10% of the sequences were essentially unmutated with the majority of cells containing a large number of mutations. As expected the majority of these mutations were found within the CDRs, for each subset of sequences (**Figure 4.38B**). For the DM repertoire this was greater in CDR1 and was found to be almost similar in the PM repertoire between CDR1 and CDR2.

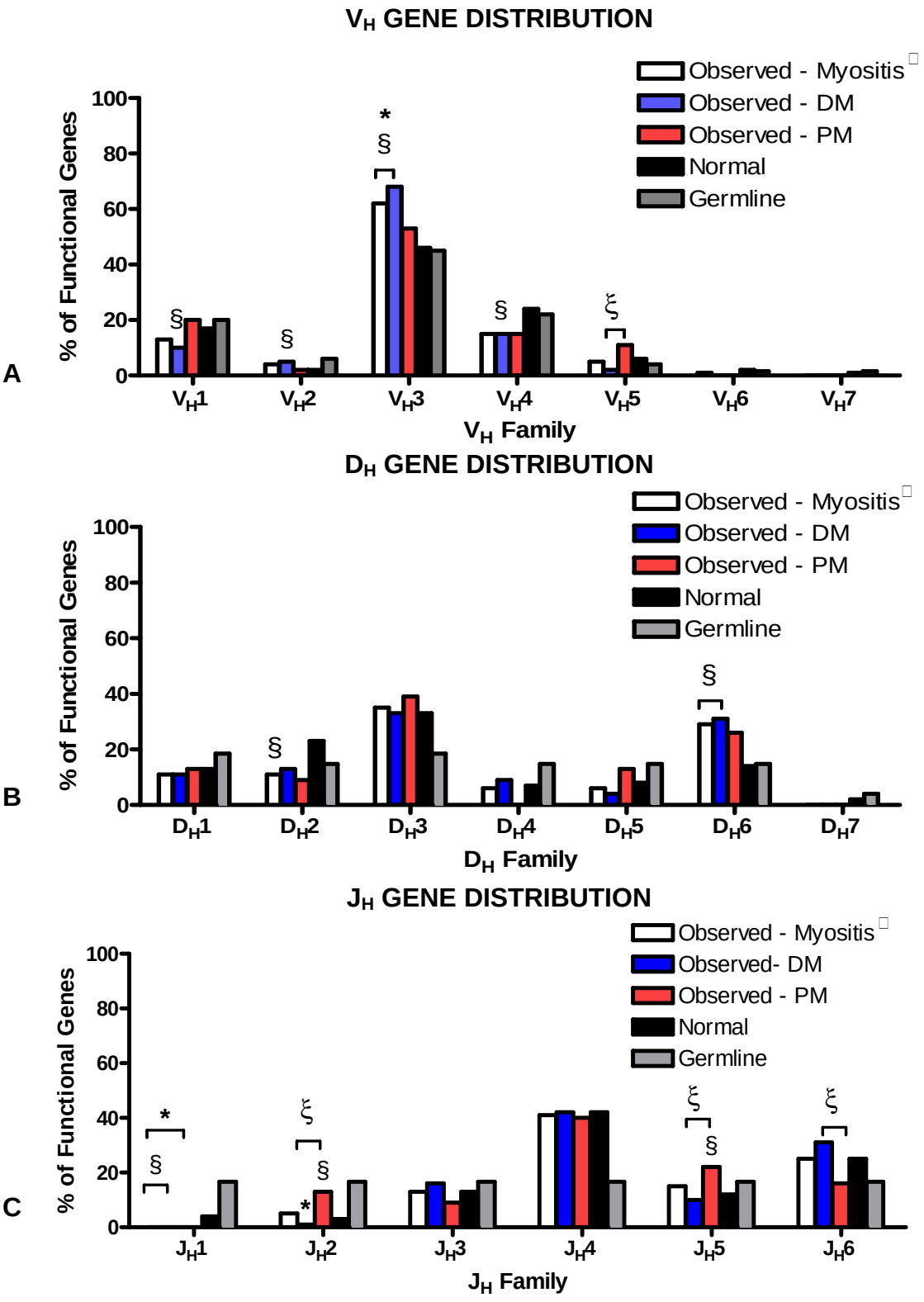

Figure 4.37 V_H Gene Family Usage in Myositis Patients

V_H gene family usage. Distribution of functional genes was compared with published normal control values from Volpe and Kepler (251) as well as the germline complexity assuming every germline gene is capable of producing a functional rearrangement. Absolute values were used in Chi Square Analysis to determine gene selections. § represent a significant difference from normal control values; * represent a significant difference from the germline; ξ represents a significant difference between DM and PM myositis subsets ($p<0.05$). □ From all DM, PM and IBM patients.

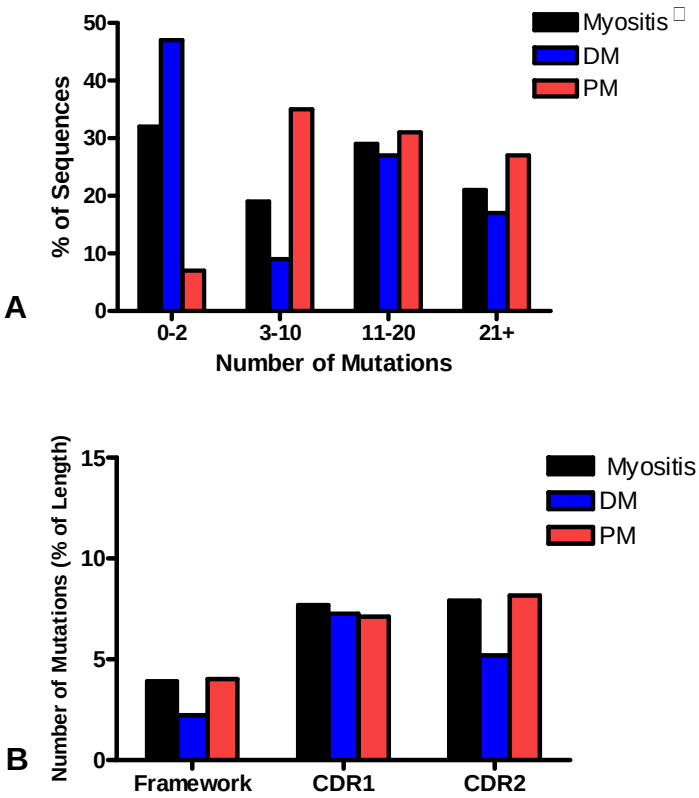

Figure 4.38 Numbers of Mutations and Mutational Distribution of Functional Sequences in Myositis Patients

Figure 4.38A - The number of mutations within functional rearranged genes were analysed collectively from all myositis patients as well as in the DM and PM subsets. Base differences within the first 24 bases of sequence were disregarded as this part of the sequence binds the 5' V_H primer. Graph demonstrates sequences collectively from myositis patients show a diverse distribution of mutational numbers while sequences from DM patients were primarily from a naïve populations and sequences from PM patients were highly mutated.

Figure 4.38B - The locations of mutations observed within functional rearranged genes were categorised as being within FR or CDR regions. The numbers of mutations within these regions were expressed as a percentage of the entire length of the region to correct for the longer lengths observed within the framework regions. Graph demonstrates a higher percentage of mutations within CDR regions compared to framework regions for all 3 groups.

□ From all DM, PM and IBM patients.

A collective summary of the mutational selections (**Table 4.30**) conducted as per Hershberg *et al* (294) revealed that sequences, with significant selections, from all 3 subsets mostly demonstrated negative selection with the FW regions in contrast to positive selection in the CDR which would be expected in an antigen-driven response. A small percentage of sequences in the myositis and PM collective sets demonstrated positive selection in the CDRs but in the myositis collective repertoire negative selection was also found within the CDRs. This negative selection in the CDRs was also observed in some sequences of the DM repertoire.

	MYO□ (n=148)				**DM (n=93)**				**PM (n=55)**			
	CDR		**FW**		**CDR**		**FW**		**CDR**		**FW**	
	#	**%**	**#**	**%**	**#**	**%**	**#**	**%**	**#**	**%**	**#**	**%**
Positive Selection	3	**2.0**	0	**0**	0	**0**	0	**0**	3	**5.5**	0	**0**
Negative Selection	2	**1.4**	21	**14.2**	2	**2.2**	10	**10.8**	0	**0**	11	**20**

Table 4.30 Summary Table of Myositis Sequences with Significant Selection

The total number of sequences with significant selection, positive or negative, in CDR or FW regions was calculated (#) and the percentage (%) calculated for each myositis category to reveal a higher percentage of sequences contained negative selection in the FW regions compared to other selections within the Ig sequences. □ From all DM, PM and IBM patients.

In each set of sequences no significant differences in CDR3 length was observed and a similar CDR3 length was observed for all functional and non-functional sequences in each group (**Table 4.31**). Analysis of these CDR3 lengths in correlation with the V_H mutational numbers revealed no significant differences between the CDR3 length in unmutated and mutated sequences for the myositis and DM collective repertoires (**Figure 4.39**). A significantly shorter CDR3 length was observed in the PM collective repertoire for the group of sequences containing 21+ mutations in comparison to the sequences with between 11 and 20 mutations. For the additional of P nucleotides there was a significant increase observed at the VD junction between functional and non-functional populations in the myositis and DM sequence sets. No significant differences in N nucleotide additions were observed for any group of sequences except the increased addition of N nucleotides in the DJ junction of functional sequences in the PM sequence set compared to the VD junction. A similar pattern of exonuclease activity was observed for all 3 groups, an increase in exonuclease activity was observed and the 5'D_H and 5'J_H regions of the junction compared to the 3'V_H region. No significant differences were observed, for any group of sequences, between the 5' and 3'D_H regions or the 3'D_H and 5'J_H regions of the DJ junction.

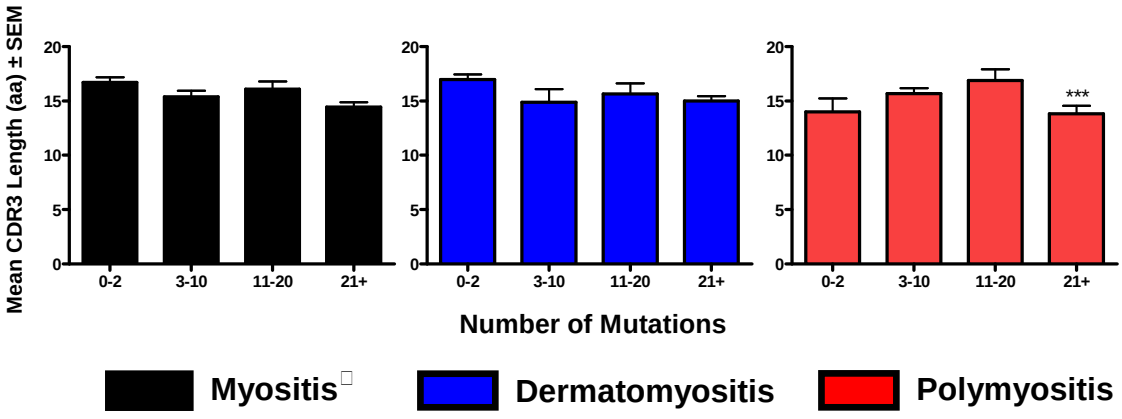

Figure 4.39 Mean CDR3 Lengths in Relation to V_H Mutational Numbers

The mean CDR3 length was calculated for immunoglobulin sequences according the number of mutations within the V_H segment of the gene rearrangement to establish any relationship between mutational number and CDR3 length. Results are given as Mean amino acid CDR3 length ± SEM. Groups within each myositis category were compared for statistical significance using the Tukey-Kramer test for multiple comparisons. *** represents a significant difference from 11-20 mutations. p-values <0.05 were deemed significant. □ From all DM, PM and IBM patients.

CDR3 Length	**MYO**	**Functional**	15.7 ± 0.3			
		Non-Functional	15.8 ± 1.7			
	DM	**Functional**	15.8 ± 0.4			
		Non-Functional	15.8 ± 1.7			
	PM	**Functional**	15.4 ± 0.5			
		Non-Functional	N/A			
			VD Junction		**DJ Junction**	
P Nucleotide Additions	**MYO**	**Functional**	0.5 ± 0.1		0.4 ± 0.1	
		Non-Functional	1.4 ± 0.7*		0.4 ± 0.4	
	DM	**Functional**	0.5 ± 0.1		0.5 ± 0.1	
		Non-Functional	1.4 ± 0.7*		0.4 ± 0.4	
	PM	**Functional**	0.4 ± 0.2		0.3 ± 0.1	
		Non-Functional	N/A		N/A	
N Nucleotide Additions	**MYO**	**Functional**	7.4 ± 0.5		8.5 ± 0.5	
		Non-Functional	6.0 ± 0.5		10.2 ± 4.1	
	DM	**Functional**	7.9 ± 0.7		8.1 ± 0.7	
		Non-Functional	6.0 ± 1.5		10.2 ± 4.1	
	PM	**Functional**	6.2 ± 1.0		9.4 ± 0.6**	
		Non-Functional	N/A		N/A	
			3' V_H	**5' D_H**	**3' D_H**	**5'J_H**
Exonuclease Activity	**MYO**	**Functional**	1.2 ± 0.2	5.0 ± 0.5 $^{\theta}$	3.9 ± 0.4	4.8 ± 0.4 $^{\theta}$
		Non-Functional	2.0 ± 0.7	2.2 ± 1.2 $^{\theta}$	6.2 ± 2.9	4.6 ± 1.6 $^{\theta}$
	DM	**Functional**	1.1 ± 0.2	5.2 ± 0.6 $^{\theta}$	4.1 ± 0.4	4.6 ± 0.5 $^{\theta}$
		Non-Functional	2.0 ± 0.7	2.2 ± 1.2 $^{\theta}$	6.2 ± 2.9	4.6 ± 1.6 $^{\theta}$
	PM	**Functional**	1.2 ± 0.2	4.7 ± 1.3 $^{\theta}$	3.2 ± 0.8	5.3 ± 0.6 $^{\theta}$
		Non-Functional	N/A	N/A	N/A	N/A

Table 4.31 CDR3 and Junctional Analysis in Myositis

The mean amino acid length of the CDR3, the mean nucleotide numbers corresponding to P and N nucleotides as well as the mean number of germline nucleotides lost due to exonuclease activity were calculated from the junctional regions of all myositis immunoglobulin sequences as well as in DM and PM subsets. Results are given as the Mean ± SEM. Instances where no non-functional sequences were identified and values could not be calculated were recorded as non applicable (N/A). * indicates a significant difference between functional and non-functional sequences while ** indicates a significant difference between the VD and DJ junctions established using an unpaired t-test. Θ represents a significant difference from 3'V_H.

A total of 9 clonally related sets of sequences were found in approximately a third of all myositis patients. Both DM patients, MYO1 and MYO16, contained clonally related sets of sequences, 1 from sample MYO1 and 2 from sample MYO16, although due to the detection of a deletion in the clonally related sequences of sample MYO1 this set of clonally related sequences may not be valid depending on the alignment algorithm used. Sets of clonally related sequences were found in 3 of 11 PM patients, MYO3, MYO5 and MYO23, with 4 different clonal sets in sample MYO5 and 1 each from samples MYO3 and MYO23. In each set of clonal sequences there was no positive selection observed within the CDRs, as would have been expected for clonally related and antigen-driven sequences. For 4 of the 9 clones a significant negative

selection was observed in the FW regions; remaining clones did not exhibit any significant positive or negative selection in either CDR or FW.

Comparison of the different mutations within all sequences identified common replacement mutations within a number of sequences. The replacement mutation at amino acid 31 within the CDR1 region, serine to asparagine (S→N), was found within all 4 MYO5 clones. In addition to this mutation within the V_H5-51, V_H3-04, V_H3-33 and V_H3-53 sequences of MYO5, the mutation was also observed within the V_H1-69 gene in sample MYO3 and the V_H3-30 gene in sample MYO23. Other common mutations were also observed within CDR2. Silent mutations within amino acids 51 and 59, isoleucine and tyrosine respectively, were found in sequences from both MYO3 and MYO5; a replacement mutation at amino acid 65 was found in sequences from MYO3, MYO5 and MYO7. At amino acid 65 the glycine amino acid was mutated to an aspartic acid amino acid (G→D). Within the same patient these common mutations may represent that a common antigenic determinant is driving the immune response and hence the mutational patterns of the Ig genes while common mutations across different patients suggests mutational hot-spots are present within the Ig genes found in these autoimmune disorders.

4.3 Discussion

The role of B cells in myositis is still currently unresolved and it was previously thought that myositis was essentially T cell mediated, especially PM and IBM. The core aim of this study was to establish if muscle infiltrating B cells were being locally stimulated resulting in an antigen-driven response leading to tissue pathology. To address this hypothesis DNA was extracted from microdissected B cells from frozen muscle sections and identification of the gene rearrangement of Ig sequences from muscle infiltrating B cells was conducted. Analysis of these sequences determined if any gene or clonal selection process was occurring within the muscle tissue. At the start of this work no previous studies had investigated the gene repertoire or clonal diversification of B cells within muscle tissue of myositis patients.

Results from Chapter 3 verified the occurrence of B cells, and their differentiated counter-parts plasma cells, within the muscle infiltrating population of cells. The results also established a number of proliferating B cells within the inflamed muscle tissue. This suggested that muscle infiltrating B cells may be proliferating, undergoing somatic hypermutation and diversification in an antigen-driven response. Further confirmation of gene selections and diversification of the Ig repertoire from normal control values, accumulation of mutations and identification of clonally related sequences with common mutations would substantiate the hypothesis that muscle infiltrating B cells within inflamed muscle were undergoing an antigen-driven response. The results presented in this chapter support these characteristics of antigen-driven diversification as well as the hypothesis of a B cell antigen-driven response within inflamed muscle of myositis patients.

Gene selections were observed for all 3 segments of the Ig rearrangement, these were shown to be both disease specific as well as patient specific. Conclusive clonal diversification of these genes was also observed in 4 of 12 patients, 1 DM patient and 3 PM patients. Collectively these results indicate that an antigen-driven response occurs within the target tissues of these patients and that clonal B cells may play a significant role in the pathogenesis of these diseases, similar to studies in other disorders of autoimmune origin or

where ectopic lymphoid tissues have been identified (52;283-285;289;317-325). In some instances gene selection and clonal diversification could not be assessed in some patients due to the small numbers of rearrangements identified from the muscle infiltrating B cell population, a larger number of sequences may be required for these samples. This could be a result of the variations in cell phenotypes found to be infiltrating the muscle described in Chapter 3. For patients MYO1, 3, 5 and 16, where gene selections and clonal diversification were observed, a significant infiltrating population of B cells was observed within frozen muscle sections. Conversely for other samples, MYO6, 7, 17, 19, 23, 24, C, E, a larger population of plasma cells were observed within muscle sections which could account for the diminished Ig repertoire or lack of clonal proliferation within these samples although despite the large plasma cell infiltration in sample MYO23 gene selections and clonal diversification of Ig genes were observed. The mutational analysis of some of these sequences from these patients would suggest that an antigen-driven response had occurred. It could be postulated that the plasma cells in these samples had been recruited to the sites of inflammation in their activated B cell or memory state and prior to biopsy had differentiated into plasma cells whereas in the previous samples the B cells are expanding and diversifying within the muscle and had not yet matured into plasma cells. The work conducted in this study was unable to differentiate between the B cell and plasma cell repertoires; further single cell or cell sorting analysis would need to be conducted to distinguish the two populations of cells. A re-stimulation of memory cells may also account for the diminished Ig repertoire; chronic stimulation of antigen-specific memory B cells could account for the large number of replicate sequences identified in this study, for all samples, with the same Ig rearrangement. Alternatively memory B cells could have entered a differentiation stage of proliferation without further somatic hypermutation accounting for the lack of clonal proliferation. The process used in this study could not differentiate between this chronic stimulation and repeated amplification of a single amplicon within the PCR reactions unless consecutive sections or different regions of the section were analysed in separate PCR reactions. In order to account for this repeated amplification and prevent misinterpretation of clonal expansion without mutation these sequences were

only counted once within the sample repertoire. If a chronic stimulation of antigen specific memory B cells was to occur within the inflamed muscle tissue what remains uncertain is whether these memory cells are recruited to the inflamed muscle site in this mature state or whether peripherally activated B cells are initially recruited which later mature into memory cells. It could be that the timings of the clinical investigations into the inflamed muscle have missed the initial expansion and mutation phase of the B cell antigen driven response. The use of a memory B cell marker, CD27, in the previous immunohistological studies described in Chapter 3 may have provided additional evidence of the B cell role in inflamed muscle of myositis patients. In circumstances where no clonally related sets of sequences were identified it may indicate that infiltrating B cells are not mutating within the regions of cellular infiltration but are mutating and migrating into infected tissue from other locations, presumably the draining lymph nodes, in contrast to the proposed hypothesis. Recent studies have demonstrated the expression of AID, the enzyme responsible for SHM and CSR, and the functional relationship between AID, CSR and autoantibody production within the FDC networks of ectopic GC-like structures in SS and RA patients (55;326). AID expression was not found within target tissues where no FDCs or GCs were present except for in interfollicular (IF) large B cells outwith these GC compartments where AID has been shown to be functionally active (327-329). Identification and classification of AID expressing cells within inflamed muscle would corroborate the findings of this study, SHM and clonal diversification, and provide greater insight into antigen-driven responses in autoimmune target tissues where no GC structures are present. The participation of ectopic lymphoid tissues in generating antigen specific B cell responses has also been recently described by Weinstein *et al* (330) to further substantiate that the target tissue in various autoimmune diseases are sites of active antigen-specific response rather than sites of lymphocyte accumulation.

From the results described in Chapter 3 a number of samples contained $Ki67^+$ proliferating B cells, MYO1, 17, 19, 24 and E, but evidence of clonal diversification was only observed for sample MYO1. The need for analysis of additional muscle sections may be required to fully evaluate the process of clonal diversification in these samples.

As previously described in Chapter 3 the impact of patient's therapy on cellular infiltration as well as Ig gene repertoire and identification of clonally related sequences in this chapter cannot be overlooked. As previously described in Chapter 2 (Table 2.1) and Chapter 3, section 3.3, six patients, MYO5, 19, 23, 24, C and E, were receiving steroid therapy at the time or just prior to biopsy. Additionally patient MYO5 was receiving IVIg therapy while patient MYO19 was receiving methotrexate. These therapies could have distorted the true heterogeneity of the B cell response in these patients. Despite the therapeutic interventions gene selections and clonally related sets of sequences in MYO5 and MYO23 indicate that B cell antigen-driven diversification was still occurring within the inflamed muscle tissue. This is more significant for patient MYO5 who had been receiving therapy for three years prior to the biopsy while patient MYO23 had only received a week of therapy which was stopped two weeks prior to the biopsy. As previously mentioned in Chapter 2 the biopsy for patient MYO5 used in this study was conducted approximately 3 years following the initial biopsy for clinical investigations for diagnosis. Examination of this initial biopsy would have provided interesting insights into the original Ig gene repertoire and clonal diversification sequence sets of B cells within the inflamed muscle at the onset of the disease while also revealing the impact of therapy on these two factors but unfortunately this biopsy was not available for analysis.

A surprising finding from this study was the lack of significant positive selection within CDRs. The accumulation of mutations and identification of clonally related sequences indicate the occurrence of B cell antigen-driven responses within the inflamed muscle but are not substantiated with significant positive selection in Ig sequences. Positive CDR selection was observed for a small percentage of sequences but the bulk of selection was found to be negative selection in the FW regions, although this negative selection was also observed in the CDRs (Table 4.30). Antigen driven responses have traditionally been associated with an increase in replacement mutations from expected frequencies in CDRs indicating positive selection while decreased levels of replacement mutations within FW regions indicated negative selection. The methods previously and currently used to detect selection based on the analysis of mutation patterns in Ig sequences are described in section 4.3.3. Current

analysis has indicated that previous methods have misinterpreted positive CDR selection with negative selection in the FW regions due to crosstalk which could not be differentiated in previous methods. This may indicate that studies that have previously established positive selection above expected frequencies in antigen-driven studies may be based on flawed methodology and generate false positive selection within the Ig sequences. Taking into consideration the updated parameters of analysis by Hershberg *et al* (294) which incorporate fundamental aspects of sequence variation and diversity into assigning selection, provides a more accurate assessment of selection within Ig sequences. The lack of positive selection in CDRs observed in this study may relate to findings previously described where selection against amino acid replacement in CDRs may occur to prevent the degradation of high affinity autoantibodies (331). Other possibilities may include a lower rate of SHM at ectopic sites in comparison to secondary lymph nodes (330) or a defect may occur in affinity maturation if there is less competition over lower affinity cells at ectopic sites (330) due to an abundance of self antigen or a lack of regulation outside GCs (301;332;333). This could also correspond to the absence of FDCs from a large cohort of samples in Chapter 3 and recent studies which demonstrated the expression and function of AID in FDC networks (55;326).

Analysis of the CDR3 regions, the addition of P and N nucleotides as well as exonuclease activity at the junctional regions in the current study yielded different results compared to published studies (238;241;242;251;291). Generally previous studies have demonstrated that CDR3 lengths are significantly shorter in functional rearrangements. In the current study no significant differences were observed between the CDR3 lengths in functional and non-functional populations for individual patients as well as collective analysis for the different disease subsets. In this study very few cells expressing non-functional Ig sequences were detected within the infiltrating repertoire and in some cases no non-functional sequences were examined in individual patients, therefore comparison to the non-functional repertoire could not be conducted. Analysis of a larger population of sequences may be required in order to fully determine if selection for smaller CDR3 lengths is present within functional sequences in the disease repertoires. Differences

between disease repertoires and the normal control repertoire may also account for this change in CDR3 lengths in the functional and non-functional populations. One study also demonstrated a significant decrease in CDR3 length in mutated sequences compared to unmutated sequences (238), generally within this study this pattern was not observed with exception for the collective PM sequences and sample MYO16 (Figure 4.25) where highly mutated sequences contained a significantly shorter CDR3 compared to the sequences with fewer mutations. Again this may indicate a difference in the enzymatic mechanisms and gene selections within disease models compared to normal control models, although in addition to the CDR3 length the amino acid composition of the CDR3 would also have to be considered. Previous studies have also examined the addition of P an N nucleotides as well as the exonuclease activity with the junctional regions (251;291;334). Generally a significant increase in P and N nucleotides were found within the VD junction compared to the DJ junction, a pattern that was not observed in the current study. The increased addition of N nucleotides at the VD junction is thought to relate to the increased TdT expression during the development stage of V-DJ joining. TdT was found to be initially upregulated during the D-J recombination in pre-pro-B development stage with a further increase at the V-DJ recombination stage observed in pro-B cells, it was then observed that TdT expression quickly declines (251). The results of the current study do not correspond to these findings but may relate to selection in the target tissues. Previous studies have also reported a significant decrease in exonuclease activity at the V_H region compared to the 5'D_H and J_H regions (291;334), a similar pattern to that observed in this study. These variations in exonuclease activity at various regions within the CDR3 have been thought to relate to the primary sequence of the gene rearrangements. An increased exonuclease activity was observed in D_H2, D_H3 and J_H6 genes compared to other D_H and J_H genes (334). It had been proposed that the slightly more AT rich region at the 5'J_H region is preferentially targeted by exonuclease activity (291).

One aspect of antigen-driven B cells not examined in this study was the process of isotype switching. Evidence showing the isotype switching of antibodies in these responses would further substantiate the antigen driven response in the

target tissues of myositis patients. If these studies were to continue constant region primers could be used in PCR reactions to establish the isotype of antibody produced from muscle infiltrating B cells alternatively immunohistochemical studies could be conducted with antibodies specific to the various antibody isotypes. The occurrence of isotype switching was demonstrated in a recent study by Bradshaw *et al* (90) which also examined the incidence of antigen-driven B cell responses in the target tissues of myositis patients is discussed fully in section 4.3.1. Briefly Bradshaw *et al* identified clonal variants of different antibody isotypes (IgG and IgA) in DM patient, providing further evidence of antigen-driven diversification of B cells within inflamed muscle. A recent review (335) has suggested that the constant region may also influence antibody specificity and affinity. Another aspect of the B cell response not examined in this study was the Ig repertoire and mutations of the light chains. Examination of the light chain sequences from the muscle infiltrating B cell population would have given a rounded examination of the full B cell response in this study. Amplification of lambda and kappa light chains were conducted for a number of samples in this study with successful amplification but due to the extensive nature of the work required for the light chain analysis, time constraints and the sufficient use of heavy chain sequences to determine antigen-driven clonal diversification this aspect of the response was not fully pursued but should be considered in subsequent studies. Examination of paired peripheral blood samples, taken at the time of biopsy, would also be extremely beneficial in subsequent studies. Due to the constraints of examining archival material and the difficulty in obtaining fresh muscle biopsies for this study paired blood analysis was not conducted. Such analysis would allow a comparison of any V, D or J gene selections in the peripheral blood to that observed within the muscle as well as identification of clonal rearrangements or variants from the muscle infiltrating repertoire in the blood. A study conducted by Voswinkel *et al* (336) examined and compared the B cell repertoires between the synovial tissue and peripheral blood B cell repertoire in a patient with RA. The study detected identically rearranged genes within different joints and within the PBL indicating the recirculation of B lymphocytes between joint and peripheral blood. Although affinity maturation was observed from the sequences, authors suggested that a primary selection

occurred before distribution to the joints and following migration to the joints antigen-driven diversification was continued before re-circulating into the peripheral blood B cell repertoire. Re-circulation of activated synovial B cells has also been demonstrated in another study by Souto-Carneiro *et al* (337) which described the identification of clonally related B cells at different sites of synovial inflammation. The absence of FDCs within these sites suggested to the authors that these stimulated B cells from early RA lesions migrate to other areas of inflammation and re-enter a cyclic hypermutation process. This work supports previous work (338;339) which demonstrates the cyclic re-entry of stimulated B cells. This could be a plausible situation from the work described in the current study where some samples lacked the presence of FDCs as previously described in chapter 3. Conversely Owens *et al* (340), while studying the B cell repertoires in Multiple Sclerosis plaques, found that this repertoire was distinct from the repertoire of the PBL. The results indicated that a compartmentalised humoral response was occurring and that there was no entry of the CNS sequences into the peripheral blood repertoire. Comparison of the sequences isolated from the muscle and the peripheral blood were conducted in the current study from sample MYO5 which demonstrated that no sequences with the same rearrangements were found in the two different sites, although only a small sample of the total PBL was examined. Gene selections from MYO5 PBL were observed when compared to normal control values as well as the MYO5 muscle repertoire. The peripheral blood sample obtained for patient MYO5 was obtained 3 years after the biopsy was conducted and the biopsy examined in this study was taken two years after the diagnostic biopsy so alterations in the repertoire as a result of treatments and other immune responses cannot be overlooked.

4.3.1 Somatic Hypermutation and Clonal Diversification in Myositis

At the commencement of this study no previous studies addressed if B cell antigen driven responses were occurring within the inflamed muscle of myositis patients. Recently Bradshaw *et al* (90) demonstrated that antigen specific responses were occurring in muscle of DM, PM and IBM patients. This study examined the Ig isotype usage, somatic mutations and clonal expansion of B cell and plasma cell infiltrates within myositis samples. Twelve different muscle

samples (7 IBM, 3 DM and 2 PM) were examined for the presence of B cells and plasma cells, in contrast to the results described in Chapter 3 of this study very few $CD19^+$ or $CD20^+$ cells were found within the infiltrating population. The majority of B cell derived cells present within these samples were $CD138^+$ plasma cells. The Ig sequences from these 12 patients were examined and reveal that the majority of cells infiltrating these muscle biopsies had class switched from IgM to either IgG or IgA, indicating a stimulated response as naïve cells do not perform class switching until they have encountered antigen. Conversely most of the sequences isolated from control blood samples, 2 from IBM patients and 2 from normal controls, contained sequences mostly derived from B cells producing IgM sequences. In obtaining the results for this chapter the constant regions of Ig were not accounted for but analysis of these regions may have provided evidence of class switching occurring within the myositis samples used for this study, similar to that observed by Bradshaw *et al*, to suggest a stimulated response within the muscle. No collective repertoire analysis or gene usage percentages were conducted for each patient of myositis subset by Bradshaw *et al* therefore no comparisons of V_H, D_H and J_H gene selections could be made. Mutational numbers within the sequences from the twelve patients isolated by Bradshaw *et al* demonstrated that these sequences contained considerably more mutations in comparison to blood control samples. Bradshaw *et al* demonstrated that mutational numbers within inflammatory myopathies were shown to range from between 16 mutations per sequence to 27 per sequence; this was in contrast to control sequences which contained between 2 and 17 mutations per sequence. Interestingly it was noted by the authors that approximately 50% of the IgM sequences had between 11 and 30 mutations per sequence and appeared to have undergone affinity maturation without class switching. In the current study a wide range of mutational numbers were observed from essentially naïve cells, in contrast to Bradshaw *et al*, to highly mutated cells. Clonally related sequences were found in 10 of the 12 myositis patients with up to four different clonal sets isolated from each muscle section and were not observed in any of the blood samples used from either the IBM patients or normal control patients. These clones were mostly found to consist of two clonal variants but up to six different clonal variants were observed for some clonally related sets of sequences. Similarly

up to four different clonal sets of sequences were found within muscle sections in the current study but this was only observed for sample MYO5 where the whole section was used instead of microdissected cellular aggregates from the muscle sections. In contrast only a single clonal set of sequences was isolated from each microdissected cellular aggregation which contained between 2 and 8 clonal variants. Three of the clones from Bradshaw *et al*, one from each myositis subset, were shown to be derived from V_H5-51, V_H3-23 and V_H3-30 gene rearrangements. Clonally related sets of sequences containing the V_H gene segments V_H5-51 and V_H3-30 were also found within this study which may suggest a common selection for these particular genes between different patients. Further mutational analysis of these clones isolated by Bradshaw *et al* demonstrated that a number of identical replacement mutations were found in clones of the same patient, indicating that these clonally related sets of sequences may be being driven by the same antigen, while other replacement mutations were found in many clones from different patients suggests the location of mutational hotspots within the Ig sequence as well as indicating that a common antigen may be driving the B cell response. Laser capture microdissection (LCM) experiments were used to further assess the degree of clonal expansion within inflammatory myopathy tissue. LCM was used to divide tissue sections from each of the 3 inflammatory myopathies into distinct regions from which Ig sequences were obtained and analysed. Using this method, further evidence of clonally related sets of sequences were obtained from DM and IBM samples demonstrating the presence of clonally related sets of sequences within the same and different regions of the same muscle samples indicating the expansion of B cells within inflamed muscle tissue. This could be further examined, in both studies, to incorporate additional muscle sections to determine if the clonal expansion extends into additional sections. Results of Bradshaw *et al*, together with the results presented in this chapter indicate that antigen driven B cell responses are occurring within muscle rather than in a local lymph node as is classically thought. In contrast a number of patients within the current study did not display evidence of an antigen-driven B cell response which may also indicate that these infiltrating B cells and plasma cells are mutating in other locations and migrating into these areas of infiltration but may also be the result of previous immunosuppressive therapy in some patients

as previously discussed, although four sets of clonal related sequences were isolated from sample MYO5 who had extensive therapy prior to the biopsy used in this study. None of the patients in the study by Bradshaw *et al* had received therapy prior to the study. In comparison to the entire myositis response only a small fraction of the response was assessed in several muscle sections which may underestimate the true heterogeneity of the B cell response. Clonal diversification may be occurring within other areas of muscle which were not examined.

4.3.2 Assignment of Ig Genes

Ig gene assignments in this study were conducted using the JOINSOLVER (291) as well as the IMGT/V-QUEST software (292;293). Numerous programmes are available for identification and assignment of germline genes in rearranged Ig gene sequences but as JOINSOLVER concentrates on characterisation of the CDR3, a region pivotal in identification of clonally related Ig genes which addresses the central aim of this study, this programme was deemed appropriate for the current study. To account for any anomalies between software algorithms IMGT/V-QUEST was also used in this study. Recent updates to the IMGT/V-QUEST software (293), including detection of insertions and deletions which is not carried out by the JOINSOLVER software, provided a more accurate comparison between the two algorithms. Following completion of the sequence analysis described in this chapter the JOINSOLVER algorithm was updated (The Characterization of Mutations in Complementarity Determining Region 3 of Human Ig Gene Rearrangements using JoinSolver, Nancy S. Longo, Daniel E. Russ, Eric Schloeffler and Peter E. Lipsky (manuscript in preparation)) to accommodate mutations within the D_H and J_H gene segments. This algorithm change creates a greater accuracy of gene assignment as well as assignments of P and N nucleotides, in addition to those lost by exonuclease activity. These changes correspond to the manual sequence changes conducted within this study but repeat analysis of the sequences generated may result in subtle changes to the results described. The use of the original JOINSOLVER algorithm and the updated IMGT/V-QUEST algorithm in this study generated alignments, which for the most part, corresponded to each alignment programme. A difference in gene assignment

was observed for approximately 5% of the sequences isolated from muscle infiltrating cells while only 2% of sequences contained insertions and deletions. Most of these sequences contained deletions in multiples of 3 from the CDR2 which allowed the reading frame to be maintained and productive translation of the Ig. Although rare, the process of insertions and deletions, especially in the CDRs, does create further diversification within the Ig repertoire.

The JOINSOLVER software was compared to the DNAPLOT software (Centre for Protein Engineering, www.mrc.cpe.cam.ac.uk) (291) using 144 randomly selected unmutated and mutated Ig rearrangements. For 50% of the rearrangements both programmes gave comparable D gene assignments but JOINSOLVER performed better than DNAPLOT for 22% of rearrangements either by finding a higher consecutive match or because DNAPLOT failed to identify any D gene for 25% of the rearrangements. For all sequences JOINSOLVER was able to generate some D gene alignment although this was not always significant. New algorithms have recently been described (341;342). SoDA (Somatic Diversification Analysis, http://dulci.org/soda/) (342) is a dynamic programming alignment algorithm which takes into consideration the variation around the recombination sites from nucleotide addition and exonuclease activity and allows for insertions and deletions within the gene. This algorithm was compared to both JOINSOLVER and IMGT/V-QUEST using a set of artificial Ig sequences generated using a simulation programme; all programmes use the same libraries from IMGT. The authors report that SoDA identified more rearrangements accurately compared to both JOINSOLVER and IMGT/V-QUEST and observed that JOINSOLVER did not perform as well in assigning V_H gene segments. It was also observed that IMGT/V-QUEST identified fewer D_H genes. All 3 programmes were similar in identifying J_H genes but at a 15% mutational rate in the artificial sequences both JOINSOLVER and IMGT/V-QUEST performed better. The SoDA algorithm was also tested using 30 randomly selected sequences of which some were used in the testing of JOINSOLVER (291). For 18 of these sequences all 3 programmes agreed in the gene identification and for the remaining 12 SoDA never made an identification, for the V and J genes, that was not supported by either JOINSOLVER or IMGT/V-QUEST. The iHMMune align

(www.emi.unsw.edu.au/~ihmmune/) algorithm has recently been described (341) and is an alignment application that uses a hidden Markov model (HMM) to model the processes involved in Ig gene rearrangement and maturation. This algorithm was compared to JOINSOLVER, IMGT/V-QUEST and SoDA using both clonally related and randomly selected Ig sequences. Analysis of clonally related sequences demonstrated that all four programmes agreed with the assignment of the longer V_H and J_H genes, although variations in the predicted alleles were observed. Differences were noted within the D_H gene assignments between the four programmes. Analysis of randomly selected sequences, from the same collection as previous studies was also conducted (251;291). From 662 sequences total agreement was only observed for 104 of the sequences, while agreement in the V_H, D_H and J_H gene assignments was observed for 357, 291 and 322 sequences respectively. From this analysis it was observed that iHMMune provided a more accurate identification of the rearranged germline genes as fewer disagreements were observed with this algorithm compared to the other 3 programmes and D_H gene alignments were generally longer and contained fewer mismatches. Although iHMMune accounts for modelling Ig processes that are not represented by other algorithms it does not account for insertions and deletions within germline genes.

Analysis of the sequences from this study with the SoDA and iHMMune algorithms may provide a more accurate assignment of gene as well as mutational analysis but due to time constraints and timing of publications this was not possible for the current study presented. The difficulties in assigning germline genes, especially D_H genes, to rearranged Ig genes because of germline gene similarities, somatic mutations, exonuclease and TdT activity may make it difficult to determine which algorithm would provide the most accurate gene assignments.

4.3.3 Detecting Selection of Ig Sequences

Analysis of selection in this study was conducted by the method proposed by Hershberg *et al* (294) to detect positive antigen-driven selection in the B cell Ig genes from the infiltrating B cell population in both the inflamed muscle of myositis patients and skin of vasculitis patients. Many methods and studies

have previously been conducted in order to detect selection (343-346), which are based on mutation patterns in Ig sequences. Shlomchik *et al* (346) used a binomial distribution model to study selection which was based on detecting positive selection by comparing the fraction of R mutations in the CDR to all other mutations while assuming a fixed level of negative selection. In the study by these authors it was expected that half of R mutations within FW regions would be eliminated through negative selection, therefore to compensate for this fixed level of negative selection the observed number of R mutations in the FW was doubled. The study also assumed that all V-region mutations occurred at random which was later accounted for by a revised and extended binomial test by Chang and Casali (344). This test took into consideration that codons with a higher susceptibility for R mutations were generally found within CDRs as well as removing the fixed level of negative selection from the test by allowing for the total number of mutations within the FW. Following this method Lossos *et al* (345) described a multinomial distribution test which allowed the frequency of mutations to be considered in four categories, R and S mutations in CDR and/or FW regions of the gene, which the previous binomial methods had failed to account for and were based only on two distribution possibilities. This modified method provided a more accurate method of determining antigen selection. This method consisted of a sum of all the binomial probabilities which also took into account the inherent susceptibility of the codons of the CDR and FW to R mutations. The results of this multinomial distribution were tested on 86 V_H gene sequences and were compared to that of the binomial test described by Chang and Casali. In the majority of sequences the p values obtained using both methods varied in magnitude but not in statistical significance, inconsistencies were only found in 8 sequences resulting in opposite statistical conclusions, but the authors argue that the proper multinomial test should be applied when determining selection even though results from each test proved similar. Despite the increased accuracy of this test in comparison to previous methods, the method failed to consider the presence of mutational hot-spots within the gene and assumed that mutations in the V_H genes occurred randomly which can produce the false appearance of selection. Bose and Sinha (343) also examined antigen selection using a modified Chang and Cascali / Lossos method which included the effects of hot-

spot regions in the Ig gene. While the Chang and Cascali / Lossos method assumes that an Ig gene becomes somatically mutated across its length, the Bose and Sinha method depends on the length, the codon usage as well as the built-in mutability of different regions of the Ig gene. The results of this study identified false positive results and failed to establish the role of antigen-driven selection in clonal maturation and concluded that selection can act both for and against R mutations in the CDR as well as in the FW regions depending on the relative contribution to affinity and structural integrity of the Ig. Recently Hershberg *et al* (294) have proposed a new focused binomial test for detecting selection in Ig V region sequences. This study demonstrated that the multinomial test by Lossos *et al*, referred to as a global binomial test by Hershberg *et al*, was mathematically equivalent to the previously proposed method by Chang and Cascali. The previous method produced a high frequency of Type 1 (specificity) false positives and was unable to distinguish whether a relatively high frequency of R mutations in CDR was due to positive selection in the CDR or negative selection in the FW - crosstalk between positive and negative selection. The authors also concluded that the statistical method of Bose and Sinha was also flawed as it was based on these previous methods. The study by Hershberg *et al* proposed the focused binomial test for selection which corrects for the specificity problem exhibited in the global binomial test and eliminates crosstalk. The newly proposed test fully accounts for the effects of microsequence specificity, the likelihood of each nucleotide to mutate depending on its local sequence, and incorporated the transition over transversion bias of somatic hypermutation for the first time in this type of analysis. This method of detecting selection was tested by re-analysis of sequences from diffuse large B cell lymphomas (DLBCL) by Lossos *et al* (347), re-analysis of 76 non-functional rearrangements from previously published studies and sequences generated in response to the nitrophenyl (NP) antigen in conventional Ig heavy chain transgenic mice which do not mutate or isotype switch their heavy chain loci. In this system positive selection was expected to dominate due to a fixed heavy chain which would cause all mutation and selection to be focused on the light lambda chain. Re-examination of sequences from DLBCL using the focused binomial test indicated that many false positive results were assigned; positive selection was not found in any of

the 54 sequences using the focused binomial test compared to 16 out of 54 sequences using the method proposed by Lossos *et al*. It was thought by the authors that this false positive selection was a result of crosstalk as negative selection was detected in 88% of the 16 sequences with positive selection. Studies from the transgenic mice established that positive selection could be detected while the analysis of non-functional sequences detected no selection and demonstrated that previous positive selection found in these sequences was the result of false positive errors. The results of this study demonstrate that the focused binomial test can be used to detect positive and negative selection with high specificity and increased sensitivity which can be applied to single sequences in addition to independent mutations in clonally related Ig sequences.

4.3.4 Summary

In summary, the work presented in this chapter demonstrates that B cell antigen-driven responses are occurring within the target tissues of myositis patients, even in PM patients where B cells are traditionally not thought to play a significant part in the pathological process. Ig sequence analysis from infiltrating B cells within these myositis samples established positive and negative gene selections within individual patients as well as between different myositis subsets. An accumulation of mutations was also observed in these sequences with a number of common mutations observed between various sets of sequences which share the same Ig gene rearrangements in addition to further independent V_H mutations, indicating clonal diversification. Collectively these results strongly indicate that B cells present within the inflamed muscle of myositis patients are acting in response to an antigen present at the sites of inflammation. In these samples, especially where clonally related sequences were not isolated, the mutational features of the sequences indicated the occurrence of antigen-driven diversification, possibly at another site or the re-circulation of antigen specific B cells from other sites of inflammation. Although the work conducted in this chapter demonstrates B cell antigen-driven responses in the target tissues of myositis patients and implicates B cells in the pathological process of myositis it does not identify the antigen(s) stimulating these responses.

Chapter 5 - Phenotypic Cellular Characterisation, V_H Gene Repertoire and Clonal Diversification of Skin Infiltrating B cells in Vasculitis Patients

5.1 Introduction

As previously discussed in Chapter 1, vasculitis is another inflammatory condition with unknown aetiology. Vasculitis can act both systemically or locally and in both instances vasculitis can manifest within the skin due to the abundant vascular supply. Very few studies have established a role for B cells within the vasculitis disorders but the suspected contribution of immune complexes and autoantibodies in vascular pathology, in addition to the clinical improvements observed using Rituximab B cell depletive therapy in these disorders, strongly indicates a pathogenic role for B cells in vasculitis conditions. The previous work in this study supports the hypothesis that infiltrating lymphocytes were being stimulated locally to respond to an endogenous antigen resulting in tissue damage and has established an antigen-driven role for B cells in muscle inflammation. The work of this chapter tests the same hypothesis within skin inflammation of vasculitis patients by addressing the following key aims:

- Determine the occurrence, organisation and proliferation of skin infiltrating B cells and plasma cells along with the additional cell phenotypes (T cells (CD3, CD4, and CD8), macrophages (CD68), Follicular dendritic cells (FDC), proliferating cells (Ki67) and regulatory T cell (FoxP3)) within skin biopsies.
- Establish the Ig gene repertoire and V_H mutational patterns of infiltrating B cells and plasma cells to assess sequence characteristics from infiltrating B cells and plasma cells which may indicate if clonally related B cells are present within the skin inflammatory infiltrate undergoing an antigen-driven B cell response
- Compare the Ig gene repertoire from skin infiltrating cells to the paired peripheral blood repertoire to further assess gene selections within the vasculitis patients.

The immunohistological data described in this chapter is summarised in Table 5.1.

Sample	Germinal Centre Formation	Cellular Aggregation	CD20	Plasma Cell	FDC	CD3	CD4	CD8	CD68	FoxP3	Ki67	-IgG1	-IgG2a	-IgM
VAS1	-	-	-	+++	-	++	++	+	++	+	- (+ IF only)	-	-	-
VAS6	-	+	+	+++	-	++	++	+	+++	+	++	-	-	-
VAS7	-	+	-	+++	-	+	+	+	++	+	-	-	-	-

Table 5.1 Immunohistochemistry Summary Table from Vasculitis Samples

Table 5.1 provides a summary overview of the immunohistochemistry profiles observed from each sample for each vasculitis patient. The table summarises the infiltration of each cell phenotype observed throughout the entire biopsy (n=3-7 sections for each cell phenotype depending on tissue availability) and is not based solely on the representative images presented in Figures 5.1, 5.3 and 5.5. Comparisons were made between cell phenotypes in the same patient and not between different patients. For germinal centre formation, – represents the absence of these structures within the skin sections. The extent of cellular aggregation of infiltrating cells was established for each sample and was based on semi quantitative observations; - represents no cellular aggregation with a widespread scattering of lymphocytes throughout the skin section; +, ++, +++ represents an increasing degree of aggregation of lymphocytes respectively observed within the skin sections. N/A was applied to samples where no or very little infiltration was present. Immunohistochemistry summary profiles were based on semi-quantitative observations of cellular infiltration; - indicates where cell phenotypes were absent from the infiltrating population while +, ++, +++ represent increasing numbers of cell phenotypes respectively within the skin infiltrating population. Areas highlighted in yellow indicate where proliferating cell phenotypes were observed from fluorescent double immunohistochemistry (IF) experiments, these experiments were not included in the semi quantitative analysis and were used solely to establish the population of proliferating cells.

5.2 Phenotypic Characterisation of Cellular Infiltrates in Vasculitis Patients

5.2.1 Sample VAS1

For sample VAS1 no significant regions of aggregation were observed within the skin biopsy, infiltrating cells were distributed throughout the entire biopsy (**Figure 5.1**). No clear association between infiltrating cell populations and blood vessels was observed in the sections examined. No $CD20^+$ (**A**) cells or FDCs (**B**) were present within the section; small numbers of $CD20^+$ cells were later observed in double immunofluorescent experiments (**Figure 5.2**). The major types of infiltrating cells included plasma cells (**C**), $CD3^+$ (**D**), $CD4^+$ (**E**) and $CD8^+$ (**F**) cells. As observed within myositis samples the numbers of $CD8^+$ cells appears to be reduced in comparison to the CD3 and CD4 cell markers. Unlike some of the myositis samples the number of $CD4^+$ cells did not appear to be greater than that of the $CD3^+$ cells. No proliferating cells (**G**) were observed within the VAS1 sections used in these experiments but there was a large infiltrate of $CD68^+$ (**H**) cells. FoxP3 (**I**) staining revealed a small number of $FoxP3^+$ cells were present within the biopsy. The use of negative control isotype antibodies produced no non-specific staining (**J-L**).

Analysis of $Ki67^+$ proliferating cells at a greater tissue depth to the sections used for the above experiments identified proliferating $CD4^+$ (**C**) and $CD68^+$ (**E**) cells (**Figure 5.2**). Although $FoxP3^+$ cells were identified from initial staining, Figure 5.1, no FoxP3 cells were observed during double staining experiments. Negative control staining produced no non-specific staining.

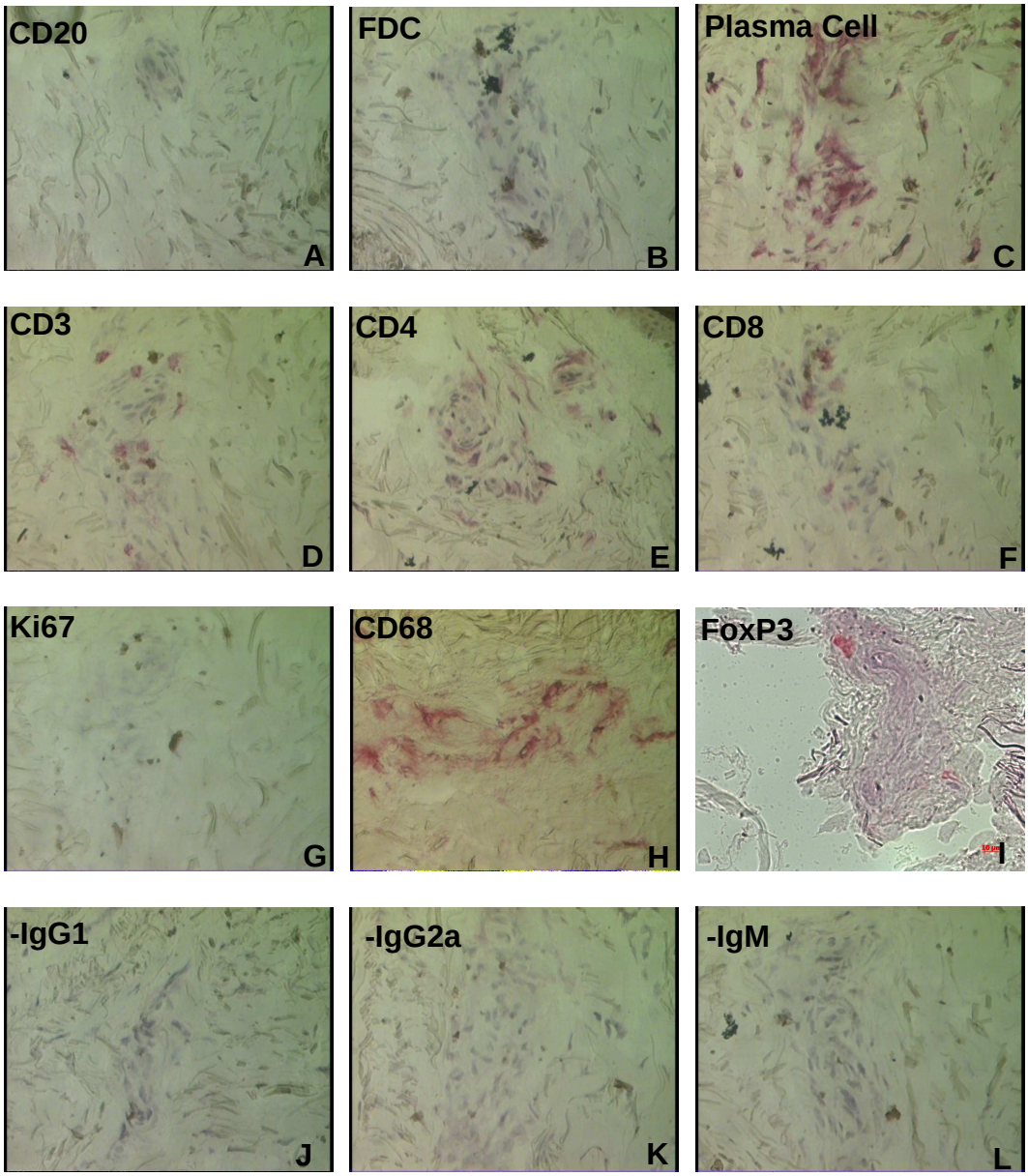

Figure 5.1 Immunohistochemistry of serial skin sections of Sample VAS1.

A representative example of serial skin sections from sample VAS1 stained for CD20 (**A**), FDC (**B**), Plasma cells (**C**), CD3 (**D**), CD4 (**E**), CD8 (**F**), Ki67 (**G**), CD68 (**H**), FoxP3 (**I**), IgG1 Negative control (**J**), IgG2a Negative control (**K**), IgM Negative control (**L**) and visualised by APAAP and New Fuschin substrate to establish cellular infiltrates within the skin section. Images A – L: 400X

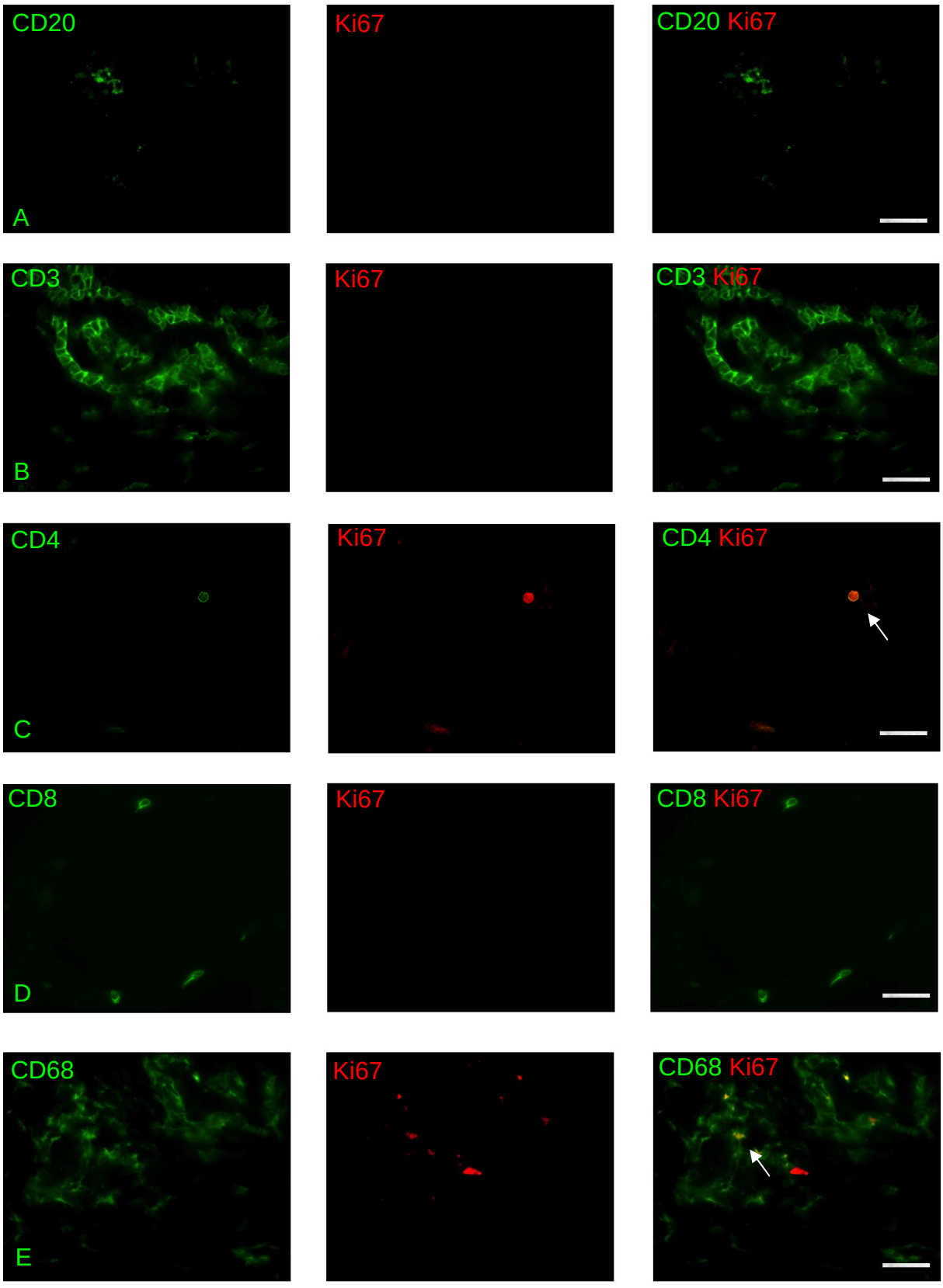

Figure 5.2 Double Immunohistochemical staining of serial vasculitis sections of sample VAS1

A representative example of serial skin sections from sample VAS1 stained for CD20 (**A**), CD3 (**B**), CD4 (**C**), CD8 (**D**), CD68 (**E**) and visualised by Fluorescein Avidin D before all sections were stained with Ki67 and visualised by Texas Red Avidin D. This allowed the type of proliferating cells within the vasculitis sample to be identified. Images were taken at 630X; Scale Bar represents 15 µm. Arrows identify proliferating cells within the sections.

5.2.2 Sample VAS6

A heavy cellular infiltrate was observed within sample VAS6 (**Figure 5.3**). These infiltrating cells formed very loose aggregates of cells in a few areas of the section but a large proportion of cells were distributed throughout the whole section. No clear association between infiltrating cell populations and blood vessels was observed in the sections examined. The dominant cell type present within sample VAS6 was identified as plasma cells (**C**). Very few $CD20^+$ (**A**) cells and no FDCs (**B**) were found within the sample. $CD20^+$ cells present in the sample did appear to form part of the aggregates of cells and were not found dispersed throughout the entire section. $CD3^+$ (**D**) and $CD4^+$ (**E**) cells were present, both within cellular aggregates as well as the other areas of infiltration. $CD8^+$ (**F**) cells were also observed but this was reduced in comparison to $CD3^+$ and $CD4^+$ cells. A considerable infiltration of $Ki67^+$ (**G**) and $CD68^+$ (**H**) cells were also present within sections of sample VAS6 as well as a number of $FoxP3^+$ (**I**) cells. As with previous staining no non-specific staining was observed within the sample (**J-L**).

In sample VAS6 proliferating cells were identified as $CD4^+$ (**C**), $CD8^+$ (**D**), $CD68^+$ (E), $FoxP3^+$ (**F**) cells with a random $CD20^+$ (**A**) cell also present within the infiltrating population (**Figure 5.4**). Negative control experiments with the antibody isotype controls showed no non-specific staining within sections.

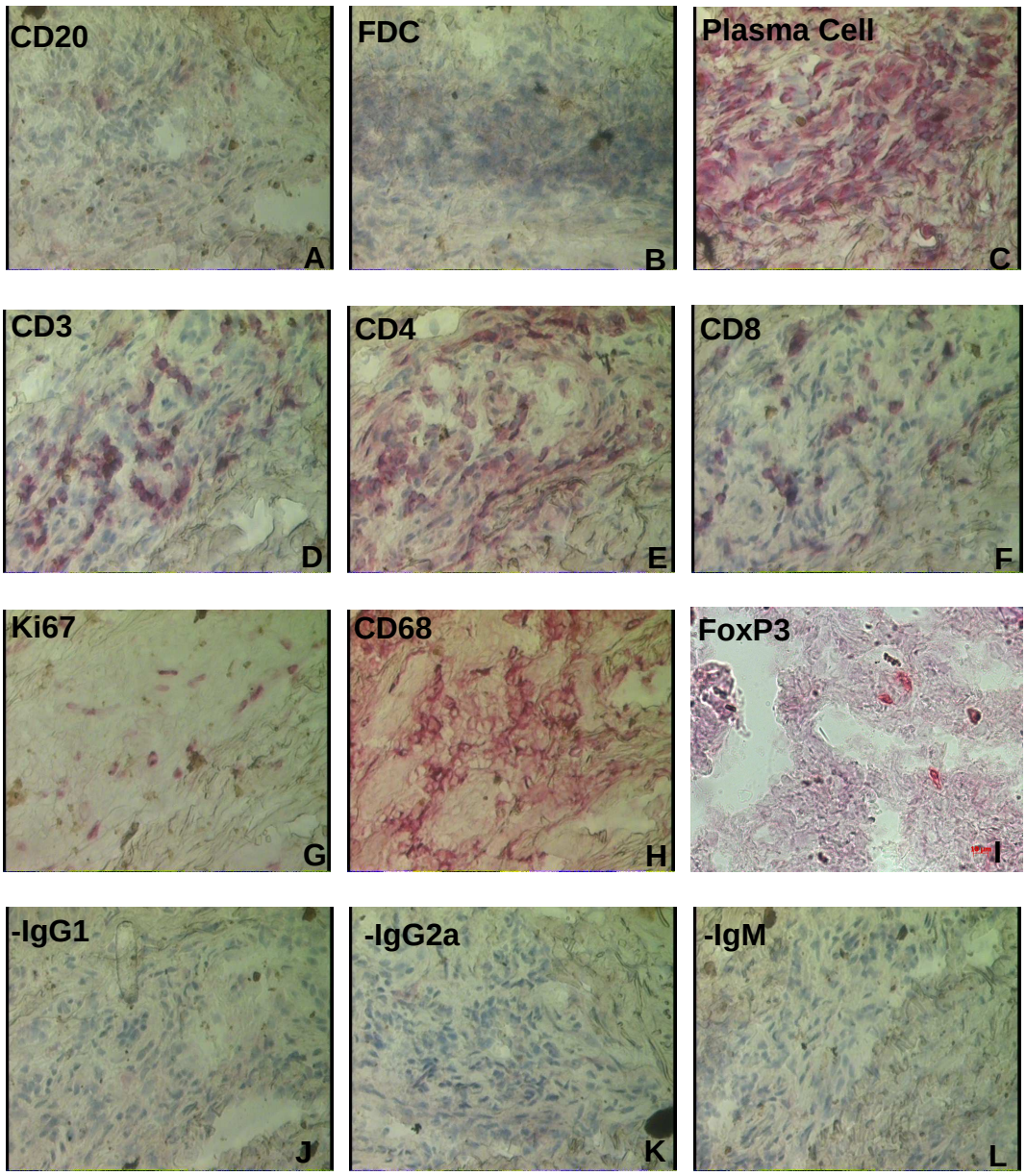

Figure 5.3 Immunohistochemistry of serial skin sections of Sample VAS6.

A representative example of serial skin sections from sample VAS6 stained for CD20 (**A**), FDC (**B**), Plasma cells (**C**), CD3 (**D**), CD4 (**E**), CD8 (**F**), Ki67 (**G**), CD68 (**H**), FoxP3 (**I**), IgG1 Negative control (**J**), IgG2a Negative control (**K**), IgM Negative control (**L**) and visualised by APAAP and New Fuschin substrate to establish cellular infiltrates within the skin section. Images A – L: 400X

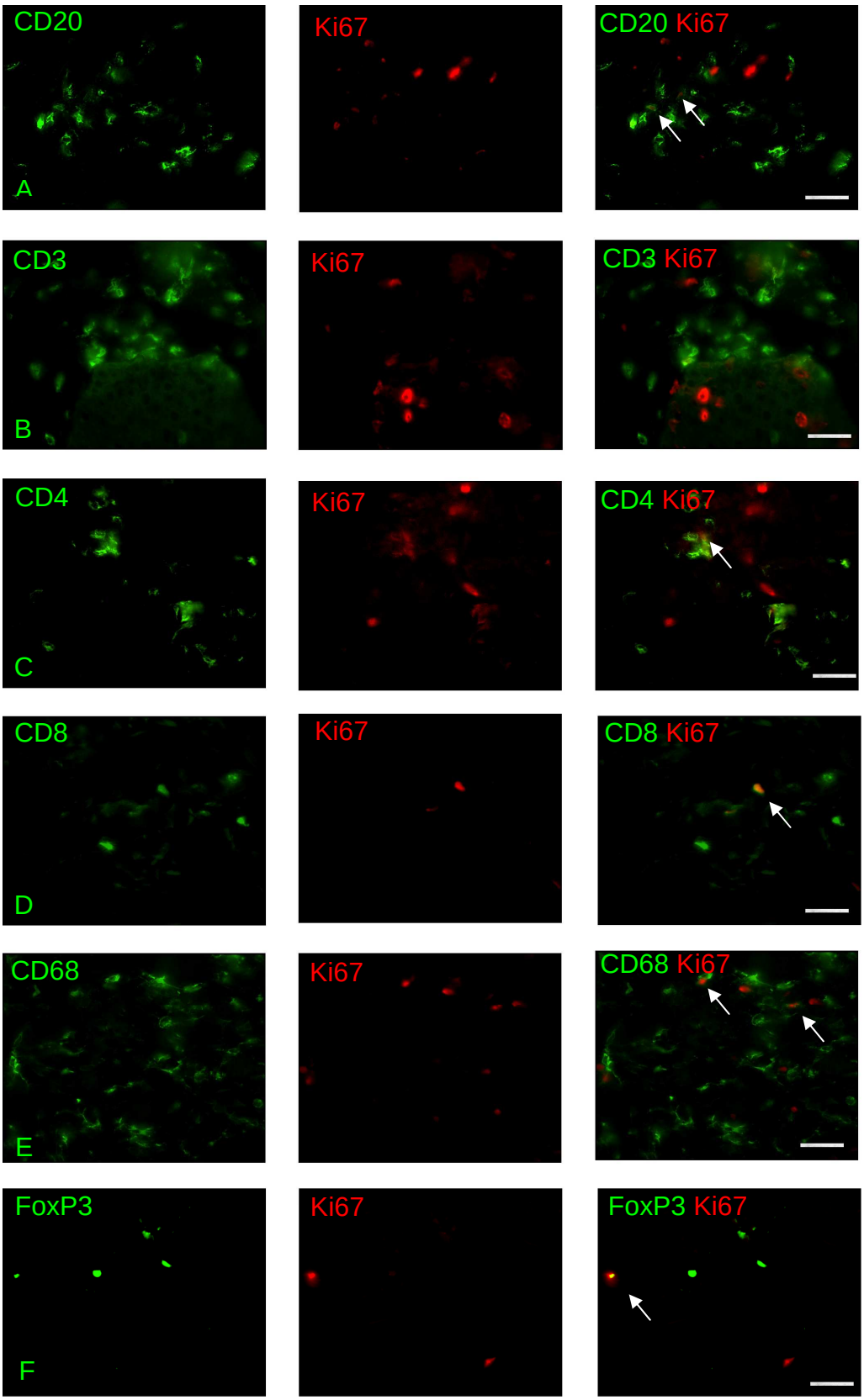

Figure 5.4 Double Immunohistochemical staining of serial vasculitis sections of sample VAS6

A representative example of serial skin sections from sample VAS6 stained for CD20 (**A**), CD3 (**B**), CD4 (**C**), CD8 (**D**), CD68 (**E**) FoxP3 (**F**) and visualised by Fluorescein Avidin D before all sections were stained with Ki67 and visualised by Texas Red Avidin D. This allowed the type of proliferating cells within the vasculitis sample to be identified. Images were taken at 630X; Scale Bar represents 15 µm. Arrows identify proliferating cells within the sections.

5.2.3 Sample VAS7

For sample VAS7 the cellular distribution and phenotypes were similar to that of the previous vasculitis sample, VAS6 (**Figure 5.5**), although a small proportion of infiltrating cell populations were shown to associate with blood vessels. Predominately plasma cells (**C**) infiltrated sample VAS7 with very few $CD20^+$ (**A**) cells or FDCs (**B**). $CD3^+$ (**D**), $CD4^+$ (**E**), $CD8^+$ (**F**) and $CD68^+$ (**H**) cells were also present within the sample as well as a number of $FoxP3^+$ (**I**) cells. VAS6 and VAS7 cellular populations were similar to each other except for the presence of $Ki67^+$ (**G**) cells. No $Ki67^+$ cells were present within these sections of VAS7 tested for cellular markers. As with previous samples no non-specific staining was observed within sample VAS7 (**J-L**).

Despite $Ki67^+$ cells being absent from the cellular infiltrate for the initial cell characterisation further sections were tested for the presence of $Ki67^+$ cells in double staining experiments (**Figure 5.6**). No further evidence of proliferating cells could be found within sample VAS7. Negative control staining produced no non-specific staining.

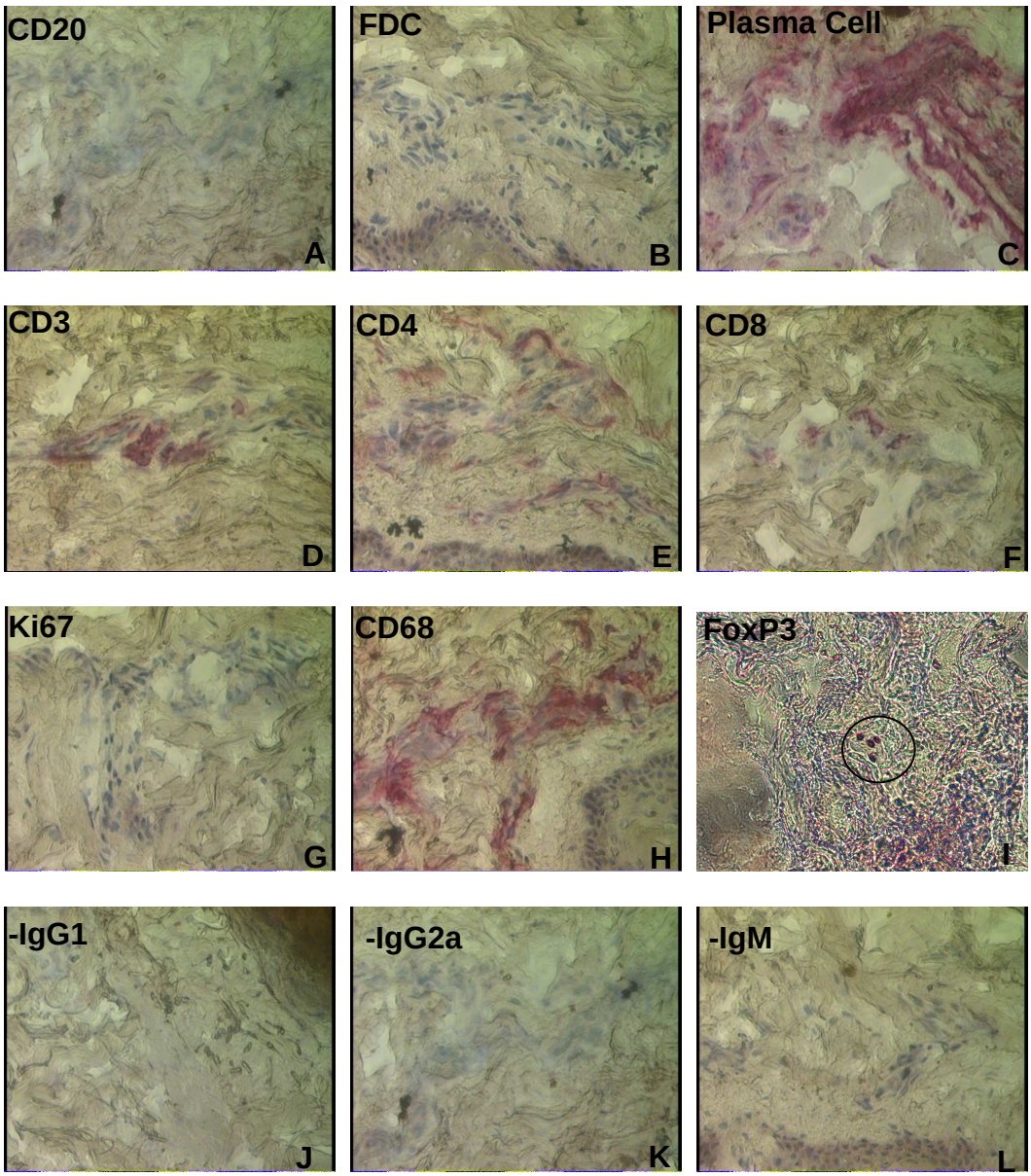

Figure 5.5 Immunohistochemistry of serial skin sections of Sample VAS7.

A representative example of serial skin sections from sample VAS7 stained for CD20 (**A**), FDC (**B**), Plasma cells (**C**), CD3 (**D**), CD4 (**E**), CD8 (**F**), Ki67 (**G**), CD68 (**H**), FoxP3, denoted by circle, (**I**), IgG1 Negative control (**J**), IgG2a Negative control (**K**), IgM Negative control (**L**) and visualised by APAAP and New Fuschin substrate to establish cellular infiltrates within the skin section. Images A – L: 400X

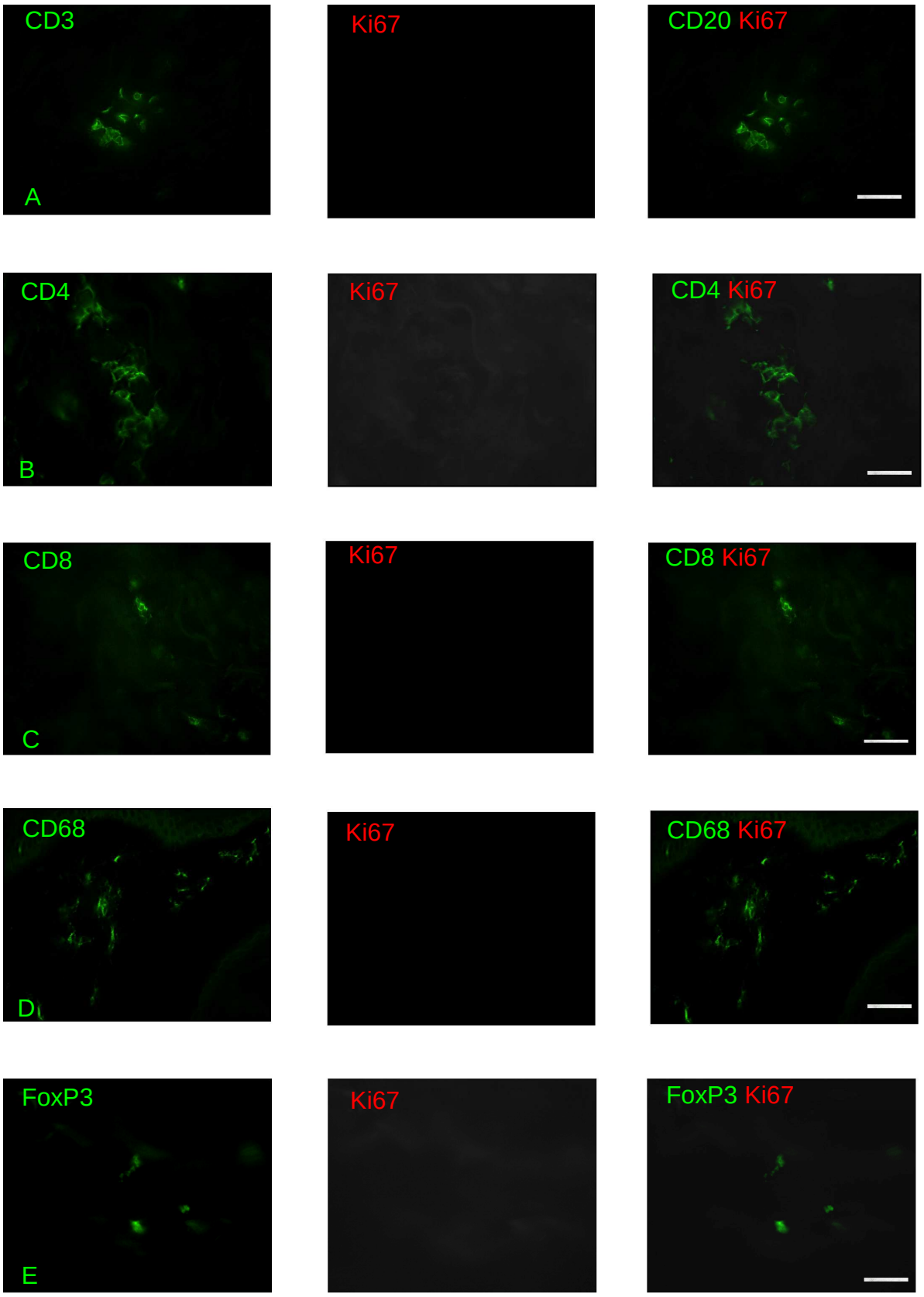

Figure 5.6 Double Immunohistochemical staining of serial vasculitis sections of sample VAS7

A representative example of serial skin sections from sample VAS7 stained for CD3(**A**), CD4 (**B**), CD8 (**C**), CD68 (**D**), FoxP3 (**E**) and visualised by Fluorescein Avidin D before all sections were stained with Ki67 and visualised by Texas Red Avidin D. This allowed the type of proliferating cells within the vasculitis sample to be identified. Images were taken at 630X; Scale Bar represents 15 µm. Arrows identify proliferating cells within the sections.

5.3 V_H Repertoire in Vasculitis Patients

5.3.1 Sample VAS1

As previously described in section 5.2.1 the cellular infiltrate of sample VAS1 contained limited $CD20^+$ B cells but plasma cells were widely distributed within the sample. Microdissection and DNA amplification was conducted to establish the Ig gene rearrangements present within these infiltrating cells (**Figure 5.7**). Three different functional gene rearrangements were isolated from infiltrating cells (**Table 5.2A**). These sequences utilised the V_H1-18*01, V_H3-23*01 and V_H3-33*01 gene segments which were highly mutated, with between 21 and 30 mutations per sequence. A D_H gene could only be assigned to 1 rearrangement, V_H1-18*01, in all other cases the number of consecutive matches was too short to statistically assign a D_H gene. J_H5, 4 and 6 gene segments were used in the V_H1-18*01, V_H3-23*01 and 3-33*01 gene segments respectively. The isolated sequences were highly mutated and the percentage of mutations present within CDR1 was comparable to that of framework regions but an increase in mutational percentages was observed within CDR2 of all of the isolated sequences. Analysis of the R and S mutations revealed that there was only significant selection for the V_H1-18*01 Ig rearrangement, where there was a significant negative selection within the FW regions (**Table 5.2B**). CDR3 lengths were found to range from 13 to 23 amino acids in these sequences. As a D_H gene assignment could only be made for the V_H1-18*01 rearrangement, this was the only Ig rearrangement where analysis of the junctional regions could be conducted. In this Ig rearrangement no P nucleotides were assigned at either the VD or DJ junction. 3 and 6 N nucleotides were assigned at the VD and DJ junctions respectively while exonuclease activity was found to remove 1, 5, 7 and 10 nucleotides respectively from the 3'V_H, 5'D_H, 3'D_H and 5'J_H gene segments of the junction. For gene rearrangements containing the V_H gene segments V_H3-23 and V_H3-33, duplicate copies of the sequence were isolated that contained different somatic mutations. These could not be deemed as clonally related sets of genes as there was only one somatic mutation difference between each set which could have occurred as a result of PCR error.

No differences in gene assignments between the JOINSOLVER and IMGT/V-QUEST were observed for any of the Ig rearrangements.

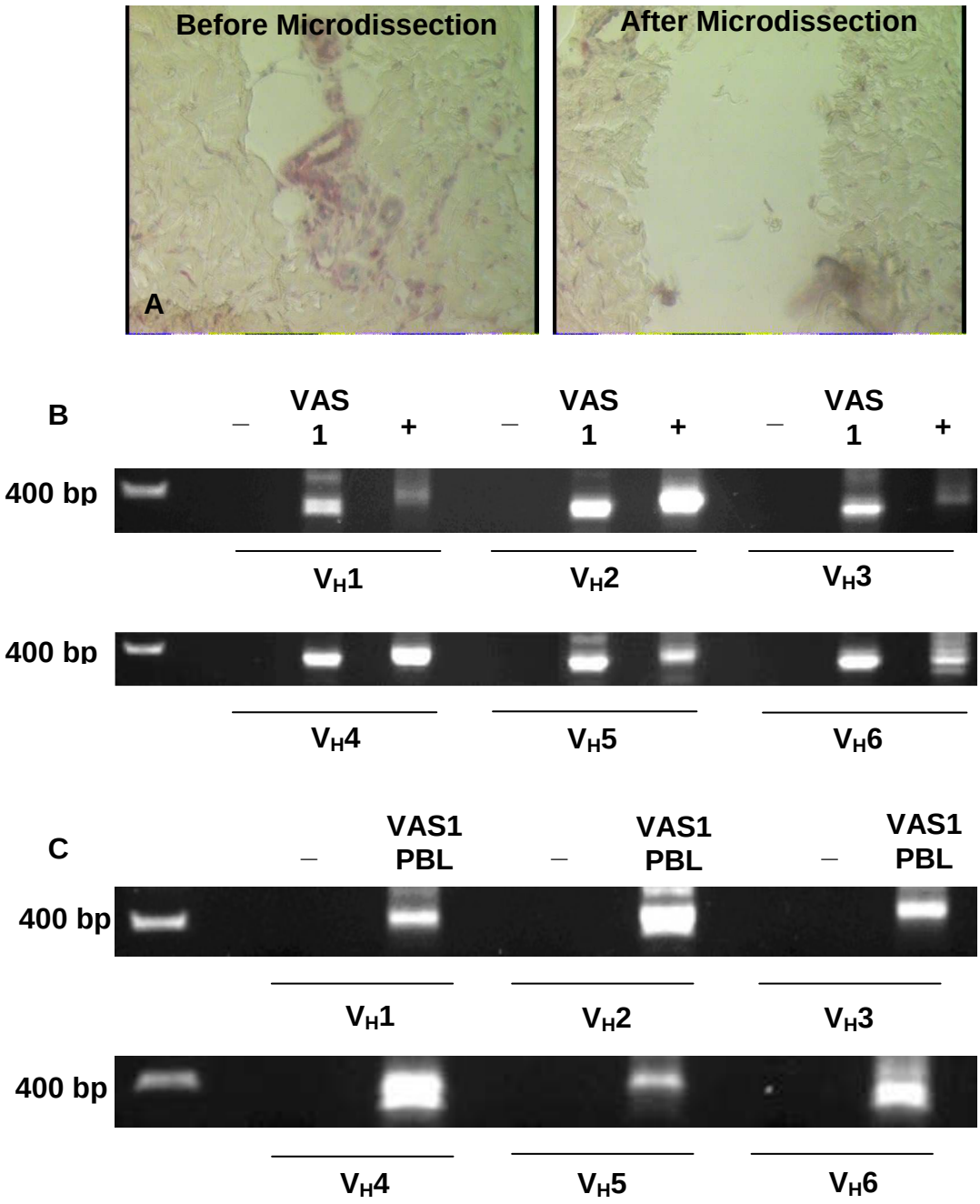

Figure 5.7 Microdissection of infiltrating B cells and amplification of V_H-gene rearrangements from Sample VAS1

The region of plasma cell infiltration was microdissected from sample VAS1. Figure 5.7A demonstrates the microdissection of the region of cellular infiltration. Images were taken at 400X. PCR reactions were conducted for DNA isolated form the muscle sections (Figure 5.7B) in addition to DNA isolated from PBL (Figure 5.7C), as previously described in Chapter 2. – indicates negative control PCR reactions where DNA was substituted with water while + indicates positive control PCR reactions using peripheral blood mononuclear cells isolated from peripheral blood of a healthy individual. Results show amplification of all V_H families.

A

V_H Gene	D_H Gene	J_H Gene	Number of Isolated Sequences	Number of Point Mutations	CDR3	CDR3 Length (aa)	Mutational Distribution (% of length)			V-J Length (bp)	Consecutive D length (bp) (+Mismatches)
							Framework	CDR1	CDR2		
1-18*01	2-2*01	5*02	1	30	ARDDCSGTSCHADL	14	7.7	13.3	20.4	33	16 (+3)
3-23*01	No D gene Assignment	4*02	2	25, 26	VKTTVINLSYFED	13	7.7, 8.1	6.7, 6.7	13, 13	36	8
3-33*01	No D gene Assignment	6*03	2	21, 22	ARAKIVAVSASPSMGSYYHYMDV	23	6.3, 6.8	6.7, 6.7	11.1, 11.1	50	9

B

V_H Gene	D_H Gene	J_H Gene	Number of Isolated Sequences	Number of Point Mutations	R-CDR	S-CDR	pCDR	p-CDR	R-FW	S-FW	pFW	p-FW
1-18*01	2-2*01	5*02	1	30	10	3	0.47674	**-0.9986**	9	8	0.68809	**-0.0303**
3-23*01	No D gene Assignment	4*02	2	25	7	1	0.45266	**0.72724**	11	6	0.65	**-0.7226**
				26	7	1	0.43496	**0.63113**	12	6	0.65077	**-0.8478**
3-33*01	No D gene Assignment	6*03	2	21	4	3	0.46759	**-0.3722**	9	5	0.67394	**-0.2219**
				22	4	3	0.46759	**-0.3722**	10	5	0.67394	**-0.299**

Table 5.2 A&B Sequence Analysis from Sample VAS1

Table 5.2A - Best matching germline sequences were identified from aligning sequences in the IMGT database using JOINSOLVER software from the VAS1 vasculitis section. Identical sequences with the same V_H, D_H, J_H, CDR3 and base mutations were only counted once. V-J lengths and consecutive D match lengths (bp) were also identified using the JOINSOLVER software and allowed assignment of the D_H genes as described in section 2.3.12.3.

The number of mutations within functional rearranged genes were analysed collectively from all region of dissected cellular infiltration. Base differences within the first 24 bases of sequence were disregarded as this part of the sequence binds the 5' V_H primer.

The locations of mutations observed within functional rearranged genes were categorised as being within FR or CDR regions. The numbers of mutations within these regions were expressed as a percentage of the entire length of the region to correct for the longer lengths observed within the framework regions.

Table 5.2B - The number of replacement and silent mutations and the presence of any positive and negative selection was conducted as per Hershberg *et al* (294) as previously described. R-CDR/FW and S-CDR/FW represent the number of replacement and silent mutations in the CDR and FW respectively. pCDR represents the probability of having a R mutation in the CDR given all the mutations in the sequence except R mutations within the FW while pFW represents the probability of having a R mutation in the FW given all the mutations in the sequence except R mutations within the CDR and p-CDR/FW represent the p-value of the focused binominal test on the CDR and FW respectively. A negative sign indicates negative selection. p-values <0.05 were deemed significant.

5.3.1.1 V_H Repertoire from VAS1 PBL

From the paired blood sample obtained at the time of biopsy, 29 functional and 2 non-functional sequences were identified (**Table 5.3**). Using Chi Square analysis, a significant selection for the use of V_H2 gene segments was observed which was significant against normal control values (**Figure 5.8A**). A selection against V_H4 gene segments was also observed, significant against both the normal control values and the baseline germline composition. No other selections for the remaining V_H families was observed, although selections for V_H1-3, 1-69, 2-26, 2-5 and 3-21 individual gene segments was observed. D_H genes could be statistically assigned in 55.2% of the sequences isolated from the blood repertoire, as described using the method in section 2.3.12.3 and the V-J lengths and consecutive D match lengths in Table 5.3. Comparing the distribution of these identified D_H gene segments against control values demonstrated a significant selection for the use of D_H3 gene segments in the Ig rearrangements, in particular D_H3-22 gene segments which was used significantly more than normal controls (**Figure 5.8B**). D_H3 family selection was significant against both control values. No other gene selections were observed within the D_H repertoire. Analysis of the J_H gene segments revealed a selection against J_H1 and J_H2 gene segments which was only significant to the baseline germline complexity (**Figure 5.8C**). Negative selection was also observed for the use of J_H4 and J_H5 gene segments, both were significant against normal control values but J_H5 was also significant against the germline values. Conversely a selection for the use of J_H3 and J_H6 gene segments was observed within the VAS1 PBL repertoire, both were significant against the normal control values only. No common gene rearrangements were observed between the infiltrating population in the skin and the peripheral blood.

The IMGT/V-QUEST found deletions in the V_H3-38*02 D_H3-9*01 J_H4*02 Ig rearrangement. Using JOINSOLVER this rearrangement was non-functional, the same arrangement was observed using IMGT/V-QUEST before the detection of deletions. 6 nucleotides were found to have been deleted from the CDR2. Once restored both algorithms identified a functional rearrangement consisting of the V_H3-23*04 D_H3-9*01 J_H4*02 gene segments with 23 V_H mutations. No other anomalies were detected.

V_H Gene	D_H Gene	J_H Gene	Number of Isolated Sequences	Number of Point Mutations	CDR3	V-J Length (bp)	Consecutive D length (bp) (+Mismatches)
1-03*01	No D gene Assignment	4*02	1	30	ARDLPDTGYFDP	27	6
1-03*01	3-10*01	4*02	1	0	ARVGVVRGDFYFDY	22	12
1-18*01	No D gene Assignment	3*02	1	3	ARASGDDDAFDI	13	6
1-46*01	3-22*01	3*02	1	0	ARRGPLAGNYYDSSGYYSGAFDI	51	28 (+3)
1-69*04	No D gene Assignment	3*02	1	0	ARGRGDAFDI	11	7
1-69*04	3-22*01	3*02	1	0	ARRGPLAGNYYDSSGYYSGAFDI	51	28 (+3)
1-69*04	3-22*01	3*02	1	0	ARGSDYYDSSGSNYEAFDI	38	22 (+1)
1-69*09	No D gene Assignment	6*03	1	1	ARVSESWEVTVAKSVHMDV	39	8
1-69*09	3-22*01	4*02	1	0	ARETGYYDSSGYWN	32	23
2-05*09	3-22*01	3*02	1	7	AHRRYSDSSGHGGAFDI	29	17 (+1)
2-05*10	5-24*01	4*02	1	0	AHTERWLPLDY	23	14 (+1)
2-05*10	No D gene Assignment	6*03	1	26	VHTPPHYYYIDV	29	6
2-26*01	No D gene Assignment	6*03	1	35	ARVQKVQLWREAYYYYLDV	43	8
3-07*01	3-10*02	4*02	1	14	ARILSGNSYDTCDF	38	14 (+2)
3-21*01	2-2*01	6*03	2	0	ARDGVYCSSTSCYLRNYYYYMDV	38	25
				1	ARDGVYCSSTSCYLRNYYYYMDV	38	25
3-21*01	3-3*01	6*03	2	0	ARDRGLYDFWSHTPNYMDV	35	14
				2	ARDRGLYDFWSHTPNYMDV	35	14
3-21*01	6-6*01	6*03	1	0	ARDTSSGIAARDYYYMDV	28	13
3-21*01	No D gene Assignment	6*03	1	0	ARVPTSRGDYYMDV	18	7
3-21*01	No D gene Assignment	6*03	1	1	ARDPPPLGNQGYYYMDV	24	7
3-23*01	2-15*01R	3*02	1	18	AKGGVAAGYSFDI	29	12
3-30*03	3-3*01	4*02	1	12	AKDGAPRTPFGVVIIFGFDY	46	18
3-38*02	3-9*01	4*02	(1)	37	AKIGNHDLSTAYYNLFDY	43	18 (+2)
3-48*02	No D gene Assignment	3*01	1	0	ARDSARQDPIL	23	5
3-66*01	No D gene Assignment	4*02	1	15	ATVSRGALDY	18	6
4-39*01	No D gene Assignment	6*03	1	0	ARCRYEVPVFYYMDV	24	6
5-51*01	2-15*01	6*03	1	0	ARLYCSGGSCKTRAPYYYYMDV	38	21
5-51*01	3-22*01	2*01	(1)	2	ARLVDYYYDSSGYSPAVLRS	40	25
5-51*01	No D gene Assignment	6*03	1	0	ARHYATVRYYYMDV	16	7
6-01*01	No D gene Assignment	3*01	1	16	VRGFRSAFDF	27	5

Table 5.3 Heavy chain genes identified from the PBL sample of vasculitis patient VAS1

Best matching germline sequences were identified from aligning sequences in the IMGT database using JOINSOLVER software from the VAS1 PBL sample. The total number of sequences isolated is given in the 4th column of the table; non-functional rearrangements indicated in brackets. Identical sequences with the same V_H, D_H, J_H, CDR3 and base mutations were only counted once. CDR3 amino acid sequences were also identified using the JOINSOLVER software. V-J lengths and consecutive D match lengths (bp) were also identified using the JOINSOLVER software and allowed assignment of the D_H genes as described in section 2.3.12.3.

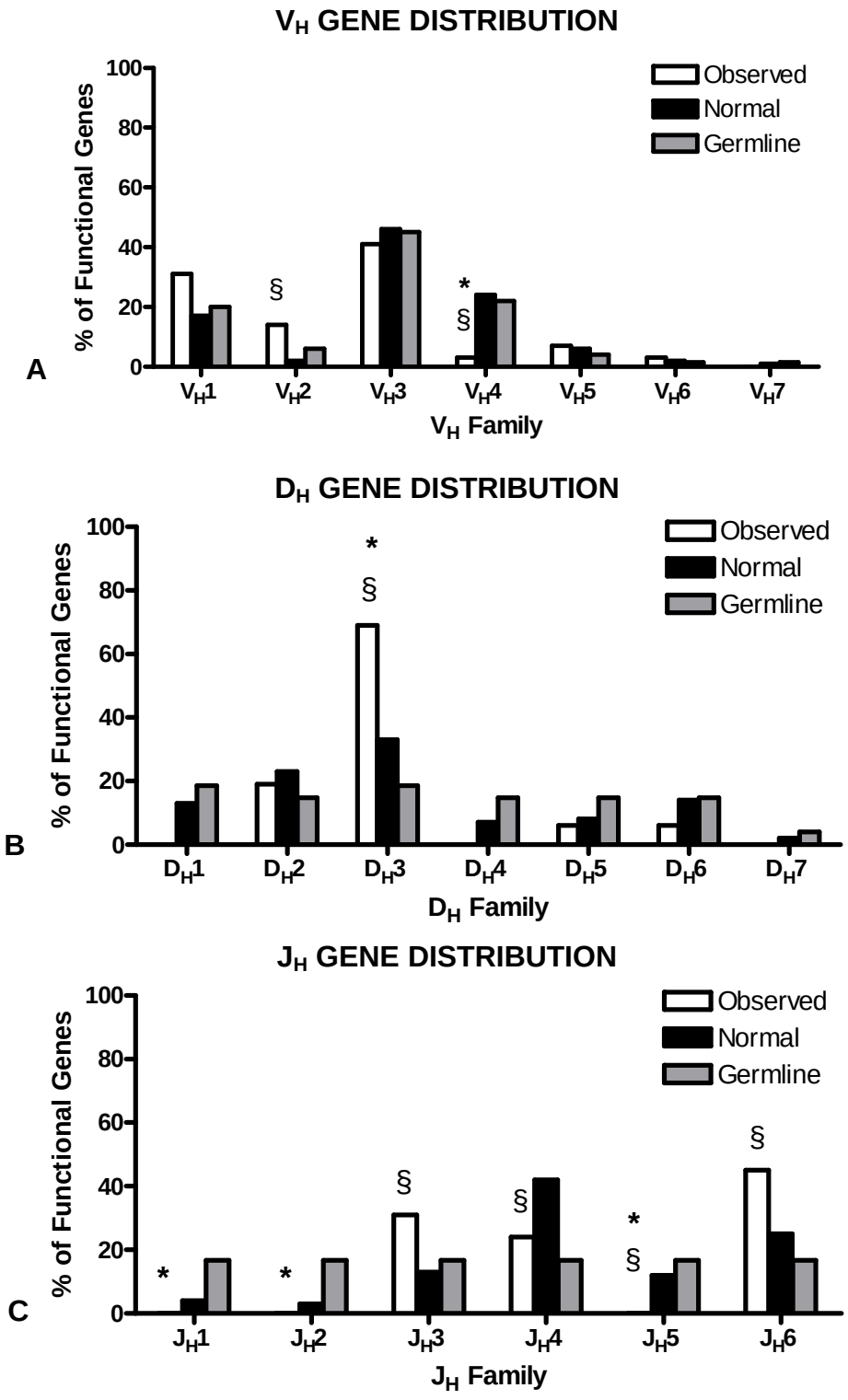

Figure 5.8 V_H Gene Family Usage of VAS1 PBL

V_H gene family usage. Distribution of functional genes was compared with published normal control values from Volpe and Kepler (251) as well as the germline complexity assuming every germline gene is capable of producing a functional rearrangement. Absolute values were used in Chi Square Analysis to determine gene selections. § represent a significant difference from normal PBL values; * represent a significant difference from the germline ($p<0.05$).

5.3.1.2 Mutational Analysis of PBL B Cell Ig Sequences of Sample VAS1

Analysis of the V_H mutations of these sequences demonstrated that approximately 65% of the sequences contained 2 or less mutations, an essentially naïve population (**Figure 5.9A**). The remainder of the sequences were highly mutated; approximately 10% of the Ig sequences from the PBL repertoire contained over 21 V_H mutations. In Ig rearrangements where mutations were observed, a slightly higher percentage of these mutations were found within CDRs compared to the FW regions (**Figure 5.9B**). Analysis of the R and S mutations to assess selection within these Ig rearrangements demonstrated that a significant selection was only observed for one Ig rearrangement (**Table 5.4**). Positive selection within the CDRs was observed for the V_H3-07*01 D_H3-10*02 J_H4*02 rearrangement, no other significant selection were observed.

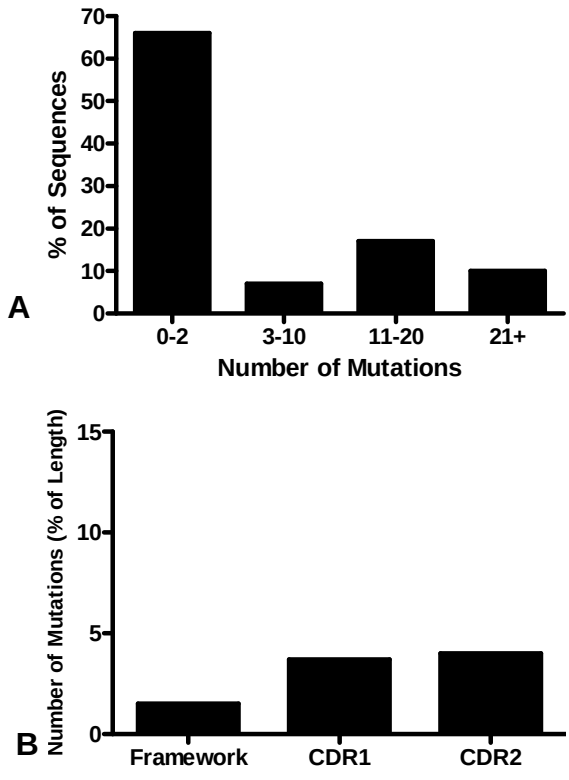

Figure 5.9 Numbers of Mutations and Mutational Distribution of Functional Sequences in VAS1 PBL

Figure 5.9A - The number of mutations within functional rearranged genes were analysed in the PBL sample of VAS1. Base differences within the first 24 bases of sequence were disregarded as this part of the sequence binds the 5' V_H primer. Graph demonstrates that PBL Ig rearrangements were essentially from a naïve population with a small percentage of highly mutated rearrangements.

Figure 5.9B - The locations of mutations observed within functional rearranged genes were categorised as being within FR or CDR regions. The numbers of mutations within these regions were expressed as a percentage of the entire length of the region to correct for the longer lengths observed within the framework regions. Graph demonstrates a higher percentage of mutations within CDR regions compared to framework regions.

5.3.1.3 CDR3 Analysis

Analysis of the VDJ junctional area of these sequences demonstrated that the functional Ig rearrangements had a mean CDR3 length of 16.1 ± 0.8 amino acids while non-functional rearrangements contained CDR3 lengths of 19 ± 1.0 amino acids, which were not significantly different (**Table 5.5**).

V_H Gene	D_H Gene	J_H Gene	Number of Isolated Sequences	Number of Point Mutations	R-CDR	S-CDR	pCDR	p-CDR	R-FW	S-FW	pFW	p-FW
1-03*01	No D gene Assignment	4*02	1	30	11	1	0.47328	**0.16256**	13	5	0.7011	**-0.8525**
1-03*01	3-10*01	4*02	1	0	-	-	-	**-**	-	-	-	**-**
1-18*01	No D gene Assignment	3*02	1	3	0	1	0.47868	**-0.2718**	1	1	0.68628	**-0.2644**
1-46*01	3-22*01	3*02	1	0	-	-	-	**-**	-	-	-	**-**
1-69*04	No D gene Assignment	3*02	1	0	-	-	-	**-**	-	-	-	**-**
1-69*04	3-22*01	3*02	1	0	-	-	-	**-**	-	-	-	**-**
1-69*04	3-22*01	3*02	1	0	-	-	-	**-**	-	-	-	**-**
1-69*09	No D gene Assignment	6*03	1	1	0	0	0.46644	**0**	1	0	0.67237	**0.67237**
2-05*09	3-22*01	3*02	1	7	5	0	0.43955	**0.17116**	0	2	0.67868	**-0.1032**
2-05*10	5-24*01	4*02	1	0	-	-	-	**-**	-	-	-	**-**
2-05*10	No D gene Assignment	6*03	1	26	5	4	0.44582	**-0.3986**	11	6	0.67963	**-0.1421**
2-26*01	No D gene Assignment	6*03	1	35	10	4	0.46467	**-0.6477**	11	10	0.68234	**-0.0138**
3-07*01	3-10*02	4*02	1	14	10	0	0.44584	**0.02267**	1	3	0.668	**-0.1221**
3-21*01	2-2*01	6*03	2	0	-	-	-	**-**	-	-	-	**-**
				1	0	0	0.49844	**0**	1	0	0.65896	**0.65896**
3-21*01	3-3*01	6*03	2	0	-	-	-	**-**	-	-	-	**-**
				2	0	0	0.49844	**-0.5016**	2	1	0.65896	**1.01654**
3-21*01	6-6*01	6*03	1	0	-	-	-	**-**	-	-	-	**-**
3-21*01	No D gene Assignment	6*03	1	0	-	-	-	**-**	-	-	-	**-**
3-21*01	No D gene Assignment	6*03	1	1	0	0	0.49844	**0**	1	0	0.65896	**0.65896**

Cont…

V_H Gene	D_H Gene	J_H Gene	Number of Isolated Sequences	Number of Point Mutations	R-CDR	S-CDR	pCDR	p-CDR	R-FW	S-FW	pFW	p-FW
3-23*01	2-15*01R	3*02	1	18	8	0	0.45436	**0.39523**	4	6	0.64769	**-0.1247**
3-30*03	3-3*01	4*02	1	12	5	0	0.46794	**0.09263**	6	1	0.6723	**0.33596**
3-38*02	3-9*01	4*02	(1)	37	13	2	0.4377	**0.31463**	13	9	0.66934	**-0.1977**
3-48*02	No D gene Assignment	3*01	1	0	-	-	-	**-**	-	-	-	**-**
3-66*01	No D gene Assignment	4*02	1	15	8	1	0.46708	**0.18261**	3	3	0.66604	**-0.2199**
4-39*01	No D gene Assignment	6*03	1	0	-	-	-	**-**	-	-	-	**-**
5-51*01	2-15*01	6*03	1	0	-	-	-	**-**	-	-	-	**-**
5-51*01	3-22*01	2*01	(1)	2	1	0	0.43336	**0.43336**	1	0	0.69901	**0.69901**
5-51*01	No D gene Assignment	6*03	1	0	-	-	-	**-**	-	-	-	**-**
6-01*01	No D gene Assignment	3*01	1	16	6	1	0.47428	**0.65021**	5	4	0.65306	**-0.3332**

Table 5.4 Analysis of Replacement and Silent Mutations and Positive and Negative Selection in Sample VAS1 PBL

Replacement and silent mutations within the immunoglobulin sequences and antigen-driven selection were determined according to Hershberg *et al* (294) and the corresponding computer programme (http://clip.med.yale.edu/selection). This improved method of analysis uses a focused binomial test to establish positive or negative mutational selections within the sequence with high specificity and increased sensitivity accounting for known biases within the immunoglobulin gene sequence. R-CDR and S-CDR represents the number of replacement and silent mutations within the CDR respectively. pCDR represents the probability of having a R mutation in the CDR given all the mutations in the sequence except R mutations within the FW while p-CDR is the p-value of the focused binominal test on the CDR. Conversely R-FW and S-FW represents the number of replacement and silent mutations within the FW respectively. pFW represent the probability of having a R mutation in the FW given all the mutations in the sequence except R mutations within the CDR while p-FW is the p-value of the focused binominal test on the FW. If the number of R mutations is less than expected the software will test for negative selection and p-values will be preceded by a negative sign or if the number of mutations is more than expected the software will test for positive selection. p-values <0.05 are highlighted in yellow and were deemed significant for selection.

Analysis of these CDR3 lengths in comparison to the V_H mutational numbers did not reveal any significant changes to the CDR3 lengths in the different mutational groups (**Figure 5.10**). Further analysis of the junctional areas demonstrated that there were an increased number of P nucleotides at the VD junction in functional sequences compared to the DJ junction. A significant increase in exonuclease activity was found at the 3'V_H gene portion of the junction in non-functional rearrangements compared to the functional population. This reduced exonuclease activity at the 3'V_H gene portion of the junction was also significantly reduced compared to the 5'D_H and 5'J_H gene portions of the junction.

CDR3 Length	**Functional**	16.1 ± 0.8			
	Non-Functional	19 ± 1.0			
		VD Junction		**DJ Junction**	
P Nucleotide	**Functional**	0.8 ± 0.2**		0.2 ± 0.1	
	Non-Functional	0.5 ± 0.5		0.5 ± 0.5	
N Nucleotide	**Functional**	8 ± 1.5		7 ± 0.9	
	Non-Functional	13.5 ± 5.5		4.5 ± 1.5	
		3' V_H	**5' D_H**	**3' D_H**	**5'J_H**
Exonuclease Activity	**Functional**	0.9 ± 0.3*	4.3 ± 0.8 Θ	6.6 ± 1.3	7.1 ± 1 Θ
	Non-Functional	4 ± 3*	6 ± 5	2.5 ± 2.5	5 ± 0

Table 5.5 CDR3 and Junctional Analysis in VAS1 PBL

The mean amino acid length of the CDR3, the mean nucleotide numbers corresponding to P and N nucleotides as well as the mean number of germline nucleotides lost due to exonuclease activity were calculated from the junctional regions of all myositis immunoglobulin sequences as well as in DM and PM subsets. Results are given as the Mean ± SEM. Instances where no non-functional sequences were identified and values could not be calculated were recorded as non applicable (N/A). * indicates a significant difference between functional and non-functional sequences while ** indicates a significant difference between the VD and DJ junctions established using an unpaired t test. Θ represents a significant difference from 3'V_H.

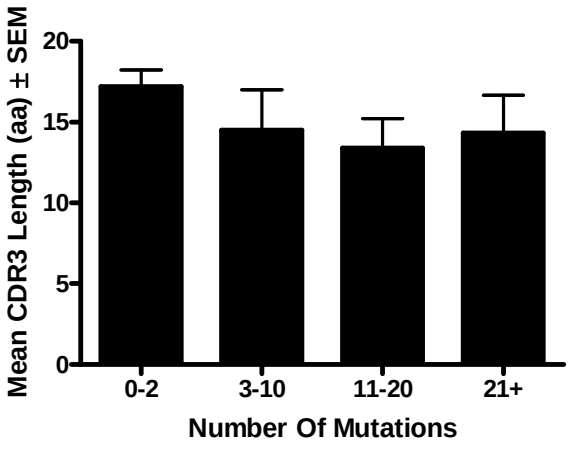

Figure 5.10 Mean CDR3 Lengths in Relation to V_H Mutational Numbers

The mean CDR3 length was calculated for immunoglobulin sequences according the number of mutations within the V_H segment of the gene rearrangement to establish any relationship between mutational number and CDR3 length. Results are given as Mean amino acid CDR3 length ± SEM. Groups were compared for statistical significance using the Tukey-Kramer test for multiple comparisons. The graph demonstrates that no significant changes in CDR3 length were observed at the various number of mutations. p-values <0.05 would have been deemed significant.

No clonally related sequences were observed in the PBL repertoire.

5.3.2 Sample VAS6

As shown in Figure 5.3 there was very little evidence of $CD20^+$ cells within sample VAS6 but there was a large infiltration of plasma cells. Nested PCR reactions (**Figure 5.11**) from 2 areas of plasma cells dissected yielded 7 functional Ig's with 4 different gene rearrangements, as shown in **Table 5.6A**. These sequences were isolated multiple times from the same vasculitis sample. As shown in Table 5.6, the infiltrating cells used V_H1, V_H3 and V_H4 family gene segments, D_H genes, D_H4-17*01 and D_H5-12*01, could only be assigned in the V_H3-30*03 and V_H4-59*01 rearrangements respectively. The remaining segments of the gene rearrangements were composed of J_H2, 4 and 6 family members. The V_H1 gene rearrangement and both sets of the V_H3 family genes were highly mutated with over 16 mutations whilst the V_H4 set of genes were essentially non-mutated with between 0 and 2 mutations. Mutational distribution within the genes showed a similar pattern to that observed within muscle biopsies; a greater percentage of mutations were evident within CDRs in comparison to framework regions for each mutated sequence, with a higher percentage of mutations within CDR2 in comparison to CDR1. Despite the large number of mutations in most of the Ig rearrangements from sample VAS6 no significant positive or negative selection was observed in either of the FW or CDRs (**Table 5.6B**). Similar CDR3 lengths were observed for these sequences with a range between 14 and 18 amino acids which may correspond to a similar epitope mediating the response within the skin of sample VAS6. Junctional analysis could be conducted on the V_H3-30*03 and V_H4-59*01 rearrangements where D_H genes could be assigned. P nucleotides, 2, were assigned at the VD junction of the V_H3-30*03 rearrangements, no other P nucleotides were identified in any other gene. For the V_H3-30*03 rearrangement 4 and 8 N nucleotides were observed at the VD and DJ junctions while 3 and 6 were observed in the V_H4-59*01 Ig genes. Exonuclease activity was only observed at the 5'J_H region of the V_H3-30*03 genes where 3 nucleotides were removed. For the V_H4-59*01 2, 8, 2 and 0 nucleotides were found to be removed at the 3'V_H, 5'D_H, 3'D_H and 5'J_H regions respectively. The different mutational patterns evident within this repertoire were not sufficient evidence for clonal diversity as the mutations present were within the PCR error rate. No differences were observed between the two gene assignment algorithms used in this study.

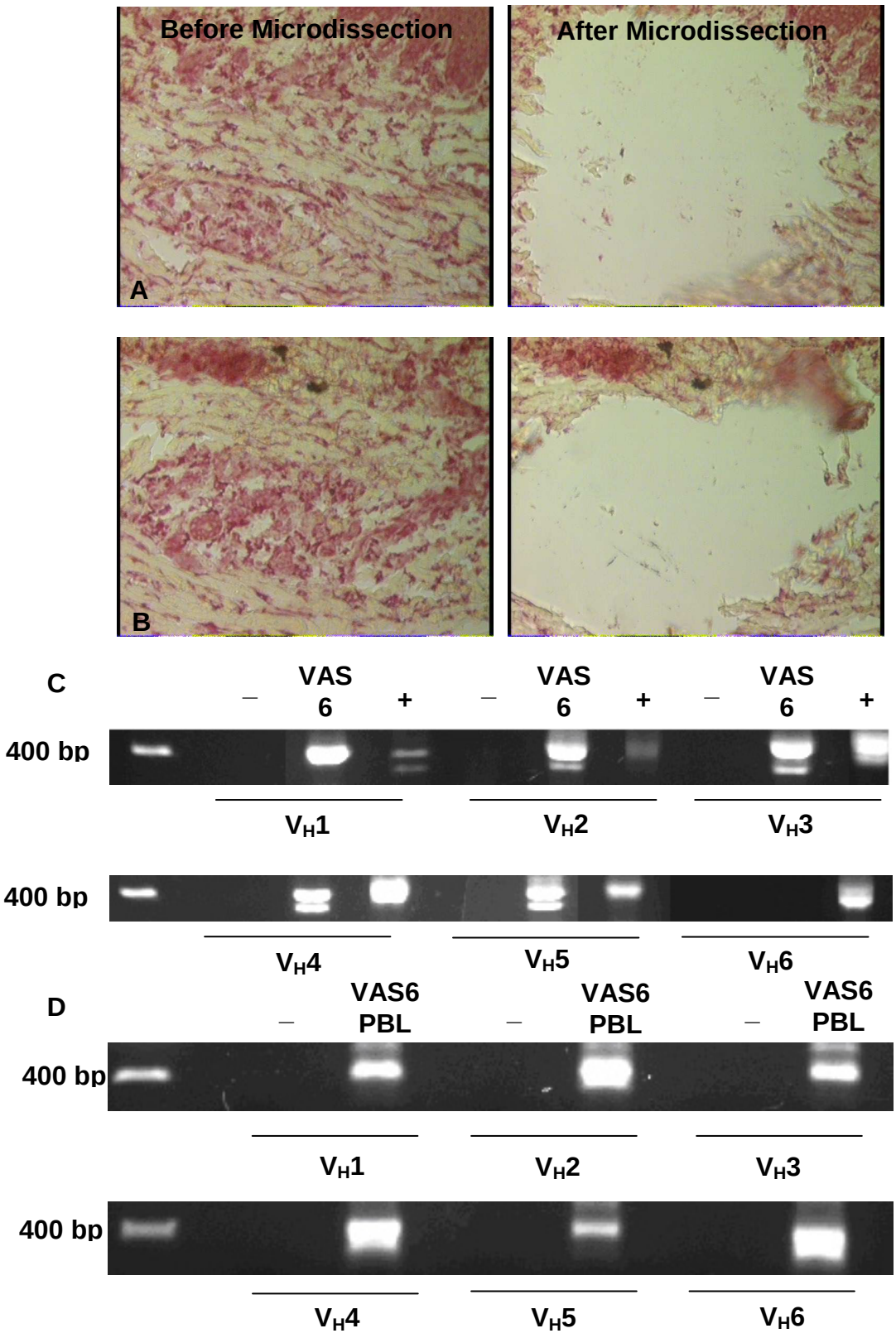

Figure 5.11 Microdissection of infiltrating B cells and amplification of V_H-gene rearrangements from Sample VAS6

Regions of plasma cell infiltration were microdissected from sample VAS6. Figure 5.11A and B demonstrates the microdissection of 2 regions of cellular infiltration. Images were taken at 400X. PCR reactions were conducted for DNA isolated form the muscle sections (Figure 5.11C) in addition to DNA isolated from PBL (Figure 5.11D), as previously described in Chapter 2. – indicates negative control PCR reactions where DNA was substituted with water while + indicates positive control PCR reactions using peripheral blood mononuclear cells isolated from peripheral blood of a healthy individual. Results show amplification of V_H1 to 5 families from muscle tissue but amplification of all 6 families from the blood sample.

A

V_H Gene	D_H Gene	J_H Gene	Number of Isolated Sequences	Number of Mutations	CDR3	CDR3 Length (aa)	Mutational Distribution (% of length)			V-J Length (bp)	Consecutive D length (bp) (+Mismatches)
							Framework	CDR1	CDR2		
1-46*02	No D gene Assignment	4*02	1	17	ARDPLDCPNNKCYLYFDH	18	3.2	13.3	14.8	44	7
3-23*01	No D gene Assignment	6*02	1	25	AKDPILRGSWRGVVAMDV	18	6.3	13.3	16.7	36	8
3-30*03	4-17*01	2*01	2	16, 17	AKEGHDYGDYFYVWLDH	17	4.5, 5	6.7, 6.7	9.3, 9.3	49	16
4-59*01	5-12*01	4*02	3	0, 2, 2	ARQSGYDSPNYFDY	14	0, 0.9, 0.5	0, 0, 0	0, 0, 2	22	13

B

V_H Gene	D_H Gene	J_H Gene	Number of Isolated Sequences	Number of Mutations	R-CDR	S-CDR	pCDR	p-CDR	R-FW	S-FW	pFW	p-FW
1-46*02	No D gene Assignment	4*02	1	17	7	3	0.47666	**0.47764**	5	2	0.67527	**-0.2639**
3-23*01	No D gene Assignment	6*02	1	25	8	3	0.44592	**0.50796**	10	4	0.65167	**-0.584**
3-30*03	4-17*01	2*01	2	16	6	0	0.46606	**0.41859**	6	4	0.67432	**-0.6176**
				17	6	0	0.46606	**0.41859**	7	4	0.67432	**-0.7755**
4-59*01	5-12*01	4*02	3	0	-	-	-	**-**	-	-	-	**-**
				2	0	0	0.44001	**-0.56**	0	2	0.65645	**-0.118**
				2	1	0	0.44001	**0.44001**	1	0	0.65645	**0.65645**

Table 5.6 A&B Sequence Analysis from Sample VAS6

Table 5.6A - Best matching germline sequences were identified from aligning sequences in the IMGT database using JOINSOLVER software from the VAS6 vasculitis section. Identical sequences with the same V_H, D_H, J_H, CDR3 and base mutations were only counted once. V-J lengths and consecutive D match lengths were also identified using the JOINSOLVER software and allowed assignment of the D_H genes as described in section 2.3.12.3.

The number of mutations within functional rearranged genes were analysed collectively from all region of dissected cellular infiltration. Base differences within the first 24 bases of sequence were disregarded as this part of the sequence binds the 5' V_H primer.

The locations of mutations observed within functional rearranged genes were categorised as being within FR or CDR regions. The numbers of mutations within these regions were expressed as a percentage of the entire length of the region to correct for the longer lengths observed within the framework regions.

Table 5.6B - The number of replacement and silent mutations and the presence of any positive and negative selection was conducted as per Hershberg *et al* (294) as previously described. R-CDR/FW and S-CDR/FW represent the number of replacement and silent mutations in the CDR and FW respectively. pCDR represents the probability of having a R mutation in the CDR given all the mutations in the sequence except R mutations within the FW while pFW represents the probability of having a R mutation in the FW given all the mutations in the sequence except R mutations within the CDR and p-CDR/FW represent the p-value of the focused binominal test on the CDR and FW respectively. A negative sign indicates negative selection. p-values <0.05 were deemed significant.

5.3.2.1 V_H Repertoire from VAS6 PBL

In addition to Ig analysis from the skin infiltrating repertoire of sample VAS6, the Ig repertoire of the patient's peripheral blood was also assessed from a paired blood sample at the time of biopsy. From this sample 36 functional and 9 non-functional sequences were identified (**Table 5.7**). Gene usage analysis of these functional rearrangements demonstrated a positive selection for the use of V_H2 gene segments which was significant against both normal control values and the baseline germline complexity (**Figure 5.12A**). In addition to this positive selection, a selection for V_H7 gene segments was also observed within the PBL repertoire which was significant against normal control values. A selection against V_H3 and V_H4 gene segments was also observed, these were both significant against normal control values while the declined use of V_H4 gene segments was also significant against the baseline germline complexity. The selection for V_H2 and against V_H4 gene segments was also observed from the PBL sample of patient VAS1 (Figure 5.8A). Analysis for the use of individual gene segments demonstrated a significant selection for the use of the V_H1-3, 1-69 and 2-5 gene segments, these gene selections were also observed within the PBL sample of patient VAS1. In this sample D_H genes could be statistically assigned in 66.7% of the Ig rearrangements. From these assignments a positive selection was observed for D_H3 gene but this was only significant against the germline complexity and not against normal control values (**Figure 5.12B**). The use of all other D_H gene family segments mirrored the use of the normal control values. Comparing the use of the individual D_H gene segments to the normal control values, a selection for the use of D_H3-9, 5-12 and 6-13 gene segments was observed. The repertoire for the use of the J_H segments also mirrored the normal control repertoire with the exception of the J_H2 gene segments. Analysis of this sample demonstrated that there was a significant selection for the use of these gene segments. This selection was significant against normal control values but not the baseline germline complexity. No common gene rearrangements were observed between the infiltrating population in the skin and the peripheral blood.

No differences in gene assignments from the JOINSOLVER and IMGT/V-QUEST algorithms were observed for this sample.

V_H Gene	D_H Gene	J_H Gene	Number of Isolated Sequences	Number of Point Mutations	CDR3	V-J Length (bp)	Consecutive D length (bp) (+Mismatches)
1-03*01	2-2*01	3*02	1	0	ARDRKVVPALDAFDI	21	12
1-03*01	5-12*01	6*02	1	1	ARVDIVASNSYYYGMDV	23	14
1-69*01	2-21*02	3*02	1	0	AREALAYCGGDCYSRDAFDI	37	28
1-69*01	3-10*01	4*02	1	17	ATEIGDMDRGVTRPEF	43	16 (+1)
1-69*01	6-13*01	6*02	1	2	ARATGYSSRYYYYGMDV	20	14
1-69*01	6-19*01	3*02	(1)	0	ARGGSHAKYPRIAVAGTPSRGWMLLLI	58	19
1-69*01	No D gene Assignment	2*01	1	24	ASVRFGESWYFDL	36	8
1-69*01	No D gene Assignment	5*02	(1)	1	ARDLG*VYQLSHTPEDPTGST	41	9
1-69*02	3-10*01	3*02	1	0	ARVLDLGYGSGSYYNVFDAFDI	44	24
2-05*04	3-9*01	5*02	1	20	AHRRNPEYSLTGVNWFDP	41	10
2-05*04	No D gene Assignment	4*02	1	20	AHRLSISYYFDF	34	7
2-05*10	1-26*01	5*02	1	13	AHSPSGTYHKQYNWFDP	30	12 (+1)
2-05*10	3-10*01	1*01	1	0	ARLTPTITMVRGVIITTGEYFQH	49	29
2-05*10	3-16*02	2*01	1	0	AHWSYDYVWGSYRSPISDWYFDL	48	28
2-05*10	3-22*01	4*02	1	8	VLLTYYDSSVYPYS	40	21 (+1)
2-05*10	No D gene Assignment	4*01	1	7	AHRRGAPGYFDY	19	7
2-05*10	No D gene Assignment	4*02	(1)	1	AHPTELTILARL	27	7
2-05*10	No D gene Assignment	4*02	1	2	AVAANADYFDY	16	7
3-11*03	3-22*01	3*02	1	1	ARGVYDSSGYTAFDI	26	18
3-15*01	No D gene Assignment	4*02	1	10	TTEEYTFGYYIDY	25	7
3-15*01	No D gene Assignment	4*02	1	9	STVDD	13	7
3-21*01	5-12*01	4*02	1	0	ARDVEVVATEPDY	24	11
3-21*01	6-13*01	6*02	1	0	AREGDSSSWGRGGGKYGMDV	37	14
3-30*03	3-10*01	6*02	1	0	AKRRGSGSYYKLYYYYGMDV	32	20
3-33*01	No D gene Assignment	2*01	1	12	ARDPPISISVAVSYWYFDL	30	9
3-49*01	2-15*01	2*01	1	1	AREGPGLLTPYCSGGSCLYWYFDL	53	22
3-66*01	3-10*01	5*02	(1)	31	SPITMVRGVIITSCLL*FLVRP	54	29
3-66*01	4-23*01	4*02	1	27	ARVGNSCGIEY	28	10
4-34*01	3-22*01	1*01	1	1	ARYRLTPNYYDSREGQEDQH	47	16
4-34*01	3-22*01	6*02	(1)	1	ASRRITMIVVVPQVWT	33	23
4-34*03	3-22*01	3*02	1	31	ARDAYGEEGYYDSSGYYYSLQDAFDI	63	27
5-51*01	No D gene Assignment	2*01	1	13	ARGNTGWSEYWYFDL	21	8
5-51*03	3-10*01	5*02	(1)	0	VNAGRITMVRGVIRPSTTGST	47	27
5-51*03	4-17*01	2*01	1	0	ARVNDYGDSWYFDL	21	12
6-01*01	No D gene Assignment	3*02	1	10	VRDSGIGLDAFDI	23	7
6*01-01	No D gene Assignment	3*02	(1)	0	ARRGS*APMMLLI	23	8
6-01*01	6-19*01	4*02	(1)	0	ARDLWQWLACTTLT	22	11

Cont…

V_H Gene	D_H Gene	J_H Gene	Number of Isolated Sequences	Number of Point Mutations	CDR3	V-J Length (bp)	Consecutive D length (bp) (+Mismatches)
6-01*01	6-13*01	6*02	1	1	ARGGAAAGTDYYYYGMDV	21	15
7-04-1*01	2-2*03	6*02	(1)	0	APLGTWRA**YQLLWGMPTTTTVWT	50	20
7-04-1*02	No D gene Assignment	1*01	1	14	AREGSIEVTAPGYFQH	27	9
7-04-1*02	No D gene Assignment	5*02	1	1	ARDEKGFGFDP	14	7
7-04-1*02	No D gene Assignment	6*02	1	1	AREGGHVYMDV	15	6
7-04-1*02	3-9*01	4*02	2	1	AREHYDILTGYYEWRGPDYFDY	44	26
				2	AREHYDILTGYYEWRGPDYFDY	44	26
7-04-1*02	6-13*01R	3*02	1	0	ARDFRYQLPHDAFDI	21	11

Table 5.7 Heavy chain genes identified from the PBL sample of vasculitis patient VAS6

Best matching germline sequences were identified from aligning sequences in the IMGT database using JOINSOLVER software from the VAS6 PBL sample. The total number of sequences isolated is given in the 4th column of the table; non-functional rearrangements indicated in brackets. Identical sequences with the same V_H, D_H, J_H, CDR3 and base mutations were only counted once. CDR3 amino acid sequences were also identified using the JOINSOLVER software; * indicates the presence of a stop codon within the CDR3. V-J lengths and consecutive D match lengths (bp) were also identified using the JOINSOLVER software and allowed assignment of the D_H genes as described in section 2.3.12.3.

5.3.2.2 Mutational Analysis of PBL B Cell Ig Sequences of Sample VAS6

As observed within the PBL sample of VAS1 the majority of cells within the blood sample VAS6 were essentially from a naïve population; approximately 60% of the sequences contained between 0 and 2 mutations within the V_H region (**Figure 5.13A**). The remaining sequences contained from 3 mutations per sequence to over 21 mutations per sequence. Most of these remaining sequences, approximately 20%, contained between 11 and 20 mutations. A higher percentage of these mutations were located within the CDRs of the Ig rearrangements, with a higher percentage observed in CDR1 compared to CDR2 (**Figure 5.13B**). Further analysis of these mutations in assessing the selection within these genes demonstrated that a significant selection was observed in 4 different gene rearrangements within the PBL samples of VAS6 (**Table 5.8**). As shown in Table 5.8 this selection was observed in 3 functional genes and 1 non-functional gene. All Ig rearrangements contained a negative selection within the FW regions. Other positive and negative selections were observed in all the sequences in both the FW and CDRs but they were not statistically significant.

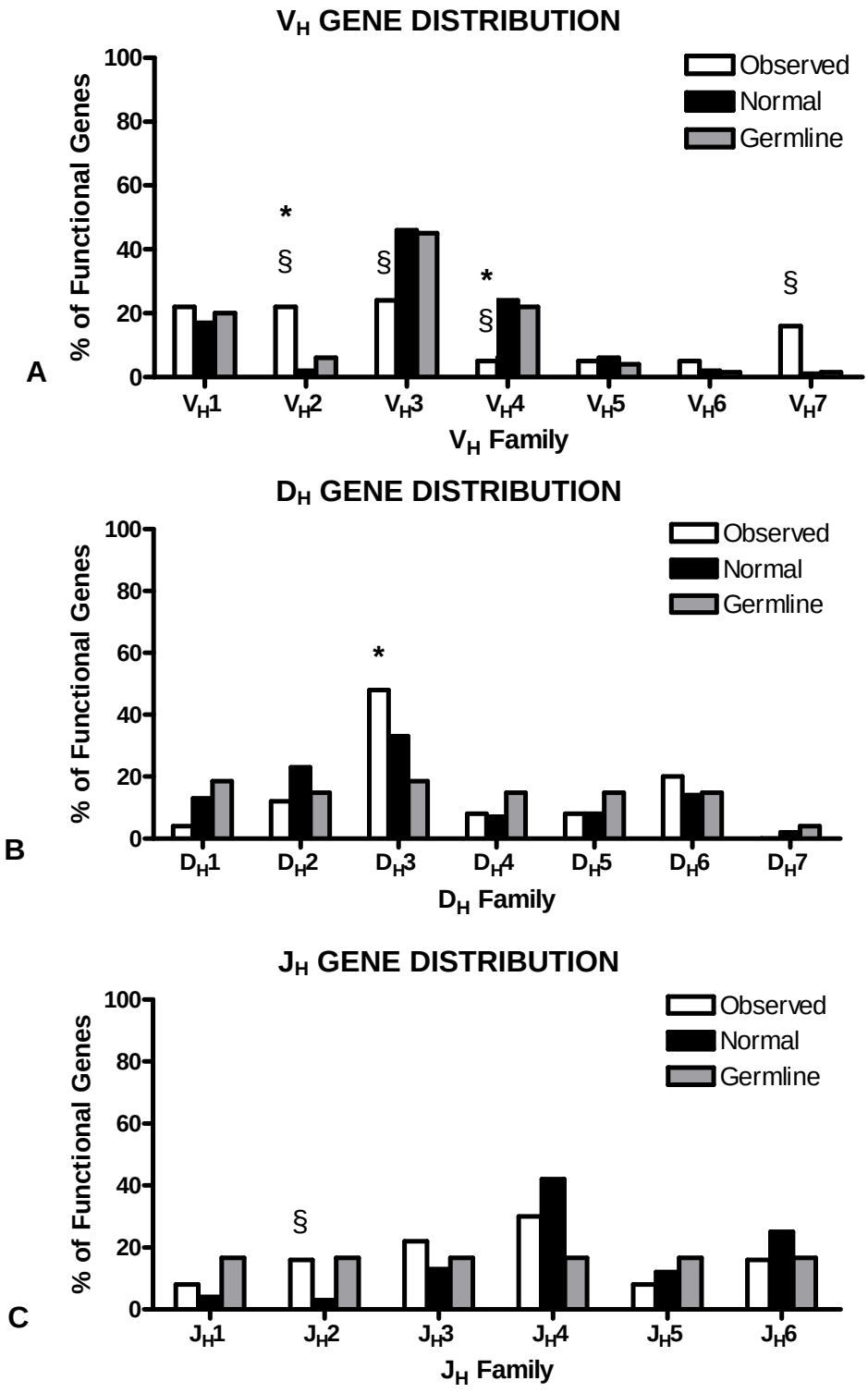

Figure 5.12 V_H Gene Family Usage of VAS6 PBL

V_H gene family usage. Distribution of functional genes was compared with published normal control values from Volpe and Kepler (251) as well as the germline complexity assuming every germline gene is capable of producing a functional rearrangement. Absolute values were used in Chi Square Analysis to determine gene selections. § represent a significant difference from normal PBL values; * represent a significant difference from the germline ($p<0.05$).

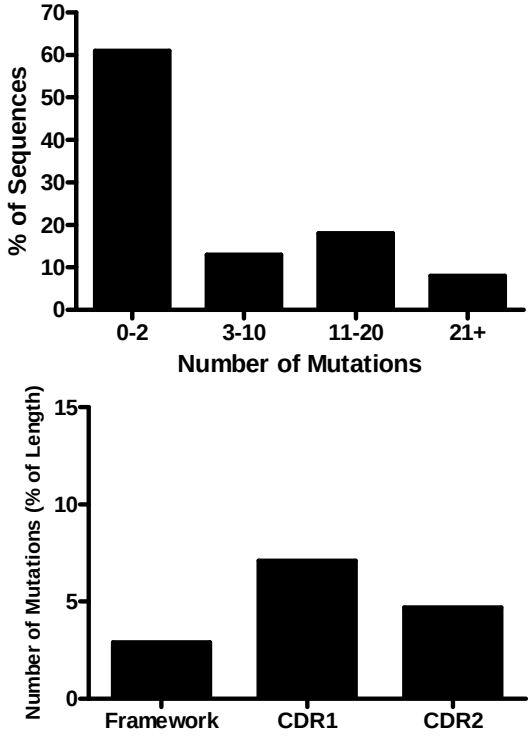

Figure 5.13 Numbers of Mutations and Mutational Distribution of Functional Sequences in VAS6 PBL

Figure 5.13A - The number of mutations within functional rearranged genes were analysed in the PBL sample of VAS6 PBL. Base differences within the first 24 bases of sequence were disregarded as this part of the sequence binds the 5' V_H primer. Graph demonstrates that PBL Ig rearrangements were essentially from a naïve population with a small percentage of highly mutated rearrangements.

Figure 5.13B - The locations of mutations observed within functional rearranged genes were categorised as being within FR or CDR regions. The numbers of mutations within these regions were expressed as a percentage of the entire length of the region to correct for the longer lengths observed within the framework regions. Graph demonstrates a higher percentage of mutations within CDR regions compared to framework regions.

5.3.2.3 CDR3 Analysis

No significant differences in the mean CDR3 amino acid length were observed in these sequences between the functional and non-functional populations (**Table 5.9**). Despite these results a significant decrease in CDR3 length was observed for the sequences containing between 3 and 10 mutations (**Figure 5.14**). This significance was only against sequences containing 2 or less mutations and not significant against sequences with more than 10 mutations per sequence. Further analysis of the CDR3 region examined the addition of P and N nucleotides at the VD and DJ junctions as well as the exonuclease activity at the gene segment ends, 3'V_H, 5'D_H, 3'D_H and 5'J_H, within the VDJ junction. Within these sequences no significant differences were observed between the VD and DJ junction, or between functional and non-functional sequences, for the addition of P and N nucleotides at these regions. Conversely a significant difference in exonuclease activity was observed at the 3'V_H gene segment of the junction between the functional and non-functional Ig rearrangements, with a significant reduced exonuclease activity in functional rearrangements. This reduced enzyme activity was also significant against the 5'D_H and 5'J_H regions in functional rearrangements.

V_H Gene	D_H Gene	J_H Gene	Number of Isolated Sequences	Number of Point Mutations	R-CDR	S-CDR	pCDR	p-CDR	R-FW	S-FW	pFW	p-FW
1-03*01	2-2*01	3*02	1	0	-	-	-	-	-	-	-	-
1-03*01	5-12*01	6*02	1	1	0	0	0.47328	**0**	1	0	0.7011	**0.7011**
1-69*01	2-21*01	3*02	1	0	-	-	-	-	-	-	-	-
1-69*01	3-10*01	4*02	1	17	5	1	0.45038	**0.5459**	8	3	0.66893	**-0.9625**
1-69*01	6-13*01	6*02	1	2	1	0	0.45038	**0.45038**	1	0	0.66893	**0.66893**
1-69*01	6-19*01	3*02	1	0	-	-	-	-	-	-	-	-
1-69*01	No D gene Assignment	2*01	1	24	7	1	0.45038	**0.53682**	11	5	0.66893	**-0.8331**
1-69*01	No D gene Assignment	5*02	(1)	1	0	0	0.45038	**0**	1	0	0.66893	**0.69488**
1-69*02	3-10*01	3*02	1	0	-	-	-	-	-	-	-	-
2-05*04	3-9*01	5*02	1	20	5	2	0.44921	**-0.5082**	6	7	0.67583	**-0.0325**
2-05*04	No D gene Assignment	4*02	1	20	4	1	0.44921	**-0.2326**	6	9	0.67583	**-0.0161**
2-05*10	1-26*01	5*02	1	13	6	0	0.44582	**0.20661**	4	3	0.67963	**-0.5535**
2-05*10	3-10*01	1*01	1	0	-	-	-	-	-	-	-	-
2-05*10	3-16*01	2*01	1	0	-	-	-	-	-	-	-	-
2-05*10	3-22*01	4*02	1	8	2	0	0.44582	**0.19875**	6	0	0.67963	**0.09855**
2-05*10	No D gene Assignment	4*01	1	7	1	0	0.44582	**-0.4922**	3	3	0.67963	**-0.3821**
2-05*10	No D gene Assignment	4*02	(1)	1	0	0	0.44582	**0**	1	0	0.67963	**0.67963**
2-05*10	No D gene Assignment	4*02	1	2	1	0	0.44582	**0.67963**	1	0	0.67963	**0.67963**
3-11*03	3-22*01	3*02	1	1	0	0	0.45384	**-0.5462**	0	1	0.66416	**-0.3358**
3-15*01	No D gene Assignment	4*02	1	10	3	2	0.44151	**0.78267**	4	1	0.65731	**-0.6389**
3-15*01	No D gene Assignment	4*02	1	9	2	1	0.44151	**-0.633**	3	3	0.65731	**-0.2389**
3-21*01	5-12*01	4*02	1	0	-	-	-	-	-	-	-	-

Cont…

V_H Gene	D_H Gene	J_H Gene	Number of Isolated Sequences	Number of Point Mutations	R-CDR	S-CDR	pCDR	p-CDR	R-FW	S-FW	pFW	p-FW
3-21*01	6-13*01	6*02	1	0	-	-	-	-	-	-	-	-
3-30*03	3-10*01	6*02	1	0	-	-	-	-	-	-	-	-
3-33*01	No D gene Assignment	2*01	1	12	6	3	0.46949	**0.43089**	2	1	0.67189	**-0.1116**
3-49*01	2-15*01	2*01	1	1	0	0	0.44792	**-0.5521**	0	1	0.66152	**-0.3385**
3-66*01	3-10*01	5*02	(1)	31	13	4	0.46708	**0.35578**	5	6	0.66604	**-0.0105**
3-66*01	4-23*01	4*02	1	27	7	1	0.46166	**0.41664**	15	4	0.66979	**0.46598**
4-34*01	3-22*01	1*01	1	1	0	0	0.42295	**-0.5771**	0	1	0.65147	**-0.3485**
4-34*01	3-22*01	6*02	(1)	1	0	0	0.42295	**0**	1	0	0.65147	**0.65147**
4-34*03	3-22*01	3*02	1	31	9	3	0.42279	**0.6563**	12	7	0.6487	**-0.3217**
5-51*01	No D gene Assignment	2*01	1	13	6	0	0.43336	**0.08806**	5	2	0.69901	**0.97214**
5-51*03	3-10*01	5*02	(1)	0	-	-	-	-	-	-	-	-
5-51*03	4-17*01	2*01	1	0	-	-	-	-	-	-	-	-
6-01*01	No D gene Assignment	3*02	1	10	2	2	0.47428	**-0.5285**	4	2	0.65306	**-0.3897**
6*01-01	No D gene Assignment	3*02	(1)	0	-	-	-	-	-	-	-	-
6-01*01	6-19*01	4*02	(1)	0	-	-	-	-	-	-	-	-
6-01*01	6-13*01	6*02	1	1	0	0	0.47428	**0**	1	0	0.65306	**0.65306**
7-04-1*01	2-2*03	6*02	(1)	0	-	-	-	-	-	-	-	-
7-04-1*02	No D gene Assignment	1*01	1	14	4	0	0.42769	**-0.533**	2	8	0.66832	**-0.0036**
7-04-1*02	No D gene Assignment	5*02	1	1	1	0	0.42587	**0.42587**	0	0	0.67038	-
7-04-1*02	No D gene Assignment	6*02	1	1	0	0	0.42587	**-0.57412**	0	1	0.67038	**-0.32961**
7-04-1*02	3-9*01	4*02	2	1	0	1	0.42587	**-0.54412**	0	0	0.67038	**-0.32961**
				2	1	0	0.42769	**0.42769**	1	0	0.66832	**0.66832**
7-04-1*02	6-13*01R	3*02	1	0	-	-	-	-	-	-	-	-

Table 5.8 Analysis of Replacement and Silent Mutations and Positive and Negative Selection in Sample VAS6 PBL

Replacement and silent mutations within the immunoglobulin sequences and antigen-driven selection were determined according as per Hershberg *et al* (294) and the corresponding computer programme (http://clip.med.yale.edu/selection). This improved method of analysis uses a focused binomial test to establish positive or negative mutational selections within the sequence with high specificity and increased sensitivity accounting for known biases within the immunoglobulin gene sequence. R-CDR and S-CDR represents the number of replacement and silent mutations within the CDR respectively. pCDR represents the probability of having a R mutation in the CDR given all the mutations in the sequence except R mutations within the FW while p-CDR is the p-value of the focused binominal test on the CDR. Conversely R-FW and S-FW represents the number of replacement and silent mutations within the FW respectively. pFW represent the probability of having a R mutation in the FW given all the mutations in the sequence except R mutations within the CDR while p-FW is the p-value of the focused binominal test on the FW. If the number of R mutations is less than expected the software will test for negative selection and p-values will be preceded by a negative sign or if the number of mutations is more than expected the software will test for positive selection. p-values <0.05 are highlighted in yellow and were deemed significant for selection.

CDR3 Length	Functional	16.5 ± 0.8			
	Non-Functional	19 ± 1.8			
		VD Junction		DJ Junction	
P Nucleotide	Functional	0.8 ± 0.2		0.4 ± 0.1	
	Non-Functional	1.6 ± 0.7		1 ± 0.8	
N Nucleotide	Functional	8.8 ± 1.5		7 ± 1.1	
	Non-Functional	8.6 ± 3.6		8 ± 3	
		3' V_H	5' D_H	3' D_H	5'J_H
Exonuclease Activity	Functional	1.1 ± 0.3*	4.4 ± 0.7 Θ	4.1 ± 0.7	3.8 ± 0.8 Θ
	Non-Functional	4 ± 1.3*	3.6 ± 1.9	3.4 ± 1.3	5 ± 3.1

Table 5.9 CDR3 and Junctional Analysis in VAS6 PBL

The mean amino acid length of the CDR3, the mean nucleotide numbers corresponding to P and N nucleotides as well as the mean number of germline nucleotides lost due to exonuclease activity were calculated from the junctional regions of all myositis immunoglobulin sequences as well as in DM and PM subsets. Results are given as the Mean ± SEM. Instances where no non-functional sequences were identified and values could not be calculated were recorded as non applicable (N/A). * indicates a significant difference between functional and non-functional sequences using an unpaired t test. Θ represents a significant difference from 3'V_H.

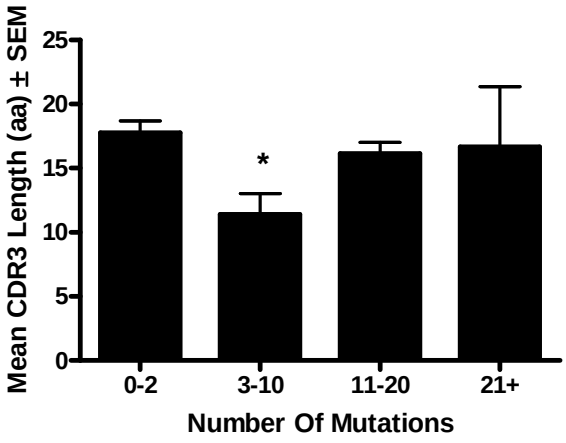

Figure 5.14 Mean CDR3 Lengths in Relation to V_H Mutational Numbers

The mean CDR3 length was calculated for immunoglobulin sequences according the number of mutations within the V_H segment of the gene rearrangement to establish any relationship between mutational number and CDR3 length. Results are given as Mean amino acid CDR3 length ± SEM. Groups were compared for statistical significance using the Tukey-Kramer test for multiple comparisons. The graph demonstrates that no significant changes in CDR3 length were observed at the various number of mutations. p-values <0.05 would have been deemed significant.

No clonally related sequences were observed in the repertoire isolated from the PBL, but as only a small sample of the whole repertoire was isolated and identified clonally related sequences were not expected within the Ig repertoire.

5.3.3 Sample VAS7

As previously described in section 5.2.3 very few B cells were present within the cellular infiltrates of sample VAS7, but plasma cells were shown to be present within cellular aggregates. A similar observation to that observed in the other vasculitis samples. **Figure 5.15** demonstrates the microdissection and DNA amplification from these cells which was used to establish the gene repertoire these infiltrating cells. Five different functional gene rearrangements were amplified from DNA released from the VAS7 microdissection (**Table 5.10A**). Two of the amplified genes contained V_H1 gene segments, 1-46*01 and 1-69*09, while the remaining 3 gene rearrangements contained V_H3 gene segments, 3-12*01, 3-30*03 and 3-73*01. D_H3-10*01 could only be assigned in the V_H1-46*01 gene rearrangement. J_H1, 4 and 5 gene segments were also assigned. Mutational numbers were high in the gene rearrangements containing the V_H1-46*01, 3-21*01 and 3-73*01 gene segments with over 15 mutations per sequence. The remaining two sequences isolated from VAS7 sections contained less than 10 mutations per sequence. Location analysis of these mutations demonstrated that the majority of mutations occurred within the CDR compared to framework regions. Table 5.10A demonstrates that these were largely found within CDR1 compared to CDR2. No significant selection could be assigned to any of the gene rearrangements regardless of the large number of mutations within the V_H region of the sequence (**Table 5.10B**). For these sequences isolated from the skin infiltrating population, CDR3 lengths were found to range from 9 to 17 amino acids. Junctional analysis in the V_H1-46*01 gene rearrangement where a D_H gene could be assigned demonstrated that no P nucleotides were present at either the VD or DJ junction. On the contrary 17 and 3 N nucleotides were assigned respectively at the VD and DJ regions of the junction. Analysis of the exonuclease activity demonstrated that 0, 8, 8 and 6 nucleotides were removed from the respective 3'V_H, 5'D_H, 3'D_H and 5'J_H gene segments of the junction. No clonally related sets of sequences were found within the infiltrating cells and all gene assignments from the JOINSOLVER algorithm corresponded to the gene assignments of IMGT/V-QUEST.

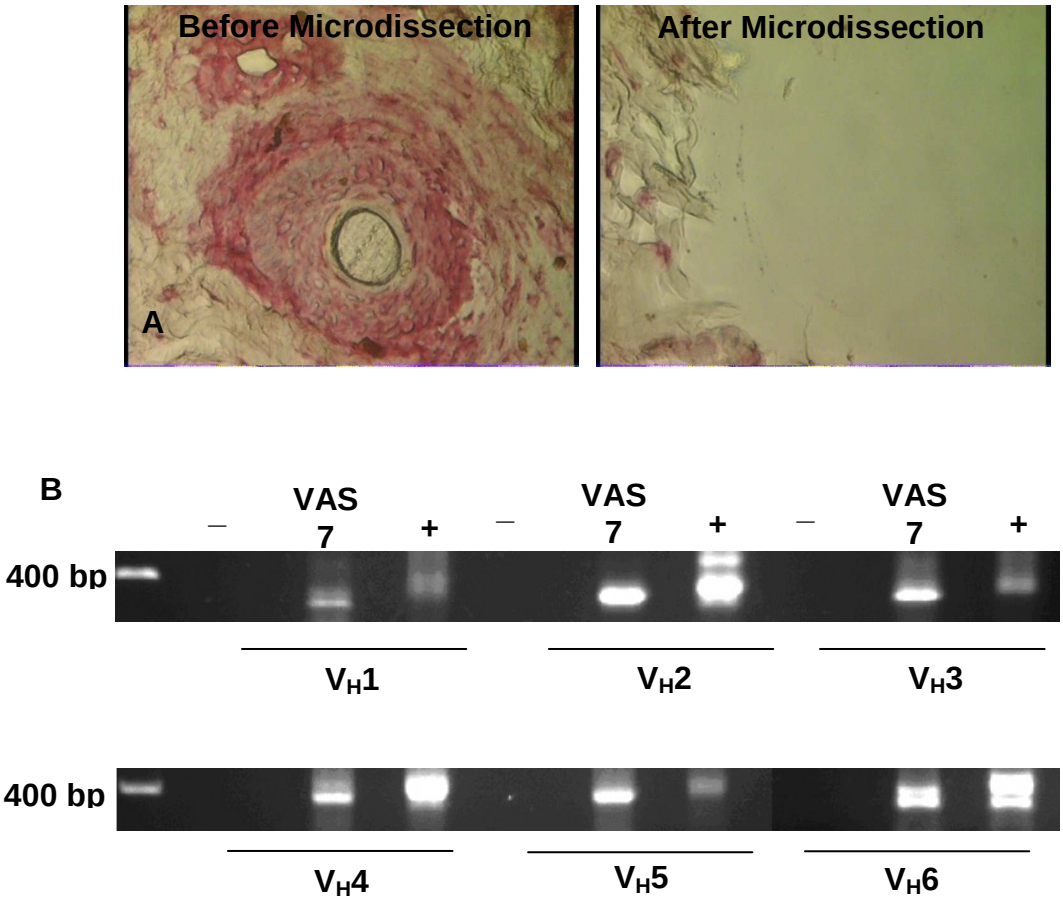

Figure 5.15 Microdissection of infiltrating B cells and amplification of V_H-gene rearrangements from Sample VAS7

A region of plasma cell infiltration was microdissected from sample VAS7. Figure 5.15A demonstrates the microdissection of 2 regions of cellular infiltration. Images were taken at 400X. DNA released from these microdissections was amplified using a Nested PCR system (Figure 5.15B), as previously described in Chapter 2. – indicates negative control PCR reactions where DNA was substituted with water while + indicates positive control PCR reactions using peripheral blood mononuclear cells isolated from peripheral blood of a healthy individual. Results show amplification of all 6 V_H families.

A

V_H Gene	D_H Gene	J_H Gene	Number of Isolated Sequences	Number of Point Mutations	CDR3	CDR3 Length (aa)	Mutational Distribution (% of length)			V-J Length (bp)	Consecutive D length (bp) (+Mismatches)
							Framework	CDR1	CDR2		
1-46*01	3-10*01	4*02	1	16	ARESIIFADGSGSYGDY	17	5	33.3	0	37	17
1-69*09	No D gene Assignment	1*01	1	2	VIHLIQLST	9	0.5	0	2	25	7
3-21*01	No D gene Assignment	4*02	1	24	AREHWELLRGNDYYLDY	17	6.3	20	13.7	43	6
3-30*03	No D gene Assignment	4*02	1	8	ARRGYLNSVDY	11	0.9	20	5.9	20	8
3-73*01	No D gene Assignment	5*02	1	21	TRREDGSGSFSA	12	6.3	13.3	9.8	28	8

B

V_H Gene	D_H Gene	J_H Gene	Number of Isolated Sequences	Number of Point Mutations	R-CDR	S-CDR	pCDR	p-CDR	R-FW	S-FW	pFW	p-FW
1-46*01	3-10*01	4*02	1	16	5	0	0.47813	**0.65911**	7	4	0.67198	**-0.788**
1-69*09	No D gene Assignment	1*01	1	2	0	1	0.46644	**-0.2847**	0	1	0.67237	**-0.1073**
3-21*01	No D gene Assignment	4*02	1	24	6	4	0.51535	**-0.3872**	9	5	0.65709	**-0.1773**
3-30*03	No D gene Assignment	4*02	1	8	5	1	0.46794	**0.09263**	2	0	0.6723	**-0.9479**
3-73*01	No D gene Assignment	5*02	1	21	5	2	0.47451	**-0.5352**	8	6	0.66316	**-0.1863**

Table 5.10 A&B Sequence Analysis from Sample VAS7

Table 5.10A - Best matching germline sequences were identified from aligning sequences in the IMGT database using JOINSOLVER software from the VAS7 vasculitis section. Identical sequences with the same V_H, D_H, J_H, CDR3 and base mutations were only counted once. V-J lengths and consecutive D match lengths (bp) were also identified using the JOINSOLVER software and allowed assignment of the D_H genes as described in section 2.3.12.3.

The number of mutations within functional rearranged genes were analysed collectively from all region of dissected cellular infiltration. Base differences within the first 24 bases of sequence were disregarded as this part of the sequence binds the 5' V_H primer.

The locations of mutations observed within functional rearranged genes were categorised as being within FR or CDR regions. The numbers of mutations within these regions were expressed as a percentage of the entire length of the region to correct for the longer lengths observed within the framework regions.

Table 5.10B - The number of replacement and silent mutations and the presence of any positive and negative selection was conducted as per Hershberg *et al* (294) as previously described. R-CDR/FW and S-CDR/FW represent the number of replacement and silent mutations in the CDR and FW respectively. pCDR represents the probability of having a R mutation in the CDR given all the mutations in the sequence except R mutations within the FW while pFW represents the probability of having a R mutation in the FW given all the mutations in the sequence except R mutations within the CDR and p-CDR/FW represent the p-value of the focused binominal test on the CDR and FW respectively. A negative sign indicates negative selection. p-values <0.05 were deemed significant.

5.3.4 V_H Repertoire in Vasculitis

As a limited number of Ig sequences were obtained from skin infiltrating cells in each individual vasculitis patient, the results from all three patients were pooled to establish if a common pattern of gene usage and mutational patterns occurred. The results demonstrated that the collective repertoire of V_H gene usage mirrored the normal control values as well as the baseline germline complexity (**Figure 5.16A**). These findings are in contrast to those observed within the PBL repertoire of samples VAS1 and VAS6 where a common selection for the use of V_H2 gene segments and selection against V_H4 gene segments was observed in both samples. Despite the lack of selection for the different V_H gene families as a whole within the skin, selections were observed for the use of V_H1-46, 3-33, 3-73 and 4-59 individual gene segments. From the Ig repertoire from skin infiltrating cells D_H genes could be assigned in 41.2% of gene rearrangements. From this a selection for the use of D_H4 and D_H5 gene segments was observed which was significant against normal control values, in particular the D_H4-17 and 5-12 gene segments which were significantly selected (**Figure 5.16B**). Similar to the V_H repertoire these selections were in contrast to that observed within the two paired blood samples. The positive selection for the use of D_H3 gene segments within the PBL was not observed in the Ig rearrangements from the cellular infiltrates within the skin. J_H2 gene segments were found to be over-represented in the 3 vasculitis patients, which was significant against the normal control values but not the baseline germline complexity (**Figure 5.16C**). This selection was also observed within the repertoire from one of the peripheral blood samples, VAS6, but is in contrast to the results from the second blood sample, VAS1.

5.3.4.1 Mutational Analysis in Vasculitis

Analysis of mutational numbers from the 17 functional Ig rearrangements isolated demonstrated that approximately a quarter of the sequences isolated were essentially non-mutated and from a naïve population (**Figure 5.17A**). The remaining sequences were highly mutated with over 50% of the sequences containing over 11 mutations per sequence. These mutations were largely observed in the CDRs compared to FW regions, with a slightly higher percentage within CDR1 compared to CDR2 (**Figure 5.17B**).

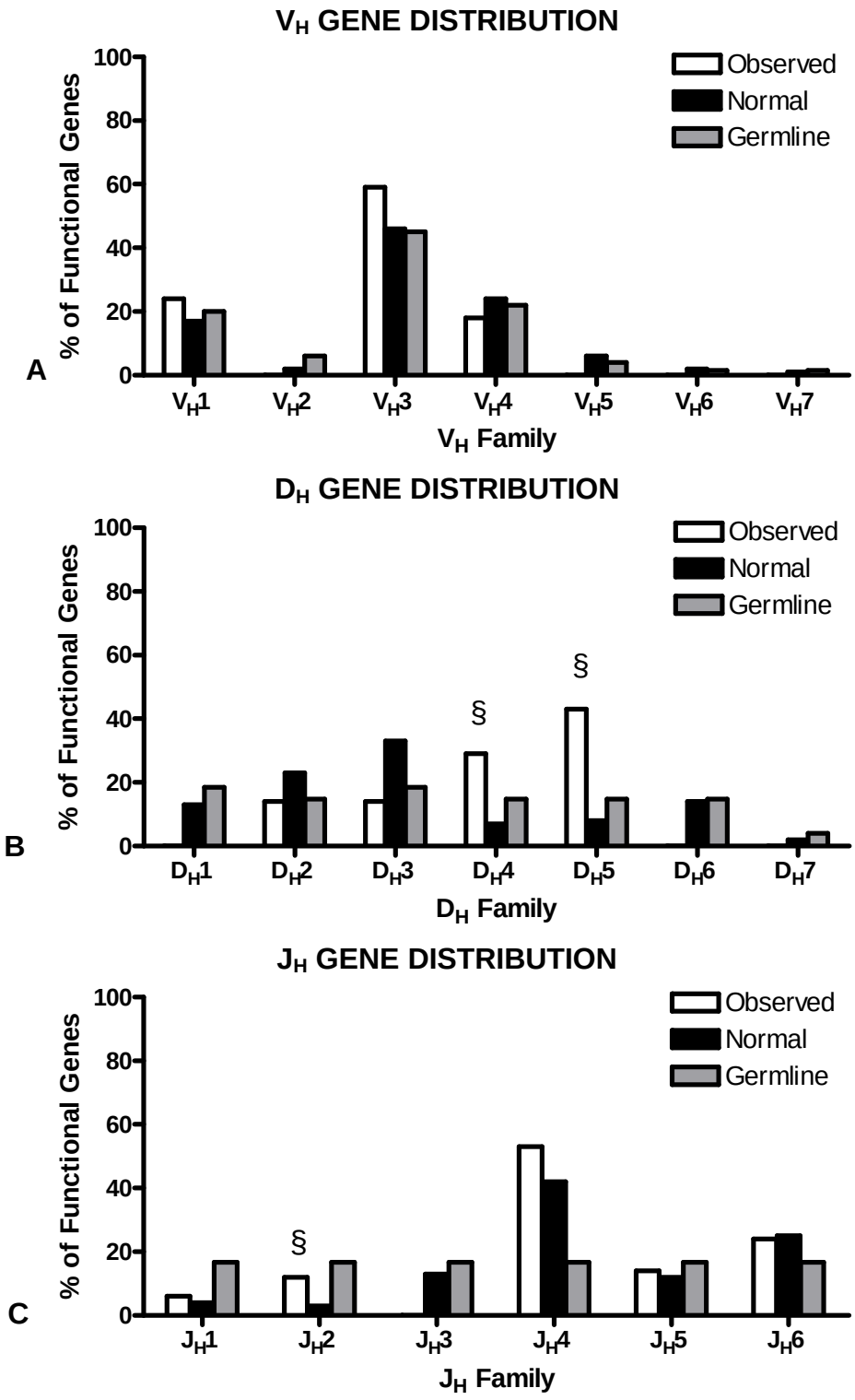

Figure 5.16 V_H Gene Family Usage of Vasculitis samples

V_H gene family usage. Distribution of functional genes was compared with published normal control values from Volpe and Kepler (251) as well as the germline complexity assuming every germline gene is capable of producing a functional rearrangement. Absolute values were used in Chi Square Analysis to determine gene selections. § represent a significant difference from normal PBL values; * represent a significant difference from the germline ($p<0.05$).

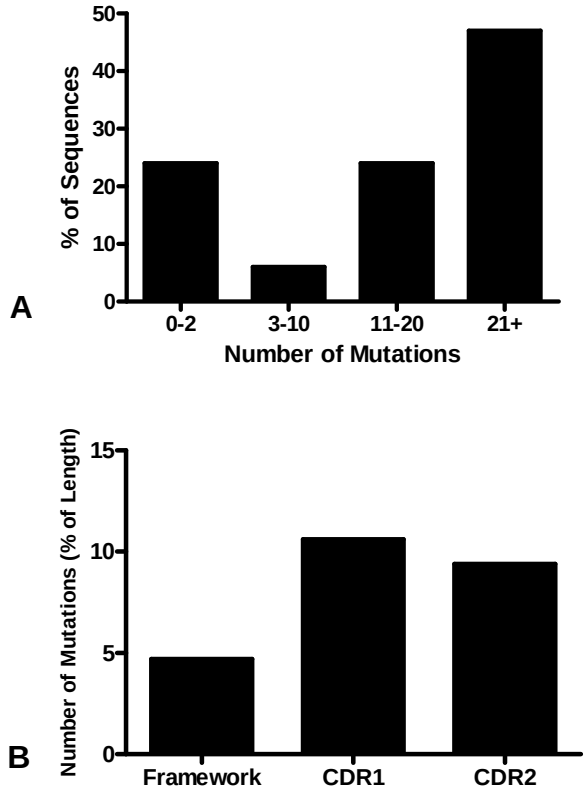

Figure 5.17 Numbers of Mutations and Mutational Distribution of Functional Sequences in Vasculitis Patients

Figure 5.17A - The number of mutations within functional rearranged genes were analysed collectively from all vasculitis patients. Base differences within the first 24 bases of sequence were disregarded as this part of the sequence binds the 5' V_H primer. Graph demonstrates sequences within cellular infiltrates show a diverse distribution of mutational numbers.

Figure 5.17B - The locations of mutations observed within functional rearranged genes were categorised as being within FR or CDR regions. The numbers of mutations within these regions were expressed as a percentage of the entire length of the region to correct for the longer lengths observed within the framework regions. Graph demonstrates a higher percentage of mutations within CDR regions compared to framework regions.

From the collective repertoire of 17 functional sequences, selection was only significantly observed in 1 functional Ig rearrangement. In this Ig rearrangement negative selection was observed in the FW region, no other significant selection was observed from any other rearrangement.

5.3.4.2 CDR3 Analysis

In the isolated repertoire from the vasculitis samples no non-functional Ig rearrangements were identified, therefore significant differences in the junctional characteristics between functional and non-functional sequences could not be established. For the functional repertoire the mean amino acid CDR3 length was 15.5 ± 0.9 amino acids (**Table 5.11**) and no significant difference in CDR3 length was observed within the various mutational groups of sequences (**Figure 5.18**). The addition of P and N nucleotides at the VD and DJ junctions were not found to be significantly different within the functional population of sequences. Examination of the exonuclease activity at the various gene segments of the junctional area demonstrated a significant decline in the enzymatic activity at the 3'V_H region compared to the 5'D_H region in the VD region of the junction. No other significant differences were observed.

CDR3 Length	**Functional**	15.5 ± 0.9			
	Non-Functional	N/A			
		VD Junction		**DJ Junction**	
P Nucleotide	**Functional**	0.8 ± 0.4		0	
	Non-Functional	N/A		N/A	
N Nucleotide	**Functional**	5.3 ± 2		6.1 ± 0.6	
	Non-Functional	N/A		N/A	
		3' V_H	**5' D_H**	**3' D_H**	**5'J_H**
Exonuclease Activity	**Functional**	1 ± 0.4	5.3 ± 1.4 $^{\Theta}$	2.7 ± 1.1	3.4 ± 1.5
	Non-Functional	N/A	N/A	N/A	N/A

Table 5.11 CDR3 and Junctional Analysis in Vasculitis

The mean amino acid length of the CDR3, the mean nucleotide numbers corresponding to P and N nucleotides as well as the mean number of germline nucleotides lost due to exonuclease activity were calculated from the junctional regions of all vasculitis immunoglobulin sequences as well as in DM and PM subsets. Results are given as the Mean ± SEM, statistical significance was established using an unpaired t-test. Instances where no non-functional sequences were identified and values could not be calculated were recorded as non applicable (N/A). Θ represents a significant difference from 3'V_H.

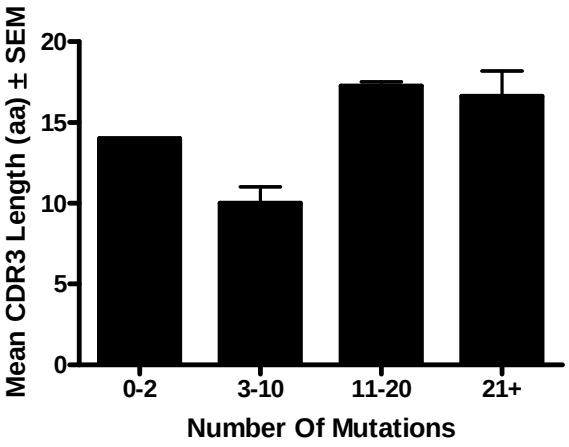

Figure 5.18 Mean CDR3 Lengths in Relation to V_H Mutational Numbers

The mean CDR3 length was calculated for immunoglobulin sequences according the number of mutations within the V_H segment of the gene rearrangement to establish any relationship between mutational number and CDR3 length. Results are given as Mean amino acid CDR3 length ± SEM. Groups were compared for statistical significance using the Tukey-Kramer test for multiple comparisons. The graph demonstrates that no significant changes in CDR3 length were observed at the various number of mutations. p-values <0.05 would have been deemed significant.

One common replacement mutation was observed between the V_H1-18*****01 gene isolated from sample VAS1 and the V_H1-46*01 gene isolated from sample VAS6. At amino acid 69, situated close to CDR2, a replacement mutation occurred within both sequences converting the methionine to a valine amino acid (M→V). The serine to asparagine replacement mutation (S→N), amino acid 31, which was observed within some of the myositis samples was also observed within the V_H3-33*01 isolated from sample VAS1.

5.4 Discussion

In a similar situation to myositis, the role of B cells in the inflammatory process of vasculitis is unknown. Pathological manifestations within vasculitic disorders have been attributed to the activation of T cells but the presence and contribution of immune complexes and autoantibodies within these inflammatory disorders strongly implicates a pathological role for B cells. This is substantiated by the clinical improvement observed in patients undergoing B cell depletive therapy as previously described. Previous work in this study aimed to define a possible role for B cells in muscle inflammation by testing the hypothesis that muscle infiltrating B cells were being locally stimulated resulting in an antigen-driven response contributing to tissue pathology. This hypothesis was also tested for skin infiltrating lymphocytes in vasculitis patients using the same procedures described for muscle infiltrating cells to determine if antigen-driven Ig sequence characteristics such as gene selection, mutational accumulation and clonal diversification were present within the Ig gene rearrangements expressed on skin infiltrating B cells.

Initially the identification and organisation of skin infiltrating cells was determined. In contrast to some of the muscle samples very few B cells were present within the infiltrating population and the vast majority of infiltrating cells were plasma cells. Skin infiltrating cells were widely distributed throughout the entire biopsy with very little aggregation and likewise to the organisation observed within myositis samples no ectopic germinal centre type structures were observed. Other cell markers were also identified, CD3, CD4, CD8, CD68 and FoxP3, while FDCs were entirely absent from the infiltrating population for all samples. Very few $Ki67^+$ proliferating cells were identified, collectively these results may indicate that an active antigen-driven response is not occurring within the skin and the infiltrating cell population is present as a result of inflammatory mediator gradients.

The lack of B cells, FDCs and ectopic germinal centre structures in the samples of the current study is in contrast to studies by Voswinkel *et al* (348;349) in Wegener's granulomatosis (WG), a disease of unknown aetiology characterised by necrotising granulomatosus inflammation and systemic vasculitis

predominately affecting small vessels. Voswinkel *et al* (348) observed different lymphocytic phenotypes ranging from diffusely infiltrating cells to cellular aggregates of T and/or B cells without FDCs in addition to germinal centre type structures containing FDCs. The initial study (348) identified B lymphocyte containing infiltrates in endonasal biopsies of all 6 WG patients studied. Approximately 30% of the cells within the follicle-like structures were identified as $CD20^+$ B cells; plasma cells were also evident but did not appear to be as substantial to the infiltrating plasma cell population in the three vasculitis patients used within the current study. The findings of Voswinkel *et al* are also supported by additional studies (350). The variations in immunohistological findings between these studies and the current study may represent different disease and B cell mechanisms occurring at various target sites of vasculitis.

To address the hypothesis that skin infiltrating B cells are being stimulated locally in an antigen-driven response the sequence characteristics of Ig rearrangements expressed on infiltrating cells was assessed. Within each individual patient a limited number of rearrangements were identified. Due to the low numbers a comparison of gene usage could not be conducted on each individual patient, therefore a collective analysis was required to determine the sequence characteristics of the Ig rearrangements. The different methods used to assign gene segments within the Ig rearrangements which may result in alterations in gene assignments, previously discussed in section 4.3.2, are also relevant to this part of the study. From the collective repertoire gene selections were observed for D_H and J_H gene segments and mutations were found in approximately 75% of sequences with over 40% of sequences containing 21 or more mutations. These results would indicate that antigen-driven diversification of B cells had occurred but the lack of V_H selection and clonal related sequences from the infiltrating lymphocytes contradicts the proposed hypothesis of this study. Analysis of a larger number of sequences from a larger cohort of patients may be required to fully assess B cell antigen driven diversification. Modifications to the Ig repertoire from patient therapies, Table 2.1, must also be considered. The sequence results could relate to the previous immunohistological studies in these samples. As previously described a large number of plasma cells were found within the infiltrating populations

along with a limited proliferating population of cells. Taken together the Ig rearrangements identified may correspond to the highest affinity, antigen-specific and clonally diversified rearrangements from B cells which have terminally differentiated into plasma cells and infiltrated into target areas of the skin with the secreted antibodies from these cells contributing to the tissue pathology. In such a situation it would be expected that the sequences isolated would exhibit positive selection based on the R and S mutation within the sequence. Selection in this study was based on the newly proposed method described by Hershberg *et al* (294), which was previously discussed in section 4.3.3. Using this method selection was only detected in 1 Ig rearrangement, which was found within the FW regions and was significant for negative selection. The lack of positive selection, in a similar situation to myositis Ig rearrangements discussed in section 4.3, may be the result of the improved parameters used to assign selection which now account for the fundamental aspects of sequence variation and diversity.

It could also be postulated that the accumulation of plasma cells observed within these samples is simply a consequence of the immune response which, as a result of inflammatory mediators, had provided a suitable niche for plasma cells within the inflamed skin and that the cells do not bear Ig rearrangements which are specific to a vasculitis specific or associated antigen. Alternatively the work of this study may suggest a different B cell mechanism in contrast to the proposed hypothesis of this study. Initiation of inflammation within the skin, in response to a vasculitis specific autoantigen, may generate a favourable environment for the migration and transition of high affinity pre-plasma cells which have the capacity to generate long-lived plasma cells and secrete pathogenic autoantibodies. Identification of the antigen specificity of antibodies secreted from plasma cells within the 3 vasculitis samples of this study would help clarify the mechanism of these cells in inflamed skin. This hypothesis may result in the limited Ig repertoire observed within this study and substantiates the significance of these B cell derived cells in the pathogenesis of vasculitis. The importance of modulating production, survival and mechanisms of plasma cells in vasculitis disorders is substantiated by previous studies which demonstrate the importance of these cells and the antibodies they produce in

the pathogenesis of vasculitis (6;171;178;188;202;351-355), reviewed (149;157;179;185;356).

As well as analysing the gene segment usage and mutational patterns of Ig rearrangements identified from vasculitis biopsies, the different mechanisms at the junctional regions of VDJ recombination were examined. Within this repertoire of sequences no non-functional sequences were isolated so significant differences between CDR3 lengths in functional and non-functional populations could not be examined to support previous findings (238;241;242;251;291). There was also no significant difference between CDR3 lengths in different mutational groups in contrast to previous studies (238). The addition of P and N nucleotides between the VD and DJ junctions was also found not to be significant between the two regions of the junction, as previously observed (251;291;334), while a significant decrease in exonuclease activity at the 3'V_H region was found compared to the 5'D_H region. These results mirror that found within the Ig gene isolated from inflamed muscle and may correlate differences within diseased repertoires compared to normal control repertoires.

In contrast to the work of Chapter 4, paired blood samples were obtained for two of the vasculitis patients. Both Ig gene repertoires demonstrated both positive and negative gene selections when compared to normal control values, with common selections observed in both patients. These selections were not observed in the repertoire from Ig expressed on skin infiltrating cells. From these samples identically rearranged genes were not found in both the peripheral blood and inflamed skin which may represent a compartmentalisation of the immune response within the skin, although analysis from a larger number of patients and of a larger number of sequences from both sources may be required to fully examine the differences between peripheral blood repertoires and the repertoires observed within the target tissues of autoimmune diseases. These results are in contrast to previous studies where recirculation of activated B cells was observed in the synovial membranes and peripheral blood repertoires of RA patients (336). Patient VAS6 had a past medical history of ankylosing spondylitis (AS). A previous study has demonstrated that antigen-driven B cell responses occurred within synovial membranes of an AS patient

(320), it would be interesting to assess the repertoires from different sites in this patient to fully assess the mechanisms involved in gene selection as well as recirculation and maturation of activated B cells. Collectively these results would indicate whether clones isolated from the skin have recirculated from the synovial membranes and the skin infiltration is non-specific and the vasculitis is secondary to the chronic inflammation of the ankylosing spondylitis.

Studies by Voswinkel *et al* (348;349) have demonstrated the antigen-driven and clonal diversification of B cells in WG, a subset of vasculitis. B lymphocyte infiltrates, in various organisations as described above, were observed in all 6 endonasal biopsies tested from which 184 V_H rearrangements were compared to healthy V_H repertoires (348). Five samples displayed a V_H repertoire with prevalence for V_H3 and V_H4 gene rearrangements with a predominance of V_H3-30, V_H3-23, V_H4-34 and V_H4-59 genes. A high proportion of mutations within sequences were observed compared to healthy repertoires which were found to relate to an increased disease activity and clonally related sets of sequences were found in 4 of the 6 patients suggesting antigen-driven affinity maturation. These results were substantiated by the presence of autoantigen specific $PR3^+$ cells within the cellular infiltrate. Another recent study by this group has analysed the Ig rearrangements from single B cells laser dissected from frozen sections from endonasal biopsies of WG patients (349). The results confirm the previous study but also allowed characterisation of individual B cell receptors by analysing the L chain sequences and pairings from these cells. Both studies conclude the selection and maturation of antigen-specific B cells in an autoimmune response of WG, a disease characterised by vasculitis, but a direct comparison cannot be made to the study of this chapter as different responses may occur at different sites of inflammation and the stimulating antigen may also be different at various locations and between different patients.

In summary, these results suggest that antigen-driven B cell responses may play a role in the inflamed skin of these vasculitis patients but with very few B cells and no clonally related sequences identified, the primary responses may be occurring at other sites of inflammation, or secondary lymphoid organs, resulting in migration of high affinity antigen-specific cells into inflamed skin.

Chapter 6 - Identification of Antigens Driving the Immune Response in Myositis Patients

6.1 Introduction

Previous results within this study, Chapters 4 & 5, have demonstrated the presence of antigen-driven diversified cells at the sites of inflammation within the target tissues of myositis and vasculitis. Gene selections and mutational analysis of the Ig gene rearrangements, where no clonally related sequences were identified, indicate that cells had undergone an antigen-driven diversification and were possibly stimulated by antigen at other locations, presumably the draining lymph node, and migrating into the sites of inflammation while identification of clonally related sequences suggested that infiltrating cells were being stimulated locally by antigens present at these sites of inflammation. Although the results have demonstrated the occurrence of an antigen-driven response they do not indicate the identity of the antigen(s) stimulating the response.

Autoantibodies were detected in the sera of five myositis patients, Table 2.1. To summarise patient MYO3 and MYO23 were Jo-1^{+} while patient MYO3 also tested positive for Sm/RNP antibodies. Two of the myositis patients, MYO16 & MYO19, tested positive for anti-nuclear antigens (ANA). The nucleolar pattern of staining indicated that the antigen may be topoisomerase 1 (Scl70) which is normally found within systemic sclerosis patients (113;357). Anti-DNA antibodies were also found in serum samples of patient MYOE, a characteristic of SLE patients. Therefore to identify the stimulating antigens occurring within the target tissues of these patients, biotinylated recombinant antigens were used to establish the following aims of the chapter:

- Identify antigen-specific muscle infiltrating lymphocytes.
- Establish the phenotype of these antigen specific cells as B cells and/or plasma cells using double immunohistochemical experiments.
- Use laser capture microdissection to isolate antigen specific cells and determine the Ig gene rearrangements of these cells.

The results described in this chapter were in preliminary stages and were intended as provisional for future work in autoantigen identification.

6.2 Identification of Antigen-Specific Cells within Cellular Infiltrates in Myositis Muscle Biopsies

6.2.1 Sample MYO3

Patient MYO3 was positive for both serum Sm/RNP and Jo-1 antibodies. Staining with these biotinylated antigens provided two very diverse patterns of staining (**Figure 6.1**). Staining for Jo-1 (**Figure 6.1A-B**) demonstrated that Jo-1^+ cells were located sporadically throughout the muscle section. In some cases a small cluster of Jo-1^+ cells were found but it also appeared that single Jo-1^+ cells were also located within the sample. The use of biotinylated Sm/RNP (**Figure 6.1C-D**) showed extensive staining throughout the whole biopsy located between the muscle fibres. Negative control staining showed no non-specific staining as did the use of biotinylated Sm/RNP on tonsil sections (data not shown). Single cells were not able to be identified within the extensive staining of Sm/RNP. Extensive staining with the Sm/RNP antigen may have occurred as a result of large numbers of anti-Sm/RNP antibodies secreted by infiltrating plasma cells in the inflamed muscle.

Double immunofluorescence experiments with the recombinant antigens revealed that the Jo-1 specific cells were mostly $CD20^+$ cells (**Figure 6.2A-B**) while the Sm/RNP^+ cells were found to be mostly plasma cells (**Figure 6.2C-D**). The extensive staining of Sm/RNP in areas of plasma cell infiltration made it difficult to identify isolated single antigen-specific cells, but a small cluster of plasma cells were found within that large area of Sm/RNP staining.

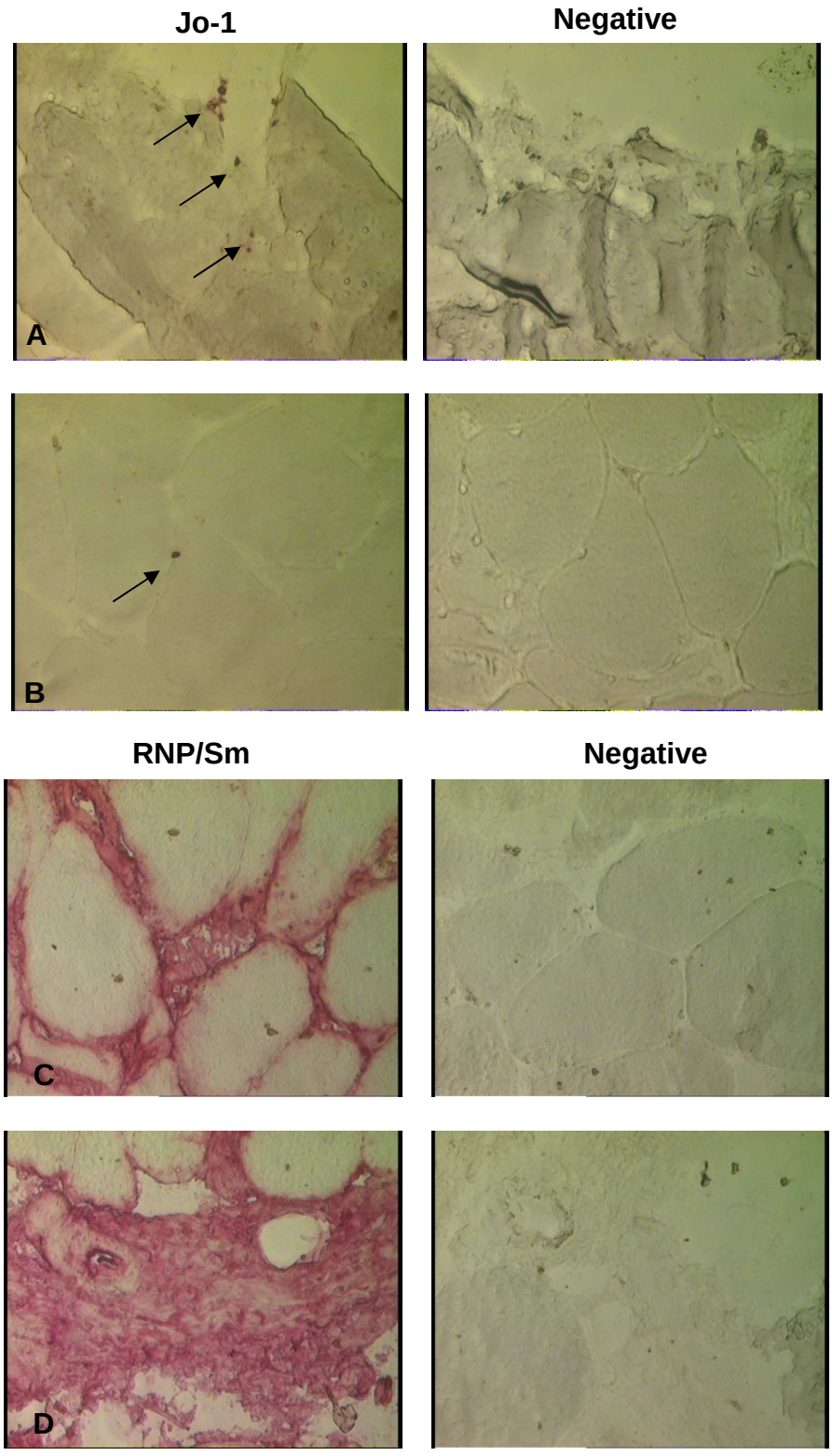

Figure 6.1 Immunohistochemical staining using biotinylated antigen in Sample MYO3

Muscle sections from sample MYO3 were stained with biotinylated antigen, Jo-1 (**A-B**) and Sm/RNP (**C-D**), and visualised by APAAP and New Fuschin substrate to establish if antigen specific cells were present within the muscle section. Biotinylated BSA was used as a negative control protein. Images taken at 400X.

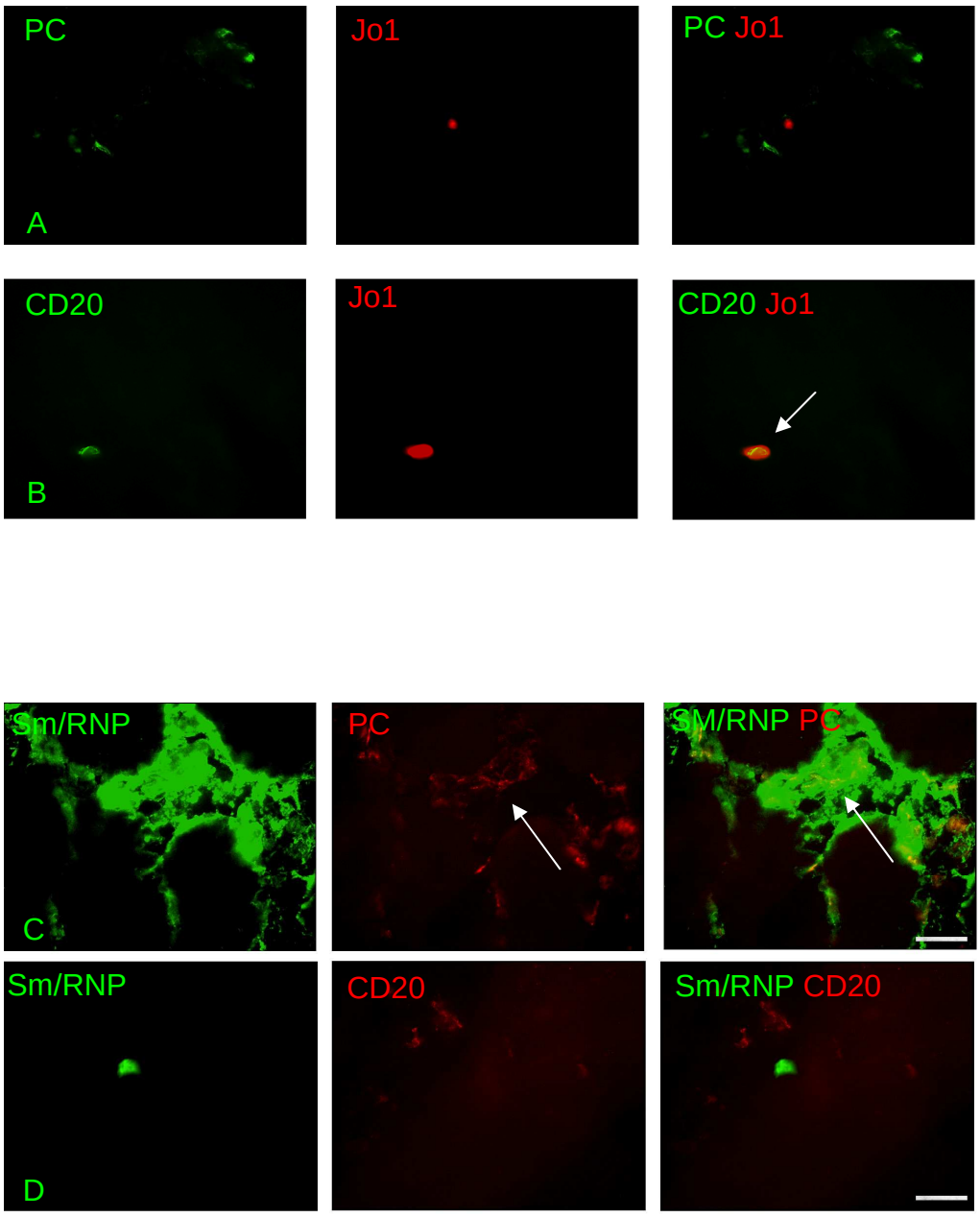

Figure 6.2 Double Immunohistochemical staining using biotinylated antigens in sample MYO3

Muscle sections from sample MYO3 were stained for Plasma cells (**A&C**) and CD20 (**B&D**) and biotinylated antigen; Jo-1 (**A-B**) and Sm/RNP (**C-D**). Cell phenotypes were visualised by Texas Red Avidin D and antigen-specific cells by Fluorescein Avidin D. This allowed the phenotype of antigen-specific cells within the myositis sample to be identified. Images were taken at 630X; Scale Bar represents 15 µm. Arrows identify antigen specific cells within the sections.

6.2.2 Sample MYO16

Patient MYO16 was positive for anti-nuclear antigens (ANA), the nucleolar pattern of staining indicated that the antigen may be Scl70 (Topoisomerase 1). Recombinant Scl70 used for staining the muscle sections demonstrated the occurrence of small clusters of $Scl70^+$ cells within the sample (**Figure 6.3.1A&B**). In comparison to the levels of infiltrating B cells and plasma cells within the sample, identified in Chapter 3, it appears that Scl70 may not be the only antigen stimulating a response within patient MYO16. Double staining experiments with recombinant Scl70 indicated that the antigen-specific cells were plasma cells (**Figure 6.3.2A&B**), there was no evidence of any antigen specific B cells within the sections used for staining. For B cell staining very few infiltrating cells were observed, this is in contrast to the staining experiments used in Chapter 3 where a very dense cluster of B cells was observed. Although these experiments were conducted on serial sections, these sections were at a greater depth of tissue than the sections described in Chapter 3, which may explain the absence of B cell infiltration in later sections. Clonally related sets of sequences observed within this patient may be in response to Scl70.

6.2.3 Sample MYO19

For sample MYO19, who also tested positive for ANA with a nucleolar pattern, results were similar to that of patient MYO16. Small clusters of $Scl70^+$ cells were observed throughout the sample (**Figure 6.4.1 A&B**). In double staining experiments both antigen-specific B cells and plasma cells were observed (**Figure 6.4.2 A&B**). The lack of clonally related sets within patient MYO19 may suggest, like the other samples, that B cells are stimulated by the antigen at another location which then migrate into inflamed muscle. As with MYO16 the frequency of antigen-specific cells in comparison to the frequency of B cells and plasma cells previously found within the sample sections indicates that other antigens may be participating in the response.

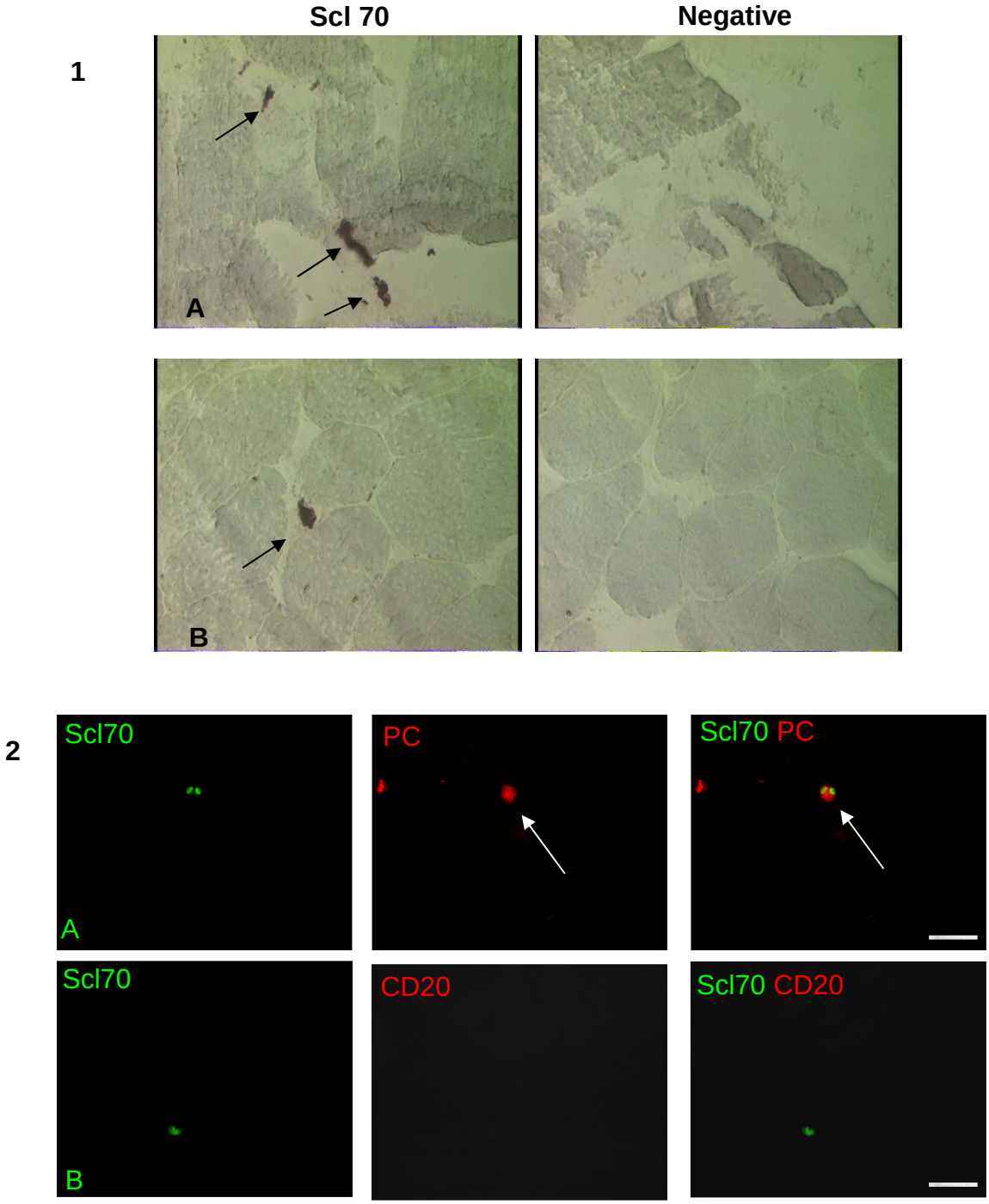

Figure 6.3 Immunohistochemical staining using biotinylated antigen in Sample MYO16

Figure 6.3.1 - Muscle sections from sample MYO16 were stained with biotinylated antigen, Scl70, (**A&B**) and visualised by APAAP and New Fuschin substrate to establish if antigen specific cells were present within the muscle section. Biotinylated BSA was used as a negative control protein. Images taken at 400X.

Figure 6.3.2 - Muscle sections from sample MYO16 were stained for Plasma cells (**A**) and CD20 (**B**) and biotinylated Scl70. Cell phenotypes were visualised by Texas Red Avidin D and antigen specific cells by Fluorescein Avidin D. This allowed the phenotype of antigen-specific cells within the myositis sample to be identified. Images were taken at 630X; Scale Bar represents 15 µm. Arrows identify antigen specific cells within the sections.

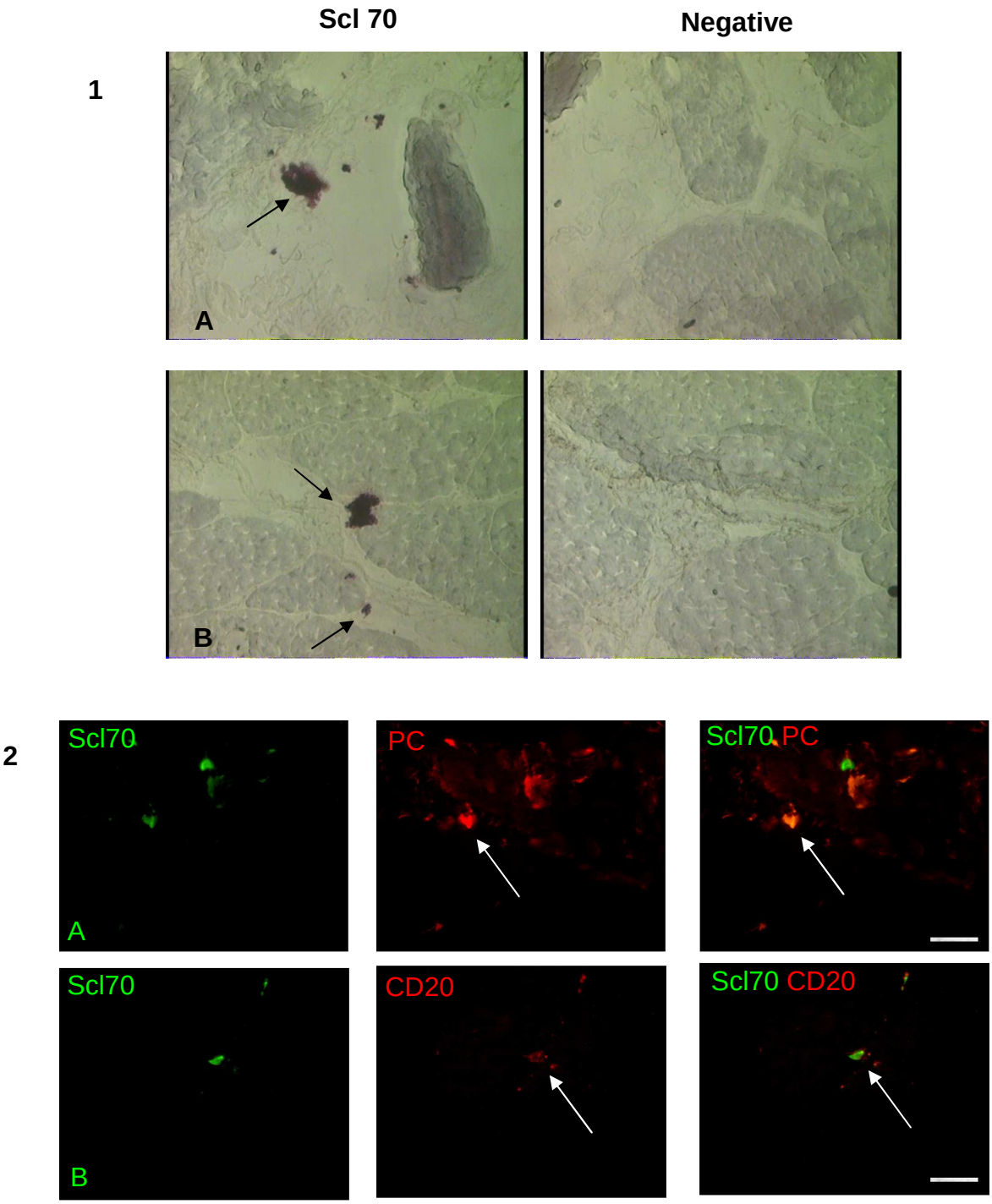

Figure 6.4 Immunohistochemical staining using biotinylated antigen in Sample MYO19

Figure 6.4.1 - Muscle sections from sample MYO19 were stained with biotinylated antigen, Scl70, (**A&B**) and visualised by APAAP and New Fuschin substrate to establish if antigen specific cells were present within the muscle section. Biotinylated BSA was used as a negative control protein. Images taken at 400X.

Figure 6.4.2 - Muscle sections from sample MYO19 were stained for Plasma cells (**A**) and CD20 (**B**) and biotinylated Scl70. Cell phenotypes were visualised by Texas Red Avidin D and antigen specific cells by Fluorescein Avidin D. This allowed the phenotype of antigen-specific cells within the myositis sample to be identified. Images were taken at 630X; Scale Bar represents 15 µm. Arrows identify antigen specific cells within the sections.

6.2.4 Sample MYO23

Patient MYO23 tested positive for serum Jo-1 autoantibodies. Staining with recombinant Jo-1 identified antigen positive cells within the sample (**Figure 6.5.1A&B**). In contrast to sample MYO3 these mostly appeared to be isolated single cells. Double staining experiments on MYO23 (**Figure 6.5.2A&B**) sections showed the presence of antigen-specific plasma cells within the sample. Antigen-specific B cells were not observed in the samples tested for by double immunofluorescence staining using recombinant antigen, but this does not exclude their presence in other sections of the sample but as very few B cells were identified in the initial cell phenotype staining this suggests that the antigen-specific cells may solely be infiltrating plasma cells. Clonally related sets of sequences were observed within this patient, which may be in response to Jo-1.

6.2.5 Sample MYOE

As shown in Table 2.1 patient MYOE tested positive for anti-DNA antibodies. Staining MYOE sections with biotinylated ds-DNA identified a small number of DNA^+ cells within the infiltrating population (**Figure 6.6.1A&B**). The occurrence of anti-DNA^+ cells was reduced in comparison to other types of antigen specific cells identified in the other myositis patients, although no direct quantification was conducted. Some of these DNA^+ cells appeared to form small aggregated clusters. Double staining experiments established the phenotype of antigen-specific cells as plasma cells (**Figure 6.6.2A&B**). The low frequency of DNA^+ cells infiltrating the sample and the low numbers of infiltrating B and plasma cells identified in Chapter 3 meant very few antigen positive cells could be identified.

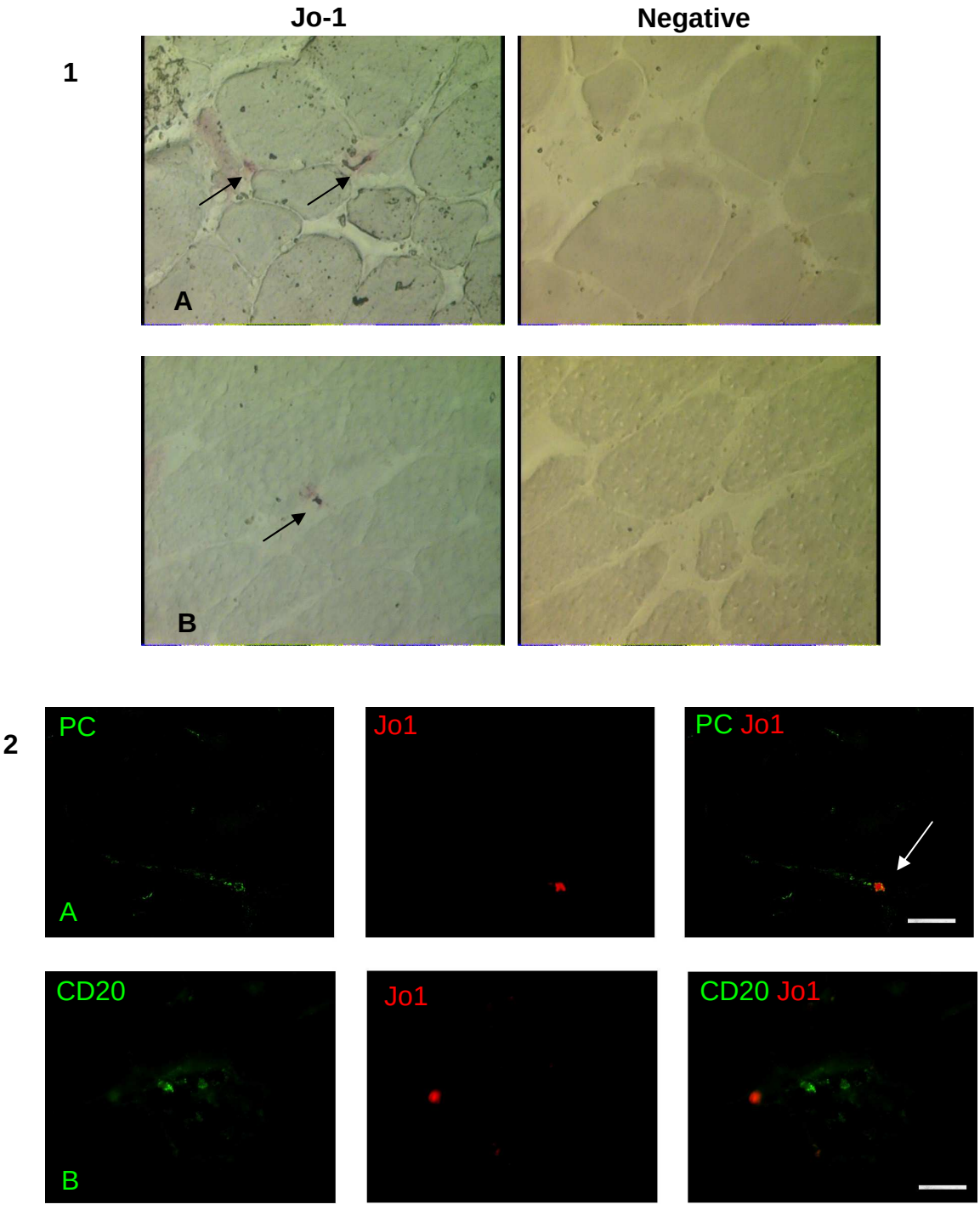

Figure 6.5 Immunohistochemical staining using biotinylated antigen in Sample MYO23

Figure 6.5.1 - Muscle sections from sample MYO23 were stained with biotinylated antigen, Jo-1, (**A&B**) and visualised by APAAP and New Fuschin substrate to establish if antigen specific cells were present within the muscle section. Biotinylated BSA was used as a negative control protein. Images taken at 400X.

Figure 6.5.2 - Muscle sections from sample MYO23 were stained for Plasma cells (**A**) and CD20 (**B**) and biotinylated Jo-1. Cell phenotypes were visualised by Fluorescein Avidin D and antigen specific cells by Texas Red Avidin D. This allowed the phenotype of antigen-specific cells within the myositis sample to be identified. Images were taken at 630X; Scale Bar represents 15 µm. Arrows identify antigen specific cells within the sections.

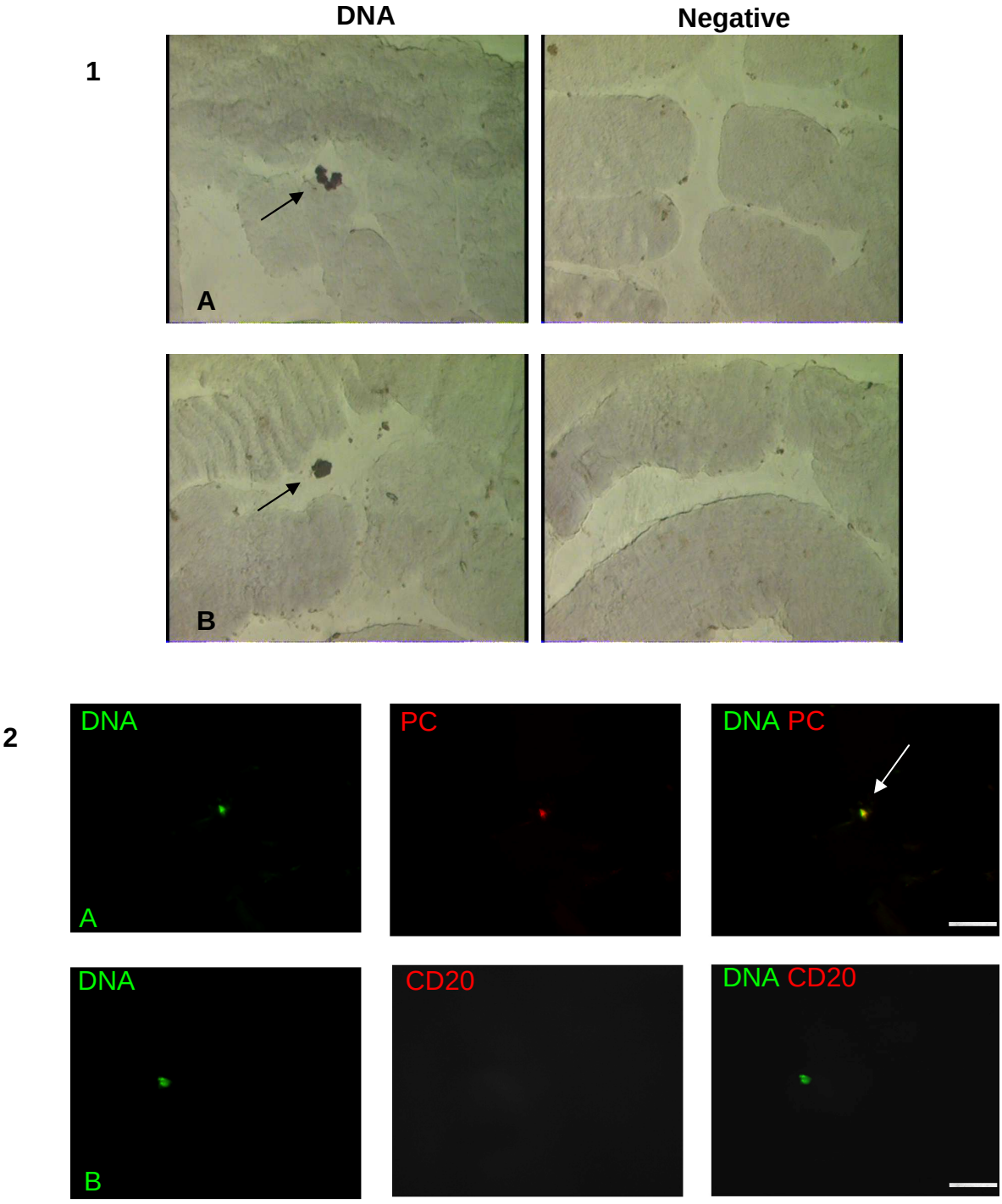

Figure 6.6 Immunohistochemical staining using biotinylated antigen in Sample MYOE

Figure 6.6.1 - Muscle sections from sample MYOE were stained with biotinylated antigen, DNA, (**A&B**) and visualised by APAAP and New Fuschin substrate to establish if antigen specific cells were present within the muscle section. Biotinylated BSA was used as a negative control protein. Images taken at 400X.

Figure 6.6.2 - Muscle sections from sample MYOE were stained for Plasma cells (**A**) and CD20 (**B**) and biotinylated DNA. Cell phenotypes were visualised by Texas Red Avidin D and antigen specific cells by Fluorescein Avidin D. This allowed the phenotype of antigen-specific cells within the myositis sample to be identified. Images were taken at 630X; Scale Bar represents 15 µm. Arrows identify antigen specific cells within the sections.

6.3 Sequence Identification of Antigen-Specific Cells

After identification of antigen specific cells within these 5 myositis patients, and the confirmation of these cells as B cells or plasma cells by double staining immunofluorescence experiments, further nested PCR reactions were conducted to identify the immunoglobulin genes of these antigen-specific cells. Antigen-specific cells were isolated using laser capture microdissection (**Figure 6.7**) and the Ig genes were amplified from the RNA released from these cells using the methods described in Chapter 2. These experiments were only in the primary stages and from the microdissections from Figure 6.7 a rearranged immunoglobulin sequence was isolated from sample MYO16 for a $Scl70^{+}$ cell which displayed sequence characteristics of an antigen-driven response (**Table 6.1**). This V_H5-51 gene rearrangement contained 14 different point mutations which were concentrated within the CDR, mostly CDR1; a sequence characteristic of a B cell from antigen-driven response or a memory B cell. Despite this no significant selection was observed in either the CDR or FW regions of the sequence. This gene rearrangement was not observed in any other patients, including MYO16 which could be the result of using tissue sections from different depths of the biopsy and also cannot be a result of contamination. Additional isolation and amplification of immunoglobulin genes for antigen-specific cells would provide greater insight into the gene rearrangements of cells specific for autoantigens.

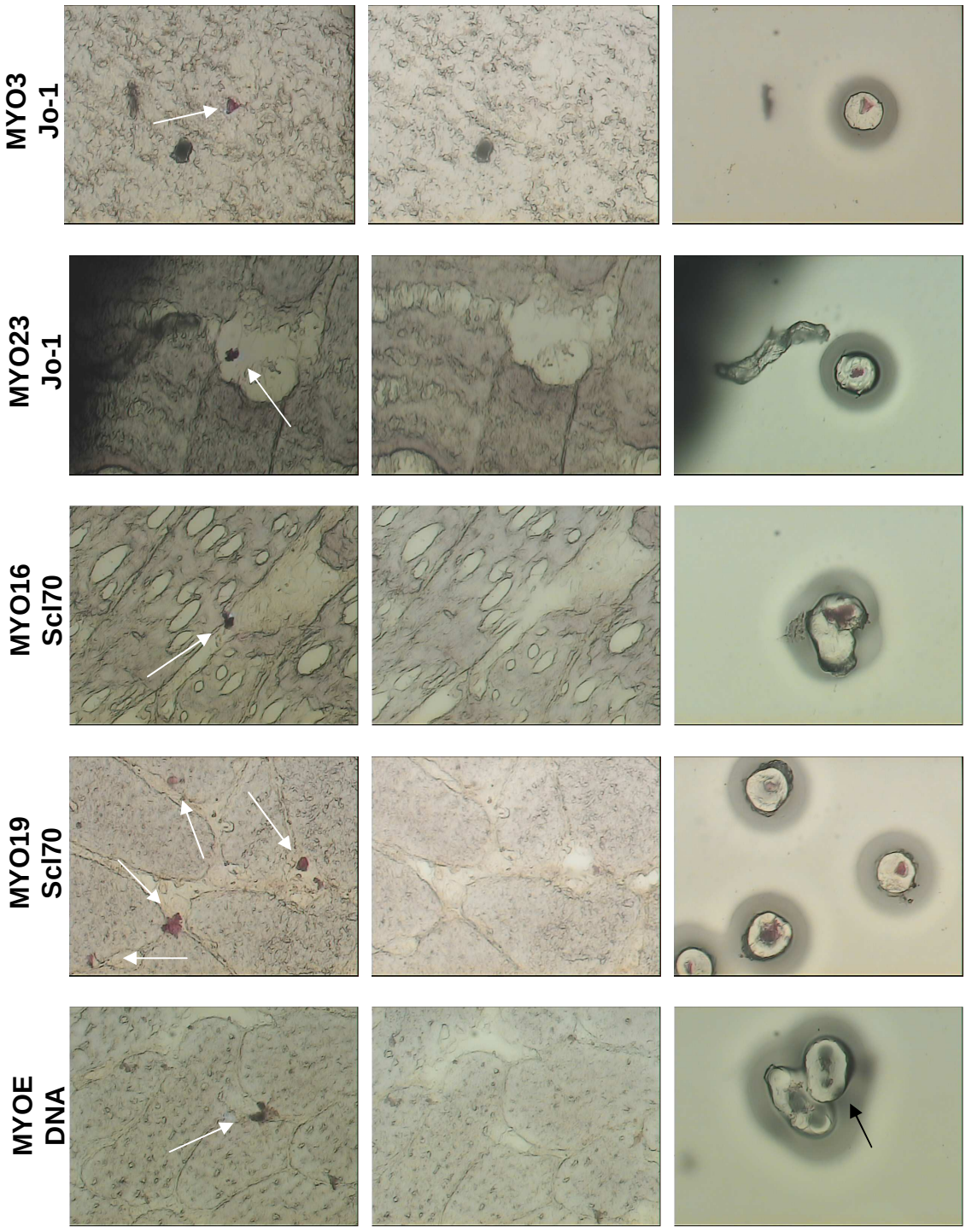

Figure 6.7 Laser Capture Microscopy for Antigen-Specific Cells in Myositis Patients

Laser-capture microscopy for single antigen specific cells identified by APAAP staining using biotinylated recombinant antigens. Arrows denote antigen-specific cells to be microdissected. Images taken after antigen specific cells have been microdissected, both in the muscle section (middle column) and on the LCM HS Cap (right-hand column). All images taken at x400.

V_H Gene	D_H Gene	J_H Gene	Number of Mutations	V-J Length (bp)	Consecutive D Match Length (bp)
5-51*01	No D Gene Assignment	2*01	14	28	7

CDR3	Mutational Distribution (% of length)		
	Framework	CDR1	CDR2
ARREDSGPLHWFFDL (15aa)	3.6	20	6

R-CDR	S-CDR	pCDR	p-CDR	R-FW	S-FW	pFW	p-FW
6	0	0.4336	0.18182	5	3	0.69714	-0.6548

Table 6.1 Sequence Analysis from Scl70 Positive Cell from Patient MYO16

Best matching germline sequences were identified from aligning sequences in the IMGT database using JOINSOLVER software. V-J lengths and consecutive D match lengths (bp) were also identified using the JOINSOLVER software to allow assignment of the D_H genes as described in section 2.3.12.3. The number of mutations within functional rearranged V_H genes were analysed, base differences within the first 24 bases of sequence were disregarded as this part of the sequence binds the 5' V_H primer. The locations of V_H mutations were categorised as being within FR or CDR regions. The numbers of mutations were expressed as a percentage of the entire length of the region to correct for the longer lengths observed within the framework regions. The number of replacement and silent mutations and the presence of any positive and negative selection was conducted as per Hershberg *et al* (294) as previously described. R-CDR/FW and S-CDR/FW represent the number of replacement and silent mutations in the CDR and FW respectively. pCDR represents the probability of having a R mutation in the CDR given all the mutations in the sequence except R mutations within the FW while pFW represents the probability of having a R mutation in the FW given all the mutations in the sequence except R mutations within the CDR and p-CDR/FW represent the p-value of the focused binominal test on the CDR and FW respectively. A negative sign indicates negative selection. p-values <0.05 were deemed significant.

6.4 Discussion

Previous results in this study have demonstrated antigen-driven diversification of infiltrating cells within the target tissues of myositis and vasculitis patients either by the identification of clonally related sequences or antigen-driven sequence characteristics such as gene selection and mutational patterns. Collectively the results may indicate local antigen stimulation within the target tissues and/or stimulation at other sites, presumably the draining lymph nodes, resulting in migration of affinity matured lymphocytes into the target tissues of these autoinflammatory disorders. Regardless of the location of antigen stimulation, the results presented thus far do not provide information on the identity of the stimulating antigen. In some of the myositis cases, autoantibodies were detected in serum samples from the patients therefore the presence of antigen positive cells for these autoantibodies within myositis samples was tested. Biotinylated recombinant antigens were used to determine if antigen specific cells were part of the infiltrating repertoire of myositis samples.

The results presented in this chapter demonstrate that autoantigen-specific cells were included within the inflammatory infiltrating cell population in myositis samples. Antigen positive cells were identified in each of the five myositis cases for all four antigens tested and were identified as a combination of B cells and plasma cells. Most of the antigen specific cells formed small clusters of cells or existed as single isolated cells. Staining for Sm/RNP produced a very different pattern of staining, extensive staining was observed throughout the entire section between the muscle fibres. Individual antigen positive cells could not be observed amongst the widespread staining which may have occurred due to enhanced antibody secretion from infiltrating plasma cells. Taking the frequency of the other antigen-positive cells in comparison to the number of B cell or plasma cell infiltration, identified in Chapter 3, results from these experiments may indicate that other antigens are also participating in the inflammatory response. In most of the cases described in this chapter there was a small number of antigen positive cells in comparison to the number of infiltrating B cells or plasma cells observed in Chapter 3. A wide range of additional antigens or modified version of the antigens used in these experiments may be responsible for some of the remaining infiltrating cells. The other autoantigens tested for in these five patients have also been observed in other disorders and may indicate myositis as a secondary disorder within these patients; DNA, in the form of dsDNA, and Sm are specific for SLE, which is also associated with RNP autoantibodies and Scl70 antibodies are generally observed within systemic sclerosis (scleroderma) patients.

The presence of antigen-specific plasma cells could indicate that B cells were stimulated and underwent diversification in other locations and that antigen specific plasma cells migrated into areas of muscle inflammation. It is also possible that B cells are being stimulated directly within the muscle and the B cells are also undergoing maturation and diversification into plasma cells at the sites of inflammation within the muscle. Following the confirmation of the phenotypes of the antigen specific cells, the cells were isolated by laser capture microdissection to establish the immunoglobulin gene rearrangements used by these antigen-specific cells. These experiments were only in the primary stages and only a few samples were tested prior to completion of this study. From the

samples tested a single gene rearrangement was isolated from Scl70^{+} cells in patient MYO16. This gene rearrangement or gene family was not observed in the original gene repertoire described in Chapter 4 where selection against V_H5 gene segments was also observed. Variations in the gene rearrangements isolated for MYO16 could be attributed to different serial sections being used for the different experiments; each section could possibly contain B cells expressing alternative gene rearrangements not observed in previous sections. Due to the difficulty for successful Ig amplification from a small number of antigen specific cells, additional testing of isolated antigen-specific cells would establish if this gene rearrangement is specific for Scl70 antigen positive cells or if additional gene rearrangements are specific for the Scl70 antigen. Also, additional testing of the other antigen positive cells would allow the gene rearrangements specific for the other antigens to be assessed. Similar studies could also be conducted on two of the vasculitis patients as these patients tested positive for Ro, La and c-ANCA autoantibodies (Table 2.3); these patients were not included in the original study due to a lack of recombinant antigen.

Similar studies to those discussed in this chapter have been conducted in other autoimmune disorders, SS, MG, WG, Hashimoto's Thyroiditis (HT) and most recently in RA. Tengnér *et al* (358) demonstrated the presence of Ro/SSA and La/SSB antibody producing cells in salivary gland biopsies from SS patients indicating that anti-Ro/SSA and anti-La/SSB autoantibodies were produced and present at the sites of inflammation implicating their involvement within the disorder. Biotinylated antigens were used to identify antigen positive cells which were thought to exhibit plasma cell morphology. These antigen-specific cells appeared scattered, singularly or in clusters primarily within the inflammatory infiltrates, findings similar to that presented in this chapter. The study also established that patients with higher levels of serum autoantibodies contained higher numbers of autoantibody producing cells within the salivary glands. Salomonsson *et al* (359), in a later study into the ectopic germinal centre formation in SS, also used biotinylated recombinant antigens (Ro and La) as probes and located antigen-specific cells within salivary gland biopsies of SS patients. The frequency of these positive cells was significantly higher in

patients with germinal centre formation compared to those without germinal centres. The study demonstrated that these antigen-specific cells were located at the periphery of the inflammatory infiltrates and also demonstrated a strong correlation between local salivary gland production and serum autoantibodies. Although present at the sites of inflammation it has also been shown that some autoantibody producing cells for Ro/SSA and La/SSB are present in the circulating peripheral blood (360).

Antigen-specific cells have also been identified in the thymus of Myasthenia Gravis patients (52;361). MG is mediated by autoantibodies directed against various epitopes of the adult acetylcholine receptor (AchR) at the neuromusclular junction, resulting in muscle weakness. These autoantibodies can also bind to the foetal AchR also present in the thymus. Sims *et al* (52) used complexes containing an antagonist of AchR function, ^{125}I-αBungarotoxin (αBuTx), to identify the occurrence of AchR antigen-specific cells within the thymus. Approximately 50% of the germinal centres present within the thymus contained antigen positive cells, in a similar pattern to the FDC network. Results demonstrated that the germinal centres containing these antigen-specific cells were undergoing antigen-driven clonal proliferation, somatic hypermutation and selection. In a subsequent study Matthews *et al* (361) demonstrated that autoantibodies directed towards the foetal AchR were significantly more common in females sampled after pregnancy than those who present before pregnancy suggesting that they may be induced by the foetus. Cloning the Fabs of these high affinity antibodies demonstrated that these antibodies used the V_H3-07, 4-61, 3-23 and 3-21 gene segments. These antibodies were shown to undergo clonal diversification and antigen-driven selection.

While analysing the V_H gene repertoires of infiltrating B cells from endonasal lesions in WG patients Voswinkel *et al* (348) identified PR3-ANCA positive cells in the vicinity of B cell-rich follicle-like structures and plasma cells. The authors suggest that potentially PR3-ANCA producing cells might be selected in PR3$^+$ granulomatous lesions starting in localised WG and continuing in generalised WG. Armengol *et al* (54) demonstrated the presence of antigen-specific cells

within active intrathyrodial germinal centres of Hashimoto thyroditis patients, an autoimmune thyroid disease. Antigen specific cells to two thyroid-specific antigens were found to be present within GCs, thyroglobulin (Tg) and thyroperoxidase (TPO). The results showed that two types of cells bound the thyroid antigens; numerous small cells, which demonstrated a similar distribution to B cells, as well as strongly positive cells with a strong cytoplasmic staining scattered all over the lymphoid follicles within the thymus, plasma cells. Double staining experiments revealed that most of the antigen specific cells were also IgG^+. Results of this study suggest that intrathyrodial lymphoid follicles were committed to thyroid antigen immune responses. Recently anti-citrullinated protein/peptide antibody (ACPA) producing plasma cells were identified in the synovial tissue of RA patients using biotinylated citrullinated fibrinogen in double immunofluorescence experiments (55). These antibodies are highly specific markers for RA and are potentially pathogenic.

In summary, the work presented in this chapter demonstrated that antigen-specific B cells and plasma cells are present within sites of inflammation in myositis patients and support previous studies where antigen specific cells were found at ectopic sites in autoimmune diseases. These results in conjunction with those of Chapter 4, identifying clonally related sets of genes, indicate that B cells may be stimulated at the site of inflammation demonstrating that an antigen-driven response occurs within the muscle but it may also be possible that cells are also stimulated at other sites and migrate into the sites of inflammation within the muscle. Additional, but extremely preliminary, experiments to identify the immunoglobulin genes of these antigen-specific cells isolated the gene rearrangements and sequence of a $Scl70^+$ cell. The mutational characteristics of the isolated gene support the occurrence of an antigen-driven response, possibly within sites of muscle inflammation but as previously mentioned these reactions may also occur at other sites leading to migration of antigen specific cells into inflamed muscle. Further analysis of immunoglobulin genes from antigen-specific cells would be required to provide further insight into the gene rearrangements, sequence mutations and clonal diversification mechanisms occurring within inflamed muscle specific to autoantigens.

Chapter 7 – General Discussion

Of paramount importance in the understanding of autoimmune inflammatory disorders is whether highly specific B cell antigen-driven adaptive immune responses are present within the target tissues of these disorders. In the current study this question was addressed in the target tissues, muscle and skin, of myositis and vasculitis patients respectively by examining the Ig repertoire and mutational characteristics of tissue infiltrating B and plasma cells and establishing if clonal diversification and affinity maturation mechanisms were ongoing within the target tissues. Collectively the data presented in this thesis demonstrated that antigen-driven B cell responses were occurring within inflamed muscle of the various myopathy subsets. Ig gene selections and oligoclonal expansion of B cells were observed in these samples signifying that muscle infiltrating B cells were being stimulated by antigen(s) within the muscle and could contribute to the pathological mechanisms in play at the sites of inflammation. Conversely in inflamed skin, gene selections and oligoclonal expansion were not observed from the sequences isolated from skin infiltrating cells indicating that there is no antigen driven B cell responses occurring within the inflamed skin but infiltrating plasma cells, outwith their normal bone marrow residence, may be contributing to the response and the pathology within the skin through the secretion of autoantibodies. Ig sequences isolated from these cells contained antigen-driven sequence characteristics. At the commencement of this work no other study had established these antigen-driven responses within these target tissues and despite the different outcomes of both disorders of this study the results presented do suggest the active participation of antigen-driven responses in the target tissues of autoimmune disorders as well as a role for B cells in the pathophysiology of these diseases.

The main objective of this work was to test the hypothesis that B cells play an antigen-driven role within these disorders. In some instances disorders are characterised as B cell mediated due to the presence of autoantibodies which are implicated in the associated pathology of the disease. In others, despite the presence of autoantibodies, disorders are categorised, or previously have been categorised, as T cell mediated disorders and the true involvement of B cells within these disorders was not fully recognised until studies, similar to the

current study, have identified biased gene repertoires and oligoclonal expansion of B cells within target tissues. Such studies support the involvement of B cells within the complex immune responses in the target tissues of these disorders which could be associated with the pathological mechanisms involved and provide a greater understanding into the course of autoimmune disease. Such studies have been conducted in a number of diseases including SLE, RA, MG, SS, MS, OS and AS (52;283;284;289;317-325;362). Despite the different methodologies and source tissues involved in all these studies, the results are in parallel with those described in this study, particularly in the myositis disorders. In each study a bias in the Ig gene repertoires was found along with the identification of gene segments which were clonally expanded in immune reactions within the target tissues, providing insights into the usage of preferred V_H gene families and possible gene dysregulation in response to antigen within these autoimmune disorders. Additional studies could indicate if certain gene combinations are prone to mutations which result in high affinity autoantibodies or are associated with pathogenicity. Subsequent to this, work has been conducted which has used the sequences generated in such studies to analyse the lineage trees generated from the clonally expanded B cells (363-366). Lineage trees were constructed from published Ig sequences from ectopic germinal centres or affected tissue B cell clones in patients with various autoimmune disorders using the IgTree© algorithm (366). These were then compared to lineage trees from normal PBL and germinal centre samples using MTree©, a computer aided algorithm for the measurement of graphical shape properties of lineage trees. This method allowed the interplay between somatic hypermutation and antigen-driven selection in different lymphoid tissues and disease situations to be assessed while alleviating the effects of different experimental protocols between research groups. Comparing lineage trees from diseased states with normal controls demonstrated that lineage trees generated from autoimmune disorders were larger than in normal controls. Analysis of mutational characteristics suggested a more vigorous diversification process and accumulation of more mutations within autoimmune disorders compared with normal controls; lineage trees from autoimmune disorders demonstrated a longer diversification process. The changes in B cell selection were also assessed from clonal trees based on the degree of tree branching

and were found to be similar between normal controls and autoimmune disorders suggesting a normal selection strength acting on the B cells within autoimmune disorders. However a recent study (367) by this group in ulcerative colitis (UC) using these methodologies revealed no significant difference in tree shape properties between sequences isolated from UC samples and control samples. In this study normal Ig gene diversification and trafficking of clones between the gut and associated lymph nodes was observed.

Antigen-driven reactions are typically thought to occur within the confinements of GC structures in secondary lymphoid organs but are commonly found in the target tissues of several autoimmune diseases. As previously described, the functionality and potential contribution of these GC reactions in disease pathogenesis has recently been described in SS and RA patients (55;326). In addition to these GC reactions the enzyme required for SHM and CSR, AID, has been observed and found to be functional in a subset of B cells outside GCs. Prior to this, studies have described antigen-driven reactions occurring outside GCs. These reactions were found to occur outside GC structures in areas lacking a FDC network in autoimmune murine models (301;332;333). It has been postulated that such reactions give rise to autoreactive B cells which are not governed by the protective mechanisms that occur within GCs. The cells participating in these extrafollicular reactions were found to be activated B cells as well as plasmablasts, the dominant producer of autoantibodies in these models (333;368;369). These findings have been extended to mice with normal backgrounds and collectively implicate that factors such as antigen density, T cell help, BCR affinity and TLR signals may regulate the occurrence of extrafollicular responses and GC responses (332;370-372). Another study has demonstrated affinity maturation by SHM in a lymphotoxin-α mouse models which fails to develop germinal centres (255). In the current study clonal diversification of B cells has been observed within the target tissues of myositis patients although no GC structures were observed. Such studies do not exclude the involvement of GC reactions but indicate an alternative pathway for the disease mechanisms generating autoantibodies towards self antigens. Contrary to this Cantaert *et al* concluded that synovial lymphoid neogenesis

was a process associated with inflammation and was independent to B lymphocyte autoimmunity (373).

As well as identification of clonally expanded B cells the outcomes of such studies also provide insight into the mechanisms of diversification in play during autoimmune reactions. Mechanisms such as receptor revision and codon insertions and deletions can also be examined to establish if defects or irregularities in these mechanisms contribute to the repertoire and pathogenicity of autoimmune reactions. Class switching is another mechanism which can be analysed from gene repertoire studies, providing that constant region primers have been used. As previously described in Chapter 4, section 4.3.1, class switching to other isotypes, including IgA, is evident within the infiltrating B and plasma cell populations in myositis samples (90) and authors hypothesised that the different Ig isotypes may have a broader role in autoimmunity, especially IgA which would normally reside on mucosal surfaces. Class switching has been identified by various methods in a number of myositis studies by this group (89;90) and the presence of isotype switched secreting plasma cells (IgA, IgG and IgM) has also been observed in MS (374). IgA secreting plasma cells, as previously described, are also thought to contribute to the pathology associated with a subset of vasculitis, KD (171). The work of Bradshaw *et al* (90) demonstrated that this class switching was occurring within the muscle with the identification of clonal variants with different isotypes. The process of class switching in target tissue of autoimmune disorders has recently been substantiated by the identification if AID in the target tissues of SS and RA patients (326). The findings of such studies enhance the understanding of immune mechanisms within the target tissues of autoimmune disorders and indicate that these responses are occurring within the target tissues and not solely within the periphery resulting in infiltration into target tissues. This would be especially significant in the two disorders of the current study where no classic germinal centre structures, the typical site of class switch recombination, were observed. Identification of Ig gene repertoires and oligoclonal expansion of autoreactive B cells can also provide the foundation for examining the mechanism of somatic hypermutation and the influence of particular mutations on antigen affinity within these sequences. Studies have been conducted on

anti-dsDNA antibodies isolated from SLE patients which demonstrate the influence of particular mutations on antigen affinity (375-379). Li *et al* (375) established that the binding activity of a monoclonal anti-DNA antibody, with 11 somatic mutations, to its target antigen was mediated through Arg105 and Arg107. Conversion of each of these residues, independently, to glycine resulted in comparable binding efficiency to ssDNA and to that of the original antibody but the binding efficiency to dsDNA was lost, indicating that both arginine residues were required for dsDNA binding but either was sufficient for ssDNA binding. More recently (376) a combinational library was constructed from splenic lymphocytes of a male patient with active SLE. Selection against dsDNA isolated 15 IgG Fabs where a strong correlation was observed between the R:S ratios on the CDRs 1 and 2 and affinities for ssDNA and dsDNA; high R:S ratios correlated with increased affinity. Subsequent studies have also linked arginine mutations to DNA antigen affinity but have also gone onto demonstrate the relationship between somatic mutations that influence the affinity to multiple antigens rather than focussing on one antigen (377-379). Specific heavy chain and light chain mutations have been found that can either enhance an antibody affinity to DNA or eliminate the affinity. For the light chains involved in these experiments arginine residues at position 94 (CDR3) in one light chain abolished DNA binding while somatic mutations resulting in an arginine residue at position 92 in two other light chains had the opposite effect. The work of this group also observed that a mutation to an arginine residue at position 27 within CDR1 played a role in binding to histones, further enhancing the affinity for dsDNA and was confirmed by a reduction in binding when the residue was altered to serine. In the heavy chain of these anti-DNA antibodies an arginine residue at position 53 (CDR2) was found to contribute to the enhanced DNA binding. Conversion of this residue to 3 other variants by site directed mutagenesis and the germline configuration of the gene resulted in reduced binding to DNA. A mutation within the germline at position 53 was also found to be insufficient for binding indicating that other mutations or sequence characteristics are required. The mutation at position 53 was also shown to enhance the antibody binding to a number of other antigens, α-actinin and glycoproteins which are significant in the pathogenesis of antiphospholipid syndrome (APS). Such studies examine the effects of somatic hypermutation

on the relationship between sequence, structure and antigen binding and highlight the influence of individual somatic mutations in autoantibodies.

As previously described in Chapter 1 the B cell depletive therapy, Rituximab, has emerged as an influential therapeutic strategy in the treatment of both myositis and vasculitis, in addition to a number of other autoimmune disorders where clinical improvements, stabilisation and remission are observed in patients (140-145;147;148;150-152;159;202;203;205;206;355;380-384). This is further substantiated by the emergence of alternative B cell depletive therapies which are targeting B cells from alternate approaches (385) and fully illustrates the importance and contribution of B cells within these disorders. Although this therapy has been found effective in various studies the emergence of B cell populations associated with clinical relapses, variations in autoantibody and autoantigen levels, which may suggest that some of the underlying disease mechanisms are still ongoing, and the wider immunological effects such as cellular modulations (386;387) illustrates the complexity of the B cell role within autoimmune disorders. In the context of this study, many studies examining the Ig gene repertoire and diversification of B cells within target tissues or peripheral blood of autoimmune patients are conducted prior to specifically targeted therapeutic interventions and the impact of therapies like Rituximab on the repertoire and diversification of B cells within target tissues or peripheral blood have not been extensively studied. Studies have been conducted in RA which examined the peripheral blood repertoire following Rituximab therapy (388) which illustrated that the use of Rituximab resulted in subtle modulation of the RA repertoire. Although the objective of this therapy is removal of $CD20^+$ populations of B cells, the influence and modulatory effect of Rituximab on the Ig repertoires of the remaining $CD20^-$ population of B cells along with the re-emerging $CD20^+$ populations would be of interest to study. Such studies would aid the understanding of Ig gene profiles associated with clinical remission and relapse as well as highlighting those Ig sequences that are of importance within the disorders.

The work presented in this thesis has focussed in on the antigen-driven role and diversification of B cells within the target tissues of myositis and vasculitis

patients but multifunctional roles have been attributed to B cells within immune responses, which influence and are influenced by an extensive number of parameters of the immune response. B cells are also capable of acting as antigen presenting, regulatory and stimulatory cells. Antigen-specific B cells are capable of taking up, internalising, processing and presenting antigen to T cells as well as other cells and may be the primary role of B cells in contributing to pathogenesis. These functions have been implicated in the initiation of immune responses, particularly those that are autoimmune. Antigen presentation by B cells could enhance the antibody production and expansion of antigen specific B and T cells, thus intensify the immune response to self antigens. Studies have shown that antigen specific B cells can capture soluble antigen and initiate a T cell response earlier than DCs and recently the transfer of antigen from B cells to other antigen presenting cells, macrophages, has been observed which could possibly lead to amplification or editing of antigen specific immune responses resulting in chronic autoimmune responses (313;389). The B cell receptor (BCR) is proposed to play a significant role in antigen presentation by B cells; antigens are internalised by receptor-mediated endocytosis in B cells, a mechanism carried out by the BCR. Two features of antigen processing within B cells are not observed within other APCs. Firstly BCR ligation with antigen induces internalisation and directs the BCR–antigen complex through the endocytic pathway towards MHC class II rich compartments promoting the formation of MHC class II-peptide complexes (390). The signalling resulting from BCR ligation upregulates MHC class II expression and stimulates their traffic through the same compartments used by the antigen-BCR complexes (391). These methods allow B cells to combine antigen recognition with the complexes in charge of its processing, favouring presentation of these internalised antigens in comparison to antigens internalised by pinocytosis. Secondly, antigen processing within B cells has been shown to induce the expression of HLA-DO, a non-classical MHC class II molecule which functions to inhibit the actions of HLA-DM, which favours presentation of peptides derived from antigen internalised through the BCR (392). Receptor-mediated endocytosis through the BCR also allows the concentration of very small quantities of antigen for efficient presentation. It has been reported that BCR affinity is directly proportional to the capacity of the B cell to participate in

antigen presentation to $CD4^+$ T cells (393). The study also demonstrated that presentation via the pinocytosis method required a 5000 fold increase in antigen concentration. In SLE, B cells have been shown to act as APCs of the target antigen snRNP (394). Transfer of B cells obtained from mice primed with snRNP from a different species lead to autoreactive $CD4^+$ T cell activation. Transgenic mice expressing a BCR specific for snRNP was also used in studies to demonstrate that high numbers of autoantigen-specific B cells can activate $CD4^+$ T cells in an autoimmune background and tolerize them in a wild-type background, supporting the role of B cells as pathogenic APCs (395). Anti-DNA B cells in lupus have also been shown to act as APCs (396).

In addition to their possible role as antigen presenting cells, B cells have been shown to exert effects through possible regulation of immune responses in autoimmune disorders. A subset of B cells, regulatory B cells, exist that suppress the exacerbation of and/or enhance the recovery from acquired immune-mediated inflammations by mechanisms that include IL-10 and TGF-β1 production, secondary antigen presentation and interaction with other immune cells either directly or through secreted antibodies (397). B cells have the ability to produce detectable quantities of immunoregulatory cytokines such as IL-2, IFN-γ, IL-12 and IL-4 in addition to IL-6, TNF-α and IL-10 which have a long term association with B cells (398). Two populations of effector B cells were identified, Be1 and Be2. Both cell types produced IL-2, IL-6 and IL-10 upon restimulation but higher levels were observed within Be2 cell populations, Be2 cell populations also produced IL-4 while Be1 cells produced IFN-γ; only trace amounts of IFN-γ were observed in Be2 cells while IL-4 was completely absent from Be1 populations. The role of these cytokine profiles in regulating T cell differentiation was studied by addition of cytokine-blocking antibodies to cultures of effector B cells and naïve T cells. Anti-IFN-γ added to cultures containing Be1 cells and T cells severely reduced the IFN-γ production produced by the effector T cells, suggesting that IFN-γ produced by Be1 cells was sufficient to differentiate T cells into IFN-γ producing effector-cells. Similar cultures containing Be2 cells and anti-IL-4 antibodies demonstrated the requirement of IL-4 to differentiate T cells to Th2-like cells. The use of anti-IL-4 antibodies resulted in no detectable levels of IL-4, IL-5, IL-6 or IL-10, but

conversely produced increased levels of IFN-γ indicating that Be2 cells may negatively regulate the differentiation of T cells into IFN-γ producing cells. Results suggest that like other APCs, effector B cells have the capacity to regulate the type of immune response generated in response to antigen.

With a focus on the inflammatory myopathies, widespread studies have been conducted examining the various cell phenotypes within myositis, as well as other autoimmune disorders, as previously described in Chapter 3. Such studies demonstrate the complex nature of immune responses and are required to analyse the B cell response in context with the overall immune mechanisms. The influence of cytokines and chemokines on the responses involved in autoimmune disorders is also of interest. In recent studies levels of BAFF/BLys (B cell activating factor/B lymphocyte stimulator), which is crucial in B cell maturation and survival and is also thought to play a role in autoantibody production, have been examined in serum samples of myositis patients (42). Serum levels were found to be elevated in myositis patients compared to control individuals and it was also noted that patients with DM or anti-Jo-1 autoantibodies had higher serum levels compared to other myositis subsets or other patients without any specific autoantibodies respectively. BAFF levels were also shown to correlate positively with CK levels and negatively with glucocorticoid treatment. This study demonstrates the important role of B cells, and BAFF, in myositis patients and provides further insights into the mechanisms involved within the muscle but could also relate to mechanisms of other disorders such as vasculitis. Following Rituximab therapy in SS patients, the repopulation of B cells has been shown to be modulated by BAFF (399) which again demonstrates the importance for further studies on B cells within autoimmune disorders. A marked increase in BAFF levels have also been observed in RA and SLE patients following Rituximab therapy which declined with the re-emergence of B cells (380;400). It has been suggested that elevated BAFF levels in myositis samples are induced by the type I IFN system produced by PDCs (42); levels of type I IFN cytokines in DM and PM have been found to correlate with disease activity (305). As described in Chapter 3 these cell phenotypes have been identified within myositis patients and in addition to influencing BAFF serum levels these cells and their products have been shown

to act in the differentiation of plasma cells as well as antigen presenting cells, all of which could contribute to the functions and actions of B cells as well as the pathophysiology with inflamed muscle. Recently IFN-α stimulation has been shown to up-regulate Ro52, at both the messenger and protein levels (401); autoantibodies to Ro52 are found in correlation with anti-Jo-1 antibodies in myositis patients as well as in other autoimmune disorders. This stimulation was also shown to result in translocation of the Ro52 protein into the nuclear compartment from the cytoplasm which could contribute to the pathological mechanisms observed in myositis and other autoimmune disorders. A correlation, and possible link to disease mechanisms, between IFN-α and immune complexes containing anti-Ro52 autoantibodies has also been shown be Elorenta *et al* (123). Another cytokine, and cell phenotype, that is reported to contribute to the development of germinal centre derived autoantibodies and play a role in autoimmune disease is IL-17, produced by Th-17 cells which are a distinct population of $CD4^+$ T helper effector cell population that differs in phenotype and function from classical T helper cells (402-405). Initially IL-17 was characterised as a potent proinflammatory cytokine coordinating local tissue inflammation but it has also been linked with the induction of autoimmunity. Reduced or eliminated levels of this cytokine have been associated with a reduced autoantibody response, the cytokine has been associated with the development of RA, MS and inflammatory bowel disease and IL-17 had been found to accelerate and stabilise germinal centre reactions and autoantibody formation of enhanced somatic hypermutation although the exact mechanisms are unresolved. Continued characterisation of autoimmune reactions provides greater insight into the mechanisms involved in these diseases and how these may influence the roles and actions of B cells within these disorders.

In addition to the number of factors of the immune system which might regulate the immune response within the muscle of the myositis patients described in this study the muscle cells themselves are also thought to contribute to the responses. It has been proposed that muscle cells themselves may act as antigen presenting cells during inflammatory reactions (406), as well as modulating the function of other APCs (407) present within the muscle during

immune responses. Antigen presentation capabilities were demonstrated in human myoblasts, cultured from muscle which constitutively express MHC class I molecules but no detectable amounts of MHC class II. IFN-γ and TNF-α stimulation induced MHC class II expression which was necessary but not sufficient for functional antigen presentation to $CD4^+$ T cells. These functions of muscle cells have been shown to be mediated through expression of MHC and co-stimulatory molecules such as CD40, ICOSL and B7 ligands (408-415), mostly recently B7-H3 which was shown to be expressed on muscle cells from different myositis subsets and was found to be a potent inhibitor of immune $CD8^+$ mediated lysis of muscle cells (411). The active participation of muscle cells in immune responses is also supported by the variety of cytokines and chemokine secreted from muscle cells and the expression of cell adhesion molecules, ICAM-1, which results in the interaction between muscle and immune cells (406). As well as antigen presenting functions human skeletal muscle derived myoblasts were found to increase the phagocytic capacity of macrophages and modulate DC maturation (407).

Nagaraju *et al* (79) demonstrated that the sustained up-regulation of MHC Class I molecules in mice leads to self-sustaining myositis, with similar features to human myositis, and the production of MSAs. Results suggest that autoimmune myositis may occur as a consequence of an apparently non-specific event, like the sustained up-regulation of MHC Class I molecules.

Besides the study of antigen-specific immune responses, non-immune mechanisms are also thought to contribute to the pathology associated with myopathies. These mechanisms could also be related to the pathology in other target tissues such as the skin (86;416). One such nonimmune mechanism may be the endoplasmic reticulum (ER) stress response. The ER plays a critical role in the synthesis, folding, processing and exporting of newly synthesised proteins. The ER stress response occurs when there is an excess accumulation of proteins within the ER, which is greater than the muscle cells ability to process. Ischaemia, hyperhomocysteinemia, viral infections and mutations that impair protein processing may also result in the ER stress response. Cells have a variety of self-protection responses to ER stress and

include the up-regulation of the NF-κB pathway, up-regulation of protein assembly associated proteins to prevent further accumulation of proteins within the ER, reduction in protein translation to prevent further accumulation and cell death. This ER stress response has recently been proposed to participate in the pathological mechanisms associated with myositis. Nagaraju *et al* (86) demonstrated, using human myositis samples and tissue from class I MHC-transgenic mice, that ER stress responses are highly activated in both samples of myositis. Data also demonstrated that the NF-κB pathway is highly activated in myositis samples in response to ER stress. Activated NF-κB induces target genes including class 1 MHC which in turn further exacerbates the ER stress response, thus initiating a self-sustained loop. This pathway and its role in pathogenesis of myositis have also recently been demonstrated by Grundtman and Lundberg (416).

The work of this study has established an antigen-driven role for B cells in the target tissues of myositis and has demonstrated the potential influence of B cell antigen driven mechanisms from other sites on the target tissues of vasculitis patients where no direct and active mechanisms were observed. These findings are substantiated and correlate with other studies examining the role of B cells in such mechanisms. Despite this a number of questions still need to be explored to fully understand the mechanisms occurring within these autoimmune diseases. From the work of this study identification of the stimulating antigen(s), epitopes and sequence characteristics of the responding high-affinity antibodies would provide a greater insight into pathological mechanisms. Sequence characteristics of antigen specific cells were very transiently explored and examined in this study, Chapter 6, but further identification of Ig rearrangements and mutational characteristics of antigen-specific cells would greatly enhance the understanding of the antibody response to autoantigens. Alternative approaches could include the use of phage-display technologies (417-420) or production of recombinant antibody molecules to isolate high-affinity antibodies. Such methods have been used in the characterisation of antibodies in Wegener's granulomatosis to PR3 (421), SLE to DNA (422) and in subacute sclerosing panencephalitis (423). Antigen specificity, antibody affinity characteristics and the effects of individual

mutations on specificity or affinity between different members of the same clonally related set of Ig V-gene sequences could then be assessed in these antibodies. Computer modelling techniques could also be used on isolated antibodies to establish important characteristics of these antibodies such as selected mutations which contribute to autoantibody specificity and affinity. Patients with autoimmune disorders could mount immune responses to various and some as yet unidentified antigens and produce a wide range of pathogenic and non-pathogenic antibodies as a result. Characterisation of pathogenic antibodies and their stimulating antigens could assist the understanding of why some protein targets are selected in autoimmune disorders resulting in a loss of B cell tolerance and how the pathogenic antibodies mediate their actions which result in pathology. Such studies would also provide a greater insight into the initiation of such reactions and determine the compartmentalisation within target tissues or widespread actions of these reactions in the periphery. Wider studies could address the promotion and regulation of autoreactive B cells and how other cell phenotypes, cytokines and co-stimulatory molecules contribute to the development and maintenance of these autoreactive B cells. Ultimately further work is required to fully ascertain the role of B cells and their antibodies within the target tissues of autoimmune disorders as greater understanding of these roles will facilitate the diagnosis, treatment and management of disorders.

To conclude, the work of this study has examined the antigen-driven B cell responses in the target tissues of myositis and vasculitis patients and demonstrated that these responses are present and active within inflamed muscle of myositis patients but absent from inflamed skin of vasculitis patients. Despite this, pathological mechanisms in the skin, secretion of potentially pathogenic autoantibodies from infiltrating plasma cells for example, could still be influenced by antigen-driven B cell responses occurring at alternative sites, presumably in peripheral lymphoid organs or at other ectopic locations. The results of this study highlight the involvement of B cells within the target tissues of autoimmune disorders and provide a foundation for future characterisation of autoantibodies, autoantigens and the autoimmune reactions of these disorders.

Reference List

(1) Murphy K, Travers P, Walport M, Shlomchik M. Janeway's Immunobiology. Seventh ed. New York: Garland Science, 2008.

(2) Garrood T, Lee L, Pitzalis C. Molecular mechanisms of cell recruitment to inflammatory sites: general and tissue-specific pathways. Rheumatology (Oxford) 2006; 45(3):250-260.

(3) Ley K, Laudanna C, Cybulsky MI, Nourshargh S. Getting to the site of inflammation: the leukocyte adhesion cascade updated. Nat Rev Immunol 2007; 7(9):678-689.

(4) Springer TA. Traffic signals for lymphocyte recirculation and leukocyte emigration: the multistep paradigm. Cell 1994; 76(2):301-314.

(5) Weber C, Fraemohs L, Dejana E. The role of junctional adhesion molecules in vascular inflammation. Nat Rev Immunol 2007; 7(6):467-477.

(6) Pankhurst T, Savage CO. Pathogenic role of anti-neutrophil cytoplasmic antibodies in vasculitis. Curr Opin Pharmacol 2006; 6(2):190-196.

(7) Tesfamariam B, DeFelice AF. Endothelial injury in the initiation and progression of vascular disorders. Vascul Pharmacol 2007; 46(4):229-237.

(8) Woywodt A, Streiber F, de Groot K, Regelsberger H, Haller H, Haubitz M. Circulating endothelial cells as markers for ANCA-associated small-vessel vasculitis. Lancet 2003; 361(9353):206-210.

(9) Woywodt A, Goldberg C, Kirsch T, de Groot K, Erdbruegger U, Haller H, Haubitz M. Circulating endothelial cells in relapse and limited granulomatous disease due to ANCA associated vasculitis. Ann Rheum Dis 2006; 65(2):164-168.

(10) Meffre E, Wardemann H. B-cell tolerance checkpoints in health and autoimmunity. Curr Opin Immunol 2008; 20(6):632-638.

(11) Goodnow CC. Multistep pathogenesis of autoimmune disease. Cell 2007; 130(1):25-35.

(12) Goodnow CC, Sprent J, Fazekas de St GB, Vinuesa CG. Cellular and genetic mechanisms of self tolerance and autoimmunity. Nature 2005; 435(7042):590-597.

(13) Zhang Z, Zemlin M, Wang YH, Munfus D, Huye LE, Findlay HW, Bridges SL, Jr., Roth DB, Burrows PD, Cooper MD. Contribution of VH gene replacement to the primary B cell repertoire. Immunity 2003; 19:21-31.

(14) Darlow JM, Stott DI. VH Replacement in Rearranged Immunoglobulin Genes. Immunology 2005; 114:155-165.

(15) Wang YH, Diamond B. B cell receptor revision diminishes the autoreactive B cell response after antigen activation in mice. J Clin Invest 2008; 118(8):2896-2907.

(16) Allan S. Revising Autoantibody Responses. Nat Rev Immunol 2008; 8(9):660.

(17) Girschick HJ, Grammer AC, Nanki T, Vazquez E, Lipsky PE. Expression of recombination activating genes 1 and 2 in peripheral B cells of patients with systemic lupus erythematosus. Arthritis Rheum 2002; 46(5):1255-1263.

(18) Zhang Z, Wu X, Limbaugh BH, Bridges SL, Jr. Expression of recombination-activating genes and terminal deoxynucleotidyl transferase and secondary rearrangement of immunoglobulin kappa light chains in rheumatoid arthritis synovial tissue. Arthritis Rheum 2001; 44(10):2275-2284.

(19) Ueda H, Howson JM, Esposito L, Heward J, Snook H, Chamberlain G, Rainbow DB, Hunter KM, Smith AN, Di Genova G, Herr MH, Dahlman I, Payne F, Smyth D, Lowe C, Twells RC, Howlett S, Healy B, Nutland S, Rance HE, Everett V, Smink LJ, Lam AC, Cordell HJ, Walker NM, Bordin C, Hulme J, Motzo C, Cucca F, Hess JF, Metzker ML, Rogers J, Gregory S, Allahabadia A, Nithiyananthan R, Tuomilehto-Wolf E, Tuomilehto J, Bingley P, Gillespie KM, Undlien DE, Ronningen KS, Guja C, Ionescu-Tirgoviste C, Savage DA, Maxwell AP, Carson DJ, Patterson CC, Franklyn JA, Clayton DG, Peterson LB, Wicker LS, Todd JA, Gough SC. Association of the T-cell regulatory gene CTLA4 with susceptibility to autoimmune disease. Nature 2003; 423(6939):506-511.

(20) Hippen KL, Tze LE, Behrens TW. CD5 maintains tolerance in anergic B cells. J Exp Med 2000; 191(5):883-890.

(21) Smith K, Seddon B, Purbhoo MA, Zamoyska R, Fisher AG, Merkenschlager M. Sensory adaptation in naive peripheral CD4 T cells. J Exp Med 2001; 194(9):1253-1261.

(22) Thien M, Phan TG, Gardam S, Amesbury M, Basten A, Mackay F, Brink R. Excess BAFF rescues self-reactive B cells from peripheral deletion and allows them to enter forbidden follicular and marginal zone niches. Immunity 2004; 20(6):785-798.

(23) Barthlott T, Kassiotis G, Stockinger B. T cell regulation as a side effect of homeostasis and competition. J Exp Med 2003; 197(4):451-460.

(24) Cyster JG, Hartley SB, Goodnow CC. Competition for follicular niches excludes self-reactive cells from the recirculating B-cell repertoire. Nature 1994; 371(6496):389-395.

(25) Sakaguchi S. Naturally arising Foxp3-expressing CD25+CD4+ regulatory T cells in immunological tolerance to self and non-self. Nat Immunol 2005; 6(4):345-352.

(26) von Boehmer H. Mechanisms of suppression by suppressor T cells. Nat Immunol 2005; 6(4):338-344.

(27) Misra N, Bayry J, Lacroix-Desmazes S, Kazatchkine MD, Kaveri SV. Cutting edge: human CD4+CD25+ T cells restrain the maturation and antigen-presenting function of dendritic cells. J Immunol 2004; 172(8):4676-4680.

(28) Bouaziz JD, Yanaba K, Tedder TF. Regulatory B cells as inhibitors of immune responses and inflammation. Immunol Rev 2008; 224:201-214.

(29) Jamin C, Morva A, Lemoine S, Daridon C, de Mendoza AR, Youinou P. Regulatory B lymphocytes in humans: a potential role in autoimmunity. Arthritis Rheum 2008; 58(7):1900-1906.

(30) Fillatreau S, Sweenie CH, McGeachy MJ, Gray D, Anderton SM. B cells regulate autoimmunity by provision of IL-10. Nat Immunol 2002; 3(10):944-950.

(31) Mauri C, Ehrenstein MR. The 'short' history of regulatory B cells. Trends Immunol 2008; 29(1):34-40.

(32) D'Cruz DP, Khamashta MA, Hughes GR. Systemic lupus erythematosus. Lancet 2007; 369(9561):587-596.

(33) Lahita RGe. Systemic Lupus Erythematosus. Fourth ed. London: Academic Press, 2005.

(34) Needham M, Mastaglia FL. Inclusion body myositis: current pathogenetic concepts and diagnostic and therapeutic approaches. Lancet Neurol 2007; 6(7):620-631.

(35) Brewerton DA, Hart FD, Nicholls A, Caffrey M, James DC, Sturrock RD. Ankylosing spondylitis and HL-A 27. Lancet 1973; 1(7809):904-907.

(36) Brown MA. Breakthroughs in genetic studies of ankylosing spondylitis. Rheumatology (Oxford) 2008; 47(2):132-137.

(37) Christen U, von Herrath MG. Initiation of autoimmunity. Curr Opin Immunol 2004; 16(6):759-767.

(38) Atassi MZ, Casali P. Molecular mechanisms of autoimmunity. Autoimmunity 2008; 41(2):123-132.

(39) Vang T, Miletic AV, Bottini N, Mustelin T. Protein tyrosine phosphatase PTPN22 in human autoimmunity. Autoimmunity 2007; 40(6):453-461.

(40) Anderson MS, Venanzi ES, Klein L, Chen Z, Berzins SP, Turley SJ, von Boehmer H, Bronson R, Dierich A, Benoist C, Mathis D. Projection of an immunological self shadow within the thymus by the aire protein. Science 2002; 298(5597):1395-1401.

(41) Mackay F, Silveira PA, Brink R. B cells and the BAFF/APRIL axis: fast-forward on autoimmunity and signaling. Curr Opin Immunol 2007; 19(3):327-336.

(42) Krystufkova O, Vallerskog T, Barbasso HS, Mann H, Putova I, Belacek J, Malmstrom V, Trollmo C, Vencovsky J, Lundberg IE. Increased serum levels of B-cell activating factor (BAFF) in subsets of patients with idiopathic inflammatory myopathies. Ann Rheum Dis 2008.

(43) Valencia X, Yarboro C, Illei G, Lipsky PE. Deficient CD4+CD25high T regulatory cell function in patients with active systemic lupus erythematosus. J Immunol 2007; 178(4):2579-2588.

(44) Viglietta V, Baecher-Allan C, Weiner HL, Hafler DA. Loss of functional suppression by CD4+CD25+ regulatory T cells in patients with multiple sclerosis. J Exp Med 2004; 199(7):971-979.

(45) Lidar M, Lipschitz N, Langevitz P, Shoenfeld Y. The infectious etiology of vasculitis. Autoimmunity 9 A.D.; 42(5):432-438.

(46) Ang CW, Jacobs BC, Laman JD. The Guillain-Barre syndrome: a true case of molecular mimicry. Trends Immunol 2004; 25(2):61-66.

(47) Willison HJ. The immunobiology of Guillain-Barre syndromes. J Peripher Nerv Syst 2005; 10(2):94-112.

(48) Vanderlugt CL, Miller SD. Epitope spreading in immune-mediated diseases: implications for immunotherapy. Nat Rev Immunol 2002; 2(2):85-95.

(49) Christopher-Stine L. Statin myopathy: an update. Curr Opin Rheumatol 2006; 18(6):647-653.

(50) Leadbetter EA, Rifkin IR, Hohlbaum AM, Beaudette BC, Shlomchik MJ, Marshak-Rothstein A. Chromatin-IgG complexes activate B cells by dual engagement of IgM and Toll-like receptors. Nature 2002; 416(6881):603-607.

(51) Aloisi F, Pujol-Borrell R. Lymphoid neogenesis in chronic inflammatory diseases. Nat Rev Immunol 2006; 6(3):205-217.

(52) Sims GP, Shiono H, Willcox N, Stott DI. Somatic Hypermutation and Selection of B Cells in Thymic Germinal Centers Responding to Acetylcholine Receptor in Myasthenia Gravis. J Immunol 2001; 167(4):1935-1944.

(53) Salomonsson S, Jonsson MV, Skarstein K, Brokstad KA, Hjelmstrom P, Wahren-Herlenius M, Jonsson R. Cellular basis of ectopic germinal center formation and autoantibody production in the target organ of patients with Sjogren's syndrome. Arthritis Rheum 2003; 48(11):3187-3201.

(54) Armengol MP, Juan M, Lucas-Martin A, Fernandez-Figueras MT, Jaraquemada D, Gallart T, Pujol-Borrell R. Thyroid autoimmune disease: demonstration of thyroid antigen-specific B cells and recombination-activating gene expression in chemokine-containing active intrathyroidal germinal centers. Am J Pathol 2001; 159(3):861-873.

(55) Humby F, Bombardieri M, Manzo A, Kelly S, Blades MC, Kirkham B, Spencer J, Pitzalis C. Ectopic Lymphoid Structures Support Ongoing Production of Class-Switched Autoantibodies in Rheumatoid Synovium. PLoS Medicine 6[1], 0001-0017. 2009.

(56) Christopher-Stine L, Plotz PH. Adult inflammatory myopathies. Best Practice & Research Clinical Rheumatology 2004; 18(3):331-344.

(57) Christopher-Stine L, Plotz PH. Myositis: an update on pathogenesis. Current Opinion in Rheumatology 2004; 16(6):700-706.

(58) Dalakas MC, Hohlfeld R. Polymyositis and dermatomyositis. Lancet 362(9388):971-82, 2003.

(59) Dalakas MC. The molecular pathophysiology in inflammatory myopathies. La Revue de Medecine Interne 2004; 25(Supplement 1):S14-S16.

(60) Dalakas MC. Update on the molecular pathogenesis of inflammatory myopathies. Autoimmunity Reviews 2004; 3(Suppl. 1):S37-S39.

(61) Garton MJ, Isenberg DA. Clinical features of lupus myositis versus idiopathic myositis: a review of 30 cases. Rheumatology 1997; 36(10):1067-1074.

(62) Plotz P. The place of autoimmunity in myositis. Autoimmunity Reviews 3 Suppl 1:S36, 2004.

(63) Briani C, Doria A, Sarzi-Puttini P, Dalakas MC. Update on idiopathic inflammatory myopathies. Autoimmunity 2006; 39(3):161-170.

(64) Greenberg SA. Proposed immunologic models of the inflammatory myopathies and potential therapeutic implications. Neurology 2007; 69(21):2008-2019.

(65) Grundtman C, Malmstrom V, Lundberg IE. Immune mechanisms in the pathogenesis of idiopathic inflammatory myopathies. Arthritis Res Ther 2007; 9(2):208.

(66) Hewer E, Goebel HH. Myopathology of non-infectious inflammatory myopathies - the current status. Pathol Res Pract 2008; 204(9):609-623.

(67) Lundberg IE, Grundtman C. Developments in the scientific and clinical understanding of inflammatory myopathies. Arthritis Res Ther 2008; 10(5):220.

(68) Hilton-Jones D. Myopathies. Reviews in Clinical Gerontology 2001; 11:131-147.

(69) Harper CR, Jacobson TA. The broad spectrum of statin myopathy: from myalgia to rhabdomyolysis. Curr Opin Lipidol 2007; 18(4):401-408.

(70) Mukhtar RY, Reckless JP. Statin-induced myositis: a commonly encountered or rare side effect? Curr Opin Lipidol 2005; 16(6):640-647.

(71) Greenberg SA. Inflammatory myopathies: evaluation and management. Semin Neurol 2008; 28(2):241-249.

(72) Bohan A, Peter JB. Polymyositis and dermatomyositis (first of two parts). N Engl J Med 1975; 292(7):344-347.

(73) Bohan A, Peter JB. Polymyositis and dermatomyositis (second of two parts). N Engl J Med 1975; 292(8):403-407.

(74) Dalakas MC, Sivakumar K. The immunopathologic and inflammatory differences between dermatomyositis, polymyositis and sporadic inclusion body myositis. Curr Opin Neurol 1996; 9(3):235-239.

(75) Kovacs SO, Kovacs SC. Dermatomyositis. J Am Acad Dermatol 1998; 39(6):899-920.

(76) Gerami P, Schope JM, McDonald L, Walling HW, Sontheimer RD. A systematic review of adult-onset clinically amyopathic dermatomyositis (dermatomyositis sine myositis): a missing link within the spectrum of the idiopathic inflammatory myopathies. J Am Acad Dermatol 2006; 54(4):597-613.

(77) Sontheimer RD. Cutaneous features of classic dermatomyositis and amyopathic dermatomyositis. Curr Opin Rheumatol 1999; 11(6):475-482.

(78) Rider LG. The heterogeneity of juvenile myositis. Autoimmun Rev 2007; 6(4):241-247.

(79) Nagaraju K, Raben N, Loeffler L, Parker T, Rochon PJ, Lee E, Danning C, Wada R, Thompson C, Bahtiyar G, Craft J, Hooft van Huijsduijnen R, Plotz P. Conditional up-regulation of MHC class I in skeletal muscle leads to self-sustaining autoimmune myositis and myositis-specific autoantibodies. PNAS 2000; 97(16):9209-9214.

(80) Mantegazza R, Bernasconi P, Confalonieri P, Cornelio F. Inflammatory myopathies and systemic disorders: a review of immunopathogenetic mechanisms and clinical features. J Neurol 1997; 244(5):277-287.

(81) Seitz S, Schneider CK, Malotka J, Nong X, Engel AG, Wekerle H, Hohlfeld R, Dornmair K. Reconstitution of paired T cell receptor alpha- and beta-chains from microdissected single cells of human inflammatory tissues. Proc Natl Acad Sci U S A 2006; 103(32):12057-12062.

(82) Hofbauer M, Wiesener S, Babbe H, Roers A, Wekerle H, Dornmair K, Hohlfeld R, Goebels N. Clonal tracking of autoaggressive T cells in polymyositis by combining laser microdissection, single-cell PCR, and CDR3-spectratype analysis. Proc Natl Acad Sci U S A 2003; 100(7):4090-4095.

(83) Benveniste O, Cherin P, Maisonobe T, Merat R, Chosidow O, Mouthon L, Guillevin L, Flahault A, Burland MC, Klatzmann D, Herson S, Boyer O. Severe perturbations of the blood T cell repertoire in polymyositis, but not dermatomyositis patients. J Immunol 2001; 167(6):3521-3529.

(84) Mantegazza R, Andreetta F, Bernasconi P, Baggi F, Oksenberg JR, Simoncini O, Mora M, Cornelio F, Steinman L. Analysis of T cell receptor repertoire of muscle-infiltrating T lymphocytes in polymyositis. Restricted V alpha/beta rearrangements may indicate antigen-driven selection. J Clin Invest 1993; 91(6):2880-2886.

(85) Goebels N, Michaelis D, Engelhardt M, Huber S, Bender A, Pongratz D, Johnson MA, Wekerle H, Tschopp J, Jenne D, Hohlfeld R. Differential expression of perforin in muscle-infiltrating T cells in polymyositis and dermatomyositis. J Clin Invest 1996; 97(12):2905-2910.

(86) Nagaraju K, Casciola-Rosen L, Lundberg I, Rawat R, Cutting S, Thapliyal R, Chang J, Dwivedi S, Mitsak M, Chen YW, Plotz P, Rosen A, Hoffman E, Raben N. Activation of the endoplasmic reticulum stress response in autoimmune myositis: potential role in muscle fiber damage and dysfunction. Arthritis Rheum 2005; 52(6):1824-1835.

(87) Arahata K, Engel AG. Monoclonal antibody analysis of mononuclear cells in myopathies. I: Quantitation of subsets according to diagnosis and sites of accumulation and demonstration and counts of muscle fibers invaded by T cells. Ann Neurol 1984; 16(2):193-208.

(88) Engel AG, Arahata K. Monoclonal antibody analysis of mononuclear cells in myopathies. II: Phenotypes of autoinvasive cells in polymyositis and inclusion body myositis. Ann Neurol 1984; 16(2):209-215.

(89) Greenberg SA, Bradshaw EM, Pinkus JL, Pinkus GS, Burleson T, Due B, Bregoli L, O'Connor KC, Amato AA. Plasma cells in muscle in inclusion body myositis and polymyositis. Neurology 2005; 65(11):1782-1787.

(90) Bradshaw EM, Orihuela A, McArdel SL, Salajegheh M, Amato AA, Hafler DA, Greenberg SA, O'Connor KC. A local antigen-driven humoral response is present in the inflammatory myopathies. J Immunol 2007; 178(1):547-556.

(91) Wiendl H. Idiopathic inflammatory myopathies: current and future therapeutic options. Neurotherapeutics 2008; 5(4):548-557.

(92) Amemiya K, Granger RP, Dalakas MC. Clonal restriction of T-cell receptor expression by infiltrating lymphocytes in inclusion body myositis persists over time. Studies in repeated muscle biopsies. Brain 2000; 123 (Pt 10):2030-2039.

(93) Dimitri D, Benveniste O, Dubourg O, Maisonobe T, Eymard B, Amoura Z, Jean L, Tiev K, Piette JC, Klatzmann D, Herson S, Boyer O. Shared blood and muscle CD8+ T-cell expansions in inclusion body myositis. Brain 2006; 129(Pt 4):986-995.

(94) Fyhr IM, Moslemi AR, Mosavi AA, Lindberg C, Tarkowski A, Oldfors A. Oligoclonal expansion of muscle infiltrating T cells in inclusion body myositis. J Neuroimmunol 1997; 79(2):185-189.

(95) Sordet C, Goetz J, Sibilia J. Contribution of autoantibodies to the diagnosis and nosology of inflammatory muscle disease. Joint Bone Spine 2006; 73(6):646-654.

(96) Targoff INM. Update on myositis-specific and myositis-associated autoantibodies. Current Opinion in Rheumatology 2000; 12(6):475-481.

(97) Dalakas MC, Illa I, Gallardo E, Juarez C. Inclusion body myositis and paraproteinemia: incidence and immunopathologic correlations. Ann Neurol 1997; 41(1):100-104.

(98) Casciola-Rosen L, Nagaraju K, Plotz P, Wang K, Levine S, Gabrielson E, Corse A, Rosen A. Enhanced autoantigen expression in regenerating muscle cells in idiopathic inflammatory myopathy. J Exp Med 2005; 201(4):591-601.

(99) Casciola-Rosen L, Andrade F, Ulanet D, Wong WB, Rosen A. Cleavage by Granzyme B Is Strongly Predictive of Autoantigen Status: Implications for Initiation of Autoimmunity. J Exp Med 1999; 190(6):815-826.

(100) Hengstman GJD, van Engelen BGM, Vree Egberts WTM, van Venrooij WJP. Myositis-specific autoantibodies: overview and recent developments. Current Opinion in Rheumatology 2001; 13(6):476-482.

(101) Gomard-Mennesson E, Fabien N, Cordier J, Ninet J, Tebib J, Rousset H. Clinical Significance of Anti-Histidyl-tRNA Synthetase (Jo1) Autoantibodies. Ann N Y Acad Sci 2007; 1109:414-420.

(102) Frank MB, McCubbin V, Trieu E, Wu Y, Isenberg DA, Targoff IN. The association of anti-Ro52 autoantibodies with myositis and scleroderma autoantibodies. J Autoimmun 1999; 12(2):137-142.

(103) Mielnik P, Wiesik-Szewczyk E, Olesinska M, Chwalinska-Sadowska H, Zabek J. Clinical features and prognosis of patients with idiopathic inflammatory myopathies and anti-Jo-1 antibodies. Autoimmunity 2006; 39(3):243-247.

(104) Zampieri S, Ghirardello A, Iaccarino L, Tarricone E, Gambari PF, Doria A. Anti-Jo-1 antibodies. Autoimmunity 2005; 38(1):73-78.

(105) Hirakata M. Autoantibodies to aminoacyl-tRNA synthetases. Intern Med 2005; 44(6):527-528.

(106) Hirakata M, Suwa A, Takada T, Sato S, Nagai S, Genth E, Song YW, Mimori T, Targoff IN. Clinical and immunogenetic features of patients with autoantibodies to asparaginyl-transfer RNA synthetase. Arthritis Rheum 2007; 56(4):1295-1303.

(107) Levine SM, Raben N, Xie D, Askin FB, Tuder R, Mullins M, Rosen A, Casciola-Rosen LA. Novel conformation of histidyl-transfer RNA synthetase in the lung: the target tissue in Jo-1 autoantibody-associated myositis. Arthritis Rheum 2007; 56(8):2729-2739.

(108) Friedman AW, Targoff IN, Arnett FC. Interstitial lung disease with autoantibodies against aminoacyl-tRNA synthetases in the absence of clinically apparent myositis. Semin Arthritis Rheum 1996; 26(1):459-467.

(109) Betteridge Z, Gunawardena H, North J, Slinn J, McHugh N. Anti-synthetase syndrome: a new autoantibody to phenylalanyl transfer RNA synthetase (anti-Zo) associated with polymyositis and interstitial pneumonia. Rheumatology (Oxford) 2007.

(110) Hashish L, Trieu E, Sadanandan P, Targoff IN. Identification of autoantibodies to tyrosyl-tRNA synthetase in dermatomyositis with feature consistent with anti-synthetase syndrome (abstract). Arthritis & Rheumatism 2005; 52(Suppl.9):S312.

(111) Howard OM, Dong HF, Yang D, Raben N, Nagaraju K, Rosen A, Casciola-Rosen L, Hartlein M, Kron M, Yang D, Yiadom K, Dwivedi S, Plotz PH, Oppenheim JJ. Histidyl-tRNA synthetase and asparaginyl-tRNA synthetase, autoantigens in myositis, activate chemokine receptors on T lymphocytes and immature dendritic cells. J Exp Med 2002; 196(6):781-791.

(112) Oppenheim JJ, Dong HF, Plotz P, Caspi RR, Dykstra M, Pierce S, Martin R, Carlos C, Finn O, Koul O, Howard OM. Autoantigens act as tissue-specific chemoattractants. J Leukoc Biol 2005; 77(6):854-861.

(113) Routsias JG, Vlachoyiannopoulos PG, Tzioufas AG. Autoantibodies to intracellular autoantigens and their B-cell epitopes: molecular probes to study the autoimmune response. Crit Rev Clin Lab Sci 2006; 43(3):203-248.

(114) Stone KB, Oddis CV, Fertig N, Katsumata Y, Lucas M, Vogt M, Domsic R, Ascherman DP. Anti-Jo-1 antibody levels correlate with disease activity in idiopathic inflammatory myopathy. Arthritis Rheum 2007; 56(9):3125-3131.

(115) Zampieri S, Ghirardello A, Iaccarino L, Briani C, Sarzi-Puttini P, Atzeni F, Arienti S, Todesco S, Doria A. Polymyositis-dermatomyositis and infections. Autoimmunity 2006; 39(3):191-196.

(116) Miller FW, Waite KA, Biswas T, Plotz PH. The role of an autoantigen, histidyl-tRNA synthetase, in the induction and maintenance of autoimmunity. Proc Natl Acad Sci U S A 1990; 87(24):9933-9937.

(117) Arbuckle MR, McClain MT, Rubertone MV, Scofield RH, Dennis GJ, James JA, Harley JB. Development of Autoantibodies before the Clinical Onset of Systemic Lupus Erythematosus. N Engl J Med 2003; 349(16):1526-1533.

(118) Stone KB, Oddis CV, Fertig N, Katsumata Y, Lucas M, Vogt M, Domsic R, Ascherman DP. Anti-Jo-1 antibody levels correlate with disease activity in idiopathic inflammatory myopathy. Arthritis Rheum 2007; 56(9):3125-3131.

(119) Venables PJ. Antibodies to Jo-1 and Ro-52: why do they go together? Clin Exp Immunol 1997; 109(3):403-405.

(120) Rutjes SA, Vree Egberts WT, Jongen P, Van Den HF, Pruijn GJ, van Venrooij WJ. Anti-Ro52 antibodies frequently co-occur with anti-Jo-1 antibodies in sera from patients with idiopathic inflammatory myopathy. Clin Exp Immunol 1997; 109(1):32-40.

(121) Limaye VS, Cassidy J, Scott G, Roberts-Thomson PJ, Gillis D. Anti-Ro52 antibodies, antisynthetase antibodies, and antisynthetase syndrome. Clin Rheumatol 2007.

(122) Hassan AB, Fathi M, Dastmalchi M, Lundberg IE, Padyukov L. Genetically determined imbalance between serum levels of tumour necrosis factor (TNF) and interleukin (IL)-10 is associated with anti-Jo-1 and anti-Ro52 autoantibodies in patients with poly- and dermatomyositis. J Autoimmun 2006; 27(1):62-68.

(123) Eloranta ML, Helmers SB, Ulfgren AK, Ronnblom L, Alm GV, Lundberg IE. A possible mechanism for endogenous activation of the type I interferon system in myositis patients with anti-Jo-1 or anti-Ro 52/anti-Ro 60 autoantibodies. Arthritis Rheum 2007; 56(9):3112-3124.

(124) Ghirardello A, Zampieri S, Iaccarino L, Tarricone E, Bendo R, Gambari PF, Doria A. Anti-Mi-2 antibodies. Autoimmunity 2005; 38(1):79-83.

(125) Targoff IN, Reichlin M. The association between Mi-2 antibodies and dermatomyositis. Arthritis Rheum 1985; 28(7):796-803.

(126) Brouwer R, Hengstman GJ, Vree EW, Ehrfeld H, Bozic B, Ghirardello A, Grondal G, Hietarinta M, Isenberg D, Kalden JR, Lundberg I, Moutsopoulos H, Roux-Lombard P, Vencovsky J, Wikman A, Seelig HP, van Engelen BG, van Venrooij WJ. Autoantibody profiles in the sera of European patients with myositis. Ann Rheum Dis 2001; 60(2):116-123.

(127) Hengstman GJ, Vree Egberts WT, Seelig HP, Lundberg IE, Moutsopoulos HM, Doria A, Mosca M, Vencovsky J, van Venrooij WJ, van Engelen BG. Clinical characteristics of patients with myositis and autoantibodies to different fragments of the Mi-2 beta antigen. Ann Rheum Dis 2006; 65(2):242-245.

(128) Hengstman GJ, ter Laak HJ, Vree Egberts WT, Lundberg IE, Moutsopoulos HM, Vencovsky J, Doria A, Mosca M, van Venrooij WJ, van Engelen BG. Anti-signal recognition particle autoantibodies: marker of a necrotising myopathy. Ann Rheum Dis 2006; 65(12):1635-1638.

(129) Gunawardena H, Betteridge ZE, McHugh NJ. Newly identified autoantibodies: relationship to idiopathic inflammatory myopathy subsets and pathogenesis. Curr Opin Rheumatol 2008; 20(6):675-680.

(130) Sato S, Hirakata M, Kuwana M, Suwa A, Inada S, Mimori T, Nishikawa T, Oddis CV, Ikeda Y. Autoantibodies to a 140-kd polypeptide, CADM-140, in Japanese patients with clinically amyopathic dermatomyositis. Arthritis Rheum 2005; 52(5):1571-1576.

(131) Mimori T, Imura Y, Nakashima R, Yoshifuji H. Autoantibodies in idiopathic inflammatory myopathy: an update on clinical and pathophysiological significance. Curr Opin Rheumatol 2007; 19(6):523-529.

(132) Targoff IN, Mamyrova G, Trieu EP, Perurena O, Koneru B, O'Hanlon TP, Miller FW, Rider LG. A novel autoantibody to a 155-kd protein is associated with dermatomyositis. Arthritis Rheum 2006; 54(11):3682-3689.

(133) Kaji K, Fujimoto M, Hasegawa M, Kondo M, Saito Y, Komura K, Matsushita T, Orito H, Hamaguchi Y, Yanaba K, Itoh M, Asano Y, Seishima M, Ogawa F, Sato S, Takehara K. Identification of a novel autoantibody reactive with 155 and 140 kDa nuclear proteins in patients with dermatomyositis: an association with malignancy. Rheumatology (Oxford) 2007; 46(1):25-28.

(134) Betteridge Z, Gunawardena H, North J, Slinn J, McHugh N. Identification of a novel autoantibody directed against small ubiquitin-like modifier activating enzyme in dermatomyositis. Arthritis Rheum 2007; 56(9):3132-3137.

(135) Cordeiro AC, Isenberg DA. Treatment of inflammatory myopathies. Postgrad Med J 2006; 82(969):417-424.

(136) Choy EH, Isenberg DA. Treatment of dermatomyositis and polymyositis. Rheumatology (Oxford) 2002; 41(1):7-13.

(137) Kalla R, Soumakiyan M, Tuck S. A case of inclusion body myositis responsive to prednisolone therapy. Clin Rheumatol 2008.

(138) Cherin P, Pelletier S, Teixeira A, Laforet P, Genereau T, Simon A, Maisonobe T, Eymard B, Herson S. Results and long-term followup of intravenous immunoglobulin infusions in chronic, refractory polymyositis: an open study with thirty-five adult patients. Arthritis Rheum 2002; 46(2):467-474.

(139) Dalakas MC. Intravenous immunoglobulin in autoimmune neuromuscular diseases. JAMA 2004; 291(19):2367-2375.

(140) Anolik JH, Barnard J, Cappione A, Pugh-Bernard AE, Felgar RE, Looney RJ, Sanz I. Rituximab improves peripheral B cell abnormalities in human systemic lupus erythematosus. Arthritis Rheum 2004; 50(11):3580-3590.

(141) Arkfeld DG. The potential utility of B cell-directed biologic therapy in autoimmune diseases. Rheumatol Int 2008; 28(3):205-215.

(142) Cambridge G, Leandro MJ, Edwards JC, Ehrenstein MR, Salden M, Bodman-Smith M, Webster AD. Serologic changes following B lymphocyte depletion therapy for rheumatoid arthritis. Arthritis Rheum 2003; 48(8):2146-2154.

(143) Eisenberg R. SLE: Rituximab in lupus. Arthritis Res Ther 2003; 5(4):157-159.

(144) Gorman C, Leandro M, Isenberg DA. B cell depletion in autoimmune diseases. Arthritis Research & Therapy 2003; 5(Suppl 4):S17-S21.

(145) Looney RJM, Anolik JHM, Campbell DR, Felgar REMP, Young FM, Arend LJM, Sloand JAM, Rosenblatt JM, Sanz IM. B Cell Depletion as a Novel Treatment for Systemic Lupus Erythematosus: A Phase I/II Dose-Escalation Trial of Rituximab. Arthritis & Rheumatism 2004; 50(8):2580-2589.

(146) Pers JO, Daridon C, Bendaoud B, Devauchelle V, Berthou C, Saraux A, Youinou P. B-cell depletion and repopulation in autoimmune diseases. Clin Rev Allergy Immunol 2008; 34(1):50-55.

(147) Silverman GJ. Targeting of B cells in SLE: rationale and therapeutic opportunities. Bull NYU Hosp Jt Dis 2006; 64(1-2):51-56.

(148) Walsh M, Jayne D. Rituximab in the treatment of anti-neutrophil cytoplasm antibody associated vasculitis and systemic lupus erythematosus: past, present and future. Kidney Int 2007; 72(6):676-682.

(149) Pitashny M, Shoenfeld Y. B cell depletion in autoimmune rheumatic diseases. Autoimmun Rev 2005; 4(7):436-441.

(150) Chung L, Genovese MC, Fiorentino DF. A pilot trial of rituximab in the treatment of patients with dermatomyositis. Arch Dermatol 2007; 143(6):763-767.

(151) Levine TDM. Rituximab in the Treatment of Dermatomyositis: An Open-Label Pilot Study. Arthritis & Rheumatism 2005; 52(2):601-607.

(152) Cooper MA, Willingham DL, Brown DE, French AR, Shih FF, White AJ. Rituximab for the treatment of juvenile dermatomyositis: a report of four pediatric patients. Arthritis Rheum 2007; 56(9):3107-3111.

(153) Cambridge G, Leandro MJ, Teodorescu M, Manson J, Rahman A, Isenberg DA, Edwards JC. B cell depletion therapy in systemic lupus erythematosus: effect on autoantibody and antimicrobial antibody profiles. Arthritis Rheum 2006; 54(11):3612-3622.

(154) Dalakas MC. Invited article: inhibition of B cell functions: implications for neurology. Neurology 2008; 70(23):2252-2260.

(155) Dorner T, Burmester GR. New approaches of B-cell-directed therapy: beyond rituximab. Curr Opin Rheumatol 2008; 20(3):263-268.

(156) Amato AA, Griggs RC. Treatment of idiopathic inflammatory myopathies. Curr Opin Neurol 2003; 16(5):569-575.

(157) Carlson JA, Cavaliere LF, Grant-Kels JM. Cutaneous vasculitis: diagnosis and management. Clin Dermatol 2006; 24(5):414-429.

(158) Csernok E, Gross WL. Primary vasculitides and vasculitis confined to skin: clinical features and new pathogenic aspects. Arch Dermatol Res 2000; 292(9):427-436.

(159) Guillevin L, Dorner T. Vasculitis: mechanisms involved and clinical manifestations. Arthritis Res Ther 2007; 9 Suppl 2:S9.

(160) Ramos-Casals M, Nardi N, Lagrutta M, Brito-Zeron P, Bove A, Delgado G, Cervera R, Ingelmo M, Font J. Vasculitis in systemic lupus erythematosus: prevalence and clinical characteristics in 670 patients. Medicine (Baltimore) 2006; 85(2):95-104.

(161) Grzeszkiewicz TM, Fiorentino DF. Update on cutaneous vasculitis. Semin Cutan Med Surg 2006; 25(4):221-225.

(162) Carlson JA, Ng BT, Chen KR. Cutaneous vasculitis update: diagnostic criteria, classification, epidemiology, etiology, pathogenesis, evaluation and prognosis. Am J Dermatopathol 2005; 27(6):504-528.

(163) Fries JF, Hunder GG, Bloch DA, Michel BA, Arend WP, Calabrese LH, Fauci AS, Leavitt RY, Lie JT, Lightfoot RW, Jr., . The American College of Rheumatology 1990 criteria for the classification of vasculitis. Summary. Arthritis Rheum 1990; 33(8):1135-1136.

(164) Jennette JC, Falk RJ. Small-vessel vasculitis. N Engl J Med 1997; 337(21):1512-1523.

(165) Jennette JC, Falk RJ, Andrassy K, Bacon PA, Churg J, Gross WL, Hagen EC, Hoffman GS, Hunder GG, Kallenberg CG, . Nomenclature of systemic vasculitides. Proposal of an international consensus conference. Arthritis Rheum 1994; 37(2):187-192.

(166) Savage CO, Harper L, Adu D. Primary systemic vasculitis. Lancet 1997; 349(9051):553-558.

(167) Xu LY, Esparza EM, Anadkat MJ, Crone KG, Brasington RD. Cutaneous Manifestations of Vasculitis: A Visual Guide. Semin Arthritis Rheum 2008.

(168) Katsambas A, Stefanaki C. Life-threatening purpura and vasculitis. Clinics in Dermatology 2005; 23(3):227-237.

(169) Weyand CM, Goronzy JJ. Medium- and large-vessel vasculitis. N Engl J Med 2003; 349(2):160-169.

(170) Carlson JA, Chen KR. Cutaneous vasculitis update: neutrophilic muscular vessel and eosinophilic, granulomatous, and lymphocytic vasculitis syndromes. Am J Dermatopathol 2007; 29(1):32-43.

(171) Rowley AH, Shulman ST. New developments in the search for the etiologic agent of Kawasaki disease. Curr Opin Pediatr 2007; 19(1):71-74.

(172) Fiorentino DF. Cutaneous vasculitis. Journal of the American Academy of Dermatology 2003; 48(3):311-340.

(173) Calamia KT, Balabanova M. Vasculitis in systemic lupus erythematosis. Clinics in Dermatology 2004; 22(2):148-156.

(174) Tseng MT, Hsieh SC, Shun CT, Lee KL, Pan CL, Lin WM, Lin YH, Yu CL, Hsieh ST. Skin denervation and cutaneous vasculitis in systemic lupus erythematosus. Brain 2006.

(175) Carlson JA, Chen KR. Cutaneous vasculitis update: small vessel neutrophilic vasculitis syndromes. Am J Dermatopathol 2006; 28(6):486-506.

(176) Kallenberg CG. Antineutrophil cytoplasmic autoantibody-associated small-vessel vasculitis. Curr Opin Rheumatol 2007; 19(1):17-24.

(177) Bosch X, Guilabert A, Espinosa G, Mirapeix E. Immunotherapy for antineutrophil cytoplasmic antibody-associated vasculitis: challenging the therapeutic status quo? Trends Immunol 2008; 29(6):280-289.

(178) Bosch X, Guilabert A, Font J. Antineutrophil cytoplasmic antibodies. Lancet 2006; 368(9533):404-418.

(179) Kallenberg CG, Rarok A, Stegeman CA, Limburg PC. New insights into the pathogenesis of antineutrophil cytoplasmic autoantibody-associated vasculitis. Autoimmun Rev 2002; 1(1-2):61-66.

(180) Sanders JS, Huitma MG, Kallenberg CG, Stegeman CA. Prediction of relapses in PR3-ANCA-associated vasculitis by assessing responses of ANCA titres to treatment. Rheumatology (Oxford) 2006.

(181) Terrier B, Saadoun D, Sene D, Ghillani-Dalbin P, Amoura Z, Deray G, Fautrel B, Piette JC, Cacoub P. Anti-myeloperoxidase antibodies are a useful marker of disease activity in ANCA-associated vasculitides. Ann Rheum Dis 2008.

(182) Radice A, Sinico RA. Antineutrophil cytoplasmic antibodies (ANCA). Autoimmunity 2005; 38(1):93-103.

(183) Falk RJ, Terrell RS, Charles LA, Jennette JC. Anti-neutrophil cytoplasmic autoantibodies induce neutrophils to degranulate and produce oxygen radicals in vitro. Proc Natl Acad Sci U S A 1990; 87(11):4115-4119.

(184) Ohlsson S, Hellmark T, Pieters K, Sturfelt G, Wieslander J, Segelmark M. Increased monocyte transcription of the proteinase 3 gene in small vessel vasculitis. Clin Exp Immunol 2005; 141(1):174-182.

(185) Kallenberg CG, Heeringa P, Stegeman CA. Mechanisms of Disease: pathogenesis and treatment of ANCA-associated vasculitides. Nat Clin Pract Rheumatol 2006; 2(12):661-670.

(186) Matsumoto T, Kaneko T, Wada H, Kobayashi T, Abe Y, Nobori T, Shiku H, Stearns-Kurosawa DJ, Kurosawa S. Proteinase 3 expression on neutrophil membranes from patients with infectious disease. Shock 2006; 26(2):128-133.

(187) Xiao H, Heeringa P, Hu P, Liu Z, Zhao M, Aratani Y, Maeda N, Falk RJ, Jennette JC. Antineutrophil cytoplasmic autoantibodies specific for myeloperoxidase cause glomerulonephritis and vasculitis in mice. J Clin Invest 2002; 110(7):955-963.

(188) Jennette JC, Xiao H, Falk RJ. Pathogenesis of vascular inflammation by anti-neutrophil cytoplasmic antibodies. J Am Soc Nephrol 2006; 17(5):1235-1242.

(189) Pendergraft WF, III, Preston GA, Shah RR, Tropsha A, Carter CW, Jr., Jennette JC, Falk RJ. Autoimmunity is triggered by cPR-3(105-201), a protein complementary to human autoantigen proteinase-3. Nat Med 2004; 10(1):72-79.

(190) Shoenfeld Y. The idiotypic network in autoimmunity: antibodies that bind antibodies that bind antibodies. Nat Med 2004; 10(1):17-18.

(191) Belizna C, Duijvestijn A, Hamidou M, Cohen Tervaert JW. Antiendothelial cell antibodies in vasculitis and connective tissue disease. Ann Rheum Dis 2006; 65(12):1545-1550.

(192) Buckley CD, Ed RG, Nash GB, Raza K. Endothelial cells, fibroblasts and vasculitis. Rheumatology (Oxford) 2005; 44(7):860-863.

(193) Baiu DC, Barger B, Sandor M, Fabry Z, Hart MN. Autoantibodies to vascular smooth muscle are pathogenic for vasculitis. Am J Pathol 2005; 166(6):1851-1860.

(194) Unger L, Kayser M, Nusslein HG. Successful treatment of severe rheumatoid vasculitis by infliximab. Ann Rheum Dis 2003; 62(6):587-588.

(195) Booth AD, Jayne DR, Kharbanda RK, McEniery CM, Mackenzie IS, Brown J, Wilkinson IB. Infliximab improves endothelial dysfunction in systemic vasculitis: a model of vascular inflammation. Circulation 2004; 109(14):1718-1723.

(196) Booth A, Harper L, Hammad T, Bacon P, Griffith M, Levy J, Savage C, Pusey C, Jayne D. Prospective study of TNFalpha blockade with infliximab in anti-neutrophil cytoplasmic antibody-associated systemic vasculitis. J Am Soc Nephrol 2004; 15(3):717-721.

(197) Bartolucci P, Ramanoelina J, Cohen P, Mahr A, Godmer P, Le Hello C, Guillevin L. Efficacy of the anti-TNF-alpha antibody infliximab against refractory systemic vasculitides: an open pilot study on 10 patients. Rheumatology (Oxford) 2002; 41(10):1126-1132.

(198) Stone J.H. Etanercept plus standard therapy for Wegener's Granulomatosis. N Engl J Med 2005; 352(4):351-361.

(199) Raza K, Carruthers DM, Stevens R, Filer AD, Townend JN, Bacon PA. Infliximab leads to a rapid but transient improvement in endothelial function in patients with primary systemic vasculitis. Ann Rheum Dis 2006; 65:946-948.

(200) Ramos-Casals M, Brito-Zeron P, Soto MJ, Cuadrado MJ, Khamashta MA. Autoimmune diseases induced by TNF-targeted therapies. Best Pract Res Clin Rheumatol 2008; 22(5):847-861.

(201) Ramos-Casals M, Brito-Zeron P, Cuadrado MJ, Khamashta MA. Vasculitis induced by tumor necrosis factor-targeted therapies. Curr Rheumatol Rep 2008; 10(6):442-448.

(202) Smith KG, Jones RB, Burns SM, Jayne DR. Long-term comparison of rituximab treatment for refractory systemic lupus erythematosus and vasculitis: Remission, relapse, and re-treatment. Arthritis Rheum 2006; 54(9):2970-2982.

(203) Lovric S, Erdbruegger U, Kumpers P, Woywodt A, Koenecke C, Wedemeyer H, Haller H, Haubitz M. Rituximab as rescue therapy in anti-neutrophil cytoplasmic antibody-associated vasculitis: single centre experience with 15 patients. Nephrol Dial Transplant 2008.

(204) Ferraro AJ, Drayson MT, Savage CO, MacLennan IC. Levels of autoantibodies, unlike antibodies to all extrinsic antigen groups, fall following B cell depletion with Rituximab. Eur J Immunol 2008; 38(1):292-298.

(205) Specks U, Fervenza FC, McDonald TJ, Hogan MC. Response of Wegener's granulomatosis to anti-CD20 chimeric monoclonal antibody therapy. Arthritis Rheum 2001; 44(12):2836-2840.

(206) Keogh KA, Wylam ME, Stone JH, Specks U. Induction of remission by B lymphocyte depletion in eleven patients with refractory antineutrophil cytoplasmic antibody-associated vasculitis. Arthritis Rheum 2005; 52(1):262-268.

(207) Ollila J, Vihinen M. B cells. The International Journal of Biochemistry & Cell Biology 2005; 37(3):518-523.

(208) Nutt SL, Kee BL. The transcriptional regulation of B cell lineage commitment. Immunity 2007; 26(6):715-725.

(209) Dalakas MC. B cells in the pathophysiology of autoimmune neurological disorders: A credible therapeutic target. Pharmacol Ther 2006.

(210) Hardy RR, Hayakawa K. B cell development pathways. Annu Rev Immunol 2001; 19:595-621.

(211) Hardy RR, Kincade PW, Dorshkind K. The protean nature of cells in the B lymphocyte lineage. Immunity 2007; 26(6):703-714.

(212) LeBien TW. Fates of human B-cell precursors. Blood 2000; 96(1):9-23.

(213) Monson NL. The natural history of B cells. Curr Opin Neurol 2008; 21 Suppl 1:S3-S8.

(214) O'Connor BP, Gleeson MW, Noelle RJ, Erickson LD. The rise and fall of long-lived humoral immunity: terminal differentiation of plasma cells in health and disease. Immunol Rev 2003; 194:61-76.

(215) Slifka MK, Antia R, Whitmire JK, Ahmed R. Humoral immunity due to long-lived plasma cells. Immunity 1998; 8(3):363-372.

(216) Tarlinton D, Radbruch A, Hiepe F, Dorner T. Plasma cell differentiation and survival. Curr Opin Immunol 2008; 20(2):162-169.

(217) Fuxa M, Skok JA. Transcriptional regulation in early B cell development. Curr Opin Immunol 2007; 19(2):129-136.

(218) Hagman J, Lukin K. Transcription factors drive B cell development. Curr Opin Immunol 2006; 18(2):127-134.

(219) Laiosa CV, Stadtfeld M, Graf T. Determinants of lymphoid-myeloid lineage diversification. Annu Rev Immunol 2006; 24:705-738.

(220) Mix E, Goertsches R, Zettl UK. Immunoglobulins - Basic Considerations. Journal of Neurology 2006; 253:V/9-V/17.

(221) Cook GP, Tomlinson IM. The human immunoglobulin VH repertoire. Immunol Today 1995; 16(5):237-242.

(222) Cook GP, Tomlinson IM, Walter G, Riethman H, Carter NP, Buluwela L, Winter G, Rabbitts TH. A map of the human immunoglobulin VH locus completed by analysis of the telomeric region of chromosome 14q. Nat Genet 1994; 7(2):162-168.

(223) Ichihara Y, Matsuoka H, Kurosawa Y. Organization of human immunoglobulin heavy chain diversity gene loci. EMBO J 1988; 7(13):4141-4150.

(224) Matsuda F, Ishii K, Bourvagnet P, Kuma K, Hayashida H, Miyata T, Honjo T. The complete nucleotide sequence of the human immunoglobulin heavy chain variable region locus. J Exp Med 1998; 188(11):2151-2162.

(225) Kodaira M, Kinashi T, Umemura I, Matsuda F, Noma T, Ono Y, Honjo T. Organization and evolution of variable region genes of the human immunoglobulin heavy chain. J Mol Biol 1986; 190(4):529-541.

(226) Lee KH, Matsuda F, Kinashi T, Kodaira M, Honjo T. A novel family of variable region genes of the human immunoglobulin heavy chain. J Mol Biol 1987; 195(4):761-768.

(227) Tomlinson IM, Walter G, Marks JD, Llewelyn MB, Winter G. The repertoire of human germline VH sequences reveals about fifty groups of VH segments with different hypervariable loops. J Mol Biol 1992; 227(3):776-798.

(228) Willems van Dijk K, Mortari F, Kirkham PM, Schroeder HW, Jr., Milner EC. The human immunoglubulin VH7 gene family consists of a small, polymorphic group of six to eight gene segments dispersed throughout the VH locus. Eur J Immunol 1993; 23:832-839.

(229) Corbett SJ, Tomlinson IM, Sonnhammer EL, Buck D, Winter G. Sequence of the human immunoglobulin diversity (D) segment locus: a systematic analysis provides no evidence for the use of DIR segments, inverted D segments, "minor" D segments or D-D recombination. J Mol Biol 1997; 270(4):587-597.

(230) Fanning LJ, Connor AM, Wu GE. Development of the immunoglobulin repertoire. Clin Immunol Immunopathol 1996; 79(1):1-14.

(231) Grawunder U, Harfst E. How to make ends meet in V(D)J recombination. Current Opinion in Immunology 2001; 13(2):186-194.

(232) Jung D, Giallourakis C, Mostoslavsky R, Alt FW. Mechanism and control of V(D)J recombination at the immunoglobulin heavy chain locus. Annu Rev Immunol 2006; 24:541-570.

(233) Zhang Z, Burrows PD, Cooper MD. The molecular basis and biological significance of VH replacement. Immunol Rev 2004; 197:231-242.

(234) Tonegawa S. Somatic generation of antibody diversity. Nature 1983; 302(5909):575-581.

(235) Nemazee D. Receptor editing in lymphocyte development and central tolerance. Nat Rev Immunol 2006; 6(10):728-740.

(236) Zhang Z. VH replacement in mice and humans. Trends in Immunology 2007; 28(3):132-137.

(237) Schroeder HW, Jr., Ippolito GC, Shiokawa S. Regulation of the antibody repertoire through control of HCDR3 diversity. Vaccine 1998; 16(14-15):1383-1390.

(238) Rosner K, Winter DB, Tarone RE, Skovgaard GL, Bohr VA, Gearhart PJ. Third complementarity-determining region of mutated VH immunoglobulin genes contains shorter V, D, J, P, and N components than non-mutated genes. Immunology 2001; 103(2):179-187.

(239) Wilson PC, Wilson K, Liu YJ, Banchereau J, Pascual V, Capra JD. Receptor revision of immunoglobulin heavy chain variable region genes in normal human B lymphocytes. J Exp Med 2000; 191(11):1881-1894.

(240) Klonowski KD, Monestier M. Ig heavy-chain gene revision: leaping towards autoimmunity. Trends in Immunology 2001; 22(7):400-405.

(241) Brezinschek HP, Brezinschek RI, Lipsky PE. Analysis of the heavy chain repertoire of human peripheral B cells using single-cell polymerase chain reaction. J Immunol 1995; 155(1):190-202.

(242) Brezinschek HP, Foster SJ, Brezinschek RI, Dorner T, Domiati-Saad R, Lipsky PE. Analysis of the Human VH Gene Repertoire . Differential Effects of Selection and Somatic Hypermutation on Human Peripheral CD5+/IgM+ and CD5-/IgM+ B cells. J Clin Invest 1997; 99(10):2488-2501.

(243) Dorner T, Lipsky PE. Molecular basis of immunoglobulin variable region gene usage in systemic autoimmunity. Clin Exp Med 2005; 4(4):159-169.

(244) Dorner T, Lipsky PE. Immunoglobulin Variable-Region Gene Usage in Systemic Autoimmune Diseases. Arthritis & Rheumatism 2001; 44(12):2715-2727.

(245) Guigou V, Cuisinier AM, Tonnelle C, Moinier D, Fougereau M, Fumoux F. Human immunoglobulin VH and VK repertoire revealed by in situ hybridization. Mol Immunol 1990; 27(9):935-940.

(246) Huang C, Stewart AK, Schwartz RS, Stollar BD. Immunoglobulin heavy chain gene expression in peripheral blood B lymphocytes. J Clin Invest 1992; 89(4):1331-1343.

(247) Kraj P, Friedman DF, Stevenson F, Silberstein LE. Evidence for the overexpression of the VH4-34 (VH4.21) Ig gene segment in the normal adult human peripheral blood B cell repertoire. J Immunol 1995; 154(12):6406-6420.

(248) Kraj P, Rao SP, Glas AM, Hardy RR, Milner EC, Silberstein LE. The human heavy chain Ig V region gene repertoire is biased at all stages of B cell ontogeny, including early pre-B cells. J Immunol 1997; 158(12):5824-5832.

(249) Stewart AK, Huang C, Stollar BD, Schwartz RS. High-frequency representation of a single VH gene in the expressed human B cell repertoire. J Exp Med 1993; 177(4):1227.

(250) Suzuki I, Pfister L, Glas A, Nottenburg C, Milner EC. Representation of rearranged VH gene segments in the human adult antibody repertoire. J Immunol 1995; 154(8):3902-3911.

(251) Volpe JM, Kepler TB. Large-scale analysis of human heavy chain V(D)J recombination patterns. Immunome Res 2008; 4(1):3.

(252) Perlmutter RM, Kearney JF, Chang SP, Hood LE. Developmentally controlled expression of immunoglobulin VH genes. Science 1985; 227(4694):1597-1601.

(253) Yancopoulos GD, Desiderio SV, Paskind M, Kearney JF, Baltimore D, Alt FW. Preferential utilization of the most JH-proximal VH gene segments in pre-B-cell lines. Nature 1984; 311(5988):727-733.

(254) Gu H, Tarlinton D, Muller W, Rajewsky K, Forster I. Most peripheral B cells in mice are ligand selected. J Exp Med 1991; 173(6):1357-1371.

(255) Matsumoto M, Lo SF, Carruthers CJ, Min J, Mariathasan S, Huang G, Plas DR, Martin SM, Geha RS, Nahm MH, Chaplin DD. Affinity maturation without germinal centres in lymphotoxin-alpha-deficient mice. Nature 1996; 382(6590):462-466.

(256) Zheng NY, Wilson K, Jared M, Wilson PC. Intricate targeting of immunoglobulin somatic hypermutation maximizes the efficiency of affinity maturation. J Exp Med 2005; 201(9):1467-1478.

(257) Muramatsu M, Kinoshita K, Fagarasan S, Yamada S, Shinkai Y, Honjo T. Class switch recombination and hypermutation require activation-induced cytidine deaminase (AID), a potential RNA editing enzyme. Cell 2000; 102(5):553-563.

(258) Neuberger MS, Harris RS, Di Noia J, Petersen-Mahrt SK. Immunity through DNA deamination. Trends Biochem Sci 2003; 28(6):305-312.

(259) Longerich S, Basu U, Alt F, Storb U. AID in somatic hypermutation and class switch recombination. Curr Opin Immunol 2006; 18(2):164-174.

(260) Diaz M, Casali P. Somatic immunoglobulin hypermutation. Curr Opin Immunol 2002; 14(2):235-240.

(261) Goodman MF, Scharff MD, Romesberg FE. AID-initiated purposeful mutations in immunoglobulin genes. Adv Immunol 2007; 94:127-155.

(262) Odegard VH, Schatz DG. Targeting of somatic hypermutation. Nat Rev Immunol 2006; 6(8):573-583.

(263) Neuberger MS, Milstein C. Somatic hypermutation. Curr Opin Immunol 1995; 7(2):248-254.

(264) Teng G, Papavasiliou FN. Immunoglobulin Somatic Hypermutation. Annu Rev Genet 2007.

(265) Edry E, Melamed D. Class switch recombination: a friend and a foe. Clin Immunol 2007; 123(3):244-251.

(266) Han JH, Akira S, Calame K, Beutler B, Selsing E, Imanishi-Kari T. Class switch recombination and somatic hypermutation in early mouse B cells are mediated by B cell and Toll-like receptors. Immunity 2007; 27(1):64-75.

(267) Kelsoe G. Life and death in germinal centers (redux). Immunity 1996; 4(2):107-111.

(268) MacLennan IC. Germinal centers. Annu Rev Immunol 1994; 12:117-139.

(269) Han S, Zheng B, Takahasi Y, Kelsoe G. Distinctive characteristics of germinal center B cells. Seminars in Immunology 1997; 9:255-260.

(270) Garside P, Ingulli E, Merica RR, Johnson JG, Noelle RJ, Jenkins MK. Visualization of specific B and T lymphocyte interactions in the lymph node. Science 1998; 281(5373):96-99.

(271) Camacho SA, Kosco-Vilbois MH, Berek C. The dynamic structure of the germinal center. Immunology Today 1998; 19(11):511-514.

(272) Manser T. Textbook germinal centers? J Immunol 2004; 172(6):3369-3375.

(273) van Nierop K, de Groot C. Human follicular dendritic cells: function, origin and development. Seminars in Immunology 2002; 14(4):251-257.

(274) Hauser AE, Shlomchik MJ, Haberman AM. In vivo imaging studies shed light on germinal-centre development. Nat Rev Immunol 2007; 7(7):499-504.

(275) Allen CD, Ansel KM, Low C, Lesley R, Tamamura H, Fujii N, Cyster JG. Germinal center dark and light zone organization is mediated by CXCR4 and CXCR5. Nat Immunol 2004; 5(9):943-952.

(276) Allen CD, Okada T, Tang HL, Cyster JG. Imaging of germinal center selection events during affinity maturation. Science 2007; 315(5811):528-531.

(277) Hauser AE, Junt T, Mempel TR, Sneddon MW, Kleinstein SH, Henrickson SE, von Andrian UH, Shlomchik MJ, Haberman AM. Definition of germinal-center B cell migration in vivo reveals predominant intrazonal circulation patterns. Immunity 2007; 26(5):655-667.

(278) Schwickert TA, Lindquist RL, Shakhar G, Livshits G, Skokos D, Kosco-Vilbois MH, Dustin ML, Nussenzweig MC. In vivo imaging of germinal centres reveals a dynamic open structure. Nature 2007; 446(7131):83-87.

(279) Allen CD, Okada T, Cyster JG. Germinal-center organization and cellular dynamics. Immunity 2007; 27(2):190-202.

(280) Brink R. Germinal-center B cells in the zone. Immunity 2007; 26(5):552-554.

(281) Bende RJ, van Maldegem F, Triesscheijn M, Wormhoudt TA, Guijt R, van Noesel CJ. Germinal centers in human lymph nodes contain reactivated memory B cells. J Exp Med 2007.

(282) Figge MT, Garin A, Gunzer M, Kosco-Vilbois M, Toellner KM, Meyer-Hermann M. Deriving a germinal center lymphocyte migration model from two-photon data. J Exp Med 2008; 205(13):3019-3029.

(283) Stott DI, Hiepe F, Hummel M, Steinhauser G, Berek C. Antigen-driven Clonal Proliferation of B Cells within the Target Tissue of an Autoimmune Disease . The Salivary Glands of Patients with Sjogren's Syndrome. J Clin Invest 1998; 102(5):938-946.

(284) Schroder AE, Greiner A, Seyfert C, Berek C. Differentiation of B cells in the nonlymphoid tissue of the synovial membrane of patients with rheumatoid arthritis. PNAS 1996; 93(1):221-225.

(285) Nzula S, Going JJ, Stott DI. Antigen-driven Clonal Proliferation, Somatic Hypermutation, and Selection of B Lymphocytes Infiltrating Human Ductal Breast Carcinomas. Cancer Res 2003; 63(12):3275-3280.

(286) Grammer AC, Slota R, Fischer R, Gur H, Girschick H, Yarboro C, Illei GG, Lipsky PE. Abnormal germinal center reactions in systemic lupus erythematosus demonstrated by blockade of CD154-CD40 interactions. J Clin Invest 2003; 112(10):1506-1520.

(287) Kikuchi Y, Koarada S, Tada Y, Ushiyama O, Morito F, Suzuki N, Ohta A, Horiuchi T, Miyake K, Nagasawa K. Difference in B cell activation between dermatomyositis and polymyositis: analysis of the expression of RP105 on peripheral blood B cells. Ann Rheum Dis 2001; 60(12):1137-1140.

(288) Tada Y, Koarada S, Morito F, Mitamura M, Inoue H, Suematsu R, Ohta A, Miyake K, Nagasawa K. Toll-like receptor homolog RP105 modulates the antigen-presenting cell function and regulates the development of collagen-induced arthritis. Arthritis Res Ther 2008; 10(5):R121.

(289) Fraser NL, Rowley G, Field M, Stott DI. The VH gene repertoire of splenic B cells and somatic hypermutation in systemic lupus erythematosus. Arthritis Research & Therapy 5(2):R114-21, 2003.

(290) Le Rouzix E. Contamination-pipetting: relative efficiency of filter tips comapred to Microman positive displacement pipette. Nature Methods 2006; 3(6):iii-iv.

(291) Souto-Carneiro MM, Longo NS, Russ DE, Sun Hw, Lipsky PE. Characterization of the Human Ig Heavy Chain Antigen Binding Complementarity Determining Region 3 Using a Newly Developed Software Algorithm, JOINSOLVER. J Immunol 2004; 172(11):6790-6802.

(292) Giudicelli V, Chaume D, Lefranc MP. IMGT/V-QUEST, an integrated software program for immunoglobulin and T cell receptor V-J and V-D-J rearrangement analysis. Nucleic Acids Res 2004; 32(Web Server issue):W435-W440.

(293) Brochet X, Lefranc MP, Giudicelli V. IMGT/V-QUEST: the highly customized and integrated system for IG and TR standardized V-J and V-D-J sequence analysis. Nucleic Acids Res 2008; 36(Web Server issue):W503-W508.

(294) Hershberg U, Uduman M, Shlomchik MJ, Kleinstein SH. Improved methods for detecting selection by mutation analysis of Ig V region sequences. Int Immunol 2008; 20(5):683-694.

(295) Wang K., Lau TY, Morales M., Mont EK., Straus SE. Laser-capture microdissection: refining estimates of the quantity and distribution of latent herpes simplex virus 1 and varicella-zoster virus DNA in human trigeminal Ganglia at the single-cell level. Journal of Virology 2005; 79(22):14079-14087.

(296) Wang X, Stollar BD. Human immunoglobulin variable region gene analysis by single cell RT-PCR. J Immunol Methods 2000; 244(1-2):217-225.

(297) Greenberg SA, Pinkus JL, Pinkus GS, Burleson T, Sanoudou D, Tawil R, Barohn RJ, Saperstein DS, Briemberg HR, Ericsson M, Park P, Amato AA. Interferon-alpha/beta-mediated innate immune mechanisms in dermatomyositis. Ann Neurol 2005; 57(5):664-678.

(298) Greenberg SA, Pinkus GS, Amato AA, Pinkus JL. Myeloid dendritic cells in inclusion-body myositis and polymyositis. Muscle Nerve 2007; 35(1):17-23.

(299) Greenberg SA, Sanoudou D, Haslett JN, Kohane IS, Kunkel LM, Beggs AH, Amato AA. Molecular profiles of inflammatory myopathies. Neurology 2002; 59(8):1170-1182.

(300) Raju R, Dalakas MC. Gene expression profile in the muscles of patients with inflammatory myopathies: effect of therapy with IVIg and biological validation of clinically relevant genes. Brain 2005; 128(Pt 8):1887-1896.

(301) William J, Euler C, Christensen S, Shlomchik MJ. Evolution of autoantibody responses via somatic hypermutation outside of germinal centers. Science 2002; 297(5589):2066-2070.

(302) Nagaraju K, Casciola-Rosen L, Rosen A, Thompson C, Loeffler L, Parker T, Danning C, Rochon PJ, Gillespie J, Plotz P. The Inhibition of Apoptosis in Myositis and in Normal Muscle Cells. J Immunol 2000; 164(10):5459-5465.

(303) Marinova E, Han S, Zheng B. Germinal center helper T cells are dual functional regulatory cells with suppressive activity to conventional CD4+ T cells. J Immunol 2007; 178(8):5010-5017.

(304) Baechler EC, Bauer JW, Slattery CA, Ortmann WA, Espe KJ, Novitzke J, Ytterberg SR, Gregersen PK, Behrens TW, Reed AM. An interferon signature in the peripheral blood of dermatomyositis patients is associated with disease activity. Mol Med 2007; 13(1-2):59-68.

(305) Walsh RJ, Kong SW, Yao Y, Jallal B, Kiener PA, Pinkus JL, Beggs AH, Amato AA, Greenberg SA. Type I interferon-inducible gene expression in blood is present and reflects disease activity in dermatomyositis and polymyositis. Arthritis Rheum 2007; 56(11):3784-3792.

(306) Wenzel J, Schmidt R, Proelss J, Zahn S, Bieber T, Tuting T. Type I interferon-associated skin recruitment of CXCR3+ lymphocytes in dermatomyositis. Clin Exp Dermatol 2006; 31(4):576-582.

(307) McNiff JM, Kaplan DH. Plasmacytoid dendritic cells are present in cutaneous dermatomyositis lesions in a pattern distinct from lupus erythematosus. J Cutan Pathol 2008; 35(5):452-456.

(308) Lopez de Padilla CM, Vallejo AN, McNallan KT, Vehe R, Smith SA, Dietz AB, Vuk-Pavlovic S, Reed AM. Plasmacytoid dendritic cells in inflamed muscle of patients with juvenile dermatomyositis. Arthritis Rheum 2007; 56(5):1658-1668.

(309) Villadangos JA, Young L. Antigen-presentation properties of plasmacytoid dendritic cells. Immunity 2008; 29(3):352-361.

(310) Jego G, Palucka AK, Blanck JP, Chalouni C, Pascual V, Banchereau J. Plasmacytoid dendritic cells induce plasma cell differentiation through type I interferon and interleukin 6. Immunity 2003; 19(2):225-234.

(311) Kumanovics G, Magyarlaki T, Komocsi A, Szekeres G, Czirjak L. Simultaneous presence of neutrophil alveolitis and Ki-67 positivity of alveolar macrophages in dermato-/polymyositis and systemic sclerosis. Rheumatol Int 2003; 23(1):6-10.

(312) Kim WJ, Kim H, Suk K, Lee WH. Macrophages express granzyme B in the lesion areas of atherosclerosis and rheumatoid arthritis. Immunol Lett 2007; 111(1):57-65.

(313) Harvey BP, Quan TE, Rudenga BJ, Roman RM, Craft J, Mamula MJ. Editing antigen presentation: antigen transfer between human B lymphocytes and macrophages mediated by class A scavenger receptors. J Immunol 2008; 181(6):4043-4051.

(314) Butler WT, Rossen RD. Effects of corticosteroids on immunity in man. I. Decreased serum IgG concentration caused by 3 or 5 days of high doses of methylprednisolone. J Clin Invest 1973; 52(10):2629-2640.

(315) McMillan R, Longmire R, Yelenosky R. The effect of corticosteroids on human IgG synthesis. J Immunol 1976; 116(6):1592-1595.

(316) Boor PP, Metselaar HJ, Mancham S, Tilanus HW, Kusters JG, Kwekkeboom J. Prednisolone suppresses the function and promotes apoptosis of plasmacytoid dendritic cells. Am J Transplant 2006; 6(10):2332-2341.

(317) Hansen A, Dorner T, Lipsky PE. Use of immunoglobulin variable-region genes by normal subjects and patients with systemic lupus erythematosus. Int Arch Allergy Immunol 2000; 123:36-45.

(318) Jacobi AM, Hansen A, Burmester GR, Abramson SB, Dorner T, Lipsky PE. Enhanced mutational activity and disturbed selection of mutations in VH gene rearrangements on a patient with systemic lupus erythematosus. Autoimmunity 2001; 33:61-76.

(319) Owens GP, Ritchie AM, Burgoon MP, Williamson RA, Corboy JR, Gilden DH. Single-cell repertoire analysis demonstrates that clonal expansion is a prominent feature of the B cell response in multiple sclerosis cerebrospinal fluid. J Immunol 2003; 171(5):2725-2733.

(320) Voswinkel J, Weisgerber K, Pfreundschuh M, Gause A. B lymphocyte involvement in ankylosing spondylitis: the heavy chain variable segment gene

repertoire of B lymphocytes from germinal center-like foci in the synovial membrane indicates antigen selection. Arthritis Res 2001; 3(3):189-195.

(321) Gerhard N, Krenn V, Magalhaes R, Morawietz L, Brandlein S, Konig A. IgVH-genes analysis from psoriatic arthritis shows involvement of antigen-activated synovial B-lymphocytes. Z Rheumatol 2002; 61(6):718-727.

(322) Da RR, Qin Y, Baeten D, Zhang Y. B cell clonal expansion and somatic hypermutation of Ig variable heavy chain genes in the synovial membrane of patients with osteoarthritis. J Immunol 2007; 178(1):557-565.

(323) Shiokawa S, Matsumoto N, Nishimura J. Clonal analysis of B cells in the osteoarthritis synovium. Ann Rheum Dis 2001; 60(8):802-805.

(324) Kim HJ, Krenn V, Steinhauser G, Berek C. Plasma cell development in synovial germinal centers in patients with rheumatoid and reactive arthritis. J Immunol 1999; 162(5):3053-3062.

(325) Owens GP, Winges KM, Ritchie AM, Edwards S, Burgoon MP, Lehnhoff L, Nielsen K, Corboy J, Gilden DH, Bennett JL. VH4 Gene Segments Dominate the Intrathecal Humoral Immune Response in Multiple Sclerosis. J Immunol 2007; 179(9):6343-6351.

(326) Bombardieri M, Barone F, Humby F, Kelly S, McGurk M, Morgan P, Challacombe S, De Vita S, Valesini G, Spencer J, Pitzalis C. Activation-induced cytidine deaminase expression in follicular dendritic cell networks and interfollicular large B cells supports functionality of ectopic lymphoid neogenesis in autoimmune sialoadenitis and MALT lymphoma in Sjogren's syndrome. J Immunol 2007; 179(7):4929-4938.

(327) Cattoretti G, Buttner M, Shaknovich R, Kremmer E, Alobeid B, Niedobitek G. Nuclear and cytoplasmic AID in extrafollicular and germinal center B cells. Blood 2006; 107(10):3967-3975.

(328) Marafioti T, Jones M, Facchetti F, Diss TC, Du MQ, Isaacson PG, Pozzobon M, Pileri SA, Strickson AJ, Tan SY, Watkins F, Mason DY. Phenotype and genotype of interfollicular large B cells, a subpopulation of lymphocytes often with dendritic morphology. Blood 2003; 102(8):2868-2876.

(329) Moldenhauer G, Popov SW, Wotschke B, Bruderlein S, Riedl P, Fissolo N, Schirmbeck R, Ritz O, Moller P, Leithauser F. AID expression identifies interfollicular large B cells as putative precursors of mature B-cell malignancies. Blood 2006; 107(6):2470-2473.

(330) Weinstein JS, Nacionales DC, Lee PY, Kelly-Scumpia KM, Yan XJ, Scumpia PO, Vale-Cruz DS, Sobel E, Satoh M, Chiorazzi N, Reeves WH. Colocalization of antigen-specific B and T cells within ectopic lymphoid tissue following immunization with exogenous antigen. J Immunol 2008; 181(5):3259-3267.

(331) Borretzen M, Randen I, Zdarsky E, Forre O, Natvig JB, Thompson KM. Control of autoantibody affinity by selection against amino acid replacements in the complementarity-determining regions. Proc Natl Acad Sci U S A 1994; 91(26):12917-12921.

(332) Shlomchik MJ. Sites and stages of autoreactive B cell activation and regulation. Immunity 2008; 28(1):18-28.

(333) William J, Euler C, Leadbetter E, Marshak-Rothstein A, Shlomchik MJ. Visualizing the onset and evolution of an autoantibody response in systemic autoimmunity. J Immunol 2005; 174(11):6872-6878.

(334) Jackson KJ, Gaeta B, Sewell W, Collins AM. Exonuclease activity and P nucleotide addition in the generation of the expressed immunoglobulin repertoire. BMC Immunol 2004; 5:19.

(335) Torres M, Casadevall A. The immunoglobulin constant region contributes to affinity and specificity. Trends Immunol 2008; 29(2):91-97.

(336) Voswinkel J, Weisgerber K, Pfreundschuh M, Gause A. The B lymphocyte in rheumatoid arthritis: recirculation of B lymphocytes between different joints and blood. Autoimmunity 1999; 31(1):25-34.

(337) Souto-Carneiro MM, Krenn V, Hermann R, Konig A, Muller-Hermelink HK. IgVH genes from different anatomical regions, with different histopathological patterns, of a rheumatoid arthritis patient suggest cyclic re-entry of mature synovial B-cells in the hypermutation process. Arthritis Res 2000; 2(4):303-314.

(338) Oprea M, Perelson AS. Somatic mutation leads to efficient affinity maturation when centrocytes recycle back to centroblasts. J Immunol 1997; 158(11):5155-5162.

(339) Kepler TB, Perelson AS. Cyclic re-entry of germinal center B cells and the efficiency of affinity maturation. Immunol Today 1993; 14(8):412-415.

(340) Owens GP, Burgoon MP, Anthony J, Kleinschmidt-DeMasters BK, Gilden DH. The immunoglobulin G heavy chain repertoire in multiple sclerosis plaques is distinct from the heavy chain repertoire in peripheral blood lymphocytes. Clin Immunol 2001; 98(2):258-263.

(341) Gaeta BA, Malming HR, Jackson KJ, Bain ME, Wilson P, Collins AM. iHMMune-align: hidden Markov model-based alignment and identification of germline genes in rearranged immunoglobulin gene sequences. Bioinformatics 2007; 23(13):1580-1587.

(342) Volpe JM, Cowell LG, Kepler TB. SoDA: implementation of a 3D alignment algorithm for inference of antigen receptor recombinations. Bioinformatics 2006; 22(4):438-444.

(343) Bose B, Sinha S. Problems in using statistical analysis of replacement and silent mutations in antibody genes for determining antigen-driven affinity selection. Immunology 2005; 116(2):172-183.

(344) Chang B, Casali P. The CDR1 sequences of a major proportion of human germline Ig VH genes are inherently susceptible to amino acid replacement. Immunol Today 1994; 15(8):367-373.

(345) Lossos IS, Tibshirani R, Narasimhan B, Levy R. The inference of antigen selection on Ig genes. J Immunol 2000; 165(9):5122-5126.

(346) Shlomchik MJ, Aucoin AH, Pisetsky DS, Weigert MG. Structure and function of anti-DNA autoantibodies derived from a single autoimmune mouse. Proc Natl Acad Sci U S A 1987; 84(24):9150-9154.

(347) Lossos IS, Okada CY, Tibshirani R, Warnke R, Vose JM, Greiner TC, Levy R. Molecular analysis of immunoglobulin genes in diffuse large B-cell lymphomas. Blood 2000; 95(5):1797-1803.

(348) Voswinkel J, Mueller A, Kraemer JA, Lamprecht P, Herlyn K, Holl-Ulrich K, Feller AC, Pitann S, Gause A, Gross WL. B lymphocyte maturation in Wegener's granulomatosis: a comparative analysis of VH genes from endonasal lesions. Ann Rheum Dis 2006; 65(7):859-864.

(349) Voswinkel J, Assmann G, Held G, Pitann S, Gross WL, Holl-Ulrich K, Herlyn K, Mueller A. Single cell analysis of B lymphocytes from Wegener's granulomatosis: B cell receptors display affinity maturation within the granulomatous lesions. Clin Exp Immunol 2008.

(350) Mueller A, Holl-Ulrich K, Lamprecht P, Gross WL. Germinal centre-like structures in Wegener's granuloma: the morphological basis for autoimmunity? Rheumatology (Oxford) 2008; 47(8):1111-1113.

(351) Keogh KA, Wylam ME, Stone JH, Specks U. Induction of remission by B lymphocyte depletion in eleven patients with refractory antineutrophil cytoplasmic antibody-associated vasculitis. Arthritis Rheum 2005; 52(1):262-268.

(352) Keogh KA, Ytterberg SR, Fervenza FC, Carlson KA, Schroeder DR, Specks U. Rituximab for refractory Wegener's granulomatosis: report of a prospective, open-label pilot trial. Am J Respir Crit Care Med 2006; 173(2):180-187.

(353) Sneller MC. Rituximab and Wegener's granulomatosis: are B cells a target in vasculitis treatment? Arthritis Rheum 2005; 52(1):1-5.

(354) Specks U, Fervenza FC, McDonald TJ, Hogan MC. Response of Wegener's granulomatosis to anti-CD20 chimeric monoclonal antibody therapy. Arthritis Rheum 2001; 44(12):2836-2840.

(355) Ferraro AJ, Drayson MT, Savage COS, MacLennan IC. Levels of autoantibodies, unlike antibodies to all extrinsic antigen groups, fall following B cell depletion with Rituximab. Eur.J.Immunol. 38, 292-298. 25-10-2007.

(356) Chan AT, Flossmann O, Mukhtyar C, Jayne DR, Luqmani RA. The role of biologic therapies in the management of systemic vasculitis. Autoimmun Rev 2006; 5(4):273-278.

(357) Basu D, Reveille JD. Anti-scl-70. Autoimmunity 2005; 38(1):65-72.

(358) Tengner P, Halse AK, Haga HJ, Jonsson R, Wahren-Herlenius M. Detection of anti-Ro/SSA and anti-La/SSB autoantibody-producing cells in salivary glands from patients with Sjogren's syndrome. Arthritis Rheum 1998; 41(12):2238-2248.

(359) Salomonsson S, Jonsson MV, Skarstein K, Brokstad KA, Hjelmstrom P, Wahren-Herlenius M, Jonsson R. Cellular basis of ectopic germinal center formation and autoantibody production in the target organ of patients with Sjogren's syndrome. Arthritis Rheum 2003; 48(11):3187-3201.

(360) Halse A, Wahren-Herlenius M, Jonsson R. Ro/SS-A- and La/SS-B-reactive B lymphocytes in peripheral blood of patients with Sjogren's syndrome. Clin Exp Immunol 1999; 115(1):208-213.

(361) Matthews I, Sims G, Ledwidge S, Stott D, Beeson D, Willcox N, Vincent A. Antibodies to acetylcholine receptor in parous women with myasthenia: evidence for immunization by fetal antigen. Lab Invest 2002; 82(10):1407-1417.

(362) von Budingen HC, Harrer MD, Kuenzle S, Meier M, Goebels N. Clonally expanded plasma cells in the cerebrospinal fluid of MS patients produce myelin-specific antibodies. Eur J Immunol 2008; 38(7):2014-2023.

(363) Steiman-Shimony A, Edelman H, Hutzler A, Barak M, Zuckerman NS, Shahaf G, Dunn-Walters D, Stott DI, Abraham RS, Mehr R. Lineage tree analysis of immunoglobulin variable-region gene mutations in autoimmune diseases: chronic activation, normal selection. Cell Immunol 2006; 244(2):130-136.

(364) Steiman-Shimony A, Edelman H, Barak M, Shahaf G, Dunn-Walters D, Stott DI, Abraham RS, Mehr R. Immunoglobulin variable-region gene mutational lineage tree analysis: application to autoimmune diseases. Autoimmun Rev 2006; 5(4):242-251.

(365) Shahaf G, Barak M, Zuckerman NS, Swerdlin N, Gorfine M, Mehr R. Antigen-driven selection in germinal centers as reflected by the shape characteristics of immunoglobulin gene lineage trees: a large-scale simulation study. J Theor Biol 2008; 255(2):210-222.

(366) Barak M, Zuckerman NS, Edelman H, Unger R, Mehr R. IgTree: creating Immunoglobulin variable region gene lineage trees. J Immunol Methods 2008; 338(1-2):67-74.

(367) Tabibian-Keissar H, Zuckerman NS, Barak M, Dunn-Walters DK, Steiman-Shimony A, Chowers Y, Ofek E, Rosenblatt K, Schiby G, Mehr R, Barshack I. B-cell clonal diversification and gut-lymph node trafficking in ulcerative colitis revealed using lineage tree analysis. Eur J Immunol 2008; 38(9):2600-2609.

(368) William J, Euler C, Primarolo N, Shlomchik MJ. B cell tolerance checkpoints that restrict pathways of antigen-driven differentiation. J Immunol 2006; 176(4):2142-2151.

(369) William J, Euler C, Shlomchik MJ. Short-lived plasmablasts dominate the early spontaneous rheumatoid factor response: differentiation pathways, hypermutating cell types, and affinity maturation outside the germinal center. J Immunol 2005; 174(11):6879-6887.

(370) Weisel F, Wellmann U, Winkler TH. Autoreactive B cells get activated in extrafollicular sites. Eur J Immunol 2007; 37(12):3330-3333.

(371) Herlands RA, William J, Hershberg U, Shlomchik MJ. Anti-chromatin antibodies drive in vivo antigen-specific activation and somatic hypermutation of rheumatoid factor B cells at extrafollicular sites. Eur J Immunol 2007; 37(12):3339-3351.

(372) Herlands RA, Christensen SR, Sweet RA, Hershberg U, Shlomchik MJ. T Cell-Independent and Toll-like Receptor-Dependent Antigen-Driven Activation of Autoreactive B Cells. Immunity 2008; 29(2):249-260.

(373) Cantaert T, Kolln J, Timmer T, van der Pouw Kraan TC, Vandooren B, Thurlings RM, Canete JD, Catrina AI, Out T, Verweij CL, Zhang Y, Tak PP, Baeten D. B lymphocyte autoimmunity in rheumatoid synovitis is independent of ectopic lymphoid neogenesis. J Immunol 2008; 181(1):785-794.

(374) Zhang Y, Da RR, Hilgenberg LG, Tourtellotte WW, Sobel RA, Smith MA, Olek M, Nagra R, Sudhir G, van den NS, Qin Y. Clonal expansion of IgA-positive plasma cells and axon-reactive antibodies in MS lesions. J Neuroimmunol 2005; 167(1-2):120-130.

(375) Li Z, Schettino EW, Padlan EA, Ikenatsu H, Casali P. Structure-function analysis of a lupus anti-DNA autoantibody: central role of the heavy chain complementary-determining region 3 Arg in binding of double- and single-stranded DNA. Eur J Immunol 2000; 30:2015-2026.

(376) BEHRENDT M, PARTRIDGE LJ, GRIFFITHS B, GOODFIELD M, SNAITH M, LINDSEY NJ. The role of somatic mutation in determining the affinity of anti-DNA antibodies. Clinical and Experimental Immunology 2003; 131(1):182-189.

(377) Lambrianides A, Giles I, Ioannou Y, Mason L, Latchman DS, Manson JJ, Isenberg DA, Rahman A. Arginine mutation alters binding of a human monoclonal antibody to antigens linked to systemic lupus erythematosus and the antiphospholipid syndrome. Arthritis Rheum 2007; 56(7):2392-2401.

(378) Haley J, Mason LJ, Nagl S, Giles I, Latchman DS, Isenberg DA, Rahman A. Somatic mutations to arginine residues affect the binding of human monoclonal antibodies to DNA, histones, SmD and Ro antigen. Mol Immunol 2004; 40(11):745-758.

(379) Rahman A, Haley J, Radway-Bright E, Nagl S, Low DG, Latchman DS, Isenberg DA. The importance of somatic mutations in the V(lambda) gene 2a2 in human monoclonal anti-DNA antibodies. J Mol Biol 2001; 307(1):149-160.

(380) Cambridge G, Isenberg DA, Edwards JC, Leandro MJ, Migone TS, Teodorescu M, Stohl W. B cell depletion therapy in systemic lupus erythematosus: relationships among serum B lymphocyte stimulator levels, autoantibody profile and clinical response. Ann Rheum Dis 2008; 67(7):1011-1016.

(381) Ioannou Y, Lambrianides A, Cambridge G, Leandro MJ, Edwards JC, Isenberg DA. B cell depletion therapy for patients with systemic lupus erythematosus results in a significant drop in anticardiolipin antibody titres. Ann Rheum Dis 2008; 67(3):425-426.

(382) Walsh M, Jayne D. Targeting the B cell in vasculitis. Pediatr Nephrol 2008.

(383) Cambridge G, Leandro MJ, Teodorescu M, Manson J, Rahman A, Isenberg DA, Edwards JC. B cell depletion therapy in systemic lupus erythematosus: effect on autoantibody and antimicrobial antibody profiles. Arthritis Rheum 2006; 54(11):3612-3622.

(384) Edwards JC, Cambridge G. B-cell targeting in rheumatoid arthritis and other autoimmune diseases. Nat Rev Immunol 2006; 6(5):394-403.

(385) Dorner T, Burmester GR. New approaches of B-cell-directed therapy: beyond rituximab. Curr Opin Rheumatol 2008; 20(3):263-268.

(386) Sfikakis PP, Souliotis VL, Fragiadaki KG, Moutsopoulos HM, Boletis JN, Theofilopoulos AN. Increased expression of the FoxP3 functional marker of regulatory T cells following B cell depletion with rituximab in patients with lupus nephritis. Clin Immunol 2007; 123(1):66-73.

(387) Vallerskog T, Gunnarsson I, Widhe M, Risselada A, Klareskog L, van Vollenhoven R, Malmstrom V, Trollmo C. Treatment with rituximab affects both the cellular and the humoral arm of the immune system in patients with SLE. Clin Immunol 2007; 122(1):62-74.

(388) Rouziere AS, Kneitz C, Palanichamy A, Dorner T, Tony P. Regeneration of the immunoglobulin heavy-chain repertoire after transient B-cell depletion with an anti-CD20 antibody. Arthritis Research & Therapy 2005; 7:R714-R724.

(389) Harvey BP, Gee RJ, Haberman AM, Shlomchik MJ, Mamula MJ. Antigen presentation and transfer between B cells and macrophages. Eur J Immunol 2007; 37(7):1739-1751.

(390) Aluvihare VR, Khamlichi AA, Williams GT, Adorini L, Neuberger MS. Acceleration of intracellular targeting of antigen by the B-cell antigen receptor: importance depends on the nature of the antigen-antibody interaction. EMBO J 1997; 16(12):3553-3562.

(391) Cheng PC, Steele CR, Gu L, Song W, Pierce SK. MHC class II antigen processing in B cells: accelerated intracellular targeting of antigens. J Immunol 1999; 162(12):7171-7180.

(392) Karlsson L, Surh CD, Sprent J, Peterson PA. A novel class II MHC molecule with unusual tissue distribution. Nature 1991; 351(6326):485-488.

(393) Batista FD, Neuberger MS. Affinity dependence of the B cell response to antigen: a threshold, a ceiling, and the importance of off-rate. Immunity 1998; 8(6):751-759.

(394) Mamula MJ, Fatenejad S, Craft J. B cells process and present lupus autoantigens that initiate autoimmune T cell responses. J Immunol 1994; 152(3):1453-1461.

(395) Yan J, Mamula MJ. B and T cell tolerance and autoimmunity in autoantibody transgenic mice. Int Immunol 2002; 14(8):963-971.

(396) Datta SK, Zhang L, Xu L. T-helper cell intrinsic defects in lupus that break peripheral tolerance to nuclear autoantigens. J Mol Med 2005; 83(4):267-278.

(397) Mizoguchi A, Bhan AK. A case for regulatory B cells. J Immunol 2006; 176(2):705-710.

(398) Harris DP, Haynes L, Sayles PC, Duso DK, Eaton SM, Lepak NM, Johnson LL, Swain SL, Lund FE. Reciprocal regulation of polarized cytokine production by effector B and T cells. Nat Immunol 2000; 1(6):475-482.

(399) Pers JO, Devauchelle V, Daridon C, Bendaoud B, Le Berre R, Bordron A, Hutin P, Renaudineau Y, Dueymes M, Loisel S, Berthou C, Saraux A, Youinou P.

BAFF-modulated repopulation of B lymphocytes in the blood and salivary glands of rituximab-treated patients with Sjogren's syndrome. Arthritis Rheum 2007; 56(5):1464-1477.

(400) Cambridge G, Stohl W, Leandro MJ, Migone TS, Hilbert DM, Edwards JC. Circulating levels of B lymphocyte stimulator in patients with rheumatoid arthritis following rituximab treatment: relationships with B cell depletion, circulating antibodies, and clinical relapse. Arthritis Rheum 2006; 54(3):723-732.

(401) Strandberg L, Ambrosi A, Espinosa A, Ottosson L, Eloranta ML, Zhou W, Elfving A, Greenfield E, Kuchroo VK, Wahren-Herlenius M. Interferon-alpha induces up-regulation and nuclear translocation of the Ro52 autoantigen as detected by a panel of novel Ro52-specific monoclonal antibodies. J Clin Immunol 2008; 28(3):220-231.

(402) Hsu HC, Yang P, Wang J, Wu Q, Myers R, Chen J, Yi J, Guentert T, Tousson A, Stanus AL, Le TV, Lorenz RG, Xu H, Kolls JK, Carter RH, Chaplin DD, Williams RW, Mountz JD. Interleukin 17-producing T helper cells and interleukin 17 orchestrate autoreactive germinal center development in autoimmune BXD2 mice. Nat Immunol 2008; 9(2):166-175.

(403) Tarlinton D. IL-17 drives germinal center B cells? Nat Immunol 2008; 9(2):124-126.

(404) Bettelli E, Oukka M, Kuchroo VK. T(H)-17 cells in the circle of immunity and autoimmunity. Nat Immunol 2007; 8(4):345-350.

(405) Kolls JK, Linden A. Interleukin-17 family members and inflammation. Immunity 2004; 21(4):467-476.

(406) Goebels N, Michaelis D, Wekerle H, Hohlfeld R. Human myoblasts as antigen-presenting cells. J Immunol 1992; 149(2):661-667.

(407) Schwab N, Waschbisch A, Wrobel B, Lochmuller H, Sommer C, Wiendl H. Human myoblasts modulate the function of antigen-presenting cells. J Neuroimmunol 2008; 200(1-2):62-70.

(408) Sugiura T, Kawaguchi Y, Harigai M, Takagi K, Ohta S, Fukasawa C, Hara M, Kamatani N. Increased CD40 expression on muscle cells of polymyositis and dermatomyositis: role of CD40-CD40 ligand interaction in IL-6, IL-8, IL-15, and monocyte chemoattractant protein-1 production. J Immunol 2000; 164(12):6593-6600.

(409) Murata K, Dalakas MC. Expression of the costimulatory molecule BB-1, the ligands CTLA-4 and CD28, and their mRNA in inflammatory myopathies. Am J Pathol 1999; 155(2):453-460.

(410) Wiendl H, Mitsdoerffer M, Schneider D, Melms A, Lochmuller H, Hohlfeld R, Weller M. Muscle fibres and cultured muscle cells express the B7.1/2-related inducible co-stimulatory molecule, ICOSL: implications for the pathogenesis of inflammatory myopathies. Brain 2003; 126(Pt 5):1026-1035.

(411) Waschbisch A, Wintterle S, Lochmuller H, Walter MC, Wischhusen J, Kieseier BC, Wiendl H. Human muscle cells express the costimulatory molecule B7-H3,

which modulates muscle-immune interactions. Arthritis Rheum 2008; 58(11):3600-3608.

(412) Wiendl H, Mitsdoerffer M, Schneider D, Chen L, Lochmuller H, Melms A, Weller M. Human muscle cells express a B7-related molecule, B7-H1, with strong negative immune regulatory potential: a novel mechanism of counterbalancing the immune attack in idiopathic inflammatory myopathies. FASEB J 2003; 17(13):1892-1894.

(413) Wiendl H, Mitsdoerffer M, Hofmeister V, Wischhusen J, Weiss EH, Dichgans J, Lochmuller H, Hohlfeld R, Melms A, Weller M. The non-classical MHC molecule HLA-G protects human muscle cells from immune-mediated lysis: implications for myoblast transplantation and gene therapy. Brain 2003; 126(Pt 1):176-185.

(414) Wiendl H, Hohlfeld R, Kieseier BC. Muscle-derived positive and negative regulators of the immune response. Curr Opin Rheumatol 2005; 17(6):714-719.

(415) Wiendl H, Hohlfeld R, Kieseier BC. Immunobiology of muscle: advances in understanding an immunological microenvironment. Trends Immunol 2005; 26(7):373-380.

(416) Grundtman C, Lundberg IE. Pathogenesis of idiopathic inflammatory myopathies. Curr Rheumatol Rep 2006; 8(3):188-195.

(417) Azzazy HME, Highsmith J. Phage display technology: clinical applications and recent innovations. Clinical Biochemistry 2002; 35(6):425-445.

(418) Hoogenboom HR, de Bruine AP, Hufton SE, Hoet RM, Arends J, Roovers RC. Antibody phage display technology and its applications. Immunotechnology 1998; 4:1-20.

(419) Smothers JF, Henikoff S, Carter P. Affinity selection from biological libraries. Science 2002; 298:621-622.

(420) Vaccaro P, Pavoni E, Monteriu G, Andrea P, Felici F, Minenkova O. Efficient display of scFv antibodies on bacteriophage lambda. Journal of Immunological Methods 2006; 310:149-158.

(421) Voswinkel J, Kerkdijk AJ, Mueller A, Assmann G, Pfreundschuh M, Held G. A novel system to test for specificity of B cell receptors from tissue of Wegener's granulomatosis patients. Clin Exp Rheumatol 2008; 26(3 Suppl 49):S90-S96.

(422) Zhang J, Jacobi AM, Mackay M, Aranow C, Wang T, Chinnasamy P, Diamond B. Identification of DNA-reactive B cells in patients with systemic lupus erythematosus. J Immunol Methods 2008; 338(1-2):79-84.

(423) Burgoon MP, Keays KM, Owens GP, Ritchie AM, Rai PR, Cool CD, Gilden DH. Laser-capture microdissection of plasma cells from subacute sclerosing panencephalitis brain reveals intrathecal disease-relevant antibodies. PNAS 2005; 102(20):7245-7250.

Appendix 1 – Ig DNA Sequence Alignments using the JOINSOLVER Software

The JOINSOLVER algorithm (http://joinsolver.niams.nih.gov) (241) was used to match the isolated Ig DNA sequences from myositis and vasculitis samples to the corresponding germline genes. The software was used with the default parameters. For illustration purposes only the alignments for the assigned genes have been shown, in most instances this was the best matching and highest scoring alignment but where alternative, lower scoring, matches have been assigned the higher scoring alignments have also been given with the assigned gene highlighted in yellow. Assignment of D_H genes and junctional analysis was conducted as described in section 2.3.12.3. Primer regions, the first 24 bases at the 5' V_H region, were disregarded; for illustration purposes in the sequence alignments below and on the attached CD these regions were converted back to germline configurations once the best matching germline gene had been assigned to allow mutational numbers to correspond to those used in the analysis of these sequences in Chapters 4 and 5. Junctional nucleotides highlighted in yellow illustrate the P and N nucleotides used in the analysis of these regions after manual analysis of the D gene assignment and junctional regions.

In addition to JOINSOLVER the IMGT/V-QUEST algorithm was also used match the isolated Ig DNA sequences to the corresponding germline genes. Any anomalies between the two alignment algorithms are given within the results section of Chapters 4 and 5. The IMGT/V-QUEST algorithm has the capability of searching the isolated sequence for the presence of insertions and deletions of nucleotides, which is not available using the JOINSOLVER algorithm. Where insertions and deletions were detected the corresponding alignments from the IMGT/V-QUEST algorithm are provided in addition to the subsequent alignments, using both programmes, following restoration of the insertions or deletions.

Sequence alignments to gene assignments for all sequences used in this study can be found on the attached CD; alignments from one patient from each principal disorder of this study are shown below.

Sample MYO17
Sequence – V_H3-30*03, D_H3-9*01, J_H4*02

Raw Sequence

```
CAGGTGCAGCTGGTGGAGTCTGGGGGAGGCGTGGTCCAGCCTGGGAGGTCTCTGAGACTCTCCTGTGCAGCCTCTGGATTCACCTTCAGTACCTATGCCATGCACTGGGTCCGCCAGG
CTCCAGGCAAGGGGCTGGAGTGGCTGGCAATTATTTCATATGATGGAGGTAATAAATACTATGCAGACTCCGTGAAGGGCCGATTCACCATTTCCAGAGACAATTCCAAGAATACGCT
GTATCTGCAAATGAACAGCCTGAGAGCTGAGGACACGGCTGTATATTGGTGTGCGACAGGCGCGTATTATGATATTTTGAGTGGTGCTCGGCCGTTTGACTACTGGGGCCAGGGAACC
CTGGTCACCGTCTCCTA
```

Joinsolver Alignment

Summary

```
Amino acid translation of the sequence:
QVQLVESGGGVVQPGRSLRLSCAASGFTFSTYAMHWVRQAPGKGLEWLAIISYDGGNKYYADSVKGRFTISRDNSKNTLYLQMNSLRAED
TAVYWCATGAYYDILSGARPFDYWGQGTLVTVS

JoinSolver
Rearrangement is productive:

Highest scoring matches:
V: IGHV3-30*03  D:IGHD3-9*01  J: IGHJ4*02
The VH segment has 12 mutations
CDR3 Length:  51
 A   T   G   A   Y   Y   D   I   L   S   G   A   R   P   F   D   Y
GCG ACA GGC GCG TAT TAT GAT ATT TTG AGT GGT GCT CGG CCG TTT GAC TAC
```

V Match Results

```
                  ----------------------------------------------------------FR1-----------
                   1   2   3   4   5   6   7   8   9   10  11  12  13  14  15  16  17  18
                   Q   V   Q   L   V   E   S   G   G   G   V   V   Q   P   G   R   S   L
            score CAG GTG CAG CTG GTG GAG TCT GGG GGA GGC GTG GTC CAG CCT GGG AGG TCT CTG
IGHV3-30*03  1317 ... ... ... ... ... ... ... ... ... ... ... ... ... ... ... ... ..C ...

                  ------------------------------------------------ ___________CDR1_________
                   19  20  21  22  23  24  25  26  27  28  29  30  31 31a 31b  32  33  34
                   R   L   S   C   A   A   S   G   F   T   F   S   T           Y   A   M
                  AGA CTC TCC TGT GCA GCC TCT GGA TTC ACC TTC AGT ACC --- --- TAT GCC ATG
IGHV3-30*03       ... ... ... ... ... ... ... ... ... ... ... ... .G. --- --- ... .G. ...
```

```
                  ___ --------------------------------FR2------------------- ___________
                   35  36  37  38  39  40  41  42  43  44  45  46  47  48  49  50  51  52
                   H   W   V   R   Q   A   P   G   K   G   L   E   W   L   A   I   I   S
                  CAC TGG GTC CGC CAG GCT CCA GGC AAG GGG CTG GAG TGG CTG GCA ATT ATT TCA
IGHV3-30*03       ... ... ... ... ... ... ... ... ... ... ... ... ... G.. ... G.. ..A ...

                  ____________________________CDR2_____________________________________ --------
                  52a 52b 52c  53  54  55  56  57  58  59  60  61  62  63  64  65  66  67
                   Y           D   G   G   N   K   Y   Y   A   D   S   V   K   G   R   F
                  TAT --- --- GAT GGA GGT AAT AAA TAC TAT GCA GAC TCC GTG AAG GGC CGA TTC
IGHV3-30*03       ... --- --- ... ... A.. ... ... ... ... ... ... ... ... ... ... ... ...

                  ------------------FR3-------------------------------------------------------
                   68  69  70  71  72  73  74  75  76  77  78  79  80  81  82 82a 82b 82c
                   T   I   S   R   D   N   S   K   N   T   L   Y   L   Q   M   N   S   L
                  ACC ATT TCC AGA GAC AAT TCC AAG AAT ACG CTG TAT CTG CAA ATG AAC AGC CTG
IGHV3-30*03       ... ..C ... ... ... ... ... ... ..C ... ... ... ... ... ... ... ... ...

                  ------------------------------------ ___CDR3_____
                   83  84  85  86  87  88  89  90  91  92  93  94  95
                   R   A   E   D   T   A   V   Y   W   C   A   T   G
                  AGA GCT GAG GAC ACG GCT GTA TAT TGG TGT GCG ACA GGC
IGHV3-30*03       ... ... ... ... ... ... ..G ... .AC ... ... .G. .A
```

D Match Results

```
                    A   T   G   A   Y   Y   D   I   L   S   G   A   R   P   F   D   Y   W   G   Q   G   T   L   V   T   V   S
          len|rf    GCG ACA GGC GCG TAT TAT GAT ATT TTG AGT GGT GCT CGG CCG TTT GAC TAC TGG GGC CAG GGA ACC CTG GTC ACC GTC TCC TA
IGHD3-    10|2                  . ... ..C ... ... ... .C. ... TA. TAT AAC
9*01
```

J Match Results

```
                    A   T   G   A   Y   Y   D   I   L   S   G   A   R   P   F   D   Y   W   G   Q   G   T   L   V   T   V   S
          scoreGCG ACA GGC GCG TAT TAT GAT ATT TTG AGT GGT GCT CGG CCG TTT GAC TAC TGG GGC CAG GGA ACC CTG GTC ACC GTC TCC TA
IGHJ4*02  176                                                 AC TAC ... ... ... ... ... ... ... ... ... ... ... ... ... .CA G
```

Junction Analysis

```
V Match: IGHV3-30*03  D Match: IGHD3-9*01  J Match: IGHJ4*02
  V-J Distance: 38
VD Junction: # of P,N Nucleotides: (0,14)  CAGGCGCGTATTAT
DJ Junction: # of P,N Nucleotides: (0,14)  GTGGTGCTCGGCCG
```

Sequence – V_H6-01*01, No D Gene Assignment, J_H5*02

Raw Sequence

CAGGTACAGCTGCAGCAGTCAGGTCCAGGACTGGTGAAGCCCTCGCAGACCCTCTCACTCACCTGTGCCATCTCCGGGGACAGTGTCTCTAGCAACAGTGCTGCTTGGAACTGGATCA
GGCAGTCCCCATCGAGAGGCCTTGAGTGGCTGGCAAGGACATACTACAGGTCCAAGTGGTATAATGATTATGCAGTATCTGTGAAAAGCCGAATAACCATCAACCCAGACACATCCAA
GAACCAGTTCTCCCTGCAGCTGAACTCTGTGATTCCCGAAGACACGGCTGTCTATTACTGTGTAAGATCCCCCCTTAAGCAGTGGCTGGAACCCTGGGGCAAGGGAACCCTGGTCACC
GTCTCCTCAA

Joinsolver Alignment

Summary

Amino acid translation of the sequence:
QVQLQQSGPGLVKPSQTLSLTCAISGDSVSSNSAAWNWIRQSPSRGLEWLARTYYRSKWYNDYAVSVKSRITINPDTSKNQFSLQLNSVI
PEDTAVYYCVRSPLKQWLEPWGKGTLVTVSS

JoinSolver
Rearrangement is productive:
Highest scoring matches:
V: IGHV6-01*01 D:IGHD3-16*02R J: IGHJ5*02
The VH segment has 5 mutations
CDR3 Length: 33

```
 V   R   S   P   L   K   Q   W   L   E   P
GTA AGA TCC CCC CTT AAG CAG TGG CTG GAA CCC
```

V Match Results

```
                  ----------------------------------------------------------FR1-----------
                   1   2   3   4   5   6   7   8   9   10  11  12  13  14  15  16  17  18
                   Q   V   Q   L   Q   Q   S   G   P   G   L   V   K   P   S   Q   T   L
            score CAG GTA CAG CTG CAG CAG TCA GGT CCA GGA CTG GTG AAG CCC TCG CAG ACC CTC
IGHV6-01*01 1425  ... ... ... ... ... ... ... ... ... ... ... ... ... ... ... ... ... ...

                  ------------------------------------------------ ___________CDR1_________
                   19  20  21  22  23  24  25  26  27  28  29  30  31 31a 31b  32  33  34
                   S   L   T   C   A   I   S   G   D   S   V   S   S   N   S   A   A   W
                  TCA CTC ACC TGT GCC ATC TCC GGG GAC AGT GTC TCT AGC AAC AGT GCT GCT TGG
IGHV6-01*01       ... ... ... ... ... ... ... ... ... ... ... ... ... ... ... ... ... ...

                  ___ --------------------------------FR2-------------------- ___________
                   35  36  37  38  39  40  41  42  43  44  45  46  47  48  49  50  51  52
                   N   W   I   R   Q   S   P   S   R   G   L   E   W   L   A   R   T   Y
                  AAC TGG ATC AGG CAG TCC CCA TCG AGA GGC CTT GAG TGG CTG GCA AGG ACA TAC
IGHV6-01*01       ... ... ... ... ... ... ... ... ... ... ... ... ... ... .G. ... ... ...
```

```
                        _____________________CDR2_____________________________________ --------
                        52a 52b 52c  53  54  55  56  57  58  59  60  61  62  63  64  65  66  67
                         Y   R       S   K   W   Y   N   D   Y   A   V   S   V   K   S   R   I
                        TAC AGG --- TCC AAG TGG TAT AAT GAT TAT GCA GTA TCT GTG AAA AGC CGA ATA
IGHV6-01*01             ... ... --- ... ... ... ... ... ... ... ... ... ... ... ... ..T ... ...

                        ------------------FR3-----------------------------------------------------
                         68  69  70  71  72  73  74  75  76  77  78  79  80  81  82 82a 82b 82c
                         T   I   N   P   D   T   S   K   N   Q   F   S   L   Q   L   N   S   V
                        ACC ATC AAC CCA GAC ACA TCC AAG AAC CAG TTC TCC CTG CAG CTG AAC TCT GTG
IGHV6-01*01             ... ... ... ... ... ... ... ... ... ... ... ... ... ... ... ... ... ...

                        ------------------------------------ ___CDR3_____
                         83  84  85  86  87  88  89  90  91  92  93  94  95
                         I   P   E   D   T   A   V   Y   Y   C   V   R   S
                        ATT CCC GAA GAC ACG GCT GTC TAT TAC TGT GTA AGA TCC
IGHV6-01*01             .C. ... ..G ... ... ... ..G ... ... ... .C. ... GA
```

D Match Results

```
                         V   R   S   P   L   K   Q   W   L   E   P   W   G   K   G   T   L   V   T   V   S   S
                len|rf   GTA AGA TCC CCC CTT AAG CAG TGG CTG GAA CCC TGG GGC AAG GGA ACC CTG GTC ACC GTC TCC TCA A
IGHD3-16*02R    6|3      .AT .AC ... ... AAA CGT A.T CAT AAT AC
```

J Match Results

```
                         V   R   S   P   L   K   Q   W   L   E   P   W   G   K   G   T   L   V   T   V   S   S
               score    GTA AGA TCC CCC CTT AAG CAG TGG CTG GAA CCC TGG GGC AAG GGA ACC CTG GTC ACC GTC TCC TCA A
IGHJ5*02       183                       .C A.C ... T.C ..C ... ... ... C.. ... ... ... ... ... ... ... ... G
```

Junction Analysis

```
V Match: IGHV6-01*01   D Match: IGHD3-16*02R  J Match: IGHJ5*02
  V-J Distance: 29
VD Junction: # of P,N Nucleotides: (2,3)  TAAga(tc)
DJ Junction: # of P,N Nucleotides: (0,18)  CTTAAGCAGTGGCTGGAA
```

Sample VAS1
Sequence – V_H1-18*01, D_H2-2*01, J_H5*02

Raw Sequence

```
CAGGTTCAGCTGGTGCAGTCTGGAGCTGAGGTGAAGAAGCCTGGGGCCTCAGTGACGGTCTCCTGCACGGCCTCTGGTTACACCTTTACCAGCTATGCTGTCAGCTGGGTGCGACAGG
CCCCTGGACAAGGTCTTGAGTGGATGGCGTGGATCAGCACTTACTATGATGATGCAAAATATGCGCCGAAATTCCAGGGCAGACTTTCCGTGACCACGGACACATCCACGAGCACAGC
CTACATGGAACTGAGGAGCCTGAGATCTGACGACACGGCCAGATACTTCTGTGCGAGAGACGATTGTTCTGGTACCAGCTGTCATGCCGACCTCTGGGGCCAGGGAACCCTGGTCACC
AAGCCG
```

Joinsolver Alignment

Summary

```
Amino acid translation of the sequence:
QVQLVQSGAEVKKPGASVTVSCTASGYTFTSYAVSWVRQAPGQGLEWMAWISTYYDDAKYAPKFQGRLSVTTDTSTSTAYMELRSLRSDD
TARYFCARDDCSGTSCHADLWGQGTLVTK

JoinSolver
Rearrangement is productive:

Highest scoring matches:
V: IGHV1-18*01  D:IGHD2-2*01  J: IGHJ5*02
The VH segment has 30 mutations
CDR3 Length:  42
 A   R   D   D   C   S   G   T   S   C   H   A   D   L
GCG AGA GAC GAT TGT TCT GGT ACC AGC TGT CAT GCC GAC CTC
```

V Match Results

```
                  ----------------------------------------------------------FR1-----------
                   1   2   3   4   5   6   7   8   9   10  11  12  13  14  15  16  17  18
                   Q   V   Q   L   V   Q   S   G   A   E   V   K   K   P   G   A   S   V
            score CAG GTT CAG CTG GTG CAG TCT GGA GCT GAG GTG AAG AAG CCT GGG GCC TCA GTG
IGHV1-18*01 1155  ... ... ... ... ... ... ... ... ... ... ... ... ... ... ... ... ... ...

                  ------------------------------------------------ __________CDR1_________
                   19  20  21  22  23  24  25  26  27  28  29  30  31 31a 31b  32  33  34
                   T   V   S   C   T   A   S   G   Y   T   F   T   S           Y   A   V
                  ACG GTC TCC TGC ACG GCC TCT GGT TAC ACC TTT ACC AGC --- --- TAT GCT GTC
IGHV1-18*01       .A. ... ... ... .A. ..T ... ... ... ... ... ... ... --- --- ... .G. A..
```

```
                ___ ------------------------------FR2------------------- ___________
                 35  36  37  38  39  40  41  42  43  44  45  46  47  48  49  50  51  52
                 S   W   V   R   Q   A   P   G   Q   G   L   E   W   M   A   W   I   S
                AGC TGG GTG CGA CAG GCC CCT GGA CAA GGT CTT GAG TGG ATG GCG TGG ATC AGC
IGHV1-18*01     ... ... ... ... ... ... ... ... ... ..G ... ... ... ... .GA ... ... ...

                ___________________________CDR2_____________________________________ --------
                52a 52b 52c  53  54  55  56  57  58  59  60  61  62  63  64  65  66  67
                 T           Y   Y   D   D   A   K   Y   A   P   K   F   Q   G   R   L
                ACT --- --- TAC TAT GAT GAT GCA AAA TAT GCG CCG AAA TTC CAG GGC AGA CTT
IGHV1-18*01     G.. --- --- ... A.. .G. A.C A.. ..C ... ..A .A. ..G C.. ... ... ... G.C

                ------------------FR3-----------------------------------------------------
                 68  69  70  71  72  73  74  75  76  77  78  79  80  81  82 82a 82b 82c
                 S   V   T   T   D   T   S   T   S   T   A   Y   M   E   L   R   S   L
                TCC GTG ACC ACG GAC ACA TCC ACG AGC ACA GCC TAC ATG GAA CTG AGG AGC CTG
IGHV1-18*01     A.. A.. ... ..A ... ... ... ... ... ... ... ... ... ..G ... ... ... ...

                ------------------------------------ ___CDR3_____
                 83  84  85  86  87  88  89  90  91  92  93  94  95
                 R   S   D   D   T   A   R   Y   F   C   A   R   D
                AGA TCT GAC GAC ACG GCC AGA TAC TTC TGT GCG AGA GAC
IGHV1-18*01     ... ... ... ... ... ... GTG ..T .A. ... ... ... ..
```

D Match Results

```
                  A   R   D   D   C   S   G   T   S   C   H   A   D   L   W   G   Q   G   T   L   V   T   K   P
          len|rf  GCG AGA GAC GAT TGT TCT GGT ACC AGC TGT CAT GCC GAC CTC TGG GGC CAG GGA ACC CTG GTC ACC AAG CCG
IGHD2-2*01 10|2     . .GA T.. ... AG. A.. ... ... ..C T.. ...
```

J Match Results

```
                  A   R   D   D   C   S   G   T   S   C   H   A   D   L   W   G   Q   G   T   L   V   T   K   P
          score GCG AGA GAC GAT TGT TCT GGT ACC AGC TGT CAT GCC GAC CTC TGG GGC CAG GGA ACC CTG GTC ACC AAG CCG
IGHJ5*02  100                             A. AAC TGG TT. ... .C. ... ... ... ... ... ... ... ... GTC T.C TCA G
```

Junction Analysis

```
V Match: IGHV1-18*01  D Match: IGHD2-2*01  J Match: IGHJ5*02
  V-J Distance: 33
VD Junction: # of P,N Nucleotides: (0,11)  CGATTGTTCTG
DJ Junction: # of P,N Nucleotides: (0,12)  TCATGCCGACCT
```

Sequence – V_H3-23*01, No D Gene Assignment, J_H4*02 (25 Mutations)

Raw Sequence

GAGGTGCAGCTGTTGGAGTCTGGGGGAGGCTTGGTAGAGGTTGGGGGGTCCCTGAGACTCTCCTGTGCGGCCTCTGGACTCCCCTTTAGAAGCTCTGCCATGAGCTGGGTCCGCCAGG
CTCCAGGGAAGGGGCTGGAGTGGGTCTCAAGTATTAGTAGTAGTGGCAGTACCACATACTACGCAGACTCCGCGAAGGGCCGGTTCACCGTCTCCAGAGACAATTCCAGGAACACTTT
ATTTCTGCAATTGAACAGCCTGAGAGCCGAGGACACGGCCATATACTACTGCGTGAAGACCACGGTTATAAACCTGTCGTACTTTGAAGACTGGGGCCGGGGGACCACGGTCACCGTC
TCCTCAGGAACCCTGGTCACCGTCTCCTCAA

Joinsolver Alignment

Summary

Amino acid translation of the sequence:
EVQLLESGGGLVEVGGSLRLSCAASGLPFRSSAMSWVRQAPGKGLEWVSSISSSGSTTYYADSAKGRFTVSRDNSRNTLFLQLNSLRAED
TAIYYCVKTTVINLSYFEDWGRGTTVTVSSGTLVTVSS

JoinSolver
Rearrangement is productive:
Highest scoring matches:
V: IGHV3-23*01 D:IGHD1-14*01R J: IGHJ4*02
The VH segment has 25 mutations
CDR3 Length: 39

```
 V   K   T   T   V   I   N   L   S   Y   F   E   D
GTG AAG ACC ACG GTT ATA AAC CTG TCG TAC TTT GAA GAC
```

V Match Results

```
                  ------------------------------------------------------------FR1-----------
                   1   2   3   4   5   6   7   8   9   10  11  12  13  14  15  16  17  18
                   E   V   Q   L   L   E   S   G   G   G   L   V   E   V   G   G   S   L
             score GAG GTG CAG CTG TTG GAG TCT GGG GGA GGC TTG GTA GAG GTT GGG GGG TCC CTG
IGHV3-23*01  1209  ... ... ... ... ... ... ... ... ... ... ... ... C.. CC. ... ... ... ...

                  ---------------------------------------------- ___________CDR1_________
                   19  20  21  22  23  24  25  26  27  28  29  30  31 31a 31b  32  33  34
                   R   L   S   C   A   A   S   G   L   P   F   R   S           S   A   M
                  AGA CTC TCC TGT GCG GCC TCT GGA CTC CCC TTT AGA AGC --- --- TCT GCC ATG
IGHV3-23*01       ... ... ... ... ..A ... ... ... T.. A.. ... ..C ... --- --- .A. ... ...

                  ___ --------------------------------FR2------------------- ___________
                   35  36  37  38  39  40  41  42  43  44  45  46  47  48  49  50  51  52
                   S   W   V   R   Q   A   P   G   K   G   L   E   W   V   S   S   I   S
                  AGC TGG GTC CGC CAG GCT CCA GGG AAG GGG CTG GAG TGG GTC TCA AGT ATT AGT
IGHV3-23*01       ... ... ... ... ... ... ... ... ... ... ... ... ... ... ... GC. ... ...
```

```
                          _____________________CDR2_____________________________________ --------
                          52a 52b 52c  53  54  55  56  57  58  59  60  61  62  63  64  65  66  67
                           S           S   G   S   T   T   Y   Y   A   D   S   A   K   G   R   F
                          AGT --- --- AGT GGC AGT ACC ACA TAC TAC GCA GAC TCC GCG AAG GGC CGG TTC
IGHV3-23*01               G.. --- --- ... ..T G.. .G. ... ... ... ... ... ... .T. ... ... ... ...

                          ------------------FR3-----------------------------------------------------
                           68  69  70  71  72  73  74  75  76  77  78  79  80  81  82 82a 82b 82c
                           T   V   S   R   D   N   S   R   N   T   L   F   L   Q   L   N   S   L
                          ACC GTC TCC AGA GAC AAT TCC AGG AAC ACT TTA TTT CTG CAA TTG AAC AGC CTG
IGHV3-23*01               ... A.. ... ... ... ... ... .A. ... ..G C.G .A. ... ... A.. ... ... ...

                          ------------------------------------ ___CDR3_____
                           83  84  85  86  87  88  89  90  91  92  93  94  95
                           R   A   E   D   T   A   I   Y   Y   C   V   K   T
                          AGA GCC GAG GAC ACG GCC ATA TAC TAC TGC GTG AAG ACC
IGHV3-23*01               ... ... ... ... ... ... G.. ..T ... ..T .C. ..A GA
```

D Match Results

```
                                V   K   T   T   V   I   N   L   S   Y   F   E   D   W   G   R   G   T   T   V   T   V   S   S   G   T   L   V   T   V   S   S

                          len|rf GTG AAG ACC ACG GTT ATA AAC CTG TCG TAC TTT GAA GAC TGG GGC CGG GGG ACC ACG GTC ACC GTC TCC TCA GGA ACC CTG GTC ACC GTC TCC TCA A

IGHD1-14*01R              8|1      GT. GTT C.. ... ... CC
```

J Match Results

```
                                V   K   T   T   V   I   N   L   S   Y   F   E   D   W   G   R   G   T   T   V   T   V   S   S   G   T   L   V   T   V   S   S

                          scoreGTG AAG ACC ACG GTT ATA AAC CTG TCG TAC TTT GAA GAC TGG GGC CGG GGG ACC ACG GTC ACC GTC TCC TCA GGA ACC CTG GTC ACC GTC TCC TCA A

IGHJ4*02                  168                                 AC ... ... ..C T.. ... ... .A. ..A ... CT. ... ... ... ... ... .
```

Junction Analysis

```
V Match: IGHV3-23*01  D Match: IGHD1-14*01R  J Match: IGHJ4*02
  V-J Distance: 36
VD Junction: # of P,N Nucleotides: (0,9)  TGAAGACCA
DJ Junction: # of P,N Nucleotides: (0,19)  AACCTGTCGTACTTTGAAG
```

Sequence – V_H3-23*01, No D Gene Assignment, J_H4*02 (26 Mutations)

Raw Sequence

GAGGTGCAGCTGTTGGAGTCTGGGGGAGGCTTGGTAGAGGTTGGGGGGTCCCTGAGACTCTCCTGTGCGGCCTCTGGACTCCCCTTTAGAAGCTCTGCCATGAGCTGGGTCCGCCAGG
CTCCAGGGAAGGGGCTGGAGTGGGTCTCAAGTATTAGTAGTAGTGGCAGTACCACATACTACGCAGACTCCGCGAAGGGCCGGTTCACCGTCTCCAGAGACAATTCCAGGAACACTTC
ATTTCTGCAATTGAACAGCCTGAGAGCCGAGGACACGGCCATATACTACTGCGTGAAGACCACGGTTATAAACCTGTCGTACTTTGAAGACTGGGGCCGGGGGACCACGGTCACCGTC
TCCTCAA

Joinsolver Alignment

Summary

Amino acid translation of the sequence:
EVQLLESGGGLVEVGGSLRLSCAASGLPFRSSAMSWVRQAPGKGLEWVSSISSSGSTTYYADSAKGRFTVSRDNSRNTSFLQLNSLRAED
TAIYYCVKTTVINLSYFEDWGRGTTVTVSS

JoinSolver
Rearrangement is productive:
Highest scoring matches:
V: IGHV3-23*01 D:IGHD1-14*01R J: IGHJ4*02
The VH segment has 26 mutations
CDR3 Length: 39

```
 V   K   T   T   V   I   N   L   S   Y   F   E   D
GTG AAG ACC ACG GTT ATA AAC CTG TCG TAC TTT GAA GAC
```

V Match Results

```
                  ----------------------------------------------------------FR1-----------
                   1   2   3   4   5   6   7   8   9   10  11  12  13  14  15  16  17  18
                   E   V   Q   L   L   E   S   G   G   G   L   V   E   V   G   G   S   L
             score GAG GTG CAG CTG TTG GAG TCT GGG GGA GGC TTG GTA GAG GTT GGG GGG TCC CTG
IGHV3-23*01  1200  ... ... ... ... ... ... ... ... ... ... ... ... C.. CC. ... ... ... ...

                  ---------------------------------------------- ___________CDR1_________
                   19  20  21  22  23  24  25  26  27  28  29  30  31 31a 31b  32  33  34
                   R   L   S   C   A   A   S   G   L   P   F   R   S           S   A   M
                  AGA CTC TCC TGT GCG GCC TCT GGA CTC CCC TTT AGA AGC --- --- TCT GCC ATG
IGHV3-23*01       ... ... ... ... ..A ... ... ... T.. A.. ... ..C ... --- --- .A. ... ...

                  ___ --------------------------------FR2-------------------- ___________
                   35  36  37  38  39  40  41  42  43  44  45  46  47  48  49  50  51  52
                   S   W   V   R   Q   A   P   G   K   G   L   E   W   V   S   S   I   S
                  AGC TGG GTC CGC CAG GCT CCA GGG AAG GGG CTG GAG TGG GTC TCA AGT ATT AGT
IGHV3-23*01       ... ... ... ... ... ... ... ... ... ... ... ... ... ... ... GC. ... ...
```

```
                        _____________________CDR2_____________________________________ --------
                        52a 52b 52c  53  54  55  56  57  58  59  60  61  62  63  64  65  66  67
                         S           S   G   S   T   T   Y   Y   A   D   S   A   K   G   R   F
                        AGT --- --- AGT GGC AGT ACC ACA TAC TAC GCA GAC TCC GCG AAG GGC CGG TTC
IGHV3-23*01             G.. --- --- ... ..T G.. .G. ... ... ... ... ... ... .T. ... ... ... ...

                        ------------------FR3-----------------------------------------------------
                         68  69  70  71  72  73  74  75  76  77  78  79  80  81  82 82a 82b 82c
                         T   V   S   R   D   N   S   R   N   T   S   F   L   Q   L   N   S   L
                        ACC GTC TCC AGA GAC AAT TCC AGG AAC ACT TCA TTT CTG CAA TTG AAC AGC CTG
IGHV3-23*01             ... A.. ... ... ... ... ... .A. ... ..G CTG .A. ... ... A.. ... ... ...

                        ------------------------------------ ___CDR3_____
                         83  84  85  86  87  88  89  90  91  92  93  94  95
                         R   A   E   D   T   A   I   Y   Y   C   V   K   T
                        AGA GCC GAG GAC ACG GCC ATA TAC TAC TGC GTG AAG ACC
IGHV3-23*01             ... ... ... ... ... ... G.. ..T ... ..T .C. ..A GA
```

D Match Results

```
                         V   K   T   T   V   I   N   L   S   Y   F   E   D   W   G   R   G   T   T   V   T   V   S   S
                len|rf   GTG AAG ACC ACG GTT ATA AAC CTG TCG TAC TTT GAA GAC TGG GGC CGG GGG ACC ACG GTC ACC GTC TCC TCA A
IGHD1-14*01R    8|1         GT. GTT C.. ... ... CC
```

J Match Results

```
                         V   K   T   T   V   I   N   L   S   Y   F   E   D   W   G   R   G   T   T   V   T   V   S   S
                score    GTG AAG ACC ACG GTT ATA AAC CTG TCG TAC TTT GAA GAC TGG GGC CGG GGG ACC ACG GTC ACC GTC TCC TCA A
IGHJ4*02        159                                     AC ... ... ..C T.. ... ... .A. ..A ... CT. ... ... ... ... ... G
```

Junction Analysis

```
V Match: IGHV3-23*01  D Match: IGHD1-14*01R  J Match: IGHJ4*02
  V-J Distance: 36
VD Junction: # of P,N Nucleotides: (0,9)  TGAAGACCA
DJ Junction: # of P,N Nucleotides: (0,19)  AACCTGTCGTACTTTGAAG
```

Sequence – V_H3-33*01, No D Gene Assignment, J_H6*03 (21 Mutations)

Raw Sequence

CAGGTGCAGCTGGTGGAGTCTGGGGGAGGCGTGGTCCAGCCTGGGACGTCCCTGAGACTCTCCTGTAAAGGCTCTGGATTCAGTTTCAGCAACTATGGCATGCACTGGGTCCGCCAGG
CTCCAGGCAAGGGGCTGGAATGGGTGGCAGTTATCTGGTACGATGGAAGTCAGAAAAATTATGCAGACTCCGTGAAGGGCCGAGTCACCATCTCCAGAGAGAATTCCAAGAACACGCT
GTATCTGGAAATGAACAGCCTGAGAGGCGAGGACACGGCTGTATATTACTGTGCGAGGGCGAAAATTGTAGCAGTTTCAGCAAGCCCGTCGATGGGCTCCTACTATCACTACATGGAC
GTCTGGGGCAAAGGGACCACGGTCACCGTCTCCTCAA

Joinsolver Alignment

Summary

Amino acid translation of the sequence:
QVQLVESGGGVVQPGTSLRLSCKGSGFSFSNYGMHWVRQAPGKGLEWVAVIWYDGSQKNYADSVKGRVTISRENSKNTLYLEMNSLRGED
TAVYYCARAKIVAVSASPSMGSYYHYMDVWGKGTTVTVSSK

JoinSolver
Rearrangement is productive:
Highest scoring matches:
V: IGHV3-33*01 D:IGHD5-24*01R J: IGHJ6*03
The VH segment has 21 mutations
CDR3 Length: 69

A	R	A	K	I	V	A	V	S	A	S	P	S	M	G	S	Y	Y	H	Y	M	D	V
GCG	AGG	GCG	AAA	ATT	GTA	GCA	GTT	TCA	GCA	AGC	CCG	TCG	ATG	GGC	TCC	TAC	TAT	CAC	TAC	ATG	GAC	GTC

V Match Results

```
                  ------------------------------------------------------------FR1-----------
                   1   2   3   4   5   6   7   8   9   10  11  12  13  14  15  16  17  18
                   Q   V   Q   L   V   E   S   G   G   G   V   V   Q   P   G   T   S   L
             score CAG GTG CAG CTG GTG GAG TCT GGG GGA GGC GTG GTC CAG CCT GGG ACG TCC CTG
IGHV3-33*01  1236  ... ... ... ... ... ... ... ... ... ... ... ... ... ... ... .G. ... ...

                  ------------------------------------------------ ___________CDR1_________
                   19  20  21  22  23  24  25  26  27  28  29  30  31 31a 31b  32  33  34
                   R   L   S   C   K   G   S   G   F   S   F   S   N           Y   G   M
                  AGA CTC TCC TGT AAA GGC TCT GGA TTC AGT TTC AGC AAC --- --- TAT GGC ATG
IGHV3-33*01       ... ... ... ... GC. .CG ... ... ... .CC ... ..T .G. --- --- ... ... ...

                  ___ --------------------------------FR2-------------------- ___________
                   35  36  37  38  39  40  41  42  43  44  45  46  47  48  49  50  51  52
                   H   W   V   R   Q   A   P   G   K   G   L   E   W   V   A   V   I   W
                  CAC TGG GTC CGC CAG GCT CCA GGC AAG GGG CTG GAA TGG GTG GCA GTT ATC TGG
IGHV3-33*01       ... ... ... ... ... ... ... ... ... ... ... ..G ... ... ... ... ..A ...
```

```
                                  _____________________CDR2_____________________________________ --------
                                  52a 52b 52c  53  54  55  56  57  58  59  60  61  62  63  64  65  66  67
                                   Y           D   G   S   Q   K   N   Y   A   D   S   V   K   G   R   V
                                  TAC --- --- GAT GGA AGT CAG AAA AAT TAT GCA GAC TCC GTG AAG GGC CGA GTC
IGHV3-33*01                       ..T --- --- ... ... ... A.T ... T.C ... ... ... ... ... ... ... ... T..

                                  ------------------FR3-----------------------------------------------------
                                   68  69  70  71  72  73  74  75  76  77  78  79  80  81  82 82a 82b 82c
                                   T   I   S   R   E   N   S   K   N   T   L   Y   L   E   M   N   S   L
                                  ACC ATC TCC AGA GAG AAT TCC AAG AAC ACG CTG TAT CTG GAA ATG AAC AGC CTG
IGHV3-33*01                       ... ... ... ... ..C ... ... ... ... ... ... ... ... C.. ... ... ... ...

                                  ------------------------------------ ___CDR3_____
                                   83  84  85  86  87  88  89  90  91  92  93  94  95
                                   R   G   E   D   T   A   V   Y   Y   C   A   R   A
                                  AGA GGC GAG GAC ACG GCT GTA TAT TAC TGT GCG AGG GCG
IGHV3-33*01                       ... .C. ... ... ... ... ..G ... ... ... ... ..A .A
```

D Match Results

```
                A   R   A   K   I   V   A   V   S   A   S   P   S   M   G   S   Y   Y   H   Y   M   D   V   W   G   K   G   T   T   V   T   V   S   S   K
          len|rf GCG AGG GCG AAA ATT GTA GCA GTT TCA GCA AGC CCG TCG ATG GGC TCC TAC TAT CAC TAC ATG GAC GTC TGG GGC AAA GGG ACC ACG GTC ACC GTC TCC TCA A
IGHD5-
24*01R    9|1             GT. ... ... ..C A.C ..T A.
```

J Match Results

```
                A   R   A   K   I   V   A   V   S   A   S   P   S   M   G   S   Y   Y   H   Y   M   D   V   W   G   K   G   T   T   V   T   V   S   S   K
          score GCG AGG GCG AAA ATT GTA GCA GTT TCA GCA AGC CCG TCG ATG GGC TCC TAC TAT CAC TAC ATG GAC GTC TGG GGC AAA GGG ACC ACG GTC ACC GTC TCC TCA A
IGHJ6*03  243                                                   AT TA. .A. ... ..C T.. ... ... ... ... ... ... ... ... ... ... ... ... ... ... ... G
```

Junction Analysis

```
V Match: IGHV3-33*01  D Match: IGHD5-24*01R  J Match: IGHJ6*03
  V-J Distance: 50
VD Junction: # of P,N Nucleotides: (0,6)  GGCGAA
DJ Junction: # of P,N Nucleotides: (0,35)  AGTTTCAGCAAGCCCGTCGATGGGCTCCTACTATC
```

Sequence – V_H3-33*01, No D Gene Assignment, J_H6*03 (22 Mutations)

Raw Sequence

CAGGTGCAGCTGGTGGAGTCTGGGGGAGGCGTGGTCCAGCCTGGGACGTCCCTGAGACTCTCCTGTAAAGGCCCTGGATTCAGTTTCAGCAACTATGGCATGCACTGGGTCCGCCAGG
CTCCAGGCAAGGGGCTGGAATGGGTGGCAGTTATCTGGTACGATGGAAGTCAGAAAAATTATGCAGACTCCGTGAAGGGCCGAGTCACCATCTCCAGAGAGAATTCCAAGAACACGCT
GTATCTGGAAATGAACAGCCTGAGAGGCGAGGACACGGCTGTATATTACTGTGCGAGGGCGAAAATTGTAGCAGTTTCAGCAAGCCCGTCGATGGGCTCCTACTATCACTACATGGAC
GTCTGGGGCAAAGGGACCACGGTCACCGTCTCCTCAA

Joinsolver Alignment

Summary

Amino acid translation of the sequence:
QVQLVESGGGVVQPGTSLRLSCKGPGFSFSNYGMHWVRQAPGKGLEWVAVIWYDGSQKNYADSVKGRVTISRENSKNTLYLEMNSLRGED
TAVYYCARAKIVAVSASPSMGSYYHYMDVWGKGTTVTVSS

JoinSolver
Rearrangement is productive:
Highest scoring matches:
V: IGHV3-33*01 D:IGHD5-24*01R J: IGHJ6*03
The VH segment has 22 mutations
CDR3 Length: 69

```
 A   R   A   K   I   V   A   V   S   A   S   P   S   M   G   S   Y   Y   H   Y   M   D   V
GCG AGG GCG AAA ATT GTA GCA GTT TCA GCA AGC CCG TCG ATG GGC TCC TAC TAT CAC TAC ATG GAC GTC
```

V Match Results

```
                  ------------------------------------------------------------FR1-----------
                   1   2   3   4   5   6   7   8   9   10  11  12  13  14  15  16  17  18
                   Q   V   Q   L   V   E   S   G   G   G   V   V   Q   P   G   T   S   L
             score CAG GTG CAG CTG GTG GAG TCT GGG GGA GGC GTG GTC CAG CCT GGG ACG TCC CTG
IGHV3-33*01  1227  ... ... ... ... ... ... ... ... ... ... ... ... ... ... ... .G. ... ...

                  ---------------------------------------------- __________CDR1_________
                   19  20  21  22  23  24  25  26  27  28  29  30  31 31a 31b  32  33  34
                   R   L   S   C   K   G   P   G   F   S   F   S   N           Y   G   M
                  AGA CTC TCC TGT AAA GGC CCT GGA TTC AGT TTC AGC AAC --- --- TAT GGC ATG
IGHV3-33*01       ... ... ... ... GC. .CG T.. ... ... .CC ... ..T .G. --- --- ... ... ...

                  ___ --------------------------------FR2------------------- ___________
                   35  36  37  38  39  40  41  42  43  44  45  46  47  48  49  50  51  52
                   H   W   V   R   Q   A   P   G   K   G   L   E   W   V   A   V   I   W
                  CAC TGG GTC CGC CAG GCT CCA GGC AAG GGG CTG GAA TGG GTG GCA GTT ATC TGG
IGHV3-33*01       ... ... ... ... ... ... ... ... ... ... ... ..G ... ... ... ... ..A ...
```

```
                                  _____________________CDR2_____________________________________ --------
                                  52a 52b 52c  53  54  55  56  57  58  59  60  61  62  63  64  65  66  67
                                   Y           D   G   S   Q   K   N   Y   A   D   S   V   K   G   R   V
                                  TAC --- --- GAT GGA AGT CAG AAA AAT TAT GCA GAC TCC GTG AAG GGC CGA GTC
IGHV3-33*01                       ..T --- --- ... ... ... A.T ... T.C ... ... ... ... ... ... ... ... T..

                                  ------------------FR3-----------------------------------------------------
                                   68  69  70  71  72  73  74  75  76  77  78  79  80  81  82 82a 82b 82c
                                   T   I   S   R   E   N   S   K   N   T   L   Y   L   E   M   N   S   L
                                  ACC ATC TCC AGA GAG AAT TCC AAG AAC ACG CTG TAT CTG GAA ATG AAC AGC CTG
IGHV3-33*01                       ... ... ... ... ..C ... ... ... ... ... ... ... ... C.. ... ... ... ...

                                  ------------------------------------ ___CDR3_____
                                   83  84  85  86  87  88  89  90  91  92  93  94  95
                                   R   G   E   D   T   A   V   Y   Y   C   A   R   A
                                  AGA GGC GAG GAC ACG GCT GTA TAT TAC TGT GCG AGG GCG
IGHV3-33*01                       ... .C. ... ... ... ... ..G ... ... ... ... ..A .A
```

D Match Results

```
                    A   R   A   K   I   V   A   V   S   A   S   P   S   M   G   S   Y   Y   H   Y   M   D   V   W   G   K   G   T   T   V   T   V   S   S
          len|rf    GCG AGG GCG AAA ATT GTA GCA GTT TCA GCA AGC CCG TCG ATG GGC TCC TAC TAT CAC TAC ATG GAC GTC TGG GGC AAA GGG ACC ACG GTC ACC GTC TCC TCA A
IGHD5-
24*01R    9|1               GT. ... ... ..C A.C ..T A.
```

J Match Results

```
                    A   R   A   K   I   V   A   V   S   A   S   P   S   M   G   S   Y   Y   H   Y   M   D   V   W   G   K   G   T   T   V   T   V   S   S
          score     GCG AGG GCG AAA ATT GTA GCA GTT TCA GCA AGC CCG TCG ATG GGC TCC TAC TAT CAC TAC ATG GAC GTC TGG GGC AAA GGG ACC ACG GTC ACC GTC TCC TCA A
IGHJ6*03  243                                                       AT TA. .A. ... ..C T.. ... ... ... ... ... ... ... ... ... ... ... ... ... ... ... G
```

Junction Analysis

```
V Match: IGHV3-33*01  D Match: IGHD5-24*01R  J Match: IGHJ6*03
  V-J Distance: 50
VD Junction: # of P,N Nucleotides: (0,6)  GGCGAA
DJ Junction: # of P,N Nucleotides: (0,35)  AGTTTCAGCAAGCCCGTCGATGGGCTCCTACTATC
```

Appendix 2- Statistical Analysis Results

Statistical analysis, as described in section 2.3.13 was conducted using GraphPad Prism 4 (GraphPad Software Inc., San Diego CA, USA). The following tables present the p-values obtained from each statistical test conducted in the analysis of results presented in this study. Areas highlighted in yellow indicate where a statistically significant difference was observed and the p-values obtained were less than 0.05. 'N/A' or '–' illustrate where statistical analysis could not be conducted either because a non-productive repertoire was not identified within the samples or where numbers were not sufficient to allow the respective statistical analysis to be conducted.

Table 1a - Results (p-values) from Chi Square Test in the Statistical Analysis of Functional Ig Gene Distributions from Muscle Infiltrating B Cells in Individual Myositis Patients Compared with PBL or Germline V-gene Frequencies.

	MYO1		MYO3		MYO5			MYO5 PBL		MYO16		MYO23	
	PBL	Germline	PBL	Germline	PBL	Germline	MYO5 PBL	PBL	Germline	PBL	Germline	PBL	Germline
VH1	0.3048	0.2966	<0.0001	0.0021	0.0311	0.0254	0.0016	0.0028	0.0949	0.0603	0.0612	0.1678	0.1456
VH2	0.0003	0.567	0.5556	0.3064	0.3965	0.8179	0.3506	<0.0001	0.32	0.391	0.1386	0.668	0.4554
VH3	0.0381	0.1305	0.0645	0.1155	0.7001	0.7	0.9848	0.0801	0.2151	<0.0001	0.0009	0.0097	0.0154
VH4	0.1418	0.4402	0.5317	0.7291	0.514	0.7424	0.4177	0.0029	0.0179	0.1513	0.3625	0.3611	0.4696
VH5	0.4842	0.9097	0.3128	0.4072	<0.0001	0.0034	0.0574	0.303	0.2877	0.1419	0.2339	0.4627	0.5457
VH6	0.2377	0.2882	0.519	0.5608	0.5084	0.5084	0.21	0.0566	0.23	0.348	0.3981	0.6389	0.6718
VH7	0.4696	0.2882	0.6929	0.5608	0.6532	0.5084	-	0.53	0.3559	0.5655	0.3981	0.7738	0.6718
DH1	0.6003	0.7725	0.9148	0.7935	0.4064	0.8079	0.0377	0.1022	0.0528	0.1122	0.0595	N/A Expected frequency for observed values was below 5 therefore Chi Square Analysis could not be conducted.	
DH2	0.1395	0.8488	0.5723	0.9719	0.0982	0.2207	0.1939	0.5053	0.8667	0.2605	0.7741		
DH3	0.6692	0.1095	0.1867	0.039	0.9886	0.3545	0.4113	0.1403	0.0254	0.3817	0.6883		
DH4	0.4237	0.604	0.4623	0.2783	0.4046	0.2207	0.2987	0.5171	0.7203	0.8377	0.3633		
DH5	0.559	0.1899	0.5237	0.9719	0.1079	0.6056	0.4436	0.6027	0.0723	0.2301	0.096		
DH6	0.3954	0.7024	0.2925	0.2783	0.4554	0.6056	0.4436	0.7525	0.0723	<0.0001	0.0023		
DH7	0.4383	0.2319	0.7394	0.6053	0.706	0.5582	-	0.5937	0.409	0.6042	0.4222		
JH1	0.1165	0.0019	0.3913	0.0852	0.3294	0.0512	-	0.1728	0.0068	0.2122	0.0132	0.5328	0.2049
JH2	0.5385	0.0475	0.5285	0.4202	0.3946	0.0512	0.096	0.0019	0.7243	0.2762	0.0132	<0.0001	0.132
JH3	0.3074	0.5309	0.1051	0.0852	0.5102	0.9315	0.9668	0.3174	0.9086	0.0117	0.5666	0.2382	0.2049
JH4	0.6287	0.1729	0.7	0.1897	0.2513	0.0991	0.1817	0.4895	0.332	0.4439	0.3496	0.01	0.2049
JH5	0.5898	0.8609	0.0238	0.541	0.7013	0.5949	0.1637	0.0195	0.7171	0.0955	0.1391	0.0023	0.2636
JH6	0.0849	0.3421	0.4781	0.9566	0.4539	0.9315	0.3025	0.017	0.5767	0.2572	0.4136	0.0824	0.2049

Table 1b - Results (p-values) from Chi Square Test in the Statistical Analysis of Functional Ig Gene Distributions from Different Myositis Subsets Compared with PBL, Germline V-gene Frequencies or Between Myositis Subsets.

	MYO		DM		PM		
	PBL	Germline	PBL	Germline	PBL	Germline	DM vs PM
VH1	0.5548	0.2773	0.0491	0.0922	0.621	0.9596	0.0759
VH2	0.0878	0.5744	0.0227	0.8991	0.9223	0.2726	0.2889
VH3	<0.0001	0.0348	<0.0001	0.0081	0.3118	0.4324	0.0688
VH4	0.0071	0.2504	0.0416	0.3236	0.0972	0.3462	0.9331
VH5	0.8661	0.6687	0.1446	0.5362	0.0942	0.1736	0.0228
VH6	0.1687	0.4212	0.1315	0.1754	0.2461	0.2968	N/A
VH7	0.2408	0.0856	0.3557	0.1754	0.4775	0.2968	N/A
DH1	0.6589	0.3451	0.6566	0.342	0.9868	0.5987	0.7879
DH2	0.0126	0.6398	0.0641	0.7944	0.0977	0.5069	0.6113
DH3	0.7246	0.1011	0.8965	0.1783	0.5722	0.1057	0.5878
DH4	0.7094	0.1535	0.5817	0.4358	0.1828	0.0543	0.135
DH5	0.5649	0.1535	0.2495	0.0677	0.3512	0.8572	0.1219
DH6	<0.0001	0.141	0.0002	0.1166	0.0839	0.3206	0.6702
DH7	0.2638	0.0857	0.3511	0.151	0.5465	0.3512	N/A
JH1	0.0109	<0.0001	0.045	<0.0001	0.1231	0.0023	N/A
JH2	0.1425	0.243	0.2471	0.0085	<0.0001	0.7861	0.0025
JH3	0.984	0.8145	0.4417	0.9723	0.3507	0.5541	0.2262
JH4	0.7873	0.2272	0.923	0.2215	0.716	0.2628	0.8172
JH5	0.2695	0.8922	0.5417	0.5819	0.0209	0.7698	0.0408
JH6	0.9515	0.6307	0.1809	0.4533	0.1358	0.9848	0.0461

Table 2 - Results (p-values) from Chi Square Test in the Statistical Analysis of Functional Ig Gene Distributions Collectively from Skin Infiltrating B cells and Two Paired Peripheral Blood Samples or Germline DNA.

	VAS		VAS1 PBL		VAS6 PBL	
	PBL	**Germline**	**PBL**	**Germline**	**PBL**	**Germline**
VH1	0.5103	0.7291	0.0551	0.2483	0.7542	0.9849
VH2	0.5556	0.3064	<0.0001	0.1418	<0.0001	0.0239
VH3	0.2856	0.3268	0.6258	0.7472	0.0121	0.0555
VH4	0.5317	0.7291	0.0093	0.0291	0.0092	0.0391
VH5	0.3128	0.4072	0.7728	0.5573	0.9795	0.72
VH6	0.519	0.5608	0.7094	0.6821	0.2162	0.3654
VH7	0.6926	0.5608	0.606	0.4524	<0.0001	0.013
DH1	0.308	0.2177	0.1233	0.0616	0.2012	0.1123
DH2	0.5723	0.9719	0.6663	0.7763	0.2018	0.8105
DH3	0.2804	0.7935	0.0029	0.001	0.0888	0.0173
DH4	0.0284	0.3949	0.2665	0.0991	0.8247	0.4733
DH5	0.0006	0.102	0.8161	0.3747	0.9243	0.4733
DH6	0.2925	0.2783	0.3881	0.3747	0.6695	0.856
DH7	0.7394	0.6053	0.615	0.4272	0.5379	0.341
JH1	0.7198	0.4202	0.2628	0.0257	0.2098	0.5197
JH2	0.0452	0.7592	0.3284	0.0257	<0.0001	1
JH3	0.1051	0.0852	0.0055	0.4782	0.2879	0.8725
JH4	0.0787	0.1233	0.0466	0.6919	0.1503	0.4857
JH5	0.4543	0.4202	0.0497	0.0257	0.5278	0.5197
JH6	0.8803	0.7261	0.0147	0.2	0.2434	1

Table 3 - Results (p-values) from Chi Square Test in the Statistical Analysis of Individual V_H Gene Distributions from both disorders and paired peripheral blood samples compared to normal control values of Volpe and Kepler (251).

V_H Gene	MYO	DM	PM	MYO5 PBL	VAS	VAS1 PBL	VAS6 PBL
1~18*01	0.2268	0.9154	0.1895	0.7867	0.4949	0.8972	0.2885
1~2*01	0.016	0.0578	0.1445	0.1969	0.4171	0.2893	0.2377
1~24*01	0.3813	0.4906	0.596	0.6392	0.7682	0.7003	0.668
1~3*01	0.6717	0.3359	0.0501	0.0166	0.6807	0.0015	0.0063
1~45*02	0.7338	0.7889	0.8368	0.8555	0.9089	0.8811	0.8677
1~46*01	0.2187	0.3674	0.3598	0.3582	0.0034	0.5524	0.4005
1~58*01	0.6304	0.7048	0.7708	0.7967	0.8713	0.8325	0.8137
1~69*01	0.7845	0.3407	0.0797	0.197	0.9428	0.0057	0.0278
1~8*01	0.4461	0.2502	0.3765	0.4342	0.6229	0.5208	0.4743
1~f*01	0.127	0.7048	0.0027	0.7967	0.8713	0.8325	0.8137
2~26*01	0.4436	0.5487	0.6447	<0.0001	0.7976	0.009	0.7091
2~5*01	0.1336	0.0076	0.328	0.3454	0.5865	0.0004	<0.0001
2~70*01	0.4252	0.2424	0.8194	0.4257	0.6164	0.513	0.4661
3~11*01	0.004	<0.0001	0.7979	0.3099	0.5232	0.4043	0.8632
3~13*01	0.4652	0.5652	0.6583	0.6958	0.8058	0.7481	0.7205
3~15*01	0.0468	0.0007	0.264	0.3233	0.5346	0.4173	0.177
3~19*01	-	-	-	-	-	-	-
3~20*01	0.3886	0.4973	0.6016	0.6444	0.7716	0.7046	0.6728
3~21*01	0.1189	0.1044	0.6713	0.9997	0.4328	<0.0001	0.3081
3~23*01	0.0052	0.0971	0.0175	0.293	0.2389	0.2771	0.0545
3~30*01	0.0018	0.0374	0.0382	0.6037	0.335	0.4311	0.302
3~30-3*01	0.06761	0.1493	0.2673	0.3267	0.5375	0.4206	0.3695
3~33*01	0.0131	0.5004	0.0009	0.2423	0.0393	0.337	0.9162
3~35*01	0.8326	0.8655	0.8964	0.9083	0.9432	0.9247	0.9161
3~38*02	0.8792	0.9047	0.9266	0.9351	0.9592	0.9467	0.9406
3~43*01	0.5069	0.6013	0.6878	0.7198	0.8232	0.7704	0.7451
3~48*01	0.8864	0.2184	0.1827	0.098	0.4555	0.9212	0.281
3~49*01	0.826	0.9533	0.6281	0.4813	0.6579	0.563	0.3579
3~53*01	0.7962	0.3071	0.0776	0.4874	0.6623	0.5684	0.5251
3~64*01	0.3685	0.4714	0.5797	0.6243	0.7581	0.6575	0.6541
3~66*01	0.0052	0.0044	0.3201	0.9877	0.7305	0.077	0.136
3~7*01	<0.0001	<0.0001	0.2511	0.5476	0.3903	0.848	0.2113
3~72*01	0.0617	0.5569	0.0001	0.6895	0.8017	0.7428	0.7147
3~73*01	0.7165	0.5111	0.1447	0.0764	0.0012	0.7136	0.6826
3~74*01	0.2483	0.1697	0.9285	0.3504	0.5571	0.4432	0.3929
3~9*01	0.0774	0.0195	0.941	0.3543	0.5602	0.4468	0.3967
4~28*01	0.7923	0.8357	0.8733	0.8879	0.9293	0.9078	0.8973
4~30-2*01	0.142	0.2476	0.3729	0.4317	0.621	0.5184	0.4719
4~30-4*01	-	-	-	-	-	-	-
4~31*01	0.1532	0.1229	0.2354	0.2941	0.5095	0.3889	0.3371
4~34*01	0.039	0.0402	0.8627	0.4301	0.2271	0.1147	0.6022
4~39*01	0.1075	0.162	0.429	0.1876	0.4073	0.9038	0.2279
4~4*01	0.7927	0.9109	0.8031	0.3315	0.5246	0.4059	0.3545
4~55*01	-	-	-	-	-	-	-
4~59*01	0.1753	0.0676	0.9386	0.1903	0.0032	0.2821	0.2308

Cont…

V_H Gene	MYO	DM	PM	MYO5 PBL	VAS	VAS1 PBL	VAS6 PBL
4~61*01	0.3315	0.6449	0.3302	0.3892	0.5882	0.4785	0.4308
4~b*01	0.8836	0.4865	0.585	0.6292	0.7614	0.6917	0.6586
5~51*01	0.8413	0.1238	0.0176	0.1116	0.3804	0.4985	0.7188
5~a*01	0.4832	0.8241	0.3901	0.4473	0.6328	0.5326	0.4869
6~1*01	0.1687	0.1315	0.2461	0.0509	0.519	0.7094	0.2162
7~4-1*01	0.2249	0.3598	0.4813	0.5355	0.6954	0.6091	<0.0001
7~81*01	0.8792	0.9047	0.9266	0.9351	0.9592	0.9467	0.9406

Table 4 - Results (p-values) from Chi Square Test in the Statistical Analysis of Individual D_H Gene Distributions from both disorders and paired peripheral blood samples compared to normal control values of Volpe and Kepler (251).

	MYO	DM	PM	MYO5 PBL	VAS	VAS1 PBL	VAS6 PBL
0~IR*01	0.3465	0.4364	0.6115	0.6532	0.7793	0.6718	0.6038
1~1*01	0.2781	0.0721	0.4879	0.5394	0.702	0.5629	0.4786
1~14*01	0.407	0.493	0.6546	0.6922	0.805	0.709	0.6476
1~20*01	0.727	0.1728	0.8506	0.8676	0.9172	0.8751	0.8474
1~26*01	0.8431	0.0721	0.793	0.3011	0.519	0.3296	0.7592
1~7*01	0.47	0.3604	0.0055	0.5975	0.7419	0.6186	0.5421
1~IR1*01	0.2813	0.373	0.561	0.607	0.7484	0.6277	0.5526
1~OR15*1	0.7142	0.7621	0.8434	0.8612	0.9132	0.8691	0.84
2~15*01	0.2017	0.1273	0.9581	0.3786	0.5829	0.0936	0.9972
2~2*01	0.0075	0.0511	0.2377	0.3735	0.8862	0.9996	0.2176
2~21*01	0.0648	0.0721	0.4127	0.488	0.6513	0.4945	0.6951
2~8*01	0.647	0.9432	0.4946	0.28	0.7063	0.5689	0.4854
2~IR2*01	0.5252	0.5994	0.7317	0.7617	0.85	0.7749	0.7262
2~OF15*2	0.2974	0.389	0.5739	0.6189	0.7564	0.6391	0.5657
3~10*01	0.8907	0.4803	0.4816	0.6612	0.5773	0.5584	0.1477
3~16*01	0.3435	0.702	0.2804	0.3396	0.5515	0.3679	0.8809
3~22*01	0.0229	0.7604	<0.0001	0.6429	0.4316	0.0007	0.1267
3~3*01	0.6988	0.9417	0.5495	0.0008	0.4456	0.0969	0.1579
3~9*01	0.5596	0.4566	0.3412	0.3997	0.5995	0.4272	0.0263
3~OR15*3	0.4478	0.5303	0.6821	0.7171	0.8212	0.7326	0.6756
4~17*01	0.909	0.0721	0.3244	0.6975	0.001	0.4111	0.9774
4~23*01	0.8925	0.805	0.561	0.607	0.7484	0.6277	0.2675
4~4*01	0.9586	0.6631	0.5968	0.6398	0.7704	0.6591	0.589
4~OR15*4	0.5447	0.6165	0.7438	0.7725	0.8569	0.7852	0.7385
5~12*01	0.0904	0.4619	0.0362	0.3381	<0.0001	0.5468	0.0434
5~24*01	0.5239	0.2536	0.0465	0.3727	0.681	0.3063	0.4465
5~5*01	0.1208	0.1995	0.4024	0.4588	0.6441	0.4849	0.3924
5~OR15*5	0.6393	0.6984	0.8003	0.823	0.889	0.8329	0.7961
6~13*01	0.4175	0.0091	0.2954	0.3546	0.5637	0.3828	0.0046
6~19*01	0.0022	0.1783	0.0002	0.435	0.4837	0.2897	0.6376
6~25*01	0.573	0.6412	0.761	0.7879	0.8667	0.7997	0.756
6~6*01	0.0012	<0.0001	0.4748	0.5272	0.6934	0.2649	0.4654
7~27*01	0.2638	0.3556	0.5465	0.5937	0.7394	0.615	0.5379

Table 5 – Results (p-values) from Two Tailed Unpaired t-tests in Individual Patients, Paired Peripheral Blood Samples, Collective Patients and Disease Subsets of both Myositis and Vasculitic Disorders in Comparison of CDR3 Lengths in the Functional and Non-Functional Repertoires.

	MYO1	MYO5 PBL	MYO	MYO DM	MYO PM	VAS	VAS1 PBL	VAS6 PBL
CDR3 Length P vs NP	0.661	0.5017	0.9529	0.9461	N/A	0.0716	0.3613	0.1632

Table 6 – Results (p-values) from Two Tailed Unpaired t-tests in Individual Patients, Paired Peripheral Blood Samples, Collective Patients and Disease Subsets of the Myositis Disorders in Comparison of P and N Nucleotide Lengths at Different Regions of the Ig Gene Recombination Junction and in the Functional and Non-Functional Repertoires.

		MYO1		MYO3		MYO5		MYO5 PBL		MYO16		MYO23		MYO		MYO DM		MYO PM	
		VD vs DJ		VD vs DJ		VD vs DJ		VD vs DJ		VD vs DJ		VD vs DJ		VD vs DJ		VD vs DJ		VD vs DJ	
P Nucleotide	**Productive**	0.3758		0.3615		0.6239		0.5886		0.5262		N/A		0.6342		0.7839		0.6309	
	Non-Productive	0.2725		N/A		N/A		N/A		N/A		N/A		0.2725		0.2725		N/A	
		VD	**DJ**	**VD**	**DJ**	**VD**	**DJ**	**VD**	**DJ**	**VD**	**DJ**	**VD**	**DJ**	**VD**	**DJ**	**VD**	**DJ**	**VD**	**DJ**
	P vs NP	0.039	0.9447	N/A	N/A	N/A	N/A	0.2679	N/A	N/A	N/A	N/A	N/A	0.0124	0.9314	0.0239	0.7963	N/A	N/A
N Nucleotide	**Productive**	0.4064		0.2261		0.3495		0.9787		0.0596		N/A		0.1654		0.8557		0.0073	
	Non-Productive	0.364		N/A		N/A		0.2589		N/A		N/A		0.364		0.364		N/A	
		VD	**DJ**	**VD**	**DJ**	**VD**	**DJ**	**VD**	**DJ**	**VD**	**DJ**	**VD**	**DJ**	**VD**	**DJ**	**VD**	**DJ**	**VD**	**DJ**
	P vs NP	0.2658	0.3928	N/A	N/A	N/A	N/A	0.4129	0.3212	N/A	N/A	N/A	N/A	0.5242	0.4644	0.4043	0.432	N/A	N/A

Table 7 – Results (p-values) from Two Tailed Unpaired t-tests in Collective Vasculitis Patients and Paired Peripheral Blood Samples in Comparison of P and N Nucleotide Lengths at Different Regions of the Ig Gene Recombination Junction and in the Functional and Non-Functional Repertoires.

		VAS		VAS1 PBL		VAS6 PBL	
		VD vs DJ		VD vs DJ		VD vs DJ	
P Nucleotide	Productive	N/A		0.0343		0.202	
	Non-Productive	N/A		1		0.5761	
		VD	DJ	VD	DJ	VD	DJ
	P vs NP	N/A	N/A	0.721	0.3453	0.13	0.229
N Nucleotide	Productive	0.6487		0.5394		0.3282	
	Non-Productive	N/A		0.2552		0.9017	
		VD	DJ	VD	DJ	VD	DJ
	P vs NP	N/A	N/A	0.238	0.3662	0.975	0.715

Results (p-values) from Two Tailed Unpaired t-tests in Comparison of Exonuclease Activity at Different Regions of the Ig Gene Recombination Junction and in the Functional and Non-Functional Repertoires.

Table 8a

		MYO1				MYO3				MYO5				MYO5 PBL			
		3' VH	5' DH	3'DH	5' JH	3' VH	5' DH	3'DH	5' JH	3' VH	5' DH	3'DH	5' JH	3' VH	5' DH	3'DH	5' JH
Exonuclease Activity	P vs NP	0.2468	0.1282	0.3957	0.8798	N/A	N/A	N/A	N/A	N/A	N/A	N/A	N/A	0.016	0.9219	0.8556	0.2724
	VH vs JH	<0.0001				0.0002				0.0008				0.0002			
	5'DH vs3'DH	0.3414				0.8507				0.0787				0.6078			
	VH vs 5'DH	<0.0001				0.0925				0.0472				0.0004			
	3'DH vs JH	0.8918				0.7814				0.0035				0.4661			

Table 8b

		MYO16				MYO23				MYO				MYO DM				MYO PM			
		3' VH	5' DH	3'DH	5' JH	3' VH	5' DH	3'DH	5' JH	3' VH	5' DH	3'DH	5' JH	3' VH	5' DH	3'DH	5' JH	3' VH	5' DH	3'DH	5' JH
Exonuclease Activity	P vs NP	N/A	N/A	N/A	N/A	N/A	N/A	N/A	N/A	0.238	0.2155	0.181	0.9035	0.249	0.1359	0.2073	0.9947	N/A	N/A	N/A	N/A
	VH vs JH	0.0006				N/A				<0.0001				<0.0001				<0.0001			
	5'DH vs3'DH	0.1346				N/A				0.1058				0.1286				0.3309			
	VH vs 5'DH	0.0006				N/A				<0.0001				<0.0001				0.0103			
	3'DH vs JH	0.1917				N/A				0.0923				0.4023				0.0593			

Table 9

		VAS				VAS1 PBL				VAS6 PBL			
		3' VH	5' DH	3'DH	5' JH	3' VH	5' DH	3'DH	5' JH	3' VH	5' DH	3'DH	5' JH
Exonuclease Activity	P vs NP	N/A	N/A	N/A	N/A	0.027	0.528	0.29	N/A*	0.003	0.6796	0.639	0.5869
	VH vs JH	0.1518				<0.0001				0.0021			
	5'DH vs3'DH	0.1758				0.1333				0.7844			
	VH vs 5'DH	0.0132				0.0007				0.0001			
	3'DH vs JH	0.075				0.7324				0.7912			

Table 10 – Results (p-values) from One-Way Analysis of Variance Test Used In Conjunction with the Tukey-Kramer Multiple Comparison Post Test in Individual Patients, Paired Peripheral Blood Samples, Collective Patients and Disease Subsets of both Myositis and Vasculitic Disorders to Determine Statistical Difference Between Mean CDR3 Lengths in Mutated Sequences.

	0-2 vs 3-10	0-2 vs 11-20	0-2 vs 20+	3-10 vs 11-20	3-10 vs20+	11-20 vs 20+
MYO1	>0.05	>0.05	>0.05	>0.05	>0.05	>0.05
MYO3	>0.05	>0.05	>0.05	>0.05	>0.05	>0.05
MYO5	N/A	N/A	N/A	>0.05	>0.05	>0.05
MYO5 PBL	>0.05	>0.05	>0.05	>0.05	>0.05	>0.05
MYO16	>0.05	>0.05	<0.0001	>0.05	<0.05	<0.05
MYO	>0.05	>0.05	<0.05	>0.05	>0.05	>0.05
MYO DM	>0.05	>0.05	>0.05	>0.05	>0.05	>0.05
MYO PM	>0.05	>0.05	>0.05	>0.05	>0.05	<0.05
VAS	>0.05	>0.05	>0.05	>0.05	>0.05	>0.05
VAS1 PBL	>0.05	>0.05	>0.05	>0.05	>0.05	>0.05
VAS6 PBL	<0.05	>0.05	>0.05	>0.05	>0.05	>0.05